Advanced Composite Materials for Aerospace Engineering

Processing, Properties and Applications

Edited by Sohel Rana and Raul Fangueiro

Related titles

Modelling of Failure in Advanced Composite Materials
(ISBN 978-0-08100-332-9)
Recent Advances in Smart Self-healing Polymers and Composites
(ISBN 978-1-78242-280-8)
Predicting Structural Integrity and Durability in Advanced Composite Materials
(ISBN 978-0-08100-137-0)

Woodhead Publishing Series in Composites Science and Engineering: Number 70

Advanced Composite Materials for Aerospace Engineering

Processing, Properties and Applications

Edited by

Sohel Rana

Raul Fangueiro

For information on all Woodhead Publishing publications
visit our website at https://www.elsevier.com/

Working together
to grow libraries in
developing countries

www.elsevier.com • www.bookaid.org

*Dedicated to my mentor and dearest grandfather, **Md. Abdur Razzaque** and my lovely wife, **Gargi** whose love and inspiration are always behind every piece of my work, including this book.*
― Sohel Rana

*Dedicated to my wife **Ana** and my daughters **Carolina**, **Ana João** and **Inês**…with you everything is possible!*
― Raul Fangueiro

List of contributors

R.D. Anandjiwala   CSIR Materials Science and Manufacturing, Port Elizabeth, South Africa; Faculty of Science, Nelson Mandela Metropolitan University, Port Elizabeth, South Africa

C. Ayranci   University of Alberta, Edmonton, AB, Canada

P. Balakrishnan   Mahatma Gandhi University, Kottayam, Kerala, India

A.M. Baptista   University of Porto, Porto, Portugal

J.P. Carey   University of Alberta, Edmonton, AB, Canada

U. Chatterjee   Indian Institute of Technology, New Delhi, India

B. Cheung   University of Alberta, Edmonton, AB, Canada

D.D.L. Chung   State University of New York, Buffalo, NY, United States

R. Das   University of Auckland, Auckland, New Zealand

M. de Araujo   University of Minho, Guimarães, Portugal

R. Fangueiro   School of Engineering, University of Minho, Guimarães, Portugal

Z. Fawaz   Ryerson University, Toronto, ON, Canada

K.V.N. Gopal   Indian Institute of Technology Madras, Chennai, India

H. Hu   Hong Kong Polytechnic University, Kowloon, Hong Kong

A. Hunt   University of Alberta, Edmonton, AB, Canada

M. Ivey   University of Alberta, Edmonton, AB, Canada

M.J. John   CSIR Materials Science and Manufacturing, Port Elizabeth, South Africa

M. Joshi   Indian Institute of Technology, New Delhi, India

K.M. Karumbaiah   University of Auckland, Auckland, New Zealand

L.Z. Linganiso   CSIR Materials Science and Manufacturing, Port Elizabeth, South Africa

F.J. Lino Alves   University of Porto, Porto, Portugal

Y. Liu   Hong Kong Polytechnic University, Kowloon, Hong Kong

A.T. Marques   University of Porto, Porto, Portugal

C. Melchior   National Polytechnic Institute of Chemical Engineering and Technology (INP-ENSIACET), Toulouse, France

G.W. Melenka   University of Alberta, Edmonton, AB, Canada

J.P. Nunes   Minho University, Guimaraes, Portugal

S. Parveen   School of Engineering, University of Minho, Guimarães, Portugal

L. Pothen   Bishop Moore College, Alleppey, Kerala, India

S. Rana   School of Engineering, University of Minho, Guimarães, Portugal

C. Scarponi   "La Sapienza" University of Rome, Rome, Italy

J.F. Silva   Polytechnic Institute of Porto, Porto, Portugal

M.S. Sreekala   Sree Sankara College Kalady, Enakulam, Kerala, India

S. Thomas   Mahatma Gandhi University, Kottayam, Kerala, India

Z. Wang   Hong Kong Polytechnic University, Kowloon, Hong Kong

A. Zulifqar   Hong Kong Polytechnic University, Kowloon, Hong Kong

Woodhead Publishing Series in Composites Science and Engineering

Editors' biographies

Dr Sohel Rana is currently a Senior Scientist at Fibrous Materials Research Group, University of Minho, Portugal. He obtained his bachelor's degree in Textile Technology from University of Calcutta, India and a master's degree and PhD in Fibre Science and Technology from Indian Institute of Technology (IIT, Delhi), India. His current research areas are advanced fibrous and composite materials, natural fibres, nanocomposites, electrospinning, multifunctional and bio-composite materials and so on. He is author of one book, edited four books and contributed 14 book chapters, six keynote and invited papers, and about 100 publications in various refereed journals and international conferences. He has also participated in the editorial board of several scientific journals and is a potential reviewer for numerous scientific journals, including *Composite Science and Technology*, *Composites Part A*, *Composite Interfaces*, *Journal of Composite Materials*, *Journal of Reinforced Plastics and Composites*, *Powder Technology*, *Journal of Nanomaterials*, *Journal of Applied Polymer Science* and others.

Prof. Raul Fangueiro is currently professor and senior researcher in the School of Engineering at the University of Minho, Portugal. He is the Head of the Fibrous Materials Research Group of the same university with expertise in advanced materials (nano, smart and composite) and structures (3D, auxetic and multiscale) with 25 researchers. He is the mentor and the coordinator of the Fibrenamics International Platform (www.fibrenamics.com) including 200 partners developing promotion, dissemination, technology transfer and research activities on fibre-based advanced materials. He has more than 110 published papers in international reputed scientific journals, 320 conference publications, 36 books and 14 patents. He is the scientific coordinator of several national and international research projects on advanced fibrous and composite materials, mainly for building, architectural and health care applications. He supervised various PhD and post-doctoral scientific works, and is an expert of the European Technological Textile Platform and member of the editorial board of several leading international scientific journals on composite and fibrous materials.

Preface

Currently, the aerospace industry is looking for alternative materials to reduce fuel consumption and improve safety and performance. Fibre-reinforced composites offer a wide range of properties by combining fibres from different materials (eg, polymeric, inorganic or metallic), scales (macro, micro or nano) and forms (tubes, particles, short fibres, tows or fabrics) with various matrix materials. Advanced composite materials can address all the demands asked for in aerospace materials, and, consequently, their use in the aerospace industry is steadily increasing.

This book focusses predominantly on advanced composite materials and their use in aerospace applications. It discusses the basic and advanced requirements of these materials that are necessary for various applications in the aerospace sector. All the main types of commercial composites such as laminates, sandwich composites, braided composites, ceramic and metal matrix composites and carbon−carbon composites are discussed and compared to metals. Various aspects, including the type of fibre, matrix, structure, properties, modelling, testing and mechanical and structural behaviour are discussed. The introductory chapter (chapter: Advanced composites in aerospace engineering) provides brief discussion on the main requirements of the aerospace materials and how advanced composites can fulfil these demands. Also, this chapter introduces different types of composite materials which are already in use or have future prospects in the aerospace industry. Detailed discussions on these various composite materials are presented separately in subsequent chapters.

Besides materials, architecture of reinforcements also has strong influence on the performance of composites. The use of advanced fibrous architectures in composite materials is increasing to address the demands of advanced technical sectors. In consideration of this, chapter "Advanced fibrous architectures for composites in aerospace engineering" has been dedicated to advanced 2D and 3D fibrous structures manufactured by weaving and knitting technologies. Their production methods, properties and applications are discussed in detail.

There are several new types of composite materials that have huge potential for applications in the aerospace sector, such as nanocomposites, and multiscale and auxetic composites; these are also explored in detail. Like other industrial sectors, nanotechnology has also shown huge promise to develop outstanding high-performance and multifunctional materials. Nanocomposites and multiscale composites are such advanced materials with great prospects in the aerospace sector. The concepts, production, processing, challenges, modelling and applications of these composites are presented in chapters "Polymer nanocomposite: an advanced material for aerospace

applications and Multiscale composites for aerospace engineering". Auxetic composites are also new and show excellent characteristics for considering them in aerospace applications. Details on these composites have been presented in chapter "Auxetic composites in aerospace engineering".

Self-sensing of damage and its automatic healing are essential characteristics which can greatly improve the safety, reduce maintenance and improve performance of aerospace materials. Chapters "Self-sensing structural composites in aerospace engineering and Self-healing composites for aerospace applications" present detailed information on the concept, types, mechanisms and properties of various self-sensing and self-healing composites and their application in aerospace engineering. Looking at the environmental benefits and sustainability, natural fibre and bio-composites can also find potential applications in the aerospace industry, and these important materials are discussed in chapter "Natural fibre and polymer matrix composites and their applications in aerospace engineering".

Quality control is an important task for materials used in aerospace engineering, which demands high safety. Quality control for aerospace materials begins with the inspection of the raw materials and continues through the monitoring of the production process and characterization of the final structural parts. All these essential steps of quality control for aerospace composites are discussed in detail in chapter "Quality control and testing methods for advanced composite materials in aerospace engineering".

The book's main strength is that it covers the design, processing, properties, modelling and application potential of these materials. What sets the book apart from other published titles is that it is completely dedicated to the use of advanced composite materials in aerospace applications. It discusses the overall requirements for these materials, the different types that are currently available, structures, properties, testing, modelling and product design examples. The book discusses all the existing types of advanced composite materials currently available as well as novel materials that are still in the initial stages of research. We strongly believe that this book will be essential reading for engineers and scientists currently working in this field of research as well as students taking selected courses on advanced composite materials.

Sohel Rana and Raul Fangueiro
University of Minho

Advanced composites in aerospace engineering

1

S. Rana, R. Fangueiro
School of Engineering, University of Minho, Guimarães, Portugal

1.1   Introduction and current scenario

Aerospace engineering is a branch of engineering dealing with development of aircrafts and space crafts. Similar to many other engineering disciplines, materials science and engineering are integral parts of aerospace engineering dealing with the materials for constructing aerospace structures. Although metals are mostly used in the construction of aerospace structures, advances in materials science, especially in composites science and technology, allowed the development of promising new materials for aerospace engineering. Composites are hybrid materials developed by combining two or more components, in order to utilize the advantageous features of each component. Recently, fibre-reinforced polymer composites (FRPs), developed by reinforcing different types of matrices (eg, polymeric, ceramic, metallic etc.), with fibrous materials are gaining tremendous attention in aerospace engineering. In today's aerospace industry, the consumption of composite materials has increased more than 50% (Brown, 2014). Composite materials have been used in the aerospace industry in primary and secondary structural parts, including rocket motor castings, radomes, antenna dishes, engine nacelles, horizontal and vertical stabilizers, centre wing boxes, aircraft wings, pressure bulkheads, landing gear doors, engine cowls, floor beams, tall cones, flap track panels, vertical and horizontal stabilizers and so on. Fig. 1.1 shows the growth of composite materials' usage in commercial aircrafts. The Boeing 777, which is a long-range twin-engine jet airliner with capacity over 300 passengers launched in 2000, used 11% composite materials (Table 1.1). The Boeing 787 Dreamliner, launched in 2007, used more than 50% composites (approximately 32,000 kg of carbon fibre composites manufactured with 23 tons of carbon fibre). Fig. 1.2 shows the use of composites materials in the Boeing 787. In 2014, approximately 1680 MT of composite materials, worth more than US\$1.1 billion, were used in the engine components. This estimate will reach to 2665 MT composites, worth US\$1.7 billion, by 2023 (Red, 2015). Looking at the high temperature requirements, it is expected that ceramic matrix composites will have huge prospects for aircraft engine components.

The substantial growth in the use of FRPs in the past few years is attributed to the fact that advanced FRPs can address most of the following important requirements for
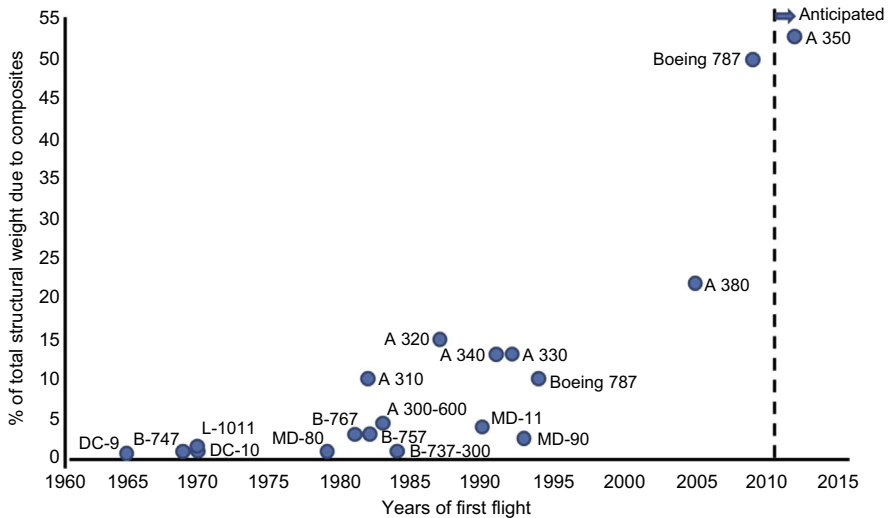
Figure 1.1 Increased growth of composite use in aircrafts over the years (Brown, 2014).

Table 1.1 Increased use of fibre-reinforced polymer composites in aircraft structures

Boeing 777	Boeing 787 Dreamliner
Launched in 2000	Launched in 2007
11% FRPs	50% FRPs
70% Aluminium	20% Aluminium
7% Titanium	15% Titanium
11% Steel	10% Steel
1% Others	5% Others

aerospace materials (Koski et al., 2009; Nurhaniza et al., 2010; Mouritz, 2012; Alderliesten, 2015; Pevitt and Alam, 2014; Huda and Edi, 2013):

- Light weight: FRPs are much lighter in weight as compared to metals. In the context of addressing the increasing price of fuels, a strong demand exists to reduce the weight of aerospace structures in order to achieve considerable fuel savings. The use of composite materials led to more than 30% weight reduction of aircraft structures. Additionally, lower fuel consumption will help to reduce the emission of greenhouse gases.
- Composite materials used in aerospace structures should have high static strength. Some parts of the structures, for example aircraft wings, should be resistant to extreme forces due to wind shear and other high transient forces.
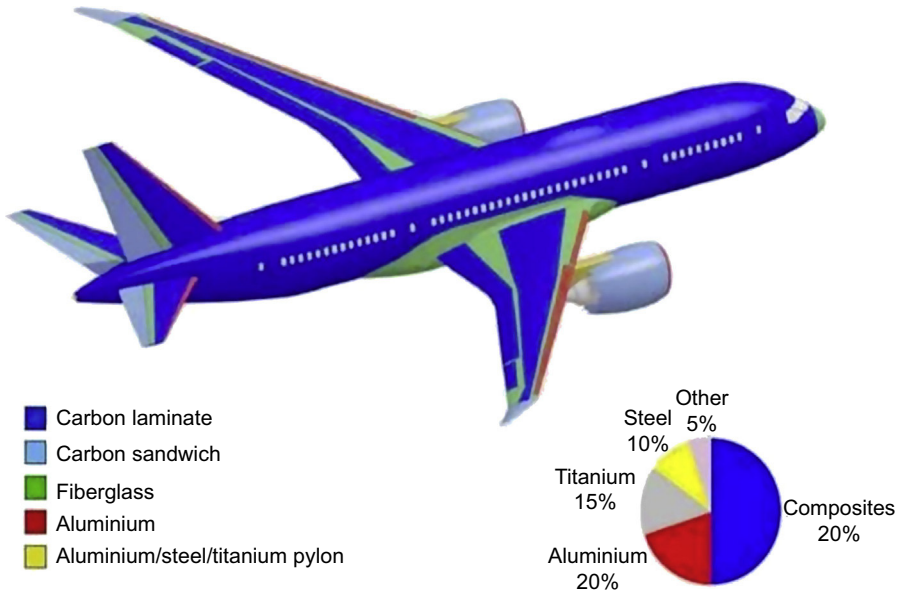
Figure 1.2 Use of composites in the Boeing 787 (Brown, 2014).

- Good fatigue performance is another important requirement for composites used in aerospace engineering. The lifetime of the aerospace structures strongly depends on their fatigue performance. Good fatigue properties increase the lifetime of aerospace structures, reduce the maintenance frequency and cost and enhance the safety.
- Composites for aerospace engineering should also possess high fracture toughness and damage tolerance. The cracks and flaws present in the structures should not grow quickly leading to sudden failure of the structures.
- High-impact energy is another essential requirement of aerospace composites to resist against sudden impacts of various types (eg, bird strikes, foreign objects, etc.).
- Aerospace composites should provide shielding of electromagnetic waves.
- Multifunctionality is an important requirement of aerospace composites. Composites should provide excellent dimensional stability under a wide range of temperatures (starting from freezing to high temperatures), resistance to lightning strikes, hail, corrosive environments (eg, fluids such as jet fuel, lubricants and paint strippers) and improved fire, smoke and toxicity performance.
- Structural health monitoring (SHM) is also an essential need for aerospace composite materials. This is necessary for online monitoring of damage in the aerospace structures in order to carry out timely maintenance activities. This would help to reduce the maintenance cost and improve the safety of aerospace structures.
- Availability of affordable and easy designing and manufacturing techniques as well as reliable analysis and prediction tools are also highly essential, in order to compete with other materials used in aerospace engineering.

Today's advanced composites can fulfil all the requirements listed above. In addition to that, as compared to metals, composite materials require fewer joints and rivets, leading to higher aircraft reliability and lower susceptibility to the structural fatigue

cracks. As an example, the use of composites in LCA Tejas led to 40% fewer parts as compared to the metallic design, half of the total number of fasteners and about 2000 fewer drilled holes in the airframe; this resulted in significant cost saving and shorter time to assemble the aircraft (only 7 months as compared to 11 months for the metallic design) (http://www.tejas.gov.in/technology/composite_materials.html). Additionally, composite materials offer the possibility to design green flights by reducing the greenhouse gas emissions as well as by offering the possibility to recycle or biodegrade (in the case of green composites) the materials after the end of the life cycle.

However, a few challenges exist regarding the use of composite materials in modern aircrafts and space crafts. One problem with composite materials is the limited information on the behaviour of composite airframe structures due to less experience on composite airframes as compared to metallic designs. The engineers rely on prediction tools to know the behaviour of the composite airframe structures. Another concern with the aerospace composites is the complex structure of composite materials which leads to difficulty in detecting various damages, especially the impact damages which may not be visible. Repair of composite structures also takes more time as compared to repair to the metallic frames, again due to less experience with these materials on the part of the technicians. The composite technology for aerospace structures is quite immature, and there is a lack in the standardization of these materials. Therefore, future efforts should be directed to tackle these challenges in order to maintain the steady growth in composites' use in aerospace industry.

1.2 Types of advanced composite materials

1.2.1 Laminated composites

Laminated composites are the most frequently used composite materials in different industrial applications. This type of composites is fabricated by assembling a number of fibrous layers and combing them with the matrix materials. Fig. 1.3 illustrates the structure of laminated composites.
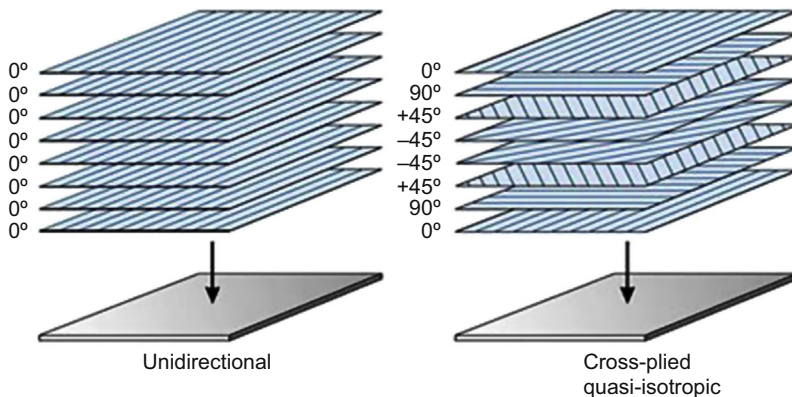
Figure 1.3 Schematic representation of laminated composites.
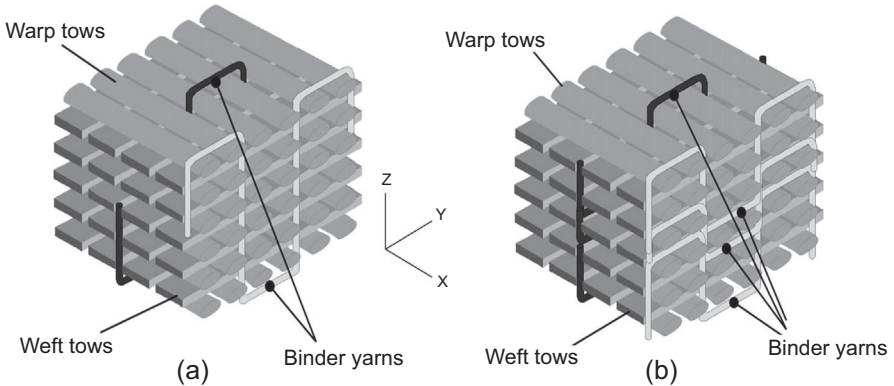
Figure 1.4 3D woven fibre architectures: (a) orthogonal and (b) layer interlock.
Mouritz, A.P., et al., 1999. Review of applications for advanced three-dimensional fibre textile composites. Composites Part A: Applied Science and Manufacturing 30 (12), 1445−1461.

The fibrous layers can be arranged in various orientations with respect to the axis of the composites, as shown in Fig. 1.1; accordingly, their in-plane properties can be tailored in different directions. Laminated composites can be characterized by high in-plane strength and stiffness. However, the principal drawback of laminated composites is their poor performance in through-the-thickness direction. Delamination of different layers under loading conditions is one of the main failure modes of laminated composites. Different ply-stitching methods are used to reduce the delamination problem, but at the cost of reduced in-plane properties of laminates. More recently, different types of three-dimensional (3D) fibre architectures containing through-the-thickness yarns are being utilized to produce composite laminates with enhanced Z-directional properties (Rana and Fangueiro, 2015). Fig. 1.4 presents the schematic of 3D woven fibre architecture with through-the-thickness binder yarns. Composites fabricated using different 3D fibrous architectures possess superior fracture toughness, damage tolerance and impact properties and can produce complex and near-net-shape composite preforms.

1.2.2 Sandwich composites

Sandwich composites are fabricated by combining two thin and strong skins with thick and light-weight core materials. Fig. 1.5 shows the schematic of sandwich composites.

Typically, the faces are high-strength composites, which are bonded to different types of core materials (honeycombs, balsa wood, foam etc.) using adhesives. Sandwich composites present several advantages as compared to the composite laminates, such as (Velosa, 2012):

- Light weight,
- High bending stiffness,
- Cost-effectiveness,

Figure 1.5 Schematic illustration of sandwich composites (Velosa, 2012).

Face or skin
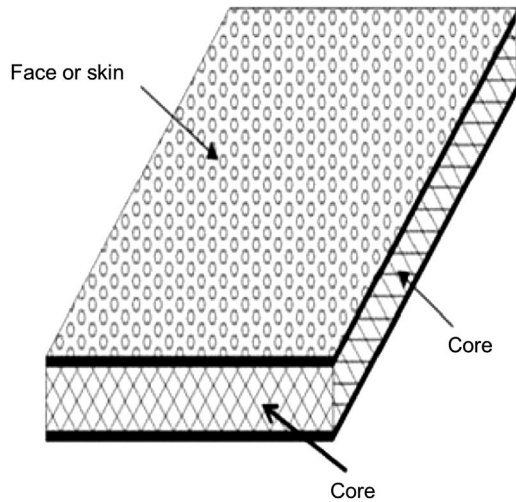
Core

Core

- Thermal insulation,
- Noise insulation, and
- Vibration damping.

Similar to laminated composites, one major problem with the sandwich composites is the debonding between the core and face materials. Recently, several types of sandwich fibrous architectures with integrated face and skin (eg, woven and knitted spacer fabrics) have been developed. These fibrous architectures are used as preforms of sandwich composites to avoid debonding problems between face and core materials.

1.2.3   Braided composites

Braided composites are produced from fibrous architectures developed using braiding technology (Rana, 2015). Braided structures are produced by intertwining two or more yarns and are distinguished from other fibrous architectures by the yarns aligned diagonally to the structure axis. Fig. 1.6 shows a braided structure, illustrating the braiding angle and other structural parameters.

Braided structures can be 2D, 3D or multidimensional and have huge flexibility in producing different shapes such as hollow tubular, stuffed tubular, flat, solid square and irregularly shaped or fashioned solids. Additionally, numerous complex profiles can be produced such as I beams, H beams, delta beams, channel beams, angle beams, ribbed and solid columns, tubes, plates and the like, which can be utilized for fabricating braided composites. Braided composites possess a number of advantageous features, such as:

- High shear and torsional strength and stiffness,
- High transverse strength and modulus,
- Damage tolerance and fatigue life,
- Notch insensitivity,
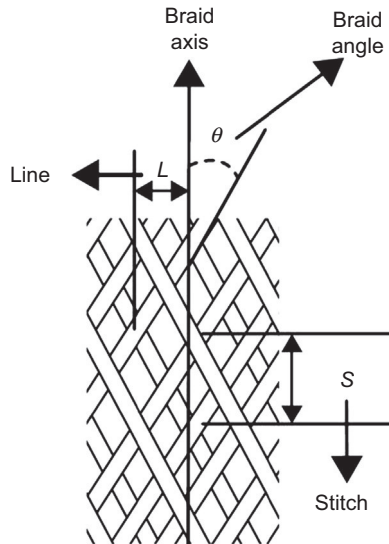
Figure 1.6 Schematic representation of a braided structure showing different structural parameters.
Sohel Rana, Raul Fangueiro, 2015. Braided Structures and Composites: Production, Properties, Mechanics and Technical Applications, CRC Press.

- High fracture toughness, and
- Possibility to develop complex and near-net-shape composites.

1.2.4 Auxetic composites

Auxetic materials and composites possess a negative Poisson's ratio (ie, unlike conventional materials, they expand in the transverse direction when loaded in the longitudinal direction) (Subramani, 2014). This behaviour is illustrated in Fig. 1.7.

Due to this unusual characteristic, auxetic materials possess several advantages such as:

- High shear modulus,
- Synclastic curvature,
- High damping resistance,
- High fracture toughness,
- Enhanced crack growth resistance, and
- High energy absorption capability.

Auxetic composites can be produced through different techniques: (a) using auxetic reinforcements in the form of auxetic fabrics (eg, produced through knitting technology) or auxetic yarns (eg, double-helix yarns) and (b) the angle ply method, in which a number of nonauxetic composite layers are arranged in a special sequence so that the resulting composites show auxetic behaviour.
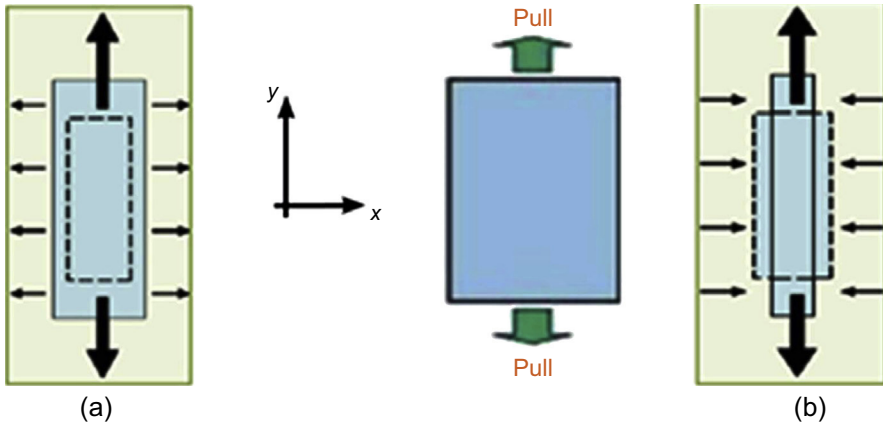
Figure 1.7 Behaviour of (a) auxetic and (b) conventional material under tensile loading (Uzum, 2012).

1.2.5 Ceramic and metal matrix composites

Ceramic matrix composites are developed by reinforcing ceramics using continuous fibres, particles or whiskers (Robert et al., 1988). Some common type of reinforcements for ceramic matrix composites include silicon carbide (SiC), titanium carbide (TiC) and boron carbide (B_4C), silicon nitrides (Si_3N_4) and boron nitrides (BN), alumina (Al_2O_3) and zirconia (ZrO_2), and carbon (graphite or partially amorphous) and boron. Ceramic matrix composites possess the following advantageous features:

- High fracture toughness,
- Resistance to catastrophic failure,
- High strength,
- Light weight,
- Low thermal expansion,
- Ability to withstand high temperature, and
- High oxidation resistance.

Metallic matrix composites are fabricated by reinforcing different types of metallic matrices such as aluminium, magnesium, titanium, copper and so on (Miracle, 2005). Typical reinforcements for metallic matrix composites are ceramic particles or fibres, carbon fibres and metallic fibres. Different processing techniques are used for metal matrix composites such as liquid metal (electroplating and electroforming, stir casting, pressure infiltration, squeeze casting, spray deposition and reactive processing) and powder metallurgy. Various merits of metallic matrix composites are:

- High transverse strength and stiffness,
- High ductility and fracture toughness,
- High temperature resistance,
- High fire resistance,

- High electrical and thermal conductivities,
- No moisture absorption, and
- Better radiation protection.

1.2.6   Nanocomposites

Nanocomposites are the class of composite materials in which nanomaterials are used either for the reinforcement purpose or for enhancing the functionalities of the composites (Thostenson, 2005). As reinforcement, nanomaterials present several advantages such as:

- High surface area and better interface,
- Smaller defects, and
- Low volume fraction required for property enhancement.

Some nanomaterials which have remarkable mechanical properties are carbon nanotubes and nanofibres. The have been proved to be excellent reinforcing materials. These nanomaterials have shown high capability to improve various properties of different types of matrix (polymeric, ceramic, metallic and cementitious) such as in-plane strength and stiffness, fracture toughness, fatigue properties, impact properties, dynamic mechanical properties, thermal stability and so on. Nanographite, nanoclay and metal nanoparticles are other nanomaterials which are used for reinforcement. In addition to that, nanocomposites with many other functionalities have been developed, such as electrical and thermal conductivity, electromagnetic inteference shielding, strain and damage sensing, gas barrier properties, fire resistance and others.

Several methods of preparation of nanocomposites are in use, such as dispersion, melt extrusion, in situ polymerization, electrospinning and more. In the case of the dispersion method, nanomaterials are directly dispersed in different types of matrices through ultrasonication, stirring, calendaring or other mechanical techniques. In the extrusion process, nanomaterials are mixed with thermoplastic matrices using extruders. Also, nanomaterials can be mixed with monomers, and subsequently polymerization occurs due to catalytic action of some functional groups present on the nanomaterial surface. An electrospinning process can also be used to produce functional nanocomposite fibres. For this purpose, nanomaterials are mixed to the polymer solution and then electrospun in the form of nanocomposite fibre webs or continuous yarns. Nanomaterials are used to improve the mechanical stability of the nanofibre web/yarn and introduce several functionalities.

1.2.7   Multiscale composites

Multiscale composites are a new class of hybrid composites which have been developed by combining reinforcements from different length scales (eg, macro, micro or nano) (Rana et al., 2014, 2015). Nanomaterials have been either added as filers within a matrix of conventional FRPs or incorporated within the fibre system prior to introducing them within the matrix. Nanomaterials are introduced within the matrix by using a dispersion process through various mechanical techniques such as

ultrasonication, mechanical stirring, calendaring and ball milling, or sometimes by using chemical dispersing agents such as surfactants, polymers or the like during the mechanical treatment. Alternatively, nanomaterials are incorporated within the fibre system through directly growing, coating, sizing, spraying, electrophoretic deposition or chemical grafting processes.

Various types of nanomaterials are commonly used to fabricate multiscale composites such as carbon nanomaterials (eg, CNT, CNF, nanographite etc.), nanoclay, metal nanoparticles (eg, nano-Al$_2$O3) and so on, resulting in different properties and characteristics, as listed below:

- Enhanced in-plane mechanical properties,
- Improved fracture toughness,
- High thermal stability,
- Excellent electrical and thermal conductivity,
- Electromagnetic shielding effectiveness,
- High impact resistance,
- Self-sensing characteristics,
- Gas barrier properties, and
- Fire resistance.

1.2.8 Carbon−carbon composites

Carbon−carbon (C−C) composites are developed by reinforcing carbonaceous matrix with carbon fibres or, more recently, with carbon nanotubes (CNTs). C−C composites possess high specific mechanical properties of carbon fibres with the high temperature resistance of a carbon matrix (Manocha, 2003). The advantageous properties of C−C composites are as follows:

- High specific strength,
- High specific stiffness,
- Retention of mechanical properties at high temperature,
- Biocompatibility, and
- Chemical inertness.

C−C composites are produced mainly by two techniques: (1) by carbonization through pyrolysis of an organic matrix (both thermosetting and thermoplastic), and (2) through the chemical vapour deposition (CVD) method using a hydrocarbon gas.

1.2.9 Natural fibre composites

In recent times, tremendous interest is being paid to various natural plant fibres (eg, sisal, jute, flax, hemp, coir etc.) by both the scientific community and industrial sectors for various applications, including construction, automobiles, sports, aerospace and geotechnical engineering. The global natural fibre composites market reached €1.6 billion in 2010, with a compound annual growth rate of 15% in the past five years. By 2016, the natural fibre composite market is expected to reach €2.8 billion. Natural fibres are low cost, lightweight, nonhazardous, eco-friendly, renewable

materials possessing high specific mechanical properties and requiring lower energy during their growth and applications (Rana et al., 2014). These materials have huge potential to reduce the consumption of nonrenewable, non-environmentally friendly, energy-consuming materials such as concrete, metals or synthetic fibres in the above applications. However, despite all of these attractive properties, natural fibres cannot often meet the requirements of many applications due to some inherent drawbacks. A major problem with natural fibres is their high moisture absorption which leads to swelling and subsequent degradation and strength loss. Poor resistance to chemicals, high temperature and fire are other major drawbacks. Additionally, natural fibres present poor interfacial properties when combined with different matrices (polymeric or cementitious) and also lead to formation of cracks in brittle matrices due to their swelling properties. Therefore, the durability of natural fibres and the structures made with natural fibres are questionable, and this fact is limiting the full utilization of these wonderful materials in various sectors.

More commonly, natural fibres are treated with various chemicals such as alkali, water repellents, silane, peroxides, permanganates and so on, to reduce their moisture absorption and improve their compatibility with various matrices (Relves et al., 2015). However, although these chemical treatments are quite efficient, they are not environmentally favourable due to production of waste chemicals and effluents. Recently, plasma surface modification has come out as a clean and dry surface modification technique of various polymeric fibres including natural fibres. Although plasma treatment can provide different types of functionalized surfaces depending on the type of gas used in the plasma reactor (air, oxygen, nitrogen etc.), this technique has limitations in terms of variety of surface modifications and stability of surface functional groups. Therefore, grafting of various polymers has also been carried out at the plasma functionalized surfaces in order to produce stable varieties of functional groups as per the applications. However, this process contains a chemical reaction step (grafting) and therefore is associated with environmental pollution. The grafting step can be eliminated by using the plasma polymerization process in which surface activation and polymerization occur simultaneously. Plasma polymerization has been used extensively in anticorrosive surfaces and in scratch-resistant, chemical barrier and water-repellent coatings since this is a clean and green (ie, no-solvent) process that is reliable, reproducible and suitable for wide varieties of monomers, different surfaces and sample geometries. Therefore, these advanced surface treatment methods can overcome the inherent problems of natural fibres as well as introduce many other functionalities that enhance their applicability in various industrial sectors.

1.2.10   Self-sensing composites

Self-sensing composites are capable of sensing their strain, damage, temperature and so on (Rana et al., 2014; Wang and Chung, 2013). Currently, self-sensing composites are receiving special attention for various structural applications in which they are used to improve safety. The existing approaches of sensing the condition of structural parts are mostly based on using external sensors. For strain and damage sensing, fibre-optic and piezoelectric sensors have been researched widely and are also commercially
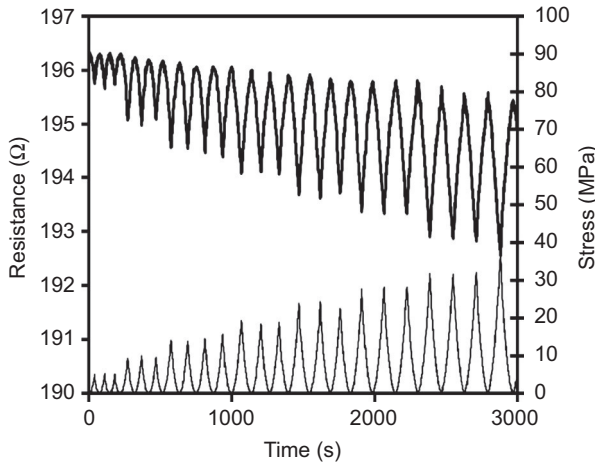
Figure 1.8 Change in through-thickness resistance (thick upper curve) with stress of continuous carbon fibre epoxy—matrix composite.

Wang, D., Chung, D.D.L., 2013. Through-thickness piezoresistivity in a carbon fiber polymer-matrix structural composite for electrical-resistance-based through-thickness strain sensing. Carbon 60 (1), 129—138.

available. However, these sensing systems have some inherent drawbacks such as high cost, necessity of skilled personnel, fragile nature, inaccessibility to remote places and so on. To address these problems, self-sensing composites are rising in prominence. These composites are capable of sensing strain or damage in the structures which are constructed using these composites. Fig. 1.8 shows the response from a self-sensing composite made of carbon fibres.

Self-sensing composites usually work on the piezoresistive principle (ie, they change their electrical resistivity with strain or damage). These composites contain a conducting component such as carbon fibres or carbon particles or nanotubes. The change of resistivity is due to the change in electrical contact points between the conducting elements. Upon tensile loading, electrical resistivity increases due to reduction in electrical contact points between the conductive short fibres, particles or nanotubes. The opposite is the case when the composite is subjected to compressive loading. However, in the case of long fibre composites, decrease in resistivity has been noted during tensile loading due to fibre alignment and increase in electrical contact points; however, the extent of resistance change is generally low.

As long as fibre composites are mostly used in aerospace and other technical applications, developing long fibre composites with good sensing performance is challenging. Recently, hybrid composites of carbon and other nonconducting low-strength fibres have been developed to perform sensing of composite damage. These composites can show a sharp change in the electrical resistance well before the complete breakage of the composites. However, they can perform strain sensing with sufficient sensitivity only in the prestressed conditions. To overcome this problem, carbon
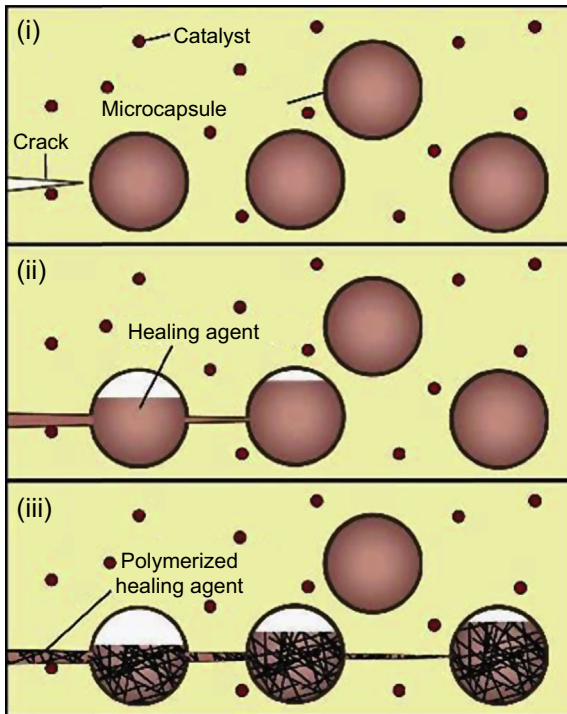
Figure 1.9 Microcapsule-based healing mechanism. Garcia, S.J., Fischer, H.R., 2014. 9-Self-healing polymer systems: properties, synthesis and applications. In: Aguilar, M.R., Román, J.S. (Eds.), Smart Polymers and Their Applications, Woodhead Publishing. pp. 271–298.

particles or nanomaterials like CNTs have been used to achieve good sensing performance. The composites based on CNTs can detect the microscale damages in the composite structures and, therefore, are highly promising for self-sensing of aerospace structures.

1.2.11 Self-healing composites

Self-healing composite materials are those which can repair the damage initiated within their structure automatically (Blaiszik et al., 2010). The self-healing of damage can be extrinsic (ie, the composite materials contain an external healing agent for damage repair). The healing agent can be contained within microcapsules, hollow fibres or vascular networks. Due to initiation of cracks, these systems that contain healing agents break, releasing the healing material and repairing the cracks. Fig. 1.9 shows a microcapsule-based healing mechanism.

Self-healing can also occur by several intrinsic mechanisms. In cases of intrinsic self-healing, the composites contain some polymers which can exhibit reversible interactions by the action of some external stimulus such as heat, light, radiation or the like. Therefore, upon initiation of damage, the external stimuli can induce different types of reversible interactions (eg, a reversible change of phase in cases of thermoplastics,

reversible chemical bonding like retro-Diels−Alder (rDA) reactions, reversible physical interactions in ionomeric polymers, reversible supramolecular interactions, shape memory type interactions etc.) and repair the cracks. The healing efficiency of composites is calculated using the following equation:

$$\eta = \frac{f_{\text{healed}} - f_{\text{damaged}}}{f_{\text{virgin}} - f_{\text{damaged}}}$$

where f is the property of interest. The self-healing composites can repair the following properties:

- Fracture property,
- Fatigue property,
- Impact energy, and
- Barrier and corrosion property.

1.3   Conclusion

The use of advanced composite materials in the aerospace sector is growing steadily due to several advantages of composites over metals, such as composites' light weight, high strength, corrosion resistance and superior fatigue and fracture properties, as well as multifunctional performances such as SHM and self-healing. A few types of composites have been already in use in the aerospace industry such as laminates, sandwich composites, braided composites, C−C composites and metallic and ceramic matrix composites, and other novel types such as nanocomposites, auxetic composites and multiscale composites also have huge prospects in the aerospace sector due to their numerous attractive properties. Self-sensing and self-healing composite technology will also be explored extensively to fulfil the current demands of the aerospace industry. However, a strong need exists for reliable inspection and prediction tools, repairing techniques and standardization of aerospace composites, and future efforts should be directed to solve these important issues.

References

Alderliesten, R.C., 2015. Design for damage tolerance in aerospace: a hybrid material technology. Materials and Design 66, 421−428.

Blaiszik, B.J., et al., 2010. Self-healing polymers and composites. Annual Review of Materials Research 40 (1), 179−211.

Brown, G., 2014. The use of composites in aircraft construction. http://vandaair.com/2014/04/14/the-use-of-composites-in-aircraft-construction.

Garcia, S.J., Fischer, H.R., 2014. 9-Self-healing polymer systems: properties, synthesis and applications. In: Aguilar, M.R., Román, J.S. (Eds.), Smart Polymers and Their Applications, Woodhead Publishing. pp. 271−298.

Huda, Z., Edi, P., 2013. Materials and Design 46, 552.

Koski, K., Siljander, A., Backstronm, M., Liukkonen, S., Juntunen, J., Sarkimo, M., Lahdenpera, K., Tikka, J., Lahtinen, R., 2009. Fatigue, residual strength and non-destructive tests of an aging aircraft's wing detail. International Journal of Fatigue 31, 1089−1094.

Manocha, Lalit M., February/April 2003. High performance carbon−carbon composites. Sadhana 28 (Parts 1 & 2), 349−358.

Miracle, D.B., 2005. Metal matrix composites − from science to technological significance. Composites Science and Technology 65, 2526−2540.

Mouritz, A.P., et al., 1999. Review of applications for advanced three-dimensional fibre textile composites. Composites Part A: Applied Science and Manufacturing 30 (12), 1445−1461.

Mouritz, A., 2012. Introduction to aerospace materials. Technology and Engineering 39.

Nurhaniza, M., Ariffin, M.K.A., Ali, Aidy, Mustapha, F., Noraini, A.W., 2010. Finite element analysis of composites materials for aerospace applications. In: IOP Conference Series: Materials Science and Engineering, vol. 11, no. 1. IOP Publishing, p. 012010.

Pevitt, C., Alam, F., 2014. Computer and Fluids 100, 155.

Rana, Sohel, Fangueiro, Raul, 2015. Braided Structures and Composites: Production, Properties, Mechanics and Technical Applications. CRC Press.

Rana, S., Zdraveva, E., Pereira, C., Fangueiro, R., Correia, A.G., 2014. Development of hybrid braided composite rods for reinforcement and health monitoring of structures. The Scientific World Journal 2014, 1−9.

Rana, Sohel, Parveen, Shama, Fangueiro, Raul, 2015. Advanced carbon nanotube reinforced multi-scale composites. In: Bakerpur, Ehsan (Ed.), Advanced Composite Materials: Manufacturing, Properties, and Applications. De Gruyter Open.

Red, C., 2015. Composites in commercial aircraft engines, 2014-2023. http://www.compositesworld.com/articles/composites-in-commercial-aircraft-engines-2014-2023.

Relves, Catia, Rana, Sohel, Fangueiro, Raul, Castro, Gaston, 2015. Characterization of physical, mechanical and chemical properties of quiscal fibres. Plasma Chemistry and Plasma Processing 35, 863−878.

Robert, Ruh, Palazotto, N., Watt, George, 1988. Introduction to ceramic composites in aerospace applications. Journal of Aerospace Engineering 1 (2), 65−73.

Subramani, P., Rana, Sohel, Oliveira, Daniel V., Fangueiro, Raul, Xavier, Jose, 2014. Development of novel auxetic structures based on braided composites. Materials and Design 61, 286−295.

Thostenson, E., Li, C., Chou, T., 2005. Review nanocomposites in context. Journal of Composites Science and Technology 65, 491−516.

Uzum, M., 2012. Mechanical properties of auxetic and conventional polypropylene random short fiber reinforced composites. Fibres and Textiles in Eastern Europe 5 (94), 70−74.

Velosa, J.C., Rana, S., Fangueiro, Raúl, Van Hattum, F.W.J., Soutinho, F., Marques, S., 2012. Mechanical behavior of novel sandwich composite panels based on 3D-knitted spacer fabrics. Journal of Reinforced Plastics and Composites 31 (2), 95−105.

Wang, D., Chung, D.D.L., 2013. Through-thickness piezoresistivity in a carbon fiber polymer-matrix structural composite for electrical-resistance-based through-thickness strain sensing. Carbon 60 (1), 129−138.

Advanced fibrous architectures for composites in aerospace engineering

2

Y. Liu [1], M. de Araujo [2], H. Hu [1]

[1]Hong Kong Polytechnic University, Kowloon, Hong Kong; [2]University of Minho, Guimarães, Portugal

2.1 Introduction

In 2013, the output of the composites industry is estimated to have been worth €95 billion (US$126 billion) at the finished parts stage, and a growth of 9−10% per annum is projected up to 2020 and beyond. Until recently, investments have been driven by the aerospace industry with a focus on reducing the weight of the aircraft. At the moment, the emphasis appears to be on reducing the weight of passenger cars and other vehicles (Anon, 2014).

Due to the higher stiffness-to-weight and strength-to-weight ratios of some fibres (Table 2.1), as compared to other materials, such as metals, they are favourite candidates in many applications in aerospace engineering.

A *fibre* is a unit of matter characterized by flexibility, fineness and a high ratio of length to thickness (Anon, 1963). Because fibres have a high surface-to-volume ratio, they can be extremely strong materials.

Table 2.1 Specific properties of some high-performance fibres in comparison with some metals

Specific properties	Carbon HM	Para-aramid HM	E-Glass	Aluminium	Steel
Specific modulus: E/ρ (N m/kg)[a]	256	80	28	26	27
Specific strength: σ/ρ (N m/kg)[b]	1.2	2	0.775	0.05−0.23	0.04−0.27

ρ = density.
σ = tensile strength.
E = Young's modulus.
HM = high modulus.
[a]Also known as the stiffness-to-weight ratio.
[b]Also known as the strength-to-weight ratio.

The fibres used to form structures which are useful for the reinforcing of composite materials used in aerospace engineering are *high-performance fibres*. These are mostly organic and inorganic man-made fibres that are engineered for specific applications that require very high performance in terms of strength, stiffness, heat resistance or chemical resistance. These fibres have generally higher tenacity and higher modulus than standard fibres. The most important of these fibres are carbon, aramid and glass fibres.

Fibres are anisotropic materials, and they normally are very strong and stiff along the fibre length but may bend under their own weight. Fibres have low bending and torsional rigidities, and they buckle easily.

As the term implies, *textile structural composites* are rigid textile-containing materials designed for structural or load-bearing applications.

The specific assemblage of flexible fibrous materials (fibres, yarns and fabrics) is known as the textile composite *preform*. Textile preforms vary considerably in terms of fibre orientation, entanglement and geometry. Moreover, a textile preform architecture can vary from a simple planar sheet to a complex three-dimensional (3D) net shape.

For aircraft, rockets and other applications wherein the stiffness-to-weight ratio (modulus-to-weight ratio) is the major consideration, carbon fibres have become the dominant material. Where the tensile strength-to-weight ratio is the major consideration, aramid fibres are the chosen ones (Scardino, 1989).

The structure and properties of the various high-performance fibres: tenacity, modulus, toughness, thermal resistance, chemical resistance and so on must be transferred (translated) into yarn and fabric structures in order to produce preforms with the desired properties for an application. In the case of the mechanical properties, the translation efficiency will very much depend on the degree of orientation of the fibres in the yarn and fabric structures developed. It should be noted that the structure and geometry of fabrics also play a major role in achieving particular properties (ie, thermal resistance and porosity).

Fig. 2.1 illustrates how fibre properties are translated or transferred to a final application (ie, a composite material).

Textile fabrics designed for composite materials for load-bearing functions, such as in aerospace applications, are often required to exhibit functional elements in multiple directions. In this context, a biaxial woven fabric, being orthotropic, exhibits high strength and poor compliance in the axial and radial directions and the opposite in the bias directions. The same is true for a Raschel-knitted fabric incorporating warp and weft inlays. A braided fabric, on the other hand, exhibits low strength and high compliance in the axial and radial directions and the opposite in the bias directions. Many nonwoven fabrics made up of randomly oriented constituent elements enjoy a degree of isotropy. However, conventional products of all four fabric formation systems are invariably planar sheets, having no functional element in the thickness direction. Even if these planar sheets are joined one on top of the other, as in laminates, the functional elements in the third direction do not exist.
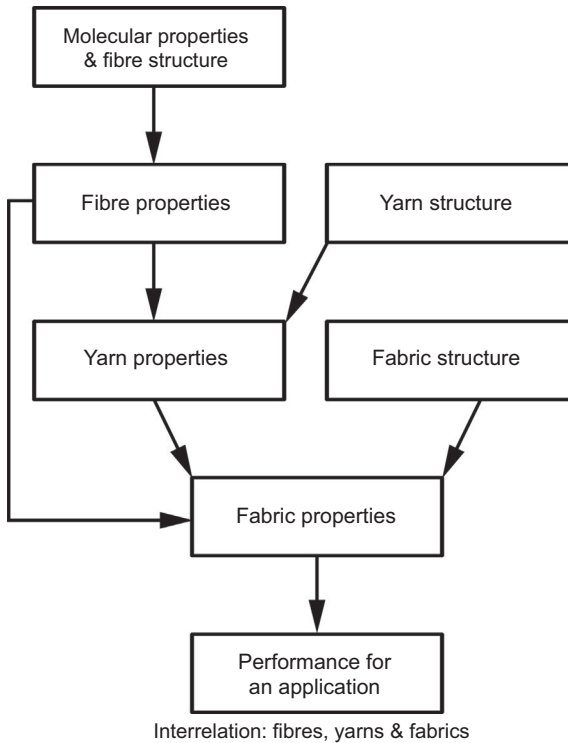
Figure 2.1 Transference of fibre properties to a final application.

In order to achieve an improved planar isotropy in woven, braided and knitted fabrics, yarns may be introduced in different directions. This approach results in triaxial woven and triaxial braided fabrics as well as multi-axial woven and knitted fabrics. The introduction of load-bearing elements in the third direction in woven, knitted and braided structures has led to the 3D fabric formation systems (Banerjee, 2014).

2.2 Types of fibrous architectures

A fibre is a 1D material which can be engineered to form various 1D, 2D and 3D fibrous architectures through textile processes. The formed fibrous architectures can be classified in different ways, either based on structural integrity and fibre linearity and continuity, or based on the fabric formation techniques.

Fibrous architectures can be classified into four categories by considering structural integrity and fibre linearity and continuity: 2D discrete, 2D continuous, 2D planar interlaced or intermeshed and 3D fully integrated structures (Ko, 1999). A 2D discrete fibrous architecture with randomly distributed staple fibres has no material continuity. Its structural integrity comes from the interfibre friction, thereby giving low strength translation efficiency. A 2D continuous fibrous architecture is a unidirectional or

multidirectional fibre system which is realized by aligning continuous filaments. It has the highest level of fibre continuity and linearity, and therefore has the highest level of strength translation efficiency. However, this fibrous architecture without in-plane and out-of-plane yarn interlacing has intra- and interlaminar weaknesses. To overcome the intralaminar failure problem, 2D planar interlaced and intermeshed fibrous architectures using continuous filaments are developed, but their interlaminar strength is still limited owing to the lack of through-thickness fibre reinforcement. Unlike the 2D fibrous systems, the 3D fully integrated fibrous architectures have fibres oriented in various in-plane and out-of-plane directions. The additional reinforcement in the through-thickness direction makes the composite virtually delamination-free.

With the exception of the 2D continuous fibrous architectures for filament wound and angle ply tape lay-up structures, the other 2D and 3D fibrous architectures can be realized using industrialized textile processes and therefore can be classified into woven, nonwoven, knitted and braided structures. While 2D discrete fibrous architectures can be formed by nonwoven techniques, the other 2D and 3D fibrous architectures can be fabricated by weaving, knitting and braiding techniques. Since this chapter focuses on the fibrous architectures for composites in aerospace engineering, only the architectures that have been used or have potential to be used in aerospace-related composites will be covered.

2.3   2D fibrous architectures

2D discrete (nonwoven) and continuous fibrous architectures with intralaminar weakness are not included in the discussion because they are not suitable for aerospace applications. In this section, four types of 2D fibrous architectures are briefly introduced: woven structures, knitted structures, directionally oriented structures (DOS) and braided structures.

2.3.1   Woven structures

Conventional 2D woven structures are formed by interlacing warp and weft thread systems. There are three basic and most regular weaves: plain, twill and satin (Fig. 2.2). The plain weave is the simplest in which each weft yarn interlaces with each warp yarn. In a twill weave, each weft yarn floats across the warp yarns in a progression of interlacings to the right or left, forming a distinct diagonal line. Compared to plain weave of the same cloth parameters, twills have longer floats, fewer intersections and a more open construction. In a satin weave, each warp yarn interlaces with each weft yarn only once, each weft yarn interlaces with each warp yarn only once, and interlacing positions can never be adjacent which leads to a smooth fabric surface. Unlike conventional 2D weaves involving two orthogonal directions of yarn, triaxial weaves consist of three sets of yarn which form 60 degree angles to each other, as shown in Fig. 2.3. Triaxial fabrics possess exceptional mechanical properties in several
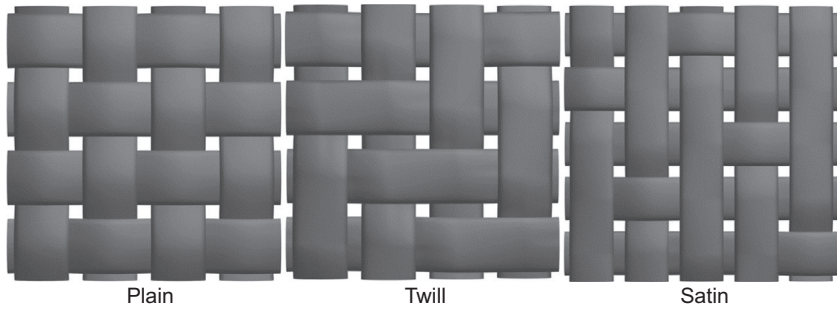
Figure 2.2 Basic 2D woven structures.
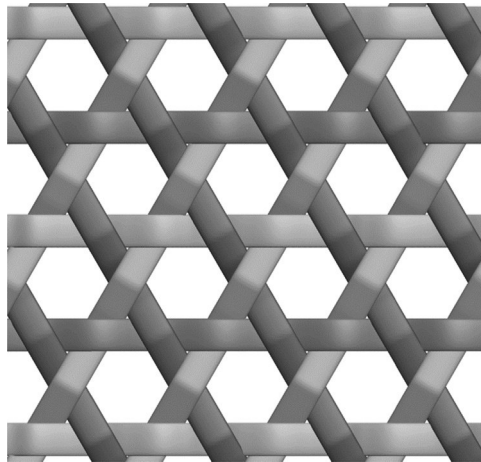
Figure 2.3 Triaxial weave.

directions. Since the interlacing points are fixed into the fabric structure, these fabrics exhibit high shear resistance.

2.3.2 Knitted structures

Knitted structures are formed from consecutive rows of intermeshed loops. The loop is the basic unit of a knitted structure. By intermeshing loops in different ways, various types of knitted stitches are formed. There are two types of knitting, namely, weft knitting and warp knitting. In weft knitting, the yarns fed into the machine form loops one by one across the fabric width (Spencer, 2001). A loop of a weft-knitted stitch consists of a head, two legs and two feet. Fig. 2.4 shows the four primary weft-knitted structures: plain, rib, interlock and purl. Each is composed of a different combination of face and reverse loop stitches. There are three basic weft-knitted stitches: loop, float and tuck, as illustrated in Fig. 2.5. Warp-knitted structures are quite different from weft-knitted structures, forming loops simultaneously at every needle in the needle

Figure 2.4 Primary base
weft-knitted structures:
(a) plain; (b) rib; (c) interlock;
(d) purl.
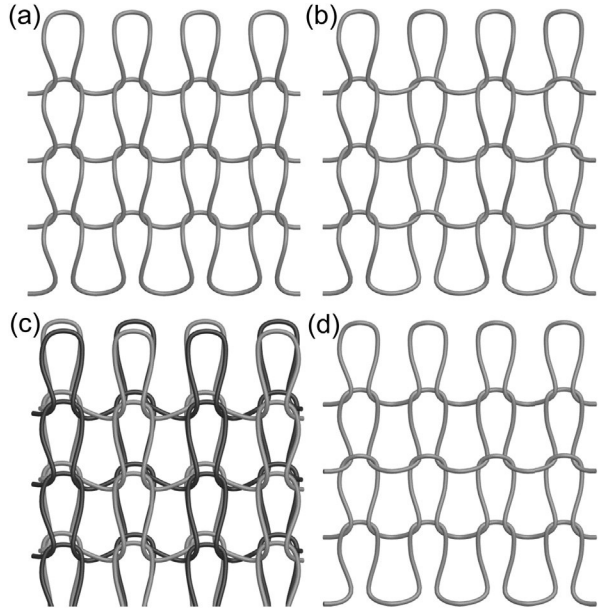
Figure 2.5 Basic knitted stitches.
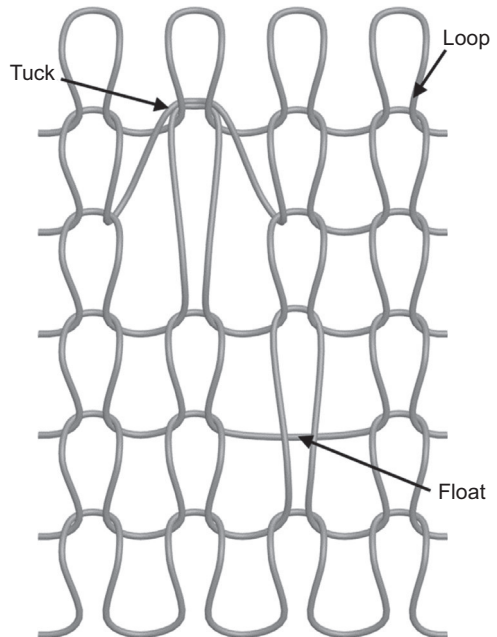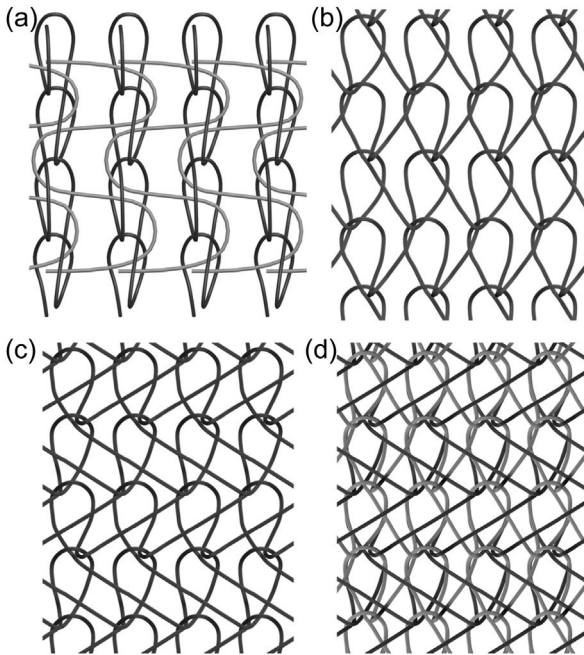
Figure 2.6 Typical warp-knitted structures: (a) pillar inlay; (b) tricot; (c) cord; (d) locknit.

bar in the fabric lengthwise direction (Spencer, 2001). The basic unit of a warp-knitted structure consists of one overlap and two underlaps, and the overlap may be open or closed. Fig. 2.6 shows four typical warp-knitted structures in which both open and closed overlaps are employed. The simplest warp-knitted structure is the pillar stitch where lappings are carried out over the same needle. Since there are no lateral connections with wales, no fabric is created. To form a complete fabric, inlay yarns are introduced by underlapping movements to connect the separate wales as shown in Fig. 2.6(a). If the laps are carried out in alternate overlap and underlap motions on two adjacent needles, then a tricot construction is produced as shown in Fig. 2.6(b). In the tricot stitch, one needle space is underlapped. By increasing one needle space for underlap motion, a cord stitch is formed as shown in Fig. 2.6(c). In this way, by employing different needle spaces for underlapping, a large family of tricot stitch derivatives is available. Tricot and cord stitches are both knitted using one guide bar. By combining tricot and cord stitches with two guide bars, a locknit structure is formed as shown in Fig. 2.6(d).

2.3.3 Directionally oriented structures

DOS are unique multiply fabrics (Au, 2011). In these structures, straight ends of absolutely parallel and noncrimped yarns are inserted into the structures at different angles (Raz, 1987). With these techniques, fabric properties can be engineered to enhance the

Monoaxial warp   Monoaxial weft   Biaxial perpendicular   Biaxial diagonal

Triaxial diagonal and weft   Triaxial diagonal and warp   Multiaxial
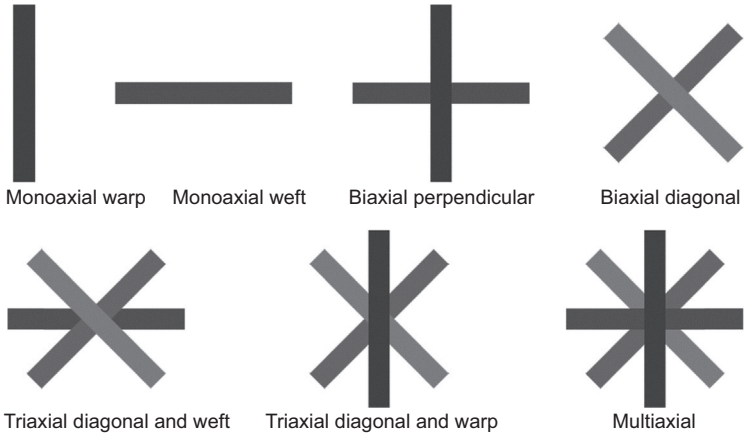
Figure 2.7 The range of DOS.

Monoaxial warp   Monoaxial weft

Biaxial perpendicular   Multiaxial
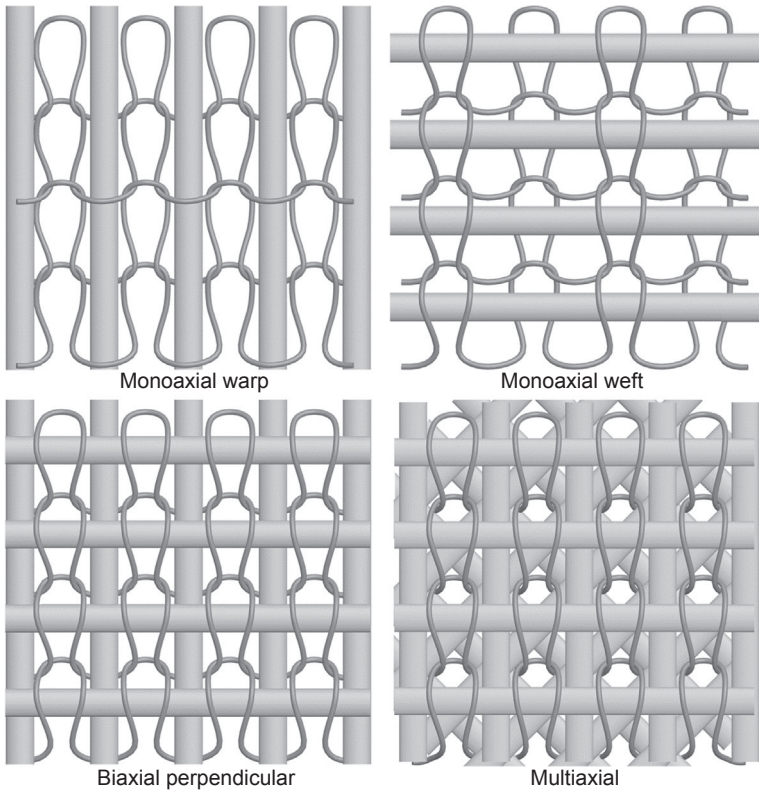
Figure 2.8 Typical weft-knitted DOS.

in-plane properties only in the required orientations, thereby producing the fabric with the ideal combination of excellent mechanical properties and cost-effective production. DOS include mono-, bi-, tri- and multiaxial structures as illustrated in Fig. 2.7, which can be produced with weft- and warp-knitting technologies.

There is a large family of weft-knitted structures suitable for manufacturing weft-knitted DOS. Some typical DOS formed by weft knitting are illustrated in Fig. 2.8. The monoaxial warp DOS uses purl as the basic structure, while the monoaxial weft DOS uses a 1×1 rib as the basic structure. Single jersey can be used to fix the biaxial perpendicular noncrimped yarns because the warp and weft yarns are interlocked within the basic structure. The multiaxial straight ends also can be bound by a single-jersey structure. It should be noted that Fig. 2.8 only gives the most simple and effective way of producing the respective DOS. There are plenty of other possibilities to fix the straight yarns for weft-knitted DOS. For instance, double-jersey structures are also able to bind the four types of DOS.

Warp knitting is the most used technology for manufacturing DOS. Warp-knitted DOS are commonly bound by pillar and tricot stitches in the warp-knitting process. Fig. 2.9 shows some typical warp-knitted mono-, bi-, tri- and multiaxial DOS bound by pillar and tricot stitches. Up to eight layers of straight ends are possible to be combined by warp-knitting technology.

2.3.4 Braided structures

In braiding, three or more threads interlace with one another in a diagonal formation, producing linear (1D), flat (2D), tubular or solid constructions (3D). Fig. 2.10 shows some typical 2D flat braids. The most common and simplest braided structure is the bias braid. Fig. 2.10(a) gives a bias with a braid angle of 45 degree. Longitudinal or axial yarns may be introduced into the braiding process to create triaxial braids. Three possible triaxial braids are illustrated in Fig. 2.10(b)−(d).

2.4 3D fibrous architectures

Laminates reinforced with 2D fibrous architectures have inferior mechanical properties, and their manufacture is expensive due to high labour requirements in the manual lay-up of plies. The application of 2D laminates in aerospace engineering has been restricted by their inferior impact damage resistance and low through-thickness mechanical properties. 3D architectures not only improve the 3D structural homogeneity but also reduce the waste of expensive materials and manufacturing costs due to the elimination of cutting and making-up operations. Composites reinforced by 3D fibrous architectures provide better through-thickness mechanical properties than those made with the traditional 2D fibrous architectures. This section briefly reviews 3D woven, knitted and braided fibrous architectures.
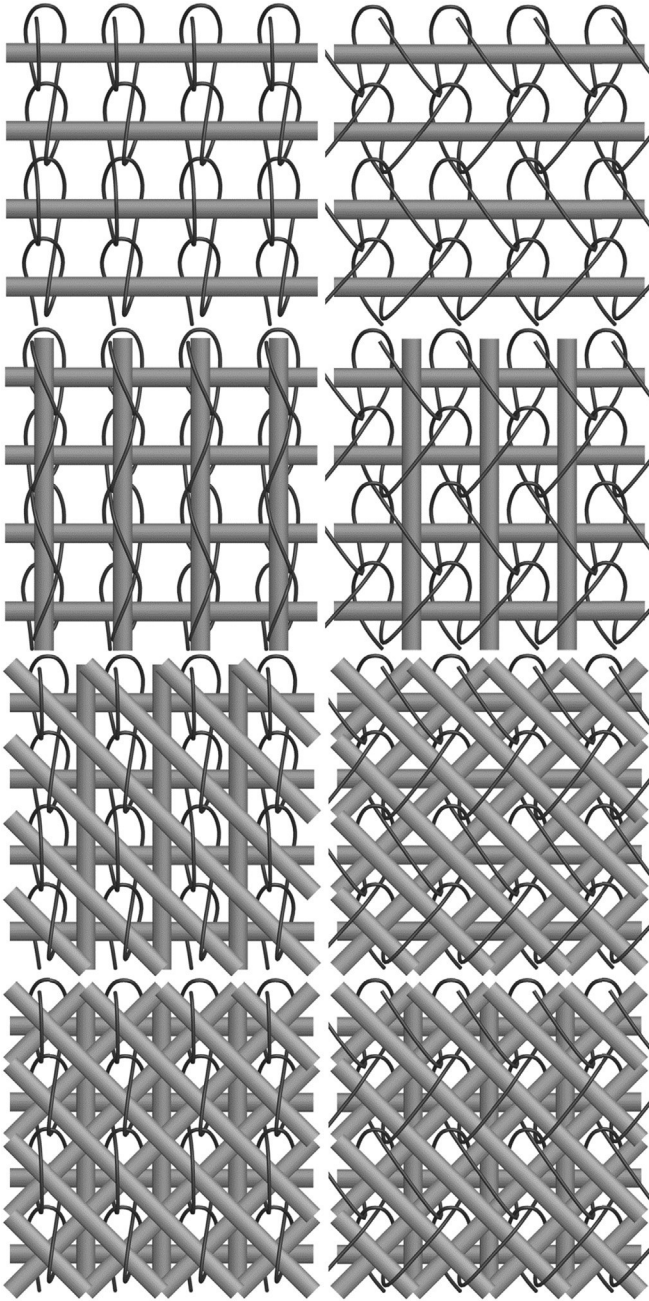
Figure 2.9 Typical warp-knitted DOS.
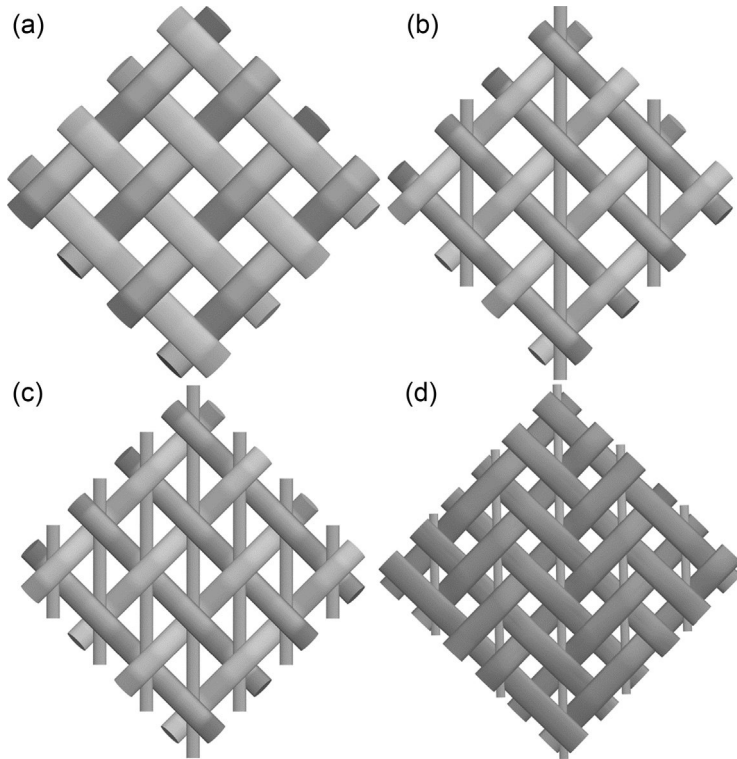
Figure 2.10 Typical 2D braided structures: (a) 1×1 bias; (b) 1×1 triaxial, axial yarns at alternate cross-overs; (c) 1×1 triaxial, axial yarns at each cross-over; (d) 2×2 triaxial.

2.4.1 3D woven structures

The weaving technology is capable of constructing 3D fibrous architectures with many different geometrical features. 3D woven structures can be classified into four categories: solid, hollow, shell and nodal as listed in Table 2.2.

3D solid woven structures consist of warp and weft yarns in the in-plane directions and z-binder yarns in the through-thickness direction. There are three types of 3D solid woven structures according to the binding pattern: orthogonal, angle interlock and fully interlaced (Chen et al., 2011). Angle interlock structures are also of two types: through-thickness and layer-to-layer. Fig. 2.11 shows a typical example for each type of the 3D woven structures. The x- and y-yarns of the orthogonal and angle interlock structures are not interlaced, whereas the x-yarns are interlaced with both y- and z-yarns in the fully interlaced structure (Stig and Hallström, 2012). The angle of the z-binder yarns can be adjusted to form a variety of angle interlock structures. In addition, combinations of angle interlock and orthogonal structures can evolve into four basic binding possibilities: angle interlock/through-thickness binding (A/T), angle

Table 2.2 **3D woven fibrous architectures**

Structure	Architecture	Production techniques
Solid	Orthogonal	2D weaving, 3D weaving
	Angle interlock	2D weaving
	Fully interlaced	3D weaving
Hollow	Spacer structure of a fabric spacer layer	2D weaving
	Spacer structure of a yarn spacer layer	Face-to-face weaving
	Honeycomb	2D weaving
Shell	Double curvature	2D weaving
Nodal	Tubular network with or without flanges	2D weaving
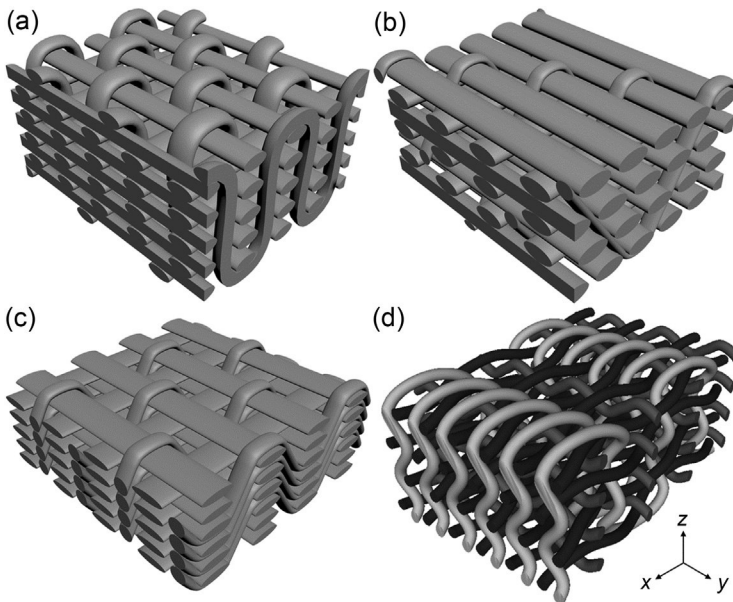
Figure 2.11 3D woven structures: (a) orthogonal; (b) through-thickness angle interlock; (c) layer-to-layer angle interlock; (d) fully interlaced.
Adapted from Stig, F., Hallström, S., 2012. Spatial modelling of 3D-woven textiles. Composite Structures 94, 1495−1502.

interlock/layer-to-layer binding (A/L), orthogonal interlock/through-thickness binding (O/T) and orthogonal interlock/layer-to-layer binding (O/L) as illustrated in Fig. 2.12 (Hu, 2008). Orthogonal and fully interlaced structures can be woven to form various profiled structures in solid, shell, tubular and a combination of these types directly.
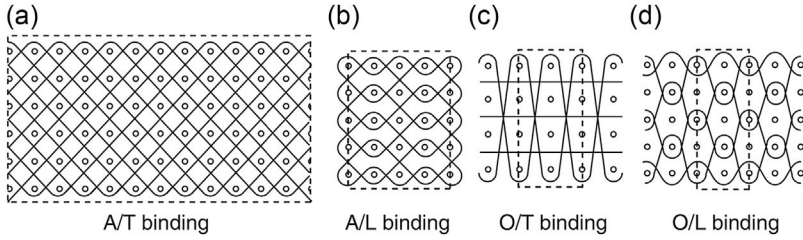
Figure 2.12 3D angle interlock woven structures: (a) angle interlock/through-thickness binding; (b) angle interlock/layer-to-layer binding; (c) orthogonal interlock/through-thickness binding; (d) orthogonal interlock/layer-to-layer binding.
Adapted from Hu, J.L., 2008. 3D Fibrous Assemblies Properties, Applications and Modelling of Three-dimensional Textile Structures. Woodhead, Cambridge, pp. 104−130.

3D hollow woven structures can be divided into two types: spacer structure and honeycomb structure. The spacer structure has normally three layers: two surface layers connected by a spacer layer. The spacer layer can be formed either by fabrics or by spacer yarns. In the case fabrics are used in the spacer layer, the cross-section of the woven spacer structure can be trapezoidal, triangular or rectangular as illustrated in Fig. 2.13, in which a fabric construction for the triangular woven spacer structure is also given. Fig. 2.14 shows a typical woven spacer structure whose two surface layers are joined together by spacer yarns. The 3D hollow honeycomb structure is a multi-layer cellular architecture where adjacent layers of fabrics are joined and separated
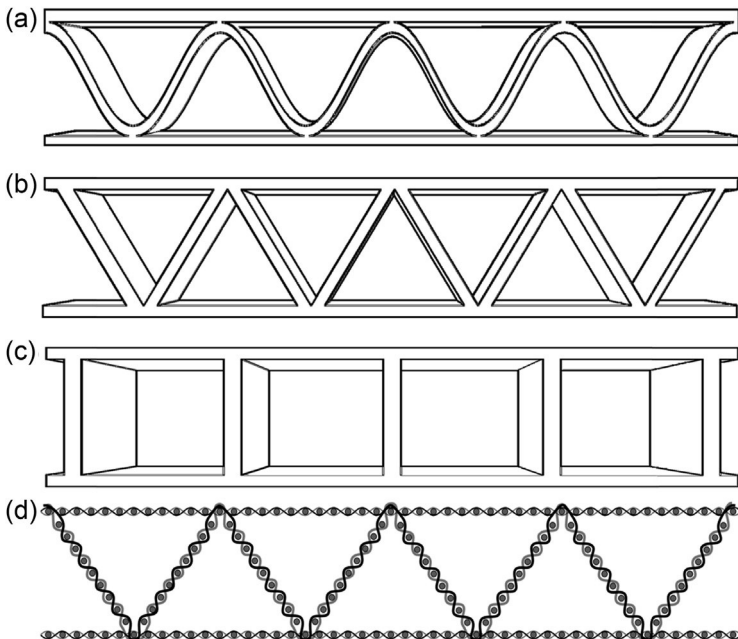
Figure 2.13 3D woven spacer structures with a fabric spacer layer: (a) trapezoidal; (b) triangular; (c) rectangular; (d) fabric construction for a triangular structure.
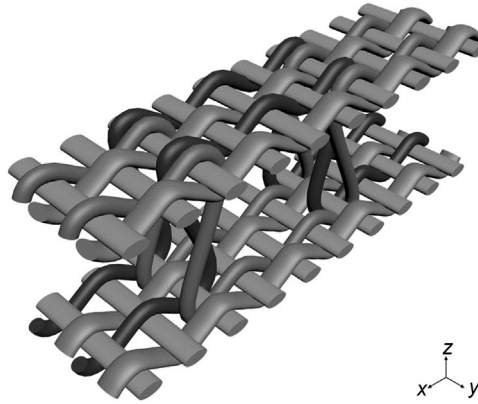
Figure 2.14 3D woven spacer structure with a yarn spacer layer.
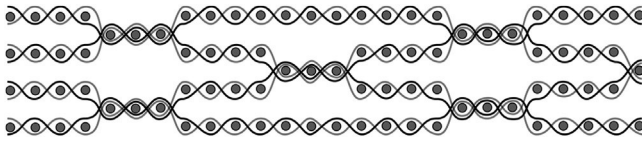
Figure 2.15 3D woven honeycomb structure.

at arranged intervals as shown in Fig. 2.15. The special connection between adjacent layers makes the fabric structure open up to form a cellular honeycomb structure after it is taken off the machine.

3D shell woven structures normally have doubly curved surfaces which can be formed by weaving with profiled take-up systems or a combination of different weaves. The profiled take-up of the fabric results in double curvatures in the fabric. Fig. 2.16 shows an example of using a combination of short-float weaves and long-float weaves to form a dome structure (Chen and Tayyar, 2003).

3D nodal woven structures are a network formed by deferent tubular or solid members (Chen et al., 2011). Fig. 2.17 shows some typical nodal woven structures with or without flanges. The basic weaves for constituting 3D nodal woven structures can be plain, twill and satin weaves.

2.4.2   3D knitted structures

3D knitted fibrous architectures, including net-shape structures and spacer structures, are produced by either the weft-knitting or warp-knitting processes. Weft knitting is very flexible to produce net-shape tubular structures and spatial shells. Fig. 2.18 gives some typical knitted tubular structures produced on a computerized flat knitting machine with two needle beds. The basic knit stitch for these tubular structures is plain knit. It is also possible to knit 3D tubular structures with flanges similar to the 3D
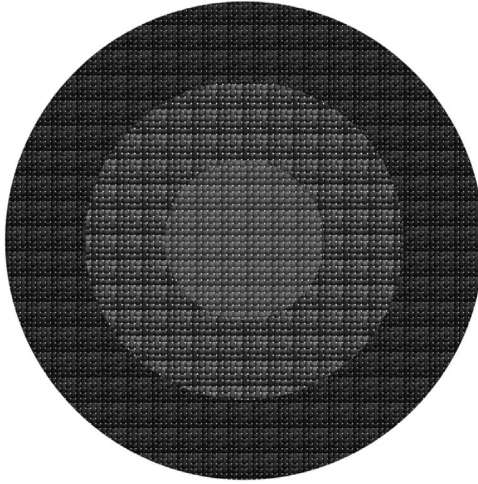
Figure 2.16 A design for a 3D dome structure by combining plain, twill and satin weaves.
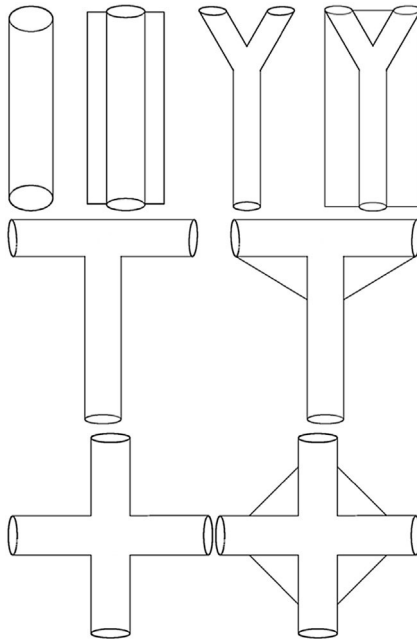
Figure 2.17 3D woven nodal structures.

woven nodal structures, as shown in Fig. 2.17. Flat weft-knitting technology is also able to produce 3D shell structures, such as a 3D dome structure and a box structure as shown in Fig. 2.19. The capability of individual needle controlling offers the greatest potential of computerized flat knitting machines to form a variety of 3D net-shape
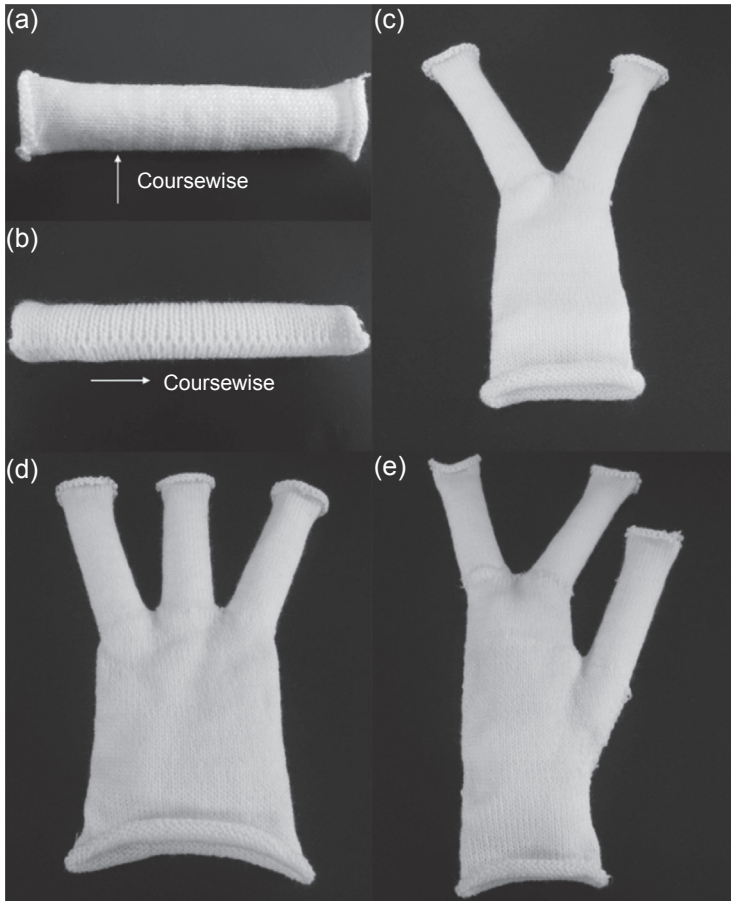
Figure 2.18 3D knitted tubular structures: (a) single tube knitted parallel to transverse direction; (b) single tube knitted parallel to axial direction; (c) bifurcated tube; (d) trifurcate tube branched at the same course; (e) trifurcate tube branched at different courses.
Adapted from Liu, Y.P., Hu, H., 2015. Three-dimensional Knitted Textiles in Advances in 3D Textiles. Woodhead, Cambridge, pp. 125−152.

forms. Warp-knitting machines equipped with double needle bars can also be used to form various 3D tubular structures of more compact, uniform and fine construction.

The spacer structure is another type of 3D knitted structure which consists of two separate surface layers joined together but kept apart by spacer yarns or a fabric spacer layer (Hu et al., 1996). Both weft- and warp-knitting technologies are able to produce spacer structures in which surface layers are connected by spacer yarns. Fig. 2.20 shows a typical warp-knitted spacer structure and a typical weft-knitted spacer structure. The surface layers of the warp-knitted spacer structure are based on the reverse locknit structure, whereas those of the weft-knitted spacer structure are based on a
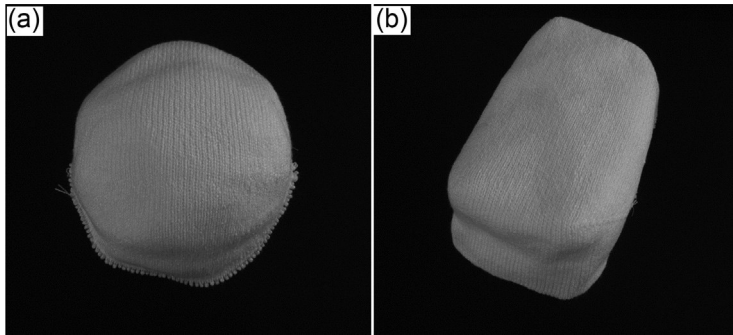
Figure 2.19 3D knitted shell structures: (a) A 3D knitted dome and (b) a 3D knitted box. Adapted from Liu, Y.P., Hu, H., 2015. Three-dimensional Knitted Textiles in Advances in 3D Textiles. Woodhead, Cambridge, pp. 125−152.

plain-knit structure. The two surface layers of warp-knitted spacer structures can either be the same or different; either both surfaces or only one can be of mesh structure, even with different mesh sizes on each side. The thickness of warp-knitted, flat weft-knitted and circular weft-knitted spacer structures can be 1−65 mm, 3−12 mm and 1.5−5.5 mm, respectively (Liu, 2012). Flat weft-knitting machines are also able to produce spacer structures whose spacer layers are fabrics similar to 3D woven spacer structures with fabric spacer layers as shown in Fig. 2.13.

2.4.3   3D braided structures

3D braiding technology is an extension of the well-established 2D braiding technology wherein the fabric is constructed by the intertwining of two or more yarn systems to form an integral structure. 3D braiding is capable of manufacturing a wide variety of tubular and complex solid constructions. Some examples are given in Fig. 2.21.

2.5   Hybrid fibrous architectures

Hybrid structures are formed by combining different kinds of textile structures to balance some characteristics or weaknesses of the individual structure. From the synergy of the properties of each structure, a fibrous architecture with improved properties is obtained. Fig. 2.22 shows a typical hybrid structure by combining two nonwoven fabrics and a multiaxial DOS produced on a Liba warp-knitting machine (Kruse and Gries, 2011). Fig. 2.23 illustrates a stitched woven-knitted fibrous structure consisting of two outer layers of a plain-woven fabric and two inner layers of weft-knitted fabrics (Hu et al., 2010). Fig. 2.24 shows a co-woven-knitted structure in which both knitted and woven structures are combined in a single fabric construction (Xu et al., 2011).
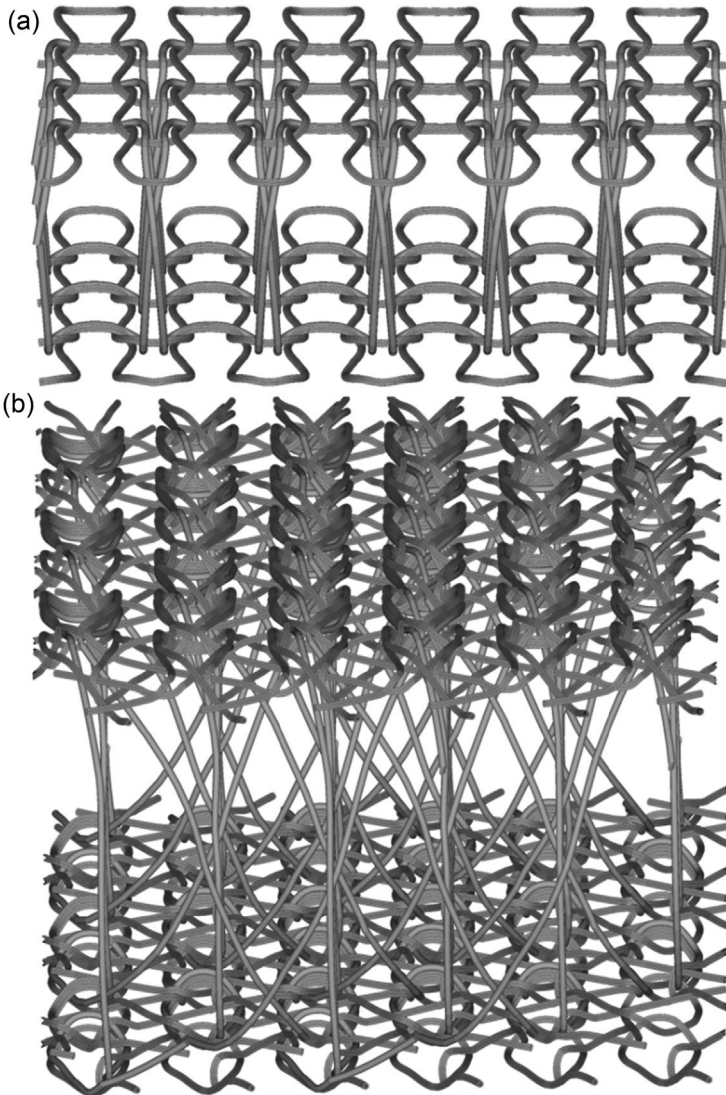
Figure 2.20 3D spacer structures: (a) weft-knitted; (b) warp-knitted.

2.6 Production techniques

This section describes the production techniques of the 2D and 3D textile structures discussed above.

2.6.1 Woven structures

Conventional 2D woven fabrics are produced by interlacing warp and weft yarns to form plain, twill and satin structures on either tappet or dobby looms. There are five
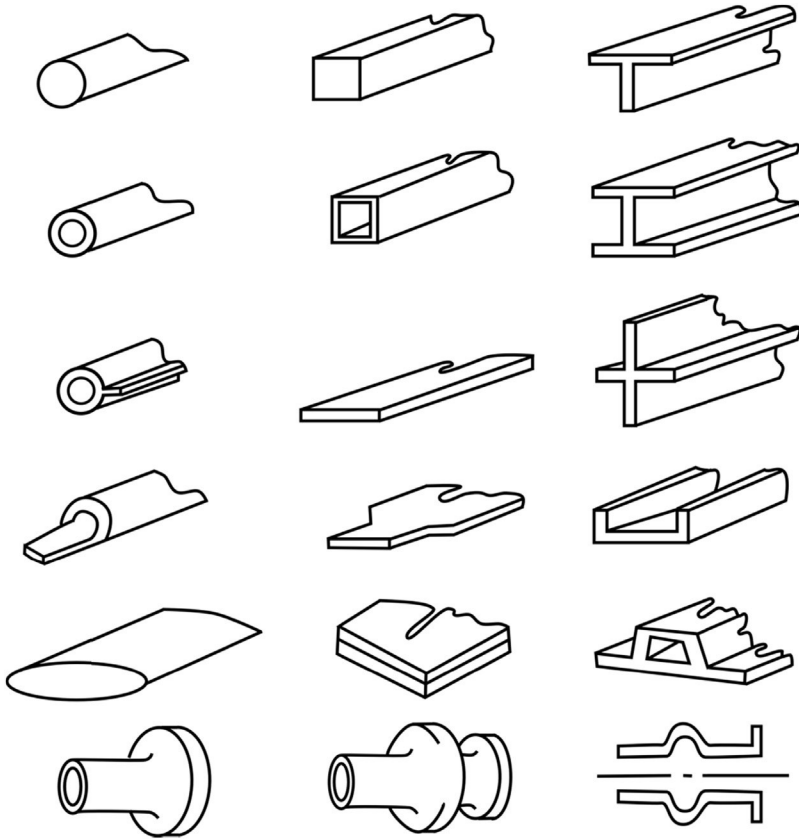
Figure 2.21 3D braided structures.
Adapted from Ko, F.K., 1989. Three-dimensional fabrics for structural composites.
In: Chou, T.W., Ko, F.K. (Eds.) Textile Structural Composites, Elsevier, Amsterdam.

basic weaving motions constituting the weaving process: let-off, shedding, weft inser-
tion, beat-up and take-up. A number of weft insertion technologies including shuttle,
rapier, projectile and air-jet are available. The 2D-weaving process employing the
mono-directional shedding is also suitable for weaving some 3D woven structures,
as described in Section 2.4.1, including 3D solid orthogonal and angle interlock struc-
tures, 3D hollow spacer structures with fabric spacer layers and honeycomb structures,
3D shell structures and 3D nodal structures. Fig. 2.25 illustrates the 2D-weaving prin-
ciple for manufacturing 2D conventional and 3D angle interlock woven structures.

   3D hollow spacer structures with spacer yarns are produced by using a velvet
face-to-face weaving technology. A velvet loom weaves warp and weft yarns into
two separate ground fabrics simultaneously (face-to-face with a space between
them), while pile warp yarns interlace alternately with the two separate ground fabrics
(Fig. 2.26).
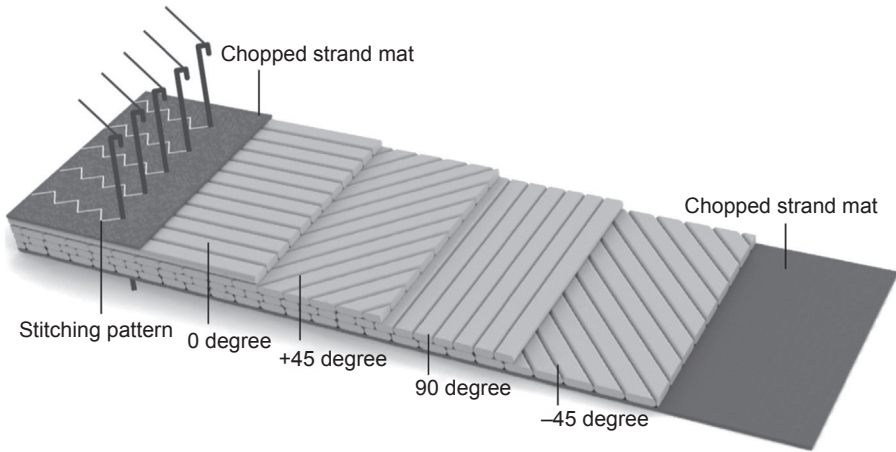
Figure 2.22 A hybrid fibrous architecture by combining nonwoven fabric and DOS using warp-knitting technology.
Adapted from Kruse, F., Gries, T., 2011. Standardisation of production technologies for non-crimp fabric composites. In: Lomov, S.V. (Ed.), Non-crimp Fabric Composites, Woodhead, Cambridge, pp. 42–66.
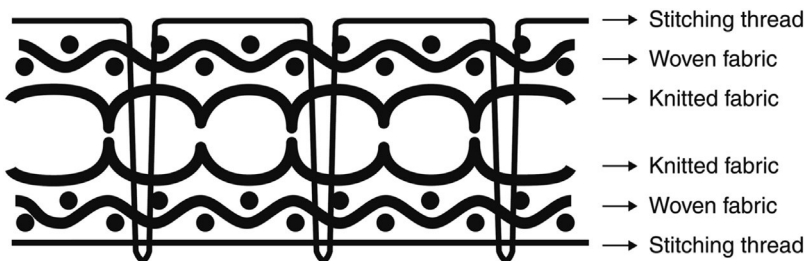
Figure 2.23 A hybrid fibrous architecture by combining woven and knitted fabrics using stitching technology.
Adapted from Hu, H., Zhang, M., Fangueiro, R., Araujo, M.D., 2010. Mechanical properties of composite materials made of 3D stitched woven-knitted preforms. Journal of Composite Materials 44, 1753–1767.
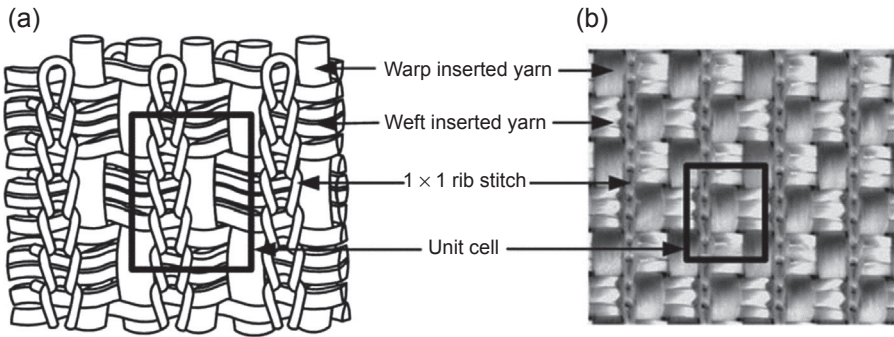
Figure 2.24 A hybrid co-woven-knitted structure: (a) structure diagram; (b) fabric.
Adapted from Xu, Y., Hu, H., Yuan, X., 2011. Geometrical analysis of co-woven-knitted preform for composite reinforcement. Journal of the Textile Institute 102, 405–418.
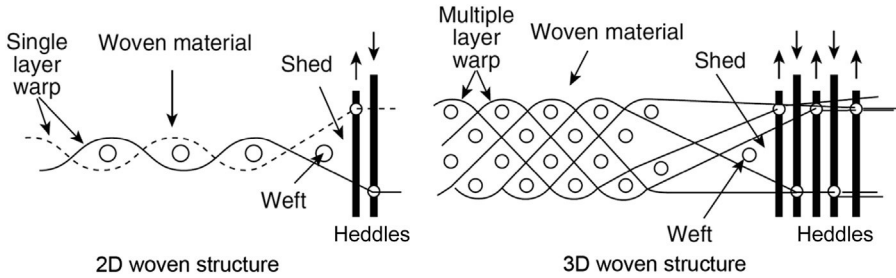
Figure 2.25 Illustration of the 2D-weaving principle for 2D and 3D woven structures. Adapted from Hu, J.L., 2008. 3D Fibrous Assemblies Properties, Applications and Modelling of Three-dimensional Textile Structures. Woodhead, Cambridge, pp. 104−130.
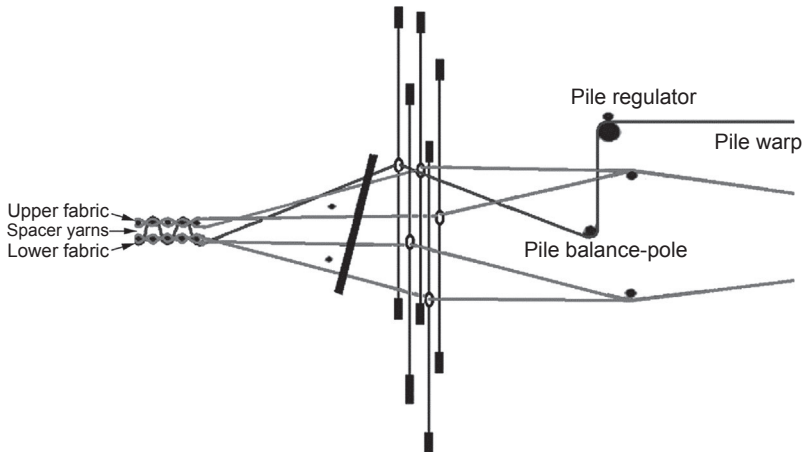
Figure 2.26 3D woven spacer fabric production on face-to-face principle.

Even though the conventional 2D-weaving process can be used to produce various 3D woven solid structures, the thickness dimension is limited. For this reason, different types of specially designed 3D-weaving machines have been developed for manufacturing 3D woven fabrics. King (1976) has developed a special weaving machine to produce orthogonal structures containing X, Y and Z yarns without interlacings as shown in Fig. 2.27. During weaving, the Z yarns are static, the X yarns are inserted first and then beaten up into place, and then the Y yarns are inserted and beaten up too. This is repeated to produce a compact structure until the desired height is achieved, producing a 3D rectangular cross-sectional configuration. There is no shedding involved in this production process. Khokar (1996) has developed a 3D-weaving machine employing a dual-directional shedding operation. Such a shedding system enables the warp yarns to interlace with both horizontal and vertical sets of weft yarns. This special 3D-weaving process also allows direct production of woven profiled materials. The 3D fully interlaced woven structures offer ultimate structural integrity even when the fabrics are cut and damaged.
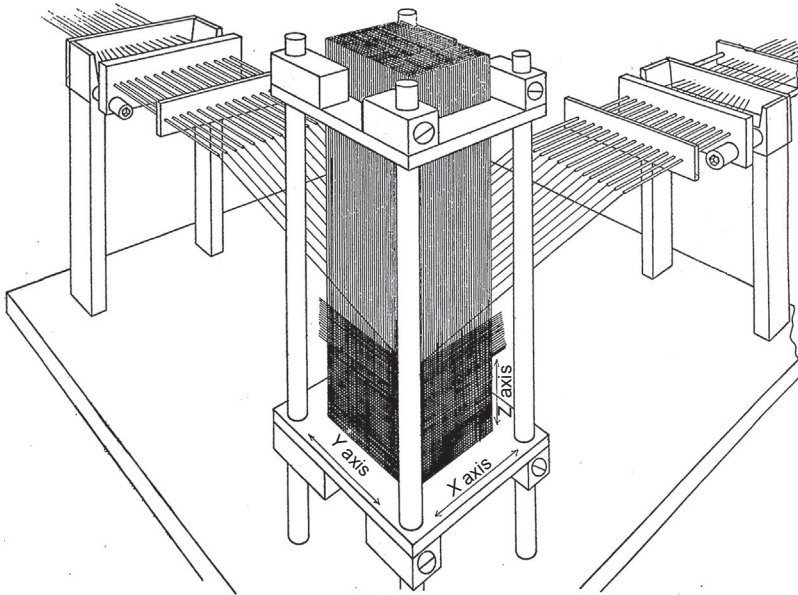
Figure 2.27 King's specially designed 3D-weaving machine for manufacturing 3D solid orthogonal structures.
Adapted from King, R.W., 1976. Apparatus for Fabricating Three-dimensional Fabric Material, US Patent No. 3955602.

The manufacture of triaxial woven structures is achieved by using techniques derived from traditional 2D-weaving and automatic braiding techniques. One typical triaxial weaving machine was designed by Dow (1975) and manufactured by Barber-Colman as illustrated in Fig. 2.28. The machine lays down warp yarns using a rotating wheel with mounted spindles. Heddles are then used to create a shed for weft insertion.

2.6.2   Knitted structures

The principles of weft knitting and warp knitting are illustrated in Fig. 2.29 (Spencer, 2001). In weft knitting, yarn feeding and loop formation occur at each needle in succession across the needle bed during the same knitting cycle. More specifically, the needles (A, B, C and D) are fed in turn with the same weft yarn so as to form a course of the fabric with loops (E, F, G and H). In warp knitting, yarn feeding and loop forming occur at every needle in the needle bar during the same knitting cycle. All needles (A, B, C and D) in the needle bar are simultaneously lapped by separate warp guides (E, F, G and H).

The key feature of circular weft knitting is to produce fabric structures in a tubular form. However, flat weft knitting is more flexible in constructing different types of tubular structures, including single, bifurcated and multibranched tubes due to the
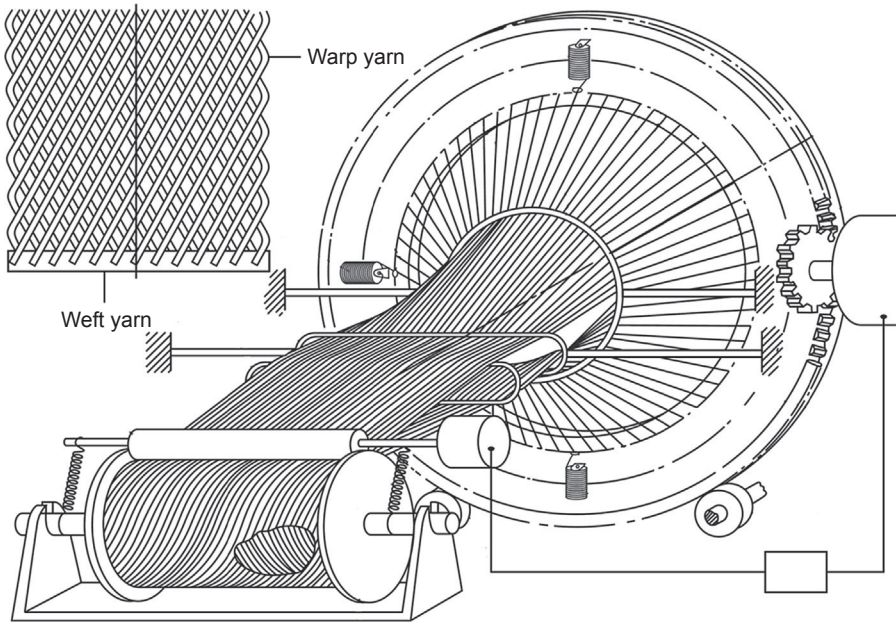
Figure 2.28 Rotating wheel with mounted spindles for manufacturing triaxial woven structures. Adapted from Dow, N.F., 1975. Warp Beam for Triaxial Weaving, US Patent No. 3884429.

capabilities of individual needle selection, loop transfer, multiple system knitting and the use of stitch pressers and holding down sinkers. Fig. 2.30 shows a single tube knitting on a computerized flat knitting machine using selected needles. Tubular knitting forms a tube by knitting one yarn on the two needle beds alternately, only passing the yarn from one needle bed to the other at the two selvages. By using tubular knitting in conjunction with intarsia technology, a number of variations from a single tube can be achieved (Fig. 2.18). Intarsia knitting technology enables knitting machines to use a number of different yarn carriers to knit different parts of the fabric. The yarn carriers can be used separately or at the same time. With this technology, a bifurcated tube can be formed by knitting a single tube of a certain length first with one yarn and then introducing an additional yarn carrier to form two tubes simultaneously with two yarns. In a similar way, by using more yarn carriers, multibranched tubular structures can be formed.

The versatility of computerized flat knitting machines offers the possibility of knitting 3D textiles with more complex shapes, such as domes, spheres and box-like shapes as shown in Fig. 2.31. A knitted dome structure can be formed by 2D repeated shaping segments (Fig. 2.31(b)). Such 2D segments were realized by repeatedly increasing and decreasing the number of needles in action. Each shaping segment represents an operation of gradually widening followed by gradually narrowing the fabric. Whereas the shaping segment type affects the angle of the dome and the height−base ratio, the number of shaping segments affects the dome shape. By changing the elliptical shaping segment for domes to a triangular segment, box-like structures can be
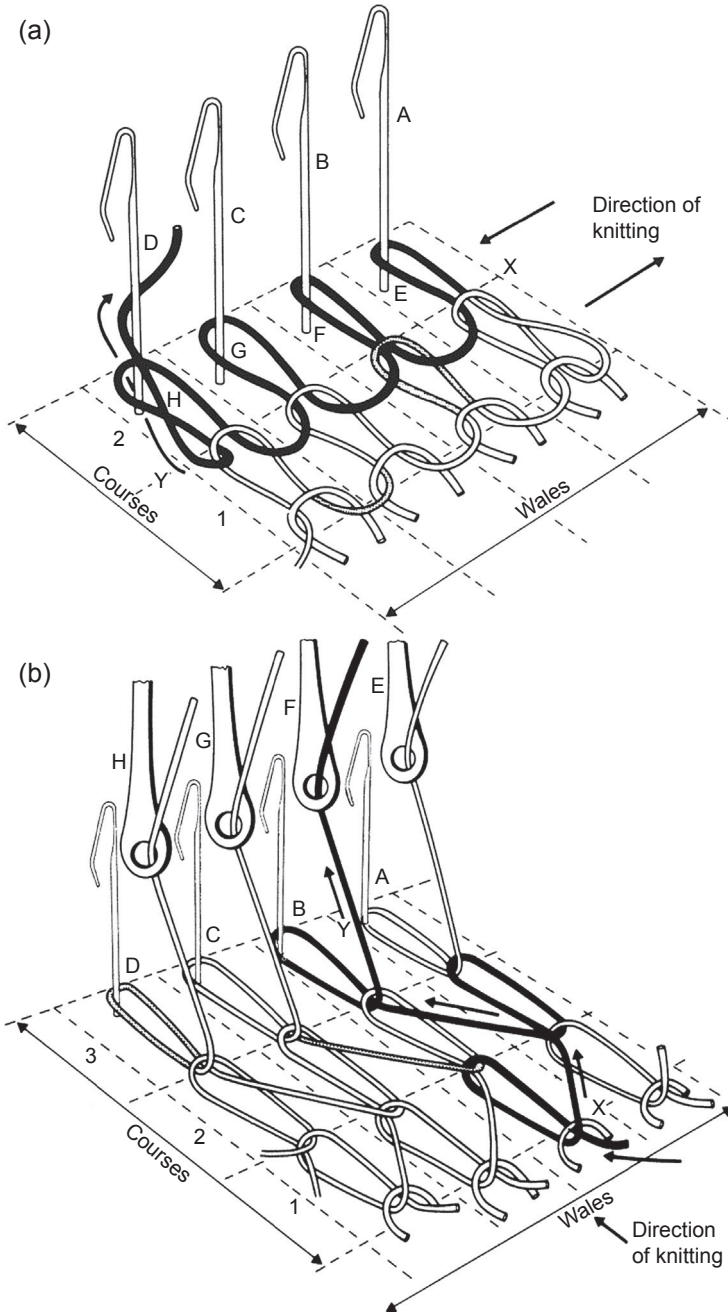
Figure 2.29 Knitting principles: (a) weft knitting; (b) warp knitting.
Adapted from Spencer, D.J., 2001. Knitting Technology, third ed. Woodhead, Cambridge.
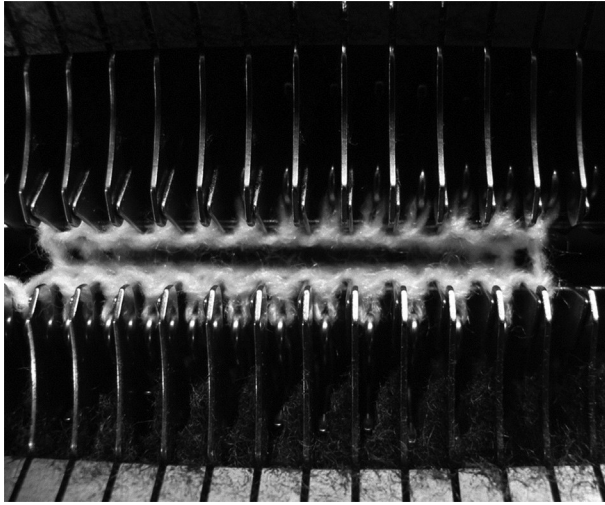
Figure 2.30 Knitting a single tube using selected needles on a computerized flat knitting machine.
Adapted from Liu, Y.P., Hu, H., 2015. Three-dimensional Knitted Textiles in Advances in 3D Textiles. Woodhead, Cambridge, pp. 125−152.
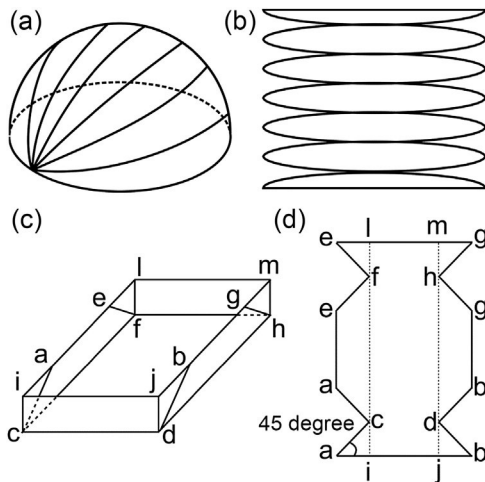
Figure 2.31 The knitting principle of 3D shells: (a) 3D theoretical form; (b) 2D pattern of a dome; (c) 3D theoretical form; (d) 2D pattern of a box.
Adapted from Liu, Y.P., Hu, H., 2015. Three-dimensional Knitted Textiles in Advances in 3D Textiles. Woodhead, Cambridge, pp. 125−152.

formed. As shown in Fig. 2.31(d), the straight lines representing the decrease or increase of the number of operating needles are linear rather than curved for the dome structure. The shaping segment type affects the angle of the box being formed. The ratio between the number of stitches being shaped and not being shaped determines the length−width ratio of the resultant box. The capability of varying the

number of knitting needles offers the greatest potential of computerized flat knitting machines to form a variety of 3D net-shape forms.

Spacer structures are produced on circular, flat weft-knitting or warp-knitting machines with two sets of needles. Circular weft-knitting machines equipped with a cylinder and a dial are able to produce the spacer fabrics whose separate outer layers are connected by yarns. Spacer fabrics on circular weft-knitting machines are produced using dial needles and cylinder needles to knit two distinctive layers of fabric separately and then connect the two fabric layers with tucks on both the dial and cylinder needles (Fig. 2.32). The distance between the two individual fabric layers can be adjusted by varying the dial height relative to the machine cylinder. Spacer fabric thicknesses pre-set in this way can vary between 1.5 and 5.5 mm (Kunde, 2004). Similar to the production of spacer fabrics on circular machines, the production of spacer fabrics with a spacer layer of yarns on flat machines is carried out by creating two independent fabric layers on the front- and back-needle beds separately and then connecting them by tucks on both the needle beds (Fig. 2.33). The distance between the two needle beds determines the spacer fabric thickness. Unlike circular weft-knitting machines, the distance between the two needle beds of a flat weft-knitting machine is normally fixed around 4 mm. The critical characteristic distinguishing warp-knitted spacer fabrics from the other kinds of spacer fabrics is that their three basic structural elements (ie, top layer, bottom layer and spacer layer) are knitted together in the same knitting cycle. Warp-knitted spacer fabrics are produced on double-needle-bar Raschel machines; the principle is schematically shown in Fig. 2.34(a). While guide bars 1 and 2 lap the front-needle bar and guide bars 5 and 6 lap the back-needle bar (to knit the top layer and the bottom layer, respectively), guide bars 3 and 4 lap the spacer yarns around both the needle bars in succession. The production of a spacer fabric on a double-bar Raschel machine, RD 6, by Karl Mayer is shown in Fig. 2.34(b).
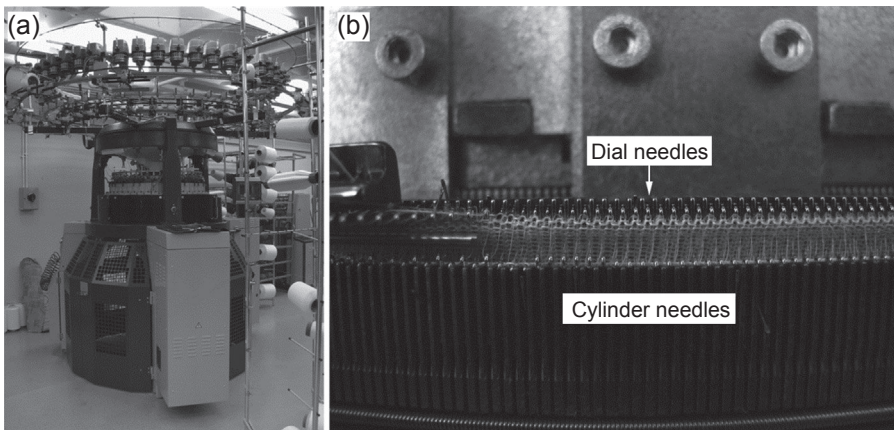
Figure 2.32 Producing a spacer fabric on a circular weft-knitting machine: (a) a Terrot double-jersey circular machine; (b) knitting a spacer fabric on the circular machine. Adapted from Liu, Y.P., Hu, H., 2015. Three-dimensional Knitted Textiles in Advances in 3D Textiles. Woodhead, Cambridge, pp. 125−152.

Figure 2.33 Producing a spacer fabric on a computerized flat knitting machine: (a) a Stoll computerized flat knitting machine; (b) knitting a spacer fabric on the flat machine.
Adapted from Liu, Y.P., Hu, H., 2015. Three-dimensional Knitted Textiles in Advances in 3D Textiles. Woodhead, Cambridge, pp. 125−152.

2.6.3   Directionally oriented structures

Weft-knitted DOS are produced on both circular and flat weft-knitting machines. Fig. 2.35 shows the knitting principle of a biaxial weft-knitted DOS on a circular knitting machine, in which straight yarns are introduced in both the wale-wise and the course-wise directions. Either single-jersey or double-jersey circular knitting machines may be selected according to the binding knitted structures desired. For the monoaxial DOS described in Fig. 2.8, a double-jersey machine may be used. While straight yarns should be introduced in the wale-wise direction for knitting the monoaxial warp DOS, straight yarns should be inserted in the course-wise direction for knitting the monoaxial weft DOS. Apart from inserting straight yarns in wale-wise and course-wise directions, it is also possible to introduce straight yarns at different angles to form multiaxial weft-knitted DOS. The knitting principle of weft-knitted DOS on flat knitting machines is similar for circular machines.

The warp-knitting technology is very productive for the manufacture of warp-knitted DOS. While a biaxial warp-knitted DOS consists of warp (0 degree) and weft (90 degree) yarns, a multiaxial DOS has additional bias ($\pm\theta$) yarns held
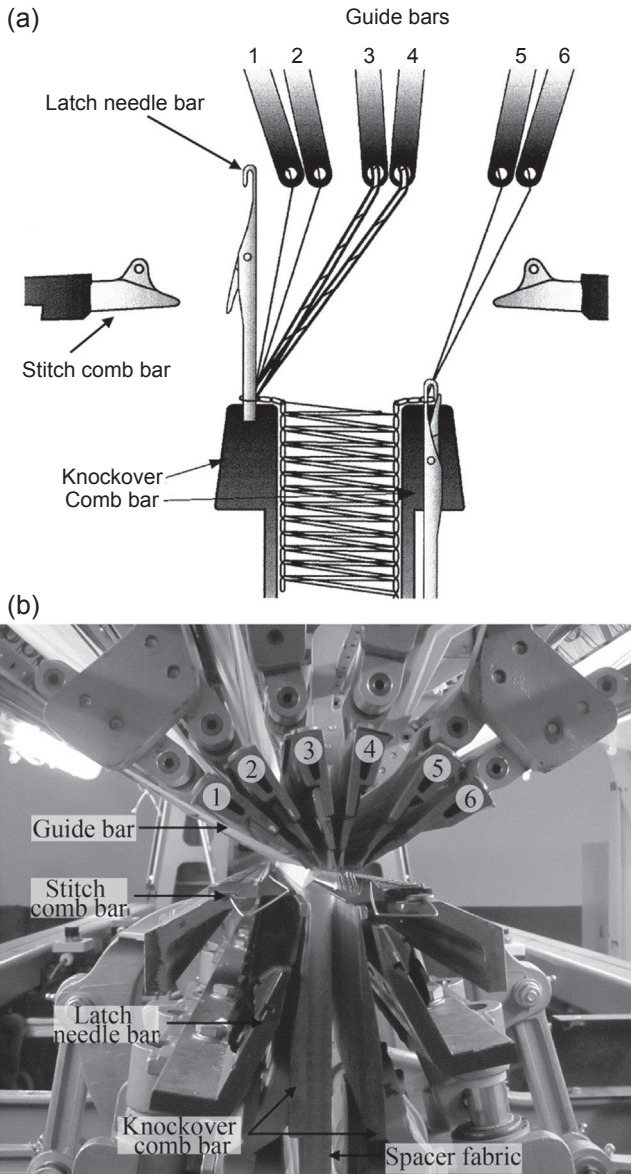
Figure 2.34 Principle of producing spacer fabrics on a double-needle-bar Raschel machine: (a) a schematic illustration; (b) RD 6 by Karl Mayer.
Adapted from Liu, Y.P., Hu, H., 2015. Three-dimensional Knitted Textiles in Advances in 3D Textiles. Woodhead, Cambridge, pp. 125–152.

together by a chain or tricot stitch through the thickness of the fabric. The warp-knitting machine used for the production of biaxial DOS can be divided into three machine modules: feeding, knitting and take-up, as illustrated in Fig. 2.36 (Schnabel and Gries, 2011). The feeding module consists of a weft insertion system,
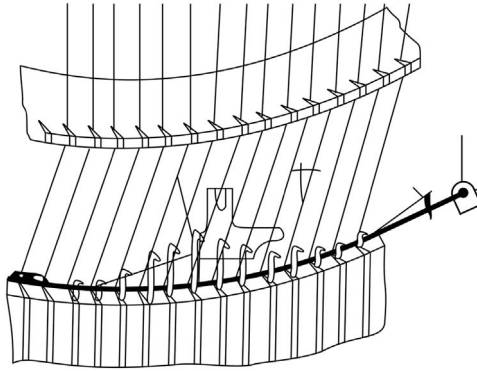
Figure 2.35 Knitting of a biaxial structure on a circular machine.
Adapted from de Araujo, M., Fangueiro, R., Hu, H., 2011. Weft-knitted structures for industrial applications in Advances in Knitting Technology, pp. 136−170.
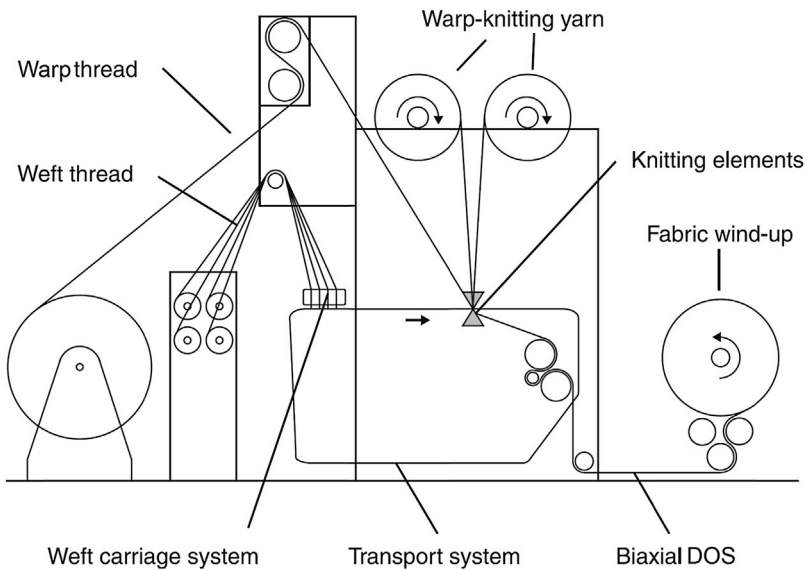
Figure 2.36 Warp-knitting principle for biaxial DOS.
Adapted from Schnabel, A., Gries, T., 2011. Production of non-crimp fabrics for composites. In: Lomov, S.V. (Ed.), Non-crimp Fabric Composites, Woodhead, Cambridge, pp. 3−41.

which is continuously feeding weft threads into the hooks or needles of two transport systems. There is one transport system on each side of the machine. The transport system continuously supplies the layers of weft straight yarns to the warp-knitting machine. The warp threads are directly fed to the needles by a yarn guide bar without both underlapping and overlapping movements. The weft and warp threads are fixed during the warp-knitting process by knitting yarns to form a biaxial DOS fabric which is subsequently wound onto the take-up module.
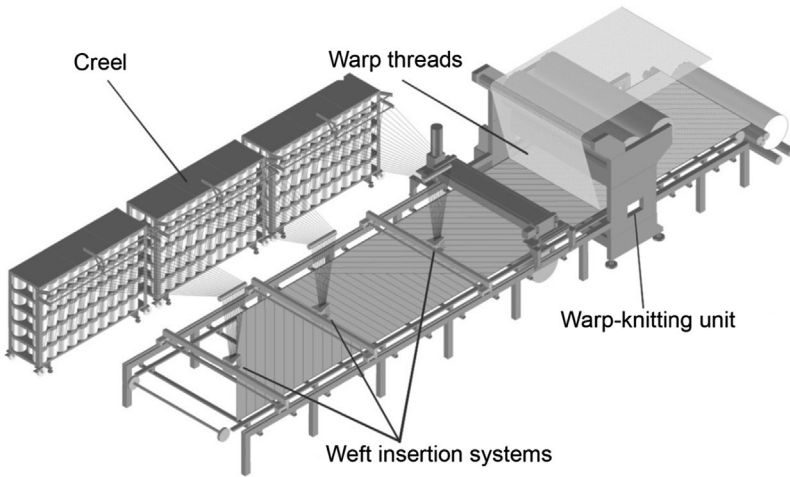
Figure 2.37 Warp-knitting principle for multiaxial DOS.
Adapted from Schnabel, A., Gries, T., 2011. Production of non-crimp fabrics for composites. In: Lomov, S.V. (Ed.), Non-crimp Fabric Composites, Woodhead, Cambridge, pp. 3−41.

The working principle of warp-knitting machines for the production of multiaxial DOS is comparable to that of biaxial DOS. The standard machine configuration consists of three weft carriage systems, which are adjustable in small ranges between −45 degree and +45 degree (Fig. 2.37). The single yarn layers are fed in consecutive steps into the weft lay-in units of the transport system. The warp threads made of rovings are supplied directly to the needles.

2.6.4   Braided structures

Braiding is a process of interlacing three or more threads diagonally to the product axis to obtain a thicker, wider or stronger product or in order to cover some profile. There are several types of braiding machines developed for manufacturing 2D and 3D braided structures. The classical and most commonly used braiding machines equipped with horn gears are known as maypole machines, which can be used to produce 1D linear, 2D flat and 3D tubular and solid braids. Fig. 2.38 demonstrates the principle of using a maypole machine to braid a linear product (Kyosev, 2015). The key parts of the machine include tracks, carriers and horn gears. The track determines the path of the motion, but the carriers are moved forwards by the horn gears. The process can be extended to more yarns to produce 2D flat and 3D tubular structures by placing a string of horn gears in an open-ended circular and complete circular form, respectively. 2D flat and 3D tubular triaxial braids can be produced by introducing inlay yarns in the braiding process. Fig. 2.39 shows a tubular braiding process with a third set of longitudinal inlay yarns. For structural composite applications, mandrel overbraiding is always employed to produce 3D tubular braids for profiled sections, as shown in Fig. 2.40 (Potluri and Nawaz, 2011). Unlike flat and tubular braids with only one
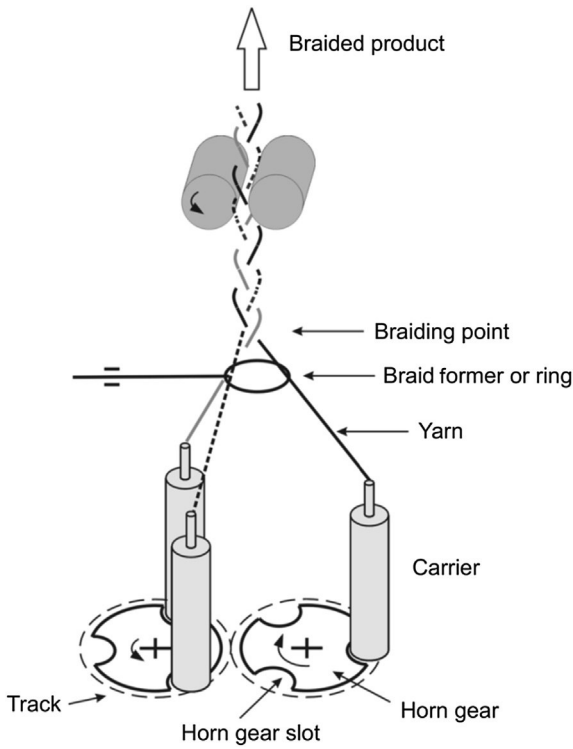
Figure 2.38 Principal construction of a maypole braiding machine.
Adapted from Kyosev, Y., 2015. Braiding Technology for Textiles, Woodhead, Cambridge.
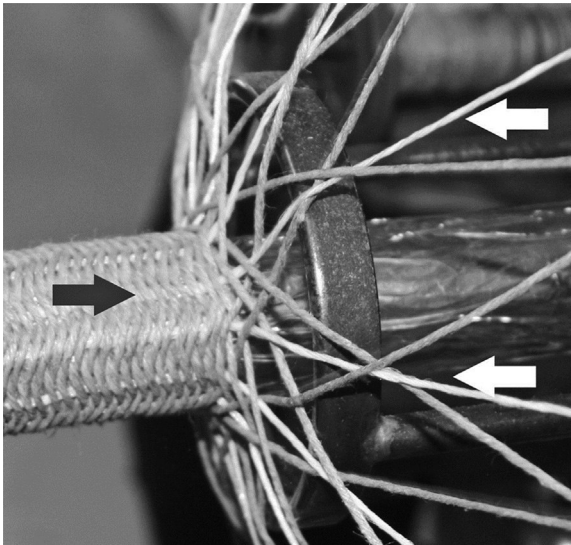
Figure 2.39 Triaxial tubular braid with inlay yarns. The arrows point to the inlay yarns. Adapted from Kyosev, Y., 2015. Braiding Technology for Textiles, Woodhead, Cambridge.
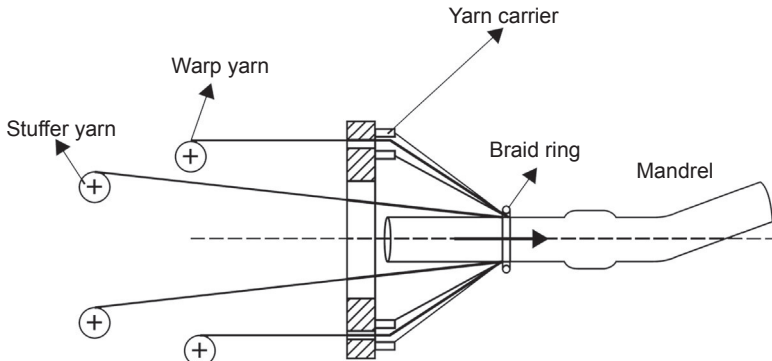
Figure 2.40 Mandrel overbraiding.
Adapted from Potluri, P., Nawaz, S., 2011. Developments in braided fabrics. In: Gong, R.H. (Ed.), Specialist Yarn and Fabric Structures, Woodhead, Cambridge, pp. 333−353.

interlaced layer, 3D solid braids have several interconnected layers. There are two basic types of machines to form a 3D solid braid: horn gear and Cartesian machines which differ only in their method of yarn carrier displacement. Similar to 2D braiding, horn-gear-based machines with square or circular arrangement can also produce 3D solid braids. To allow for more flexibility in preform size, shape and microstructure, 3D Cartesian braiding machines have been developed (Fig. 2.41). Moving carriers around a rectangular mesh, the so-called two-step and four-step braiding processes, involve the placement of the carriers over a special table into rows and columns. Motion is performed by moving an entire row or column in a given sequence, usually alternately. This process is used mainly for composite profiles with 3D cross-sections as illustrated in Fig. 2.21.
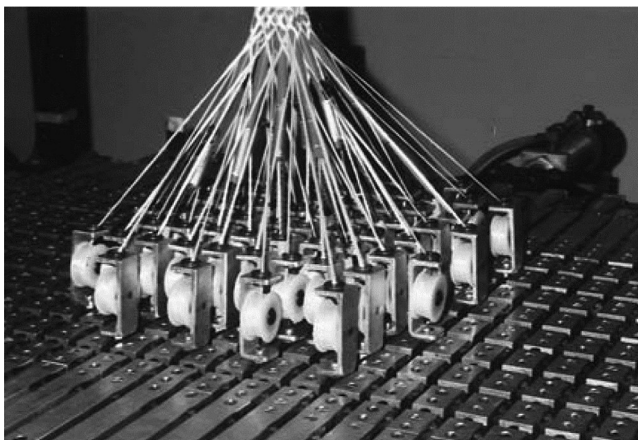
Figure 2.41 3D Cartesian braiding machine.
Adapted from Kostar, T.D., Chou, T.W, 1999. Braided structures. In: Miravete, A. (Ed.), 3D Textile Reinforcements in Composite Materials, Woodhead, Cambridge, pp. 217−240.

2.7 Properties of advanced fibrous architectures: advantages and disadvantages

The published literature regarding the mechanical properties of textile reinforcement is scarce. However, some basic principles and requirements may be discussed and taken into account.

As illustrated in Fig. 2.1, the translation efficiency of the fibre properties to the final application (i.e. a composite material) should be maximized. Therefore, it is of utmost importance to choose the appropriate structure for the application.

The use of straight, noncrimp continuous filament yarns with very low twist for the reinforcement is an important requirement. These have to be placed in 2D and 3D assemblies to form preforms.

Concerning woven structures, at least one set of yarns must have crimp and therefore is not straight. The effect of crimp on the tensile properties is well illustrated in Figs 2.42 and 2.43.

The strength of a woven fabric depends essentially on the strength of the composing yarns. There are, however, some additional effects due to the structure of the fabric. In order to achieve the maximum tensile strength at rupture, the load must be uniformly distributed by all the yarns in a particular direction (warp or weft). This is the case for the structures illustrated in Fig. 2.42: for structures (a) and (b) in both directions, and for the structure in (c) in the weft direction. However, this will not be the case for structure (c) in the warp direction as the crimp is not the same for all the yarns in the warp direction. Any load applied to (c) in the warp direction will be essentially taken up by the warp yarns without crimp. The yarns with crimp will merely contribute with a small force, just enough to straighten them out. By the time the yarns with crimp are straight and ready to support larger loads, the yarns initially without crimp will probably be at the stage of rupture. For this reason, the tensile strength at rupture of structure (c) in the warp direction will be a little more than half the tensile strength of structure (a).
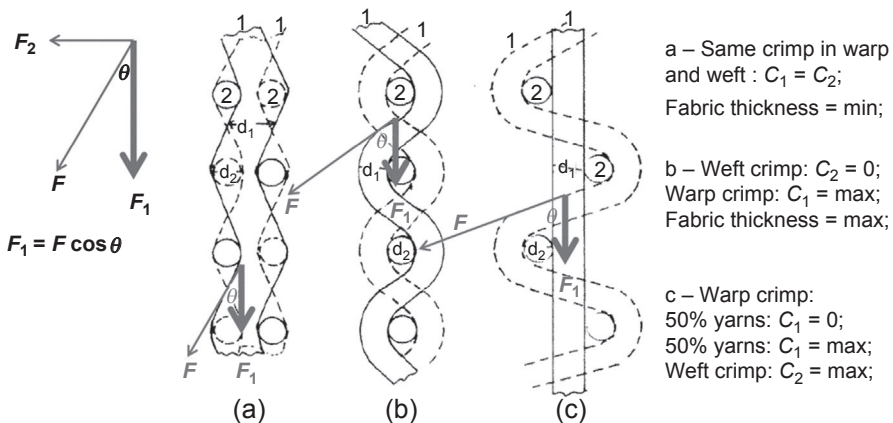
Figure 2.42 Section of a variety of plain-weave structures: effect of crimp on tensile properties (1, warp; 2, weft).

F = force applied
P = yarn spacing
l = modular length
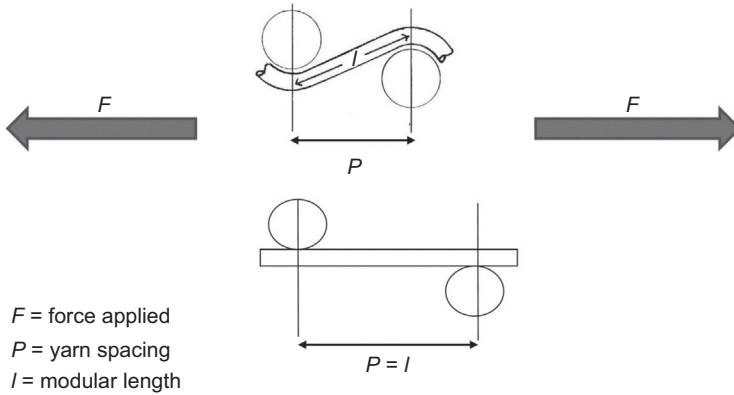
Figure 2.43 Illustration of crimp interchange in a woven fabric.

The effect of crimp interchange at the initial stage of loading is illustrated in Figs 2.43 and 2.44. Fig. 2.43 shows that when a woven fabric is extended in one direction (warp or weft), only when the modular length (l) is equal to the yarn spacing (p) does the yarn start supporting in full the load applied. Before that, the effect of the applied load is to deform the structure just enough to remove the crimp in the yarn.

The tensile behaviour of a woven fabric under a gradually increasing applied force is usually shown by the load-extension curve (Fig. 2.44) in which the slope of the primary linear region of the curve, the low-resistance region, is called the primary modulus and corresponds to the deformation of the structure. The slope of the secondary linear region of the curve, the high-resistance region, is called the secondary modulus and corresponds to the extension of the yarns. There is a nonlinear region between these two linear regions that could be affected by the fabric structure. In this
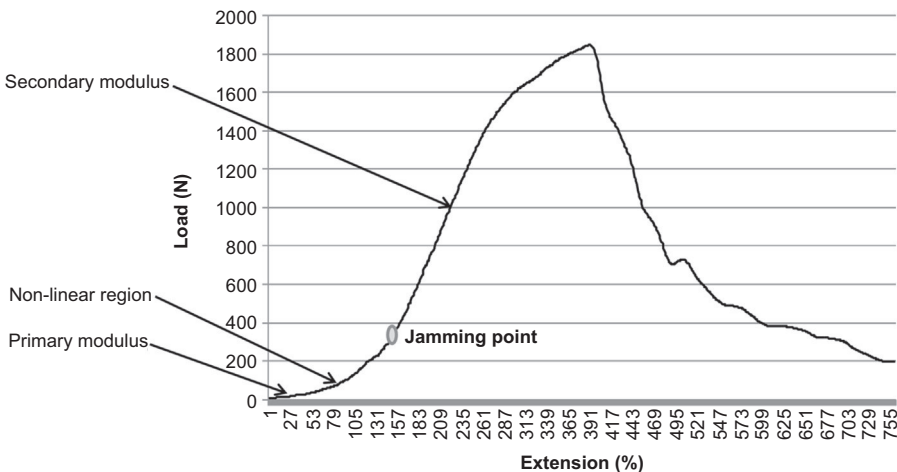
Figure 2.44 Typical load-extension curve of a woven fabric (weft direction).

latter region, a stick-slip effect due to interyarn friction may occur as yarns are displaced further. Extension of the yarn starts occurring when the structure is jammed and the yarns are straight.

To diminish the effect of crimp interchange when loading woven fabrics, flat yarns may be used instead of round ones.

DOS knitted fabrics seem to be the most successful technology for developing preforms for textile structural composites, as this technology enables the placement of straight noncrimp yarns in a variety of directions. Fig. 2.45 illustrates loading of a DOS structure with straight yarns as compared with loading a woven structure with crimped yarns. It should be noted that the greater the crimp, and consequently the greater the obliquity of the yarn, the smaller will be the contribution of the yarn to bear a load. When the same yarn is placed without crimp, as is the case of a DOS structure, it will be able to withstand greater loads.

Fig. 2.46 illustrates a typical load-extension curve of a DOS fabric in which the load is immediately borne by the yarn as soon as it is applied.

At the present time, the DOS warp-knitting-based technology is the most widely used by far, and the rate of production of these machines is very high. However, the DOS weft-knitting-based technology is much more flexible and may be of great interest in the future.

With regard to braided structures, the main limitation is fabric width, as the number of carriers needed to manufacture a wide fabric is very large and often impractical. It should be noted that problems of crimp interchange may be encountered, especially when loading in the bias directions.
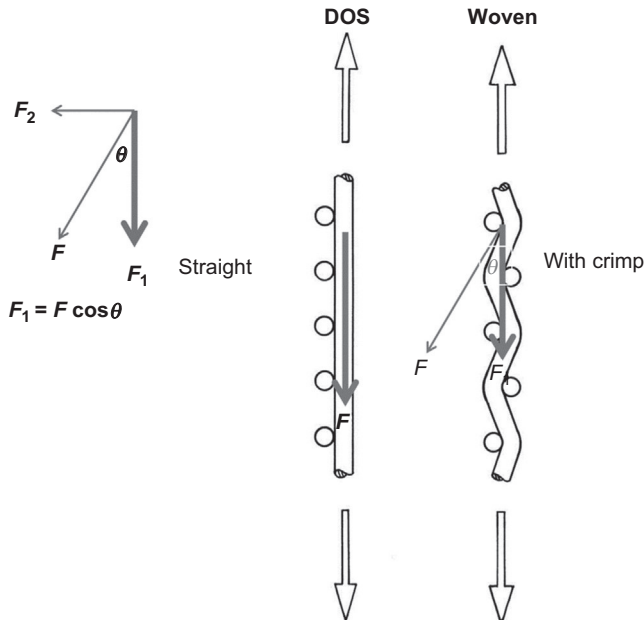
Figure 2.45 Effect of crimp on the load applied.

Figure 2.46 Typical load-extension
curve of a DOS fabric (reinforcement
yarn direction).
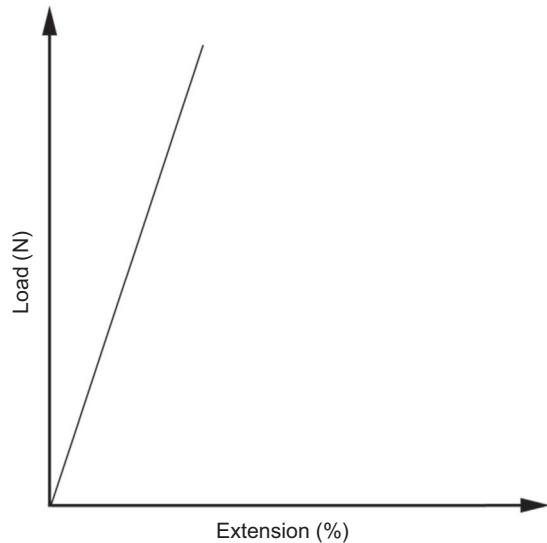
    Braided fabrics are highly deformable via the mechanism of fabric shear in the axial
and radial directions, and the opposite is true in the bias directions. It may be said that
they exhibit high compliance in the axial and radial directions and low compliance in
the bias direction. In the case of woven fabrics, the opposite of what happens in braided
fabrics is true, and so they exhibit low compliance in the axial and radial directions and
high compliance in the bias directions. In order to increase the rigidity of braided fab-
rics in the axial direction, an axial yarn may be introduced in that direction by using the
technique of triaxial braiding. In the case of woven fabrics, the rigidity in a third di-
rection may be achieved by using the triaxial weaving technique.

    Concerning the use of 3D fabrics in the composites sector, in which properties such
as high energy absorption, good impact resistance, good formability, good
through-thickness stiffness, strength, and fatigue resistance to flexural and torsional
strains along with a certain degree of isotropy and low density are required, the devel-
oped 3D products do not fully satisfy all the desired criteria. Furthermore, commercial
applications normally call for well-established design strategies that relate the func-
tional properties of a product with its structural parameters and material properties
as well as production systems that are efficient and reliable. In this respect, a consider-
able amount of development is yet to be undertaken in the area of 3D fabric technology
(Banerjee, 2014).

2.8   Applications

The drive within the aerospace composites field over the last decade has been to reduce
cost, increase component performance and reduce component weight (Lowe, 2005).

Due to their superior weight-to-specific stiffness and weight-to-specific strength ratios, and their potential for integral design, the use of textile structural composites in aerospace applications is increasing. The share of composite structures in the Airbus A340, A380 and the upcoming A350 XWB was around 17%, 25% and 50%, respectively, showing a rapidly increasing trend (Middendorf and Metzner, 2011). The in-plane mechanical performance of textile composites made by the liquid moulding method (vacuum assisted resin transfer moulding (VARTM), resin transfer moulding (RTM) or resin film infusion (RFI)) is almost equal to those made by the prepreg method. However, the out-of-plane impact resistance of textile structural composites manufactured by the liquid moulding method is lower than that developed by the prepreg method. It should be noted that glass and aramid fibres have gained relatively limited use in the aerospace sector, due to the higher density and lower stiffness of glass fibre and the high moisture absorption of aramid fibre. Hence, the majority of composite parts used in the aerospace industry are produced using the preimpregnated carbon fibre fabric with thermoset matrices. Woven, knitted, DOS, braided and other textile structures have been used in the development of composite parts for aerospace applications, whereas the most used textile structure is DOS.

2.8.1 Woven structures

One example of using woven structures in the aerospace field was realized in Japan by Kawasaki Heavy Industries, where a 380 g/m^2 2 × 2 twill carbon fibre fabric using Tenax HTS 5631 12K yarn was fabricated with a special weaving technique. The prepreg developed using this fabric has found several applications, including the Embraer ERJ 170 inboard flaps, the Embraer ERJ190 outboard flaps and wing stubs and the Boeing 737−300 winglets (Fig. 2.47).

2.8.2 Knitted structures

An example of using knitted structures in developing aerospace composite parts was conducted at Daimler-Benz. Fig. 2.48 shows a stiffened panel which was manufactured with warp-knitted skin and 3D braided stiffeners stitched together to a complex preform. The fibre structure was subsequently impregnated in an RTM process by DLR in Braunschweig (Drechsler, 1999).

Figure 2.47 Boeing 737−300 winglet programme for Aviation Partners Boeing.
Adapted from Lowe, J., 2005. Aerospace applications. In: Long, A.C. (Ed.), Design and Manufacture of Textile Composites, Woodhead, Cambridge, pp. 405−423.
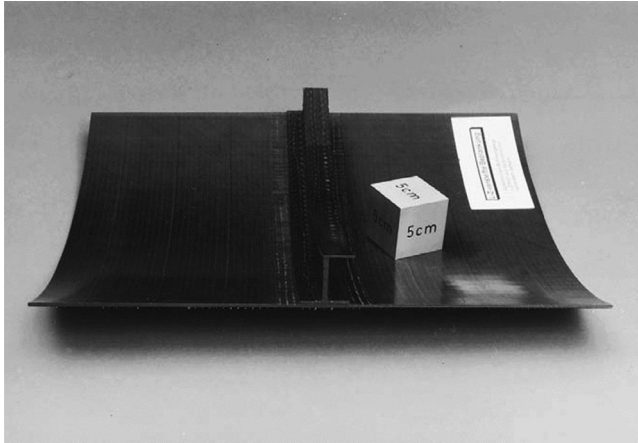
Figure 2.48 Stiffened panel consisting of braided profiles and warp-knitted skins.
Adapted from Drechsler, K., 1999. 3D textile reinforced composites for the transportation
industry. In: Miravete, A. (Ed.), 3D Textile Reinforcements in Composite Materials, Woodhead,
Cambridge, pp. 43–66.

2.8.3   Directionally oriented structures

DOS using 12K carbon fibre are the most commonly used structures in aerospace ap-
plications. There are two typical application examples: the Airbus A380 rear pressure
bulkhead (RPB) and Airbus A400M cargo door (Middendorf and Metzner, 2011). The
A380 RPB is produced at the Airbus plant in Stade, near Hamburg, using the preform
made of multiaxial carbon fibre DOS supplied by Saertex. This preform is draped over
a positive mould and then laminated using the RFI process (Fig. 2.49). After an initial
curing of the 3 mm thick basic laminate and the attachment of stringers, the part is
finally cured in an autoclave. The finished bulkhead weighs about 240 kg of size
6.2 m by 5.5 m (Middendorf and Metzner, 2011). The Airbus A400M cargo door con-
sists largely of multiaxial carbon fibre DOS with additional monoaxial DOS fabric for
local reinforcements and skin lay-up. The A400M cargo door is processed using the
EADS/Premium Aerotec patented vacuum-assisted process (VAP) infusion technol-
ogy (Fig. 2.50). The A400M cargo door is manufactured at the Premium Aerotec
site, Augsburg. Besides the large-scale structures described above, there are some
additional aerospace applications on the substructure level, such as the Airbus A380
flap track diaphragms, side shells and straps.

2.8.4   Braided structures

Large braiding machines have opened up interesting applications of braided structures
in the aerospace industry. A&P developed a Vectron sock of 2 m in diameter and 3 m
in length using an 800 carrier braiding machine (Potluri and Nawaz, 2011). Fig. 2.50
shows a prototype airlock developed for NASA using the braided sock developed by
A&P (Fig. 2.51).

Figure 2.49 Draping of the DOS fabric in the Airbus A380 rear pressure bulkhead production. Adapted from Middendorf, P., Metzner, C., 2011. Aerospace applications of non-crimp fabric composites. In: Lomov, S.V. (Ed.), Non-crimp Fabric Composites, Woodhead, Cambridge, pp. 441−448.
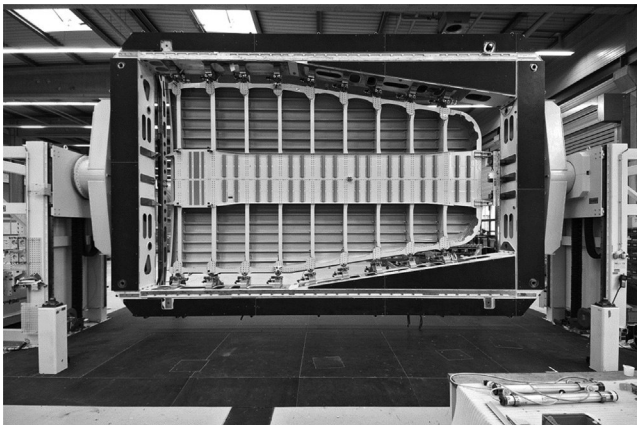
Figure 2.50 Airbus A400M cargo door manufactured at Premium Aerotec. Adapted from Middendorf, P., Metzner, C., 2011. Aerospace applications of non-crimp fabric composites. In: Lomov, S.V. (Ed.), Non-crimp Fabric Composites, Woodhead, Cambridge, pp. 441−448.

2.8.5 Future applications

The current applications of textile structures in the aerospace industry are mainly based on 2D structures using prepreg technology because 2D textile reinforcements are stronger in-plane than 3D solid textile reinforcements. The out-of-plane impact

Figure 2.51 Braided airlock developed for NASA.
Adapted from Potluri, P., Nawaz, S., 2011. Developments in braided fabrics. In: Gong, R.H. (Ed.), Specialist Yarn and Fabric Structures, Woodhead, Cambridge, pp. 333−353.
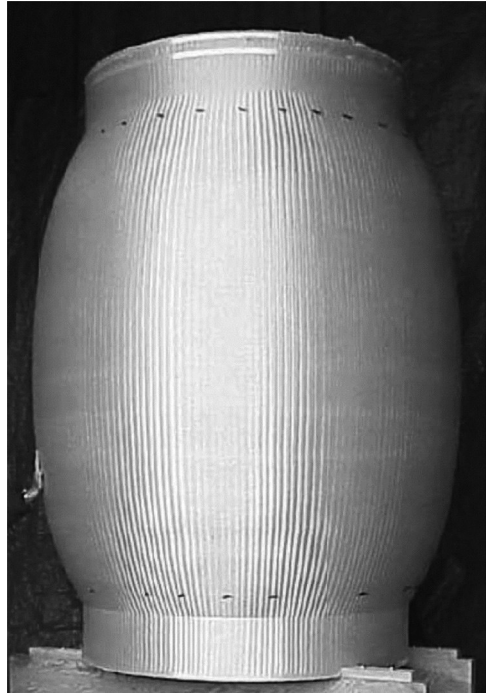
resistance is another important load case consideration in the development of aerospace composite parts. 3D solid textile structures with yarns orientated in the thickness direction give the composite very strong out-of-plane properties. Hence, the use of 3D solid textile structures is beneficial for aerospace composite parts to avoid delamination and fractures. However, especially in parts such as stiffeners and stringers, not all loads are in-plane, making the prepreg laminates less suitable. It can be expected that in the near future, 3D solid woven, knitted and braided fibrous architectures will attract great attention in the aerospace industry.

2.9 Summary and concluding remarks

The various types of advanced fibrous architectures (woven, knitted, braided and others) that are used for producing composites for various applications in aerospace engineering were discussed. The various production techniques used for advanced fibrous architectures were described, and the properties, advantages and disadvantages and applications of the various products were analysed. It was concluded that warp-knitted DOS structures using 12K carbon fibre are the most commonly used structures in aerospace applications. It is expected that in the near future, 3D solid woven, knitted and braided fibrous architectures will attract great attention in the aerospace industry.

Sources of further information

CITEC (aerospace materials), http://www.cytec.com/ (accessed 30.01.15.).
Gong, R.H., 2011. Specialist Yarn and Fabric Structures. Woodhead, Cambridge.
Long, A.C., 2005. Design and Manufacture of Textile Composites. Woodhead, Cambridge.
Lomov, S.V., 2011. Non-crimp Fabric Composites. Woodhead, Cambridge.
Miravete, A., 1999. 3D Textile Reinforcements in Composite Materials. Woodhead, Cambridge.

References

Anon, 1963. Textile Terms and Definitions. The Textile Institute, Manchester, p. 63.
Anon, 2014. A Strong Future for Carbon, Glass, Synthetic and Natural Fibre Textiles in Composites. Technical Textile Markets, p. 96.
Au, K.F., 2011. Advances in Knitting Technology. Woodhead, Cambridge.
Banerjee, P.K., 2014. Principles of Fabric Formation. CRC Press-Taylor & Francis Group, Boca Raton, FL 33487, p. 425.
Chen, X.G., Tayyar, A.E., 2003. Engineering, manufacturing, and measuring 3D domed woven fabrics. Textile Research Journal 73, 375−380.
Chen, X.G., Taylor, L.W., Tsai, L.J., 2011. An overview on fabrication of three-dimensional woven textile preforms for composites. Textile Research Journal 81, 932−944.
Dow, N.F., 1975. Warp Beam for Triaxial Weaving, US Patent No. 3884429.
Drechsler, K., 1999. 3D textile reinforced composites for the transportation industry. In: Miravete, A. (Ed.), 3D Textile Reinforcements in Composite Materials. Woodhead, Cambridge, pp. 43−66.
Hu, H., Araujo, M.D., Fangueiro, R., 1996. 3D technical fabrics. Knitting International 1232, 55−57.
Hu, J.L., 2008. 3D Fibrous Assemblies Properties, Applications and Modelling of Three-dimensional Textile Structures. Woodhead, Cambridge.
Hu, H., Zhang, M., Fangueiro, R., Araujo, M.D., 2010. Mechanical properties of composite materials made of 3D stitched woven-knitted preforms. Journal of Composite Materials 44, 1753−1767.
Khokar, N., 1996. 3D fabric-forming process: distinguishing between 2D-weaving, 3D-weaving and an unspecified non-interlacing process. Journal of the Textile Institute 87, 97−106.
King, R.W., 1976. Apparatus for Fabricating Three-dimensional Fabric Material, US Patent No. 3955602.
Ko, F.K., 1989. Three-dimensional fabrics for structural composites. In: Chou, T.W., Ko, F.K. (Eds.), Textile Structural Composites. Elsevier, Amsterdam.
Ko, F.K., 1999. 3D textile reinforcements in composite materials. In: Miravete, A. (Ed.), 3D Textile Reinforcements in Composite Materials. Woodhead, Cambridge, pp. 9−42.
Kostar, T.D., Chou, T.W., 1999. Braided structures. In: Miravete, A. (Ed.), 3D Textile Reinforcements in Composite Materials. Woodhead, Cambridge, pp. 217−240.
Kruse, F., Gries, T., 2011. Standardisation of production technologies for non-crimp fabric composites. In: Lomov, S.V. (Ed.), Non-crimp Fabric Composites. Woodhead, Cambridge, pp. 42−66.
Kunde, K., 2004. Spacer fabrics − their application and future opportunities. Melliand International 10, 283−286.
Kyosev, Y., 2015. Braiding Technology for Textiles. Woodhead, Cambridge.

Liu, Y.P., 2012. A Study of Warp-Knitted Spacer Fabrics as Cushioning Materials for Human Body Protection (Ph.D. dissertation). The Hong Kong Polytechnic University.

Lowe, J., 2005. Aerospace applications. In: Long, A.C. (Ed.), Design and Manufacture of Textile Composites. Woodhead, Cambridge, pp. 405−423.

Middendorf, P., Metzner, C., 2011. Aerospace applications of non-crimp fabric composites. In: Lomov, S.V. (Ed.), Non-crimp Fabric Composites. Woodhead, Cambridge, pp. 441−448.

Potluri, P., Nawaz, S., 2011. Developments in braided fabrics. In: Gong, R.H. (Ed.), Specialist Yarn and Fabric Structures. Woodhead, Cambridge, pp. 333−353.

Raz, S., 1987. Warp Knitting Production. Melliand Textilberichte.

Scardino, F., 1989. An introduction to textile structures and their behaviour. In: Chou, T.W., Ko, F.K. (Eds.), Textile Structural Composites. Elsevier, Amsterdam, pp. 1−24.

Schnabel, A., Gries, T., 2011. Production of non-crimp fabrics for composites. In: Lomov, S.V. (Ed.), Non-crimp Fabric Composites. Woodhead, Cambridge, pp. 3−41.

Spencer, D.J., 2001. Knitting Technology, third ed. Woodhead, Cambridge.

Stig, F., Hallström, S., 2012. Spatial modelling of 3D-woven textiles. Composite Structures 94, 1495−1502.

Xu, Y., Hu, H., Yuan, X., 2011. Geometrical analysis of co-woven-knitted preform for composite reinforcement. Journal of the Textile Institute 102, 405−418.

Metal and ceramic matrix composites in aerospace engineering

3

F.J. Lino Alves, A.M. Baptista, A.T. Marques
University of Porto, Porto, Portugal

3.1 Introduction

Ceramic matrix composites (CMCs) have the potential for high fracture toughness, resistance to catastrophic failure, high strength, light weight and low thermal expansion, and they withstand high temperature with high oxidation resistance. These types of materials exhibit much greater resistance to high temperatures and aggressive environments than metals or other conventional engineering materials.

Ceramics are nonmetallic inorganic materials, composed by metallic and nonmetallic elements connected by ionic and/or covalent bonds. Fig. 3.1 shows the two types of bonds that are present in NaCl (sodium chloride) and SiC (silicon carbide), respectively.

The ionic character of a ceramic can be determined by:

$$\% \text{ of ionic bonding} = 1 - \exp\left[-0.25 \times (X_a - X_b)^2\right] \times 100 \qquad [3.1]$$

where X_a and X_b are the electro negativities (tendency of an atom to attract electrons in the bond) of the elements a and b.
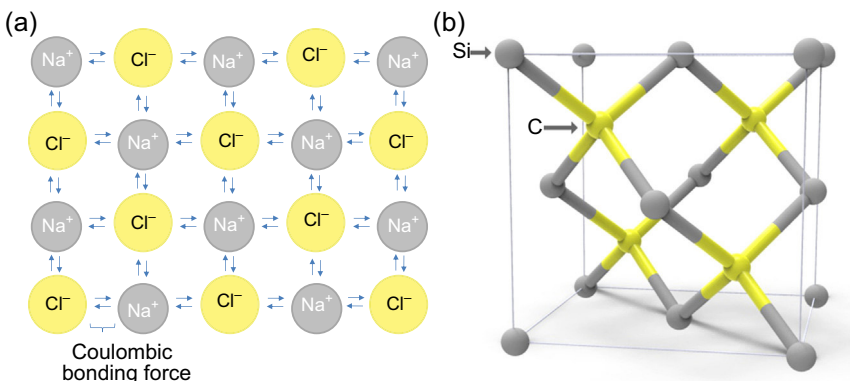
Figure 3.1 Type of bonds in ceramics: (a) ionic bond (NaCl), and (b) covalent bond (SiC).

CMCs are materials showing a chemically or physically distinct phase in large proportion (>5%), dispersed in a continuous matrix, exhibiting specific final properties. Their damage-tolerant behaviour and good mechanical properties in a broad range of temperatures can also be highlighted.

In CMCs, the matrix is a ceramic material, usually a technical ceramic that is manufactured by relatively complex processes from high-purity raw materials with small particle size (micro or nanoscale) and with good mechanical, thermal, electrical or chemical resistance. Ceramics normally form hybrid chemical bonds between covalent and ionic types, and they possess low density, chemical stability, high hardness and refractoriness (ie, they keep their mechanical resistance at high temperatures). Despite the remarkable evolution over the last two decades towards improvement of these properties, the ceramic materials with monolithic shape maintained their intrinsic limitations: limited tensile strength and low resistance to mechanical impact and thermal shock (Amaral Fortes and Ferreira, 2003).

For continued developments, there are a number of key technical needs, including new refractory matrices, new stable fibres and inert coatings for fibres, as well as affordable manufacturing techniques. A better understanding of materials is necessary, including fibre−matrix interaction, and relationships among microstructure, mechanics and properties.

Because of large temperature variations in space (-160 to $+93°C$) and the need to maintain precise alignment of communication and sensor systems, dimensional stability is a critical factor. Several CMCs can be recommended for this, such as the ones reinforced with graphite and aramid fibres (KEVLAR®), which possess a high specific strength and modulus and a low coefficient of thermal expansion (CTE). Stiffness and low thermal distortion, rather than strength, are the major considerations for space crafts, so the required material properties differ from those used in aircrafts. Other important factors for space crafts include thermal and electrical conductivity, long-term stability under vacuum, space radiation and low out-gassing (Schwartz, 1994).

Increasing the fracture toughness of ceramics has been one of the main reasons for the international scientific community's remarkable research efforts to produce ceramics with R-curve behaviour. This continuous research, fundamentally different from the conventional 'flaw elimination' approach, uses strategies that are 'flaw tolerant', 'nanoparticle dispersion strengthening' and focused on 'laminates'. In the flaw tolerant approach to ceramics that do not have phase transformations (allotropy), the microstructure is designed to promote grain-localized bridging behind the crack tip, which ideally leads to the strength being independent of flaw size. From the processing standpoint, the advantage is the strength to be less sensitive to processing defects and accidents. Improvements in flaw tolerance depend upon having a multiphase ceramic with a controlled heterogeneous microstructure. This requires a processing strategy for flaw tolerance in contrast to that for flaw elimination. In the nanoparticle-dispersion-strengthening approach, it has been reported that the incorporation of a dispersion of ultrafine (100−300 nm) second-phase particles into a matrix of higher expansion coefficient results in significant strengthening. Finally, laminar composites also provide an opportunity for tailoring the microstructure and mechanical properties of structural ceramics (Harmer et al., 1992).

While these composites are in the research and development stage, they offer structural engineers excellent rigidity, a high strength-to-weight ratio, high temperature capability and a noncatastrophic failure mode.

In the CMCs, the dispersed phase, also called the 'strengthening phase', can be continuous fibres, whiskers and particles. The properties of CMC components, as well as the respective volume fraction, frequency of distribution, orientation, size and geometry of reinforcement phases, are determinant factors for the final properties. There is, however, an additional factor which is decisive for the properties of the composites: the existence of a significant area of the reinforcement−matrix interface with its own characteristics.

Current CMC applications include turbines and internal combustion engines, aerospace structures and high-temperature leading edges and skins. The capabilities of CMCs are exploited to the extreme in the case of the thermal protection system of space shuttles that, on entry into the atmosphere at 3000 km/h, reach a temperature of 1500°C in the nose, supported only by carbon fibres in a carbon matrix composite. To protect against contact with oxygen, the carbon−carbon composite is first coated with a layer of silicon and then over-coated with a layer of silicon dioxide (Ruh et al., 1988; Richerson, 2000).

CMCs are now being introduced into many other new fields, and their range of applications will grow when the production cost will be significantly reduced. There is a strong need for the development of cost-effective SiC (silicon carbide) fibres to promote CMCs' applications where price is also a major concern.

Metal matrix composites (MMCs) are often related to light metal matrix composites. Although there is not a universally accepted definition of MMCs, we may consider MMCs as being a composite system with two distinct constituents, that is, a metallic matrix (most commonly, aluminium, magnesium or titanium) and a second material (metal, ceramic or other organic compound) acting as a reinforcement phase. The reinforcement may be considered distinct through the process history. MMCs can be considered as powder, particulate or fibre (either continuous fibres or short or chopped fibres) reinforced. The reinforcement may be used for a structural role but can also be applied to change physical properties (thermal expansion, thermal and electrical conductivity, friction, wear resistance etc.). Compatibility (chemical and thermal) between reinforcement and matrix, as well as control of interfacial properties, is essential in order to have an efficient MMC.

Bearing in mind the structure of MMCs' reinforcement (in most cases, a ceramic) in a metal matrix, their properties can be tailored and varied, covering almost the interval from metals' to ceramic's properties. In the case of structural properties, specific strength and specific stiffness are the main characteristics that MMCs will present. However, one has to consider that in MMCs with continuous reinforcements, anisotropy will bring big differences in mechanical properties with respect to orientation. In certain structural applications, ductility, toughness, fatigue and impact resistance may be fundamental requirements, implying a critical constituents selection and a process capable of controlling microstructural features (Miracle, 2005).

As far as processing is concerned, liquid metal (electroplating and electroforming, stir casting, pressure infiltration, squeeze casting, spray deposition and reactive

processing) and powder metallurgy cover the most important processes for MMCs. However, in most processing routes, there is a need for machining and finishing operations. This requires specific tools and operating parameters in order to have a cost-effective process.

From cutting tools to tank armours, brake discs (automotive and railways) and callipers as well as pistons, propulsion shafts and bicycle frames, MMCs present a large variety of applications. Automotive tyre studs, golf clubs, power electronic modules and applications in thermal management (eg, heat sinks for power amplifiers and printed circuit boards) can be found. Aerostructural, aeropropulsion and different subsystems can be reported as applications of MMCs in the aerospace industry.

The current research objectives for MMCs are to: increase yield and tensile strength at different temperatures, but keep the minimum ductility; increase creep resistance at higher temperatures as compared to conventional alloys; increase fatigue strength, mainly at high temperatures; improve thermal shock resistance; improve corrosion resistance; increase Young's modulus and reduce thermal expansion. Moreover, continuous process development is also a part of the main research activity for MMCs.

3.2   Types of matrix

3.2.1   Ceramic matrices

The fibre−matrix interfacial domain may consist of an interface or an interphase. An interphase implies the presence of at least two interfaces: one with the matrix and one with the fibre, and more when the interphase consists of a multilayer (Bansal and Lamon, 2015). There are two main types of bonding at the interface: mechanical (lower strength) or chemical bonding. Mechanical bonding results from residual stresses leading to gripping of the fibre by the matrix. Radial gripping can be enhanced when the interface is rough. Interfacial properties depend upon fibre and matrix because bonding results from chemical reactions during processing or thermal shrinkage during cooling. The prevalent assumption is that good composite behaviour requires weak fibre−matrix interfaces that de-bond upon impingement of a matrix crack. Interphases allow these limitations to be overcome, and they allow the interfacial characteristics to be tailored with respect to composite properties (Bansal and Lamon, 2015).

The more common matrices are the glasses, glass ceramics, carbon, SiC, Si_3N_4, aluminates and oxides. Table 3.1 presents the main properties of some ceramic matrices.

Advances in power generation systems for aircraft engines, land-based turbines, rockets and hypersonic missiles and flight vehicles have increased the demand for structural materials that have superior long-term mechanical properties and retain these properties under high temperature, high pressure and several environmental factors, such as moisture. Because these applications require exposure to oxidizing

Table 3.1 Physical and mechanical properties of different ceramic matrices (Granta, 2015)

Property or matrice	Aluminosilicate 1720	Glass ceramics, nonmachinable 9606	Carbon industrial	SiC HP	Si$_3$N$_4$ HP	Alumina 99	Mullite
Density (g/cm^3)	2.49−2.54	2.57−2.62	1.3−1.8	3.14−3.21	3.16−3.23	3.65−3.93	2.7−3
Price (€/kg)	1.06−1.24	1.55−9.31	8.39−12.7	10.9−15.5	26.3−40.2	20.3−30.6	6.21−7.76
Young's modulus (GPa)	84.8−89.1	115−121	6−15	390−410	302−318	360−380	110−220
Tensile strength (MPa)	39.9−43.9	109−120	8−16	476−525	476−525	257−284	55−132
Strain to failure (%)	0.04−0.05	0.09−0.1	0.05−0.27	0.12−0.13	0.15−0.17	0.07−0.08	0.02−0.12
Flexural modulus (GPa)	84.8−89.1	115−121	6−15	390−410	302−318	360−380	110−220
Flexural strength (MPa)	51.9−57.1	131−145	35−50	571−630	952−1050	381−420	175−250
Hardness Vickers (HV)	476−525	588−648	24−48	2380−2630	1810−2000	1520−1680	243−268
Fracture toughness (MPa m$^{1/2}$)	0.71−0.73	1.4−1.7	0.5−1.3	3−3.5	2.6−3.2	3.8−4.2	2.1−2.3
Maximum service temperature (°C)	200−650	686−714	2580−2690	1500−1650	1080−1230	1170−1230	1500−1700
Thermal conductivity (W/m °C)	1−1.5	3.25−3.51	5−30	76.9−83.2	31.7−34.3	30−36	2−6
Thermal expansion coefficient (μstrain/°C)	4.11−4.28	5.58−5.81	1.3−5	4.9−5.1	3.6−3.7	4.5−8.3	3.5−5

environments, the thermodynamic stability and oxidation resistance of CMCs are vital issues. The need for environmentally stable composites motivated the development of CMCs based on environmentally stable oxide constituents (Bansal and Lamon, 2015).

3.2.2 Metallic matrices

In theory, any metallic alloy can be used to produce an MMC. In reality, only a few are used: aluminium, magnesium and titanium, and eventually copper for superconducting magnets. In aerospace applications, weight savings are critical, and that is the reason to use light metal alloys. In recent years, the use of aluminium matrix composites has been widespread in structural and thermal management components for aeronautics and aerospace, due to their excellent specific strength and stiffness as well as their good thermal properties and corrosion resistance (Miracle, 2001; Chawla and Chawla, 2006). Among all, precipitation-hardenable alloys, like Al−Cu−Mg and Al−Zn−Mg−Cu, are especially important (Chawla and Chawla, 2006).

For the production of SiC−Al composites, Yana et al. (2008) suggest the use of an aluminium alloy with high silicon content in order to control the formation of Al_4C_3 in the reinforcement−matrix interface. This compound is considered as the most detrimental reaction product in this type of composites. Titanium and its alloys present relatively high strength and modulus-to-weight ratios. Titanium has a melting point of 1672°C and retains strength at high temperatures with good corrosion and oxidation resistance. Ti6Al4V, also known as grade 5, Ti-6Al-4V or Ti 6-4, is the most commonly used titanium alloy, with extensive applications in aerospace air frame and engine components (http://www.aerospacemetals.com/titanium-ti-6al-4v-ams-4911.html). Magnesium is one of the lightest metals (1.74 g/cm^3) (Chawla and Chawla, 2006), with a strength-to-weight ratio similar to that of aluminium alloys. Magnesium and its alloys also have a high vibration damping capacity that makes them an ideal material choice for many high-speed applications (http://www.intlmag.org/magnesiumbasics/advantages.cfm). The main properties of MMC matrices are shown in Table 3.2, and the main properties of different ceramic fibres are shown in Table 3.3.

3.3 Types of fibre

CMCs and MMCs can be fabricated with different types of reinforcements which strongly influence the ease of fabrication and the resulting properties. Components are chosen on the basis of chemical stability and compatibility and thermo-physical and mechanical properties, since final composite properties are in large part governed by the properties of components. There are three general types of ceramic and metal matrix composites: particulate-reinforced; whisker-reinforced and filament (continuous or discontinuous)-reinforced.

In continuous fibre-reinforced ceramics, only those fibres that withstand the high temperatures of matrix processing (above 1000°C) may be used. Other

Table 3.2 Physical and mechanical properties of MMC matrices

Property	ρ g/cm^3	CTE 10^{-6} K^{-1}	Thermal conductivity W/m K	Yield stress (tensile) MPa	Ultimate tensile stress MPa	Young's modulus GPa	Elongation %	References
Matrices								
Al 2024	2.78	22.7	120			70		Yana et al. (2008)
Al 2024	2.77	22.9	151			72		Parsonage (1999)
Al 6061/T6	2.71	23.2	160	193	227	69	10	Speer and Es-Said (2004)
Al 6061/T6	2.70	23.6	180	–	290	69/70	–	Parsonage (1999) and U.S. Congress (1988)
AlBeMet	2.1	13.9	240	282	338	199	10	Speer and Es-Said (2004)
AlBeMet162	2.1	13.9	210	221–328	288–439	193	10	Parsonage (1999)
Ti TC4	4.44	9.2	6.8			109		Yana et al. (2008)
Ti 6Al4V	4.43	8.8	7.2	827	896	110	10	Speer and Es-Said (2004)
Ti 6Al4V					1170	114		U.S. Congress (1988)
Ti 6Al4V	4.42	8.6–9.7	6.7	880	950–1000	110	14	http://www. aerospacemetals.com/ titanium-ti-6al-4v- ams-4911.html
Mg Al6Mn	1.78	26	62	130	220	45	8	http://www.makeitfrom. com/material-properties/ AM60A-AM60A-F- MgAl6Mn-M10600- Magnesium/
Mg				30	115		6.08	Sun et al. (2012)
Mg + Ni5%				58	146		3	Sun et al. (2012)

Table 3.3 Main properties of different ceramic fibres (Granta, 2015)

Fibre	SiC fibre 140 μm	SiC whisker	Alumina whisker	C fibres high modulus
Property				
Density (g/cm^3)	3.15−3.20	3.15−3.21	3.95−3.97	1.8−1.85
Price (€/kg)	4040−4060	1400−1550	3880−4660	31.3−37.6
Young's modulus (GPa)	440−480	440−480	445−460	370−390
Tensile strength (MPa)	2250−2300	6000−8000	1660−2340	2400−2410
Strain to failure (%)	0.2−0.25	0.2−0.25	0.2−0.25	1.8−2
Flexural modulus (GPa)	440−480	440−480	445−460	370−390
Flexural strength (MPa)	2250−2300	6000−8000	2000−2800	2200−5200
Hardness Vickers (HV)	3200−3300	900−1000	2300−2400	660−810
Fracture toughness (MPa m$^{1/2}$)	2.2−3	2.25−3.25	3−5.9	1−2
Maximum service temperature (°C)	1030−1080	1130−1180	977−1030	530−580
Thermal conductivity (W/m °C)	60−100	6−100	20−25.6	80−200
Thermal expansion coefficient (μstrain/°C)	4.4−4.8	4−4.2	7.7−8.6	0.2−0.4

high-temperature requirements to be met include long-term stability, creep and oxidation resistance. A wide spectrum of continuous fibre-reinforced CMCs and MMCs can be foreseen. Common examples of reinforcement phases are silicon carbide (SiC), titanium carbide (TiC) and boron carbide (B_4C); silicon nitrides (Si_3N_4) and boron nitrides (BNs); alumina (Al_2O_3) and zirconia (ZrO_2); and carbon (graphite or partially amorphous) and boron (Amaral Fortes and Ferreira, 2003; Bansal and Lamon, 2015; Clauss, 2008). Nonoxide fibres exhibit superior strength and creep resistance as compared to the oxides (Granta, 2015). Typical reinforcements for MMCs are: ceramic particles or ceramic fibres; carbons fibres and metallic fibres which tend to fail due to high density and affinity of reaction with a matrix alloy. One of the first MMCs used boron filament as a reinforcement. The main properties of typical fibres used in MMCs are presented in Table 3.4.

3.3.1 Particulate reinforcements

In particulate-reinforced composites, particles of a second phase are incorporated in a continuous matrix. These composites can easily be fabricated by sintering or hot pressing well-dispersed mixtures of the two components.

Table 3.4 Physical and mechanical properties of different fibres used with MMCs

Property	ρ (g/cm³)	CTE µstrain/ °C	Thermal conductivity (W/m °C)	Young's modulus (GPa)	Tensile strength (MPa)	Strain to failure (%)	Fracture toughness (MPa m^{1/2})	Hardness Vickers (HV)	Maximum service temperature (°C)	Price (€/kg)
Fibre										
Alumina fibre (f)	3−4	7−9	20−25	220−390	2000−2400	0.8−1	1.5−2	600−700	970−1000	1210−4000
Alumina whisker or particulate (p)	3.94−3.97	7.5−8.5	20−25	445−460	1660−2340/ 1500−1600	0.2−0.25	3−6	2300−2400/ 900−1000	970−1000	3900−4660
Aluminium nitride (p)										
Borsic	2.7−2.8	~5	~38	~400	~3000	0.75	2−4	800−1000	~550	2700−3200
Graphite	1.9−2	0.01−0.3	80−200	600−800	2000−2400	0.5−0.8	1−2	600−800	500−600	50−55
SiC whisker	3.15−3.21	~4	60−100	440−480	6000−8000	0.2−0.25	2.25−3.25	900−1000	~1150	1400−1550
SiC (p)	~3.18	~4	60−100	450−480	2500−300	0.2−0.25	2−3.5	~3250	~1050	23−40
Boron	~2.5	~5.6	~19	~400	~2400	0.5−0.8	2−4	800−1000	~550	400−500
Boron carbide (p/f)										
Beryllium	~1.86	11	~ ~185	~307	~965	3−4	11−15	200−320	250−300	225−340
Titanium diboride (p)	~4.5	~4.7	~73	500−550	~320	~0.15	~5.5	2500−3000	~1475	15−30

CTE, coefficient of thermal expansion; *f*, fibres; *p*, particles; ρ, density.
Adapted from Granta, 2015. CES Edupack, Granta Design.

3.3.2   Continuous fibres

Ceramic filament reinforced composite can use different types of filaments. Examples can be a graphite filament, an Al_2O_3 filament or a mullite or SiC monofilament produced by an organometallic polymer route. In fact, using continuous refractory fibres is the most efficient way to obtain strong and tough CMCs at high temperature.

3.3.3   Short fibres

Short fibre-reinforced composites are fabricated by hot pressing well-dispersed whiskers in powder matrices. Some anisotropy of properties is seen as the whiskers tend to orient perpendicularly to the hot pressing direction. Al_2O_3-SiC and mullite$-SiC$ whiskers composites have been fabricated by ultrasonic dispersion of the whiskers in the powder, followed by hot pressing (Bansal and Lamon, 2015).

3.3.3.1   Glass fibres

This earlier developed synthetic reinforcements begun to be incorporated in polymeric matrices in the 1940s. A decisive feature for the ease in processing and incorporation is their great flexibility, which results from their high aspect ratio (>100), low modulus of elasticity and extremely thin diameter. The most common examples of glass fibres are E type, a good electrical insulator, C type with high corrosion resistance and the more refractory glass S (or R, in Europe) type with a high silica content. As typical values of properties of E glass fibres, one can reference the density of 2.55 g/cm^3, the tensile strength of 1.75 GPa, a Young's modulus of 70 GPa and a thermal expansion coefficient of 4.7×10^{-6} K^{-1} (Amaral Fortes and Ferreira, 2003). Although they can be used as reinforcements of CMCs or MMCs, due to their low service temperatures they are hardly found as reinforcements for those types of composites. They are quoted here as a historic reference. However, for nondemanding structural and thermal applications, they have been used for a long time.

3.3.3.2   Boron fibres

Boron nitride is a very important inert material which has excellent thermal shock resistance, anisotropic thermal properties, good dielectric properties and low strength. It has been used as a reinforcement phase for silicon nitride, improving the maximum temperature in thermal shock from 600°C to 700$-$900°C (Ruh et al., 1988). Boron fibres are very resistant, with a high Young's modulus of 420 GPa and tensile strength up to 5.7 GPa, but they need highly expensive processing, which is a great disadvantage. It is possible to grow thin fibres (25 μm diameter) by laser chemical vapour deposition (LCVD), a process in which only the top of the filament is heated by the laser's focal point, unlike the conventional technique in which the entire tungsten (W) wire is kept at the same temperature (Amaral Fortes and Ferreira, 2003). Silicon carbide$-$boron nitride composites have been investigated to exhibit improved thermal shock resistance (Granta, 2015).

3.3.3.3 Carbon fibres

Carbon, graphite and their modifications are typical high-temperature materials. Their intrinsic high thermal stability (above 3000°C) and very low density (~ 1.9 g/cm^3) make carbon-based materials one of the most promising candidates for high-temperature applications. The particular advantage of carbon fibres is the extremely high specific stiffness and strength (Granta, 2015). Strictly speaking, graphite fibres are a special case resulting from the total conversion, by heat treatment, of the near-crystalline structure of carbon into graphite, giving them highly anisotropic properties (the Young's modulus varies from 1000 GPa in the basal plane to 35 GPa in the c-axis direction) (Amaral Fortes and Ferreira, 2003).

Nonoxide CMCs reinforced by nonoxide fibres have been mostly studied. The reason for this is that carbon and silicon carbide fibres display the highest properties for use at high temperatures. Second, for compatibility reasons, nonoxide fibres can be combined essentially to nonoxide matrices. However, carbon fibres degrade in oxidizing atmosphere at temperatures as low as 450°C, and they must be protected. SiC-based fibres are much more resistant to oxidation (Amaral Fortes and Ferreira, 2003).

Among the reinforcements of the CMCs, carbon fibres have the highest values of specific tensile strength ($\sigma/\rho = 2.8$ GPa/g cm^3) and specific modulus ($E/\rho = 380$ GPa/g cm^3). They are produced from the pyrolysis of an organic precursor: cellulose, rayon, synthetic polymer polyacrylonitrile (PAN) and pitch from petroleum (Fig. 3.2). The production of carbon fibres from the first two types of precursor fibres involves an initial oxidation step to strengthen the polymer, followed by pyrolysis for decomposition of the organic carbon precursor. The following step is the final stage involving graphitization in Ar or N$_2$ at 2400−3000°C (Amaral Fortes and Ferreira, 2003).

Carbon fibres are excellent in inert atmosphere, but in air they oxidize starting from 500°C. A useful property of C fibres is the negative thermal expansion coefficient in the longitudinal direction ($\alpha = -1.4 \times 10^{-6}$ K^{-1}), and this allowed them to be used in polymer matrix composites (PMCs) with a zero thermal expansion coefficient. A more recent type of carbon fibre is the carbon fibre grown in the gas phase (vapour-grown carbon fibres), obtained by decomposition of a hydrocarbon in a substrate (C, Si or quartz), when it is heated in the presence of a metal catalyst (Fe, Ni or Co) at temperatures higher than 1000°C. In this process, the catalyst is continuously removed from the static substrate, and the carbon fibre grows between the catalyst and the substrate. The great advantage of this technique is the production of fibres that have high mechanical resistance (up to 20 GPa) and are free from defects (Amaral Fortes and Ferreira, 2003).

3.3.3.4 Oxide fibres

Oxide fibres are inherently resistant to oxidation, but they have limited creep resistance and undergo grain growth at high temperatures, which causes strength degradation. They display much higher densities than carbon and SiC-based fibres. Despite these drawbacks, alumina-based CMCs have been extensively studied (Granta, 2015).
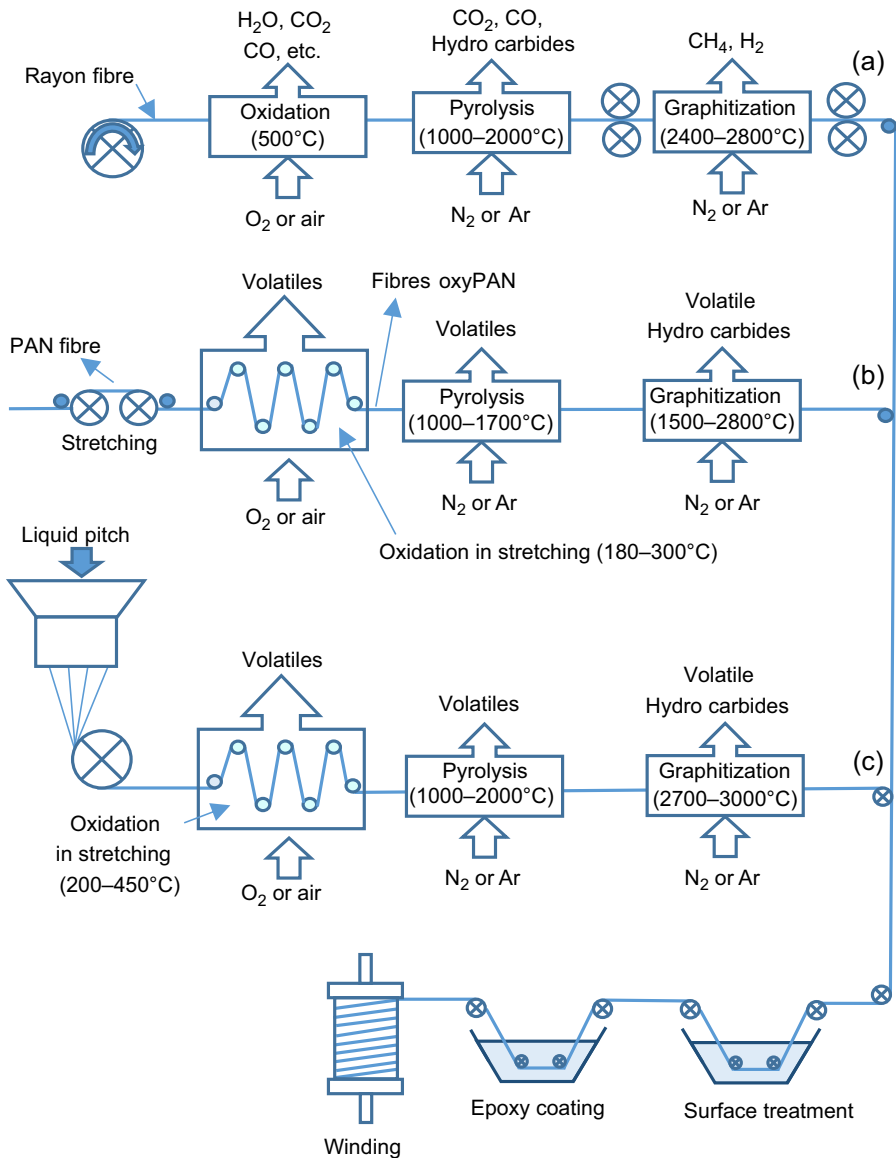
Figure 3.2 Sequence of manufacturing carbon fibres starting from different precursors; (a) rayon; (b) polyacrylonitrile (PAN); (c) pitch for oil.
Adapted from Amaral Fortes, M., Ferreira, P.J. (Eds.), 2003. Materiais Dois Mil. IST Press (in Portuguese). ISBN:972-8469-26-8.
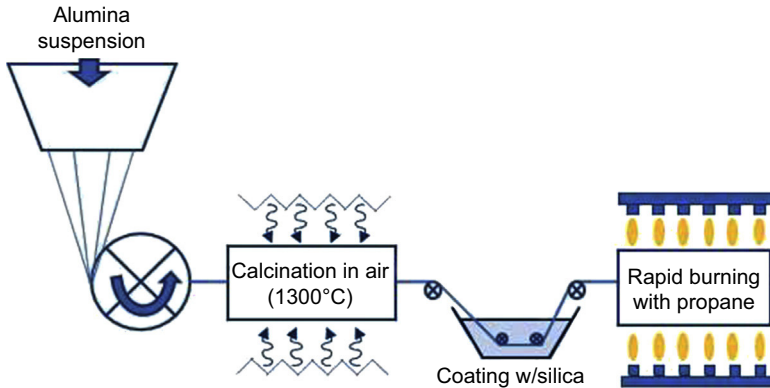
Figure 3.3 Basic process of manufacture of α alumina fibres.
Adapted from Amaral Fortes, M., Ferreira, P.J. (Eds.), 2003. Materiais Dois Mil. IST Press (in Portuguese). ISBN:972-8469-26-8.

Alumina α fibres (the stable phase of alumina) are the most common ceramic fibres based on oxides. The basic manufacturing process involves five steps (Fig. 3.3): (1) formulation of a suspension of alumina particles and additives in aqueous solution; (2) stretch the 'green' fibres from the suspension, with drying; (3) slow burning for alumina densification; (4) fibre coating with a shallow cover of silica to block surface cracks; and (5) fast final sintering with propane flame (Amaral Fortes and Ferreira, 2003). The advantage of mono-crystalline filaments is their high creep resistance, due to the absence of grain boundaries. The typical characteristics of α-Al_2O_3 fibres are a 10 μm diameter, 0.5 μm grain size, tensile strength of 1.8 GPa and Young's modulus of 320 GPa (Amaral Fortes and Ferreira, 2003). Sapphire (single-crystal Al_2O_3) fibres are no longer available; their cost and diameter (>50 μm) limit their use in composites (Granta, 2015).

3.3.3.5 Fibres of covalent ceramics

The covalent ceramic fibres include the SiC ones. One of the techniques of production of these fibres is the chemical vapour deposition (CVD) process on tungsten (W) or carbon (C) substrates, as with boron (B) fibres, from mixtures of hydrogen and silanes. Typical properties include the tensile strength of 3.5 GPa and Young's modulus of 430 GPa. SiC fibres obtained by CVD are fragile, hence an alternative processing technique came up leading to the production of more flexible fibres: controlled pyrolysis of a polymeric precursor. The steps involved in this technique are: (1) drawing at 350°C of a polymeric precursor fibre (eg, polycarbosilane $[-Si(CH_3)_2-CH_2-]_n$); (2) cure and polymer stabilization at 190 °C in air or at room temperature in ozone; and (3) pyrolysis in vacuum at 1300°C of the fibre precursor to produce the final ceramic fibre (Amaral Fortes and Ferreira, 2003).

There are several commercial fibres with compositions near SiC, such as Nicalon: a mixture of nano crystalline β-SiC$-$SiC (~ 1.7 nm), SiO_2 and free C, but with a creep

resistance lower than that of CVD fibres with 100% SiC, but more flexible (fracture elongation of 1.6%). A negative feature of the fibres obtained by pyrolysis is the presence of residual porosity (5−25%) of nanometre dimensions. Polymer pyrolysis processing is still used for the production of Si_3N_4−SiC fibres or even pure Si_3N_4. For example, Si_3N_4 fibres with 10 μm diameter are obtained from the PHS polymer (perhydropolisilizane) dissolved in xylene, and extruded and pyrolized at 1400°C in N_2, with good tensile strength (2.5 GPa) (Amaral Fortes and Ferreira, 2003).

Si_3N_4 fibres can also be obtained by CVD, as described for boron (B) and SiC fibres, from the reactants $SiCl_4$ and NH_3, but they are also costly. The fibres of $SiCl_4$ and NH_3 resist oxidation up to 1300°C, presenting the best mechanical resistance values (2.0 GPa) up to that temperature. Other covalent fibres are BN and boron carbide (B_4C). BN fibres have superior oxidation resistance compared to carbon fibres and are derived from a precursor fibre of boron oxide (B_2O_3) which is converted to nitride by ammonia and thermally stabilized. B_4C fibres are obtained over C substrates by a CVD process, from mixtures of BCl_3 and H_2, according to the following reaction: $BCl_3 + 6H_2 + C \rightarrow B_4C + 12HCl$ (Amaral Fortes and Ferreira, 2003).

Zirconium diborides (ZrB_2) and hafnium diborides (HfB_2) belong to the refractory transition metal diborides from the fourth to sixth groups of the periodic table. Most of these diborides have melting points above 3000°C, high thermal and electric conductivities, chemical inertness against molten metals and good thermal shock resistance. Although various kinds of ZrB_2- and HfB_2-based composites are already available, poor fracture toughness is still an open problem, and further research is demanded (Granta, 2015).

3.3.3.6   Particles and whiskers

The variety of reinforcements in particle shape is much more extensive than in fibres, because almost all materials can be obtained in powders. The whiskers are a particular type of reinforcement characterized by short single-crystal fibres with high mechanical resistance, given the absence of grain boundaries and low density of crystalline defects. Typically, they feature some micrometre diameters (0.5−10 μm) and are a few microns to a few centimetres in length, with aspect ratios between 50 and 10,000 (Amaral Fortes and Ferreira, 2003; Lamon, 2010). Fig. 3.4 shows some examples of whiskers (Soltani et al., 2015).

Whiskers are usually obtained by growth in the vapour phase; a pioneering process used since 1970 is the production of SiC whiskers from rice husks. This raw material represents about 20% of rice processing and contains cellulose, silica and other organic and inorganic compounds. The shells are heated in the absence of oxygen at 700°C to release volatiles, and are then subjected to auto-carburization (combination of carbon from cellulose with silica) for 1 h at 1500−1600°C, forming SiC (Amaral Fortes and Ferreira, 2003; Richerson, 1992).

Particles are separated from the whiskers by sedimentation, having an average aspect ratio of about 75. An alternative process is the vapour−liquid−steam technique (VLS), where the whiskers are obtained from SiO and CH_4 gases, originating dissolved species of Si and C in a metallic liquid catalyst, and subsequently getting
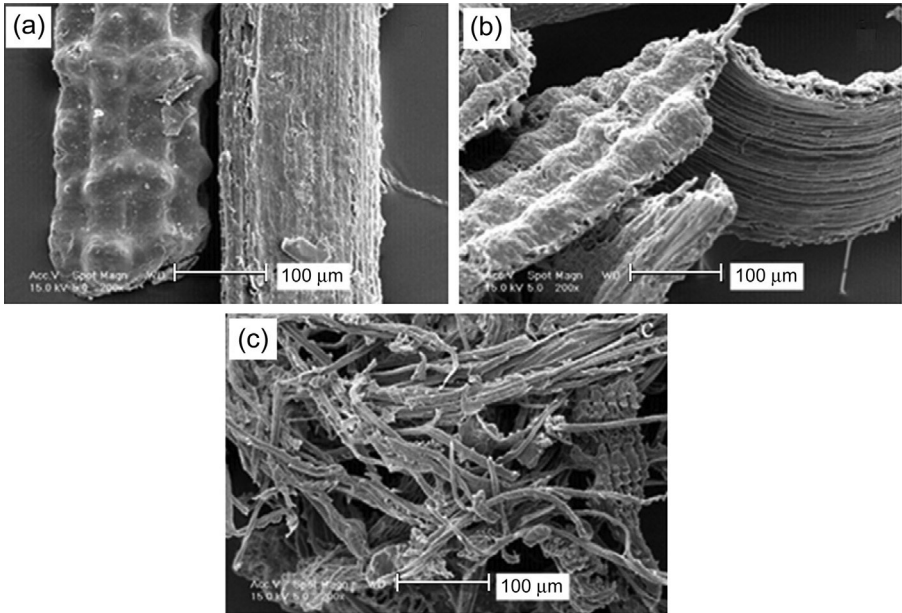
Figure 3.4 Scanning electron micrograph of (a) untreated rice husk fibres; (b) alkali-treated rice husk fibres; and (c) bleached rice husk fibres.
Reproduced from Soltani, N., Bahrami, A., Pech-Canul, M.I., Gonzalez, L.A., 2015. Review on the physicochemical treatments of rice husk for production of advanced materials. Chemical Engineering Journal 264, 899−935.

precipitated in vapour−liquid surface in the form of SiC. Examples of tensile strength and Young's modulus values are 8.4 and 580 GPa for medium-length fibres of 10 mm and 6 μm diameter, respectively. As a general rule, the whiskers cost about 5× more than the particles of the same composition, whereas, for instance, SiC fibres have 100× higher cost than the simple particles (Amaral Fortes and Ferreira, 2003).

3.4 Processing techniques

3.4.1 Manufacturing of CMCs

Several approaches are available for processing CMCs using liquid, gaseous or solid precursors. CMCs are manufactured by conventional manufacturing techniques of ceramic materials or by specific processes. The first include the steps known as the densification of powders (consolidation by cold pressing followed by sintering or, in one step, hot pressing). During sintering, the reinforcement phases can inhibit the densification by formation of rigid structures, and thereby preclude the shrinkage and sealing of porosity. Depending on the thermal expansion coefficient differences, tensile stresses are induced in the matrix around the reinforcements that inhibit

densification. For this reason, the amount of reinforcement is normally kept less than 40% by volume (Amaral Fortes and Ferreira, 2003).

The most common technique for the production of glass fibre composites is infiltration by suspension (Fig. 3.5), in which the fibres are impregnated with a suspension of the matrix phase, and then stacked in layers forming preforms, which are cut, calcinated and finally consolidated by hot pressing. In the case of composites of SiC fibre in a Si_3N_4 matrix, one can use a specific technique which combines the reactive sintering with hot pressing: alternately stack Si layers mixed with a polymeric binder and layers of SiC fibres, followed by the steps of burning of the binder and sintering under pressure in N_2 atmosphere at $1100-1400°C$ for nitration of silicon (Amaral Fortes and Ferreira, 2003).

In the field of reactive sintering for production of CMCs, there stands out a commercial material (REFEL®) that is manufactured by infiltration at $1700°C$, at low pressure, of liquid Si into fibres or carbon particles; Si reacts with carbon, resulting in a thin array with less than 10% vol of Si reinforced by SiC, and with excellent thermo-chemical compatibility between the matrix and reinforcement. Nonconventional techniques of production of CMCs are still liquid infiltration, direct oxidation, polymeric pyrolysis, the CVD process, the sol−gel method and self-propagating high-temperature synthesis (SHS) (Amaral Fortes and Ferreira, 2003).

The infiltration method by liquid is very similar to the techniques used for infiltration of metals or polymers: a pre-form reinforcing phase is infiltrated by a liquid or a matrix precursor suspension by capillary action, in vacuum or under exterior pressure.
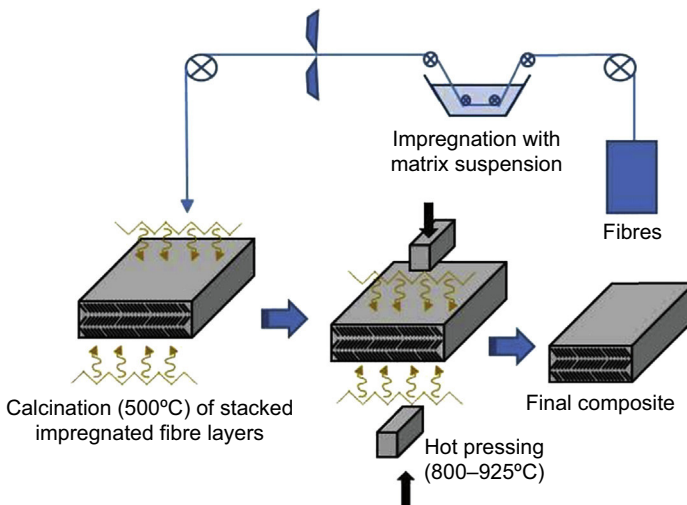
Figure 3.5 Production scheme for ceramic fibre−matrix composites using the infiltration technique with suspension.
Adapted from Amaral Fortes, M., Ferreira, P.J. (Eds.), 2003. Materiais Dois Mil. IST Press (in Portuguese). ISBN:972-8469-26-8.

An example of this process is the production of glassy matrix composites with various fibres (SiC, C, Al_2O_3 and mullite) which are drawn inside a crucible with molten glass. Other materials are the ones that result from infiltration with organometallic polymers or with hydrocarbons (pitch or phenolic resins), later pyrolized and resulting in matrices of SiC and carbon, respectively. The following is a final step of hot pressing for total densification. The method of direct oxidation (the Lanxide™ process) is a variant of impregnation, in which a ceramic (eg, SiC) pre-form of the reinforcement phase is infiltrated with liquid metal (eg, Al) that is simultaneously oxidized (Amaral Fortes and Ferreira, 2003).

The chemical vapour infiltration (CVI) process is a low-temperature technique compared to liquid infiltration. However, the gas flow inside the preforms can lead to occlusion of pores, which requires multiple impregnations and machining cycles for the complete closure of porosity. CVI was first used for the fabrication of carbon−carbon composites via pyrolysis of CH_4 at 1000−2000°C. CVI of fibre pre-forms is a method used in CMCs with matrices of SiC, Si_3N_4, C, B_4C, TiC and Al_2O_3, and re-inforcements of Nicalon (SiC) and Nextel (α-Al_2O_3). The CVI has been studied since the 1960s, as an extension of CVD technology. When the CVD is used to incorporate rather large amounts of matrix materials in fibrous preforms, it is called chemical vapour impregnation or infiltration (Amaral Fortes and Ferreira, 2003).

Another technique, the sol−gel process, has the advantages of low processing temperature and high compositional homogeneity. However, the differential shrinkage between reinforcement and matrix is significant and may result in the development of cracking. Finally, self-propagating high-temperature synthesis (SHS) technology, known mainly for the manufacture of porous refractories, can be used for the production of CMCs such as SiC (whiskers)−Al_2O_3. In this case, pressure is applied during or shortly after the internal exothermic reaction of matrix, for the densification of the material (Amaral Fortes and Ferreira, 2003).

3.4.1.1 Interface between reinforcement−matrix and mechanical properties

The ceramic materials rarely display plastic deformation below 1000°C, with the mechanical resistance determined by the catastrophic propagation of cracks generated by: (1) processing defects; (2) the geometry of parts; and (3) degradation in service. The crack resistance can be increased by reducing the size of defects or increasing the fracture toughness. The second alternative is the main goal of the CMCs. Ideally, the interface should present less mechanical strength than the intrinsic resistance of the constituent phases of composites, making it the preferred route for the spread of cracks and enhancing the fracture toughness of the material. The stress−strain curve of a CMC with aligned fibres along the length of the specimen may be analogous to that of a metallic alloy with a yield region (Fig. 3.6(a)): (1) initial elastic behaviour; (2) within the limit of elastic proportionality, the matrix cracks, and the slope of the curve begins to decrease; (3) the matrix yields by multiple cracking, perpendicular to the axis of the test piece, while the remaining load is transmitted and supported by fibres until it reaches the maximum tension value; and (4) rupture or extraction
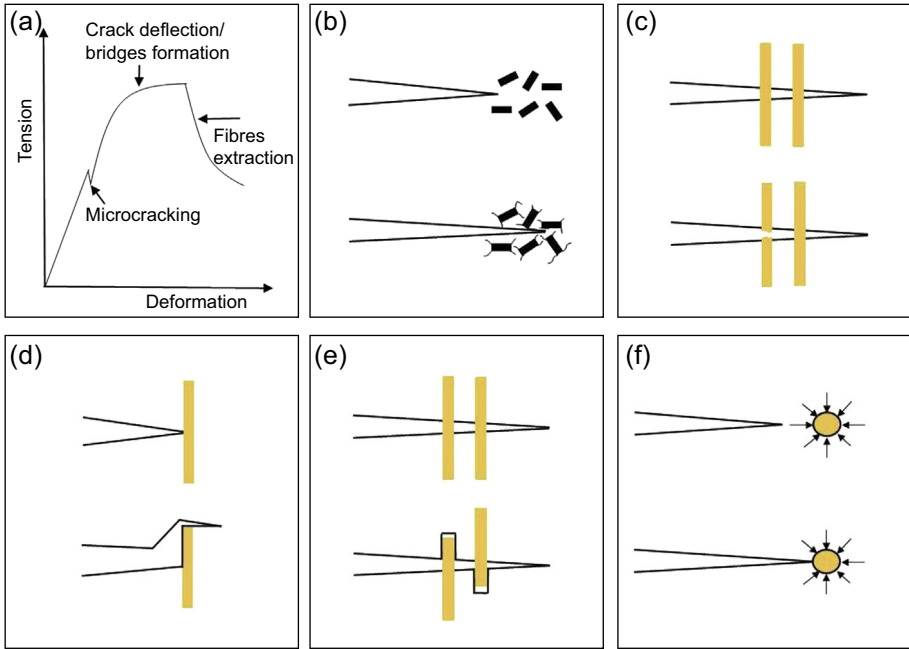
Figure 3.6 (a) Characteristic stress−strain curve of a CMC reinforced with fibres. Toughness mechanisms: (b) micro-crack toughening; (c) formation of bridges between the sides of the cracks; (d) crack de-flexion; (e) extraction of reinforcing fibres); and (f) slowdown or stoppage of the cracks.

Adapted from Amaral Fortes, M., Ferreira, P.J. (Eds.), 2003. Materiais Dois Mil. IST Press (in Portuguese). ISBN:972-8469-26-8.

of fibres in a noncatastrophic way until the complete fracture of the sample. The main outcome of this behaviour is greater toughness of the material.

Micro-cracking of the matrix (Fig. 3.6(b)) is an example of a toughness mechanism. It is favoured by the presence of the fibres, which stems from the expression deduced to the minimum spacing (x) between cracks that can be developed:

$$x = (V_m \sigma_m r)/(2 V_f \tau) \tag{3.2}$$

where V_m and V_f are, respectively, the mass fractions of matrix and fibre; σ_m is the tensile strength of the matrix; r is the radius of the fibre; and τ is the interfacial shearing resistance.

Micro-cracking occurs at the crack tip, decreasing the stress concentration intensity factor. However, extensive micro-cracking of the matrix, besides reducing the modulus of elasticity, can enable the internal oxidation of the material; and so, if their relative importance is considerable, the composite is not reliable for high-temperature applications.

Another mechanism, the formation of fibre bridges between the faces of the cracks, is crucial in materials like the aluminas reinforced with whiskers of SiC. A high value of friction between reinforcement and matrix, a high amount of fibres, its diameter and, above all, its tensile strength contribute positively to this phenomenon. In this mechanism, the fibres act against the crack opening, and their rupture occurs at a certain distance 'behind' the crack tip (Fig. 3.6(c)). The decohesion of the interface is a prerequisite for the other two mechanisms: the deflection of the cracks and the extraction of fibres (Fig. 3.6(d) and (e)).

For the extraction mechanism of fibres, a simple balance of forces determines that the fibre is pulled out of the matrix, in the condition $l/d \geq \sigma_{fl}/(4\tau_i)$, in which l/d is the fibre aspect ratio, σ_{fl} the tensile strength and τ_i the interface resistance. It should be noted that the fracture toughness of a CMC can result from the combination of all these mechanisms, reaching a maximum for an optimum amount of reinforcement phase. In the case of composites reinforced with particles of dimensions in the range of $1-10$ nm, the increase of fracture toughness is due, in part, to the arrest or even stopping of crack propagation by the action of the compression stress field surrounding the particles (Fig. 3.3(f)) (Amaral Fortes and Ferreira, 2003).

Toughening mechanisms are the result of careful control of the reinforcement−matrix interface. The interface characteristics result from the selection of the phases itself, as regards thermodynamic stability during processing and service, and also the eventual coating of the reinforcement phase. Ideally, this coat should not react with the fibre or the matrix, and must be stable at the manufacturing and usage temperatures of composites. The most common coating thicknesses are $0.1-1$ μm, and the most commonly used coatings are carbon, BN, SiC, ZrO_2 and SnO_2. For example, BN avoids chemical bonding between a ZrO_2 matrix and surface silica of SiC fibres, making the interface less brittle.

Although the primary objective of the formulation of the CMCs is not the increase in the modulus of elasticity or tensile strength by addition of second phases, this effect is not negligible, especially in CMCs of a glassy matrix. Increments in Young's modulus proportional to the relative volume of the fibres are known for Nicalon−glass or carbon−glass composites, up to a 55% reinforcement volume, above which the porosity in the matrix increases and the Young's modulus decreases.

Also, the thermal expansion coefficient of composites (α_c) depends upon their internal structure and the values of this property for its constituents. In the case of a particulate composite, this parameter does not follow a simple law of mixtures, depending on the volumetric module (K) of the components:

$$\alpha_c = (\alpha_m V_m K_m + \alpha_p V_p K_p)/(V_m K_m + V_p K_p) \qquad [3.3]$$

Properties such as thermal conductivity k and dielectric permittivity ε_r present more complex dependencies on the microstructure. The density (ρ) is the only property for which the rule of mixtures works regardless of the geometry of reinforcement phases. It is important to know these materials' resistance to fatigue. In the case of the CMCs, this property is much more complex, due to the presence of the toughness mechanisms

mentioned before. The fatigue resistance of the CMCs is best described by replacing the conventional parameter 'crack length increment' (*da*) of the Paris law

$$da/dN = A(\Delta K)^{\mathrm{m}}$$
[3.4]

by the 'crack density increment' or by the *dE−dN* gradient.

CMCs respond, typically, to cyclical loads with an initial increase in the density of cracks, suffering a deceleration of the degradation in the intermediate stage corresponding to the multiplication of such mechanisms operating in subcritical crack growth. In polycrystalline ceramics, inter-granular sliding and diffusion of defects are phenomena that in most cases control the creep behaviour. In the CMCs, these mechanisms are also determinants, but the creep resistance may be higher. Comparing the creep resistance of a monolithic alumina with an alumina reinforced by 20% vol of SiC whiskers, the deformation speed of the composite in the temperature range 1200−1400°C is two orders of magnitude lower due to inter-granular alumina slip retardation by SiC whiskers. This mechanism is crucial for obtaining values of creep resistance around 1.08 GPa at 1400°C, in the case of nanocomposites of $SiC-Si_3N_4$. The same system, but with SiC fibres, offers increased creep resistance if the fibres are aligned along the load axis. However, as mentioned, covalent phases such as SiC, Si_3N_4 and carbon are susceptible to oxidation, so CMCs based on oxides, as is the case in the $Al_2O_3-SiO_2$ system, confer greater stability at high temperature in air (Amaral Fortes and Ferreira, 2003; Harmer et al., 1992; Richerson, 2000).

3.4.2   Manufacturing of MMCs

A simple classification of MMCs manufacturing is based on the matrix state in the processing technique: liquid, solid or gaseous.

3.4.2.1   Liquid state processing

When using relatively low-melting-temperature alloys, like Mg or Al, liquid state routes are very convenient as near-net shapes can be produced and usually production costs are lower.

Reinforcement (short) fibres or particles can be mixed to the melted matrix prior to casting to obtain a composite part. Usually, stirring is needed to ensure less heterogeneity in the resulting material. Centrifugal casting allows finished parts with intentionally segregated reinforcement, like a brake disk reinforced in the periphery and without reinforcement in the central hub which is very advantageous from a machining or performance perspective (Chawla and Chawla, 2006).

Conventional casting is used to produce composite foundry ingots that can be processed to obtain extrusion billets or rolling blanks for further processing. Continuous casting can also be used to produce long semiproducts with a constant section, rod or bar. A common problem with those techniques is the resulting heterogeneity, as presented in Fig. 3.7; clustering of reinforcement elements and regions with less concentration that can be reduced by deformation processing. Sun et al. (2012) uses ultrasonic
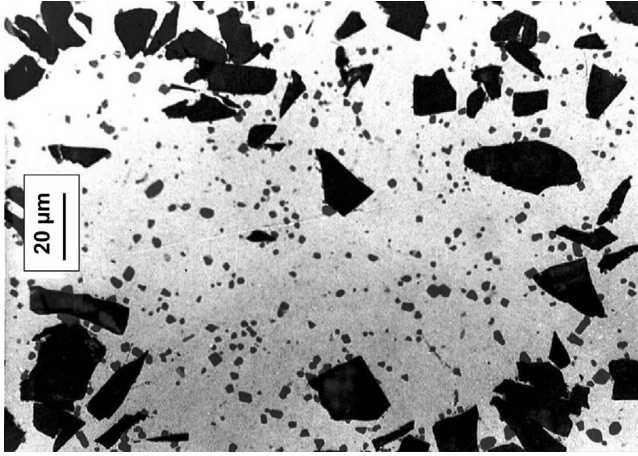
Figure 3.7 Continuous cast aluminium matrix composite − A356/20%SiCp-T6. Notice SiC
[**AU1**] particles clustering and less reinforced central region.
Paulo Davim, J., 1997 (Ph.D. thesis).

cavitation for dispersion and processing of C-coated Ni nanoparticles in molten Mg to
produce a fine reinforced composite up to 4.9 wt% Ni.

Another route uses reinforcement preforms to be infiltrated by the liquid metal.
Pressure-less infiltration, low-pressure infiltration and squeeze casting (Fig. 3.8) or
pressure infiltration are different possible options. Pressure-less infiltration, as
described by Yana et al. (2008), uses a SiC particle pre-form with 40−70% volume
and an aluminium alloy ingot which is placed over it and heated to 790−810°C for
2−12 h depending on the thickness of SiC powder beds. Squeeze casting is a

Figure 3.8 Squeeze cast aluminium matrix composite − AA383/Al$_2$O$_3$/20f. Alumina fibres in
the pre-form present a three-dimensional (3D) distribution.
Paulo Davim, J., 1997 (Ph.D. thesis).

pressure-assisted infiltration method of short fibre or particulate preforms by liquid metal. The advantages over conventional infiltration are the shorter processing time, ability to produce relatively complex shapes, minimal porosity or shrinkage (due to applied pressure) and minimization of interfacial reactions (Chawla and Chawla, 2006).

Spray co-deposition consists of projecting particles or short fibres on a melted alloy spray, resulting in a rapid solidified composite. One advantage of this technique is the high production rate (6−10 kg/min) that can be achieved and the rapid solidification that minimizes interfacial reactions between matrix and reinforcement (Chawla and Chawla, 2006).

3.4.2.2   Solid-state processing

Most of the solid-state-based processes are based on powder metallurgy (PM). Reinforcement and metal alloy in fine powder form are closely mixed together and then cold pressed/sintered or hot pressed. Secondary operations like forging or extrusion are often used to obtain fully compacted composites with better properties due to grain and fibre alignment. PM is useful to produce discontinuous fibre-reinforced composites, eventually with nanoparticles. A good advantage of this method is its ability to produce near-net-shape parts. It is also possible to get functionally graded materials by using a progressive increment or reduction of reinforcement volume in specific regions of the part to be produced. A drawback is associated with difficulty in controlling the reinforcement dispersion, resulting in clustering and less reinforced regions.

For long or continuous fibre-reinforced products, co-extrusion and roll bonding are often applied (Miracle, 2001). In titanium matrix composite (TiMC) manufacturing, the foil−fibre−foil (FFF) method, matrix-coated monotape (MCM) method and matrix-coated fibre (MCF) method are currently in use. A vacuum hot-pressing MCF method is described by Peng (2005) for the production of SiC-reinforced TiMCs. SiC monofilaments, 140 μm in diameter, are Ti-6Al-4V coated with ∼50 μm thickness covering and then packed together in square and hexagonal arrangements. Regular fibre distribution has been achieved in both preparations.

3.4.2.3   Vapour deposition

Gaseous state processing is mainly executed by plasma spraying, for example to metal coat fibres to be used in the MCF method. In this process, the matrix is deposited on the individual fibre from the vapour phase. The composite fabrication is completed with a hot isostatic pressure operation.

3.5   Joining and repair techniques

Joining is a discontinuity, a potential region for crack initiation and future failure, and hence it must be avoided. However, sometimes it cannot be avoided. Welding CMCs to themselves and to dissimilar materials is impossible because of the inexistence of electrical conductivity. However, typical mechanical solutions are available, like

fasteners, rivets, bolts, screws and the like, or the use of adhesives. Brazing and some joining materials and methods, used in restricted applications areas, are still at the research phase. These techniques can be used in some CMC applications if the general parameters are adapted for these particular materials.

One of the problems in joining is the different CTEs of materials that have to be joined. Different approaches have been proposed, such as suitable design to minimize stress concentration, metallic interlayers, graded joints or mechanical structuring of the surface to be joined (Fergurson et al., 2014). A combination of suitable joining material, machining or laser structuring, surface modification by chemical reactions and selective removal of the composite matrix can be developed and tailored to specific applications.

3.5.1   Mechanical joining and integration of CMC

Mechanical joining could be a problem if some drilling or other processes that induce stress concentration are used. Screw−nut and bolt−rivet systems are available to join CMCs, but the working temperature of the best metallic systems (super-alloys) is much lower than the expected one required for the CMCs. They can be replaced by some ceramics that have higher melting temperatures, but the possibilities are limited. CMC components can be integrated to the nanocomposite structure mechanically with metal or composite threaded fasteners, C, C 'T' joints, Miller fasteners, and round braided CMC fasteners. Mechanically locked joints are interesting for ease of assembly and disassembly, in comparison with other joining techniques. An interesting improvement in mechanical joining for CMCs is the coupling with modified adhesives or other joining materials (brazing alloys or glasses/glass-ceramics) to give reliable and hermetic joints. Actually, adhesives coupled with screws are used to join metallic or polymeric parts; its adaptation to CMCs is a challenging but promising concept (Granta, 2015).

3.5.2   Adhesive joining

Due to the high-temperature applications of CMC and MMCs, the use of adhesives is restricted. However, they can be interesting for low temperature components. Furthermore, they can be modified to increase their temperature resistance, which can be achieved by adding ceramic particles, fibres, or carbon nanotubes.

C−SiC and C/C−SiC composites can be complex shaped in thin-walled structures that can be produced via in situ joining. Thereby, the structure is divided into several subcomponents, which can be manufactured easily via the near-net-shape technique. After pyrolysis, the subcomponents are assembled by using a slight pressure or by adhesive bonding the components with a joining paste, based on phenolic resin and carbon powder. To assure a tight fit, the joint areas of the components are usually machined before assembly. The joining itself is performed in situ, during the siliconization of the assembled C−C structure. Thereby, the SiC matrix is built up in the joint, bonding together the components permanently to an integral structure (Granta, 2015). Several joining techniques cannot be used to join Si−Al−O−N ceramics because of

their tendency to decompose rather than melt at high temperatures. Si$-$Al$-$O$-$N contains a small percentage of inter-granular glassy phase that melts around 1350°C, and this can be utilized for joining these components (Schwartz, 1994).

3.5.3   Hot-pressing diffusion bonding

CMCs of Si_3N_4 matrix reinforced with SiC monofilament have led to outstanding resistance to temperatures exceeding 1350°C. Joining two panels of these materials was obtained with direct bonding using hot pressing with a monolithic monolayer as a high-temperature stable bonding agent. Some work centred on aerofoil applications is referred to in the References (see Schwartz, 1994). To produce this complex shape, it was necessary for the pre-form tape to conform to the curvature of the part to achieve multidirectional reinforcement. The tape contained 75 μm diameter fibre (SCS-9; high-purity β-SiC deposited on a 33 μm pitch-derived carbon fibre pre-coated with a thin layer of pyrolytic carbon (Peng, 2005)), which resulted in easier wrapping of the tape around the leading edge of the aerofoil. Other plies were wrapped at opposite orientation angles and along the axis of the aerofoil to give balanced and multidirectional reinforcement. Fabrication was performed by hot pressing (Schwartz, 1994). Recent studies have centred on the use of high isostatic pressing (HIP) for consolidation of parts (Schwartz, 1994).

3.5.4   Brazing

Brazing alloys can be considered as a sort of metallic 'high-temperature glue'. High-temperature brazing alloys are based on gold, nickel and copper and are often used for joining CMC to cobalt or nickel-based super-alloys. The critical issues in brazing CMCs are wettability of the braze on the substrates, the chemical interactions between the braze and the CMC, and the possible reaction products at the interface. The thermodynamic stability (affected by barrier coatings) of the brazing alloy towards CMC and the intrinsic lower melting temperature of the brazing alloy compared to the CMC or the metal to be joined and CTE mismatch are also very important considerations. Functional gradient materials can be used to accommodate CTE mismatch. Active filler materials have been developed to the point where reliable joints can be produced.

Presently there are investigations with other joining systems, such as nonoxide composites and oxide composites, to correlate with the processing conditions, interlayer microstructure and mechanical properties, and simultaneously to develop brazing materials for temperatures higher than 1230°C (Granta, 2015). Joints accomplished by brazing methods can have a number of advantages over mechanically fastened joints, including the size and weight of brazed assemblies can be significantly less; use of design involving small, compact, multipart components; use of high-temperature braze materials allows components with brazed joints to function at higher operating temperatures (Schwartz, 1994). The braze alloy which has a melting point lower than those of the CMCs is placed between the parts to be joined and is heated above its melting temperature.

3.5.5 Phosphate bonding

This process is desired as an alternative to HP or HIP, processes that are expensive and demand high-temperature sintering. Phosphate binder systems have been used in common refractories for many years, but their use in high-performance composites, especially nonoxides, remains relatively unexplored. The general concept is that a continuous tow or cloth is combined with a liquid or paste matrix precursor, and with time and heat (temperatures varying from room temperature to 300 °C), this matrix material solidifies. Phosphate bonding avoids the problems of inhibition of matrix shrinkage during densification due to fibres (Schwartz, 1994).

3.5.6 Other joining processes

A liquid silicon infiltration (LSI) used to join carbon-based CMCs, ARCJOINT, uses a carbonaceous mixture and silicon or silicon-based paste or tape, and other 'exotic' techniques like transient-liquid-phase bonding (TLPB), nano powder infiltration and transient eutectic phase (NITE), spark plasma sintering (SPS), microwave-assisted joining, laser-assisted joining, glass and glass–ceramic as joining materials for CMCs. Solid-state displacement reactions and pre-ceramic–polymer joints are also referred to in the literature as being developed only at the research phase (Granta, 2015).

3.5.7 Repairing techniques

For CMCs and MMCs, repair is not an easy task. In fact, the processes will, in most cases, involve high temperatures and/or very specific environmental conditions. However, one may consider the possibility of repairing these structural components by using the principles of joining techniques. Nowadays, there is an increasing tendency to develop self-healing techniques that may self-repair damage in inorganic materials. The following techniques can be used, particularly for MMCs (Mallick, 1997): precipitation healing; shape memory alloy-based healing; composite materials reinforced with a healing agent; electrochemical healing; self-healing solder; and others.

3.6 Properties

3.6.1 CMCs

CMCs were developed to enhance damage-tolerant quasi-ductile behaviour, whilst keeping the other advantages of ceramics, particularly at high temperatures. Their properties are very different from those of conventional ceramics, as they have anisotropy, lower rupture elongation (up to 1%), improved toughness, dynamic load capability and higher thermal shock resistance. Table 3.5 shows a set of important properties, physical, thermal and mechanical, for some CMCs.

Table 3.5 Physical and mechanical properties of CMCs

Property / Material		ρ g/cm	CTE 10^{-6} C^{-1}	Thermal conductivity W/m C	Bulk modulus GPa	Ultimate tensile stress MPa	Young's modulus GPa	Elongation %	Fracture toughness MPa m$^{0.5}$	Hardness (Vickers)
Alumina	Boron carbide	3.2−3.5	5−6	19−24	190−225	490−550	340−400	0.1−0.18	4−5.5	2e3−2.5e3
	Silicon nitride	∼3.8	∼5.5	∼760	∼214	∼390	∼360	∼0.08	∼3.1	∼2.42e3
	Titanium carbide	∼4.25	∼7.5	∼16−22	220−280	390−700	380−420	0.1−0.2	3.7−4.5	1e3−2.5e3
	Titanium dioxide	∼4	∼6.15	∼25	∼275	∼410	∼395	∼0.1	∼4	∼1.25e3
Alumino silicate	Alumina mullite fibre 'woven'	∼2.53	1.95−6	2.5−4	∼85	65−225	130−150	0.05−0.2	40−70	475−530
Carbon	Carbon	∼1.7	0.5−9.5	10−70	65−95	14−25	70−100	0.01−0.04	∼6	40−75
	Metal	∼2.5	∼3.5	15−80	12−35	10−40	15−40	0.02−0.25	∼13.5	30−100
	Resin	∼1.8	1−5	5−30	10−18	10−25	12−25	0.05−0.2	∼1.5	35−75

Silicon carbide	Silicon carbide 'woven'	~2.6	3−6	6−20	~135	205−370	130−270	0.05−0.3	25−35	2e3−3.5e3
Titanium carbide	Nickel-bonded titanium carbide	5.4−6	8−9.5	16−17.5	225−265	1e3−1.3e3	370−430	0.3−0.8	8.5−12	845−1.8e3
Tungsten carbide	Carbon	1.2−1.35	5−6	35−65	310−335	1.7e3−2.2e3	525−565	~0.6	9.5−11.5	1.4e3−1.65e3
	Cobalt	1.25−1.55	5−6.5	55−105	300−400	1.5e3−3e3	465−675	~0.6	7−24	800−2e3
	Nickel	~1.47	4.5−5.5	85−100	345−400	1.4e3−1.6e3	560−640	~0.6	~10	1.45e3−1.65e3
	Nickel−chrome bonded	1.4−1.5	4.7−5	55−75	330−355	2e3−2.5e3	585−645	~0.6	~10	1.3e3−1.6e3
	Titanium carbide	~1.15	6−7	25−75	275−305	1.5e3−1.9e3	445−500	~0.6	8.5−12.5	1.45e3−1.75e3

3.6.2   MMCs

One of the major advantages of MMCs over organic matrix composites is the maximum operating temperature. Boron−aluminium composites can be used up to 510°C, whereas an equivalent boron−epoxy composite is limited to 190°C (Peng, 2005). MMCs have also much higher thermal conductivity. Table 3.6 shows a set of important properties − physical, thermal and mechanical − for some metallic alloys and MMCs.

3.7   Modelling

The fibre or particle−matrix interfacial region is a decisive constituent of fibre-reinforced ceramic and metallic matrices. Depending upon the characteristics of this region, the type of matrix and the fibre arrangement, the composite will be a brittle ceramic, a pseudo-plastic composite or a damage-tolerant composite. The key role of the interfacial region is to protect the reinforcing fibres against fracture. Several requirements that may appear contradictory have to be met:

- fibres have to be bonded to the matrix, in order to ensure material integrity and to end up with a continuous medium;
- fibre failures have to be prevented when the matrix cracks;
- after deflection, the loads still have to be transferred efficiently through the interfacial domain, to limit fibre overloading induced by matrix cracking; and
- in aggressive environments, fibres should not be exposed to aggressive materials that diffuse through the matrix.

Analytical or numerical modelling can be used to predict elastic properties, strength and fracture, fatigue behaviour, thermal performance, the integrated structural behaviour of a given component or structure, process simulation and virtual testing. In order to speed up high-performance composite materials development, one has to understand and control constituents, interfaces and microstructures, evaluating also their effects on different properties (Materials Genome, 2011). Multiscale modelling is used more and more frequently to consider multiphase structures and heterogeneity, in order to have an optimized solution.

3.7.1   Elastic and plastic properties

The linear theory of elasticity of anisotropic and isotropic materials (determining elastic constants through classical lamination theory or other analytical and more or less empirical or statistical tools) and the micromechanical modelling for prediction of the mechanical or thermal properties of composites, with respect to those of constituent materials at a given temperature, are generally used to predict elastic properties of either metal or ceramic matrix composites. Based upon Mori-Tanaka, inverse Mori-Tanaka and pseudo-grain discretized Mori-Tanaka formulations, new approaches have been developed for a multistep procedure for materials with a hierarchical microstructure and first-choice homogenization (Beneviste, 1987;

Table 3.6 **Physical and mechanical properties of Al, Ti and Mg alloys and MMCs**

Material	ρ g/cm^3	CTE 10^{-6} K^{-1}	Thermal conductivity W/m K	Yield stress (tensile) MPa	Ultimate tensile stress MPa	Young's modulus GPa	Elongation %	References
Al + SiC$_p$ 17% vol	2.8	16.4	165		461	100		Rawal (2001)
Al + SiC$_p$ 56% vol	2.94	8	235			220		Yana et al. (2008)
Al + SiC$_p$ 63% vol	3.01	7.9	175		253	220		Rawal (2001)
Al + Al$_2$O$_3$ 10% vol	2.795	20.9	161	335		83		Badiey and Abedian (2010)
Al + Al$_2$O$_3$ 15% vol	2.839	19.8	141	340		88		Badiey and Abedian (2010)
Al + Al$_2$O$_3$ 20% vol	2.860			365		95		Badiey and Abedian (2010)
Al + TiB$_2$ 10% vol	2.6			317		91		Badiey and Abedian (2010)
Al4Li + SiC$_w$ 20% vol T6				250	320		0.4	Kobayashi et al. (1988)
Mg + Ni5%C-coated nanocomposite				85	160		5.8	Parsonage (1999)

Table 3.6 **Continued**

Material	ρ g/cm^3	CTE 10^{-6} K^{-1}	Thermal conductivity W/m K	Yield stress (tensile) MPa	Ultimate tensile stress MPa	Young's modulus GPa	Elongation %	References
UD C P100 42%/Al 6061	2.5	−049	320 L		905 L	342 L		Rawal (2001)
UD−C, B, SiC or Al$_2$O$_3$ 50%/Al 6061	2.5−3.2				620−1240 L 30−170 T	130−450 L 34−140 T		U.S. Congress (1988)
UD B 50%/Al	2.7	5.8			1100 L	235 L		Rawal (2001)
UD C P100 43%/ A791C Mg	1.97	0.54	189 L		710 L	324 L		Rawal (2001)
UD−SiC 50%/Ti					1720 L 340 T	260 L 173 T		U.S. Congress (1988)

Beneviste et al., 1989; Atul et al., 2013). Moreover, the calculation of effective tensile moduli can be done with reasonable precision, for instance with polycrystalline alumina and zirconia from monocrystal data, using the Voigt−Reuss−Hill average estimate for ceramic composites (Pabst et al., 2004).

An interesting application of Mori-Tanaka and inversed Mori-Tanaka micromechanical modelling is given in Ziegler et al. (2010) for the elastic behaviour of metal−ceramic composites with lamellar domains. A Mori-Tanaka model is presented (Ziegler et al., 2010) to give the effective stiffness tensor of a given domain following Eq. [3.5]:

$$C^{\mathrm{dom}} = C^{\mathrm{c}} + f_{\mathrm{m}}(C^{\mathrm{m}} - C^{\mathrm{c}}) : A^{\mathrm{m}}{}_{(\mathrm{MT})}$$

$$A^{\mathrm{m}}{}_{(\mathrm{MT})} = \left[f_{\mathrm{m}}I^4 + f_{\mathrm{c}}S_{\mathrm{c}} : (C^{\mathrm{m}} - C^{\mathrm{c}}) \right]^{-1}$$

[3.5]

where I^4 is the symmetric fourth-order unit tensor; and C^{m}, C^{c} and f_{c}, f_{m} are stiffness tensors and volume fractions of ceramic and metallic phases, respectively.

In the modelling process, to obtain certain effective properties and consider different scales, one has to look into the relevant representative volume element (RVE) for an equivalent homogeneous continuum. The mean-field approach (Hill, 1963) is frequently used as the homogenization process. To determine the nonlinear stress−strain behaviour, it is critical to model fragmentation. The chain-of-segment-model, the fragment dichotomy model and the Bayesian model can be applied (Lamon, 2010). In the chain-of-segment model, after determining the average number of flaws (see Eq. [3.6] from Hui et al. (1995)) per unit length

$$N(\sigma) = L_0^{-1}(\sigma/\sigma_0)^{\mathrm{m}}$$

[3.6]

where σ_0 is the scale parameter referred to the test length L_0, and m is a positive constant, a similar Weibull distribution is applied to fibre elements or a single fibre. The fibre length is subdivided in N_{e} segments, and to each is randomly assigned a strength following a probability distribution given by:

$$P(\sigma \cdot (L/N_{\mathrm{e}}) = 1 - \exp[(-L/N_{\mathrm{e}}L_0) \cdot (\sigma/\sigma_0)^{\mathrm{m}}]$$

[3.7]

The fragment dichotomy model considers fragments, and for the most severe situation (Lamon, 2010), the fragment strength can be given by:

$$\sigma^i_{\mathrm{ref}} = \lambda[(V_0/V_i K)\ln(1/(1 - P_i))^{\mathrm{m}}]$$

[3.8]

where V_i is the volume of the ith fragment; and P_i is the respective probability of failure. In the Bayesian model, the fragmentation is considered as progressive multiple failures of chain elements (Lamon, 2010), being the stress at the formation of kth crack is given by:

$$S_k = S_0 k^{1/P}(V/V)^{1/P}[-\ln(1 - P_\alpha)]^{1/P}$$

[3.9]

3.7.2   Strength, damage and fracture

The first requirement for a CMC is the ability to display strength properties that are high enough to permit a component to achieve its desired service life. Like a metallic hot section, ceramic components for aeropropulsion gas turbine engines will typically be designed to be thin-walled and cooled using conventional approaches such as film cooling (vanes and blades) and backside convective cooling (combustion liners and shrouds). Thus, component stresses typically arise from a combination of mechanical, aerodynamic and thermal-gradient loads that produce both in-plane and through-thickness stress−temperature distributions that vary with time within the component walls and attachment areas. Under these stress conditions, over a time period that s generally equivalent to the component inspection cycle, the SiC−SiC composite's in-plane matrix cracking strength (MCS) should be sufficiently high enough to reliably avoid cracks that propagate into and across the component wall, thereby preventing aggressive application environments from reaching and degrading the crack-bridging fibres. Of additional importance is the ability of the CMCs to avoid the occurrence of delamination cracks within the wall because these can significantly reduce the through-thickness thermal conductivity, further increasing the thermal-gradient stresses and the probability of wall separation. Thus, the constituents and geometries of the as-produced CMC should be optimized to ensure that both the in-plane and through-thickness composites sufficiently exceed the expected component service stresses in these directions.

The basic requirement for a tough ceramic composite is crack deflection at or near the fibre−matrix interface. As the crack is deflected along the fibre, the primary matrix crack eventually moves on around the fibre, leaving it bridging the matrix crack and reducing the stress intensity at the matrix crack tip. The fibre ultimately fractures at a point away from the crack plane and begins to be pulled out from the matrix upon continued loading on the composite. The toughening mechanism of fibre debonding and non-coplanar fracture of the constituents is often called the 'distributed damage mechanism'. The pull-out of the fibre requires some work to overcome the roughness and frictional effects. This provides further toughening to the composite. Each fibre acts more or less independently; the fracture of one imposes only a modest increase in stress on its neighbours (Bansal and Lamon, 2015).

In contrast, matrix cracks in a composite with excessive fibre−matrix bonding propagate directly through fibres, and the composite behaves as if it is a monolithic ceramic. The load deflection behaviour of a good composite exhibits nonlinear pseudo-ductile behaviour, whilst a bad one with excessive fibre−matrix bonding is perfectly elastic and typically not very strong. This load deflection behaviour has led to fairly common use of the terms 'nonbrittle' and 'brittle' to describe the two cases. The terms are understood to refer to the presence or lack of the desired nonlinear load deflection behaviour (Bansal and Lamon, 2015).

The two basic mechanisms utilized for crack deflection in CMCs are the use of a sufficiently weak (porous) matrix or the use of a weak engineered interface, which typically involves a fibre coating. The term 'sufficiently weak', in this context, is in

comparison to the fibre strength in the final composite. Crack behaviour results from a competition between a fracture in the fibre, coating (if present) and the matrix (Bansal and Lamon, 2015).

Continuum damage mechanics can be applied for damage modelling. An anisotropic damage theory has to be considered with a thermodynamic framework (Ladevèze, 2000; Ladevèze et al., 2001). Energy potential and state laws as well as damage evolution laws (eg, micro-cracking with Mode I or II) that define damage kinematics or coupling damage with plasticity or visco-plasticity may be used for different damage situations, including micro defects. They may be considered at different scales and to cater for load direction, fibre direction (if applicable) and different temperatures.

3.7.3 Fatigue

Although not fully accepted, Paris law has been used by several authors for classical fatigue analysis and subcritical cracking. It must be said that the fatigue behaviour of CMCs and MMCs strongly depends on the type of matrix, type of fibre, volume content of constituents, orientation of fibres, porosity, type of loading, frequency and environmental conditions. Besides the Paris law, continuous damage mechanics models and thermo-mechanical (reinforcement modelled as a thermo-elastic behaviour and the matrix as thermos-elastoviscoplastic) models can also be used. For CMCs, the following models may be considered (Bansal and Lamon, 2015):

- Fatigue damage evolution laws
- Fatigue inelastic strain evolution law
- Crack density indicator
- Crack opening indicator
- Damage macro models (ie, an additive damage law based on Miner's law).

From a different perspective, and to illustrate the variability of fatigue behaviour of CMCs and MMCs, the concept of fatigue strength can be used. It is associated with an endurance limit for some materials. It is related to a maximum cyclic stress that the material can support up to 10^7 cycles. Table 3.7 shows typical fatigue strength values of CMCs and MMCs. The greatest variations correspond to properties in the longitudinal and transverse direction loading with respect to the fibre.

3.7.4 Virtual testing

More and more simulations of testing are performed to avoid excessive costs with real engineering tests. Virtual testing needs to combine simulation with damage evolution laws and calibration with real advanced experiments. Hence, computational simulations may include stochastic approaches for specimen generation, together with new augmented finite element analysis (FEA) to cater for arbitrary systems, such as crack initiation, damage evolution, bifurcation and coalescence (Cox et al., 2014). Applying FEA and using a mesh that may represent the characteristics of microstructure, it can also represent an alternative to microscopy for loaded specimens.

Table 3.7 Fatigue strength of CMCs and MMCs

	CMCs						MMCs		
	Alumina	**Alumino silicate**	**Carbon**	**Silicon carbide**	**Titanium carbide**	**Tungsten carbide**	**Aluminium**	**Magnesium**	**Titanium**
Fatigue strength at 10^7 cycles (MPa)	230−600	35−65	11−19	110−230	850−1350	1350−2200	35−1100	90−330	160−500

Adapted from Granta, 2015. CES Edupack, Granta Design.

3.7.5 *Process simulation*

Thermo-mechanical models can be used in finite elements simulations to predict residual stresses due to differences between fibre and matrices thermal expansion coefficients. Fibres may have a thermo-elastic behaviour, whereas matrices (metallic, ceramic, hybrid etc.), according to their nature, may behave in a thermo-elastic, thermo-elastoplastic or even thermo-viscoelastic manner.

Pastore and Gowayed (1994) described the 'fabric geometry model' (FGM). It is based on the idea that the elastic properties of the composite can be calculated as a function of the relative proportion of the properties of the fibres, at specific directions, and the matrix. The thermal properties were also calculated on the basis of average properties from the individual constituents, using FGM. The rule of mixtures may be a fair approximation to predict the coefficient of thermal expansion of a composite, if there is no phase interaction.

In order to have accurate process modelling, there is a need to develop complex multiphysic mathematical models. They must cater to process-focussed constitutive modelling. In other words, they go from simple models (even using elastic material properties) to large and inelastic deformations, chemical and thermal interactions with nonlinear contact and friction, and electro-magnetic effects when applicable, coupled with size effects and different processing parameters. The intrinsic nature of CMCs and MMCs, with a large range of properties involving features from nano to macro-scale and leading to very different types of damage and failure modes, implies the development of consistent methodologies, based on sound theories, that are capable of integrating the interaction of mechanical, thermal, electrical, chemical and magnetic properties with heat transfer and fluid mechanics, diffusion and solidification, as well as microstructure evolution.

The phase field theory, dynamic and stochastic process modelling as well as more advanced friction models are possible modelling tools where different phases and transformation and dynamic processes occur; the aim is to perform realistic process modelling.

3.8 Applications and future

Low (2014) discusses the recent development of composites based on MAX phases, a new class of nanolayered, hexagonal ceramics with the general formula $M_{n+1}AX_n$ (where $n = 1-3$), M is an early transition metal, A is a group A element and X is carbon or nitrogen). These compounds represent a new class of solids that combine some of the best attributes of metals and ceramics (creep, fatigue and corrosion resistant and ultra-low friction). In terms of processes, spark plasma sintering and strong magnetic field alignment are highlighted as emerging techniques for the synthesis and densification of ceramic matrix composites.

The aerospace industry requires for aeroplanes high reliability on mechanical response of all components, increasingly higher cruise speeds, the highest altitude, less vibration, increase in the time interval between inspections and less emission of

harmful gases. These goals can only be matched with materials that have high-strength and specific stiffness at extreme temperatures. It is anticipated that the future large civil transport (high speed civil transport (HSCT)), a supersonic plane that is two times bigger than the Concorde, will use a wide variety of CMCs and MMCs (Fig. 3.9).

The military aviation industry is already a consumer of CMCs, both in turbines and in missile construction. An example are the turbine blades of carbon−carbon (CC) composites that can withstand temperatures of turbine exhaust gases of about 1050°C without losing strength and are extremely light; these features will make it possible for the aircrafts to reach Mach 10 speeds. For comparison, the titanium matrix composites allow them to achieve only Mach 3.8 ($\sim$450°C of the working temperature). The CC composites are the materials with the best high-temperature mechanical behaviour ever developed, with an ability to withstand temperatures as high as 2000°C in an inert atmosphere or in vacuum. This feature is more remarkable considering the respective specific values: the specific tensile strength (σ/ρ) of a CC composite, manufactured with alternated layers of unidirectional fibres and carbon blankets, can reach 160 MPa/g cm^3 at 2000°C, whereas a conventional ceramic reaches 40 MPa/g cm^3 only until 1200°C (Bansal and Lamon, 2015).

CMCs of SiC(w)−Al$_2$O$_3$ or SiC(fibres)−Si$_3$N$_4$ are alternatives to C−C composites, but with less spectacular properties (60 MPa/(g cm^3)). The aerospace industry is also a consumer of these composites of carbon fibres coated with SiC in carbon matrices. They are used on US space shuttles' thermal protection for the re-entry into the

Figure 3.9 This oxide CMC exhaust ground test demonstrator consists of a 1.60-m diameter nozzle and 1.14-m diameter × 2.34-m conical centre body with a titanium end cap inspection portal.
Destefan, J., May 14, 2013. Ceramic matrix composites make inroads in aerospace. IJACT. The Advanced Ceramic Society, Credit: Steyer.

atmosphere, where the outer layer is sacrificed. Société Européenne de Propulsion (SEP) laboratories already developed 2D and 3D composites of C and SiC fibres in SiC matrices through CVI, with exceptional properties at high temperature (1400°C, $E = 100$ GPa, $\sigma = 700$ MPa and $K_{ic} = 32$ MPam$^{1/2}$) for the future panels of the European shuttle *Hermes*, and these withstand considerable mechanical stresses at 1300°C. CC plates will cover the Huygens probe that will explore Titan, due to the atmosphere of Saturn's (75% hydrogen and 25% helium with traces of other substances like methane and water ice) satellite (Bansal and Lamon, 2015).

The braking systems are currently an important field of application of CC composites in aviation and automotive industries. When triggered, the brakes respond to the hydraulic pressure through disks (rotors and stators) in which the developed friction leads to surface temperatures as high as 3000°C and 1500°C in component volume. An additional advantage of CC composites relative to conventional systems (sintered metal against high-strength steel) is the reduction of weight: in a commercial airliner, there is economy weight saving from 1100 to 700 kg if composite materials are used in braking systems.

Application areas for CMCs have been expanded, and novel application areas, such as rocket propulsion and aircraft brakes, could be opened in the coming years. This was mainly possible due to continuous improvement of manufacturing processes. Thereby, not only the increase of material performance, like strength or environment stability, has been the focus, but also process reliability and reproducibility as well as reducing manufacturing cost (Bansal and Lamon, 2015).

The use of oxide−oxide (Ox−Ox) CMC exhaust nozzles in subsonic jet engines to improve component durability (in comparison with titanium) and avoid weight increases associated with switching to heavier metallic alloys such as Inconel is being evaluated by several companies, including Rolls-Royce Liberty Works (RRLW) and Boeing (Bansal and Lamon, 2015). The Boeing Company is working to produce an acoustic Nextel 610/aluminosilicate composite centre body and exhaust nozzle for commercial aircrafts. GE aviation has significantly invested in oxide−oxide composites, and their Ox−Ox material was first used as a divergent exhaust seal for the F414 engine. More recently, GE announced the incorporation of their Ox−Ox material in multiple components in the Passport engine for Bombardier Global 7000 and 8000 aircrafts, including the exhaust mixer, centre body and core cowls (Bansal and Lamon, 2015).

A recent program in Germany, high-performance oxide composites (HIPOCs), which began in 2009, focused on the development of various oxide-based CMCs for use in hot section applications for either land-based or aerospace turbine engines (Bansal and Lamon, 2015).

Alternative uses include semistructural applications, such as thermal protection systems (TPSs), which typically combine various elements, including insulation, to protect the underlying structure from exposure to high temperature and hot gases (Bansal and Lamon, 2015).

There have been continued industrial efforts to improve Ox−Ox TPS systems through innovative design and fabrication. BOEING has developed and improved shuttle type tile insulation, where an Ox−Ox CMC sheet is bonded to the surface of

lightweight ceramic foam insulation. The CMC provides wear protection, impact damage resistance, improved thermal resistance and a smooth surface. ATK-COIC patented an advanced non-tile-based TPS component that uses a bonded mortise and tenon system to fabricate honeycomb-like CMC panels that are mechanically fastened to the substructure (Bansal and Lamon, 2015).

The key limitation of Ox−Ox composites is their inferior interlaminar properties and low creep resistance. The most straightforward way to improve the creep resistance of these materials is by introducing higher temperature-resistant fibres. There are some initiatives for the development of higher temperature, fine-diameter oxide fibres. YAG is the most creep-resistant oxide reported and therefore a good candidate for a fibre. Mullite, spinel and zircon are other possible compositions worth exploring (Bansal and Lamon, 2015).

The matrix-dominated properties, such as resistance to wear, abrasion and uneven thermal loads, will require significant increases in matrix density, which will necessitate an oxide- or oxidation-resistant interface that debonds readily.

Besides material development, the modelling and design of structural components will require careful allowance for the matrix-dominated properties and careful placement of fibres in all loading directions. This implies a high degree of sophistication in component design and, in many cases, designing and producing weavable 3D fibre architectures (Bansal and Lamon, 2015).

CMCs were developed to enhance damage-tolerant quasi-ductile behaviour while keeping the other advantages of ceramics, particularly at high temperatures. The potential of CMC exploitation has a very wide perspective, particularly for applications with extremely demanding thermal and mechanical requirements. CMCs dominate in a broad range of intermediate properties, where the manufacturers seek low specific weight versus stiffness, and in fracture energies.

MMCs can be seen in applications such as: the Pratt and Whitney 4000 series engine fan exit guide vanes; Motorola's Iridium Satellites and GM EV-1 electronic packaging applications; F-16 fighter aircraft ventral fins and fuel access covers; the mid-fuselage structure of Space Shuttle *Orbiter* boron−aluminium tubes; and P100/6061 Al high-gain antenna wave guides and boom for the Hubble Space Telescope (HST).

Hybridization may bring other opportunities to CMCs and MMCs. Despite their potential, as well as that of PMCs, in order to satisfy the higher and higher requirements of more demanding applications, the concept of hybrid composites has to be considered. Hybridization can be seen from different perspectives. It may be different types of fibres in the same matrix (eg, aluminium−silicon hybrid composites reinforced with Ti and SiC particulates) (Miranda et al., 2015), using one type of fibre up to saturation with the addition of other types for further improvements. It can also be the same type of fibres with different matrices or even multi-material approaches: CMCs with MMCs; PMCs with either CMCs or MMCs; and other combinations. In the multi-material approach, the joining technology (eg, adhesive, bolted, riveted, 'weld bonding', self-piercing rivets, bolted/co-cured hybrid joining or Surfi-Sculpt®) is the key parameter for a successful application.

Bearing in mind the need to reduce the carbon footprint in air transport, it is expected that the next generation of engines for aeroplanes in the years 2025−30
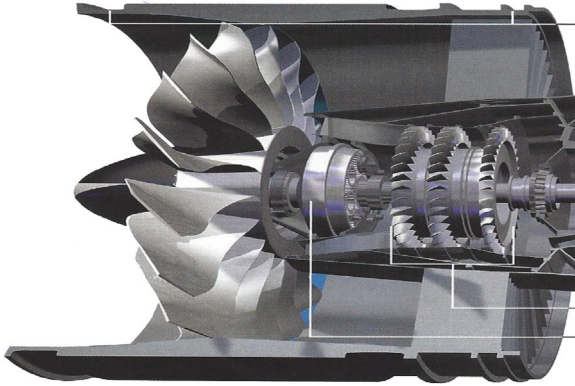
Figure 3.10 PUREPOWER 1000G (Pratt & Whitney): possible applications (carter, gear boxes and monobloc discs) of MMCs.
Leap versus PUREPOWER moteurs: le match au sommet. S&V Aviation, 2015.

will be made of a mixture of super-alloys and composites (Leap versus PUREPOWER moteurs, 2015), as can be seen in Fig. 3.10. More efficient manufacturing processes are needed for CMCs and MMCs, as well as new and more efficient self-healing techniques for maintaining strength and functionalities.

3.9   Conclusions

CMCs and MMCs, although they have already a wide range of applications, are still far from being fully exploited. In the medium and long term, the challenges, particularly in aeronautics and aerospace applications, will be such that the exploitation of tailor-made materials will imply an intensive R&D effort. Different matrices and fibres will be exploited with an adequate interface that aims for a set of requirements. Generally speaking, CMCs and MMCs are heterogeneous composite systems, with the heterogeneity characterized by size, shape, spatial distribution and different properties of the constituents. It is likely to be present in different numbers of solid phases, like fibres, aggregates and hard inclusions.

   To speed up the development of new types of CMCs and MMCs, reliable modelling and simulation tools have to be present from the beginning, in order to adequately predict at different size (nano/micro/meso and macro) and time (short, medium and long-term) scales the structural behaviour, and to control the performance (mechanical, thermal, chemical, physical and fire) characteristics of interest in advanced structures. Simultaneously, more advanced multiphysical and mathematical theoretical models are needed for more accurate process simulation. New numerical approaches have to be developed for products and process that, after the requirements definition, will identify the ideal composite system performance, the respective material production roadmap and the processing methodology to reach the required 'structural' behaviour.

References

Amaral Fortes, M., Ferreira, P.J. (Eds.), 2003. Materiais Dois Mil. IST Press (in Portuguese). ISBN 972-8469-26-8.

Atul, J., Lomov, S., Abdin, Y., Verpoest, I., Paepegem, W.V., 2013. Pseudo-grain discretization and full Mori-Tanaka formulation for random heterogeneous media: predictive abilities for stresses in individual inclusions and the matrix. Composites Science and Technology 87, 86−93.

Badiey, M., Abedian, A., 2010. Application of metal matrix composites in a satellite boom to reduce weight and vibrations as a multidisciplinary optimization. In: 27th International Congress of the Aeronautical Sciences.

Bansal, N.P., Lamon, J., 2015. Ceramic Matrix Composites Materials, Modelling and Technology. American Ceramic Society, John Wiley & Sons, Inc.

Beneviste, Y., Dvorak, G.J., Chen, T., 1989. Stress fields in composites with coated inclusions. Mechanic of Materials 7 (4), 305−317.

Beneviste, Y., 1987. A new approach to the application of Mori-Tanaka's theory in composite materials. Mechanic of Materials 6, 147−157.

Chawla, N., Chawla, K.K., 2006. In: Metal Matrix Composites. Springer.

Clauss, B., 2008. Chapter 1. Fibres for ceramic matrix composites. In: Krenkel, W. (Ed.), Ceramic Matrix Composites: Fibre Reinforced Ceramic and Their Applications. Wiley-VCH, Weinheim, Germany, pp. 1−19.

Cox, B.N., Bale, H.A., Begley, M., Blacklock, M., Do, B.-C., Fast, T., Naderi, M., Novak, M., Rajan, V.P., Rinaldi, R.G., Ritghie, R.O., Rossol, M.N., Shaw, J.H., Sudre, O., Yang, Q., Zok, F.W., Marshall, D.B., 2014. Stochastic virtual tests for high-temperature ceramic matrix composites. Annual Review of Materials Research 44, 479−529.

Destefan, J., May 14, 2013. Ceramic matrix composites make inroads in aerospace. IJACT. The Advanced Ceramic Society, Credit: Steyer.

Fergurson, J.B., Schultz, B.F., Rohatig, P.K., 2014. Self-healing metals and metal matrix composites. JOM 66 (6), 866−871.

Granta, 2015. CES Edupack. Granta Design.

Harmer, M.P., Chan, H., Miller, G.A., 1992. Unique opportunities for microstructural engineering with duplex and laminar composites. Journal of the American Ceramic Society 75 (7), 1715−1728.

Hill, R., 1963. Elastic properties of reinforced solids: some theoretical principles. Journal of Mechanics and Physics Solids 11, 357−372.

Hui, C.Y., Phoenix, S.L., Ibnabdeljalil, M., Smith, R.L., 1995. An exact closed form solution for fragmentation of Weibull fibers in single filament composite with applications to fiber-reinforced ceramics. Journal of the Mechanics and Physics of Solids 43 (10), 291−303.

Kobayashi, T., Yosino, M., Iwanari, H., Niinomi, M., Yamamoto, K., 1988. Mechanical properties of SiC reinforced aluminum alloys fabricated by pressure casting method. In: Fishman, S.G., Dhingra, A.K. (Eds.), Cast Reinforced Metal Composites. ASM International.

Ladevèze, P., Letombe, S., Cluzel, C., October 1−3, 2001. A CMC damage model based on micro and macromechanics for high-temperature and composite loading. In: 4th International Conference on High Temperature Ceramic Matrix Composites, Munich, Germany.

Ladevèze, P., October 22−27, 2000. An anisotropic damage theory including unilateral effects. In: International Bimestre on Damage Mechanics, Symposium on Continuum Damage and Fracture, Cachan, France.

Lamon, J., 2010. Stochastic models of fragmentation of brittle fibres or matrix in composites. Composites Science and Technology 70, 743−751.

Leap versus PUREPOWER moteurs: le match au sommet, 2015. S&V Aviation.

Low, I.M., 2014. Advances in Ceramic Matrix Composites. Woodhead Publishing Limited, Woodhead Publishing Series in Composite Science and Engineering: number 45, Cambridge, UK.

Mallick, P.K., 1997. Composites Engineering Handbook. Marcel Dekker, Inc., NY.

Materials Genome Initiative for Global Competitiveness, June 2011. National Science and Technology Council, Washington, USA.

Miracle, D.B., 2001. Aeronautical applications of metal-matrix composites. In: Henry, S.D., et al. (Eds.), ASM Handbook. ASM International, Ohio, USA.

Miracle, D.B., 2005. Metal matrix composites − from science to technological significance. Composites Science and Technology 65, 2526−2540.

Miranda, G., Buciumeanu, M., Madeira, S., Carvalho, O., Soares, D., Silva, F.S., 2015. Hybrid composites − metallic and ceramic reinforcements influence on mechanical and wear behaviour. Composites Part B 74, 153−165.

Pabst, W., Gregorová, E., Tichá, G., Týnová, E., 2004. Effective elastic properties of alumina-zirconia composite ceramics part 4. Tensile modulus of porous alumina-zirconia. Ceramics − Silikáty 48 (4), 165−174.

Parsonage, T., December 8−9, 1999. Beryllium metal matrix composites for aerospace & commercial applications. In: VII Conference on Metal Matrix Composites. IoM, London, U.K.

Pastore, C.M., Gowayed, Y.A., 1994. A self-consistent fabric geometry model: modification and application of a fabric geometry model to predict the elastic properties of textile composites. Journal of Composites Technology and Research 16 (1), 32−36C.

Paulo Davim, J., 1997 (Ph.D. thesis).

Peng, H.-X., 2005. Manufacturing titanium metal matrix composites by consolidating matrix coated fibres. Journal of Materials Science & Technology 21 (5), 647−651.

Rawal, S., 2001. Metal-matrix composites for space applications. JOM 53 (4), 14−17.

Richerson, D.W., 1992. Modern Ceramic Engineering, second ed. Marcel Dekker Inc.

Richerson, D.W., 2000. The Magics of Ceramics. American Ceramic Society, Westerville, Ohio, USA.

Ruh, R., Palazotto, N., Watt, G., 1988. Introduction to ceramic composites in aerospace applications. Journal of Aerospace Engineering 1 (2), 65−73.

Schwartz, M.M., 1994. Joining of Composite Matrix Materials. ASM International, Ohio, USA.

Soltani, N., Bahrami, A., Pech-Canul, M.I., Gonzalez, L.A., 2015. Review on the physico-chemical treatments of rice husk for production of advanced materials. Chemical Engineering Journal 264, 899−935.

Speer, W., Es-Said, O.S., 2004. Applications of an aluminum−beryllium composite for structural aerospace components. Engineering Failure Analysis 11, 895−902.

Sun, Y., Choi, H., Konishi, H., Pikhovich, V., Hathaway, R., Chen, L., Li, X., 2012. Effect of core-shelled nanoparticles of carbon-coated nickel on magnesium. Materials Science and Engineering A 546, 284−290.

U.S. Congress, June 1988. Office of Technology Assessment, Advanced Materials by Design, OTA-E-351. U.S. Government Printing Office, Washington, DC.

Yana, C., Wang, L., Jianyue, R., 2008. Multi-functional SiC/Al composites for aerospace applications. Chinese Journal of Aeronautics 21, 578−584.

Ziegler, T., Neubrand, A., Pait, R., 2010. Multiscale homogenization models for the elastic behavior of metal/ceramic composites with lamellar domains. Composites Science and Technology 70, 664−670.

Fibre-reinforced laminates in aerospace engineering

4

L.Z. Linganiso [1], *R.D. Anandjiwala* [1,2]

[1]CSIR Materials Science and Manufacturing, Port Elizabeth, South Africa; [2]Faculty of Science, Nelson Mandela Metropolitan University, Port Elizabeth, South Africa

4.1 Introduction

4.1.1 The origin of advanced composite materials (ACMs)

ACMs, also known as advanced polymer matrix composites (Soutis, 2005), are excellent structural and functional materials, especially in the aerospace industry, as they represent the future of aerospace materials. In other words, there would be no modern aerospace industry if there were no advanced composites in the first place. ACMs derive their origin from the embryonic efforts of the fibreglass-reinforced plastic (FRP) industry that developed in the 1940s. The history of these special materials dates back to the 1970s in China, where research was employed and further implemented in the development of composites. ACMs were first employed in military aircrafts in the 1960s and later extended to the civil aircraft applications in the 1970s (Soutis, 2005; Edwards, 2008). But civil aircraft manufacturers were slower to utilize composites in primary structural applications until the 2000s. The application of ACMs has been extended to other applications from stealth bombers to smart cars and from bridges to oil rigs (Katnam et al., 2013). The interest and development in ACMs date back to the 1960s when the NASA (National Aeronautics Space Association) conducted research in the military field (Katnam et al., 2013). The use of ACMs in the aerospace or transport industry came into being as a result of deterioration which occurred in the transportation network over 40 years.

4.1.2 Classification of ACMs

Composite materials are mostly classified into two different group levels. These two different levels adhere to either the matrix or reinforcement. The major composite levels consist of the metal matrix composites, ceramic matrix composites and organic matrix composites. Organic matrix composites generally comprise two types of composites such as carbon matrix composites (carbon-to-carbon composites) and polymer matrix composites. The second level of composites refers to the reinforcement, which is the reinforcing filler or form. Those consist of fibre-reinforced composites, particulate composites and laminar composites. ACMs generally comprise fibrous reinforcements which are bonded together with a matrix material. The combination of the

fibrous material and the matrix material yields a high-performance composite which has improved properties. Honeycomb cores and structural adhesives are also used in the production of metallic laminates and sandwich structures. Fibres are mostly used as reinforcing filaments. On the other hand, glass, aramid and carbon fibres are used extensively in the development of composites. For applications requiring very high service temperatures, boron and other exotic fibres are used in moderate quantities. Fibres generally consist of high-strength, high-stiffness and low-density properties, and over the years fibres with excellent mechanical properties have been developed.

The matrix comprises good shear and low-density properties. This matrix provides a medium of support for fibres. It has the ability to transfer stresses which determine the degree of the fibres' mechanical properties. This also assists in determining the overall performance of the composite. The different types of composites also have subtypes. With reference to the matrix, it is made up of different polymer materials. Epoxy resins are still the most frequently used matrices in advanced polymer composites, with some matrices consisting of phenolic resins; however, epoxy resins supersede the phenolics in matrices. Bismaleimide resins are a certain class of matrices which have been accepted for commercial production, consisting of thermoplastics and carbon fibre (Sardiwal et al., 2014). Fig. 4.1 details the components of composites.

In contrast, a lamina is a flat arrangement of unidirectional (or woven) fibres incorporated in a matrix material. It is commonly assumed to be orthotropic, and its thickness depends on the material from which it is manufactured. Individual laminae are generally bonded together by a curing procedure that depends on the material system used. The mechanical response of the laminate is different from that of the individual lamina that forms it. The laminate response depends on the properties of each lamina as well as the order in which the laminae are stacked. Additionally, to develop a laminate, several laminae are used with different orientations to achieve the desired properties (Fig. 4.2). Laminates are usually laid up, following stacking-sequence notation.
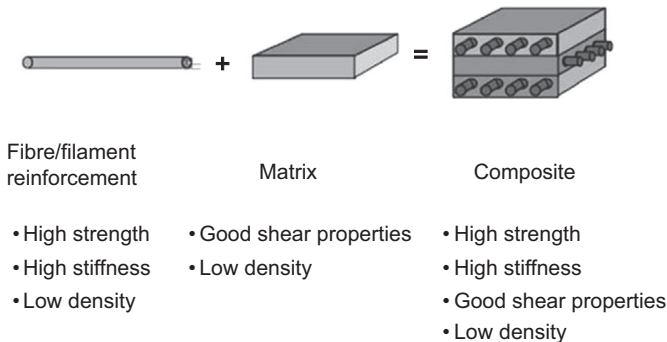

Figure 4.1 A detailed schematic of the composition of composite material.
Reproduced from Mrazova, M., 2013. Advanced composite materials of the future in aerospace industry. INCAS Bulletin 5 (3), 139−150, ISSN: 2066-8201.
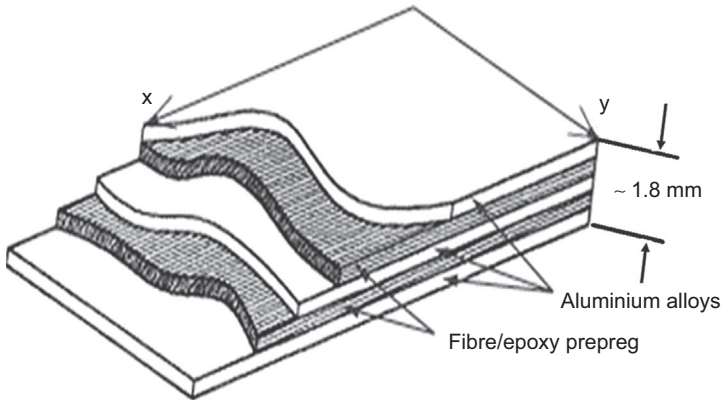
Figure 4.2 Fibre−metal−epoxy hybrid composite.
Adapted from Botelho, E.C., et al., 2006. A review on the development and properties of continuous fiber/epoxy/aluminum hybrid composites for aircraft structures. Material Research 9.

The metal laminate materials with weight reduction and improved damage tolerance characteristics were the prime drivers to develop a new family of materials for the aerospace and aeronautical industry. As a result, new lightweight fibre-metal laminates (FMLs) have been developed. The combination of metal and polymer composite laminates created a synergistic effect on many properties. The mechanical properties of FML show improvements over the properties of both aluminium alloys and composite materials individually. FMLs are used in several applications such as: wing structures, fuselage and ballistic protection. Fig. 4.3 shows an FML composite application in the Airbus A380 airplane. Several other aeronautical companies, such as Aerospatiale, NASA, Bombardier and recently, EMBRAER, have interest in substituting the traditional aluminium components with FML composites due to their prominent properties.
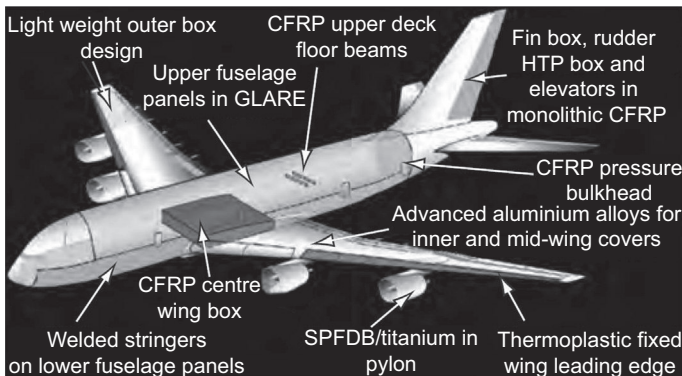

Figure 4.3 Metal−fibre applications in the A380 airplane from Airbus.
Reproduced from Botelho, E.C., et al., 2006. A review on the development and properties of continuous fiber/epoxy/aluminum hybrid composites for aircraft structures. Material Research 9.

4.1.3   Background

ACMs have been the subject of permanent interest of various specialists in recent decades. Originally, military applications in the aircraft industry prompted the commercial utilization of advanced composites after the Second World War. The innovations in the composite area have allowed significant weight reduction in structural design. Composites offer many advantages when compared to metal alloys, especially where high strength- and stiffness-to-weight ratios, excellent fatigue properties and corrosion resistance are concerned. However, they also can present some disadvantages such as low fracture toughness and moisture absorption (Botelho and Rezende, 2000; Zhang et al., 2001; Botelho et al., 2001, 2002; Bhatnagar et al., 1995; Potter, 1997; Gutowski, 1999; Matthews and Rawlings, 1999; Pardini, 2000; Hou et al., 1998). The need for continual improvement in advanced material performance is a common feature of many modern engineering endeavours. Advanced engineering structures now include a wide range of technologies from materials development, analysis, design, testing, production and maintenance. Advances in materials technologies have been largely responsible for major performance improvements in many advanced composite structures and continue to be key in determining the reliability, performance and cost-effectiveness of such systems. Lightweight, high-strength and high-stiffness fibre-reinforced composite materials are leading contenders as component materials to improve the efficiency and sustainability of many forms of transport, including those in the aerospace industry. In addition, they offer immense scope for incorporating multifunctionality due to their hierarchical internal architecture. One limiting factor in their wider exploitation is relatively poor performance under impact loading, a critical aspect of any vehicle design, leading to a significant reductions in strength, stiffness and stability (Richardson and Wisheart, 1996). Their inability to plastically deform results in energy absorption via the creation of defects and damages. This damage often manifests itself internally within the material as matrix cracks and delaminations, and can thus be difficult to detect visually. Thus, a fibre-reinforced polymer composite material could directly benefit from incorporating added functionality such as self-healing (Hillermeier and Seferis, 2001).

Also, the high stiffness of carbon fibres, for instance, allows for extremely efficient crack bridging and therefore a very low crack growth rate which leads to fatigue resistance (Rikards, 2000; Callus et al., 2006; Degallaix et al., 2002; Vlot and Gunnink, 2001; Tarnopol'skii et al., 1999). During recent decades, efforts were concentrated in the development of fatigue-resistant materials which would keep low weight and good mechanical properties. The demand for research and development of high-performance fibre-reinforced composites continues to increase as time progresses. Hypothetically, as the demand for these materials increases, the availability should also be increasing. Scientists and engineers are embarking on the development of these special materials, improving the mechanical properties of the existing ones and or developing new-generation ones to advance the development of high-performance composites for aircrafts worldwide.

The aerospace sector is the only sector that requires high levels of safety and security assurances (Hillermeier and Seferis, 2001). This is putting researchers under

pressure to develop high-quality performance materials that are certified and licenced to meet the desired requirements.

4.2   Technical requirements in the aerospace sector

ACMs are currently highly considered for aerospace applications due to the many advantages they offer, such as light weight, potential addition of functionalities and superior mechanical properties (McAdam et al., 2008). Their application spectrum has been increasing to a wider range in aerospace systems design over recent years. The aircraft applications of carbon-fibre-reinforced plastics in the centre wing box, aircraft wing, pressure bulkhead, landing gear door, engine cowl, floor beam, tall cone, flap track panels and vertical and horizontal stabilizers are a result of the outstanding properties of these composites. Standardization of the test methods for the new advanced materials is important for improving material stability and enhances their reliability (Gohardani et al., 2014). Limitations to more extensive use of advanced composites in the aerospace sector can be attributed to high materials cost, prolonged processing times and optimization of the homogeneous behaviour of the materials.

For each aerospace system designed, mechanical properties are measured in order to ensure the safety of the systems based on the environment to which the systems will be subjected. Static testing, dynamic testing and impact testing are carried out to evaluate the strength and rigidity of material structures, strength with respect to fatigue and vibrations, and impact strength and fracture properties, respectively (Koski et al., 2009; Pevitt and Alam, 2014). This section will give a summary of the aerospace sector requirements for the application of ACMs.

4.2.1   Static and fatigue

Knowledge of aerospace system characteristics such as static flow of aircrafts is critical for the design of the control systems (Koski et al., 2009). Structures such as the aircraft wing must be designed to withstand extreme loads caused by wind shear and any large transient force. Tests for static strength are therefore required for aerospace system designs in order to understand the durability of a structure over its lifetime.

Fatigue properties of the aircraft structural elements comprise a very important factor where aerospace engineering is concerned, as they greatly affect the lifetime of the aircrafts and other aerospace systems. Fatigue properties help predict the crack-growth rate and stress and determine the system's safety assessment frequency or level of safety to prevent possible accidents and minimize repair and replacement costs. The aerospace sector seeks to design structures predictably against fatigue (Pevitt and Alam, 2014), but this is challenging; therefore, research is also focussed on building damage-tolerant structures (Alderliesten, 2015). This is one of the major causes for grounding airliners, for example, as accidents have been accounted to crack growth in the past, which could have a negative effect on flight earnings due to aircrafts flying limited hours before grounding. It is therefore imperative that an aerospace system shows good fatigue properties from the production stage in order to predict long flying

hours. Good fatigue properties will be reflected by low-cost maintenance, low inspection frequency and simple repairs. The challenge in reaching maximum safety in the aerospace sector is largely affected by the production cost, operation cost and business competition. Therefore, innovation in the area of production is needed to improve designs at affordable costs. This includes clever structural design concepts, improved joints and fatigue-resistant materials necessary for designing against fatigue (Pevitt and Alam, 2014). This, however, will also imply that new theoretical data will have to be available to predict the future of the new systems.

4.2.2   Material and structural stability

Materials and structures are largely responsible for major performance improvements in the aerospace systems (Noor, 1998). Computational structural maturation and development of ACMs have improved structural performance, reduced operational risk and shortened development time (Noor and Venneri, 1997). However, future aerospace systems still need to meet demanding challenges such as affordability, safety and environmental compatibility (Noor et al., 2000). Materials used in aerospace systems (aircrafts, satellites, missiles, launchers etc.) require a combination of a range of properties such as strength, stiffness, fracture toughness, fatigue endurance and corrosion resistance (Dursun and Soutis, 2014). It is a requirement that aerospace materials must be easy to fabricate and cost-effective while at the same time are able to carry required loads of weight based on aerodynamics and structural properties (Huda and Edi, 2013).

Furthermore, aerospace materials are required to be tolerant to damage and give durability over the aircraft's design life. Aircraft structures should not crack, corrode, oxidize or suffer any form of damage while operating under adverse conditions that involve high loads, freezing, high temperatures, lightning strikes, hail and exposure to potentially corrosive fluids such as jet fuel, lubricants and paint strippers (Mouritz, 2012). In addition to these requirements, aerospace materials need to reach a much-reduced weight target for efficiency in speed and fuel consumption. Airframes reportedly contribute between 20% and 40% of the total weight for most aircrafts (Mouritz, 2012). Therefore, the use of light materials which are structurally efficient is of much importance in this target sector. Both materials and structures in the aerospace sector are required to be smart, affordable, light weight, multifunctional, operational and crashworthy in extreme environments, flexible to carry load and designed based on computational methods and simulations (Mouritz, 2012; Renton, 2001).

Improvement of material systems and structures with respect to cost, processing and performance through emerging advanced technologies and advanced joining techniques comprise key requirements for future system designs. ACMs have been a targeted technical solution in the aerospace sector, as part of structural design evolution, weight reduction and saving costs (Braga et al., 2014; Hinrichsen and Bautista, 2001; Ye et al., 2005). It is a requirement that these new-generation materials show good mechanical properties and uncompromised temperature stabilities for them to be fully reliable. Automated manufacturing technologies are recommended for cost-effective materials. Because the newly emerged composite materials differ in characteristics from the properties of the metals and alloys, construction of new damage mechanisms

is required to optimize structural efficiency (Chowdhury et al., 2015). Improved methods of design and analytical tools for simulating process and performance are also recommended for advanced and simplified future structural designs. Advanced material models for stiffness, strength and failure mechanisms are also required for the new composite materials.

4.2.3   Strength

The strength of the materials used in the design of the aerospace systems goes together with the above properties and is also required to determine structural design in aerospace systems (Williams and Starke, 2003). Strength is used to predict crack growth upon impact and monitor weight circulation in order to guarantee a long life-cycle for the systems. Composite materials are known for high strength-to-weight and stiffness-to-weight ratios which realize one of the target goals for future aerospace systems (Nurhaniza et al., 2010). The superior strength offered by the composite materials accounts for the growing demand to explore composites in the aerospace sector.

4.3   Advanced laminated composites for aerospace engineering

Laminated composite materials represent a family of hybrid materials, consisting of layers of laminae bonded using matrix materials (Fig. 4.4).
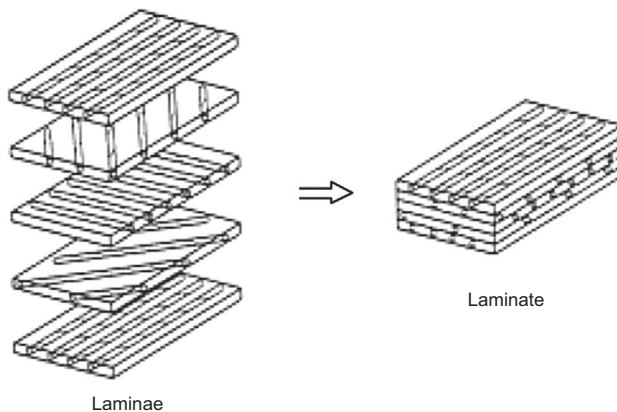

Laminae

Laminate

Figure 4.4 Tailored laminated composite.
Adapted from van Rijswijk, K., Brouwer, W.D., Beukers, A., 2003. Application of Natural Fibre Composites in the Development of Rural Societies. Delft University of Technology, FAO Corporate Document Repository, Produced by Department of Agriculture and Consumer Protection, Food and Agriculture Organisation of the United Nations, Rome.

Lamination is utilized to combine the best aspects of the constituent layers and bonding material in order to achieve a laminated composite. Some of the properties that can be improved by forming a laminated composite are:

- Strength
- Stiffness
- Low weight
- Corrosion resistance
- Wear resistance
- Beauty or attractiveness
- Thermal insulation
- Acoustical insulation

4.3.1   Common laminate definition

- Quasi-isotropic
- Balanced
- Hybrid laminates

4.3.2   Stacking-sequence notation

This concept is generally used to represent all relevant parameters such as laminate individual layer thickness, orientation and overall stacking sequence. For equal-thickness layers (regular), the listing of the layers and their orientation suffices is $[0°/90°/45°]$. If laminates are made from the same layer, the listing of the layers and their orientation suffices is $\left[90°_t/0°_{2t}/45°_{3t}\right]$. For irregular layers (which do not have the same thickness, eg, $[0°/90°/45°]$), the notation of layer thickness is appended to the previous notation. Fig. 4.5 illustrates the listing of the layers and orientation suffices.

4.3.3   Quasi-isotropic laminates

Some laminates have isotropic extensional stiffness (the same in all directions in the plane of the laminate). A quasi-isotropic laminate means a laminate which appears isotropic but is not actually isotropic. It has equal bending stiffness in all directions. Therefore, a quasi-isotropic laminate means equal extension stiffness in all in-plane directions of the laminate. All layers must be of the same material and of equal thickness. The simple example of a quasi-isotropic laminate is a three-layer laminate $[-60°/0°/60°]$ or a four-layer laminate $[0°/-45°/45°/90°]$.

4.3.4   Balanced laminates

Laminates in which all equal-thickness laminate at angle θ other than 0 degree and 90 degree to the reference axis occur only in $\pm\theta$ pairs, which are necessarily adjacent to each other. Shear extension coupling does not exist, nor does bending−extension coupling. But, bend−twist coupling does exist.
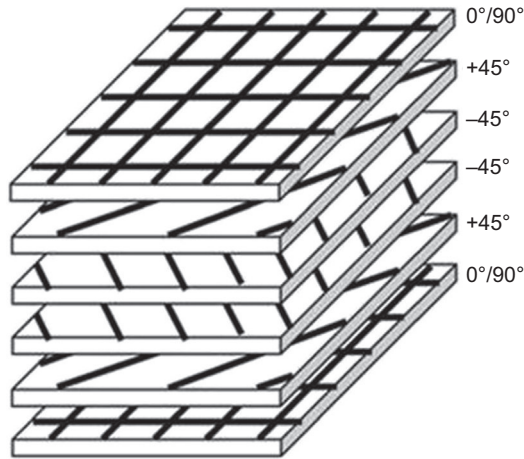
Figure 4.5 Different layers of a laminated composite and orientation suffices.
Picture: Adapted from Lanxess AG. Thermoplastic composites with multiaxial-oriented
continuous fiber layers.

4.3.5 Hybrid laminate

A hybrid laminate is a mixture of two or more material systems to form a laminate.
For example, graphite−epoxy laminate is used with Kevlar-49-epoxy laminate to
create wing-to-body fairings for the Boeing 757 and 767. Two epoxies must be
cure-compatible in order to achieve a functioning laminate. Different fibre systems
are often mixed in a hybrid laminate, but not many matrix systems can be used.

4.3.6 Background

It is now scientifically and politically acknowledged that greenhouse gas emissions
from aircraft engines contribute significantly to global climate change (Mahashabde
et al., 2011). Aircraft emissions are emitted directly into the upper troposphere and
lower stratosphere and thus have a huge impact on atmospheric composition (Lee
et al., 2009). This is against the policies conceptualized by the International Civil
Aviation Organization (ICAO), therefore the aerospace industry is aiming at reducing
emissions through weight reductions and aerodynamic improvements (Lee, 2010,
Lawrence, 2009). One of the globally recognized key technologies for significant
weight reduction to meet emission targets is the application of ACMs in aircraft design
(Mangalgiri, 1999). The lighter structures result in lower fuel consumption and thus
reduce emissions. This accelerated the demand for lightweight materials for potential
applications in the aerospace industry.

The demand in aircraft industry for high-performance, lightweight structures
stimulated a strong trend towards the development of refined models for FMLs
(Katnam et al., 2013). The existing challenges in this regard are that science and
technology must step up to account for the rising market demand of these materials,

government officials and authorities need to conceptualize the right policies and have the required standards in place for certification, while researchers need to be involved in intensive research to minimize the cost involved in the development of FMLs for aircrafts.

4.3.7 Manufacturing of laminated composites

The most important factor in manufacturing these laminates is the adhesive bonding between aluminium and FRP layers. Observations from previous work found that the damage size is greater in laminates with poor interfacial adhesion compared to that of laminates with strong adhesion between aluminium and glass layers (Ardakania et al., 2008).

FMLs are generally manufactured by stacking the composites. The stack is heated to a certain temperature under a given amount of pressure using a gear press (Fig. 4.6), before cooling slowly to room temperature. The processing temperature must be sufficient to melt the matrix without degrading the fibres in the composite. A good manufacturing technique must yield high-quality panels that exhibit very little shrinkage in the composite plies. Stacking arrangements are chosen according
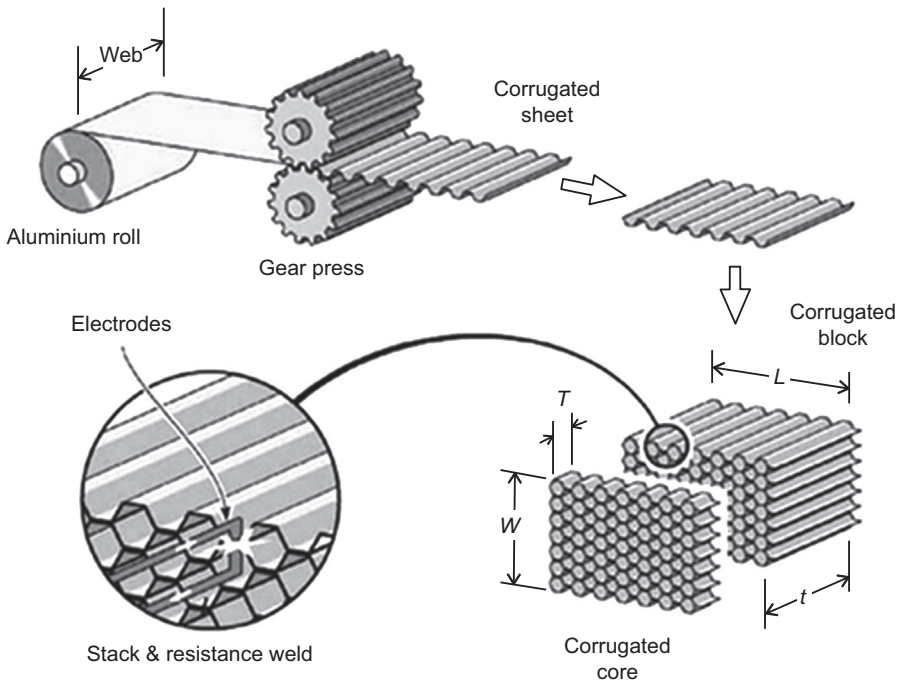

Figure 4.6 The formation of a stack manufacturing process.
Reproduced from Wadley, H.N.G., 2006. Multifunctional periodic cellular metals. Philosophical Transactions of the Royal Society A 364, 31−68. http://dx.doi.org/10.1098/rsta.2005.1697. Published online December 2, 2005.

to the desired product. The resulting films are then subject to characterization. Generally, there are two processes to manufacture thermoset laminates: low-pressure and high-pressure processes.

4.3.7.1 Low-pressure processes

Low-pressure manufacturing processes produce an excellent combination of mechanical strength, dielectric properties and thermal performance. They have an amazing ability to use a variety of fillers and additives to create a range of desirable properties from flame retardance to track resistance. Typical resins used in the low-pressure laminate manufacturing process include polyester, vinyl ester and epoxy. This manufacturing process starts with the selection of a proper resin formulation to provide the properties required for a specific application.

The low-pressure laminate manufacturing process is considered to be more cost-effective than the high-pressure laminate process due to the faster cycle time from the beginning of the process to the end.

4.3.7.2 High-pressure processes

High-pressure laminate processes use glass cloth, Kraft paper, mica paper and linen (cotton). Typical resins used in a high-pressure laminate-manufacturing process include phenolic, epoxy, melamine, silicone and polyimide. The advantages of high-pressure processes are their excellent dielectric strength and related electrical properties. A high-pressure process begins by intelligent selection of a proper resin. Kraft papers are cut to create packages of various builds depending on the sheet thickness and formulation for the product being manufactured. Resin components are mixed with filler additives; track resistance, flame retardance and thermal endurance properties are added. The resin is applied to the Kraft paper package using an automated press loading or gear press. The sheets are unloaded with automated material-handling equipment and finally inspected for quality and manufacturing tolerance with a sample being subject for characterization (Fig. 4.7).

4.3.8 Metal-based laminates (GLARE, ARALL and CARALL)

FMLs are hybrid composite materials built up from interlacing layers of thin metals and fibre-reinforced adhesives. The most commercially available FMLs are aramid-reinforced aluminium laminate (ARALL), based on aramid fibres; glass-reinforced aluminium laminate (GLARE), based on high-strength glass fibres; and carbon-reinforced aluminium laminate (CARALL), based on carbon fibres. FMLs are finding increasing use in a number of aerospace applications (Reyes and Cantwell, 2000) due to their advantages of high specific strength or stiffness, good fatigue resistance, better damage tolerance to fatigue crack growth, fire resistance, blunt notch strength, formability and repairability (Fotouhi et al., 2015). Due to their excellent properties, FMLs are being used as fuselage skin structures of the next-generation commercial aircrafts. FMLs not only provide high resistance to fatigue damage propagation, but also provide excellent
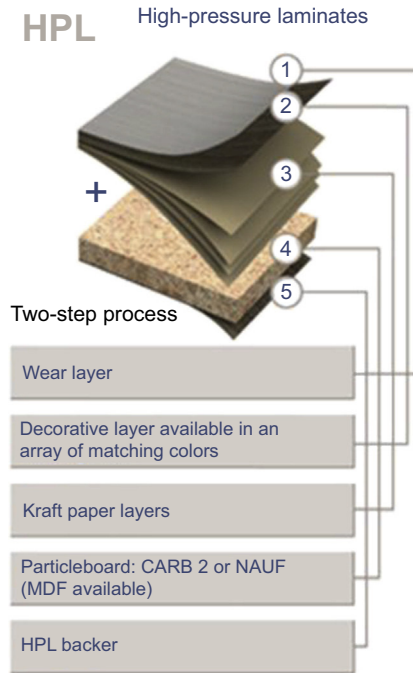
Figure 4.7 Typical example of a high-pressure laminate.
Reproduced from Thermally Fused Laminate (TFL) Panels. http://www.surfaceandpanel.com/
education/continuing-education/tfl-makes-environmentally-friendly-decorative-panels.

resistance to impacts and lightning strikes as well as high corrosion and burn-through
resistance (Vlot and Gunnink, 2001). One of the advantages of FMLs when compared
with conventional carbon fibre−epoxy composites is their low moisture absorption.
The moisture absorption in FML composites is slower when compared with polymer
composites, even under relatively harsh conditions, due to the barrier of the aluminium
outer layers. Due to this favourable properties, recently big companies such as
EMBRAER, Aerospatiale, Boeing and Airbus have started to work with this kind of ma-
terials as an alternative to save money and to guarantee the security of their aircrafts.

4.3.8.1 Aramid-reinforced aluminium laminate

Aramid fibre aluminium laminates are the first generation of FMLs to bridge the gap
between theory and operational practice. They were conceived in the late 1970s and
early 1980s. Aluminium fatigue was known to be an important material weakness
to consider in aircraft structure design, and so fatigue-insensitive aluminium was a
highly desirable material. The theory to achieve this was to use the fatigue resistance
of the newly developed, high-strength aramid fibres and to blend it in an optimal way
using the time-proven production technique of adhesive metal bonding. Some major
efforts for several applications were followed, such as for lower wing skins of the
Fokker 27 and later Fokker 50 commuter aircraft. The gap was ultimately bridged
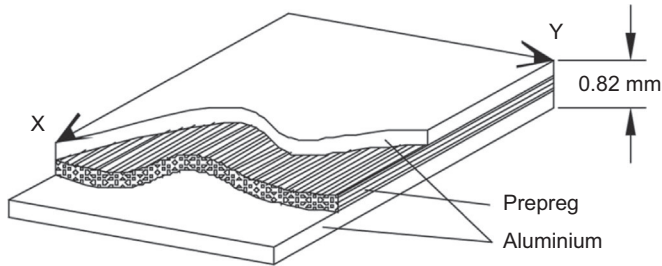
Figure 4.8 Schematic representation of ARALL laminate in 2/1 stacking.
Adapted from Castrodeza, E.M., Touça, J.M.R., Ipiña, J.E.P., Bastian, F.L., 2002. Determination of CTODC in fibre metal laminates by ASTM and Schwalbe methods. Materials Research 5, 119−125.

when ARALL was qualified for Mil Handbook 5 and was applied as skin material for the aircraft cargo door on the McDonnell Douglas C17 military air lifter (Fig. 4.8).

In 1982, the first commercial product under the trade name ARALL was launched by Alcoa (Vlot and Gunnink, 2001). The trade names ARALL 1 and ARALL 2 were standardized. The most successful product in this field was obtained at Delft University of Technology in the Netherlands, with the development of FMLs using aramid, aluminium 7475-T761 and epoxy resin (Gutowski, 1997; Hou et al., 1998; Hillermeier and Seferis, 2001). FMLs had completed their first evolutionary cycle, starting from theory; they had gone through material specification, material qualification and allowables development, design and manufacturing, finally ending in operational usage. However, aerospace demanded more than just good performance on properties; good performance on cost was also highly crucial. ALCOA commercialized ARALL in two grades: ARALL 1 with aluminium 7075 layers, stretched after curing, and ARALL 2 which had 2024 layers and was in the as-cured condition. From there, two more grades came available (1987): ARALL 3 was identical to ARALL 1 but with 7475 aluminium layers, and ARALL 4 was with a different, high-temperature adhesive for military applications (Alderliesten et al., 2003). The principal benefit of ARALL was its ability to slow and self-arrest the crack growth rate (Alderliesten et al., 2003). But, like any other material, aramid had its own disadvantages; the aramid fibres have low interface strength between the fibres and the adhesive, so it is not possible to produce laminate with a fibre volume fraction above 50% with acceptable peel strength and satisfactory interlaminar shear properties. Second, fibre failure in the crack-bridging fibre layer does occur under some fatigue load conditions, although fatigue crack growth resistance is still considerably better than that of ARALL 2. It seriously affects the efficiency of crack bridging and although post stretching can solve problems of fibre failure, it will increase the production costs. Another disadvantage was that the anisotropic properties of unidirectional fibres prohibit its application in fuselage skin where biaxial stresses occur. A more isotropic fibre composite with fibres in more than one direction was desired. ARALL has relatively poor notch behaviour, especially its blunt notch strength compared to a monolithic aluminium alloy (Asundi and Choi, 1997). Only after ARALL had been marked by Alcoa, the additional benefits

of FMLs were recognized (Vlot, 2001). In particular, the use of glass fibre instead of aramid fibres in the FMLs (Roebroeks, 1991) was tried to counteract the aforementioned disadvantages.

4.3.8.2 Glass-reinforced aluminium laminate

In 1990, another attempt to improve ARALL laminates, adopting high-strength glass fibre called GLARE instead of aramid fibres, was developed successfully (Asundi and Choi, 1997). GLARE is an FML that combines the ductile aluminium alloy 2024-T3 with S2 glass fibres embedded in FM94 epoxy (Roebroeks, 1991), as shown in Fig. 4.9. The impact properties of GLARE grades with biaxial fibre layers were better than those of aluminium, and the impact behaviour of glass fibre composites is significantly lower than that of aluminium (Alderliesten et al., 2003). GLARE properties were also better after impact than those of aluminium, resulting in the Boeing 777's first commercialization of GLARE in 1990 (Alderliesten et al., 2003). The adhesion between glass fibres were found to be better than that of aramid fibres, and glass fibres are much more resistant if loaded into compression; as a consequence, fibre failure in
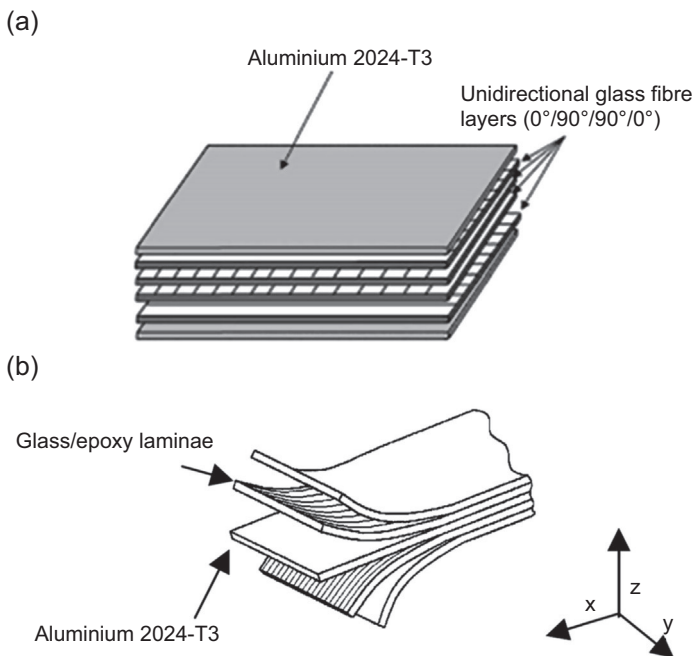

Figure 4.9 (a) Unidirectional glass fibre layers with aluminium 2024-T3 (*Hyoungseock, S., Hundley, J., Hahn, H.T., Yang, J., 2010. Numerical Simulation of Glass-Fibre-Reinforced Aluminium Laminates with Diverse Impact Damage. AIAA Journal 48 (3), 676−687.*)
(b) Configuration of continuous glass fibre−metal−epoxy hybrid composite (3/2 lay-up)
(*Reproduced from Edson, C., et al., 2008. Hygrothermal effects evaluation using the iosipescu shear test for glare laminates. Journal of the Brazilian Society of Mechanical Sciences and Engineering 30.*).

the glass fibres has rarely been observed during fatigue load. Other advantages of GLARE over ARALL were its higher tensile and compressive strength, better impact behaviour, higher ultimate strain and higher residual strength. And, due to the good bonding properties of the glass fibres to the resin, GLARE laminates with fibres are able to be built up in two directions, which is more suitable for some constructions where biaxial stresses occur (Asundi and Choi, 1997).

The manufacturing process commonly includes surface preparation of the metallic sheets like anodizing and epoxy primer painting for aluminium, and hand lay-up to build up the parts that are cured in autoclave under controlled temperature and pressure conditions; its characteristics are very suitable for aircraft external parts, like fuselage and wing skins. The reason for GLARE laminates was to obtain a material with a high fatigue crack growth resistance without fibre failure, a better notch strength and fibre lay-up in a biaxial way. This implied that the application of GLARE to the aircraft structure could lead to weight savings, improved safety, high strength, fatigue insensitivity, outstanding workshop properties, good and easy repairability, excellent damage tolerance and production simplifications. The superior behaviour of GLARE laminates could be translated into weight savings in aircraft structures combined with cost savings in production and maintenance (Asundi and Choi, 1997). The advantages of GLARE include its specific weight, which is approximately 10% lower than that of aluminium. GLARE offers the aircraft structural design damage-tolerant, lightweight, cost-effective solutions for many tension-dominated applications. Originally developed for its outstanding fatigue resistance, other characteristics of GLARE include high specific static properties, ease of manufacture, excellent impact resistance, burn-through capabilities and good corrosion resistance.

The successful introduction of GLARE hybrid material technology in the fuselage of the Airbus A380 aircraft (Pora, 2001) has constituted a major step in the mission for damage tolerance in aeronautics. Alderliesten (Alderliesten, 2015) argued that the next-generation FMLs should be tailored and designed for specific required structural properties and performance, rather than following a bottom-up approach starting from levels of FML as a material (Alderliesten, 2015). Historically, fatigue damage has been an important driver in the development and investigation of damage-tolerant material. This explains the reason why there have been vast amounts of papers on fatigue and fatigue crack propagation in FMLs (Volt, 2001). Then, the development of glass fibres instead of aramid fibres in FMLs has increased the acknowledgement of FMLs' contribution to damage tolerance.

However, damage such as matrix cracking, fibre−matrix debonding, fibre breakage and delamination can occur due to mechanical and environmental conditions during service. The impact load also induces surface damage in composite laminates; therefore, the structural composites repair technique is needed to restore the strength of a damaged component.

4.3.8.3 Carbon-reinforced aluminium laminate

CARALL composites are usually continuous carbon fibre with a polymer matrix for aerospace applications. They provide superior material properties compared to metals and thus enable lighter structural designs to be achieved (Mangalgiri, 1999).

The lighter structure results in lower fuel consumption and thus reduced emissions. Carbon-reinforced polymer composites are currently being used in aircraft design for primary and secondary structural applications (Katnam et al., 2013). In addition to the improvements in fuel efficiency and emission reduction, advanced carbon composites in aircraft design also enhance passenger comfort. Carbon-reinforced advanced composites are usually manufactured in laminate or sandwich forms for aerospace structural applications (Baker et al., 2004).

From a structural viewpoint, carbon fibre composites have advantages including a high strength-to-weight ratio, a high stiffness-to-weight ratio, improved fatigue tolerance, corrosion resistance, formability, tailored mechanical properties and low thermal expansion.

Carbon fibre−reinforced plastics can and will in the future contribute more than 50% of the structural mass of an aircraft. However, affordability is the key to survival in aerospace manufacturing, whether civil or military, and therefore effort should be devoted to analysis and computational simulation of the manufacturing and assembly process as well as simulation of the performance of the structure, since they are intimately connected.

4.3.9   Glass fibre composites (glass fibre-phenolic and glass fibre polyether ether ketone (PEEK))

4.3.9.1   Glass fibre-phenolic composites

Phenolic resins are good for high-temperature applications where parts must meet fire safety standards. Phenolic resins are used in a wide range of applications, including electronics, ballistics, mine ventilation, offshore water pipe systems, aerospace, rail and mass transit. Their key properties are low density (weight efficient), low thermal conductivity, excellent corrosion and chemical resistance, a high strength-to-weight ratio, better design flexibility, cost-effective production of complex 3D structures, excellent fatigue and impact properties, improved acoustic performance, radar/sonar transparency and low maintenance.

4.3.9.2   Glass fibre PEEK composites

This is a semicrystalline, high-temperature (up to 500°F) thermoplastic that is excellent for applications where heat, chemical and combustion properties are critical to performance. It emits little smoke or toxic gas when exposed to flame. PEEK is tough, strong and rigid and has superior creep resistance. PEEK can also resist radiation and a wide range of solvents, and with its resistance to hydrolysis, PEEK can withstand boiling water and superheated steam used with autoclave and sterilization equipment at temperatures higher than 482°F. PEEK resins are available in different grades (ie, unreinforced (or unfilled), 30% glass fibre−reinforced, 30% carbon fibre−reinforced, and high pressure-velocity (HPV)-reinforced grades), and the most common applications include those in the automotive, marine, nuclear, oil well, electronics, medical and aerospace industries.

Glass fibre PEEK is especially good for structural applications that require greater strength, stiffness or stability, especially at temperatures higher than 300°F, and the addition of glass fibre greatly reduces the expansion rate and increases the flexural modulus of the plastic. Key properties are a continuous service temperature of 500°F, low smoke and toxic-gas emissions, very low moisture absorption, superior creep resistance and excellent fatigue, stress-crack, hydrolysis and chemical resistance. They can also come in a number of different shapes or forms such as sheets, rods and tubular bars. The only limitations to PEEK are that they are costly and anisotropic (direction dependent) and require high processing temperatures. As a result, the properties should be considered in directions relative to principal laminate orientations, and they should be considered dependent on the lay-up (Alderliesten, 2015).

4.3.10 Potential applications of natural fibre composites

In past years, natural fibres have gained considerable interest in the composites area to replace petroleum-based reinforcements. Natural fibres have low density, high strength and high stiffness, and they are renewable resources. Furthermore, the developed composite materials are suitable for various applications such as automotive, construction, biomedical and aerospace.

Due to the advantages of weight, mechanical stability and price, interest in the application of natural fibre−reinforced materials is growing in the aerospace industry in the United States and Europe (Bledzki et al., 2002). However, the readiness levels of the applications of these sustainable materials are being checked for approval by the US Federal Aviation Administration (FAA) and the UK Civil Aviation Authority (Bledzki et al., 2002).

4.4 Matrix systems

The largest commercial use of polymeric material is in the manufacture of plastics. Several plastics are stable high-molecular-weight polymers, either linear or branched, and retain their chemical identity through processing and use; these are thermoplastic resins. The second large class and actually the older commercially is the thermosets, which are usually polymerized in two stages. In the first stage, they are polymerized into low-molecular-weight viscous liquids or fusible solids; in the second stage, during moulding, they are further polymerized into highly cross-linked three-dimensional structures that are then stable, insoluble and infusible. Both thermoset and thermoplastic polymers are in a variety of more complex forms such as coatings, adhesives, foams, reinforced plastics and high-temperature materials which may broadly be described as composites. The end-use application choice of these materials is based on the design consideration, material properties and process techniques for converting the material into the desired product.

Phenolic, polyesters, vinyl esters and epoxy resins are widely used thermosets reported in literature (Alves et al., 2010), and polypropylene (PP), polyvinyl alcohol, polyvinyl chloride, polylactic acid and natural rubbers are commonly used thermoplastics.

Polymeric resins are normally reinforced with fibres to improve their mechanical properties. The reinforced polymer matrix is called a composite. The end product (composite material) should have better properties (thermal, mechanical, rheological and thermo-mechanical) as compared to the starting materials (polymer matrix and reinforcement). Various reinforcements have been documented in literature to develop composites with high-performance and specific properties. The reinforcing materials, fillers and fibres could be either biobased (natural fibres) or synthetic (petroleum based). Biobased reinforcements include flax, kenaf, sisal, agave, cotton and others, and synthetic reinforcements include glass and carbon fibres. The natural fibre-reinforced composite materials are suitable for various applications such as automotive, construction, biomedical and aerospace. But glass fibres have been used extensively in the aerospace industry.

4.4.1 *Thermosetting resins*

In thermosetting plastics, the polymerization reaction is carried out in two or more stages. In the first stage, the monomers are partially polymerized to viscous liquids or low-melting-point soluble fusible solids which provide high fluidity for processing. In the final stage, the polymerization reaction is carried to completion, producing a highly cross-linked three-dimensional structure. In processing it, the liquid can be poured into a low-cost mould, but must be left there until the final polymerization reaction is complete. Fusible solids can be cured and ejected from hot moulds without cooling, but scrap is not useable. Regarding properties, the tight, rigid structure immobilizes the polymer molecules, providing high hardness, hot strength and chemical resistance, but it also makes the pure polymers inflexible and brittle, requiring fibrous reinforcement for good mechanical properties. Six major types of thermosetting are allyls, epoxy resins, polyesters, urea—formaldehyde resins, melamine—formaldehyde resins and phenol—formaldehyde resins.

Processing: The rapid cross-linking nature of the thermosetting plastics has generally limited process techniques to casting liquids and compression moulding fusible solids. In compression moulding, the fusible reactive prepolymer is pressed between the two hot mould faces until cured, then is ejected directly without the need for cooling. For improved flow and faster cure, the resin is sometimes preheated and fused in an adjacent chamber and then forced to flow through a short orifice into the final mould; this is transfer moulding. The recent improvement in both the resin and the equipment has led to the introduction of screw-injection moulding of thermoset. This has led to greater vitality and interest in the thermosetting sector of the plastic field. The resulting solution has both advantages and disadvantages. Thermoset resins are regarded as highly cross-linked amorphous resins which cannot be re-melted or dissolved. These matrices have good properties such as high strength and modulus, and good thermal and chemical resistance, and they are easily prepared. Despite the

good properties exhibited by thermoset resins, they also have displayed several short-comings, including poor cracking, brittleness and low toughness.

Much research has been conducted to address the shortcomings of thermoset resins, especially their toughness. This would be achieved by toughening the materials by incorporating liquid rubbers and linear thermoplastic polymers to better the performance and properties for the desired applications. In recent years, the demand for high-performance structural materials using thermosets has grown immensely in various applications such as aerospace, automotive, construction and biomedical.

Jute fibre was utilized to reinforce polyester to develop a frontal bonnet of a buggy. In this study, jute fibres were compared with glass fibres, and these composites were assessed by lifecycle assessment (LCA). Jute fibre composites showed better environmental performance in comparison to glass fibre composites. Jute fibre composites are regarded as a better solution for environmental concerns (Alves et al., 2010).

Feraboli and Masini investigated the development of carbon−epoxy composites for body panels and structural components of the Lamborghini Murcielago. In their study, the specifications of the composite materials were described, along with the technology required to manufacture those composites (Ferabolia et al., 2007).

Carbon−epoxy composites were developed for structural pipeline repair. The researchers investigated the thermomechanical properties by using dynamic mechanical analysis. They also compared noncured and postcured composites. It was found that the magnitude of tan delta peak of noncured composites was higher than that of post-cured composites. Also, it was noticed that the tan delta peak for postcured composites became broader and then shifted to higher temperatures. The data obtained provided an indication of what postcure temperature and time are required to develop a good structural pipeline repair (Goertzen and Kessler, 2007).

Sugita et al. (2010) developed carbon−epoxy lap joints for aerospace applications.

Cellulose nanocrystal−reinforced waterborne epoxy polymers were prepared as promising materials for structural materials and coatings. The addition of cellulose nanocrystals led to the improvement of thermomechanical, thermal and mechanical properties. Their results suggested that cellulose nanocrystals bonded well with water-borne epoxy resins (Xu et al., 2013) for potential applications in aerospace.

Most thermosets are derived from fossil fuels. Research focused on changing from petroleum-based thermoset polymers to biobased ones such as biobased epoxy is required. This is normally achieved by functionalizing plant oils with epoxidation by organic peracid or hydrogen peroxide. The benefits of using biobased thermosets are environmental friendliness and sustainability. Many studies report on synthesis and characterization of biobased thermoset polymers (Kim and Sharma, 2012, Bakare et al., 2014). The development of bioepoxy would solve environmental problems in the future.

4.4.2   Fossil fuel−based polymers

The consumption of raw materials such as coal, petroleum and natural gas fossil resources has increased steadily since the early days of industrialization. In addition to energy and heat production, fossil resources have been and still are used as basic

materials for the chemical industry, the products of which have replaced many of the renewable (generally agricultural) raw materials that have been used since antiquity. Like biobased polymers, fossil fuel−based polymers have received interest in the composites field. These polymers are utilized as polymer matrix to develop composite materials for potential applications. Fossil fuel−based polymers alone showed several drawbacks such as poor performance and properties. This necessitates the use of additives to enhance performance and properties. The additives are classified into synthetic and biobased ones; depending on the desired application and environmental concern, both types of additives could be used.

Fossil fuel polymers can be categorized into thermosets and thermoplastics. These include polyethylene, polypropylene, polyvinyl chloride, polyvinyl alcohol, polystyrene, vinyl esters, phenolic resins, epoxy resins and polyesters.

Much research focusses on the use of biobased additives to reinforce fossil fuel−based polymers to improve properties and performance. Natural fibres, agricultural residues and bacterial cellulose are commonly used reinforcements. Biobased reinforcements offer advantages such as renewability, recyclability, abundance, high strength and stiffness. These reinforcements are believed to reduce environmental problems, and they produce sustainable and environmentally compatible composite materials.

4.4.3   Thermoplastic (biobased) polymers

Thermoplastics are stable high-molecular-weight polymers that are either linear or branched. Their processability and mechanical and thermomechanical properties depend on their molecular weight, molecular flexibility, crystallinity and polarity. Their stability, solubility and permeability depend on their chemical composition and crystallinity. Examples are polyethylene, polypropylene, polystyrene, polyvinyl chloride, polytetrafluoroethylene, polymethyl methacrylate, polyoxymethylene, cellulose acetate, polysulphone and so on.

Stable high-molecular-weight linear thermoplastic polymers are converted into finished products primarily by heating them to the liquid state and applying pressure to make them flow into a mould or through a die to develop the desired shape, and then cooling below the melting or the glass transition temperature to make them retain that shape.

The public has experienced a lot of environmental concerns such as climate change and the shortage of petroleum-based resources. This necessitates the use of environmentally compatible renewable resources as an alternative. Biobased thermoplastics have drawn considerable interest to replace fossil fuel−based polymers. Biobased thermoplastics include polylactic acid (PLA), poly(hydroxybutyrate-co-valerate) (PHBV), poly(butylene adipate-co-terephthalate) (PBAT) and polybutylene succinate adipate (PBSA).

Recent studies have focussed on the development of fully biodegradable materials, also known as green composites, using biobased polymer and reinforcement. The use of biobased nanomaterials (nanofibres and nanocrystals) as reinforcements to develop bionanocomposites has been a subject of research (Reddy et al., 2013).

These materials showed advantages such as high aspect ratios, high surface area and high strength and stiffness. But they have not been applied in aircraft designs yet.

Oksman and Selin (2004) compared PLA−flax composites with PP−flax composites which have been used for automotive panels recently. They used the same procedure that is used to prepare PP−flax composites. Results showed that the strength of PLA−flax composites was 50% better than that of the currently used PP−flax composites.

Both thermoset and thermoplastic resins are often used as matrix material in the development of ACMs. However, thermosetting resins are extensively used in aircraft manufacturing due to their low manufacturing and processing costs (Soutis, 2005).

4.5 Fibre direction and stacking sequence design for FMLs

Fibre-reinforced composite materials for structural applications are often made in the form of a thin layer called a lamina. Structural elements such as bars, beams or plates are generally formed by stacking the layers to achieve their desired overall strength and stiffness. These elements are called laminates. Fibre orientation in each lamina and stacking sequence of the layers in the laminate can be chosen to achieve the desired strength and stiffness for a specific application. It is therefore very important to model the experimental loading conditions as realistically as possible.

4.5.1 The finite element model

The finite element method is one of the numerical calculations applied in various physical problems. It plays a major role in calculating the stress and deformation of the structure. Peterson and Londry (1986) applied the finite element method in the design of steel and aluminium bicycle frames. This method is also adopted to analyse the structural behaviours of composite bicycle frames (Lessard et al., 1995). To validate the results obtained from this model, experimental results such as internal delamination and dissipated energies are normally quantified.

4.5.2 The single-layer equivalent model

The single-layer equivalent model is usually adopted to simulate a multiply composite laminate. The results obtained from this model reveal which stacking can cause the highest stiffness, and they describe the regions where higher stresses occurred in the laminated composites. It is important to find the better fibre direction and stacking sequence of the FMLs.

4.5.3   Fatigue modelling strategies

According to Sendeckyj, fatigue criteria can be classified in four major categories: the macroscopic strength fatigue criteria, criteria based on residual strength, criteria based on residual stiffness and finally criteria based on actual damage mechanisms (Naik et al., 2000).

4.5.4   Fatigue life models

These models do not take into account the actual degradation mechanism but use S−N curve or Goodman-type diagrams to introduce fatigue failure criteria, and they are phenomenological models for residual stiffness and strength. Fatigue life models require extensive practical work and do not take into account the actual damage mechanisms, such as matrix cracks and fibre fracture. The main drawback of these models is their total dependency on experimental inputs for all material, lay-up and loading conditions (Schaff and Davidson, 1997).

4.5.5   Residual stiffness model

These models propose an evolution law which describes the gradual deterioration of the stiffness and strength of the composite specimen in terms of macroscopically observable properties. They account for degradation of the elastic property during fatigue. Stiffness can be measured frequently during fatigue experiments and can be measured without further degrading the material.

   Although residual strength is a meaningful measure of fatigue damage, it does not allow for nondestructive evaluation; as such, it is not possible to determine residual strength without destroying the specimen. This makes it difficult to compare damage states between two specimens.

4.5.6   Mechanistic models

This type of model was proposed to describe the deterioration of composite material in direct relation with specific damage such as transverse matrix cracks and delamination size, and quantitatively analyse the progression of actual damage mechanisms.

4.6   Future perspective and applications

ACMs have gained fame in high-performance structural designs such as aerospace applications that require lightweight components with superior mechanical properties in order to perform in demanding service conditions as well as provide energy efficiency (Katnam et al., 2013). The aerospace industry is currently using ACMs in both primary and secondary structural components. However, one of the major obstacles the aerospace industry has been facing is that the expansion of advanced composites is growing rapidly, but the authorities such as the FAA and important aviation

safety-related issues such as design rules and manufacturing processes are not in place to accelerate this transition. As a result, the aerospace industry now requires reliable technology for maintenance and repair (LLorca et al., 2011). ACMs such as FMLs have proven to be high-performance structures for aircraft design. But the cost to manufacture these structures is still very high. Intensive research and development are required to minimize costs in developing environmental friendly structures for the aerospace industry.

4.7 Conclusions

Fibrous composites have found applications in aircraft from the first flight of the Wright Brothers' *Flyer 1*, in North Carolina on 17 December 1903, to the plethora of uses now enjoyed by them in both military and civil aircraft, in addition to more exotic applications in unmanned aerial vehicles, space launchers and satellites. Their growing use has arisen from their high specific strength and stiffness, when compared to the more conventional materials, and the ability to shape and tailor their structure to produce more aerodynamically efficient structural configurations. It can be predicted that the use of carbon fibre composites will increase to more than 50% of the structural mass of an aircraft. However, to compete with the conventional materials used in aerospace engineering, efforts should be directed towards fabricating composite based aerospace parts at affordable costs and through easy manufacturing processes and to develop reliable modelling and simulation techniques for analysis of manufacturing and assembly processes as well as product's performances.

References

Alderliesten, R.C., 2015. Design for damage tolerance in aerospace: a hybrid material technology. Materials and Design 66, 421−428.

Alderliesten, R.C., Hagenbeek, M., Homam, J.J., Hooijmeijer, P.A., De Vries, T.J., Vermeeren, C.A.J.R., 2003. Fatigue and damage tolerance of Glare. Applied Composite Materials 10, 223−242.

Alves, C., Ferrão, P.M.C., Silva, A.J., Reis, L.G., Freitas, M., Rodrigues, L.B., Alves, D.E., 2010. Ecodesign of automotive components making use of natural jute fiber composites. Journal of Cleaner Production 18, 313−327.

Ardakania, M.A., Afaghi Khatibi, A., Ghazavi, S.A., 2008. A study on the manufacturing of glass-fiber-reinforced aluminum laminates and the effect of interfacial adhesive bonding on the impact behaviour. In: Proceedings of the XIth International Congress and Exposition June 2−5. Orlando, Florida, USA.

Asundi, A., Choi, A.Y.N., 1997. Fiber metal laminates: an advanced material for future aircraft. Journal of Materials Processing Technology 63, 384−389.

Bakare, F.O., Åkesson, D., Skrifvars, M., Bashir, T., Ingman, P., Srivastava, R., 2014. Synthesis and characterization of unsaturated lactic acid based thermoset bio-resins. European Polymer Journal 67 (article in press).

Baker, A., Dutton, S., Kelly, D., 2004. Composites Materials for Aircraft Structures. AIAA Education Series, Reston.

Bhatnagar, T., Ramakrishnan, N., Kaik, N.K., Komanduri, R., 1995. On the machining of fiber reinforced plastic (FRP) composite laminates. International Journal of Machine Tools and Manufacture 35 (5), 701−708.

Bledzki, A.K., Sperber, V.E., Faruk, O., 2002. Rapra review reports. Experts Overviews Covering the Science and Technology of Rubber Plastics 13 (8).

Botelho, E.C., Rezende, M.C., 2000. O uso de Compósitos Estruturais na Indústria Aeroespacial. Polímeros: Ciência e Tecnologia 10 (2), E4−E10.

Botelho, E.C., Scherbakoff, N., Rezende, M.C., Kawamoto, A.M., Sciamareli, J., 2001. Synthesis of polyamide 6/6 by interfacial polycondensation with the simultaneous impregnation of carbon fibre. Macromolecules 34 (10), 3367−3374.

Botelho, E.C., Rezende, M.C., Nogueira, C.L., 2002. Monitoring of nylon 6.6/carbon fibre composites processing by X-ray diffraction and thermal analysis. Journal of Applied Polymer Science 86, 3114−3121.

Braga, D.F.O., Tavares, S.M.O., da Silva, L.F.M., Moreira, P.M.G.P., de Castro, P.M.S.T., 2014. Advanced design for lightweight structures: review and prospects. Progress in Aerospace Sciences 69, 29−39.

Callus, P.J., Mouritz, A.P., Bannister, M.K., Leong, K.H., 2006. Tensile properties and failure mechanisms of 3D woven GRP composites. Composites Part A 30, 1277−1286.

Castrodeza, E.M., Touça, J.M.R., Ipiña, J.E.P., Bastian, F.L., 2002. Determination of CTODc in fibre metal laminates by ASTM and Schwalbe methods. Materials Research 5, 119−125.

Chowdhury, N., Chiu, W.K., Wang, J., Chang, P., 2015. Static and fatigue testing thin riveted, bonded and hybrid carbon fiber double lap joints used in aircraft structures. Composite Structures 121, 315−323.

Degallaix, G., Hassaïni, D., Vittecoq, E., 2002. Cyclic shearing behaviour of a unidirectional glass/epoxy composite. International Journal of Fatigue 24, 319−326.

Dursun, T., Soutis, C., 2014. Recent developments in advanced aircraft aluminium alloys. Materials and Design 56, 862−871.

Edson, C., et al., 2008. Hygrothermal effects evaluation using the iosipescu shear test for glare laminates. Journal of the Brazilian Society of Mechanical Sciences and Engineering 30.

Edwards, T., 2008. Composite materials revolutionise aerospace engineering. Ingenia 36, 24−28.

Ferabolia, P., Masini, A., Bonfatti, A., 2007. Advanced composites for the body and chassis of a production high performance car. International Journal of Vehicle Design 44, 233−246.

Fotouhi, M., Saeedifar, M., Sadeghi, S., Najafabadi, M.A., Minak, G., Sadeghi, M., 2015. Investigation of the damage mechanisms for model delamination growth in foam core sandwich composites using acoustic emission. Structural Health Monitoring 14 (3), 265−280.

Goertzen, W.K., Kessler, M.R., 2007. Dynamic mechanical analysis of carbon/epoxy composites for structural pipeline repair. Composites: Part B 38, 1−9.

Gohardani, O., Elola, M.C., Elizetxea, C., 2014. Potential and prospective implementation of carbon nanotubes on next generation aircraft and space vehicles: a review of current and expected applications in aerospace sciences. Progress in Aerospace Sciences 70, 42−64.

Gutowski, T.G., 1997. Advanced Composites Manufacturing, first ed. John Wiley & Sons, New York, USA.

Gutowski, T.G., 1999. Advanced Composites Manufacturing, first ed. John Wiley & Sons, New York, USA.

Hillermeier, R.W., Seferis, J.C., 2001. Interlayer toughening of resin transfer molding composites. Composites Part A 32, 721−729.

Hinrichsen, J., Bautista, C., 2001. The challenge of reducing both airframe weights and manufacturing costs. Air & Space Europe 3, 119−121.

Hou, M., Ye, L., Lee, H.J., Mai, Y.W., 1998. Manufacture of a carbon-fabric-reinforced polyetherimide (CF/PEI) composite material. Composites: Science and Technology 58 (2), 181−190.

Huda, Z., Edi, P., 2013. Materials selection in design of structures and engines of supersonic aircrafts. Materials and Design 46, 552−560.

Hyoungseock, S., Hundley, J., Hahn, H.T., Yang, J., 2010. Numerical simulation of glass-fibre-reinforced aluminium laminates with diverse impact damage. AIAA Journal 48 (3), 676−687.

Katnam, K.B., Da Silva, L.F.M., Young, T.M., 2013. Bonded repair of composite aircraft structures: a review of scientific challenges and opportunities. Progress in Aerospace Science 61, 26−42.

Kawai, M., Hachinohe, A., Takumida, K., Kawase, Y., 2001. Off-axis fatigue behaviour and its damage mechanics modelling for unidirectional fibre-metal hybrid composite: GLARE 2. Composites Part A 32, 13−19.

Kim, J.R., Sharma, S., 2012. The development and comparison of bio-thermoset plastics from epoxidized plant oils. Industrial Crops and Products 36, 485−499.

Koski, K., Siljander, A., Backstronm, M., Liukkonen, S., Juntunen, J., Sarkimo, M., Lahdenpera, K., Tikka, J., Lahtinen, R., 2009. Fatigue, residual strength and non-destructive tests of an aging aircraft's wing detail. International Journal of Fatigue 31, 1089−1094.

Lanxess AG, website. http://lanxess.com/en/corporate/home/.

Lawrence, P., 2009. Meeting the challenge of aviation emissions: an aircraft industry perspective. Technology Analysis and Strategic Management 21, 79−92.

Lee, J.J., 2010. Can we accelerate the improvement of energy efficiency in aircraft systems. Energy Conversion and Management 51, 189−196.

Lee, D.S., Fahey, D.W., Forster, P.M., Newton, P.J., Wit, R.C.N., Li, L., 2009. Aviation and global climate in the 21st century. Atmospheric Environment 43, 3520−3537.

Lessard, L.B., Nemes, J.A., Lizotte, P.L., 1995. Utilization of FEA in the design of composites bicycle frames. Composites 26, 72−74.

LLorca, J., Gonzalez, C., Molina-Aldaregurado, J., Seltzer, R., Sket, F., 2011. Multiscale modelling of composites materials: a roadmap towards virtual testing. Advanced Materials 23, 5130−5147.

Mahashabde, A., Wolfe, P., Ashok, A., Dorbian, C., He, Q., Fan, A., 2011. Assessing the environmental impacts of aircraft noise and emissions. Progress in Aerospace Science 47, 15−52.

Mangalgiri, P.D., 1999. Composite material for aerospace applications. Bulletin of Material Science 22 (3), 656−664.

Matthews, F.L., Rawlings, R.D., 1999. Composite Materials: Engineering and Science, second ed. Woodhead Publishing Limited, Cambridge, England.

McAdam, R., O'Hare, T., Moffett, S., 2008. Collaborative knowledge sharing in composite new products development: an aerospace study. Technovation 28, 245−256.

Mouritz, A., May 2012. Introduction to Aerospace Material, AIAA Education. Woodhead Publishing, ISBN 978-1-85573-946-8.

Mrazova, M., 2013. Advanced composite materials of the future in aerospace industry. INCAS Bulletin. ISSN: 2066-8201 5 (3), 139−150.

Naik, N.K., Chandra Sekher, Y., Meduri, S., 2000. Damage in woven-fabric composites subjected to low-velocity impact. Composite Science and Technology 60, 731−744.

Noor, A.K. (Ed.), 1998. Structures Technology, Historical Perspective and Evolution. AIAA, Reston, VA.

Noor, A.K., Venneri, S.L., 1997. Future aeronautical and space systems. Progressing Astronautics and Aeronautics 172, 1−5.

Noor, A.K., Venneri, S.L., Paul, D.B., Hopkins, M.A., 2000. Structures technology for future aerospace systems. Computers and Structures 74, 507−519.

Nurhaniza, M., Ariffin, M.K.A, Aidy, A., Mustapha, F., Noraini, A.W., Finite element analysis of composites materials for aerospace applications, IOP Conference Series: Materials Science and Engineering, 11 (1), 1−7.

Oksman, K., Selin, J.F., 2004. Plastics and composites from polylactic acid. Natural Fibres, Plastics and Composites 149−165.

Pardini, L.C., 2000. Tecnologia de Fabricação de Pré-Impregnados Para Compósitos Estruturais Utilizados na Indústria Aeronáutica. Polímeros: Ciência e Tecnologia 10 (2), 100−109.

Peterson, L.A., Londry, K.J., 1986. Finite-element structural analysis: a new tool for bicycle frame design. Bike Tech 5. Retrieved March 15, 2009.

Pevitt, C., Alam, F., 2014. Static computational fluid dynamics simulations around a specialised delta wing. Computers & Fluids 100, 155−164.

Pora, J., 2001. Composite materials in the airbus A380 − from history to future. In: Proceedings of ICCM13, Plenary Lecture, CD-ROM.

Potter, K., 1997. Introduction to Composite Products, first ed. Chapman & Hall, London, UK.

Reddy, M.M., Vivekanandhana, S., Misra, M., Bhatia, S.K., Mohanty, A.K., 2013. Biobased plastics and bionanocomposites: current status and future opportunities. Progress in Polymer Science 38, 1653−1689.

Renton, W.J., 2001. Aerospace structures: where are we headed? International Journal of Solids and Structures 38, 3309−3319.

Reyes, G.V., Cantwell, W.J., 2000. The mechanical properties of fibre-metal laminates based on glass fibre reinforced polypropylene. Composite Science and Technology 60, 1085−1094.

Richardson, M.O.W., Wisheart, M.J., 1996. Review of low-velocity impact properties of composite materials. Composite Part A 27, 1123−1131.

Rikards, R., 2000. Interlaminar fracture behaviour of laminated composites. Computers & Structures 76, 11−18.

Roebroeks, G.H.J.J., 1991. Towards GLARE − The Development of Fatigue Insensitive and Damage Tolerant Aircraft Material (Ph.D. dissemination). Delft University of Technology, Delft.

Sardiwal, S.K., Abdul Sami, Md, Sai Anoop, B.V., Uddin, S.A., Susmita, G., Vooturi, L., May 2014. CFD simulation and experimental study of winglets at low subsonic flow. International Journal of Engineering Research and Applications 4 (5), 184−189. www.ijera.com (Version 7). ISSN: 2248-9622.

Schaff, J.R., Davidson, B., 1997. Life prediction methodology for composites structures. Part I − Constant amplitude and two-stress level fatigue. Journal of Composite Material 31, 128−157.

Soutis, C., 2005. Carbon fibre reinforced plastic in aircraft construction. Materials Science and Engineering A 412, 171−176.

Sugita, Y., Winkelmann, C., Saponara, V.L., 2010. Environmental and chemical degradation of carbon/epoxy lap joints for aerospace applications, and effects on their mechanical performance. Composites Science and Technology 70, 829−839.

Tarnopol'skii, Y.M., Arnautov, A.K., Kulakov, V.L., 1999. Methods of determination on shear properties of textile composites. Composites Part A 30, 879−886.

Thermally Fused Laminate (TFL) Panels. http://www.surfaceandpanel.com/education/continuing-education/tfl-makes-environmentally-friendly-decorative-panels.

van Rijswijk, K., Brouwer, W.D., Beukers, A., 2003. Application of Natural Fibre Composites in the Development of Rural Societies. Delft University of Technology, FAO Corporate Document Repository, Produced by Department of Agriculture and Consumer Protection, Food and Agriculture Organisation of the United Nations, Rome.

Vlot, A., Gunnink, J.W. (Eds.), 2001. Fibre Metal Laminates − An Introduction. Kluwer Academic Publishers, Dordrecht, The Netherlands.

Volt, Ad., 2001. Glare: History of the Development of a New Aircraft Material. Kluwer Academic Publishing, Dordrecht, The Netherlands. ISBN 1-4020-0124-X.

Wadley, H.N.G., 2006. Multifunctional periodic cellular metals. Philosophical Transactions of the Royal Society A 364, 31−68. http://dx.doi.org/10.1098/rsta.2005.1697. Published online December 2, 2005.

Williams, J.C., Starke Jr., E.A., 2003. Progress in structural materials for aerospace systems. Acta Materialia 51, 5775−5799.

Xu, S., Girouard, N., Schueneman, G., Shofner, M.L., Carson Meredith, J., 2013. Mechanical and thermal properties of waterborne epoxy composites containing cellulose nanocrystals. Polymer 54, 6589−6598.

Ye, L., Lu, Y., Su, Z., Meng, G., 2005. Functionalized composite structures for new generation airframes: a review. Composites Science and Technology 65, 1436−1446.

Zhang, P.Q., Ruan, J.H., Li, W.Z., 2001. Influence of some factors on the damping property of fibre-reinforced epoxy composites at low temperature. Cryogenics 41, 245−253.

Sandwiched composites in aerospace engineering

5

J.P. Nunes [1], J.F. Silva [2]
[1]Minho University, Guimaraes, Portugal; [2]Polytechnic Institute of Porto, Porto, Portugal

5.1 Introduction

One of the biggest challenges to the design engineer in the aircraft and space industries is weight reduction. In these markets, each kilogram costs large amounts of money, and sandwiched composites became one of the most efficient solutions to conjugate the highest bending stiffness and strength-to-weight ratios in structural components (Noor, 2000; Marasco, 2005).

Typical sandwich composites consist of two thin, stiff, high-strength facing skins separated by a thick and light core (see Fig. 5.1). The skins are bonded to the core using structural adhesives strong enough to transfer loads between the two faces. The core acts like an I-beam's web, which means taking the shear loads as well as providing structural rigidity by keeping high-strength facing skins away from the neutral axis where the higher tensile and compressive stresses are developed. Sandwich structures differ from the I-beam ones mainly because they have the web spread over the entire cross-section, which provides much higher torsional rigidity than a concentrated middle-section web may offer in an I-beam (Zenkert, 1995; Mazumdar, 2001).

This chapter will review the main raw materials, manufacturing technologies and design methods applied in sandwich composite structures.
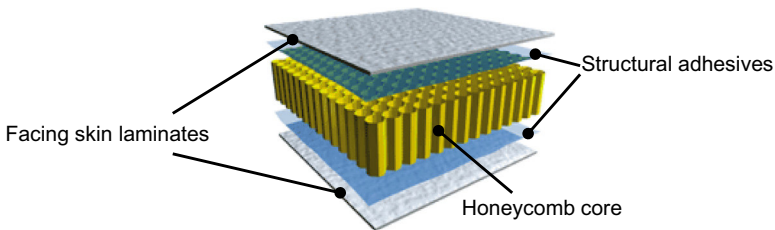
Figure 5.1 Typical sandwich composite panel.
Adapted from Sezgin, F.E., 2011. Mechanical Behavior and Modeling of Honeycomb Cored Laminated Fiber/Polymer Sandwich Structures. Master Thesis, İzmir Institute of Technology, Turkey.

5.2   Sandwiched composite structures

5.2.1   Raw materials

The relevant properties of major raw materials used as facing skinks, cores and adhesives in sandwich composite structures for aircraft and aerospace applications are summarized in this section.

5.2.1.1   Facing skins

Facing skins usually consist of polymer matrix−based fibre-reinforced composite laminates. Typical, such laminates are manufactured by using hand lay-up, autoclave, vacuum-assisted resin infusion, compression moulding, resin transfer moulding (RTM) or automated tape-laying technologies to stack polymer-based preimpregnated materials, or prepregs (unidirectional tapes, woven fabrics etc.) (Bitzer, 1997).

The selection of the matrix must be carefully considered in order to achieve the required surface properties (corrosion, temperature behaviour etc.) and manufacturing type of the composite material. Both thermosetting and thermoplastic resins are commonly used as matrices (see Table 5.1).

Epoxy, unsaturated polyester and vinyl ester are the most widely used thermosetting resins. Epoxies are almost always preferred for advanced applications, such as the aerospace and aircraft markets, where lower weight, high strength and dimensional accuracy are much more critical. Epoxies are also tougher, and they present better behaviour to heat distortion and much less shrinkage than unsaturated polyester and vinyl ester resins. Being less expansive, easy to process and superior in corrosion resistance, unsaturated polyester resins are much better adapted to more commercial and less demanding markets. Vinyl esters usually present higher corrosion behaviour than unsaturated polyesters and may be considered an intermediary solution between the epoxies and unsaturated polyesters.

Currently, thermoplastics are applied as matrix in facing-skin laminates. Compared to brittle thermosets, they present higher toughness, ductility and failure strains; enhance the fatigue, corrosion and thermal behaviours (polyetherimide (PEI) and polyetheretherketone (PEEK)); and can be much more easily recycled and reprocessed. However, it is still very difficult and expensive to manufacture stacking laminates using thermoplastic matrices because their processing requires the use of much higher temperatures and pressures. Heated compression moulding and automated tape-laying processing are the major technologies used to produce thermoplastic matrices in facing skins of sandwich composite structures.

Table 5.1 exhibits the main properties of the polymer matrices mostly used in the facing skins of sandwich structural panels. In addition to the mechanical properties, the maximum service temperature is many times the most relevant criterion for selecting the polymer matrix material to be applied in advanced composite structures for aircraft and aerospace applications.

Carbon fibres, due to their extremely low weight, high stiffness and high tensile strength, are by far the most common to be chosen to reinforce facing skin laminates

Table 5.1 **Main polymers used as matrices in sandwich-facing skins**

Material	Density (Mg/m^3)	Tensile modulus (GPa)	Tensile strength (MPa)	Maximum service temperature (°C)
Thermosetting resins				
Epoxy	1.2−1.4	2.5−5	50−130	80−215
Unsaturated polyester	1.1−1.4	1.6−4.1	35−95	60−150
Vinyl ester	1.1−1.3	3.0−3.5	73−81	60−150
Phenolic	1.1−1.4	2.7−4.1	35−60	70−120
Cyanate esters	1.1−1.3	2.6−3.5	70−125	150−250
Bismaleimide	1.2−1.3	3.9−4.6	120−180	230−320
Thermoplastics				
Polypropylene (PP)	0.9−0.91	1.15−1.57	31.0−41.9	50−135
Polyamide/(nylon) (PA)	1.12−1.42	0.25−3.84	35.2−167.6	75−150
Polycarbonate (PC)	1.20	2.20−2.41	62.7−73.3	115
Polysulphone (PSU)	1.24−1.25	2.51−2.72	60.0−74.7	150
Polyethersulphone (PES)	1.37−1.46	2.44−2.86	68.3−100.6	180
Polyimide (PI)	1.33−1.43	2.10−4.02	72.4−119.4	170
Polyphenylene sulphide (PPS)	1.35	3.28−3.42	48.3−87.3	120−220
Polyetherimide (PEI)	1.26−1.27	2.72−4.02	62.1−150.2	170
Polyether ether ketone (PEEK)	1.3−1.32	3.63	70.3−104.8	120−250

Adapted from Mazumdar, S.K., 2001. Composites Manufacturing: Materials, Product and Process Engineering. CRC Press; Muzzy, J.D., 2000. Thermoplastics − properties. In: Kelly, A., Zweben, C. Comprehensive Composite Materials. Vol. 2. Elsevier Ltd, pp. 57−76; Peters, S.K. (Ed.), 1998. Handbook of Composites, second ed. Chapman & Hall.

of sandwich structures used in aerospace and aircraft applications. Glass and aramid fibres are other reinforcements that may be used as alternatives. Glass fibres may be used in price-competitive parts that require less stiffness due to their much lower cost.

Aramid fibres, which are based on aromatic polyamide precursors and present the lowest density, may be used in facing skin laminates requiring superior wear and impact behaviour due to their excellent toughness and abrasion properties. However, the major limitations to the application of aramid fibres are their much higher price (in comparison to glass fibres), low service temperature, compressive properties and well-known lack of adhesion properties.

The typical properties of the most frequently used reinforcing fibres are shown in Table 5.2. As may be seen, carbon fibres exhibit the highest specific modulus ratio between the tensile modulus and density.

Table 5.2 **Properties of major fibres used as reinforcements in sandwich skins**

Type of fibre	Density (Mg/m^3)	Tensile modulus (E) (GPa)	Tensile strength (σ) (MPa)	Specific modulus (E/ρ) (GPa m^3/Mg)	Specific strength (σ/ρ) (MPa m^3/Mg)	Melting point (°C)	Relative cost
E-glass	2.54	70	3450	27.6	1385	≥1540	Low
S-glass	2.50	86	4500	34.4	1800	≥1540	Moderate
HM-carbon (high modulus)	1.90	400	1800	210.5	947	≥3500	High
HS-carbon (high strength)	1.70	240	2600	141.2	1529	≥3500	High
Boron	2.6	400	3500	153.8	1346	2300	High
Aramid (Kevlar® 29)	1.45	80	2800	55.2	1931	500	Moderate
Aramid (Kevlar® 49)	1.45	130	2800	89.7	1931	500	Moderate

Adapted from Mazumdar, S.K., 2001. Composites Manufacturing: Materials, Product and Process Engineering. CRC Press; Peters, S.K. (Ed.), 1998. Handbook of Composites, second ed. Chapman & Hall.

The prepregs, which present the reinforcing fibres already impregnated with the polymer matrix, are commonly used to manufacture composites of sandwich-facing skins for aircraft and aerospace structural components by using the autoclave, compression-moulding or tape-laying technologies.

Thermosetting matrix prepregs must be kept in refrigerators at low temperature to avoid the resin cure completion. In these prepregs, after impregnating the reinforcing fibres with the thermosetting matrix resin, the cure reaction is suspended by keeping the material at below-freezing temperatures. Due to that and contrarily to thermoplastic matrix prepregs, the thermosetting ones always present a limited shelf life. The typical properties of several prepreg materials that can be applied in the facing-skin sandwich composite structures may be seen in Table 5.3, which shows that prepregs can use both unidirectional fibres and woven fabrics.

5.2.1.2 Sandwich cores

While facing-skin laminates should withstand both in-plane and bending (primary loading) efforts in sandwich structures, the core must carry transverse shear loads and the compressive and crashing efforts placed on the panels. The core must also ensure an adequate transfer of loads between the two facing-skin laminates through the structural adhesives used.

Foam, solid and honeycomb cores are relatively inexpensive and may consist of balsa wood, plywood and an almost infinite selection of open- and closed-cell thermoplastic and thermosetting foams, presenting a wide variety of densities and shear moduli, and rigid, flexible or rubbery behaviour (HexWeb; Beckwith, 2008) (see Figs. 5.2 and 5.3).

Honeycomb architectures are widely used in aerospace, aircraft, transportation and marine structural applications, and the two most common types are hexagonal and square-shaped cell structures. They consist of a series of cells, nested together to form panels similar in appearance to the cross-sectional slice of a beehive. In its expanded form, honeycomb is 90−99% open space. Honeycomb is fire retardant, flexible and lightweight, and it has good impact resistance. It offers the best strength-to-weight ratio of the core materials. Honeycomb cores use both metallic and nonmetallic materials.

Aluminium is almost always the only metal used in the manufacture of honeycomb cores. Nonmetallic honeycomb cores may be made from paper or card, for less load-demanding applications, and from aramid (Nomex®), thermoplastic (polycarbonate, polypropylene, polyetherimide etc.) and other materials, such as glass-reinforced polyimide and phenolic composites Figs. 5.4 and 5.5.

Two main methods are used to manufacture honeycomb cores: expansion and corrugation. Expansion is more common, and it is used for making aluminium and aramid (Nomex®) honeycombs. The process consists of stacking together sheets of material in a block form. Before stacking, adhesive nodelines are printed on the sheets to obtain interrupted adhesive bonding. After curing the stack of sheets, slices of appropriate thickness are cut from the block and then expanded to obtain the desired cell size and shape.

Table 5.3 **Properties of prepregs applied in sandwich skins**

Type of prepreg	Fibre volume fraction (%)	Processing temperature (°C)	Tensile modulus (E) (GPa)	Tensile strength (σ) (MPa)	Maximum service temperature (°C, dry)	Shelf life ($-17.8°C$, months)	Out time at room temperature (days)
Thermosetting matrix prepregs							
Unidirectional carbon (AS4 T300)—epoxy	55−65	120	103−152	1241−2206	85−120	6−12	14−30
Unidirectional carbon (IM7)—epoxy	55−60	120	138−172	2206−3034	120	12	30
Unidirectional S2-glass—epoxy	55−63	120−177	41−55	827−1586	85−120	6	10−30
Unidirectional aramid (Kevlar®)—epoxy	55−60	120−141	69	965	85	6	10−30
Unidirectional carbon (AS4)—bismaleimide	55−62	177−246	103−152	1379−2206	232−316	6	25
Unidirectional carbon (IM7)—bismaleimide	60−66	177−227	138−172	2620−2758	232−316	6−12	25
Unidirectional carbon (IM7)—cyanate ester	55−63	120−177	138−172	690−2723	232	6	10
Unidirectional S2-glass—cyanate ester	55−60	120−177	48	1241	204	6	10
Plain-weave fabric carbon (AS4)—epoxy	57−63	120	55−70	517−855	—	6	10

Plain-weave woven fabric aramid (285K−4HS)−epoxy	60	120−140	30−31	500	85	6	10−30
Plain-weave woven fabric S-2 glass−epoxy	50−55	120	20−34.5	552−600	85	6	10
Plain-weave woven fabric glass (7781-8HS)−phenolic	55	−	20	400	−	−	−
Unidirectional carbon (IM7)−PEEK	57−63	288	179	2827	177	Unlimited	Unlimited
Unidirectional carbon (G34/700)−PA (nylon 6)	55−62	232−260	110	1489	93	Unlimited	Unlimited
Unidirectional aramid/PA (nylon 12)	52	204	47	1413	−	Unlimited	Unlimited
Unidirectional carbon (AS4)−PPS	64	232−271	121	1965	−	Unlimited	Unlimited
Unidirectional carbon (IM7)−polyimide (PI)	62	321−352	172	2620	204	Unlimited	Unlimited
Plain weave fabric carbon HM (T650-35)−polyimide (PI)	58−62	349−388	69−124	896−1069	260−316	12	Unlimited

Figure 5.2 Balsa wood core BALTEK® SBC from Airex AG Industries Balsa Wood Core.
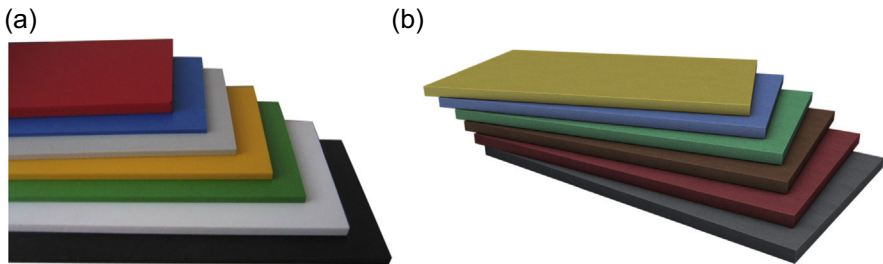
Figure 5.3 Polymer foams: (a) polyvinyl chloride (PVC) foams; (b) polyurethane foams.
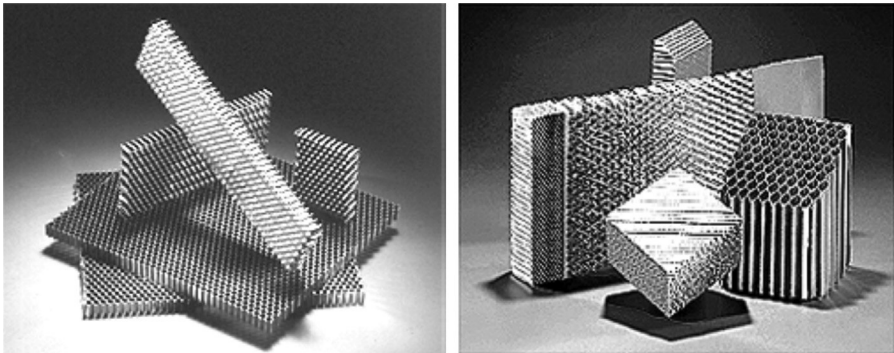
Figure 5.4 Aluminium honeycombs from Alcore Inc. − A Gill Company (Aluminium Honeycombs).

In corrugation, the sheet of material is given a corrugation form by passing through corrugating rolls. The corrugated sheets are then stacked together, bonded and cured. Finally, the honeycomb panels are cut from the block into the desired shape and size without any expansion.

In contrast, the techniques mostly used to manufacture foam cores include gas injection, blowing agents, expandable bead processes and so on. In all these processes,
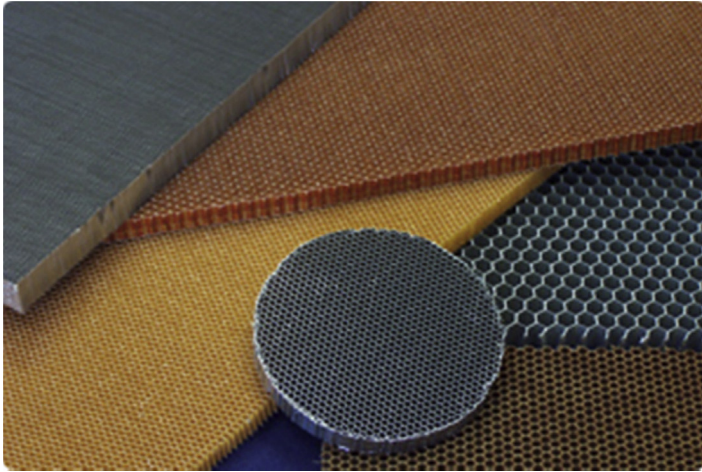
Figure 5.5 Aramid (Nomex®) honeycombs.

one gas or blowing agent is supplied to the thermoplastic or thermosetting resins to decrease its density by forming closed or open gaseous cells. The purpose of the foam is to increase the bending stiffness and thickness of the structural sandwich without increasing its weight.

The main properties of several core materials used in composite sandwich structures are summarized in Table 5.4.

Structural adhesives

The most common structural adhesives used in composite sandwiches are epoxy, acrylic and urethane resins. Typically, they are classified in three categories: (1) two-component mixed adhesives, (2) two-component unmixed adhesives and (3) one-component unmixed adhesives (Mazumdar, 2001).

The majority of epoxy and polyurethane adhesives are two-component mixed adhesives, and the acrylic and anaerobic (urethane methacrylate ester) adhesives fall into the category of two-component unmixed adhesives. The two-component mixed adhesives require the prior mixing of two components before application to the substrate surface. Once the two components are mixed, there is a limited pot life.

In two-component unmixed adhesives, the adhesive is applied on one substrate surface, and an activator, usually in a very small amount, is applied on the other substrate surface. When the two surfaces are put together, the adhesive cures by the reaction between both components.

Finally, one-component unmixed adhesives do not require mixing. Almost all these adhesives consist of a premix of two or more components such as resin, curing agent, fillers and additives. Epoxies, polyurethanes, cyanoacrylates and hot-melt, light-curable and solvent-based adhesives are examples of this type of structural adhesive.

Table 5.5 summarizes some of the main guidelines to allow selecting the appropriate adhesive to be used on a sandwich composite panel for a specific application.

Table 5.4 Properties of core materials used in sandwich composites

Honeycomb density and cell size		Compressive properties		Plate shear behaviour			
Density	Cell size[a]	Stabilized		Length direction		With direction	
Kg/m^3	mm	Strength MPa	Modulus MPa	Strength MPa	Modulus MPa	Strength MPa	Modulus MPa
3003 Aluminium							
29	19	0.9	165	0.65	110	0.4	55
37	9	1.4	240	0.8	190	0.45	90
42	13	1.5	275	0.9	220	0.5	100
54	6	2.5	540	1.4	260	0.85	130
59	9	2.6	630	1.45	280	0.9	140
83	6	4.6	1000	2.4	440	1.5	220
5052 Aluminium							
37	6	1.35	310	0.96	220	0.58	112
50	5	2.3	517	1.45	310	0.9	152
54	6	2.6	620	1.6	345	1.1	166
72	3	4.2	1034	2.3	483	1.5	214
83	6	5.2	1310	2.8	565	1.8	245
127	6	10.0	2345	4.8	896	2.9	364
130	3	11.0	2414	5.0	930	3.0	372

5056 Aluminium

37	6	1.8	400	1.2	220	0.7	103
50	3	2.4	669	1.7	310	1.1	138
50	5	2.8	669	1.8	310	1.0	138
72	3	4.7	1275	3.0	483	1.7	193

Aramid HRH10 Nomex®

29	3	0.9	60	0.5	25	0.35	17.0
32	5	1.2	75	0.7	29	0.4	19.0
32	13	1.0	75	0.75	30	0.35	19.0
48	3	2.4	138	1.25	40	0.73	25.0
48	5	2.4	140	1.2	40	0.7	25.0
64	3	3.9	190	2.0	63	1.0	35.0
64	6	5.0	190	1.55	55	0.86	33.0
80	3	5.3	250	2.25	72	1.2	40.0
96	3	7.7	400	2.6	85	1.5	50.0
123	3	11.5	500	3.0	100	1.9	60.0
144	3	15	600	3.5	115	1.9	60.0
29	5 OX	1.0	50	0.4	14	0.4	21.0
48	5 OX	2.9	120	0.8	20	0.85	35.0

Polycarbonate (PC)

127	3	4.8	379	–	–	–	–
48	6	0.8	103	–	–	–	–

Continued

Table 5.4 **Continued**

Honeycomb density and cell size		Compressive properties		Plate shear behaviour			
Density	Cell size[a]	Stabilized		Length direction		With direction	
Kg/m³	mm	Strength MPa	Modulus MPa	Strength MPa	Modulus MPa	Strength MPa	Modulus MPa
Polyetherimide (PEI)							
60−110	−	0.8−16	160−290	0.8−1.4	18−30	0.8−1.4	18−30
Glass-reinforced polyimide							
128	5	9.0	869	−	−	−	−
Glass-reinforced phenolic							
64.1	5	3.3	−	1.45	79.3	0.76	34.5
88	5	5.2−6.5	655	2.55	134.5	1.31	58.6
56.1	6	2.8	−	1.2	62	0.69	24
72	6	3.9	−	1.7	96.5	0.97	41.4
Paper honeycomb							
80	6	2.8	−	1.3	208	0.57	45
35	12.7	0.97	−	0.54	82	0.28	30.3
thead1Phenolic foam (Gillfoam®)							
112	−	1.3	−	0.71	24.8	0.71	24.8
160	−	2.3	−	1.1	44.1	1.1	44.1
288	−	8.7	−	2.2	65.5	2.2	65.5

Polyurethane foam

32	—	0.19	—	0.14	1.6	0.14	1.6
64	—	0.55	—	0.33	5.2	0.33	5.2
96	—	0.97	—	0.62	10.3	0.62	10.3
320	—	5.9	—	3.1	103	3.1	103
PVC foam, closed cell							
56	—	0.76	—	0.53	12.4	0.53	12.4
99	—	1.4	—	0.83	15.2	0.83	15.2
400	—	5.8	—	4.5	108	4.5	108
Balsa wood end grain							
96	—	5.2	—	0.97	110	0.97	110
152	—	10.3	—	1.5	193	1.5	193
250	—	26.6	—	4.9	312	4.9	312
Polystyrene (PS) foam							
30−60	—	0.3−0.9	—	0.25−0.60	4.5−20	0.25−0.60	4.5−20
Polymethacrylimide (PMI) foam							
30−300	—	0.8−16	—	0.8−7.5	19−290	0.8−7.5	19−290
Epoxy foam							
80−320	—	0.62−7.4	—	0.45−5.2	—	0.45−5.2	—
Carbon−graphite foam							
30−560	—	0.2−60	—	0.05−3.9	—	0.05−3.9	—

Table 5.5 Adhesive selection guidelines

Characteristics	Standard epoxies	Urethane	Acrylic	Silicones	Polyolefins (vinylics)
Adhesive type[a]	L1, L2, F	L, W, HM	L1, L2, W	L1, L2	F
Cure requirement	Heat, ambient	Heat, ambient	Heat, ambient	Heat, ambient	Hot melt
Curing speed	Poor	Very good	Best	Fair	Very good
Substrate flexibility	Very good	Very good	Good	Good	Fair
Shear strength	Best	Fair	Good	Poor	Poor
Peel strength	Poor to fair	Very good	Good	Very good	Fair
Impact resistance	Fair	Very good	Fair	Best	Fair
Humidity behaviour	Poor	Fair	Fair	Best	Fair
Chemical resistance	Very good	Fair	Fair	Fair	Good
Temperature resistance	Fair	Fair	Fair	Good	Poor
Gap filling	Fair	Very good	Very good	Best	Fair
Storage (months)	6	6	6	6	12

[a]Adhesive type: L1 = Liquid one part; L2 = Liquid two part; F = Film; W = Waterborne; HM = Hot melt.
Adapted from Mazumdar, S.K., 2001. Composites Manufacturing: Materials, Product and Process Engineering. CRC Press.

5.2.2 Production methods

As mentioned in Section 5.2.1, expansion and corrugation as well as gas injection, blowing agents and expandable bead processes in the case of foamed materials are the most commonly used processes to manufacture sandwich cores.

Concerning the production of final structural sandwich composite parts, there are two main possibilities: the conventional manufacturing of a composite sandwich is achieved by adhesive joining separately prepared skins to cores. The joining process during sandwich fabrication can require strict quality control. The joining process can be eliminated when the sandwich structures are manufactured by a co-cure method inside a mould. With this method, the sandwich panel adhesive and composite materials are cured simultaneously.

The most widely used production technologies include: vacuum bagging and autoclave, liquid moulding technologies (RTM, structural reaction injection moulding (S-RIM) and infusion), compression moulding, filament winding, wet lay-up and adhesive bonding. From an economical point of view, the continuous lamination manufacturing process is naturally preferable.

5.2.2.1   Liquid moulding technologies

The liquid moulding technologies include RTM, S-RIM and vacuum-injection moulding technologies, also known as infusion technologies. All these technologies are based on placing the reinforcements in the mould without any resin that is infused into the reinforcement fabrics by using pressure or vacuum. Using closed moulds, the liquid moulding technologies avoid much of closed moulds' styrene emissions problems and are suitable for producing complex shapes. In RTM, the reinforcement fabrics or mats, core materials and eventual inserts are conveniently placed in the mould that is then closed. Afterwards, the resin system is pressurized, using an injection machine that pumps and mixes in the right proportions the resin and catalysts, until full impregnation is obtained (see Fig. 5.6). The impregnation time must be lower than the resin gel-time. RTM relies on the mould–clamping structure being stiff enough to withstand the pressure of the injected resin without opening or distorting the mould. This aspect of the process can become problematic if large-scale components are moulded, with tooling sometimes becoming uneconomic simply due to its handling and clamping requirements.

Vacuum infusion (Fig. 5.7) is a wet lay-up process that is typically used to manufacture composite laminates where reinforcements are impregnated by thermosetting liquid resins. The resin sucked by vacuum is introduced into the mould, being also the bag compacted down against the laminate.

First, the reinforcement fabric layers and core are dried, laid up and precisely positioned in the mould. This may be performed manually or by automation (using robots). Next, when the resin is sucked into the mould, as the laminate is already compacted there is no room for excess resin. As very high resin-to-fibre ratios are obtained in the vacuum infusion process, high mechanical properties are usually obtained in the final composite laminate. Vacuum infusion is suitable for moulding very large structures and is considered a low-volume moulding process.

The mould may be gel-coated in the traditional fashion. After the gel coat cures, the dry reinforcement is positioned in the mould. This includes all the plies of the laminate
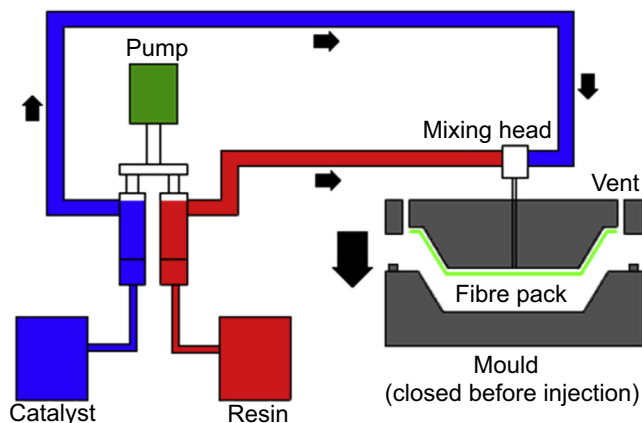
Figure 5.6 Resin transfer moulding (RTM) (Advanced Composite Manufacturing Centre).
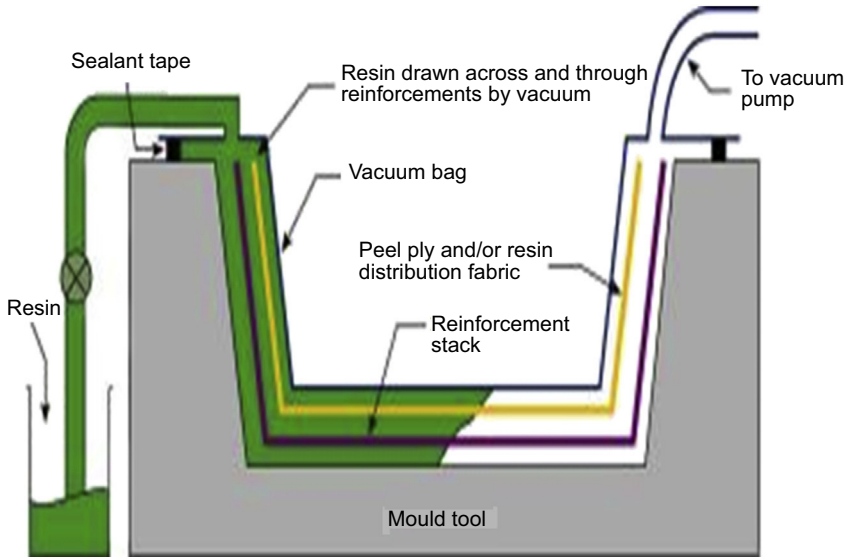
Figure 5.7 Vacuum infusion (van Paepegem).

and core material if required. A perforated release film is placed over the dry reinforce-
ment. Next, a flow medium consisting of a coarse mesh or a 'crinkle' ply is positioned,
and perforated tubing is positioned as a manifold to distribute resin across the laminate.
The vacuum bag is then positioned and sealed at the mould perimeter. A tube is con-
nected between the vacuum bag and the resin container. A vacuum is applied to consol-
idate the laminate, and the resin is pulled into the mould. In RTM and vacuum injection
moulding, conventional resin systems also used in the wet lay-up process are used. In
contrast, S-RIM employs highly reactive resins that are mixed right before injection.
Also, RTM and S-RIM technologies use matched moulds, whereas vacuum infusion
employs a one-side mould that can sometimes be seen as a modified version of the
wet lay-up technology with the mould covered by a vacuum bag to reduce the composite
voids content. The filling of resin time of RTM and vacuum infusion is in the range of a
few minutes to a few hours, enabling the production of large components before
increasing resin viscosity prohibits further impregnation. In the S-RIM technology,
the resin filling time is usually less than a minute due to the much higher resin reactivity,
meaning that only smaller components than those used with the other two processes can
be produced. The component extraction time (demoulding) can vary from a few minutes
to hours in the case of RTM, a few hours if vacuum infusion is considered and only a
few minutes in the case of S-RIM. In S-RIM, the two-component resin is mixed right
before injection in an impingement-mixing nozzle using dedicated pumps. In all pro-
cesses, multiple inlet points may be necessary for large-component production.

5.2.2.2 Bagging and autoclaving

High-performance composite materials are conventionally processed in autoclaves
which require high capital investment for the equipment. The equipment cost increases
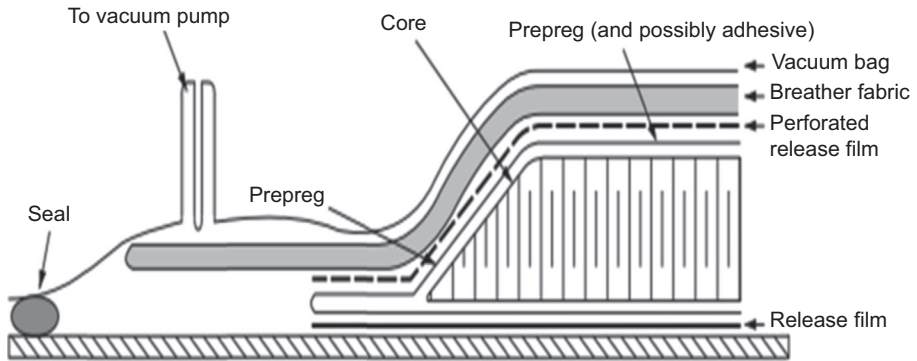
Figure 5.8 Vacuum bag lay-up example (Hexply).

exponentially with the size of the autoclave, which is one of the main constraints on the ability to fabricate large composite structures. Both monolithic laminates and sandwich structures are usually laid up using prepregs. The use of prepregs ensures good impregnation, and resins used in prepregs also tend to have better properties than the ones available for wet lay-up. Sandwich constructions can be manufactured by autoclave or vacuum bag moulding. For autoclave processing, sandwich constructions can usually be laid up and cured as a single-shot process. However, for the vacuum bag curing of large components, it may be necessary to lay up and cure in two or more stages. When using autoclave, the use of excessive pressures can led to eventual core crush.

The vacuum bag technique involves placing and sealing a flexible bag over a composite lay-up (see Fig. 5.8), evacuating all the air from under the bag. The removal of air forces the bag down onto the lay-up with a consolidation pressure of up to 1 atm. The completed assembly, with vacuum still applied, is placed inside an oven or on a heated mould, and the composite is produced after applying an appropriate temperature curing cycle.

Autoclave processing is used for the manufacture of high-quality structural components containing high fibre volume and low void contents. The autoclave technique requires a similar vacuum bag (Fig. 5.8), but the oven is replaced by an autoclave (Fig. 5.9). It allows the application of atmospheric pressure and provides the curing conditions for the composite where the application of vacuum, pressure, heat-up rate and cure temperature are controlled. Typically, high processing pressures are used for thick sections of complex shapes and lower pressures are applied for the production of sandwich structures. The curing cycle can be very long if slow heat-up rates are required to guarantee even temperature distribution on the tooling and composite components.

Manufacturing of sandwich structures made from prepregs may be accomplished in two manners. In some cases, the laminate may be laid directly onto the core in a way similar to that used in wet hand lay-up. Alternatively, previous manufactured skin laminates may be adhesively bonded to the core in a separate process. Sandwich composites manufactured using prepreg lay-up are characterized by good to excellent mechanical properties, low void contents in the laminates skins and consistent laminate quality.
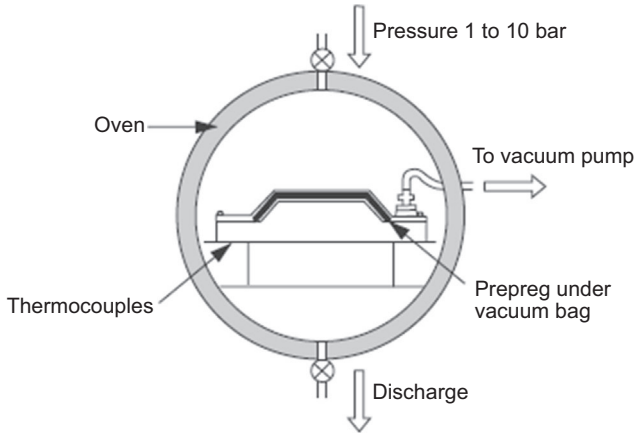
Figure 5.9 Autoclave process (Hexply).

5.2.2.3 Compression moulding

The compression-moulding technology used to manufacture sandwich structures is similar to the one used in the production of monolithic composites. If thermoplastic skins are to be used, the process starts by preheating the skins in an oven and, immediately after, placing them in a cooled mould with the core sandwiched in between. The mould must be closed fast (this requirement is essential) and pressure applied, forcing the skins to bond to the core and allowing a good surface finishing. The core material must withstand the moulding pressure and, if it is of thermoplastic nature, may further enhance bonding since heating of the face sheets will cause the core surface to melt.

This technology can be used to promote the bonding of thermosetting skins to a core panel, obtaining sandwich panels of good quality.

5.2.2.4 Wet lay-up

This is the oldest and one of the most flexible technologies for processing composites and sandwich components with composite. The wet lay-up may be performed either by hand lay-up or spray-up using labour-intensive work. This technology uses a single-side mould, which is first covered by a mould release agent. Usually, a gel coat is deposited directly onto the mould, allowing the laminate to have good environmental resistance and producing a smooth, cosmetically appealing surface. Next, the reinforcements in the form of mats (woven, knitted, stitched or bonded fabrics) are impregnated by hand with resin, with the help of brushed or nip-roller-type impregnators, for forcing the resin into the reinforcements. In the case of spray-up, fibre is chopped in a handheld gun and fed into a spray of catalysed resin directed at the mould. Laminates can cure at atmospheric conditions or with the help of vacuum bagging. The main differences between hand laid-up and sprayed-up composites are due to the differences in labour costs and mechanical properties. The lower labour

costs of spray-up implies that longer series are economically feasible, and the inferior mechanical properties achieved mean that this approach is used more commonly for commodity-type products.

5.2.2.5 Filament winding

Filament winding is a fabrication technique involving wrapping pretensioned, resin-saturated continuous reinforcements around a rotating symmetrical mould (Fig. 5.10). By changing the rotational velocity of the mandrel with the linear velocity of the guiding system, different fibre patterns can be obtained allowing the control of specific mechanical properties of the obtained composite structure. Recent filament winding equipment always uses computerized numerical control systems that can control up to six axes. Existing software can adjust all settings such as wind angle, fibre bandwidth and desired laminate thickness.

The filament winding of a sandwich structure, usually a circular pipe, begins by producing the filament-wound inner shell face and then stopping the equipment until a flexible or prefoamed core is applied to the produced skin. Then, the machine is restarted and the outer skin is produced.

5.2.2.6 Adhesive bonding

Using the bonding technique, adhesive layers are interleaved between the faces and the core, and the whole stack is subjected to a temperature and pressure cycle, depending on the adhesive resin used. For demanding applications, pressure is applied using vacuum bagging and autoclave, whereas for current applications only vacuum bagging will be enough. Hydraulic presses can also be used for pressure application in adhesive bonding. Laminate skins for bonding are normally produced using 'peel ply' fabric that is removed before bonding, ensuring a proper rugged surface. Also, it is normally necessary to prepare the surfaces to be bonded. Depending on the substrate, surfaces are prepared by one of the following procedures: (1) degrease; (2) degrease, abrade and remove loose particles; or (3) degrease and chemically pretreat. The processing sequence normally involves removing peel ply from the composite skins, preparing surfaces, applying adhesive film and placing the core material between the skins.
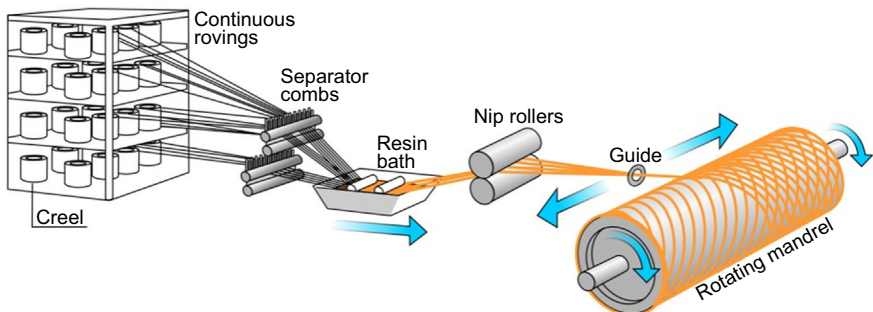
Figure 5.10 Filament winding (Nuplex).

Then, using vacuum bagging and an autoclave or an oven, apply the specified vacuum, pressure and temperature cycles. The adhesives can be used in film or liquid form, depending on the application, and are usually epoxy or polyurethane. Sandwich components manufacturing through adhesive bonding is characterized by good to excellent mechanical properties.

5.2.2.7   Continuous lamination

Continuous lamination is generally used for the large-scale manufacture of long production runs with a standard design. Sandwich panels made by continuous lamination are manufactured by bonding steel, aluminium or composite foil skins to polyurethane or polystyrene foam, mineral wool or other insulating cores. Recent continuous panel laminators or double-belt laminators have been designed to increase production speed, allowing heating and cooling of the material while at the same time subjecting it to a specified pressure. Two rolls of face sheets are first uncoiled and guided in between the belts of the press. The core is then inserted between the face sheets together with the adhesive layer. The bonding of the skins to the core material is achieved by applying convenient heating and cooling temperatures and pressure values. At the final stage, the panels will be cut at the desired lengths. The core materials can be fed in discrete blocks or, alternatively, in a continuous way by placing in situ core foam in between the skins, through injection and subsequent expansion. Another possibility is to sandwich a thermoplastic polymer film containing a foaming agent between the skins. As the polymer film melts, the foaming agent is free to expand, filling the gap between the face skins with a core foam.

5.2.3   Composite sandwich properties

Tables 5.6−5.9 present main basic, physical and mechanical properties of selected composite sandwich panels used by some major aircraft industries. Some of the characteristics presented were determined by those industries' own testing methods.

5.2.4   Major applications

Table 5.10 presents typical applications of sandwich composites in major markets.

Figs. 5.11−5.13 also show examples of applications of sandwich composites in satellites and the aerospace, aeronautical and naval industries. In satellites, Fig. 5.11 presents: (1) solar panels: carbon−epoxy prepregs as skins, aluminium honeycomb and film adhesive; (2) antenna reflectors: aramid−epoxy and carbon−cyanate prepregs in the skins and aramid−aluminium honeycomb; and (3) satellite structure: carbon−epoxy prepreg, aluminium honeycomb and film adhesive.

The following applications in the aerospace industry may be seen in Fig. 5.12(a): (1) carbon−epoxy prepregs, aluminium honeycomb and adhesives in fairings; (2) the external payload carrier assembly (Speltra); (3) carbon−epoxy prepreg in the EPS ring; (4) front skirt; (5) glass−epoxy and nonmetallic honeycomb in the booster capotage;

Table 5.6 **Basic properties of sandwich panels used by Boeing and Douglas aircraft**

Product	Core type and density	Adhesive	Facing skins	Panel thickness (mm)	Panel weight (N/m²)	Flexural strength supported in 2 points (508 mm span)		Climbing drum peel strength
						Test method: military standard 401B		
						Ultimate load (N)	Deflection at 4362.2 N (mm)	(mm N/76.2 mm width)
4409 Ty II	3 mm cell; 144.2 kg/m³ aramid honeycomb	Modified phenolic	0.25 mm unidirectional carbon–phenolic	10.2	26.3	15,093.3	10.3	24,043.6
4409 Ty III	3 mm cell; 80.1 kg/m³ aramid honeycomb	Modified phenolic	0.25 mm unidirectional carbon–phenolic	10.2	21.1	11,734.4	10.6	24,486.7
4417 Ty I	3 mm cell; 80.1 kg/m³ aramid honeycomb	Modified epoxy	0.38 mm unidirectional FRP–epoxy	10.1	24.7	11,908.9	20.2	35,456.1
4417 Ty II	3 mm cell; 144.2 kg/m³ aramid honeycomb	Modified epoxy	0.38 mm unidirectional FRP–epoxy	10.1	30.1	12,694.1	20.1	38,780.2
4417 Ty III	3 mm cell; 144.2 kg/m³ aramid honeycomb	Modified epoxy	0.56 mm unidirectional FRP–epoxy	10.2	36.3	16,663.7	13.7	34,348.2
4417 Ty IV	3 mm cell; 80.1 kg/m³ aramid honeycomb	Modified epoxy	0.38 mm unidirectional FRP–epoxy	16.7	30.5	22,596.3	6.6	35,456.1
4509 Ty 1	3 mm cell; 128.2 kg/m³ aramid honeycomb	Modified phenolic	0.30 mm unidirectional carbon–phenolic	10.0	25.0	21,811.1	6.7	28,253.9

Continued

Table 5.6 Continued

Product	Core type and density	Adhesive	Facing skins	Panel thickness (mm)	Panel weight (N/m^2)	Flexural strength supported in 2 points (508 mm span)		Climbing drum peel strength
						Test method: military standard 401B		
						Ultimate load (N)	Deflection at 4362.2 N (mm)	(mm N/76.2 mm width)
4509 Ty 2 aramid	3 mm cell; 64.1 kg/m^3 aramid honeycomb	Modified phenolic	0.30 mm unidirectional carbon–phenolic	9.9	20.0	18,932.0	7.4	26,148.8
5424 Ty I	3 mm cell; 97.7 kg/m^3, 5052 alloy, aluminium honeycomb	Modified epoxy	0.38 mm unidirectional FRP–epoxy	10.2	26.0	12,345.1	18.8	44,320.2
5424 Ty II	3 mm cell; 136.2 kg/m^3 5052 alloy, aluminium honeycomb	Modified epoxy	0.38 mm unidirectional FRP–epoxy	10.2	30.3	13,697.4	17.2	46,536.1
5433C	Fire-retardant epoxy woven FRP	Epoxy	Top face: 0.41 mm aluminium alloy 2024T3 Bottom face: 0.51 mm aluminium alloy 2024T3	1.5	35.9	NR	NR	44,320.2

FRP, fibreglass-reinforced plastic; *NR*, not required by customer specification.
Adapted from Doorway, M.C.G., 1997. Simplified Sandwich Panel Design. 34 (3), M.C. Gill Corp.

Table 5.7 **Basic properties of sandwich panels used by Airbus Industry aircraft**

Product	Core type and density	Adhesive	Facing skins	Panel thickness (mm)	Panel weight (N/m²)	Distributed surface load (N) Airbus Industrie TL 63/5000/79 (Gillfab 4105) and DAA/MBB/A1 5360 M16 000100 (Gillfab 4205, 4322 and 4323)			Concentrated load without permanent deformation (N)	Impact strength (N m)
						Load at 10.9 mm deflection	Load at 17.0 mm deflection	Ultimate load		
4105	4.8 mm cell; 96.1 kg/m³ aramid honeycomb	Modified epoxy	0.64 mm woven FRP epoxy	9.5	32.4	NA	NA	218,111	>8724.4	NA
4205	4.8 mm cell; 96.1 kg/m³ aramid honeycomb	Modified epoxy	0.64 mm fibreglass fabric−carbon fibre	9.5	33.8	43,622	76,339	196,300	>8375.5	NA
4322	4.8 mm cell; 96.1 kg/m³ aramid honeycomb	Modified epoxy	Top face: 0.61 mm fibreglass−phenolic Bottom face: 0.56 mm fibreglass−phenolic	9.5	33.4	NA	>61682	165,764	>8724.4	93.1
4323	4.8 mm cell; 96.1 kg/m³ aramid honeycomb	Modified epoxy	Top face: 0.76 mm fibreglass−phenolic Bottom face: 0.51 mm fibreglass−phenolic	12.6	36.2	NA	>106176	242,845	>8724.4	239.3

FRP, fibreglass-reinforced plastic; *NA*, not applicable.
Adapted from Doorway, M.C.G., 1997. Simplified Sandwich Panel Design. 34 (3), M.C. Gill Corp.

Table 5.8 **Physical and mechanical properties of sandwich panels used by Boeing and Douglas aircraft**

	Stabilized compressive strength (MPa)	In-plane shear strength (MPa)	2 lb Gardner impact (N mm)	Insert shear strength (N)	Roller cart (number of cycles to failure)	30-day 97% humidity soak		
						508 mm flexure strength (N)	Climbing drum peel (N mm)	
	Testing methods							
Product	Military standard 401B	BMS 4-17D	Model 11K3	Shur-Lok 5107-A3	Military standard and DAC Dwg 7954400	Military standard 401B		Specifications
4409 Ty II	13.40	2.47	21,827.7	62,423	120076/36781	13,173.9	19,994.1	Boeing BMS 4-20
4409 Ty III	5.61	2.34	22,160.0	57,669	82,300	12,170.6	21,052.0	Boeing BMS 4-20
4417 Ty I	5.83	2.65	145,148.3	80,221	83,964	10,643.8	43,212.0	Boeing BMS 4-17
4417 Ty II	14.00	3.06	119,664.2	85,368	121020/38427	10,992.8	57,616.1	Boeing BMS 4-17
4417 Ty III	15.42	2.63	183,928.5	84,234	120001/35083	12,999.4	54292.2	Boeing BMS 4-17
4417 Ty IV	5.32	2.81	140,716.3	71,986	83,804	20,066.2	55,400.2	Boeing BMS 4-17

4509 Ty 1	10.88	2.84	28,808.2	57974[a]	111,002	21,025.9	28,586.4	Douglas DAC Dwg 7954400, ty 1
4509 Ty 2	3.96	2.79	26,592.0	49380[a]	NR	17,885.1	24,597.6	Douglas DAC Dwg 7954400, ty 1
5424 Ty I	7.49	3.14	122,988.3	85,150	83570 (no failure)	10,731.1	55,400.2	Boeing BMS 4–23
5424 Ty II	12.25	3.11	190,576.5	88,248	121652 (no failure)	11,647.1	592,824.6	Boeing BMS 4–23
5433C	NR	NR	34,348	NR	NR	NR	NR	Boeing BMS 7–326 ty VII, CI 2/1

FRP, fibreglass-reinforced plastic; *NR*, not required by customer specification.
[a]Called insert membrane.
Adapted from Doorway, M.C.G., 1997. Simplified Sandwich Panel Design. 34 (3), M.C. Gill Corp.

Table 5.9 Physical and mechanical properties of sandwich panels used by Airbus Industry aircraft

Product	Compressive fatigue 2×10^6 cycles	In-plane panel shear (N)	Building fatigue lower limit 1483.2 N and upper limit 14700.7 N 2×10^6 cycles	Roller cart strength (test cycles to failure)	Insert pull-out (N)	Flammability	Smoke D, flaming 240 s nonflaming 240 s	Toxic gas emission	Heat release	Oil burner
						Testing methods				
	Airbus Industrie TL 53/5000/79 (Gillfab 4105) and DAA/MBB/A1 5360 M1B 000100 (Gillfab 4205, 4322 and 4323)					DAA/ATS 1000.001			Far 25.853/FAR 26.855	
4105	NA	29,000	NA	5583.6 N−120000 6892.3 N−35000	74,157.7	PASS	NA	NA	NA	NA
4205	PASS	24,100	PASS	5583.6 N−120000 6892.3 N−35000	100,331.0	PASS	34 2	PASS	44.4/44.3	NA
4322	NA	NA	NA	NA	74,157.7	PASS	60 3	PASS	45/45	PASS
4323	NA	NA	NA	NA	73,241.6	PASS	83 7	PASS	43.6/37	PASS

FRP, fibreglass-reinforced plastic; *NA*, not applicable.
Adapted from Doorway, M.C.G., 1997. Simplified Sandwich Panel Design. 34 (3), M.C. Gill Corp.

Table 5.10 Typical sandwich composite applications by industry

Industry				
Aircraft	**Aerospace**	**Electronics**	**Transportation**	**Construction**
Floor panels	Capsule panels	Electronic radome construction	Cargo pallets	Architectural curtain walls
Interior walls	Ablative shields for nose cones	Large antenna or disk reflectors	Shipping containers	Floor panels
Food-handling galley assemblies	Instrumentation enclosures and shelves	Military electronic instrumentation shelters	Refrigeration panels	Partitions and divider panels
Wing control surfaces			Rapid transit floor panels	
Passenger storage racks	Bulkhead panels	Shipboard electronic deck shelters	Special automobile bodies	Expandable hospital shelters
Thrust deflector assemblies	Space satellites			
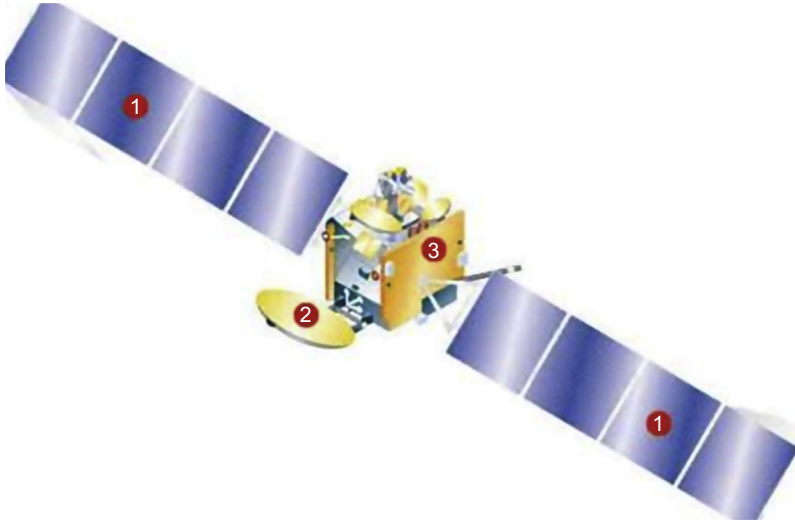
Figure 5.11 Sandwich composites applied in satellites.
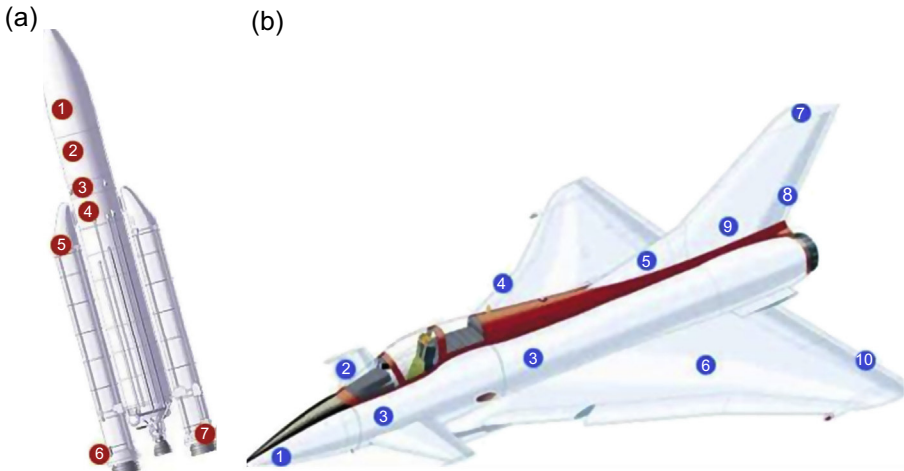
Figure 5.12 Aerospace and aeronautical applications: (a) aerospace; (b) aeronautical.

(6) carbon–epoxy filament winding in the yoke; and (7) carbon prepreg and high-temperature-resistant glass fabric in the heat shield.

Fig. 5.12(b) shows the following for the aeronautical industry: (1) epoxy or BMI prepregs and woven preforms (socks) applied in the radar transparent radomes; (2) carbon–epoxy prepregs in the foreplane canard wings; (3) carbon–epoxy prepregs, nonmetallic honeycomb cores and adhesives in the fuselage panel sections; (4) carbon
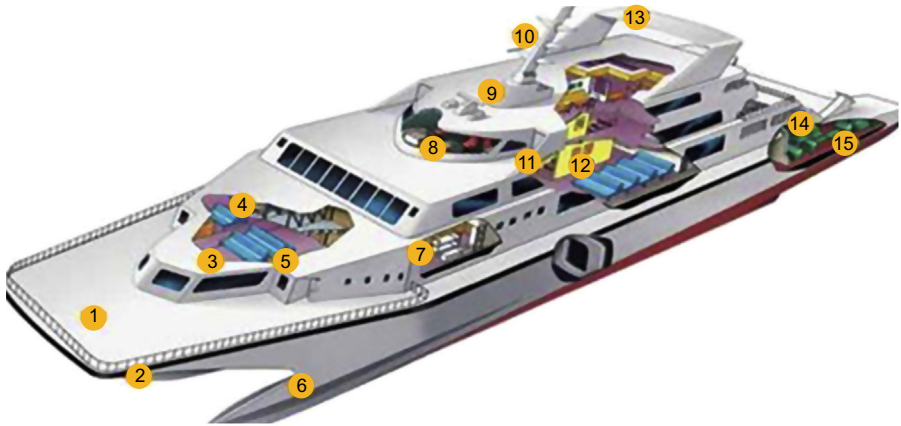
Figure 5.13 Application of sandwich composites in naval construction.

and glass—epoxy prepregs applied in the leading-edge devices; (5) fin fairings; (6) wings and ribs; (7) epoxy—quartz prepregs in fin tip; (8) rudder; (9) fin; and (10) carbon and glass—epoxy prepregs, honeycomb core and adhesives applied in the flying control surfaces.

Finally, some applications where sandwich composites are typically applied in naval construction are shown in Fig. 5.13, such as: (1) decking; (2, 6) hull skin structures; (3) lightweight floor structures; (4) suspended ceilings; (5) interior furnishings; (7) accommodation cabin units; (8) bridge deck consoles; (9) weather shields; (10) communications equipment; (11) companionway stairs; (12) partitions; (13) lightweight superstructures; (14) products for fire, smoke, and toxicity (FST) and sound attenuation in the engine room; and (15) drive shafts and couplings.

5.3 Design of sandwich structures

The suitable design of sandwich structures is one of the most important steps to enhance and ensure their best performance in service. The major analytical equations and methods that should be used to design composite sandwich structures and ensure they withstand the most relevant predictable service loadings will be addressed, presented and discussed in this chapter. As in many other cases, the design of composite sandwiches with complex geometry or submitted to combined and/or much more complex loading situations may require the application of computer-aided engineering software programmes (eg, Abaqus® or Ansys®). These software programmes allow predicting and simulating the mechanical behaviour of the structures in conditions of service by using advanced numerical methods, such as finite element analysis (FEA) or finite difference method (FDM).

This section introduces briefly some of the more relevant and simple loading situations to be considered in the mechanical design.

5.3.1 Modes of failure under flexure

Sandwich composites are primarily used as structural beams submitted to bending and must ensure they get necessary stiffness to avoid excessive deformations in load conditions. Thus, first of all, designers must verify that maximum admissible deformations (deflections) are never reached in the sandwich structure in the worst loading service conditions (Fig. 5.14). Typically, such a situation depends only on the load conditions and the sandwich panel bending and shear stiffness (HexWeb; Doorway, 1997).

Another basic design confirmation concerns the verification that both composite facing-skin laminates (see the first case in Table 5.11) and sandwich core are able to withstand the tensile, compressive and shear stresses induced in the worst service loading conditions. In the same conditions, the skin-to-core adhesive also must be capable of transferring the developed shear stresses between skin and core.

Table 5.11 summarizes the major mechanical failure modes to be verified by the designer.

In the design sandwich composite structures, two different cases also must be considered: sandwich beams or sandwich plates. In the case of sandwich beams, the width−length ratio must be lower than one-third ($b/L < 1/3$; see Fig. 5.15), and, in contrast, if this ratio is greater than one-third ($b/L \geq 1/3$), the structure must be considered a plate and the more complex and involved plate theory must be used in the calculations.

5.3.1.1 Sandwich composite beams

Consider a sandwich composite beam of span L and width b, submitted to three-point bending with a central load W per unit width in the conditions defined in Fig. 5.15.

Assuming also the same thickness, t, for both composite facing skins and a thickness, c, for the core, that the beam bends in a cylindrical manner with no curvature in the yz plane, the cross-sections remain plane and perpendicular to the longitudinal axis
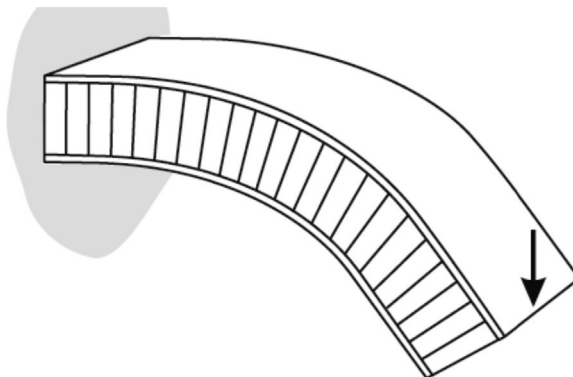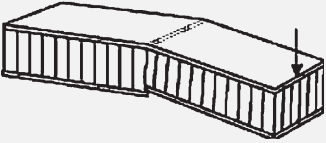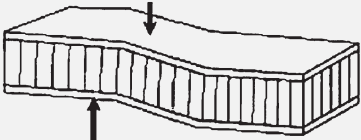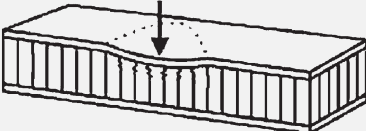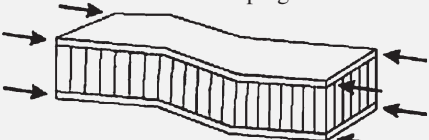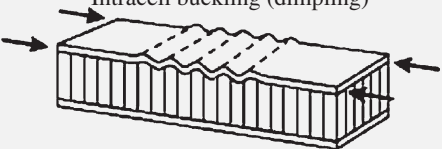
Figure 5.14 Excessive deflection in bending (HexWeb).

Table 5.11 **Major failure modes of sandwich structures**

Facing failure	Insufficient panel thickness, facing thickness or facing strength may result in failure occurring in either the compression or tensile face.
Transverse shear failure	Transverse shear failure is caused when either the shear strength of the core or panel thickness is insufficient.
Local crushing of core	Local crushing of core is caused when compressive strength of the core material is too low.
Panel buckling	Panel (or general) bucking is caused when either the panel thickness or core shear stiffness is too low.
Shear crimping	Shear crimping, which can occur as a consequence of general buckling, is caused when either the shear modulus of the core material or the shear strength of the adhesive is low.
Face wrinkling	Core compression failure (buckling inwards) or adhesive bond failure (buckling outwards) may occur depending on the relative strength of the core in compression and adhesive in flatwise tension.
Intracell buckling (dimpling)	Intracell buckling (applicable to cellular cores only) occurs where the skins or faces are very thin and the cell size is large. This effect may cause failure by propagating across adjacent cells, thereby inducing face wrinkling.

(a)

(b)
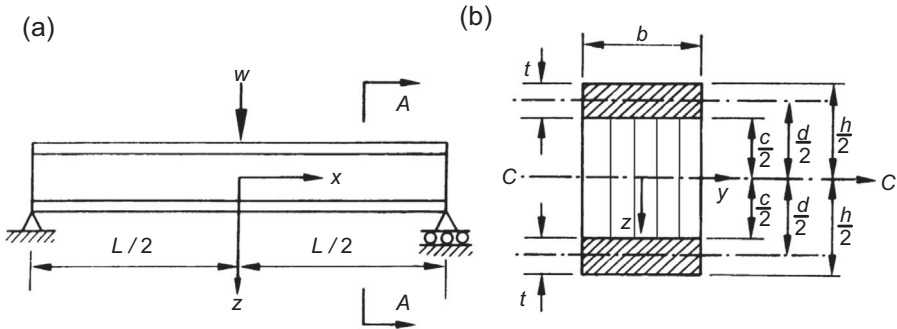
Figure 5.15 Sandwich composite beam submitted to three-point bending: (a) simple supported sandwich beam; (b) sandwich beam cross-section.

and sandwich skins remain firmly bonded to core the flexural stiffness of the sandwich beam, D, may be calculated as:

$$D = \frac{E_s \cdot b \cdot t^3}{6} + \frac{E_s \cdot b \cdot t \cdot d^2}{2} + \frac{E_c \cdot b \cdot c^3}{12} \tag{5.1}$$

where (see also Fig. 5.15):

E_s and E_c are the in-plane Young's moduli of the laminate facing skin and core in the x direction, respectively;
d is the distance between the midplanes of the upper and bottom skins; and
c is the core thickness.

In almost of cases as $\frac{d}{t} > 5.77$ and $\frac{E_s}{E_c} \cdot \frac{t}{c} \cdot \left(\frac{d}{c}\right)^2 > 16.7$, the first and third terms of Eq. [5.1] may be negligible because they amount to less than 1% of the flexural stiffness of the beam, which means it could be calculated by using the following simplified equation:

$$D = \frac{E_s \cdot b \cdot t \cdot d^2}{2} \tag{5.2}$$

The shear stiffness of the sandwich beam, S, is determined by:
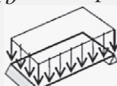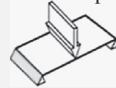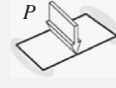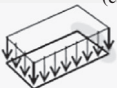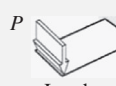
$$S = b \cdot d \cdot G_c \tag{5.3}$$

where G_c is the core shear modulus that must be considered equal, as appropriate, to the core shear modulus in the ribbon, G_L, or transverse, G_W, direction:

$$G_c = G_L \quad \text{or} \quad G_c = G_W \tag{5.4}$$

Table 5.12 shows the most common bending conditions that sandwich composite beams may withstand.

Table 5.12 Values to be used on beams loaded in different bending conditions (HexWeb)

Beam type	Maximum shear force F	Maximum bending moment M	Bending deflection coefficient k_b	Shear deflection coefficient k_s
$P = q\,l\,b$ Simple support Uniform load distribution	$P/2$	$Pl/8$	$5/384$	$1/8$
$P = q\,l\,b$ Both ends fixed Uniform load distribution	$P/2$	$Pl/2$	$1/384$	$1/8$
Simple support Central load	$P/2$	$Pl/4$	$1/48$	$1/4$
Both ends fixed P Central load	$P/2$	$Pl/8$	$1/192$	$1/4$
$P = q\,l\,b$ One end fixed (cantilever) Uniform load distribution	P	$Pl/2$	$1/8$	$1/2$
One end fixed (cantilever) P Load one end	P	Pl	$1/3$	1
$P = (q\,l\,b)/2$ One end fixed (cantilever) Triangular load distribution	P	$Pl/3$	$1/15$	$1/3$

q, the uniformly distributed load.

The maximum deflection in the sandwiched composite beam (Fig. 5.14) may be calculated as:

$$\delta = \frac{k_b \cdot P \cdot L^3}{D} + \frac{k_s \cdot P \cdot L}{S} \qquad\qquad [5.5]$$

where:

k_b and k_s are the deflection coefficients given in Table 5.12 for each bending case;
L is the total sandwich beam length; and
D and S are the sandwich beam bending and shear stiffness, respectively.

The values of the deflection calculated from Eq. [5.5] must be compared with the maximum allowable deflection required in the beam design.

5.3.1.2   Sandwich plates

As was stated in Section 5.3.1, when the ratio between the width, b, and length, a, is equal to or exceeds one-third (see Fig. 5.16), the beam theory must be replaced by the much more complex and involved plate theory.

The present text only presents solutions for the case, shown in Fig. 5.16, of a sandwich composite plate submitted to a uniformly distributed load and supported on all its four sides. In these conditions, some new coefficients and charts will be introduced and provided in the design calculations, such as:

$$\lambda = 1 - \mu^2 \qquad\qquad [5.6]$$

where:

μ is the Poisson's ratio of the facing skin material (in the previous calculations of the beam submitted to the end loading condition, it was assumed that $\lambda = 1$).
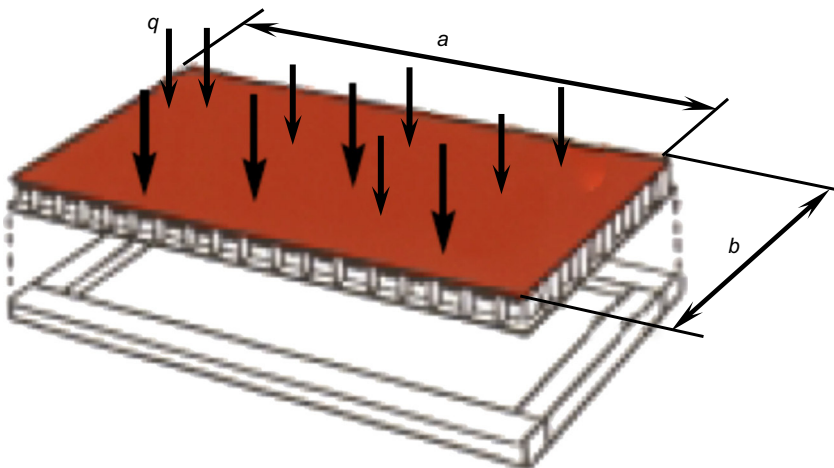
Figure 5.16 Sandwich composite plate simply supported on all four sides.

$$R = \frac{G_{\mathrm{L}}}{G_{\mathrm{W}}} \qquad [5.7]$$

where:

G_{L} and G_{W} are the core shear moduli in the ribbon and transverse directions, respectively; and

$$V = \frac{\pi^2 \cdot E_{\mathrm{S}} \cdot t \cdot d}{2 \cdot b^2 \cdot G_{\mathrm{w}} \cdot \lambda} \qquad [5.8]$$

where (see also Fig. 5.15):

E_{S} is the laminate facing skin's Young's modulus;
t is the facing skin's thickness;
d is the distance between the midplanes of the upper and bottom skins;
b is the plate width;
G_{W} is the core shear modulus in the transverse direction; and
λ is the parameter calculated by Eq. [5.13].

After determining the value of coefficient K_1 from the chart depicted in Fig. 5.17, the total deflection, δ, of the plate submitted to the uniformly distributed load, q, may be calculated by:

$$\delta = \frac{2 \cdot K_1 \cdot q \cdot b^4 \cdot \lambda}{E_{\mathrm{S}} \cdot t \cdot d^2} \qquad [5.9]$$

5.3.2 Skin failure

5.3.2.1 Sandwich beams

The maxima tensile and compressive stresses, σ_{S}, in the facing-skin laminates of the beam may be determined by Eq. [5.10]:

$$\sigma_{\mathrm{S}} = \pm \frac{M}{d \cdot t \cdot b} \qquad [5.10]$$

where:

M is the maximum bending moment the sandwich beam has to withstand. Table 5.12 presents the maximum bending moment to be considered in the most common flexion cases.

The stress calculated from Eq. [5.10] must be compared with the maximum allowable stress that the laminate facing skin can support.

End loading conditions (see Fig. 5.18) may also cause skin failure due to excessive stress, sandwich panel buckling failure (the fourth line of Table 5.11), intracell dimpling or face wrinkling (the last two cases given in Table 5.11).
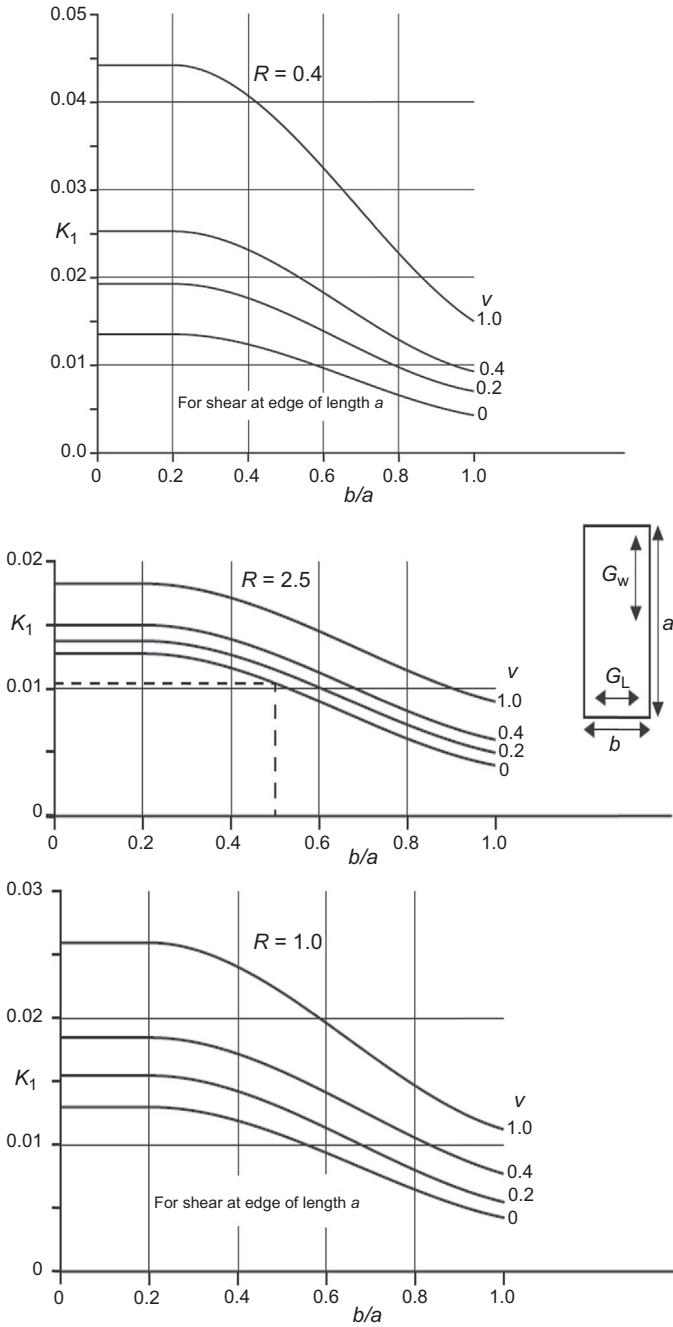
Figure 5.17 Charts for determining the coefficient K_1.
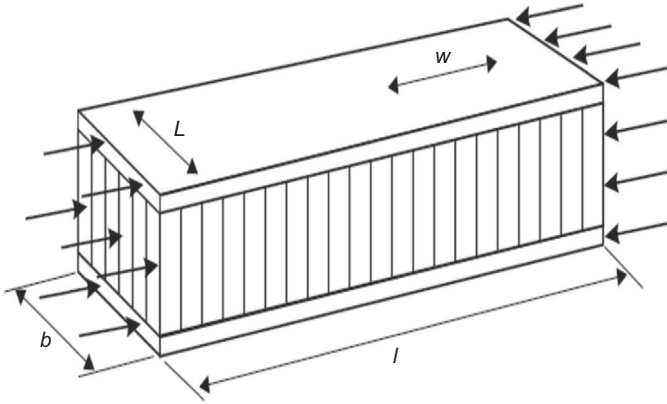
Figure 5.18 Sandwich composite beam submitted to end loading conditions.

By considering that the end applied load, P, is supported by both skins with the same thickness, t, the stress developed in the facing skins may be calculated as:

$$\sigma_S = \frac{P}{2 \cdot t \cdot b} \qquad\qquad [5.11]$$

where b is the panel width.

If the end load is applied with uniform distribution along length, q, the total load to be considered in Eq. [5.11], P, is calculated as:

$$P = q \times b \qquad\qquad [5.12]$$

As happens in bending, the stress calculated by Eq. [5.11] must be lower than the maximum allowable one that the laminate facing skins support to ensure they do not suffer failure.

It is also necessary to ensure that the compressive end load, P, does not overpass the sandwich composite beam buckling load, P_b (Table 5.11, fourth line), which may be calculated as:

$$P_b = \frac{\pi^2 \cdot D}{l^2 + \frac{\pi^2 \cdot D}{G_c \cdot d \cdot b}} \qquad\qquad [5.13]$$

and

$$|P| \le |P_b| \qquad\qquad [5.14]$$

where:

D is the panel flexural stiffness calculated from Eqs [5.1] or [5.2];
G_c is the lower value of the core shear modulus see Eq. [5.4]
l is the beam length; and
d is the distance between the midplanes of the upper and bottom skins (see Fig. 5.15).

Furthermore, to avoid buckling of the facing skins where they are unsupported by the honeycomb walls, the following intracell buckling (dimpling) stress, σ_{CR}^d, must not be exceeded in the skins:

$$\sigma_{CR}^d = 2 \times E_s \times \left[\frac{t}{s}\right]^2 \qquad [5.15]$$

where (see also Fig. 5.15):

E_s is the laminate facing skin's Young's modulus;
t is the facing skin's thickness; and
s is the size of the core cell.

Finally, wrinkling and buckling may occur in facing skins with a wavelength greater than the core cell width at higher stresses than the critical one, σ_{CR}^W, which is given by Eq. [5.16]:

$$\sigma_{CR}^W = 0.5 \times [G_c \cdot E_c \cdot E_s]^{1/3} \qquad [5.16]$$

where (see also Fig. 5.15) E_c and G_c are the core Young's and shear moduli, respectively.

5.3.2.2 Sandwich plates

In the case of sandwich composite plates, after determining the coefficient K_2 from the chart depicted in Fig. 5.19, the maximum facing-skin stress should be calculated as:

$$\sigma_s = \frac{K_2 \cdot q \cdot b^2}{d \cdot t} \qquad [5.17]$$

where K_2 is a coefficient determined from the chart depicted in Fig. 5.19.

5.3.3 Core failure

5.3.3.1 Sandwich beams

In sandwich beams under flexure, the core may fail due to excessive shear stress. Thus, the maximum value of such shear stress developed in the core caused by the transverse
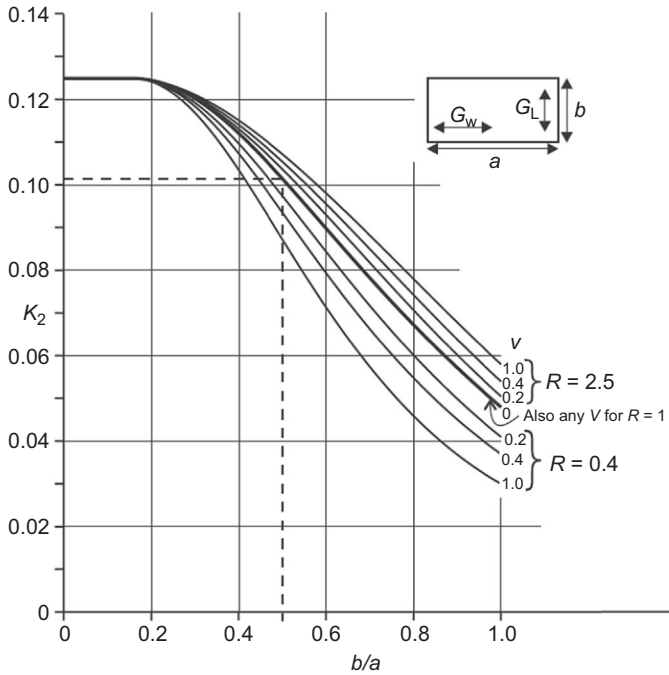
Figure 5.19 Chart for determining the coefficient K_2 for sandwich plates.

load on the beam (see the second line of Table 5.11), τ_c, calculated from Eq. [5.18], must be lower than the allowable transverse shear stress the core withstands:

$$\tau_c = \frac{F}{c \cdot b} \qquad [5.18]$$

where:

F is the maximum shear force shown in Table 5.12 for each bending case; and
c and b the core thickness and beam width, respectively.

Furthermore, the core must also resist the local compressive stress cause by the application of the transverse load, P (see the case shown in the third line of Table 5.11). Such compressive stress may be calculated by Eq. [5.19] and must be smaller than the maximum allowable compression stress the core can withstand:

$$\sigma_c = \frac{P}{A} \qquad [5.19]$$

where A is the area where the load, P, is applied.

Finally, in the case of end loading conditions (see Fig. 5.18), shear crimping failure may also occur in the core as a consequence of buckling that may be caused by a low

core shear modulus or weak adhesive shear strength. To avoid shear crimping failure, the total end load, P, applied to the sandwich beam must be smaller than the shear crimping and buckling, P_b^{SC}, determined as:

$$P_b^{SC} = c \times G_c \times b \qquad\qquad [5.20]$$

where:

   c is the core total thickness (see Fig. 5.15); and
   G_c is the lower value of the core shear modulus (see Eq. [5.4])

5.3.3.2 Sandwich plates

In the case of a sandwich composite plate submitted to a uniformly distributed load and supported on all four sides, previously presented in Fig. 5.16, the maximum shear stress developed in the core, τ_c, may be calculated from:

$$\tau_c = \frac{K_3 \cdot q \cdot b}{d} \qquad\qquad [5.21]$$

where:

   K_3 is a coefficient to be determined from the chart depicted in Fig. 5.20;
   q is the uniformly applied load;
   b is the plate width; and
   d is the distance between the midplanes of the upper and bottom beam skins.

   The core of the plate must also withstand the same local compressive stress determined for sandwich composite beams by Eq. [5.19], which results from the application of the transverse load, P (see the case shown in the third line of Table 5.11).

5.3.4 Skin and core interfacial design

Skin−core bonding must withstand, of course, at least the above-mentioned shear stress developed for the skin and core. Loads that may cause skin−core debonding only can be compared with those associated to other modes of failure (eg, face yielding, face wrinkling and core shearing) if relatively large cracks preexist at the interface. However, debonding may occur as a result of poor manufacturing, localized impact, fatigue or exposure to extremely high temperature.

   It is common to consider that skin−core debonding is avoided by ensuring that the preexistent cracks at the skin−core interface do not reach a critical length related to the adhesive critical strain energy release rates in modes I and II (G_{Ic} and G_{IIc}), normally determined by using double-cantilever beam (DCB), single-cantilever beam (SCB) and end-notched flexural (ENF) test methods, respectively. Mixed-mode fracture testing methods, which consist of a modified DCB testing setup, may allow determination of the interface fracture behaviour under simultaneous mode I and II conditions.
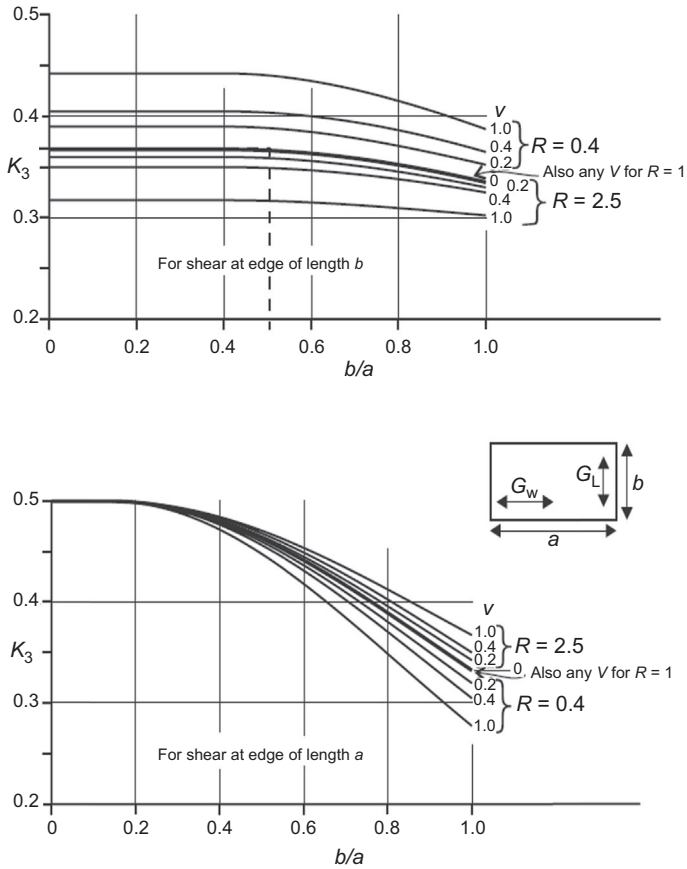
Figure 5.20 Chart for determining the coefficient K_3.

In the case of the sandwich beam under flexural concentrated load, w, depicted in Fig. 5.15, by considering that the critical strain energy release rate in mode II, G_{IIc}, was already determined as the most relevant fracture mode in the considered situation, the maximum allowable critical load that the beam may sustain, w_c, may be determined as:

$$w_c = \sqrt{X \cdot L \cdot b \cdot G_{IIc}} \qquad [5.22]$$

where:

X is a ratio between the applied load and deflection see Eq. [5.5], $\frac{w}{\delta}$; and
G_{IIc} is the critical strain energy release rate in mode II.

Experimental evidence shows that debonding is not likely to occur unless a large crack exists in the interface. Thus, a maximum allowable crack length should be defined for more liable structures in order to be adequately monitored through

nondestructive quality control tests. In complex real structures and load conditions, studies of skin−core debonding usually require the use of advanced numerical methods, such as FEA or FDM.

5.4 Quality control, maintenance, testing, inspection and repairing

This section will discuss the major aspects related to quality control during sandwiched composites manufacturing and their maintenance, testing and repairing in service. Visual, ultrasonic, X-ray, back-light and moisture detectors are some of the techniques reviewed as the main methods commonly used to detect damages in sandwich structures that are applied in aerospace and aircraft parts (Aviation Maintenance Technician Handbook, 2012).

Major manufacturing damage and defects usually include delaminations, resin-starved and resin-rich areas, cracks, blisters and air bubbles, wrinkles, voids and thermal decomposition. This section summarizes the most common nondestructive testing techniques (NDTs) used to detect such defects in quality control inspections made during manufacturing and in-service conditions of composite sandwich structures.

5.4.1 Nondestructing testing

Sandwich structures can be subjected to different impact loads that possibly create delamination and debonding damage that needs to be assessed by reliable, efficient, easy-to-use NDT methods. The damage will vary depending on the nature of the composite part, its composition and its density. The most commonly used nondestructive methods to detect damages in sandwich structures applied in aerospace are as follows (Aviation Maintenance Technician Handbook, 2012):

- Visual inspection: This is the primary method for the in-service inspection of sandwich structures. It is fast and has a large field of view, being suitable for detecting impact damages larger than 0.5 mm. It cannot detect delaminations or debondings, and it is not suited for defect sizing and defect depth estimation.
- Audible sonic testing (coin tapping) and automated tap test: This is the most common technique for detecting delamination or debondings. It is performed by tapping with a round disk or a lightweight hammer, and listening to the sound response of the sandwich structure to the hammer. A clear, sharp, ringing sound is indicative of a well-bonded solid structure, whereas a dull or thud-like sound indicates a discrepant area. This inspection must be accomplished by experienced personnel. The automated tap test is similar to the manual tap test, but instead of a hammer a solenoid is used. A transducer and recording system allows saving the force-time signal of the impactor. As the duration of the impact force can be correlated with the stiffness of the structure, a variation of such duration allows one to predict delamination and debonding damages.
- Ultrasonic inspection: This technique uses sound waves with frequencies above the audible range. Ultrasonic waves are introduced into a material where they travel in a straight line and at a constant speed until they encounter an interface (eg, a delamination). At surface interfaces, some of the wave energy is reflected and some is transmitted. The amount of reflected or transmitted energy can be detected and provides information about the damage area. Pulse-echo and through transmission (relates to whether reflected or transmitted energy is

used), normal beam and angle beam (relates to the angle that the sound energy enters the test sandwich) and contact and immersion (relates to the method of coupling the transducer to the test sandwich) are the most frequently used ultrasonic techniques. Information from ultrasonic testing can be presented in three formats: A-scan (presentation displays the amount of received ultrasonic energy as a function of time) B-scan (presentation displays a cross-section of a test specimen) and C-scan (presentation displays a plain-type view of the test specimen and discontinuities). Using this technique, porosities, inclusions, delaminations and debondings can be detected.

- Radiography: Radiography involves passing X-ray radiation through a composite part and capturing an image on the opposite side through the phenomenon of differential absorption. Areas with varying degrees of density and absorption exhibit different behaviour in terms of absorbed radiation. It can be used to identify voids, water, impact delaminations, crack-damaged cores, insufficient adhesive and entrapment of foreign material during the manufacturing process.
- Thermography: The principle of thermography is to send a heat flow on the surface of an inspected sandwich part during a certain time and then to capture the resulting thermal response. All techniques make use of the different behaviour in terms of thermal conductivity between normal and defected areas. Usually, a heat source is used to elevate the temperature of the composite under examination while observing the heating effects caused by the decrease in thermal conductivity that damaged areas exhibit. Defects such as debondings, delaminations, cracks and the presence of water can be identified.
- Moisture detector: Uses radiofrequency power loss to detect water in sandwich structures.

5.4.2   Repairing sandwich structures

Sandwich structures are bonded constructions with thin-face skins that usually can be repaired by bonding. The repair of such kinds of structures uses similar techniques for the most common types of face sheet materials, such as glass or carbon fibre composite shells. The repairs must meet the strength requirements and can be classified as temporary (limited by time; must be removed and replaced), interim (not restoring the required durability to the component and, therefore, having a different inspection interval and/or method) and permanent repairs (restoring both strength and durability). Sandwich structures with minor core damage can be repaired using a potted repair. The core material could be left in place or could be removed and filled up with a potting compound (usually filled epoxy resins) to restore some strength. This technique is also used sometimes for cosmetic repair of skin panels. Structural repair normally consists of using the following steps on the damaged component (Aviation Maintenance Technician Handbook, 2012):

- Inspect the damaged area: Use an NDT method to assess the damaged area.
- Remove the water from the damaged area: This task can be performed using breather cloths and the vacuum bag method.
- Remove the damage: The damaged area must be trimmed out, usually in circular or oval shapes. If the damaged area includes the core, this material must also be removed.
- Prepare the damaged area: The damaged and surrounding areas should be cleaned by using sandpaper, compressed air and approved solvents.
- Installation of the honeycomb core (wet lay-up): The damaged core must be replaced by a plug of the same type and shape, using an adhesive layer or resin to bond it. The vacuum bag technique can be used to cure the core replacement.
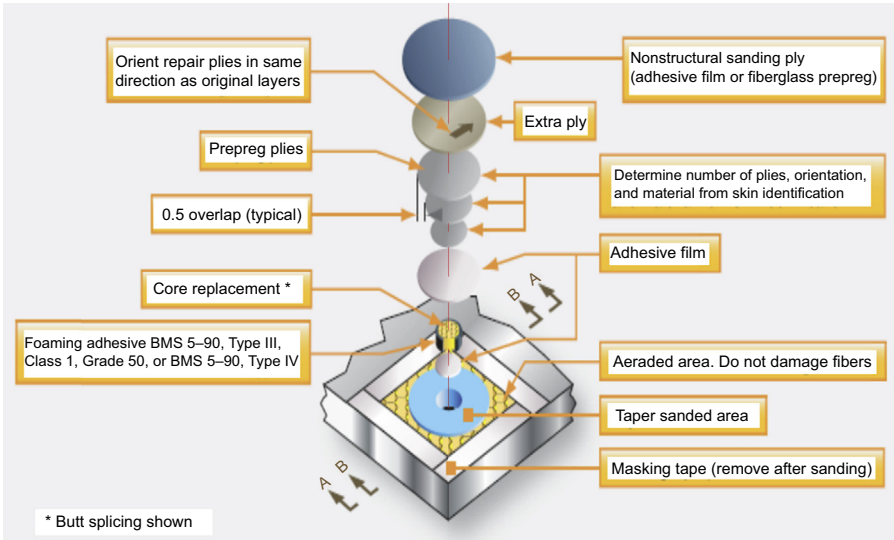
Figure 5.21 Repair ply installation (Aviation Maintenance Technician Handbook, 2012).
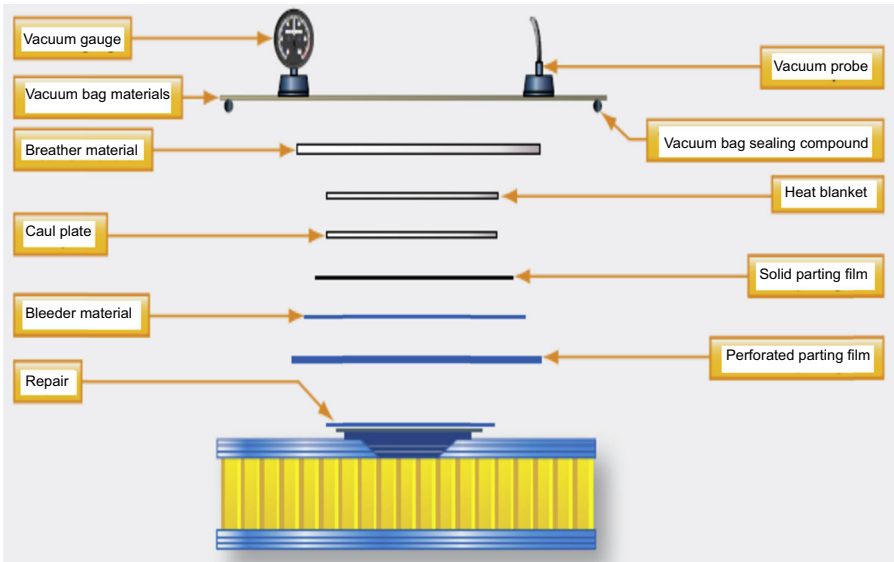
Figure 5.22 Vacuum-processing technology (Aviation Maintenance Technician Handbook, 2012).

- Prepare and install the repair plies: Impregnate or remove the backing material of the repair plies that should have the correct size and ply orientation (Fig. 5.21).
- Vacuum-bag the repair: The vacuum bag technology is usually used to remove air and to pressurize the repair for curing (Fig. 5.22).

- Cure and inspect the repair: The repair should be cured using the appropriate curing cycle. The repair should be free from pits, blisters and resin-rich and resin-starved areas. Usually, a top finishing coating is applied. Finally, an NDT technique is used to inspect the repaired area and confirm if the repair is free of defects.

5.5 Conclusions

Sandwiched composites are of particular interest and widely used because they are very suitable and amenable to the development of lightweight structures with high in-plane and flexural stiffness. In recent years, their application has increased greatly in the automotive and marine industries, and even in primary structures of commercial aircrafts (fuselage). Thus, large growth in the structural applications of those materials in the aerospace industry is forecasted for the coming years.

The main raw materials, manufacturing technologies and design methods to be considered for applying sandwich composites in aerospace structures were briefly presented and discussed in this chapter.

The chapter may be considered as an introduction that does not disregard further fundamental readings on this matter and more specific knowledge on each particular application case.

References

Advanced Composite Manufacturing Centre. <http://www.tech.plym.ac.uk http://www.tech.plym.ac.uk/sme/acmc/cpd/rtm.htm> (visited 03.06.15.).

Aluminium Honeycombs, Alcore Inc. − A Gill Company, http://www.thegillcorp.com (visit on 28.04.28.).

Aviation Maintenance Technician Handbook—Airframe. Chapter 7: Advanced Composite Materials, vol. 1, 2012. Federal Aviation Administration US Department of Transportation − Flight Standards Service.

Balsa Wood Core, Airex AG Industrie, http://www.3accorematerials.com (visit on 28.04.15.).

Beckwith, S.W., July/August 2008. Sandwich core materials & technologies − Part I. SAMPE Journal 44 (4).

Bitzer, T., 1997. Honeycomb Technology − Materials, Design, Manufacturing Applications and Testing. Chapman & Hall.

Broughton, W.R., Crocker, L.E., Gower, M.R.L., January 2002. Design Requirements for Bonded and Bolted Composite Structures. NPL Report MATC(A) 65. NPL Materials Centre − National Physical Laboratory, Middlesex, UK.

Doorway, M.C.G., 1997. Simplified Sandwich Panel Design, vol. 34 (3). M.C. Gill Corp.

Hexply-prepreg Technology, Hexcel.

HexWeb™ Honeycomb Sandwich Design Technology. Hexcel® Technology Manuals. <http://www.hexcel.com/resources/technology-manuals> (visit on 19.03.15.).

<http://www.nuplex.com/composites/processes/filament-winding> (visited on 03.06.15.).

Marasco, A.I., 2005. Analysis and Evaluation of Mechanical Performance of Reinforced Sandwich Structures: X-cor™ and K-cor™. PhD thesis. Cranfield University.

Mazumdar, S.K., 2001. Composites Manufacturing: Materials, Product and Process Engineering. CRC Press.

Muzzy, J.D., 2000. Thermoplastics − properties. In: Kelly, A., Zweben, C. (Eds.), Comprehensive Composite Materials, vol. 2. Elsevier Ltd, pp. 57−76 (Chapter 2).01.

Noor, A.K. (Ed.), 2000. Structures Technology for Future Aerospace Systems. Progress in Astronautics and Aeronautics, vol. 188. American Institute of Aeronautics and Astronautics.

Peters, S.T. (Ed.), 1998. Handbook of Composites, second ed. Chapman & Hall.

Sezgin, F.E., 2011. Mechanical Behavior and Modeling of Honeycomb Cored Laminated Fiber/Polymer Sandwich Structures. Master Thesis. İzmir Institute of Technology, Turkey.

van Paepegem, W. Home Made Composites. <http://www.composites.ugent.be/home_made_composites/organizing_your_composite_workshop.html> (visited on 27.05.15.).

Zenkert, D., 1995. An Introduction to Sandwich Construction. EMAS Publishing.

Braided composites in aerospace engineering

6

J.P. Carey, G.W. Melenka, A. Hunt, B. Cheung, M. Ivey, C. Ayranci
University of Alberta, Edmonton, AB, Canada

6.1 Introduction

Hair styles and ropes are two of the oldest examples of braids which are still widely used today. Although braiding is one of the oldest textile techniques, implementation of braids in advanced fields has been slow; the use of braids and braided composites has only recently started to appear in new areas such as the aerospace, structural reinforcement and medical fields.

Braided composites, as with their composite counterparts made by other techniques, are made of a reinforcement material (fibres) and binding materials (matrix). As a composite, braids provide superior usability, desirable and tailorable stiffness and strengths, as well as other properties, such as high specific stiffness and strengths (Ayranci and Carey, 2008).

Braids and braided composites are very useful structures stemming from the versatility of the manufacturing process and their structure patterns. Braids are quite unique and easily differentiated from other composites with their strands aligned diagonally to the structure's axis. Braids are defined by their structure as two-dimensional (2D), three-dimensional (3D) or multidirectional, and are produced as flat, tubular or 3D structures (Carey and Ayranci, 2012), all with distinct advantages.

Composite materials are being used in aircrafts; however, their use has not reached the expected levels due to their costs compared to aluminium (Baker et al.), and manufacturing and modelling challenges. Traditional hand lay-up has been used extensively in building aerospace components, from small passenger planes to the Boeing 787. Conventional applications for braided composites are overbraided fuel lines, braided air ducts, fan blades, reinforced automotive shafts, sports equipment as well as various biomedical applications, and braided composites have been considered for orthopaedic treatments (Evans and Carey, 2013). Yet, for decades, braided composites were not used extensively in the aerospace field. Some shaped braided composite structures had been manufactured for aerospace applications (Stover et al., 1971; Perez et al., 2000). As will discussed in this chapter, challenges in production and mechanical property repeatability, as well as initial capital cost for equipment, are the principal reasons for the low use of braided composites in the aerospace industry. This is largely due to the aerospace industry's stringent design standards.

The nearly nonexistent use of braided composites in aerospace changed with the development of the Airbus A350-1000 aircraft and the work by a few companies willing to meet the challenges of developing high-end braid-based components.

A number of research groups in the United States (Drexel University and University of Akron), Europe (University of Twente and Hochschule Niederrhein) and Canada (University of Alberta and University of British Columbia) also have been working on improving braided composite materials to further their use in aerospace and other heavy industrial and biomedical applications.

Herein, basic concepts and advantages of braided composite materials are first provided. This is followed by a discussion of common basic materials used to manufacture braided composites for aerospace applications. This is pursued by introducing some common manufacturing methods. Experimentally determined braided composite behaviour and means by which to model them are discussed; these sections will provide greater insight into some of the remaining challenges to greater adoption of braided composites in the aerospace field and other applications. Finally, the last section discusses early work done by Airbus on the development of the A350-1000 aircraft, as well as other currently available aerospace components.

6.2 Definition and concept

Braids have unique geometric characteristics that separate them from other textile architectures. Braids have an angle-ply fibre interlaced pattern, where the direction of the fibres is diagonal to the main structural axis. The braid angle (θ) is the characteristic angle between the strand direction and the main structural axis. Braid geometries are defined by their unit cell, a small repeating pattern characteristic of the textile architecture. The braid angle, the overall unit cell geometry and pattern, and base materials are the primary behavioural variables of braided composite materials. Aschematic example of a 2D braided architecture and an isolated unit cell are shown in Fig. 6.1.
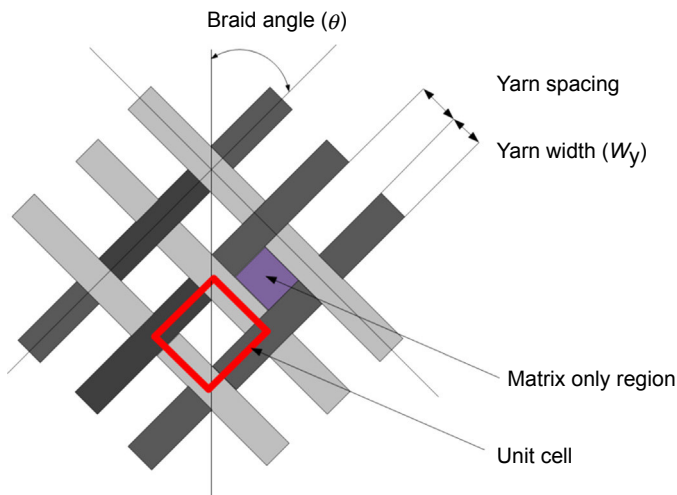
Figure 6.1 Braid geometry definition showing the angle of the braid yarns, yarn spacing and yarn width.
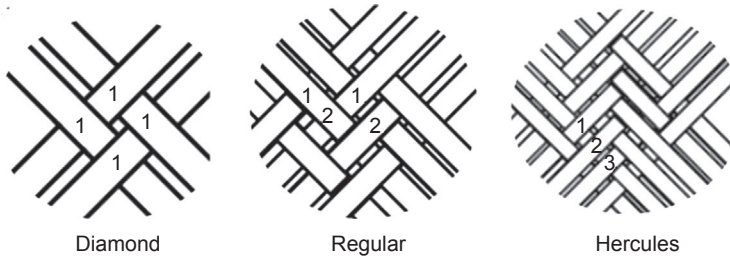
Figure 6.2 Types of braiding patterns: the diamond braid (single overlap), regular braid (double overlap) and Hercules braid (triple overlap).

2D braiding was defined as 'a readily automated, versatile and high deposition rate process best used for the production of net shape continuous fibre composite components' (Munro and Fahim, 1995). 2D braids come in diamond, regular or Hercules configurations marked by single, double or triple overlapping strand configurations, respectively (Brunschweiler, 1953; Head et al., 1989), as shown in Fig. 6.2. Axial rigidity can be increased by adding along-the-axis interlaced strands, creating triaxial braids (Fig. 6.3). 2D braiding machines can produce preforms that can be tubular, flat or more complex, shape-dependent mandrel geometries.

Adding to the versatility of the structure, the unit cells (Figs. 6.4 and 6.5) can be open- or closed-mesh. Open-meshed braided composites will have regions of neat resin (pure resin), and their properties depend more on the resin properties. Structural fibre volume fractions of open-mesh braided composites are below 35%; thus, open-mesh braided composites typically have lower stiffness properties (Carey et al., 2005; Ayranci and Carey, 2008) than closed-meshed braided composites. Therefore, open-mesh structures are used for compliant-structure applications. Reinforced polymer hoses or catheters are examples of open-mesh braids, where the reinforcement prevents excessive collapse and increases axial and torsional rigidities, but does not prevent flexion.
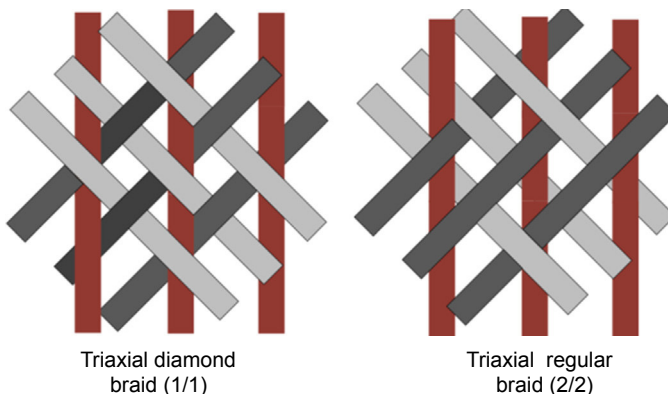
Figure 6.3 Example of triaxial braid patterns.

(a)   (b)
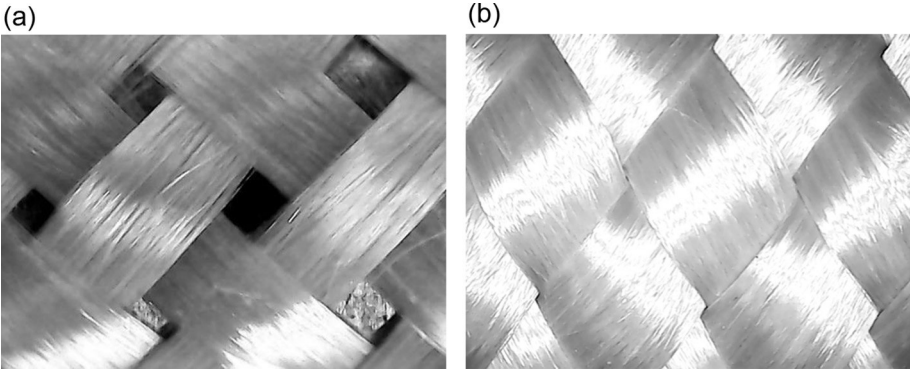
Figure 6.4 Examples of open and closed-mesh braided composite preforms. (a) Open-mesh preform; (b) closed-mesh preform. During curing, the interyarn gaps of the open-mesh braid are filled with resin, resulting in a high resin volume fraction.
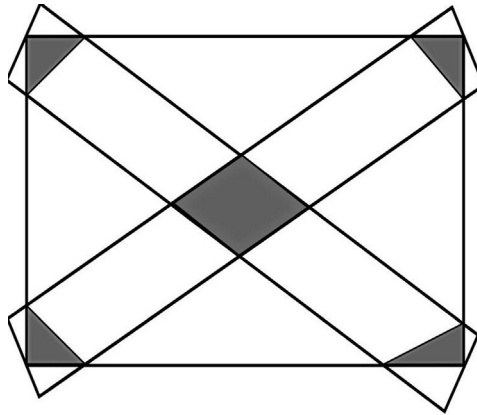
Figure 6.5 Diamond braid unit cell. Dark areas are crossover regions; top, bottom and side triangular areas are pure resin; and, rhomboids are undulation regions.

Closed-mesh braided composite behaviour is characterized by the composite material properties, in other words, that of the fibre and matrix combination. Structural fibre volume fractions of closed-mesh braided composites are greater than 50%. They are structural materials used for aerospace and other high-performance applications. Examples of open- and closed-mesh braids are shown in Fig. 6.4. In Carey et al. (2005) and Ayranci and Carey (2011), the impact of the undulation region length and thus the openness of the mesh were detailed. It was shown that classical models cannot be used to accurately predict the elastic properties of open-mesh braided composites; however, a relationship between the structural fibre volume ratios of a closed-mesh and open-mesh composite provided excellent results.

2D braids are a more general architecture than woven structures (Carey et al., 2003). Fig. 6.6 shows the 0 degree/90 degree orthogonal versus $\pm\theta$ angle ply architectural

(a)　　　　　　　　　　　　　　　(b)
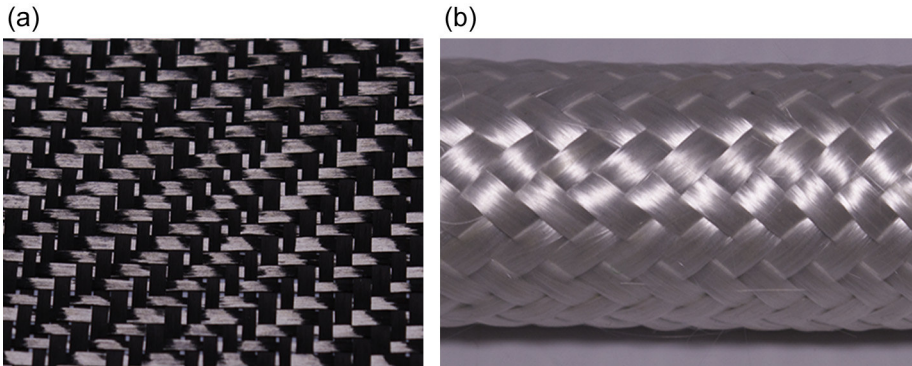
Figure 6.6 (a) Woven and (b) braided textiles.

difference in fibre alignment. 2D woven textiles and composites are characterized by their 0 degree/90 degree orthogonal interlacing, as seen in Fig. 6.6(a). Conversely, braids (Fig. 6.6(b)) have an interlaced angle ply architecture as a result of the strands being diagonally aligned with the structural axis. Woven structures are discussed in chapter Advanced Fibrous Architectures for Composites in Aerospace Engineering of this book and compared to knitted and braided structures. Braids and weaves are compared here since much of the existing testing methods were developed for woven structures. Furthermore, modelling work developed for braids is often modifications or extensions of work originally developed for weaves because of their similarities. For example, Raju and Wang (1994) developed classical laminate plate-based theories for plain-weave and five- and eight-harness satin weave structure models. 2D diamond braided unit cell composite models developed by Carey et al. (Carey et al., 2003, 2004; Ayranci and Carey, 2010; Swanek et al., 2007) evolved from these early works for weaves but were modified for angle ply structures, allowing a greater variability in assessable architectures. Woven textiles are simpler to model due to their orthogonal fixed architecture. The comparison is often made between the two textiles, especially in the case of the ±45 degree braid which is a weave rotated 45 degree.

Malkan and Ko (1989) defined 3D braiding as 'a technique for achieving 3D seamless patterns by continuous intertwining of three or more systems of yarns so that the yarns pass over one another in such a manner that each strand passes through X, Y, and Z planes-thus creating a through-the-thickness reinforcement'. This through-the-thickness reinforcement is not seen in 2D braiding. 3D braids are produced as net-shape or near-net-shape complete structures. For example, they have been produced as square or rectangular cross-sections, and as I- or C-beams. 3D braiding machines are divided into Cartesian (two-step or four-step) or rotary (multistep) machines (Chou, 1992; Kamiya et al., 2000). The geometry of a 3D braid is shown in Fig. 6.7(a). The figure shows a Cartesian 3D braid produced to form a square cross-section. The production pattern to interlace strands is shown in Fig. 6.7(b). To form a composite, the preform needs to be compacted and impregnated with a matrix.

Braided composites, as with woven and other composites, have the potential to make significant contributions to the advancement of composite materials use in the
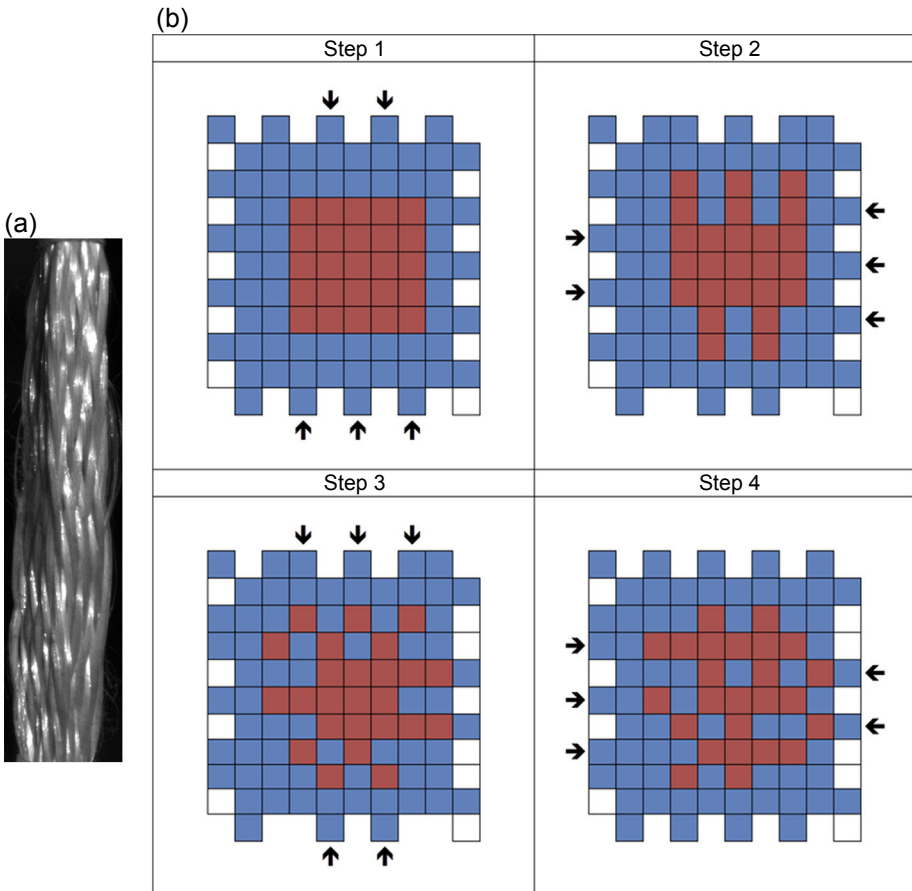
Figure 6.7 (a) 3D Cartesian braid structure and (b) production pattern for 3D Cartesian braiding.

aerospace field. Braiding's unique architecture provides uncommon versatility, adaptable to simple and complex shapes, and material property requirements.

6.3 Advantages

As stated in Carey and Ayranci (2012), the most important advantages of the braiding process are versatility of design, manufacturing, and elastic and mechanical properties. 2D and 3D braids have a number of advantages versus similar 2D architecture laminates (Munro and Fahim, 1995; Carey et al., 2003; Yang, 1990; Mouritz et al., 1999). Braiding is a rapid process that is often compared to filament winding; the interlaced structure of braids provides increased toughness compared to filament wound composites (Munro and Fahim, 1995). The versatility stems from being able to modify the orientation of the strands with respect to the preform structural axis, the unit cell configuration as well as the openness of the unit cell. Triaxial strands can be included

in 2D braid unit cells to increase axial and flexural stiffness and out-of-plane properties. Recent work has focussed on 2D braiding over carbon fibre and fibre glass cores as structural rebar (Rana et al., 2014; Ivey et al., 2014). Braids can produce near-net-shape components. 3D braided structures produce stiffer and stronger components; they increase the out-of-plane properties and provide greater resistance to delamination. It is clear that braiding can provide a panoply of properties adaptable to most applications.

2D and 3D braided composites provide greater notch resistance due to the strand interlacing. Braided structures offer superior impact resistance and toughness. Five-dimensional braids can produce near-isotropic properties (Yang, 1987). Braids have been produced on a micro scale to large industrial applications. All of the above are valuable to aerospace and ballistic applications.

Limitations of 3D (Mouritz et al., 1999) include, notably, the state of braiding equipment development; limited geometries; equipment setup time and cost; short production runs; properties are not well known and have significant scatter due to manufacturing process repeatability; laminates are stiffer and stronger; edge effects; the need for further modelling; and the lack of environmental and durability studies. However, recent advancements are tackling these issues and increasing opportunities for using braided composites in all sorts of applications.

The reader will find within this chapter a number of characteristics of braided composites, some listed above. It should be noted that, until recently, a strong argument could be made for not using braided composites in aerospace applications. Recent developments, many noted herein, show that braiding has a bright future in aerospace and other high-end applications.

6.4   Types of fibre and matrix

Typical base materials used in aerospace are required to be stiff, strong and lightweight. This makes composite materials attractive options; selection of constituent materials depends on the required component service. The current limitation to wider adoption of composite-based materials is cost. Fibres that meet the specifications of the industry are very expensive compared to metals. Braided composites can be manufactured using the same base materials as other composites; the building block is the fibre−matrix unidirectional lamina. In this section, a list of fibres (Table 6.1) and resins (Table 6.2) that have been or could be used to manufacture lamina-based braided composite aerospace components is provided. It is vital that any designer first determine needed specifications and then identify through proper calculations what material combination will meet them − which is often an optimization problem. In the following sections, basic equations are provided to determine stiffness and strength capabilities.

Here, focus is placed on three principle fibre types: glass, aramid and carbon fibres. Glass fibre composites have a high specific strength and good environmental resistance (humidity, heat, cold and corrosion), are good electrical insulators, have good dimensional stability, are easy to fabricate and cost much less than other fibres. Aramid fibres have excellent energy absorption capabilities during failure, have a low density and

Table 6.1 Typical properties of fibres used in braided composites for aerospace applications (note that designers must determine actual values for their selected materials)

Fibre	Elastic modulus (GPa)	Tensile strength (GPa)	Failure strain (%)	Density (g/cm^3)	Poisson's ratio
E-glass (Matweb, 2015a)	72	3.5	4.4−4.8	2.54−2.60	
S-glass (Matweb, 2015b)	85	4.6−4.8	5.3−5.7	2.48	
Kevlar 29 (Matweb, 2015c)	70.3	3.6	3.6	1.44	
Kevlar 49 (Matweb, 2015d)	112−138	3.6	2.4	1.44	0.35
Kevlar 149 (Matweb, 2015e)	179	3.5	1.9	1.47	
Carbon T300 (Barbaro, 1999)	230	3.5	1.5	1.75	
Carbon T600 (Toray Carbon Fibres America, 2008)	230	4.14	1.8	1.79	
Carbon AS4 (Matweb, 2015f)	231	4.5	1.8	1.79	

therefore high specific stiffness and strength, are sensitive to moisture absorption and UV, have temperature-dependent properties and will creep. Carbon fibres are the most typical fibres for aerospace structural components because these applications are weight critical. They are exceptionally lightweight, stiff and strong materials. They are available with a broad range of properties, typically differentiated between high-strength and high-stiffness carbons, but the available combinations appear vast. The fibres can operate at very high temperatures and act as electrical conductors, but operational use is limited by matrix performance.

To be functional, fibres must be reinforced by matrices, such as polymers, metals or ceramics. Matrices are critical since they hold fibres together, distribute loads throughout the composite and protect fibres from the environment and from damage. Polymers are either thermosetting (permanently set post curing) or thermoplastic (meltable and reusable). The aerospace field requires mostly thermoset matrices for structural applications.

It is always preferable that designers experimentally assess their choice of fibres and matrices following set ASTM or International Organization for Standardization (ISO) standards. Furthermore, unidirectional composite material properties need to be determined; again, ASTM standards exist to assess these, for example

Table 6.2 **Typical properties of resins (note that designers must determine the actual values for their selected materials)**

Resin	Elastic modulus (GPa)	Tensile strength (MPa)	Failure strain (%)	Density (g/cm^3)	Tg (°C)	Poisson's ratio
Thermoset						
Epoxy (Barbaro, 1999; Jones, 1998)	2.6−3.5	60−75	3.1−5.2	1.2	170−240	0.35−0.38
Polyester (Barbaro, 1999; Jones, 1998)	2.8−3.4	21−76	1.4−3.3	1.3	75−100	0.38
Thermoplastic						
Polypropylene (British Plastics Federation, 2015)	1.4	34	200	0.9	−20	
Nylon 6,6 (Gutowski, 1997)	2.8	76+	100	1.2	57	0.41
Polyether ether ketone (PEEK) (Matweb, 2015g)	3.5	100	>60	1.3	143	0.4

ASTM D3039 − Standard Test Method for Tensile Properties of Polymer Matrix Composite Materials. However, prior to performing these tests, designers can use micromechanical models to assess if the materials sufficiently meet their design criteria.

6.5 Production methods

2D braiding is a production method capable of producing near-net-shape continuous fibre composite components (Munro and Fahim, 2000). 2D and 3D braided composite production is usually performed in two steps. First, preforms are manufactured and then impregnated. In-line strand impregnation is much more prevalent than it once was (Ahmadi et al., 2009). Other means of impregnation use powder-coated yarns and/or commingled yarns (Miller et al., 1998; Alagirusamy et al., 2006) during the process. The common horizontal maypole braider can be customized for micro- to industrial-size applications. A 2D maypole braiding machine is typically composed of a central pulling device or mandrel, and a horizontal or vertical braiding head with a large number of fibre carriers (Fig. 6.8(a)). One braiding machine can produce a number of braid architectures. The number and type of horn gears, number of carriers and type of machine will determine which braided preform architecture (Fig. 6.2) will be produced (Kyosev, 2015). It is recommended that designers examine the braid pattern specifications found in their braiding machine owner's manual.

In a standard braider, one-half of the carriers move in the clockwise direction while the other half moves in the counter-clockwise direction, both in intersecting serpentine paths resulting in an interlocked structure. As depicted in Fig. 6.8(b), carriers move at an angular velocity (ω), while the mandrel is pulled at a velocity v. Convergence of strands begins at the guide plane; some braiding systems include circular guide planes to shorten the convergence distance of strands, whereas others have the convergence zone start from the carriers. Strands are deposited on the deposit plane at what is called

(a)   (b)
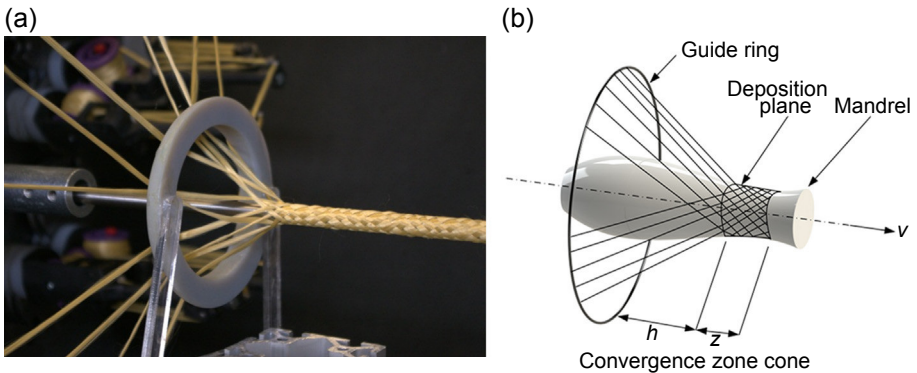
Figure 6.8 Maypole braiding process: (a) maypole braiding showing braid yarns and spools; (b) schematic of the 2D maypole braiding process with key variables and structures.

the fell point. This occurs at a distance h, the length of the convergence zone, from the guide plane. Mandrel geometry largely affects the convergence zone and, directly, the braid angle and unit cell architecture.

Kinematic models to produce specific braid unit cell geometries based on production parameters and mandrel geometry were introduced by Du and Popper (1994). Recent work by Van Ravenhorst and Akkerman (2014) and Kessels and Akkerman (2002) has elevated the level of manufacturing parameter predictions and led to downstream finite element analysis. In terms of 2D braiding production, these works provide valuable tools for the designer and manufacturing engineer. A number of assumptions are used in these models; strands are assumed to be straight, and interyarn friction is neglected. However, observation of production dynamics clearly shows that strand interactions and inertial forces should be considered. Strand paths are not straight from carrier to fell point (Fig. 6.9), and there are known strand friction-based interactions (Zhang et al., 1999) near the fell point and as the strands cross over each other.

The braid angle is the angle that the braid strands make with the principal axis (Fig. 6.1). The braid angle is largely the variable that allows for property versatility for a set fibre—matrix combination and is a function of strand dimensions, number of carriers, mandrel diameter and production variables. The preforms can be produced on simple tubular or complex-shaped mandrels or produced in flat panels using a Jacquard braider (Brunschweiler, 1953).

Fibre volume fraction V_f, a critical parameter for mechanical properties of all braided composite structures, is a measure of the content of fibre in the structure relative to the entire volume. The fibre volume fraction depends on the braid angle, fibre bundle—packing factor and fibre-packing fraction. The limiting braid angle in tension and compression is called the jam angle (Ayranci and Carey, 2008). The jammed state is a geometric state where adjacent strands prevent any further movement of strands, in tension or compression (Fig. 6.10). Examples of 2D braid preforms are schematically shown in Figs. 6.2—6.4.
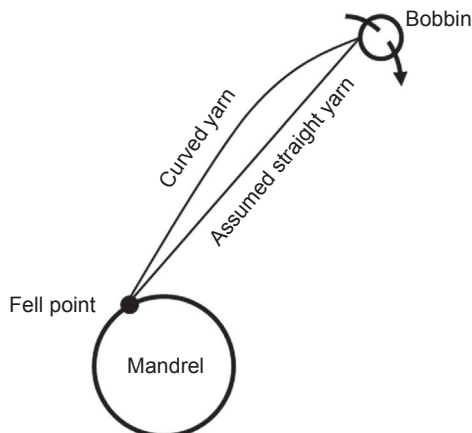
Figure 6.9 Braid production model schematic showing strand curvature.
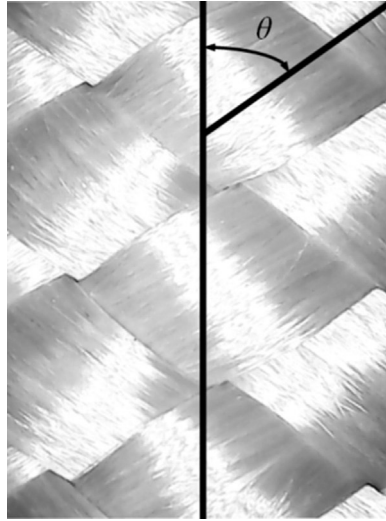
Figure 6.10 Example of braid preform in a jammed state. Braid angle is indicated by the angle of the braid yarns from the longitudinal axis.

3D braiding production includes Cartesian, rotary, triaxial, multiple interlock and five-dimensional braids, among others. Each configuration is produced using a different production process and then compacted to minimize voids. Each has different unit cells and differing through-the-thickness reinforcement leading to different, but tailorable, mechanical properties. Production processes have been used to produce a number of configurations such as I- and C-beam cross-sectional shapes, and open rectangular shells. A number of authors (Yang, 1990; Brown and Crow, 1992) detailed early 3D braid production.

In all braiding production processes, it is imperative to obtain homogeneous and thorough impregnation of braided preforms, as this significantly affects material properties. Braids are typically impregnated in line or post preform production. In-line impregnation usually involves impregnation rings or resin baths. The impregnation ring, which often acts as the guide ring, requires a peristaltic pump to force heated resin through the ring. Resin reaches edges of the ring on which strands rub during the manufacturing process. The contact of the strands on the ring separates the fibres and allows the resin to coat nearly every individual fibre. Conversely, the resin bath dips the strands a priori.

Post-impregnation commonly involves cutting the preform braid to size and massaging resin into the fibres while on a mandrel. This technique allows for vacuum systems to be used to remove excess resin as well as improve outer braid geometry.

Braiding has also long suffered geometric production inconsistency. These are the most important reasons why braided composites have not seen greater adoption in aerospace and other high-end application fields. Fortunately, new production and

modelling techniques (Van Ravenhorst and Akkerman, 2014) have been developed by a number of companies in collaboration with advanced research centres.

Production of 2D, and even more so 3D, braiding machines is expensive and time-consuming. A number of options are available to create different preforms (Table 6.3). Initial capital investment is significant. Setup time prior to a production run largely depends on the number of spools to be filled and the length of fibre required. Furthermore, in 3D braiding, unless large machines are used, the amount of fibres on each spool must be small since the entire spool must travel in confined spaces.

As with any composite material, it is imperative that designers experimentally assess the properties of their produced braided composite materials following established ASTM or ISO standards, and further test them in tailored in situ conditions. Testing under realistic combined loading conditions and fatigue life experiments ensures that components meet desired specifications and follow the strict use of safety factors specified in standards.

Table 6.3 Common braid preform shapes and production method (Carey and Ayranci, 2012; Tolosana et al., 2007; Ko, 1987)

Braid preform shape	Production process
Tubular	• 2D maypole biaxial with mandrel • 2D maypole triaxial with mandrel • 3D tubular with mandrel
Flat	• 2D maypole biaxial removing one horn gear
Stuffed tubular	• 2D maypole biaxial with inner core of bundled yarns • 2D maypole triaxial with mandrel with inner core of bundled yarns
H-beam	• 3D rotary braiding machine • Track 3D braider
I-beam	• 3D rotary braiding machine • Track 3D braider
Triangular beam	• 2D maypole biaxial with mandrel • 2D maypole triaxial with mandrel • 3D tubular
Channel beam	• 2D maypole biaxial • 2D maypole triaxial • 3D tubular
Angle beam	• 3D rotary braiding machine
Square braids and solid column	• 3D Cartesian • Track 3D braider

6.6 Properties

Braided composites are very versatile, as are the properties that can be produced with the different unit cell structures. Ayranci and Carey (2008) presented an assessment of the known state-of-the-art research in braided composite material properties. Here, only a summary (Ayranci and Carey, 2008) and more recent literature updates are provided.

Braided composite properties have been difficult to replicate. Production inconsistency leads to a wide range of obtained properties between runs and requires significant testing to determine properties; even within the same production runs, the properties can differ widely. Properties of braided composites depend on the unit cell configuration and geometry. The elastic properties of 2D braided composites, in open- and closed-mesh configurations, have been compared to those of 2D laminates with the same angle ply orientations (Carey et al., 2003). In Fig. 6.11, comparative sketches of the longitudinal (E_x), transverse (E_y) elastic and shear (G_{xy}) moduli of the three configurations are provided. Laminate properties span the full 0–90 degree angle ply range as they are not constrained by the tensile jamming (θ_{j1}) and compressive jamming (θ_{j2}) angles of the braids. Because of the geometry, the longitudinal (Fig. 6.11(a)) and transverse (Fig. 6.11(b)) elastic plots are mirror images, and the shear modulus plot (Fig. 6.11(c)) is symmetric at about 45 degree. Laminate properties span the tensile laminate elastic modulus (E_{11}) to the transverse laminate elastic properties (E_{22}). Laminate elastic constants are defined in the micromechanics portion of Section 6.7. Laminate composites properties are always greater than those of braided composites. This is due to the off-axis undulating strands that result from the interlacing in braids. Closed-mesh braided composites have greater elastic properties than those of open-mesh braided composites as matrix-rich zones dominate the properties of open-mesh structures. Comparison between 2D and 3D braided composites with 2D laminates has been performed by many authors (Carey and Ayranci, 2012; Yang, 1990; Mouritz et al., 1999).
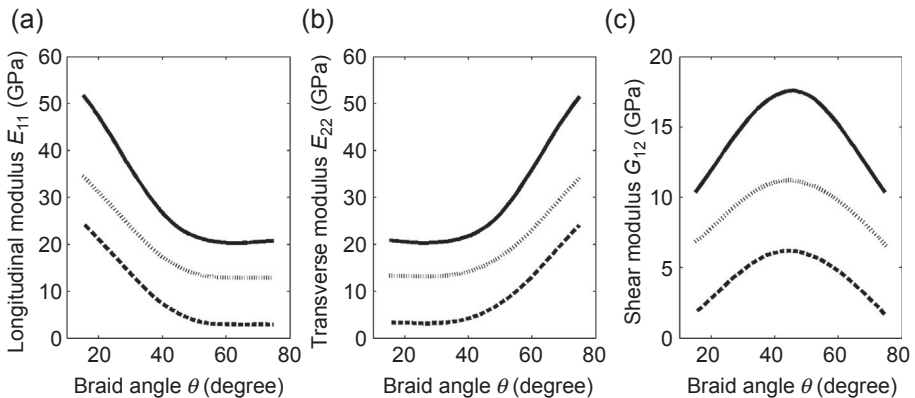
Figure 6.11 (a) Longitudinal; (b) transverse and (c) shear moduli of different composite materials, for laminates (solid line), closed-mesh braided composites (dotted line) and open-mesh braided composites (dashed line).

All braided composites, 2D and 3D, have to some degree through-the-thickness interlacing reinforcement that increases interlaminar elastic properties and strengths. Furthermore, braided composites' through-the-thickness interlacing increases delamination resistance, material toughness and impact resistance (Munro and Fahim, 1995).

Strengths of braided composites depend on the material, impregnation levels, fibre volume fraction and construction. It is not possible to provide a full assessment of the strength behaviour of all combinations. Early works found that 3D braided composites provided some valuable advantages such as increased damage resistance and toughness compared to 2D braids (Ko, 1985). Others assessed edge effects (Crane and Camponeschi, 1986; Macander et al., 1986). Wang and Zhao (2006) examined failure modes of different architectures and concluded that mechanical properties largely depended on the selected configuration. Damage resistance was greater for 3D braided composites versus their laminate counterparts, whereas strength and elastic behaviour were virtually unchanged between configurations (Gause and Alper, 1987). However, as in the case of 2D braiding, mechanical properties of 3D braided composites were lower than those of laminates with similar fibre volume fraction and lamina lay-up. This is principally due to the off-axis loading resulting from strand undulation or crimping. In the literature, the terms undulation angle and crimp angle are used interchangeably.

A recent study by Srikanth and Rao (2014) compared the strength and longitudinal elastic modulus behaviour of 2D braided and filament wound glass fibre-reinforced composites at varying angle ply angles. If the findings that are outside the feasible braiding range (ie, beyond the tensile and compressive jamming angles) are ignored, they show that braided composites have greater longitudinal elastic moduli for all angles. However, whereas at low angles (less than 30 degree) filament wound composites had greater strengths, braided composites were stronger at angles greater than 30 degree. For the aerospace industry, the nearly limitless mandrel size and length capabilities, as well as through-the-thickness reinforcement and strength and elastic properties, make braiding a more interesting choice than filament wound composites.

In compression, 2D braided composite failure occurs from diamond-shaped buckling and microfibre buckling; in torsion, and combined compression and torsion, microfibre buckling is the dominant failure mechanism (Harte and Fleck, 2000a); and in tension, the failure mode switches from fibre fracture to necking when the braid angle exceeds 45 degree (Harte and Fleck, 2000b).

2D and 3D braided composites' translaminar and interlaminar shear strengths have been compared to those of laminated composites. 2D braided composites were weaker than those of 3D braided composites due to the lack of through-the-thickness reinforcement and uneven resin-rich areas between braided layers (Knoche et al., 2006).

Fatigue behaviour of 2D braided composites was tested as a function of braid angle (Tate et al., 2006). Braided composite behaviour is quite different from that of angle ply laminated composites. It was found that 2D braided composites broke catastrophically with little to no typical warning signs such as matrix cracking or delamination in the first 90% of life. 2D braided composites were also found to have an endurance limit under tension–tension loading; the endurance strength was determined as the load

levels which allowed samples to survive 1 million cycles. Braid angle had little impact on fatigue behaviour.

Huang et al. (2005) investigated the fatigue behaviour of multilayer braided composite laminates and found different failure modes depending on the lay-up configuration. They found that a [28°/28°/28°/28°] laminate failed catastrophically under the uniaxial tensile or a high-level fatigue load as a result of fibre breakage across the specimen. In this configuration, delamination occurred only at low-level fatigue load. The [10°/10°/10°/10°] laminate's main failure mode was longitudinal splitting without delamination. Finally, the combined [28°/10°/10°/28°] laminate led to significant delamination at any applied load as well as cross-section and longitudinal splitting. Experimental work on triaxial braided composites showed that although increased temperature mitigated microscopic strand damage in the early cycling stage, heated specimen crack density exceeded that of room temperature specimens leading to decreased fatigue life (Montesano et al., 2014).

3D braided graphite–epoxy composites' fatigue behaviour was examined by Gause and Alper (1987) and compared to that of laminates. In tests that spanned a number of stress ratios, laminated composites demonstrated greater longevity and cyclic strength than braided composites. This is expected as undulating strands experience combined axial and bending loads that lead to higher stresses and early failure.

To recap this section, the findings highlighted indicate that braided composite behaviour often remains unpredictable and thus cannot yet be used widely in high-end aerospace applications. However, the performance of braided composites fares very well compared to other composite materials' production methods (Table 6.4). Prior to implementation in aerospace, thorough experimental work is required on produced braided composites. The development and use of fully validated predictive models will greatly aid in increasing braided composite use in the aerospace field.

6.7 Modelling

Modelling the properties of braided composites requires determining the geometric features of the unit cell, determining the base material properties and making some correct assumptions. In this section, a roadmap is provided for modelling the properties of braided structures.

A number of elastic constants of the selected fibre composite materials are required as input for braided composite predictive models. The elastic constants are a function of fibre (Table 6.1) and matrix (Table 6.2) properties and the fibre volume fraction. Elastic constants can be determined experimentally; however, micromechanical models can be used with candidate fibres and matrices for preliminary assessments.

A braid composed of interwoven strands is shown in Fig. 6.12. Matrix is added to form the composite. Each fibre–matrix strand is a fibre composite material in which the fibres are primarily aligned, parallel and oriented along the length of the strand idealized as a unidirectional lamina. Additional laminae-related concepts will be discussed in terms of micromechanical models in Section 6.7.1.

Table 6.4 **Comparison of composite manufacturing methods and ranked properties considering the same base materials and strand fibre volume fraction[a] (Ayranci and Carey, 2008; Carey and Ayranci, 2012; Munro and Fahim, 1995; Yang, 1990; Mouritz et al., 1999; Ko, 1985; Crane and Camponeschi, 1986; Macander et al., 1986; Wang and Zhao, 2006; Gause and Alper, 1987; Srikanth and Rao, 2014; Harte and Fleck, 2000a; Knoche et al., 2006; Tate et al., 2006; Huang et al., 2005; Montesano et al., 2014; Kaynak and Mat, 2001)**

Manufacturing method	Modulus[b]	Tensile strength[b]	Toughness	Fatigue behaviour[c]	Interlaminar resistance
2D composite structures					
Braids	2	2	Good	Good	Good in one layer, poor between laminae
Filament wound	4	3	Low		Low
Laminate	1	1	Low	Very good	Low
Woven	4	4	Good	Good	Good in one layer, poor between laminae
3D composite structures					
3D braids	Similar to laminates	Similar to laminates	Good	Good	High

[a]A rank of 1 indicates the best performance.
[b]Affected by braid or filament wound angle; results provided are for similar and commonly used angles.
[c]Fatigue behaviour is largely affected by stress levels and testing frequency, as well as ply and braid and filament wound angle arrangements.

Figure 6.12 Single overlap (diamond)-type braiding pattern being produced.

Laminae are the foundation of braided and other composite structures. A lamina is composed of stiff, strong, parallel fibres within a less stiff, weaker matrix material. Composite laminae exhibit orthotropic behaviour as a result of the difference in matrix and fibre properties, as well as the uniform fibre directionality (Agarwal et al., 2006). Although many factors affect the magnitude of lamina elastic constants, the most important one is the relative proportion of fibre and matrix, referred to as the volume fraction. For the remainder of this section, the subscripts f, m and c will be used for fibre, matrix and composite, respectively. What follows are commonly used micromechanical models; however, a number of different models exist and provide similar results.

The volume fractions of the fibre (V_f) and the matrix (V_m) are generically defined as:

$$V_i = \frac{v_i}{v_c}, \quad i = f, m \tag{6.1}$$

where v denotes constituent volumes (m^3) and $V_m = 1 - V_f$ if there are no voids in the lamina.

6.7.1 Unidirectional laminar material properties

In a lamina coordinate system, direction 1 is aligned with the fibre axis, whereas directions 2 and 3 are transverse to the fibre axis and perpendicular to each other. The required lamina elastic constants for evaluating braided composite elastic constants are longitudinal tensile (E_{11T}) and compressive (E_{11C}) moduli, transverse tensile (E_{22T}) and compressive (E_{22C}) moduli, in-plane (G_{12}) and transverse (out-of-plane) shear (G_{23}) moduli as well as major Poisson's ratio (ν_{12}) and out-of-plane Poisson's ratio (ν_{23}).

Longitudinal elastic modulus E_{11} is evaluated using a rule-of-mixtures (ROM) approach:

$$E_{11T,C} = E_f V_f + E_m V_m \tag{6.2}$$

The load sharing between the fibres and the matrix increases longitudinal properties as compared to a pure matrix. The prediction from this equation is quite accurate and is generally the accepted micromechanical model.

The major Poisson's ratio is also generally approximated by a ROM equation, and can be written as:

$$\nu_{12} = \nu_f V_f + \nu_m V_m \tag{6.3}$$

where ν_f, ν_m and ν_{12} are the fibre, matrix and lamina major Poisson's ratio, respectively. The transverse-to-longitudinal Poisson's ratio is found using the following relation:

$$\nu_{21} = \nu_{12} E_{22} / E_{11} \tag{6.4}$$

The transverse modulus of unidirectional composites E_{22} is often approximated using the following by Halpin and Tsai (Halpin, 1969):

$$\frac{E_{22}}{E_m} = \frac{1 + \xi \eta V_f}{1 - \eta V_f} \qquad [6.5]$$

where:

$$\eta = \frac{(E_f/E_m) - 1}{(E_f/E_m) + \xi} \qquad [6.6]$$

and where ξ is defined as a measure of reinforcement that depends on fibre and packing geometry and on loading conditions. It is 2 for round or square fibres, or $2a/b$ for rectangular cross-sections, where a and b are the dimensions of the rectangular cross-section.

In-plane shear modulus (G_{12}) is found from (Agarwal et al., 2006):

$$\frac{G_{12}}{G_m} = \frac{1 + \eta \xi V_f}{1 - \eta V_f} \qquad [6.7]$$

where:

$$\eta = \frac{(G_{f12}/G_m) - 1}{(G_{f12}/G_m) + \xi} \qquad [6.8]$$

where G_{f12}, G_m and G_{12} are the longitudinal shear modulus for the fibre, matrix and lamina, respectively.

Transverse shear properties are solved using the stress-partitioning parameter (SPP) technique (Barbaro, 1999) as:

$$G_{23} = G_m \frac{V_f + \eta_{23}(1 - V_f)}{\eta_{23}(1 - V_f) + V_f G_m/G_{f12}}$$

$$\eta_{23} = \frac{3 - 4\nu_m + G_m/G_{f12}}{4(1 - \nu_m)} \qquad [6.9]$$

The out-of-plane Poisson's ratio (ν_{23}) was defined (Yang, 1990) as:

$$\nu_{23} = V_f \nu_{f23} + V_m(2\nu_m - \nu_{21}) \qquad [6.10]$$

where ν_{f23} is the fibre out-of-plane Poisson's ratio.

A number of these properties are difficult to measure, and often the out-of-plane properties are assumed. For tight design considerations, it is imperative that designers

produce and test sample laminae following established methodologies as well as test end products in in situ situations.

6.7.2 Ply mechanics and macromechanics

A discussion of braided composite modelling would not be complete without mentioning other fundamental concepts, namely, ply mechanics and macromechanics. These are defined in a number of texts (Agarwal et al., 2006) and in chapter Fibre-reinforced Laminates in Aerospace Engineering of this book, and thus will not be repeated extensively here. The importance of ply mechanics is to assess the effects of off-axis loading of the lamina that form the braided composite unit cell. The strand path in a braid is not as simple as most bodies of work present it to be. The rendered image (Fig.6.13) of a tubular composite braid, reconstructed from micro−computerized tomography (micro-CT), distinctly shows fibres within a strand; and, contrary to modelling assumptions, the strand does not form an even cross-section simple to determine, replicate during production or reproduce for modelling purposes. Furthermore, a strand cross-section is typically lenticular (Fig. 6.14). However, for simplicity, the majority of models (Mouritz et al., 1999; Pickett et al., 2009; Naik and Shembekar, 1992) have assumed the strand to be rectangular or oval when untwisted, and to follow a simple sinusoidal path in the undulation region. Recent work has determined the

(a)   (b)
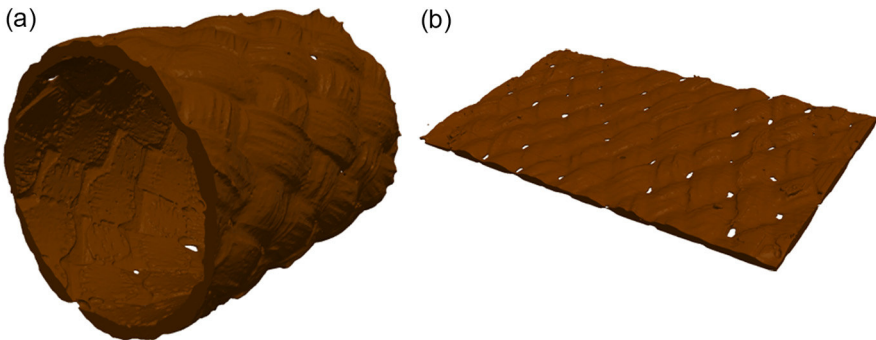
Figure 6.13 (a) Tubular braid rendering recreated from micro-CT images; (b) unwrapped image used to track the path of strands.

100 μm
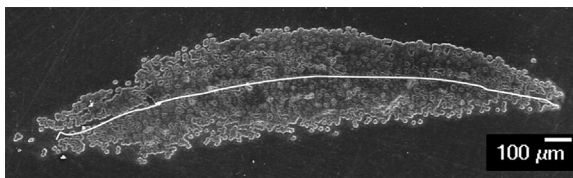
Figure 6.14 SEM of braided tube showing a single overlapping region. White line was manually incorporated to show the upper and lower strands. Each strand cross-section is near lenticular (20.0 kV, 40 × magnification).

effects of such geometric assumptions (Cheung and Carey, 2015). Using an unfolding technique, it can be clearly seen that the strand paths in the braided tube are not uniform or constant. The ply mechanics and macromechanics processes account for the strand path; proper strand path and strand cross-section are critical to proper modelling of simple 2D tubular braided composites, as in Fig. 6.13, or more complex 3D structures.

Macromechanics allows the development of constitutive equations for laminates that form the unit cell or a multilayered structure. For example, the scanning electron microscopy (SEM) in Fig. 6.14 shows overlapping strands in a braid. These overlaps must be treated using macromechanics.

6.7.3 Braided composite elastic properties

In Ayranci and Carey (2008), a number of models developed to determine braided composite material elastic properties were reviewed. Again, many were originally developed for woven composites and then modified for braided composites. There are many analytical and numerical predictive models for 2D and 3D braided composites. Numerical models (Pickett et al., 2009; Tang et al., 2003; Goyal et al., 2005; Potluri and Manan, 2007; Lomov et al., 2007; Tsai et al., 2008) are very computationally heavy, whereas analytical models provide accurate results and are quicker to solve. Finite element models are the most powerful means of analysing textile materials in two or three dimensions, but are more appropriate for strength predictions (Falzon et al., 1993). However, their complexity often limits their applicability; each application requires a new model which can take years to develop.

Analytical models focus on determining the properties of a single unit cell which is assumed to represent the behaviour of a macrostructure composed of a large number of these unit cells (Ayranci and Carey, 2008). Models (Head et al., 1989; Nakai et al., 1995) such as the finite cell model (FCM) often reduce the structure to its simplest element, a fibre bundle, and model it as a 3D structure composed of longitudinal fibre and diagonal resin truss members.

Ko et al. (Ko et al., 1986; Pastore et al., 1986) advanced the fabric geometry model (FGM), an elementary finite element method, similar in basic structure to the FCM, which defines stiffness. Overall, FGM-based models appear to predict elastic constants with accuracy; however, the approach does not model undulating strands accurately.

The classical laminate plate theory (CLPT), developed to predict in-plane properties of flat laminate composites, was modified by Ishikawa and Chou (1983, 1982) to predict stiffness and strength behaviour of woven composites. Compared to regular laminates, woven fabrics have undulations that are not accounted for in CLPT. They developed two relevant models: the mosaic model, a simplistic method of modelling the undulation by an assemblage of asymmetrical cross-ply laminates; and the fibre undulation model, which improved on the single-angle approach of FEA and accounts for continuity and undulation by using a sine function to model the strand waviness. Naik and Shembekar (Naik and Shembekar, 1992a,b; Shembekar and Naik, 1992) followed this work to address the shortcomings of the Ishikawa−Chou models, expanding the one-dimensional analysis to two dimensions. Naik and Ganesh

(1995) found that the sinusoidal approach modelled the undulation path more precisely. Naik (1996) was one of the first to implement such analyses in a program called TEXCAD for the 3D stiffness predictions of 2D triaxially braided composites using CLPT. Carey et al. (Carey et al., 2003; Ayranci and Carey, 2010; Swanek and Carey, 2006) developed CLPT-based models to calculate the elastic properties of diamond braided composites.

Redman and Douglas (1993) developed a 'CLT/rule-of-mixtures'-based model where the stiffness of each offset fibre is analysed separately and then combined to obtain the overall stiffness of the structure. Redman's model assumes a single undulation angle and open meshing. Table 6.5 provides information on a number of these approaches assessed over the years. This is in no way meant to reflect all models, or provide all information, but serves as a quick guide.

In this section, a roadmap to use an analytical model for the design of diamond braid unit cell composites, which provides sufficiently accurate results, is highlighted (Carey et al., 2003). The model can be adapted to other unit cell configurations following the same process. This model is largely sufficient and principally depends on accurately knowing the unit cell geometry, fibre volume fraction, fibre longitudinal elastic modulus E_{f11}, resin longitudinal elastic modulus E_m and shear modulus G_m. All other constituent properties have little impact on predictions. Full details and development of this model can be found in previous work (Carey et al., 2003, 2004).

The following simplifications are used in the development of these common models (Carey et al., 2004). First, the shape of the cross-sections of actual strands varies with manufacturing method. For this work, the strand is assumed to have an invariant rectangular cross-section described by the strand width W_y and the wet strand thickness h_c. Within a unit cell, it is further assumed that the strands are parallel. Second, the strand undulation geometry is defined as follows: the fibre orientation is assumed to be inclined with respect to the horizontal axis by an angle β, and the strand path is assumed to follow a cosine function. The rectangular cross-section of the unidirectional strand is inclined and always perpendicular to the fibres. The outer edges of the strand undulate as sine functions. Third, the rectangular cross-section is inclined with respect to the base plane by an angle ϕ (twist angle). Twist angle ϕ was neglected in this approach.

For a traditional multilayered laminate, the longitudinal elastic and shear moduli are determined in the following manner. The stress−strain relationship for the laminate is formulated, assuming midplane membrane strain (ε^0) and curvature (κ^0), as:

$$\left\{ \begin{matrix} N \\ M \end{matrix} \right\} = [S] \cdot \left\{ \begin{matrix} \varepsilon^0 \\ \kappa^0 \end{matrix} \right\} \qquad\qquad [6.11]$$

where:

$$[S] = \begin{bmatrix} A & B \\ B & D \end{bmatrix} \qquad\qquad [6.12]$$

Table 6.5 **Comparison of modelling methods at the root of braiding models** (Falzon et al., 1993; Ko et al., 1986; Pastore et al., 1986; Ishikawa and Chou, 1983, 1982; Nakai et al., 1996)

Method	Fabric type	Basis of model	Comparison of analytical results with experimental results	Advantages	Disadvantages
Finite cell model (FCM) and finite element method	• 3D or 2D • Any type of fabric	• Must calculate homogeneous properties with micromechanics or lamination theory • Multilevel modelling • Based on concept of fabric unit cell and structural truss analysis • Unit cell treated as 3D space truss structure • Virtual work principle • Nodal displacement • Strain energy consideration	• For woven fabric, Nastran software: upper bound shows good agreement for longitudinal and transverse moduli • Underestimates in-plane shear modulus • 50% difference in major Poisson's ratio • Poor results for torsion of braided tubes	• Best suited for strength analysis • All types of loading	• Lengthy process • Complicated programming • Memory consuming
Fabric geometry model (FGM) and angle ply undulation model	• 3D • Braid • Woven	• Stiffness of each strand calculated with Hooke's law and transformed in the general coordinates • The fractional volume of the strand determines level of influence of each strand • The total structure stiffness is the sum of all the volumetrically weighted stiffness components	For woven fabric: • Good results for longitudinal and transverse moduli • Good results for in-plane shear modulus • 50% difference in major Poisson's ratio • Provides values for other properties but not compared	• Simple analysis • Adequate accuracy for stiffness predictions • Adaptable to complex architecture	• Does not provide possibility of modelling unit cell • Unsuitable for strength analysis

Table 6.5 **Continued**

Method	Fabric type	Basis of model	Comparison of analytical results with experimental results	Advantages	Disadvantages
Classical laminate plate-based (CLPT) theories		• The CLPT assumes uniform membrane strain and uniform curvature at the midplane of the unit cell • Perfect bonding between lamina		• Simple • Provides desired E and G	• No through-the-thickness properties
Mosaic model	• 2b-Biaxial woven fabrics	Idealizes fibre waviness by laminate sections in orthogonal directions ignoring continuity (Munro and Fahim, 1995; Yang, 1990)	• For woven fabric: upper bound shows good results for longitudinal and transverse moduli of woven fabric • Underestimates in-plane shear modulus • Underestimates major Poisson's ratio • Does not predict other properties	• Simple	• In-plane properties only, no though-the-thickness properties • Poor representation of the unit cell • Too simplistic to account for all loading types
Fibre undulation model	• 3D • Woven • Braiding	• CLPT that considers the effect of the undulation regions		• Clearly defines unit cell	• In-plane properties only; no though-the-thickness properties • Does not predict failure

and where N and M are the stress and moment resultants, in GPa-m and GPa-m^2 respectively. A, B and D, the plane stress 3×3 matrices, are respectively called the extensional stiffness matrix, coupling stiffness matrix and bending stiffness matrix for the unit cell configuration. Briefly, the extensional matrix defines axial stiffness; the bending matrix defines the principal bending and torsional effects and the coupling matrix defines the influence that extensional and bending effects can have on the curvature and longitudinal deformations of the structure, respectively.

Building the A, B and D matrices is the most time-consuming task of the modelling process and relies heavily on creating proper geometric boundaries of the unit cell. The process for a simple flat braid unit cell is described in detail in Carey et al. (2003); a similar process for a braided tube, accounting for strand curvature and variable strand thickness, is described in Ayranci and Carey (2010). The A, B and D matrices are developed for each of the unit cell regions. In Carey et al. (Carey et al., 2003, 2004, 2005; Ayranci and Carey, 2010, 2011), each 2D braided composite unit cell has 13 regions: 5 regions of overlapping or crossover strands, 4 regions of pure matrix allowing for open- and close-mesh configurations and 4 regions of undulating strands. The $[A]$, $[B]$ and $[D]$ are 3×3 matrices found for each of the 13 regions as:

$$[A] = \int_x \left(\int_y \left(\int_z [\overline{Q}] dz \right) dy \right) dx$$

$$[B] = \int_x \left(\int_y \left(\int_z [\overline{Q}] \cdot z dz \right) dy \right) dx \qquad [6.13]$$

$$[D] = \int_x \left(\int_y \left([\overline{Q}] \cdot z^2 dz \right) dy \right) dx$$

where $[\overline{Q}]$ is the stiffness matrix, in the unit cell coordinate system, of the layer of resin or fibre composite strand. The matrices are added together based on an area-weighted scheme. The boundaries of the integrations in $6-12$ are defined by the geometries of the 13 regions, as done in Carey et al. (2003). Crossover regions are defined using CLPT. Strand undulation is defined as a cosine function, and numerical methods are used to evaluate A, B and D matrices' integrations over the undulation length using local solutions of CLPT at each point of the numerical integration.

The longitudinal elastic and shear moduli of the laminate, in the global x, y and z coordinate system, are found from:

$$E_x = \frac{1}{a_{11}t}$$

$$\qquad [6.14]$$

$$G_{xy} = \frac{1}{a_{66}t}$$
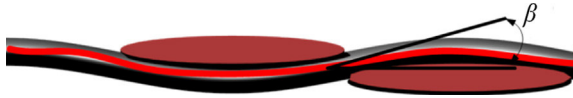
Figure 6.15 Braid undulation (crimp) angle β measured along the length of the undulating braid.
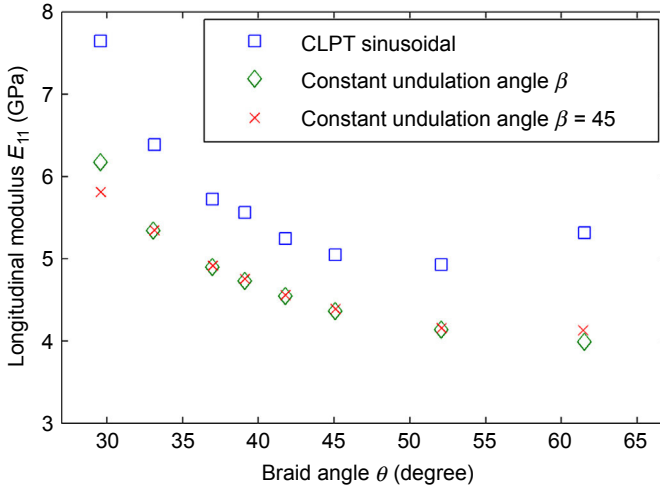
Figure 6.16 Comparison of the longitudinal elastic modulus of the undulation region of three models for the undulation region strand path.

where a_{11} and a_{66} are found in the compliance matrix $[C]$, which is the inverse of the stiffness matrix $[S]$; and t is the thickness of the braided composite.

There have been a number of questions as to the need for proper modelling of the strand undulation path (Fig. 6.15) in such analytical models. Fig. 6.16 shows the difference between three approaches: the commonly adopted sinusoidal model, a model where the undulation angle is fixed at 45 degree and one where the angle is constant based on the height and distance travelled by the strand. The sinusoidal model results are greater than those of the other two; furthermore, experimental results have been shown to closely match those of the sinusoidal path model. Fig. 6.11 showed the difference between braids and laminates.

6.7.4   Strength and failure

Strengths of braided composite materials are crucial for proper design of components in the aerospace industry and other areas. As with all design approaches for materials that have production variability and inconsistency, failure theories must be coupled with selection of stringent safety factors. Because of the complexity of braided composite structures, few works have studied their failure. For analytical models, it is

recommended to use conservative approaches. Reasonably conservative approaches consist of CLPT-based models developed earlier in this section for braided composites, in combination with first-ply failure analysis or Tsai−Wu failure analysis (Jones, 1998).

One of the most commonly used failure criteria for composite materials, the Tsai−Wu failure criterion, assumes a ply to have failed if

$$F_1\sigma_1 + F_2\sigma_2 + F_6\tau_{12} + F_{11}\sigma_1^2 + F_{22}\sigma_2^2 + F_{66}\tau_{12} + 2F_{12}\sigma_1\sigma_2 < 1 \qquad [6.15]$$

is violated. The criterion requires compressive and tensile strengths for the region of interest in terms of failure. In such analyses, it is of vital importance to determine where failure will first occur in a braided composite. For example, in the case of a 2D braided composite, the undulation region is critical. This is due in part to their off-axis geometry, causing combined loading conditions which can include axial, bending and shear loading. Furthermore, these regions possess a greater volume of neat resin which initially cracks, allowing for the undulating strand to deform and fail, followed by a scissoring effect in between the strands in the overlapping strand region. Thus, to determine conservative failure behaviour of 2D braided composites, it is recommended that the initial strength values pertinent to the failure criteria are those of the inclined lamina which forms the undulation region of the unit cell as well as those of the matrix.

By independently applying stresses equal to the various material strengths, the constants F_1, F_2, F_6, F_{11}, F_{22} and F_{66} can be found through experiment for the representative unidirectional lamina, transformed by the crimp angle using ply mechanics. The expressions for each of these constants are given below:

$$F_1 = \frac{1}{\sigma_{1,\text{ult}}^T} + \frac{1}{\sigma_{1,\text{ult}}^C} \qquad [6.16]$$

$$F_2 = \frac{1}{\sigma_{2,\text{ult}}^T} + \frac{1}{\sigma_{2,\text{ult}}^C} \qquad [6.17]$$

$$F_6 = 0 \qquad [6.18]$$

$$F_{11} = -\frac{1}{\sigma_{1,\text{ult}}^T \sigma_{1,\text{ult}}^C} \qquad [6.19]$$

$$F_{22} = -\frac{1}{\sigma_{2,\text{ult}}^T \sigma_{2,\text{ult}}^C} \qquad [6.20]$$

$$F_{66} = \frac{1}{\tau_{12,\text{ult}}^2} \qquad [6.21]$$

where the strengths are the ultimate longitudinal tensile strength ($\sigma^T_{1,\text{ult}}$), ultimate longitudinal compressive strength ($\sigma^C_{1,\text{ult}}$), ultimate transverse tensile strength ($\sigma^T_{2,\text{ult}}$), ultimate transverse compressive strength ($\sigma^C_{2,\text{ult}}$) and ultimate in-plane shear strength ($\tau_{12,\text{ult}}$) of the lamina composed of the crimped strand. Ultimate compressive strengths are included as negative values. To use these strength values in the various failure criteria, the stresses applied to the lamina must be converted first to their respective components in the local coordinate system.

The F_{12} constant requires a biaxial test with set conditions $\sigma_1 = \sigma_2 = \sigma$, with all other stresses set to 0, and can be determined by:

$$
F_{12} = \frac{1}{2\sigma^2}\left[1 - \left(\frac{1}{\sigma^T_{1,\text{ult}}} + \frac{1}{\sigma^C_{1,\text{ult}}} + \frac{1}{\sigma^T_{2,\text{ult}}} + \frac{1}{\sigma^C_{2,\text{ult}}} \right)\sigma \right.
$$
$$
\left. + \left(\frac{1}{\sigma^T_{1,\text{ult}}\sigma^C_{1,\text{ult}}} + \frac{1}{\sigma^T_{2,\text{ult}}\sigma^C_{2,\text{ult}}} \right)\sigma^2 \right]
$$

[6.22]

The Tsai–Wu and other methods have been introduced and detailed in a number of texts. In the case of open-mesh braids, the failure mechanism is most likely dominated by matrix cracking. As such, simple von Mises failure or Mohr II failure criteria could be adequate (Hu et al., 2000). No published work in the literature has been found to corroborate or refute this assumption; however, work on elastic properties of open-mesh braided composites confirmed matrix-dominated behaviours (Carey et al., 2005).

Finite element approaches also have been used for modelling strength of braided composite components. A review (Fang and Liang, 2011) reported on analytical models for 3D braided textile composites, highlighting the importance of mesostructure for analysing mechanical behaviour of 3D braided composites. Zhang et al. (2014) developed a mesoscale failure model for single-layer triaxial braided composites. Jiang et al. (2014) developed a thermo-mechanical finite element model for 3D braided composites. Lu et al. (2014) developed a nonlinear finite element model for the mesostructure of 3D full five-directional braided composites. Although typically accurate with experimental results, these models are computationally intensive and often only applicable to single structures or cases (Zhou and Zhuang, 2013).

6.7.5 Fatigue behaviour

Little has been done in terms of assessing the fatigue behaviour of braided composites, which is a burgeoning field requiring significant attention. Cyclic loading degrades the properties of all braided composite architectures. Regions of high stress concentrations, namely those with high undulation angles, largely affect the fatigue behaviour of braided composites (Wu et al., 2014).

Procedurally, fatigue behaviour is best assessed using numerical methods. This requires the development of accurate macro-, meso- and micro-geometry, critical to the process. Fang and Liang (2011) review stresses the importance of mesostructure in

analysing the fatigue behaviour of 3D braided composites; such findings are also applicable to 2D braided composites. Stresses in each strand, or unidirectional lamina, in the overall structure must be assessed within the numerical model. Critically stressed strands are compared to a fatigue failure criterion, such as the energy-based criterion proposed by Petermann and Plumtree (2001) or other criteria.

As noted in this chapter, fatigue behaviour of 2D braided composites is quite different from that of angle ply laminated composites (Tate et al., 2006). It was found by Tate et al. (2006) that, in the case of AS4−epoxy 2D braided composites, fatigue life could be modelled using sigmoidal curves. This finding is interesting and proposes a simple approach to determine fatigue behaviour of braided composites. They propose that the curve of the fatigue-to−ultimate strength ratio versus the number of cycles diagram ($S−N$ curve) is given as:

$$\frac{S_f}{S_u} = \frac{A_1 - A_2}{1 + e^{(\log_{10}N) - x_0/dx}} + A_2 \qquad [6.23]$$

where S_f is the fatigue strength; S_u is the ultimate strength of the braided composite; N is the number of cycles; and A_1, A_2, x_0 and dx are curve-fitting parameters in the equation: A_1 and A_2 provide the range of applicable strength ratio, A_1 is 1 as it is the strength for one cycle, A_2 is the endurance strength−to−ultimate strength ratio determined experimentally, x_0 is the x value at the point where the $S_f−S_u$ ratio is the average of A_1 and A_2 and, finally, dx represents the slope of the sigmoidal curve. Similar work was performed for braided and other textile composites (Kelkar et al., 2006), showing that findings are very susceptible to braid angle.

Goyal and Whitcomb (2008) used a two-scale modelling approach based on Hill's yield function for orthotropic materials to assess different biaxial braid combinations. Their findings suggest that glass braid tow is probably more susceptible to initiation of fatigue damage than a carbon braid tow of a geometrically similar braid.

A number of works have used numerical methods to improve fatigue properties of 3D braided structure designs under various loading conditions (Wu et al., 2014; Wu and Gu, 2014). Results of these works show a panoply of results that highlight the need for specific case-by-case modelling.

A vital lesson of this section is that when using modelling-based work to identify braided composite structures that meet design specifications, it is absolutely imperative to conduct experimental work to verify these findings. As stated in this chapter, braiding manufacturing processes can be inaccurate if they are not meticulously developed and if quality control is not used at every step. Therefore, braided components must undergo rigorous and standardized experimental testing prior to adopting any component in aerospace or other structures.

6.8 Joining techniques

Extensively producing large components directly from braids is impractical and would be very costly. To be useful in practical applications, braided composites must be

joined to other components. As a result of the interlaced configurations of the unit cells, braids are specifically valuable for connecting various components. During the production process and with proper design and planning, rivet or connection holes can be created. Works on braided composites with notches have shown stress distribution and failure responses that present a valuable advantage. Gause and Alper (1987) showed that tensile strength did not decrease with an open hole in the structure; it was found that bearing and transverse strength, as well as transverse stiffness properties, were lower than those of traditional laminated composites. Braided composite tensile fatigue properties were similar to those of laminates, whereas compressive fatigue properties were lower. A study that examined the difference between an integrated hole in the braided composite (ie, formed during the manufacturing process with strands surrounding the hole) vis-à-vis a hole machined into the braid specimen found greater static and fatigue strengths in the case of the formed hole (Ohki et al., 2000). These findings are expected as machined holes will cause local damage that will impact the structure when loaded. Thus, in practical terms, when including braided composites in designs, be they for aerospace or other uses, integrating the hole as part of the design and manufacturing process is imperative.

6.9   Applications

2D and 3D braiding materials and processes have not been used extensively in the aerospace industry (Baker et al.). 2D braiding is versatile and can be used to reinforce many parts. Aircraft ducts, fuselage J frames and helicopter rotor blade spars are reported applications (Baker et al.). A 3D interlock arm was reinforced with carbon fibre braided composite overlay (Staff, 2012). Braided carbon fibre structures are being considered for aircraft interior use (Calvert, 2009). However, there have not been any reported cases of 3D braided parts in use in the field. It was noted in (Baker et al.) that C-, J- and T-section panels and other components had been successfully manufactured for demonstration purposes. Based on such successful conceptual components, the slow uptake of braiding in aerospace has been perplexing. Recent industrially focussed work provided valuable insight for the use of 2D and triaxial braided composites (Kelkar and Whitcomb, 2009) impregnated using resin transfer moulding (RTM) and vacuum-assisted RTM for the small business jet industry and other applications (Roberts et al., 2009). Engineers at General Electric Aircraft Engines explored mega braiders for large-scale use in aircraft development (Braley And Dingeldin, Unpublished).

A company at the forefront of braiding technology for the aerospace field is A&P Technology. A number of aircraft parts are been redesigned using braided composite materials (Fig. 6.17). The Honeywell jet engine stator vanes are produced by A&P Technology with a layer of aramid braid followed by an overlay of carbon fibre braid (A&P Technology, 2014a). A&P also produces braid-reinforced wing flaps for Bombardier (A&P Technology, 2014b). The fan case of the GENx, a fuel-efficient, quiet and low-emissions jet engine being developed for the Boeing 787 aircraft and the Boeing 747-8, is produced by A&P Technology using an isotropic-behaviour braid pattern
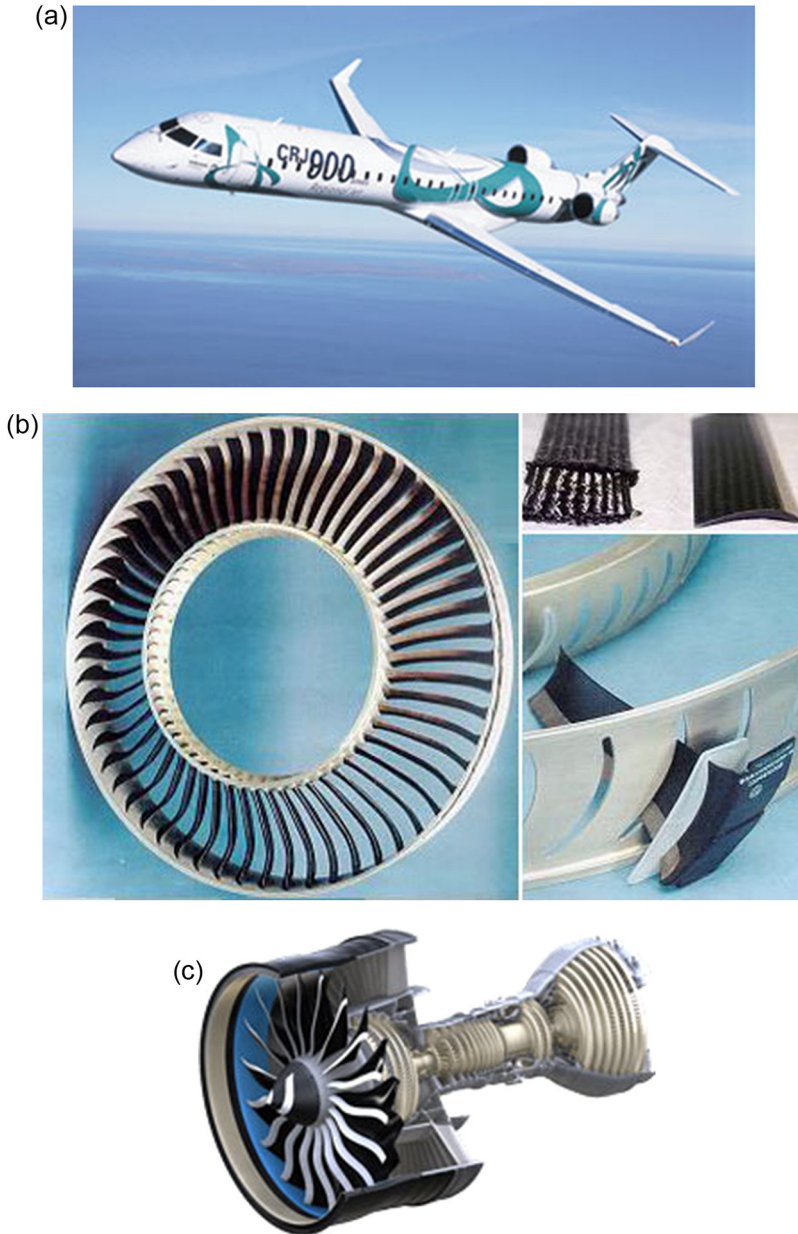
Figure 6.17 A&P Technology use of braided composites in the aerospace industry: (a) wing flaps for Bombardier; (b) jet engine stator vanes; (c) fan case of GenX turbine (images graciously provided by A&P Technology).

which provides 'better impact and better fatigue properties than other materials while greatly reducing manufacture times' (A&P Technology, 2014c).

Recent developments by Airbus in aircraft production have focussed on using braided carbon fibre-reinforced polymers for frames of the A350-1000 (Gardiner, 2012), which is scheduled to enter service in 2017 (Airbus, 2015). The process was initially selected for its low risk and high level of automation and evolved in the European Aeronautic Defence & Space Co. Innovation Works (EADS IW, Ottobrunn, Germany) developing a uniaxial braiding process (Stover et al., 1971). However, in later developments, Airbus decided to not include braided frames in the A350-1000; the reason was to take advantage as much as possible of the commonality in the processes and parts with the A350-900 (Galicia-Roquero, 2015). Braids also have seen new use in concrete reinforcement (Hajihosseini et al., 2014) and concrete confinement (Dagher et al., 2012). These exciting considerations and developments in aerospace and engineering structures demonstrate a bright future for braided composites.

Sources of further information and advice

Braided composites have begun to make their mark in the aerospace industry; however, their use is still in its infancy. Braided composites have been used in structural reinforcement and biomedical engineering applications. Some companies, such as A&P Technology and Airbus, have made highly valuable contributions to the field. These innovators will lead the way to greater discoveries and technological advancements in the aerospace field.

Before greater adoption of braided composites can occur, a greater amount of research must be invested in braided composite material technology. Braided composites are still difficult to produce with repeatability; manufacturing technology and in-line quality control are imperative. In-line preform impregnation and curing must be improved significantly for braiding to be more competitive with other composite material production methods.

Once manufactured, it is vital that properties of braided composite structures be better known, and loading and deformation, along with short and long-term behaviour, must be better understood. Material properties of the various braided structure unit cells must be further evaluated; large material properties databases need to be created. Improved analytical and numerical models need to be developed to predict properties of the different braided composite unit cells, from the simple 2D to the more complex 3D ones. Improved models will lower the cost of the large-scale testing required for using any material in the aerospace field. Although it is clear that these tests are required, proper design methodologies, based on sound modelling capabilities, will diminish the need for early testing, allow for improved part designs and focus on end products testing. There are few models in the literature on fatigue behaviour and failure theories of braided composites. Until such time as these issues are dealt with, it is unlikely that the use of braiding in aerospace will significantly increase and challenge other less versatile composite materials. It is encouraging that a number of groups are working on these issues.

Below are listed a number of seminal works for those interested in studying in greater detail braided composites and their use in aerospace applications. Dr Frank Ko is one of the pioneers in this area; his book with Dr C. Pastore and Head (Head et al., 1989) remains one of the most cited works in the area. A recent book, Braided Structures and Composites: Production, Properties, Mechanics, and Technical Applications, edited by Sohel Rana and Raul Fangueiro (CRC Press, August, 2015), is an excellent source of information on the subject. Two chapters in an encyclopaedia of composites (Carey and Ayranci, 2012), as well as the earlier version by Yang (1990), concisely provide readers much of the basic information about braided composites. Finally, the following book will be a seminal braided composite material handbook: Carey JP (author, editor) et al., Handbook of Advances in 2D and 3D Braided Composite Materials, Theory, Production, Testing and Applications; Woodhead Publishing, Elsevier, 2016.

References

Ayranci, C., Carey, J., 2008. 2D braided composites: a review for stiffness critical applications. Composite Structures 85 (1), 43−58. http://dx.doi.org/10.1016/j.compstruct.2007.10.004.

Ayranci, C., Carey, J.P., 2011. Experimental validation of a regression-based predictive model for elastic constants of open mesh tubular diamond-braid composites. Polymer Composites 32 (2), 243−251.

Ayranci, C., Carey, J.P., 2010. Predicting the longitudinal elastic modulus of braided tubular composites using a curved unit-cell geometry. Composites Part B: Engineering 41 (3), 229−235.

Ahmadi, M.S., Johari, M.S., Sadighi, M., Esfandeh, M., 2009. An experimental study on mechanical properties of GFRP braid-pultruded composite rods. Express Polymer Letters 3 (9), 560−568.

Alagirusamy, R., Fangueiro, R., Ogale, V., Padaki, N., 2006. Hybrid yarns and textile preforming for thermoplastic composites. Textile Progress 38 (4), 1−68.

Agarwal, B.D., Broutman, L.J., Chandrashekhara, K., 2006. Analysis and Performance of Fiber Composites.

A&P Technology, 2014a. Honeywell Jet Engine Stator Vane. Available: http://www.braider.com/Case-Studies/Jet-Engine-Stator-Vane.aspx.

A&P Technology, 2014b. Bombardier Wing Flap. Available: http://www.braider.com/Case-Studies/Bombardier-Wing-Flap.aspx.

A&P Technology, 2014c. GEnx Engine. Available: http://www.braider.com/Case-Studies/GEnx-Engine.aspx.

Airbus, 2015. Airbus A350-1000. Available: http://www.airbus.com/aircraftfamilies/passengeraircraft/a350xwbfamily/a350-1000/.

Baker, A., Dutton, S., Kelly, D., Composite Materials for Aircraft Structures (second ed.). Available: http://app.knovel.com/hotlink/toc/id:kpCMASE001/composite-materials-aircraft/composite-materials-aircraft.

Brunschweiler, D., 1953. Braids and braiding. Journal of the Textile Institute Proceedings 44, 666−686.

Barbaro, E.J., 1999. Introduction of Composite Materials Design. Taylor and Francis, Philadelphia, PA.

British Plastics Federation, 2015. Polypropylene (PP). Available: http://www.bpf.co.uk/plastipedia/polymers/PP.aspx.

Brown, R.T., Crow Jr., E.C., 1992. Automatic through-the-thickness braiding. In: Presented at International SAMPE Symposium and Exhibition.

Braley, M., Dingeldin, M. Advancements in Braided Materials Technology. Unpublished,.

Calvert, T., June 22, 2009. Braided fabrics for aircraft interiors use carbon reinforced PPS tapes. Available: http://www.reinforcedplastics.com/view/2263/braided-fabrics-for-aircraft-interiors-use-carbon-reinforced-pps-tapes/.

Carey, J., Ayranci, C., 2012. Processing and performance of braided composites. In: Nicolais, L., Borzacchiello, A. (Eds.), Wiley Encyclopedia of Composites. John Wiley & Sons, New Jersey, pp. 2427−2437.

Carey, J., Munro, M., Fahim, A., 2005. Regression-based model for elastic constants of 2D braided/woven open mesh angle-ply composites. Polymer Composites 26, 152−164.

Carey, J., Munro, M., Fahim, A., 2003. Longitudinal elastic modulus prediction of a 2-D braided fiber composite. Journal of Reinforced Plastics and Composites 22 (9), 813−831.

Carey, J., Fahim, A., Munro, M., 2004. Predicting elastic constants of 2D-braided fiber rigid and elastomeric-polymeric matrix composites. Journal of Reinforced Plastics and Composites 23 (17), 1845−1857.

Chou, T.W., 1992. Microstructural Design of Fiber Composites. Cambridge University Press, Cambridge.

Crane, R.M., Camponeschi Jr., E.T., 1986. Experimental and analytical characterization of multidimensionally braided graphite/epoxy composites. Experimental Mechanics 26 (3), 259−266.

Cheung, B.K.O., Carey, J., 2015. Measurement and validation of yarn geometry assumptions through digital image correlation. In: TEXCOMP-12 Conference, 26−29 May 2015, Raleigh, NS, USA.

Dagher, H.J., Bannon, D.J., Davids, W.G., Lopez-Anido, R.A., Nagy, E., Goslin, K., 2012. Bending behavior of concrete-filled tubular FRP arches for bridge structures. Construction and Building Materials 37, 432−439.

Du, G.W., Popper, P., 1994. Analysis of a circular braiding process for complex shapes. Journal of the Textile Institute 85 (3), 316−337.

Evans, K.R., Carey, J.P., 2013. Feasibility of a braided composite for orthotropic bone cast. The Open Biomedical Engineering Journal 7, 9.

Falzon, P.J., Herszberg, I., Baker, A.A., 1993. Stiffness analysis of textile composites. In: Presented at National Conference Publication − Institution of Engineers, Australia.

Fang, G., Liang, J., 2011. A review of numerical modeling of three-dimensional braided textile composites. Journal of Composite Materials 45 (23), 2415−2436.

Gutowski, T.G., 1997. Advanced Composites Manufacturing. John Wiley & Sons, Inc.

Gause, L.W., Alper, J.M., 1987. Structural properties of braided graphite/epoxy composites. Journal of Composites Technology and Research 9 (4), 141−150.

Goyal, D., Tang, X., Whitcomb, J.D., Kelkar, A.D., 2005. Effect of various parameters on effective engineering properties of 2 × 2 braided composites. Mechanics of Advanced Materials and Structures 12 (2), 113−128.

Goyal, D., Whitcomb, J.D., 2008. Effect of fiber properties on plastic behavior of 2 × 2 biaxial braided composites. Composites Science and Technology 68 (3−4), 969−977.

Gardiner, G., 2012. Airbus A350 UpdateL BRaF & FPP. Available: http://www.compositesworld.com/articles/airbus-a350-update-braf-fpp.

Galicia-Roquero, E., February 6, 2015. Personal Email, Airbus Media Relations.

Head, A.A., Ko, F.K., Pastore, C.M., 1989. Handbook of Industrial Braiding. Atkins and Pearce.

Harte, A.M., Fleck, N.A., 2000a. Deformation and failure mechanisms of braided composite tubes in compression and torsion. Acta Materialia 48 (6), 1259−1271.

Harte, A., Fleck, N.A., 2000b. On the mechanics of braided composites in tension. European Journal of Mechanics − A/Solids 19 (2), 259−275. http://dx.doi.org/10.1016/S0997-7538(99) 00164−3.

Huang, Z.M., Teng, X.C., Ramakrishna, S., 2005. Fatigue behaviour of multilayer braided fabric reinforced laminates. Polymers and Polymer Composites 13 (1), 73−81.

Halpin, J., 1969. Effects of Environmental Factors on Composite Materials. Tech. Rep. AFML-TR-67−423.

Hu, Y., Xia, Z., Ellyin, F., 2000. Mechanical behaviour of an epoxy resin under multiaxial loadings. Part I: experimental study. Polymers and Polymer Composites 8 (1), 11−18.

Hajihosseini, A., Ayranci, C., Carey, J.P.R., 2014. Simulation of the rapid curing process for braid reinforced FRP rebar in braidtrusion process using a finite element analysis. In: Presented at International SAMPE Technical Conference.

Ivey, M.A., Carey, J.P.R., Ayranci, C., 2014. Braid reinforced polymeric rebar production and characterization. In: Presented at International SAMPE Technical Conference.

Ishikawa, T., Chou, T.W., 1983. One-dimensional micromechanical analysis of woven fabric composites. AIAA Journal 21 (12), 1714−1721.

Ishikawa, T., Chou, T.W., 1982. Stiffness and strength behaviour of woven fabric composites. Journal of Materials Science 17 (11), 3211−3220.

Jones, R.M., 1998. Mechanics of Composite Materials. CRC Press.

Jiang, L.L., Xu, G.D., Cheng, S., Lu, X.M., Zeng, T., 2014. Finite element analysis of thermo-mechanical properties of 3D braided composites. Applied Composite Materials 21 (2), 325−340.

Kamiya, R., Cheeseman, B.A., Popper, P., Chou, T., 2000. Some recent advances in the fabrication and design of three-dimensional textile preforms: a review. Composites Science and Technology 60 (1), 33−47.

Kyosev, Y., 2015. 2-patterning of braided products. In: Kyosev, Y. (Ed.), Braiding Technology for Textiles. http://dx.doi.org/10.1533/9780857099211.1.29.

Kessels, J.F.A., Akkerman, R., 2002. Prediction of the yarn trajectories on complex braided preforms. Composites Part A: Applied Science and Manufacturing 33 (8), 1073−1081.

Ko, F.K., 1987. Braiding. In: Engineered Materials Handbook Anonymous. ASM International, Metals Park, OH, pp. 519−528.

Ko, F.K., 1985. Developments of High Damage Tolerant, Net Shape Composites through Textile Structural Design.

Knoche, R., Koch, D., Tushtev, K., Horvath, J., Grathwohl, G., Schmidt, S., Beyer, S., 2006. Interlaminar properties of 2D and 3D C/C composites obtained via rapid-cvi for propulsion systems. In: Presented at European Space Agency, (Special Publication) ESA SP.

Kaynak, C., Mat, O., 2001. Uniaxial fatigue behavior of filament-wound glass-fiber/epoxy composite tubes. Composites Science and Technology 61 (13), 1833−1840.

Ko, F.K., Yang, C.M., Chou, T., 1986. Structure and properties of multilayer multidirectional warp knit fabric reinforced composites. In: Composites' 86: Recent Advances in Japan and the United States, pp. 21−28.

Kelkar, A.D., Tate, J.S., Bolick, R., 2006. Structural integrity of aerospace textile composites under fatigue loading. Materials Science and Engineering B: Solid-State Materials for Advanced Technology 132 (1−2), 79−84.

Kelkar, A., Whitcomb, J.D., 2009. Characterization and Structural Behavior of Braided Composites. US Department of Transportation. Tech. Rep. DOT/FAA/AR-08/52.

Lomov, S.V., Ivanov, D.S., Verpoest, I., Zako, M., Kurashiki, T., Nakai, H., Hirosawa, S., 2007. Meso-FE modelling of textile composites: road map, data flow and algorithms. Composites Science and Technology 67 (9), 1870−1891.

Lu, Z., Wang, C., Xia, B., 2014. Failure mechanisms analysis and simulation to tensile mechanical behaviors of 3D full five-directional braided composites with interface phase. Fuhe Cailiao Xuebao/Acta Materiae Compositae Sinica 31 (1), 179−186.

Munro, M., Fahim, A., 1995. Comparison of helical filament winding and 2D braiding of fiber reinforced polymeric components. Materials and Manufacturing Processes 10 (1), 37−46.

Malkan, S.R., Ko, F.K., 1989. Effect of fiber reinforcement geometry on single-shear and fracture behavior of three-dimensionally. Journal of Composite Materials 23, 798−818.

Mouritz, A.P., Bannister, M.K., Falzon, P.J., Leong, K.H., 1999. Review of applications for advanced three-dimensional fibre textile composites. Composites Part A: Applied Science and Manufacturing 30 (12), 1445−1461.

Matweb, 2015a. E-Glass Fiber, Generic. Available: http://www.matweb.com/search/DataSheet. aspx?MatGUID=d9c18047c49147a2a7c0b0bb1743e812.

Matweb, 2015b. S-Glass Fiber, Generic. Available: http://www.matweb.com/search/DataSheet. aspx?MatGUID=6eb41a1324834878a1524129d915ca09.

Matweb, 2015c. DuPont Kevlar 29 Amarid Fiber. Available: http://www.matweb.com/search/ DataSheet.aspx?MatGUID=7323d8a43cce4fe795d772b67207eac8.

Matweb, 2015d. DuPont Kevlar 49 Aramid Fiber. Available: http://www.matweb.com/search/ DataSheet.aspx?MatGUID=77b5205f0dcc43bb8cbe6fee7d36cbb5.

Matweb, 2015e. DuPont Kevlar 149 Fiber. Available: http://www.matweb.com/search/DataSheet. aspx?MatGUID=706f16a3a8be468284571dd36bbdea35.

Matweb, 2015f. Hexcel HexTow AS4 Carbon Fiber. Available: http://www.matweb.com/ search/DataSheet.aspx?MatGUID=d875685373f14f79b6ed7bf0d9adcab6.

Matweb, 2015g. Victrex PEEK 450G General Purpose. Available: http://www.matweb.com/ search/datasheet.aspx?MatGUID=ffc10b084c4e4dd6975438d9968e1292.

Munro, M., Fahim, A., 2000. Braiding of Fiber Composite Components (Course Notes for MCG 5180). Department of Mechanical Engineering, University of Ottawa.

Miller, A.H., Dodds, N., Hale, J.M., Gibson, A.G., 1998. High speed pultrusion of thermoplastic matrix composites. Composites Part A: Applied Science and Manufacturing 29 (7), 773−782.

Macander, A.B., Crane, R.M., Camponeschi Jr., E.T., 1986. Fabrication and mechanical properteis of multidimensionally (X-D) braided composite materials. In: Presented at ASTM Special Technical Publication.

Montesano, J., Fawaz, Z., Poon, C., Behdinan, K., 2014. A microscopic investigation of failure mechanisms in a triaxially braided polyimide composite at room and elevated temperatures. Materials and Design 53, 1026−1036.

Naik, N.K., Shembekar, P.S., 1992a. Elastic behavior of woven fabric composites: I-lamina analysis. Journal of Composite Materials 26 (15), 2196−2225.

Nakai, A., Fujita, A., Yokoyama, A., Hamada, H., 1995. Design methodology for a braided cylinder. Composite Structures 32 (1−4), 501−509.

Naik, N.K., Shembekar, P.S., 1992b. Elastic behavior of woven fabric composites: III-laminate design. Journal of Composite Materials 26 (17), 2522−2541.

Naik, N.K., Ganesh, V.K., 1995. An analytical method for plain weave fabric composites. Composites 26 (4), 281−289.

Naik, R.A., 1996. Analysis of woven and braided fabric-reinforced composites. ASTM Special Technical Publication 1274, 239−263.

Nakai, H., Hamada, Hoa, S.V., 1996. Influence of braiding structure on torsional properties of braided composite tube. American Society of Mechanical Engineers, Pressure Vessels and Piping Division. PVP 326, 125−130.

Ohki, T., Ikegaki, S., Kurasiki, K., Hamada, H., Iwamoto, M., 2000. Mechanical properties of flat braided composites with a circular hole. Journal of Engineering Materials and Technology: ASME 122 (4), 420−424.

Perez, J.G., Boitnott, R.L., Johnson, E.R., 2000. Tests of braided composite fuselage frames under radial inward load. In: Presented at Collection of Technical Papers − AIAA/ASME/ASCE/AHS/ASC Structures, Structural Dynamics and Materials Conference.

Pickett, A.K., Sirtautas, J., Erber, A., 2009. Braiding simulation and prediction of mechanical properties. Applied Composite Materials 16 (6), 345−364.

Potluri, P., Manan, A., 2007. Mechanics of non-orthogonally interlaced textile composites. Composites Part A: Applied Science and Manufacturing 38 (4), 1216−1226.

Pastore, C.M., Whyte, D.W., Soebruto, H., Ko, F.K., 1986. Design and Analysis of Multiaxial Warp Knit Fabrics for Composites.

Petermann, J., Plumtree, A., 2001. Unified fatigue failure criterion for unidirectional laminates. Composites Part A: Applied Science and Manufacturing 32 (1), 107−118.

Raju, I.S., Wang, J.T., 1994. Classical laminate theory models for woven fabric composites. Journal of Composites Technology and Research 16 (4), 289−303.

Rana, S., Zdraveva, E., Pereira, C., Fangueiro, R., Correia, A.G., 2014. Development of hybrid braided composite rods for reinforcement and health monitoring of structures. The Scientific World Journal 2014. http://dx.doi.org/10.1155/2014/170187.

Van Ravenhorst, J.H., Akkerman, R., 2014. Circular braiding take-up speed generation using inverse kinematics. Composites Part a: Applied Science and Manufacturing 64, 147−158.

Redman, C.J., Douglas, C.D., 1993. Theoretical prediction of the tensile elastic properties of braided composites. Presented at 38th International SAMPE Symposium.

Roberts, G., Goldberg, R., Binienda, W., Arnold, W., Littell, J., Kohlman, L., 2009. Characterization of Triaxial Braided Composite Material Properties for Impact Simulation. Tech. Rep. NASA/TM-2009−215660.

Stover, E., Mark, W., Marfowitz, I., Mueller, W., 1971. Preparation of an Omniweave Reinforced Carbon-carbon Cylinder as a Candidate for Evaluation in the Advanced Heat Shield Screening Program. Tech. Rep. TR-70−283.

Swanek, D., Steven, S., Carey, J., 2007. Braided composite materials for the production of lightweight, high rigidity golf shafts. Sports Engineering 10, 195−208.

Srikanth, L., Rao, R.M.V.G.K., 2014. Strength and stiffness behaviour of braided and filament wound glass epoxy composites − simultaneous studies and comparison. Journal of Composite Materials 48 (4), 407−414.

Shembekar, P.S., Naik, N.K., 1992. Elastic behavior of woven fabric composites: II-laminate analysis. Journal of Composite Materials 26 (15), 2226−2246.

Swanek, D., Carey, J., 2006. Predicting the Elastic Properties of a 2D Conical Braided Composite. May 21−24. Canadian Society for Mechanical Engineering, Kananaskis.

Staff, 2012. JEC Europe 2012 Paris. Available: http://www.compositesworld.com/articles/jec-europe-2012-paris.

Toray Carbon Fibers America, 2008. "T600S Data Sheet," Technical data sheet CFA-004.

Tolosana, N., Lomov, S.V., Miravete, A., 2007. Development of a geometrical model for a 3D braiding unit cell based on braiding machine emulation. In: Finite Element Modelling of Textiles and Textile Composites, St-Petersburg, pp. 26−28, 2007.

Tate, J.S., Kelkar, A.D., Whitcomb, J.D., 2006. Effect of braid angle on fatigue performance of biaxial braided composites. International Journal of Fatigue 28 (10), 1239−1247.

Tang, X., Whitcomb, J.D., Goyal, D., Kelkar, A.D., 2003. Effect of braid angle and waviness ratio on effective moduli of 2×2 biaxial braided composites. In: Presented at Collection of Technical Papers − AIAA/ASME/ASCE/AHS/ASC Structures, Structural Dynamics and Materials Conference.

Tsai, K.H., Hwan, C.L., Chen, W.L., Chiu, C.H., 2008. A parallelogram spring model for predicting the effective elastic properties of 2D braided composites. Composite Structures 83 (3), 273−283.

Wang, Y., Zhao, D., 2006. Effect of fabric structures on the mechanical properties of 3-D textile composites. Journal of Industrial Textiles 35 (3), 239−256. http://dx.doi.org/10.1177/1528083706057595.

Wu, L., Zhang, F., Sun, B., Gu, B., 2014. Finite element analyses on three-point low-cyclic bending fatigue of 3-D braided composite materials at microstructure level. International Journal of Mechanical Sciences 84, 41−53.

Wu, L., Gu, B., 2014. Fatigue behaviors of four-step three-dimensional braided composite material: a meso-scale approach computation. Textile Research Journal 84 (18), 1915−1930.

Yang, J.M., 1990. Processing and performance of 3-D composites. In: International Encyclopedia of Composites, 4. Anonymous VCH Publishers, pp. 449−463.

Yang, J.M., 1987. Analysis and Design of Three-dimensional Composites, EM87-832. Society of Manufacturing Engineers.

Zhang, Q., Beale, D., Broughton, R.M., 1999. Analysis of circular braiding process, Part 1: theoretical investigation of kinematics of the circular braiding process. Journal of Manufacturing Science and Engineering: ASME 121 (3), 345−350.

Zhang, C., Binienda, W.K., Goldberg, R.K., Kohlman, L.W., 2014. Meso-scale failure modeling of single layer triaxial braided composite using finite element method. Composites Part A: Applied Science and Manufacturing 58, 36−46.

Zhou, L.D., Zhuang, Z., 2013. Strength analysis of three-dimensional braided T-shaped composite structures. Composite Structures 104, 162−168.

Auxetic composites in aerospace engineering

7

Z. Wang, A. Zulifqar, H. Hu
Hong Kong Polytechnic University, Kowloon, Hong Kong

7.1 Introduction

As we know, most materials laterally shrink when stretched and laterally expand when compressed in the longitudinal direction, that is, they have a positive Poisson's ratio (PR). The common example of rubber can be quoted; it becomes thinner when stretched. In contrast, there are some special materials which possess negative PR (ie, they laterally expand when stretched or laterally shrink when compressed in the longitudinal direction). The materials with negative PR are also called 'auxetics' (Evans et al., 1991), which originated from the Greek word *auxetos* meaning 'that which may be increased'. Auxetic materials can be found among natural materials such as rocks, minerals, skin and others. They can also be produced synthetically. To date, many auxetic materials have been made including auxetic foams such as polyurethane (Lakes, 1987), polytetrafluoroethylene (PTFE) (Caddock and Evans, 1989) and ultra-high-molecular-weight polyethylene (Alderson and Evans, 1992); auxetic textiles such as fibres (Ravirala et al., 2006, 2005; Alderson et al., 2002), yarns (Sloan et al., 2011) and fabrics (Wang and Hu, 2014; Liu et al., 2010; Ge and Hu, 2013; Ugbolue et al., 2011; Hu et al., 2011); auxetic composites and so on.

Auxetic materials have many enhanced properties compared to conventional materials. Auxetic materials have higher shear modulus, enabling auxetic materials to have better shear resistance. Auxetic materials have a double-curved (synclastic) property, that is, when fixed on a curved surface, the materials form a dome shape instead of the saddle shape (anticlastic) that conventional materials may form. Auxetic materials have enhanced indentation resistance and energy absorbance properties. When conventional materials are subject to an impact force, the materials flow away from the impact point, whereas the auxetic materials flow into the impact point when subject to an impact force, which makes the auxetic materials harder to be indented. Auxetic materials also have other advantages, such as enhanced fracture toughness, enhanced crack growth resistance and so on.

Due to the enhanced properties that auxetic materials possess, auxetic composites have better performance than conventional composites and have some special applications. In this chapter, the auxetic composites and their applications will be discussed in detail, especially the applications in aerospace engineering.

7.2 Definition and concept

Auxetic composites are a special kind of composites that have a negative PR. They laterally expand when stretched or laterally shrink when compressed in the longitudinal direction. They can be made from conventional materials, such as by using the laminated angle-ply method, in which the layers are stacked in a special sequence which creates a negative PR. They also can be made from auxetic materials, for example by using auxetic inclusions with different geometry, proportions and properties to make the final composites possess auxetic properties.

7.3 Advantages and disadvantages

Auxetic composites have many advantages, thanks to the auxetic behaviour they possess. As a special kind of composite, they have the same common advantages as other composites, such as high specific stiffness, high specific strength and light weight. At the same time, they also have the advantages of auxetic materials that were mentioned in Sections 7.1 and 7.2. Compared with conventional composites, the auxetic composites have higher shear modulus, enhanced indentation resistance, synclastic curvature, better crack resistance, higher damping resistance and so on. Due to these advantages, auxetic composites are very suitable for use in high-profile applications, such as automotive and aerospace engineering. The high shear modulus makes auxetic composites very suitable for aerospace engineering because most parts of the aircraft endure high shear force, such as the wings. The synclastic curvature property enables auxetic composites to have better formability than conventional composites, which makes them particularly useful in places where a complex shape needs to be formed. Auxetic composites have a high strength-to-weight ratio. We know that the weight saving is extremely important for aircraft, and that both energy consumption and pollution can be reduced by lowering the aircraft weight. Performance and safety can also be improved. Another advantage of auxetic composites is that the auxetic property and strength can be customized by changing the component's proportions. With different components and manufacturing methods, specific auxetic composites can be made for desired usages. The disadvantage of auxetic composites is that they are difficult to manufacture on a large scale. Therefore, most auxetic composites are still in theory and laboratory stages.

7.4 Types of auxetic composites

Developments in high-performance materials for applications like aerospace, automobile sports and leisure equipment have required the production of auxetic materials. Within this class of materials are the auxetic composites. Milton (1992) discussed the development of composite materials with negative PR. Auxetic composite materials can be produced either from conventional components via a specially designed

structural arrangement of the components or from auxetic components. In both cases, the fracture toughness, a mechanical property of a material which greatly depends on the PR, is reported to be enhanced as the PR approaches -1. Fracture toughness has very important implications for aerospace applications. In this section, the types of auxetic composites based on conventional components and auxetic components are discussed.

7.4.1 Laminated angle-ply auxetic composites

The idea is to transform a nonauxetic material into auxetic forms. The route closest to conventional manufacture of auxetic composites from laminated angle plies is the use of prepreg material and conventional manufacturing techniques like vacuum bag moulding. In order to achieve the auxetic effect, different stacking sequences of individual lamina are modelled, and the most suitable stacking sequence is selected. One of the most essential requirements of the individual lamina material is that it should be highly anisotropic. Therefore, carbon fibre as reinforcement is a more appropriate selection than Kevlar or glass. The majority of research work recommends the use of carbon fibre for producing auxetic composites (Alderson and Alderson, 2007). The first stage in the manufacture of auxetic composites from laminated angle plies is to design an appropriate stacking sequence of individual lamina material that could produce an auxetic effect either in plane or out of plane. This is achieved by using specially designed software. The software predicts the mechanical properties including the in-plane loading, maximum stiffness, bending strength and stability of a specific stacking sequence. To date, several different optimization approaches for the design of a suitable stacking sequence for laminated plates subjected to various stiffness and strength constraints have been established. Wenchao and Evans (1992) presented a more general approach for the optimization of stacking sequence. The FORTRAN programme they have developed enables the designers to optimize the mechanical properties of a specific stacking sequence if only the individual lamina layer properties are known. This programme is also capable of producing an optimized stacking sequence with minimum difference between properties calculated from, for example, classical laminate theory and those properties required by the designer (Alderson et al., 2005).

7.4.2 Composites with auxetic inclusions

Auxetic composites also can be manufactured by embedding different shapes with auxetic behaviour, known as inclusions, in a matrix. It must be emphasized here that the material of the inclusion has a positive PR. The auxetic behaviour is caused by the shape of the inclusion. First, an analysis for the deformation mechanism of the inclusion shape is carried out by using the finite element method. The inclusions are then embedded in a matrix to produce a composite structure. Wei and Edwards (1998) carried out an analytical and numerical study on composites with auxetic inclusions of various shapes such as discs, spheres, blades, needles and disks. It was observed that the phase properties such as inclusion volume, area fraction, matrix and inclusion PRs and Young's moduli have marked effects on the effective PR of

Figure 7.1 Periodicity cell and a
one-fourth model of a composite with
nonconvex inclusion.

Stretched →   ← Initial state
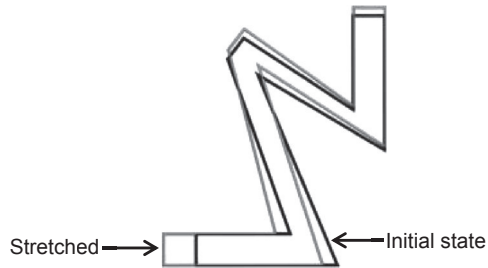
the composite with auxetic inclusions. The disk-like inclusion produced a composite
with the highest value of a negative PR. Another shape (ie, a nonconvex inclusion)
has been studied by Stavroulakis (2005). An example is shown in Fig. 7.1.
One-fourth of the periodicity cell of the nonconvex inclusion with appropriate symme-
try boundary conditions alongside the external boundaries was studied in detail with
the finite element method. In order to make the analysis simple, a very weak matrix
was assumed and then was ignored in the analysis. The results proved that loading
at the left-hand-side boundary leads to overall auxetic behaviour. This can be observed
by the deformation of the upper boundary while load is applied at the left-hand-side
boundary.

Hou et al. (2012) has reported a novel method to produce composite structures hav-
ing auxetic random inclusions and showing an isotropic auxetic effect. The re-entrant
squares and re-entrant triangles were analysed by the finite element method to observe
the deformation mechanism. The results proved that the re-entrant triangles are the best
choice as random inclusions that could be embedded in a matrix to form
two-dimensional (2D) composite structures as shown in Fig. 7.2. Different composite

(a)

Loading direction

(b)
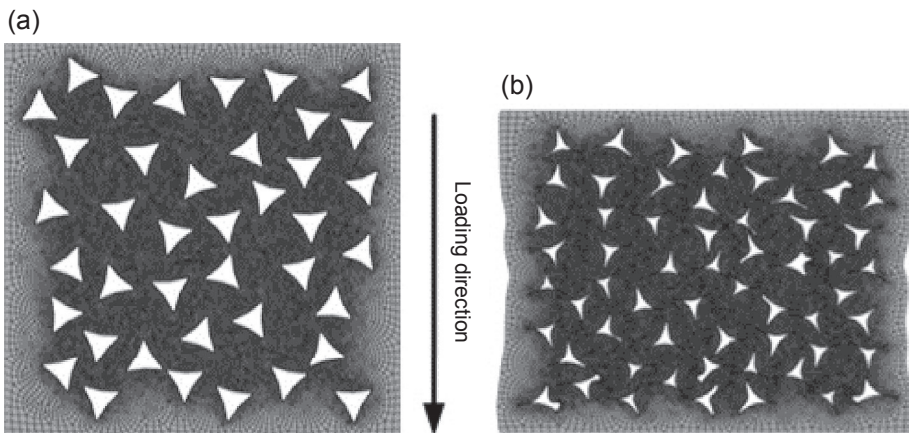
Figure 7.2 (a) Undeformed and (b) deformed finite element model with inclusions.
Hou, X., Hu, H., Silberschmidt, V., 2012. A novel concept to develop composite structures with
isotropic negative Poisson's ratio: effects of random inclusions. Composites Science and
Technology 72 (15), 1848−1854.

structures are built with different numbers (20, 40, 60 and 80) of inclusions through a parametric model. The mechanical behaviour and auxetic effect of these structures were studied using the finite element method.

The results show that by increasing the number of re-entrant inclusions into the composite structure, the isotropic auxetic effect is greatly enhanced. Therefore, the selection of an appropriate re-entrant structure as random inclusion into a matrix may lead to the development of a composite structure with an isotropic auxetic effect. Some of the re-entrant structures with orthogonal geometrical shapes can only exhibit auxetic behaviour in certain directions. As an example, the re-entrant square exhibits a positive PR behaviour when loading is applied along certain symmetry axes. On the other hand, re-entrant structures with nonorthogonal symmetrical patterns, for example a re-entrant equilateral triangle, exhibit a negative PR behaviour. The auxetic effect can also be adjusted by the re-entrant degree of the structure. The PR of a composite structure with fewer inclusions could be positive even if the inclusions have auxetic effects. However, the isotropic auxetic effect of a composite can be obtained if the number of random inclusions reaches a certain level. It was observed that if the number of inclusions surpasses 60, the isotropic auxetic effect of the composite structure can be realized from the beginning of application of compression force.

7.4.3   Auxetic composites made from preforms based on auxetic textile structures

7.4.3.1   What is a preform?

A preform is an assembly of fibres wetted with liquid resin, and it has the shape of the desired part (Hoa, 2009). After the resin is cured, a composite part is obtained. There are several advantages to making preforms of the reinforcement before loading it into the mould. Preforms speed up the process; they also improve quality and reduce part-to-part variations. Both thermoplastic and thermosetting powders can be used as preforming agents (binders). The ideal preform should be so stiff that it becomes self-locating in the production mould. In addition, the preforming agent should not decrease the permeability, the wettability or the mechanical properties of the finished part, but it should still make the preform stiff enough so that it can be handled. It is also important to consider that the mechanical properties can be knowingly reduced by the preforming operation, but they also can be close to the value without a preform binder if the preforming agent is chosen carefully. Therefore, for a given matrix system, suppliers recommend that binder or pretreated reinforcement should always be used. It should be noted that the permeability of the resin in the fibre preform depends to a great extent on the fibre volume fraction. Since the compaction pressure has great influence on the fibre volume fraction, this pressure therefore has important influence on the flow of the resin through the preforms. Different techniques such as weaving, braiding, stitching and knitting can be employed to make the preforms.

Preforms for auxetic composites can be classified into two main classes:

1. Planner auxetic preforms
2. 3D auxetic preforms

Planar auxetic assemblies

These preforms include 2D planner fabrics. The auxetic yarns can be weaved or knitted, or they may be in the form of tows and tapes arranged layer by layer at 0 degree/90 degree without a weaving or knitting process. Miller et al. (2009) reported that an auxetic composite can be produced by using a woven auxetic fabric made of auxetic yarns. The preform for an auxetic composite can be made using a double-helix yarn (DHY). The yarn consists of two components; a relatively thin but stiffer fibre is wrapped helically around a compliant, thicker, initially straight elastomeric core fibre, as shown in Fig. 7.3(a). On application of longitudinal stretch, both the components are elongated. The stiffer wrap displaces the thicker core laterally, resulting in overall lateral expansion of the yarn along the width. Initially the thicker core is a helix with zero pitch, and the stiffer wrap is a helix with an internal helical diameter equal to the outer diameter of the thicker core. When the longitudinal stretch is applied, the stiffer wrap becomes a helix with zero pitch and the thicker core becomes a helix with an internal diameter equal to the diameter of the stiffer wrap, as shown in Fig. 7.3(b). The thicker core performs two functions: when the stretch is applied it causes lateral deformation, and on removal of stretch it acts as a return spring to resume the original helix in the wrap. The auxetic behaviour of DHY yarns can be reserved in a woven fabric preform if the pitch levels between adjacent yarns in the fabric and material properties are optimized. Therefore, the DHY yarns should be woven out of register (ie, to place warp and weft yarns at alternate positions during weaving for different layers) to maximize the auxetic behaviour. Furthermore, if a matrix with a suitable matched modulus is selected, the auxetic composites can also be engineered by using woven fabric made of DHY yarns. There should be a notable difference in stiffness between the three components (ie, the wrap is an order of magnitude stiffer than the yarn), which in turn is an order of magnitude stiffer than the matrix. It is important to consider that a single-layer composite will not be auxetic; most probably, the constraint imposed by the matrix will not be sufficient to prevent the fibres from overlapping out of plane. The auxetic effect in the composite is likely to be due to the extra constraint provided by the additional layers of the DHY textile network. It is usual for composites to be multilayered. A double-layer auxetic
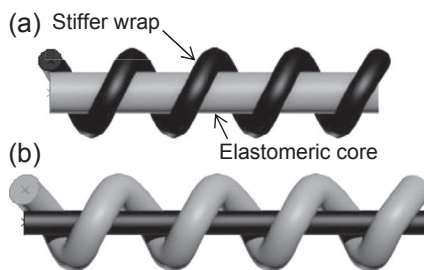
Figure 7.3 The structure of DHY: (a) initial state and (b) stretched.
Adapted from Miller, W., Hook, P., Smith, C.W., Wang, X., Evans, K.E., 2009. The manufacture and characterisation of a novel, low modulus, negative Poisson's ratio composite. Composites Science and Technology 69 (5), 651−655.

composite with an approximate PR of -0.1 can be produced using the woven fabric reinforcement manufactured from DHY yarn. The properties of DHY yarn used are given in Table 7.1. Note that the material properties of the core material are likely to be anisotropic due to the drawing process used to produce commercial fibres, and the wrap angle used is 70 degree.

The DHY yarn has a PR of -2.1. The reinforcement is a plain woven fabric. The DHY yarn is used as weft, and Meta-aramid yarn of approximately 475 dtex linear density is used as warp. The matrix material for the composite samples selected is silicone rubber gel (Dow Corning 3$-$6512, two-part elastomer).

Sloan et al. (2011) also suggested the use of helical auxetic yarns (HAYs) in a simple weave pattern to produce an auxetic textile preform, and they used this preform to manufacture a low-modulus composite. They have suggested the use of polyurethane as core fibre and polyamide as wrap fibre. The properties of the core and wrap fibres used are given in Table 7.2.

Auxetic DHY also can be used to produce a unidirectional fibre composite with both relatively high stiffness (4 GPa) and negative PR (6.8), at 30% of the fibre volume fraction, compared to other auxetic composites (Miller et al., 2012).

However, to date many auxetic knitted fabrics have been produced by using non-auxetic yarns, but no work has been reported yet about manufacturing auxetic composites based on auxetic knitted fabric preforms.

Table 7.1 Properties of DHY yarn used to manufacture auxetic composite (Miller et al., 2009)

Component	Material	Linear density (dtex)	Diameter (mm)	Young's modulus	Poisson's ratio
Wrap fibre	Twisted UHMWPE	220	0.32	6 GPa	0.5
Core fibre	Polyurethane	—	0.64	53 Mpa	0.48

UHMWPE, ultra-high-molecular-weight polyethylene.

Table 7.2 The properties of core and wrap fibres (Sloan et al., 2011)

	Polyurethane core	Polyamide wrap	Helical auxetic yarn 13 degree
Young's modulus (MPa)	30	3400	76
Ultimate tensile strength (MPa)	51	789	56
Strain at break (%)	95	17	34

7.4.3.2 3D auxetic assemblies

Ge and Hu (2013) combined the nonwoven and stitching technologies to produce a novel 3D fabric structure that could be utilized as a preform to produce auxetic composites. The novel 3D auxetic fabric structure as shown in Fig. 7.4(a) is composed of three yarn systems (ie, weft yarns, warp yarns and stitch yarns). The weft yarns and warp yarns are not interlaced, as is the case in woven fabric preforms, and therefore not crimped. Instead, they are placed at 90-degree angles upon one another and held in position by a third yarn. The warp yarns are placed one in and one out, and the positions of all of the warp yarns in two neighbouring layers are alternated by half yarn spacing. The third yarn is placed through the thickness direction and serves as the stitching yarn, as shown in Fig. 7.4(a). When the structure is compressed through the thickness direction, the weft yarns will get crimped, resulting in shrinkage of the structure in the weft directions. Since the weft yarns are fully arranged, the shape of the warp yarns remains unchanged under compression, as shown in Fig. 7.4(b), and the size of structure will not change in the warp direction. Therefore, under compression, the structure will exhibit auxetic behaviour in the weft direction and zero PR in the warp direction.

   The phenomenon of compression and shrinkage in the weft direction can be demonstrated better with the help of Fig. 7.5. Fig. 7.5(a) shows a repeating unit of the structure outlined by breaking lines. Fig. 7.5(b) demonstrates the condition under compression. The auxetic effect is mainly produced due to the spaces between the warp yarns. This may result in the reduction of the stability of the structure. As this 3D auxetic structure is developed as composite reinforcement, the compressible matrix will be filled in the spaces of the structure to make the composite. Therefore, the stability of the composite structure will be ensured. To fabricate this 3D NPR fabric structure, a special textile manufacturing process that combines both the stitching and nonwoven technologies has been proposed. It is notable that if the same type of yarn is used for both the weft and warp yarns, the auxetic effect of the structure would not be very obvious. The weft yarn should be flexible, and the warp yarn should be rigid. An elastic yarn with a smaller diameter than that of the warp and weft yarns
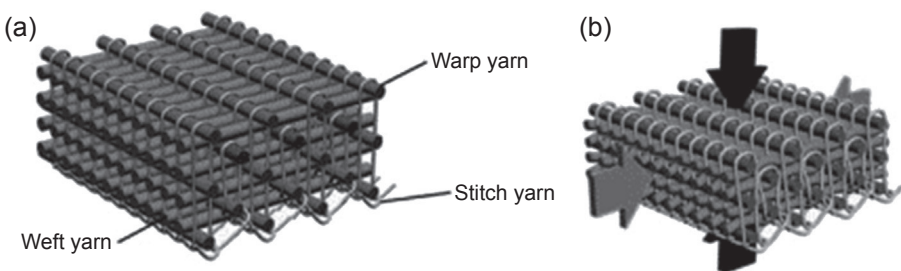
Figure 7.4 Three-dimensional negative Poisson's ratio textile structure: (a) initially and (b) under compression.
Ge, Z., Hu, H., 2013. Innovative three-dimensional fabric structure with negative Poisson's ratio for composite reinforcement. Textile Research Journal 83 (5), 543−550. Copyright © 2013 by SAGE Publications. Reprinted by permission of SAGE.
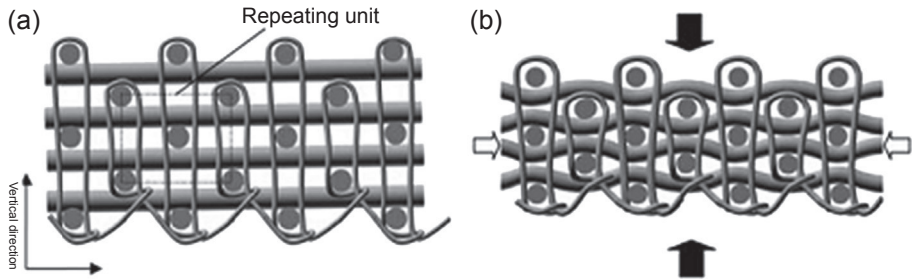
Figure 7.5 The cross-section of a three-dimensional auxetic structure: (a) initially and (b) under compression.

Ge, Z., Hu, H., 2013. Innovative three-dimensional fabric structure with negative Poisson's ratio for composite reinforcement. Textile Research Journal 83 (5), 543−550. Copyright © 2013 by SAGE Publications. Reprinted by permission of SAGE.

can be used as the stitching yarn for a better binding effect. The elasticity of the stitch yarn may be selected in such a way that the whole structure can be held by stitches without causing the obvious deformation of the weft yarns at the initial state. It is also important that under the action of the stitch yarn tension, the weft yarns cannot be kept totally straight at the initial state. So this initial effect should be taken into consideration during the analysis of the structure.

7.4.4 Fibres and matrix systems for auxetic composites

An initial study of laminated fibre-reinforced composites possessing a negative PR was carried out by Alkhalil (1990), who used a Kevlar−epoxy fibre matrix system to produce negative PR composites. The manufacture of auxetic composites by embedding an auxetic network in a conventional matrix material was first modelled numerically by Evans et al. (1992). Clarke et al. (1994) had reported that in order to enhance the value of ν, one of the elementary requirements of the individual lamina material is that it must be highly anisotropic, which makes a carbon fibre−epoxy resin system a more suitable choice for auxetic composites. Clarke et al. have also discussed the methods of increasing the value of ν, including using a prepreg with increased anisotropy (ie, using a stiffer fibre or a higher volume fraction). Furthermore, it was reported that auxetic composites can also be manufactured by using unidirectional prepreg tapes of epoxy resin reinforced with continuous carbon fibres and laminating them. The auxetic behaviour for such composites was observed for an angle of ply in the range between 15 degree and 30 degree, which was in accordance with the standard laminate theory. Unidirectional layers of glass or high-modulus carbon fibre within an epoxy resin as matrix have been used to produce angle-ply composites. Theoretical and experimental investigations showed that if there are an equal number of layers at an angle to a reference direction, a large, positive in-plane PR and a large, negative out-of-plane PR can be achieved (Hine et al., 1997). It was found that the composite would be auxetic provided the modulus of reinforcement was high and that of the

matrix material sufficiently lower. In their study, Evans et al. suggested that a negative PR would be unlikely in glass fibre composites since the fibre modulus is too low, but that a negative PR is probable in a carbon fibre composite. Later, Zhang et al. (1998) had used glass fibres as reinforcement and epoxy resin as matrix material. Evans et al. (2004) suggested the use of a continuous carbon fibre−epoxy resin system for auxetic composites in order to achieve either an in-plane or out-of-plane negative PR, provided that the fibre volume fraction and anisotropy are high enough, by selecting suitable stacking sequences. The majority of research work has been carried out on the carbon fibre composites, and it is now focussed on determining how the properties of the laminates are affected (Alderson et al., 2005). Hadi Harkati et al. (2007) had produced negative PR values of up to $\nu = -0.746$ over certain orientation angles for Kevlar and carbon reinforcements. Alderson and Coenen (2008) used the unidirectional carbon−epoxy prepreg to manufacture auxetic composites. Donoghue et al. (2009) manufactured auxetic laminates from the carbon fibre−epoxy prepreg AS4/3501-6. Bezazi et al. (2009) selected Hexcel prepreg T300/914 carbon−epoxy material to manufacture auxetic composites because of its widespread use in aerospace applications and its overall good mechanical properties (Table 7.3). Coenen and Alderson (2011) used an IM7/5882 unidirectional carbon−epoxy prepreg to produce composites with a negative through-the-thickness Poisson's ratio.

To date, all three material combinations have been investigated (Herakovich, 1984; Clarke et al., 1994; Zhang et al., 1998; Donoghue et al., 2009). In many cases, the negative PRs obtained by this route to date have been small (ie, around $\nu = -0.17$), although Miki and Murotsu (1989) had achieved a value of $\nu = -0.37$ for unbalanced, bidirectional laminates. Stagni (2001) has investigated that the Poisson ratio of composites reinforced with thinly coated hollow-cored fibres, and with osteon-like fibres, becomes negative beyond certain porosity levels. Auxetic fibre-reinforced composites can also be manufactured by composing auxetic components; for example, an auxetic matrix, auxetic reinforcement or both. This has been realized using auxetic foams previously (Chen and Lakes, 1993). A simple press-fit fastener has been developed and tested based on auxetic copper foam. Both theoretical and experimental investigation revealed that it is much more difficult to remove than conventional copper foam (Choi and Lakes, 1991). Although the work on auxetic fibre-reinforced composites of this type has recently been started with advances in the manufacture of auxetic fibres and auxetic polymers (Alderson et al., 2002, 2005; Ravirala et al., 2005), Hook et al. (2004) claimed in their patent for a fibre matrix system for auxetic composites that the reinforcement may be a fibre, rod or hollow tube, particularly of a relatively high-modulus material

Table 7.3 Mechanical properties of a T300/914 composite (Bezazi et al., 2009)

Moduli			Shear moduli			Poisson's ratio		
E_1 (GPa)	E_2 (GPa)	E_3 (GPa)	G_{12} (GPa)	G_{13} (GPa)	G_{23} (GPa)	ν_{12}	ν_{13}	ν_{23}
131.9	9.51	9.43	5.27	7.03	3.39	0.326	0.341	0.485

(natural or man-made, inorganic or organic, and may or may not be auxetic). They claimed that carbon fibre, glass fibre, polyaramids (eg, Kevlar), polyamides (eg, nylon), polyesters, polyalkylenes, polyethylene terephthalate (PET), metal wire, cotton or other material can be used as reinforcements for manufacturing auxetic composites. Furthermore, if the reinforcement is a hollow tube, the tube may contain additional materials like siloxane, liquid silicone rubber, natural rubber, nitrile rubber or any other elastomeric material (natural or man-made, and may or may not be auxetic) with an intermediate or low modulus of elasticity, and the material is capable of deformation without fracture. In addition, they have reported that the additional materials may have different properties from the tubing; the first component is of a higher modulus than the second component. The first component may have a diameter that is between 0.01 and 1 times the diameter of the second component. The first component may be between 0.001 and 1 times the cross-sectional area of the second component. They have claimed about the matrix system for auxetic composites that siloxane foams, polyurethane foams, liquid silicone rubbers, natural rubber and other low-modulus-of-elasticity materials (man-made or natural) may be used to form the matrix or act as void fillers. Alderson et al. (2005) used auxetic polypropylene fibre to produce a single fibre composite, and tests have been carried out to assess their pull-out performance from a specially designed matrix. The results have shown that it is up to four times more difficult to pull out an auxetic fibre than a similar conventional fibre. Miller et al. (2009) suggested the use of DHY along with silicone rubber gel (Dow Corning 3−6512, two-part elastomer) as the matrix material to manufacture auxetic composites. The properties of DHY yarn that they have used are shown in Table 7.1. Miller et al. (2012) in another study found low-tow-count carbon fibre (Toray T300-1K) and drawn monofilament nylon fibre adequate in order to manufacture a DHY for auxetic composites; the wrap angle of the yarn was controlled by a helical fibre guide (the yarn wrapper). The higher modulus carbon fibre 'wrap' with a diameter of 0.2 mm and Young's modulus of 143 GPa was helically wound around the lower modulus nylon 'core' which had a diameter of 0.7 mm and Young's modulus of 1.6 GPa. They have produced DHY with wrap angles of 10 degree, 20 degree and 30 degree. They have used unsaturated polyester resin (CFS Fiberglass Supplies, UK) with a modulus of 2.1 GPa and a Poisson's ratio of 0.38 as matrix to produce auxetic composites.

7.4.5 Manufacturing techniques of auxetic composites

There are a number of ways in which auxetic fibre-reinforced composites can be made. The method adopted to date by most researchers to manufacture auxetic composites is to use off-the-shelf prepreg material and the conventional vacuum bag moulding technique for manufacturing fibre-reinforced composites (Alderson and Alderson, 2007; Alderson and Coenen, 2008).

7.4.5.1 Vacuum bag moulding technique

The vacuum bag moulding technique is an extension of the wet lay-up process. In this technique, after completion of laying up, a nonadhering film of polyvinyl alcohol or

nylon is placed over the lay-up and sealed at the mould flange. A vacuum is then drawn on the bag formed by the film by a vacuum pump. In order to consolidate the laminate, up to 1 atm of vacuum pressure can be applied. The laminated composite can be cured at room or elevated temperature. In comparison to conventional manual lay-up techniques, vacuum bagging provides greater concentrations of reinforcements, better adhesion between layers, and more control over the fibre−matrix ratios. Primarily, epoxy and phenolic resin are used for this technique as polyesters and vinyl-esters may cause problems due to excessive extraction of styrene from the resin by the vacuum pump. A variety of heavy fabrics can be wet-out. Higher fibre content laminates can be achieved with vacuum bagging than with standard wet lay-up techniques. Lower void contents can be achieved than with wet lay-up, and better fibre wet-out can also be achieved because of pressure and resin flow throughout structural fibres. The amounts of volatiles emitted during cure are much lower than with other techniques. On the other hand, the extra process adds costs for labour and for disposable bagging material. In addition, a higher skill level is required for mixing and controlling resin contents. Advanced composite manufacturing, including aerospace components, cruise boats, race car components and so on, utilizes this method with preimpregnated fabrics rather than wet lay-up materials that require oven or autoclave cures (Rosato, D.V., 1997).

Alderson et al. (2005); Coenen and Alderson (2011) used the standard vacuum bag moulding technique to manufacture auxetic composites. The schematic of this technique is shown in Fig. 7.6 (Rosato, D.V., 1997).

The laminate was prepared in accordance with the required stacking sequence. Each successive ply of the prepreg was placed on top of the other at the chosen orientation on a smooth base plate. The base plate should be covered by a PTFE release material in order to facilitate removal of the specimen after curing. After completing the process of lamination, a metal top-plate covered in PTFE release material was placed on the laminate stack. A layer of breather fabric with a vacuum valve attachment fastened in a central position was placed on top in order to facilitate the passage of air efficiently. The whole assembly was then made airtight by using a high-temperature nylon bagging film and vacuum sealant. A vacuum pressure of 0.8 bar was applied overnight to consolidate the laminate. The lay-up was placed in a fan oven, and the temperature was raised at a rate of 2−3°C/min until a temperature of 180°C was achieved. This temperature was maintained for 130 min. The oven and the specimen were then slowly cooled to room temperature, the vacuum pressure was removed and the bag was
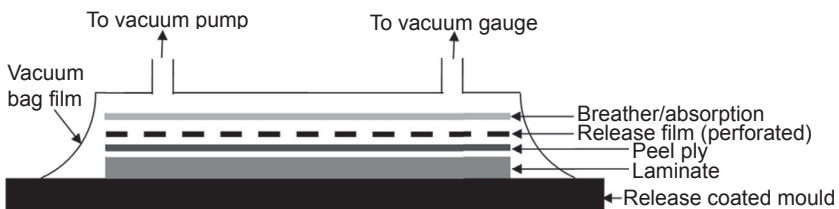
Figure 7.6 Standard vacuum bag moulding technique.

opened. The specimen was removed to measure the through-thickness PR values by using the technique of video extensometry. Donoghue et al. (2009) have reported an almost similar method to manufacture auxetic laminated composites by using the standard vacuum bagging technique. It was reported that in order to produce configurations based around a negative in-plane PR, laminates were 16 plies thick, giving an overall thickness of 2.5 mm. For configurations based around a negative through-thickness PR, laminates were 24 plies thick, giving an overall thickness of 4 mm. A vacuum pressure of 1 bar was applied to each laminate for 1 h prior to heating to consolidate the laminate. The lay-up was then placed in a fan oven, and the temperature was raised at a rate of 2.5 K/min until a temperature of 180°C was achieved. This temperature and pressure both were then maintained for 2 h until the curing stage had reached completion. The laminate was then slowly cooled at a rate of 1.5 K/min, and the vacuum pressure removed after 90 min of cooling time. The composite specimen was then removed for testing. The auxetic composites can also be produced by using DHYs. The process involves the following steps. First of all, temporarily adhering DHY fibres uniaxially within a rectangular frame is carried out in order to ensure that DHY yarns are parallel; the rectangular frame after packing with DHY fibres was then placed in a mould. It was determined that there was no easy method available to control register between DHY fibres. Therefore, the control over register between neighbouring DHY fibres was not possible. The two parts of the polyester resin are then mixed and poured into the mould and placed in a vacuum chamber for 6 min, or until no further gas bubbles evolved, and then cured in an oven at 60°C for 30 min (Miller et al., 2012).

7.4.6 Factors to be considered during auxetic composite manufacturing

In order to achieve an effective in-plane or out-of-plane negative PR, in case of continuous carbon fibre−epoxy resin composites, the fibre volume fraction and anisotropy should be high enough and appropriate stacking sequences must be selected (Evans et al., 2004). The negative in-plane PR may also be achieved by composing two plies of laminates with different fibre orientations. When the forces are applied, they will undergo the same deformation, and an internal shear will also be developed in the plies to manage the deformation. When the internal shear stress exerts to the off-axis ply, it will induce an extension because of the shear extension coupling character, and because of that extension the specimen will widen and produce a negative in-plane PR. Therefore, fibre orientation in individual plies is an important consideration during design and optimization of auxetic composites (Yeh et al., 1999). In the case of auxetic composites based on DHY reinforcements, a constant tension should be maintained during wrapping in order to prevent loss of contact between the wrap and core, and to prevent the carbon fibre from snagging which may cause rupture of individual carbon fibre strands (Miller et al., 2012). There must be a difference in stiffness of all three components for auxetic composites based on DHY reinforcements. The wrap material should be stiffer than the yarn, while the yarn should be stiffer than the matrix (Miller et al., 2009). In the case of auxetic composites based on auxetic inclusions such as

spherical, elliptic or ellipsoidal, disc-like, blade-like, sphere-like and needle-like inclusions, the auxeticity can be enhanced by increasing the inclusion volume fraction above a critical value provided that the ratio of Young's modulus of inclusion to that of a matrix falls within a definite interval (Wei and Edwards, 1998).

7.5 Properties

7.5.1 The myth of auxeticity and modulus

The auxetic system, composed of two materials with different properties, can achieve enhancements in the Young's modulus if one of the materials has a negative PR. This is not only true for Young's modulus, but also for strength, damping, indentation resistance and shear modulus. When a structure is loaded in bending, the flexural rigidity can be increased by including a core of auxetic material between these two skins to produce a sandwich structure. The key requirements for the core are normally the shear modulus and strength and compressive modulus. Light weight, acoustic insulation and thermal insulation often result from the addition of the auxetic core. The stiffness of one of the two constituents must be at least 25 times greater than that of the other constituent to obtain a PR less than zero (Munteanu et al., 2008).

Composite laminates consisting of isotropic lamina have in-plane properties that overshoot the modulus when there is a difference in PRs of individual laminas. For a fixed volume fraction of constituent materials, the in-plane modulus reduces to a minimum when the PRs for both constituents are zero. However, for laminates that consist of laminas with opposing PR signs arranged in alternative sequence, the effects of increased in-plane Young's modulus is significant and therefore must be accounted for in engineering design (Lim, 2010). In the case of composite manufactured from HAYs, the yarns with low wrap angles activate at lower strains. Higher wrap angles enable static performance to be optimized for higher strains. To optimize auxetic behaviour, the wrap should ideally be of infinitesimal diameter while maintaining a relatively high stiffness. The tensile modulus of the wrap should be higher than that of the core. In addition, while choosing core and wrap materials, the designer must consider the stiffness of these structures (ie, the combination of diameter and modulus). HAYs with core−wrap diameter ratios of around 5:1 and core−wrap tensile modulus ratios of around 1:60 are suitable for composite manufacturing (Wright et al., 2010).

In the case of composites with auxetic inclusions, if the inclusion material is sufficiently stiff (ie, has a Young's modulus more than two orders of magnitude larger than that of the matrix phase), then the overall composite may exhibit an in-plane auxetic response with auxeticity increasing with increasing Young's modulus mismatch. The elastic moduli vary significantly as the composite undergoes deformation. When the composite is stretched uniaxially, the inclusions are rotated and get aligned with loading direction, and no further rotation can occur. The composite undergoes a transition in its deformation behaviour, which gives rise to a switch from auxetic to nonauxetic behaviour. This offers a simple way to create

composites with controllable auxeticity (Kochmann and Venturini, 2013). In the composites with great auxeticity, considerably enhanced transverse moduli could be achieved without altering the longitudinal moduli. For example, changing the matrix PR from 0.3 to −0.9 and keeping all other constituent properties constant produced an almost fourfold increase in the composite transverse modulus. It has also been suggested that auxetic materials could be used in the design of hydrophones and other sensors because their low bulk modulus makes them more sensitive to hydrostatic pressure.

7.5.2   *Fracture toughness and energy absorption*

When a composite material fractures, the fibres are pulled out of the matrix. This results in the reinforcing effect being lost as the bond between the fibre and the matrix fails. It has been suggested (Evans and Alderson, 2000) that an auxetic fibre within a composite would resist fibre pull-out. When the fibre is pulled, it will expand and effectively lock into the matrix rather than contracting and pulling out easily as a conventional fibre would do (Fig. 7.7). Therefore, the fracture toughness of a composite can be enhanced by using auxetic reinforcements. With the invention of auxetic polypropylene (PP) fibres (Alderson et al., 2002), the concept of using embedded auxetic fibres in a softened epoxy resin was employed to produce a single fibre composite (Alderson et al., 2005). The fibre pull-out resistance and energy absorption were tested. In comparative tests with specimens containing positive PR fibres, the auxetic fibre-locking mechanism is shown to enable the specimen to carry more than twice the maximum load; and in terms of energy absorption, the auxetic fibre is up to three times more difficult to extract than the equivalent positive PR fibre. Donoghue et al. (2009) have reported that with auxetic fibres, pull-out is resisted because the fibres expand perpendicular to the pull-out force. This could help to resist potential failure mechanisms in the composite, such as crack growth. For a negative in-plane PR, the auxetic laminate was found to require more energy to propagate a crack when testing in tension on a double edge notched (DEN) specimen than the conventional laminate. In addition, the auxetic laminate is less notch sensitive than its conventional counterpart. For a negative through-thickness PR, the auxetic laminate was found to have higher values
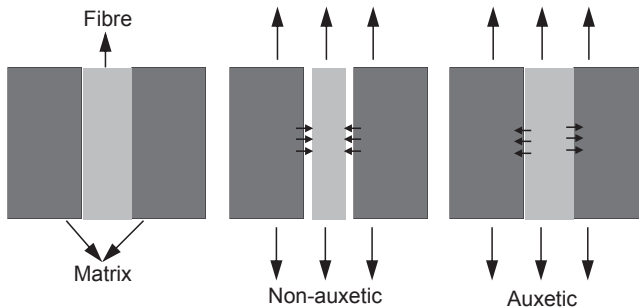
Figure 7.7 Fibre-reinforced composites.

of strain energy release rate and plane strain fracture toughness when tested using the compliance method.

7.5.3   Static indentation and low-velocity impact resistance

Some very interesting effects have also been found when static indentation and low-velocity impact of the auxetic laminates have been investigated. These properties were evaluated in comparison with laminates that have near-zero and large positive PR values with a matched through-thickness modulus. The auxetic laminates show higher loads to first failure with enhanced energy absorption in both cases. The statically tested specimens sustained higher loads and absorb more energy to catastrophic failure. The initial damage sustained is much more localized for both static and low-velocity impact testing, with a distinct lack of large delamination. This means that a smaller area of the specimen needs to be repaired. This is a clear advantage over conventional stacking sequences when the problem of impact, which is a limiting factor in the use of composites in aerospace applications, is considered (Alderson et al., 2005, Alderson and Coenen 2008).

Bezazi et al. (2009) have reported that the higher negative PRs are accompanied by strong in-plane anisotropy and high in-plane positive PR, making the depth and localization of the damage more stressed. However, strong localization of the damage is also accompanied by larger local delamination of the composite. Interlaminar shearing is often considered as key to the failure of composites under three-point bending, and the high membrane shear coupling of these auxetic laminates could be a primary source of failure during impact.

7.5.4   Synclastic deformation

Aerospace applications usually require sandwich panels which consist of stiff composite laminates of carbon or glass fibre with a light, porous sandwiched core. The net effect of this is a very strong and light material. However, the problem with these materials is that they cannot be curved, due to the positive PR of core material. Therefore, in order to form a curved panel, it is necessary to machine the required shape, which results in wastage of material, or to force the core into shape, which could result in considerable damage to the core. Conversely, when the bending moment is applied on two opposing sides of auxetic composite plates, they undergo synclastic deformation rather than anticlastic deformation. This is illustrated in Fig. 7.8(a), which
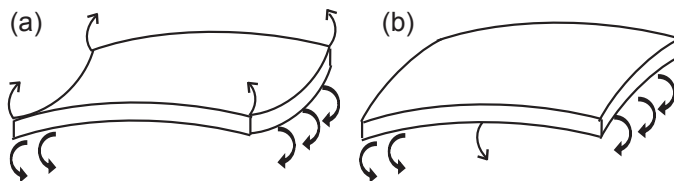
Figure 7.8 (a) Anticlastic behaviour of conventional composite plates; (b) synclastic behaviour of auxetic composite plates.

demonstrates that the core with positive PR will form a saddle shape on bending. However, Fig. 7.8(b) shows that with an auxetic material double curvatures are readily achieved, actually producing a dome. This has obvious applications in overcoming the problems described above for curved panels such as aircraft wings and other curved parts. Therefore, it is advantageous to use auxetic materials in the core of sandwich panels for curved aircraft components (Evans and Alderson, 2000).

7.6 Modelling

7.6.1 Angle-ply laminates

J.F. Clarke et al. (1994), using standard laminate theory, predicted the properties of the angle-ply laminates which are made from epoxy resin and reinforced with carbon fibres. The plies are arranged in different angles to the reference direction.

The axes of the laminates were defined as shown in Fig. 7.9. The relationship of the ε_i and σ_j is defined as:

$$\begin{bmatrix} \sigma_1 \\ \sigma_2 \\ \sigma_3 \\ \sigma_4 \\ \sigma_5 \\ \sigma_6 \end{bmatrix} = \begin{bmatrix} C_{11} & C_{12} & C_{13} & 0 & 0 & 0 \\ C_{12} & C_{22} & C_{23} & 0 & 0 & 0 \\ C_{13} & C_{23} & C_{33} & 0 & 0 & 0 \\ 0 & 0 & 0 & C_{44} & 0 & 0 \\ 0 & 0 & 0 & 0 & C_{55} & 0 \\ 0 & 0 & 0 & 0 & 0 & C_{66} \end{bmatrix} \begin{bmatrix} \varepsilon_1 \\ \varepsilon_2 \\ \varepsilon_3 \\ \varepsilon_4 \\ \varepsilon_5 \\ \varepsilon_6 \end{bmatrix}$$

where C_{ij} is the stiffness constant of the individual layer.

C'_{ij} is defined as the stiffness constant of whole laminate. Then the laminate constants (C'_{ij}) can be obtained from layer constants (C_{ij}) by the equations (Hahn and Tsai, 1980; Lee and Calgote, 1969) of the laminate theory.
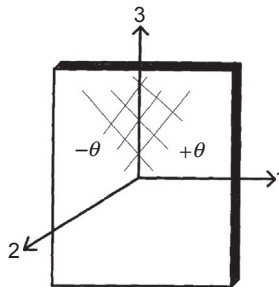
Figure 7.9 Angle-ply laminates model.
Clarke, J., Duckett, R., Hine, P., Hutchinson, I., Ward, I., 1994. Negative Poisson's ratios in angle-ply laminates: theory and experiment. Composites 25 (9), 863−868.

$$C'_{11} = C_{33}s^4 + C_{11}c^4 + 2(C_{13} + 2C_{55})s^2c^2$$

$$C'_{22} = C_{22}$$

$$C'_{33} = C_{11}s^4 + C_{33}c^4 + 2(C_{13} + 2C_{55})s^2c^2$$

$$C'_{12} = C_{12}c^2 + C_{23}s^2$$

$$C'_{13} = C_{13}(s^4 + c^4) + (C_{11} + C_{33} - 4C_{55})s^2c^2$$

$$C'_{23} = C_{12}s^2 + C_{23}c^2$$

$$C'_{44} = C_{44}c^2 + C_{66}s^2$$

$$C'_{55} = (C_{33} + C_{11} - 2C_{13} - 2C_{55})s^2c^2 + C_{55}(s^4 + c^4)$$

$$C'_{66} = C_{66}c^2 + C_{44}s^2$$

where $c = \cos\theta$ and $s = \sin\theta$.

The compliance constants of the laminate (S'_{ij}) can be determined by the stiffness matrix, and then the PR of the layers and whole laminate can be obtained by the following equations:

$$\nu_{12} = -\left(\frac{S_{12}}{S_{22}}\right) \quad \nu_{13} = -\left(\frac{S_{13}}{S_{33}}\right) \quad \nu_{23} = -\left(\frac{S_{23}}{S_{33}}\right)$$

$$\nu_{21} = -\left(\frac{S_{21}}{S_{11}}\right) \quad \nu_{31} = -\left(\frac{S_{31}}{S_{11}}\right) \quad \nu_{32} = -\left(\frac{S_{32}}{S_{22}}\right)$$

$$\nu'_{12} = \left(\frac{C'_{12}C'_{33} - C'_{23}C'_{13}}{C'_{11}C'_{33} - C'_{13}C'_{13}}\right) \quad \nu'_{13} = \left(\frac{C'_{12}C'_{23} - C'_{22}C'_{13}}{C'_{11}C'_{22} - C'_{12}C'_{12}}\right)$$

$$\nu'_{23} = \left(\frac{C'_{11}C'_{23} - C'_{12}C'_{13}}{C'_{11}C'_{22} - C'_{12}C'_{12}}\right) \quad \nu'_{21} = \left(\frac{C'_{12}C'_{33} - C'_{23}C'_{13}}{C'_{22}C'_{33} - C'_{23}C'_{23}}\right)$$

$$\nu'_{31} = \left(\frac{C'_{12}C'_{23} - C'_{22}C'_{13}}{C'_{22}C'_{33} - C'_{23}C'_{23}}\right) \quad \nu'_{32} = \left(\frac{C'_{11}C'_{23} - C'_{12}C'_{13}}{C'_{11}C'_{33} - C'_{13}C'_{13}}\right)$$

The authors used the ultrasonic velocity technique to measure the elastic properties of the angle-ply laminates, and used the theory mentioned above in order to calculate the PR of the laminates. The result shows that the theory accurately predicted the composite properties, and the laminates showed NPR for the angle θ in the range between 15 degree and 30 degree.

7.6.2 Spherical auxetic inclusions model by *Wei and Edwards (1998)*

Wei and Edwards (1998) found that the composites with spherical auxetic inclusion will show auxeticity when the inclusions reach a critical volume fraction $\phi = 1 - \phi_m$ and the ratio of inclusions to matrix Young's modulus $\delta = E/E_m$ falls within a definite interval.

The mean-field theory and two- and three-body interaction formalism were used to calculate the effective moduli of composite. It was assumed that both the inclusions and matrix are isotropic and that the spherical inclusions are dispersed in the matrix randomly. The bulk and shear modulus of inclusions and matrix are κ, μ and κ_m, μ_m, respectively. The effective moduli of the composites can be obtained by the following equations:

$$\kappa_e = \frac{(\phi_m \kappa_m + \phi \kappa P_1)}{(\phi_m + \phi P_2)}$$

$$\mu_e = \frac{(\phi_m \mu_m + \phi \mu Q_1)}{(\phi_m + \phi Q_2)}$$

where P_i and Q_i are functions of PR σ, σ_m and δ in the mean-field approximation; and $(P_1 = P_2 \geq 0, Q_1 = Q_2 \geq 0)$.

For the macroscopically isotropic composite, the effective Young's modulus and PR can be obtained by the following equations:

$$\sigma_e = \frac{(\alpha - \beta)}{(2\alpha + \beta)} \quad \text{and} \quad \delta_e = \frac{\beta(1 + \sigma_e)}{(1 + \sigma_m)}$$

where $\alpha = 3 \kappa_e/(2\mu_m)$; and $\beta = \mu_e/\mu_m$.

From the equation of PR, when $0 \leq \alpha < \beta$, the composites will show auxeticity. By using this model, the right volume fraction and ratio of Young's models of inclusions can be determined for making composites with negative PR.

7.6.3 Concentric composites model by *Strek and Jopek (2012)*

Sterk and Jopek built up a composite model with coaxial layers. The composites were defined to be formed with two different materials, and one of them is an auxetic material. The model is shown in Fig. 7.10.

The effective PR of the composites was defined as: $\nu_{eff} = -\dfrac{\overline{\varepsilon}_{transverse}}{\overline{\varepsilon}_{longitudinal}}$, where $\overline{\varepsilon}_{transverse}$ and $\overline{\varepsilon}_{longitudinal}$ are average strains in the transverse and longitudinal directions.

The effective Young's modulus was defined as: $E_{eff} = -\dfrac{\overline{\delta}_{longitudinal}}{\overline{\varepsilon}_{longitudinal}}$, where $\overline{\delta}_{longitudinal}$ is average stress in the longitudinal direction.
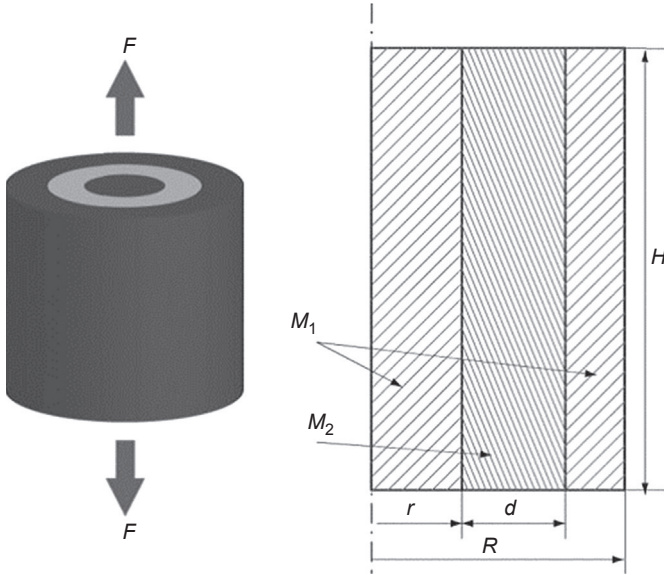
Figure 7.10 Concentric composites model.
Strek, T., Jopek, H., 2012. Effective mechanical properties of concentric cylindrical composites with auxetic phase. Physica Status Solidi (B) 249 (7), 1359−1365.

The average stress and strain are defined as:

$$\bar{\delta} = \frac{1}{S}\int_s \delta ds, \quad \bar{\varepsilon} = \frac{1}{S}\int_s \varepsilon ds$$

where S is the volume of the composite.

When the force is applied along the Z direction, the effective PR and Young's modulus in this direction are:

$$\nu_{\text{eff}} = -\frac{\bar{\varepsilon}_x}{\bar{\varepsilon}_z}, \quad E_{\text{eff}} = -\frac{\bar{\delta}_z}{\bar{\varepsilon}_z}$$

The strain and stress are calculated by using Navier's equation:

$$\rho_s \frac{\partial^2 u}{\partial t^2} - \nabla\sigma = 0$$

where u is the displacement $u = [u,v,w]$ in the x, y and z directions; and ρ_s is the density. The body force is neglected.

The relationship of stress and strain for linear conditions is:

$$\sigma = D\varepsilon$$

where σ is the stress tensor; D is the elastic matrix and ε is the small strain tensor $\varepsilon = 1/2(\nabla u + (\nabla u)^T)$.

σ and ε in vector form are:

$$\sigma = [\sigma_x \sigma_y \sigma_z \tau_{xy} \tau_{yz} \tau_{xz}]^T$$

$$\varepsilon = [\varepsilon_x \varepsilon_y \varepsilon_z \gamma_{xy} \gamma_{yz} \gamma_{xz}]^T$$

$$\lambda = \frac{E\nu}{(1+\nu)(1-2\nu)}, \quad \mu = \frac{E}{2(1+\nu)}$$

where λ and μ are Lame's constants.

The final form of the steady Navier's equation is: $\nabla(c\nabla u) = 0$, where c is the flux matrix.

The finite element method was also used to calculate the constants of the composites. The result shows that the geometry, Young's modulus and PR are the main factors to affect the final properties of the composites, and the whole composites can be engineered to have an auxetic effect by selecting the right material properties and geometries.

7.6.4 Auxetic spherical and cubic inclusions model

Shufrin et al. (2015) built two models for composites made from the isotropic conventional matrix and isotropic auxetic inclusions with spherical and cubic shapes, respectively. For the spherical model, as shown in Fig. 7.11, the inclusions were assumed in multiscale and randomly distributed in the matrix. The relationship of the properties of the composite can be expressed by the following equations (McLaughlin, 1977):

$$\begin{cases} \dfrac{dK}{dc_{NPR}} = \dfrac{(K_{NPR} - K)(3K + 4G)}{(1 - c_{NPR})(3K_{NPR} + 4G)} \\[4mm] \dfrac{dG}{dc_{NPR}} = \dfrac{(G_{NPR} - G)(6G(K + 2G) + G(9K + 8G))}{(1 - c_{NPR})(6G_{NPR}(K + 2G) + G(9K + 8G))} \end{cases}$$

$$K\Big|_{c_{NPR}=0} = K_{PPR}, \quad G\Big|_{c_{NPR}=0} = G_{PPR},$$

$$E = \frac{9KG}{3K + G}$$

$$\nu = \frac{3K - 2G}{2(3K + G)}$$

where C_{NPR} is the volumetric fraction of the auxetic inclusions; K and G is the bulk and shear moduli, respectively; E is the Young's modulus and ν is the PR.

The cubic inclusions model was considered as shown in Fig. 7.12. A finite element
software ABAQUS was used to analyse this model. The cubics are assumed to be iden-
tical and randomly distributed. E, v and G are used to represent the effective Young's
modulus, Poisson's ratio and shear modulus of the composite.

The composite is divided into a regular cubic grid as shown in Fig.7.12, and each cube is located in a different position (x,y,z). Each cube has meshes with 1, 2, 3, 4, 8, 9, 12, 18 and 27 elements per single cube (Fig. 7.13).

The effective Young's modulus and Poisson's ratio were simulated by using the boundary conditions, as shown in Fig.7.14. At external faces: face $x = L/2$: $\sigma_{xx} = \tau_{xy} = \tau_{xz} = 0$; face $y = L/2$: $\sigma_{yy} = \tau_{yx} = \tau_{yz} = 0$; and face $z = L/2$: $\sigma_{zz} = \tau_{zx} = \tau_{zy} = 0$, where σ_0 is uniformly distributed load. At internal faces (planes of symmetry), the following were specified: face $x = 0$: $u_x = 0$, $\tau_{xy} = \tau_{xz} = 0$; face $y = 0$: $u_y = 0$, $\tau_{yx} = \tau_{yz} = 0$; and face $z = 0$: $u_z = 0$, $\tau_{zx} = \tau_{zy} = 0$.

By using the displacement and strain obtained from the simulation, the effective Young's modulus and PR can be calculated by the following equations:

$$E = \frac{\sigma_0}{\varepsilon_{zz}}$$
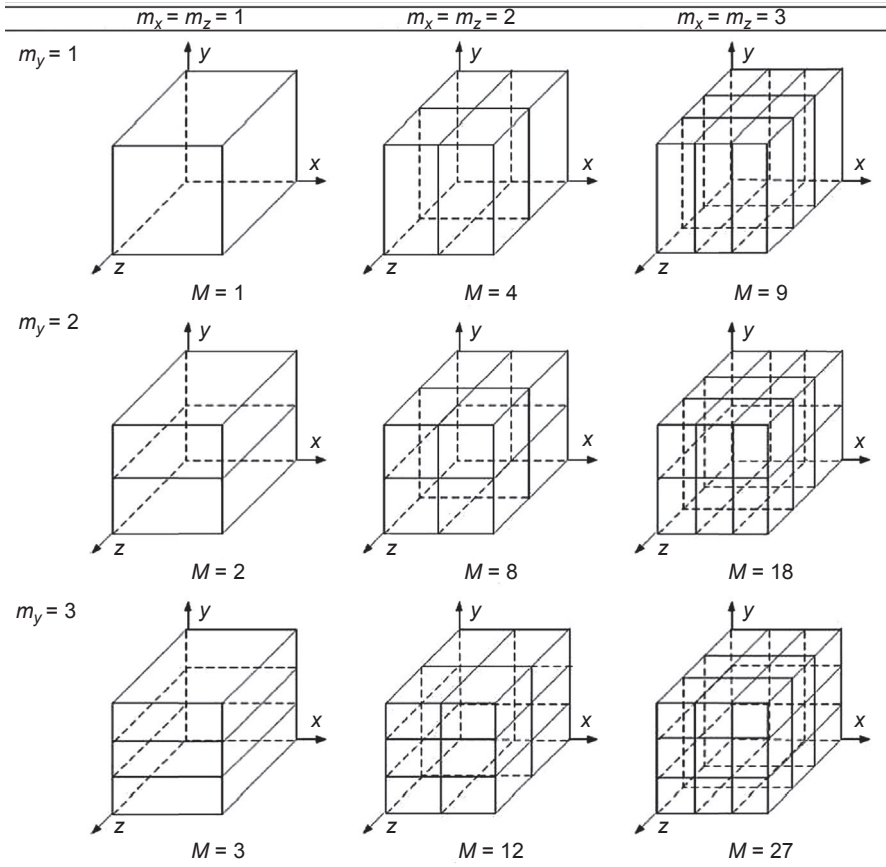
Figure 7.13 Division of a cubic grid.
Shufrin, I., Pasternak, E., Dyskin, A.V., 2015. Hybrid materials with negative Poisson's ratio inclusions. International Journal of Engineering Science 89, 100−120.
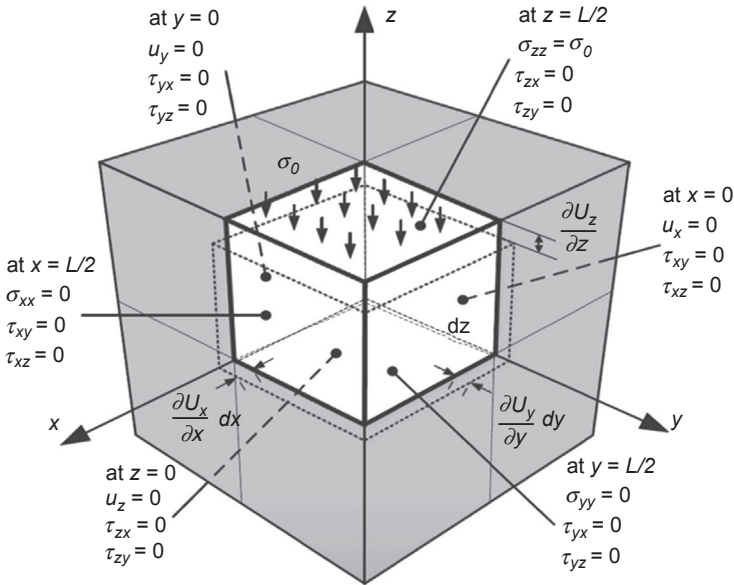
Figure 7.14 Boundary conditions of unit.
Shufrin, I., Pasternak, E., Dyskin, A.V., 2015. Hybrid materials with negative Poisson's ratio inclusions. International Journal of Engineering Science 89, 100−120.

$$\nu = -\frac{\varepsilon_{xx}}{\varepsilon_{zz}} = -\frac{\varepsilon_{yy}}{\varepsilon_{zz}}$$

The result shows that the composites can be auxetic with both kind of inclusions when their content is above a critical concentration. And the effective Young's modulus of the composites increases compared with the moduli of both phases.

7.7 Applications

7.7.1 General application

Auxetic materials can find many potential applications in many fields. The many enhanced properties of auxetic materials make them a very good choice for aerospace engineering. There are some auxetic materials which have been used in the aerospace field. For example, the pyrolytic graphite with a negative PR of −0.21 was used on the aircraft thermal protecting system (Garber, 1963). The Ni$_3$Al large single crystals with a negative PR of −0.18 were used on the aircraft engine vanes (Baughman et al., 1998; Nakamura, 1995). With the development of auxetic materials, more and more applications are found for using them in the aerospace engineering.

Auxetic materials can be used as fasten belts (Choi and Lakes, 1991) on the aircraft; when the belt is compressed, the belt becomes narrower laterally, which makes it easy

to be inserted or pulled out. When the belt is fastened, it bears the tension force, and the belt becomes fatter, which makes it tighter. Therefore, this kind of fastener will provide more safety.

Auxetic materials have better energy absorption than conventional materials. So, the cushioning effect made from the auxetic materials can help to absorb more energy and distribute the pressure more effectively; this kind of cushion is useful in aircraft components, especially the wings as they need to absorb the air thrust during flight.

7.7.2 Application of composites

Composites are being used more and more in aerospace engineering due to the advantages of high performance and relatively low weight and cost. For example, the American Boeing C-17 has used composite materials instead of aluminium in its tail from 1999, which saved more than 40,000 fasteners and 213 kg weight compared to its predecessors (Marsh, 2004). However, the conventional composites sometimes still cannot meet the high requirements of the aerospace engineering. The auxetic composites, due to their advantages, are better candidates than conventional composites to use in aerospace engineering.

One of the important properties of auxetic composites is that they have higher shear modulus. Aircrafts undertake very high shear force when flying. The materials with higher shear strength can optimize the performance of the aircraft. Most body parts of the early aircraft are made of metals which are quite heavy. With the development of the auxetic technology, auxetic composites instead of metals can be used for the aircraft components, as the auxetic composites have a higher strength-to-weight ratio than metals. Impact on the aircraft is very dangerous during flying. Tragic accidents may occur by the impact of some objects in the sky such as birds. Therefore, impact resistance is quite important for the aircraft's body.

Auxetic composites can be used for reducing noise in aircraft fuselages (Liguore and Montgomery, 2012). Wing-mounted engines on the commercial aircraft can generate high noises, and they can be transmitted to the fuselages through the stiffener and affect the passengers' comfort in the cabin. To reduce the noise, a kind of auxetic composite was invented for the stiffener, which consisted of an auxetic core, a damping layer and a constraining layer. The auxetic core should have one surface toward the structural member and a second surface away from the structural member. The damping layer could be sandwiched between the second surface of the auxetic core and a constraining layer. Compared with the conventional method, by using the thick metallic layers on the stiffener, the auxetic composites should save the weight and energy of the aircraft.

In addition, the better formability of the auxetic composites make it easier to make complex shapes and curved panels. Therefore, the auxetic composites can be a good candidate to be used in manufacturing aircraft components instead conventional composites in the future. Table 7.4 shows the advantage of auxetic composites in different parts of aircraft.

Table 7.4 Usage of auxetic composites in different parts of aircraft

Part of aircraft	Advantage of auxetic composites
Head	Enhance damping resistance.
Wings	Enhance shear resistance.
Fuselages	Reduce noise.
All the body parts	Reduce weight, good formability.

7.8 Conclusions

This chapter mainly discussed the use of auxetic composites in aerospace engineering. The auxetic composites are very good materials to be used in aircraft due to the advantages they possess. The advantages make them very useful in each part of the aircraft. For example, enhanced damping resistance can be used on the aircraft head to increase the damping property of it. Although this new breed of composites is not yet mature enough, it is believed that they will be developed and good enough to be used in aerospace engineering instead of conventional composites.

References

Alderson, A., Alderson, K., 2007. Auxetic materials. Proceedings of the Institution of Mechanical Engineers, Part G: Journal of Aerospace Engineering 221 (4), 565−575.

Alderson, K., Alderson, A., Smart, G., Simkins, V., Davies, P., 2002. Auxetic polypropylene fibres: Part 1-Manufacture and characterisation. Plastics, Rubber and Composites 31 (8), 344−349.

Alderson, K., Coenen, V., 2008. The low velocity impact response of auxetic carbon fibre laminates. Physica Status Solidi (B) 245 (3), 489−496.

Alderson, K., Evans, K., 1992. The fabrication of microporous polyethylene having a negative Poisson's ratio. Polymer 33 (20), 4435−4438.

Alderson, K., Simkins, V., Coenen, V., Davies, P., Alderson, A., Evans, K., 2005. How to make auxetic fibre reinforced composites. Physica Status Solidi (B) 242 (3), 509−518.

Alkhalil, M., 1990. Strength of Filament Wound Structures Under Complex Stresses.

Baughman, R.H., Shacklette, J.M., Zakhidov, A.A., Stafström, S., 1998. Negative Poisson's ratios as a common feature of cubic metals. Nature 392 (6674), 362−365.

Bezazi, A., Boukharouba, W., Scarpa, F., 2009. Mechanical properties of auxetic carbon/epoxy composites: static and cyclic fatigue behaviour. Physica Status Solidi (B) 246 (9), 2102−2110.

Caddock, B., Evans, K., 1989. Microporous materials with negative Poisson's ratios. I. Microstructure and mechanical properties. Journal of Physics D: Applied Physics 22 (12), 1877.

Chen, C., Lakes, R., 1993. Viscoelastic behaviour of composite materials with conventional-or negative-Poisson's-ratio foam as one phase. Journal of Materials Science 28 (16), 4288−4298.

Choi, J., Lakes, R., 1991. Design of a fastener based on negative Poisson's ratio foam. Cellular Polymers 10 (3), 205−212.

Clarke, J., Duckett, R., Hine, P., Hutchinson, I., Ward, I., 1994. Negative Poisson's ratios in angle-ply laminates: theory and experiment. Composites 25 (9), 863−868.

Coenen, V., Alderson, K., 2011. Mechanisms of failure in the static indentation resistance of auxetic carbon fibre laminates. Physica Status Solidi (b) 248 (1), 66−72.

Donoghue, J., Alderson, K., Evans, K., 2009. The fracture toughness of composite laminates with a negative Poisson's ratio. Physica Status Solidi (B) 246 (9), 2011−2017.

Evans, K., Alderson, K., 2000. Auxetic materials: the positive side of being negative. Engineering Science and Education Journal 9 (4), 148−154.

Evans, K., Donoghue, J., Alderson, K., 2004. The design, matching and manufacture of auxetic carbon fibre laminates. Journal of Composite Materials 38 (2), 95−106.

Evans, K., Nkansah, M., Hutchinson, I., 1992. Modelling negative Poisson ratio effects in network-embedded composites. Acta Metallurgica et Materialia 40 (9), 2463−2469.

Evans, K., Nkansah, M., Hutchinson, I., Rogers, S., 1991. Molecular network design. Nature 353 (6340), 124.

Garber, A., 1963. Pyrolytic materials for thermal protection systems. Aerospace Engineering 22 (1), 126−137.

Ge, Z., Hu, H., 2013. Innovative three-dimensional fabric structure with negative Poisson's ratio for composite reinforcement. Textile Research Journal 83 (5), 543−550.

Hadi Harkati, E., Bezazi, A., Scarpa, F., Alderson, K., Alderson, A., 2007. Modelling the influence of the orientation and fibre reinforcement on the negative Poisson's ratio in composite laminates. Physica Status Solidi (B) 244 (3), 883−892.

Hahn, H.T., Tsai, S.W., 1980. Introduction to Composite Materials. CRC Press.

Herakovich, C.T., 1984. Composite laminates with negative through-the-thickness Poisson's ratios. Journal of Composite Materials 18 (5), 447−455.

Hine, P., Duckett, R., Ward, I., 1997. Negative Poisson's ratios in angle-ply laminates. Journal of Materials Science Letters 16 (7), 541−544.

Hu, H., Wang, Z., Liu, S., 2011. Development of auxetic fabrics using flat knitting technology. Textile Research Journal 81 (14), 1493−1502.

Hoa, S.V., 2009. Principles of the Manufacturing of Composite Materials. DEStech Publications, Inc.

Hook, P., Evans, K., Hannington, J., Hartmann-Thompson, C., Bunce, T., 2004. Composite Materials and Structures. US patent 20070031667 A1.

Hou, X., Hu, H., Silberschmidt, V., 2012. A novel concept to develop composite structures with isotropic negative Poisson's ratio: effects of random inclusions. Composites Science and Technology 72 (15), 1848−1854.

Kochmann, D.M., Venturini, G.N., 2013. Homogenized mechanical properties of auxetic composite materials in finite-strain elasticity. Smart Materials and Structures 22 (8), 084004.

Lakes, R.S., 1987. Foam structures with a negative Poisson's ratio. Science 235, 1038−1040.

Lee, R.C., Calgote, L., 1969. The Analysis of Laminated Composite Structures.

Liguore, S.L., Montgomery, J.M., 2012. Systems and Methods for Reducing Noise in Aircraft Fuselages and Other Structures. US Patent 8297555.

Lim, T., 2010. In-plane stiffness of semiauxetic laminates. Journal of Engineering Mechanics 136 (9), 1176−1180.

Liu, Y., Hu, H., Lam, J.K., Liu, S., 2010. Negative Poisson's ratio weft-knitted fabrics. Textile Research Journal 80 (9), 856−863.

Marsh, G., 2004. Farnborough 2004−good prospects for aerospace composites. Reinforced Plastics 48 (8), 42−46.

McLaughlin, R., 1977. A study of the differential scheme in composite materials. International Journal of Engineering Science 15, 237−244.

Miki, M., Murotsu, Y., 1989. The peculiar behavior of the Poisson's ratio of laminated fibrous composites. JSME International Journal. Ser. 1, Solid Mechanics, Strength of Materials 32 (1), 67−72.

Miller, W., Hook, P., Smith, C.W., Wang, X., Evans, K.E., 2009. The manufacture and characterisation of a novel, low modulus, negative Poisson's ratio composite. Composites Science and Technology 69 (5), 651−655.

Miller, W., Ren, Z., Smith, C., Evans, K., 2012. A negative Poisson's ratio carbon fibre composite using a negative Poisson's ratio yarn reinforcement. Composites Science and Technology 72 (7), 761−766.

Milton, G.W., 1992. Composite materials with Poisson's ratios close to−1. Journal of the Mechanics and Physics of Solids 40 (5), 1105−1137.

Munteanu, L., Chiroiu, V., Dumitriu, D., Beldiman, M., 2008. On the characterization of auxetic composites. Proceedings of the Romanian Academy, Series A: Mathematics, Physics, Technical Sciences, Information Science 9 (1), 33−40.

Nakamura, M., 1995. Fundamental properties of intermetallic compounds. MRS Bulletin 20 (8), 33−39.

Ravirala, N., Alderson, A., Alderson, K., Davies, P., 2005. Expanding the range of auxetic polymeric products using a novel melt-spinning route. Physica Status Solidi (B) 242 (3), 653−664.

Ravirala, N., Alderson, K.L., Davies, P.J., Simkins, V.R., Alderson, A., 2006. Negative Poisson's ratio polyester fibers. Textile Research Journal 76 (7), 540−546.

Rosato, D.V., 1997. Designing with reinforced composites. Hanser Gardner Publications 132−133.

Shufrin, I., Pasternak, E., Dyskin, A.V., 2015. Hybrid materials with negative Poisson's ratio inclusions. International Journal of Engineering Science 89, 100−120.

Sloan, M., Wright, J., Evans, K., 2011. The helical auxetic yarn − a novel structure for composites and textiles; geometry, manufacture and mechanical properties. Mechanics of Materials 43 (9), 476−486.

Stagni, L., 2001. Effective transverse elastic moduli of a composite reinforced with multilayered hollow-cored fibers. Composites Science and Technology 61 (12), 1729−1734.

Stavroulakis, G., 2005. Auxetic behaviour: appearance and engineering applications. Physica Status Solidi (B) 242 (3), 710−720.

Strek, T., Jopek, H., 2012. Effective mechanical properties of concentric cylindrical composites with auxetic phase. Physica Status Solidi (B) 249 (7), 1359−1365.

Ugbolue, S.C., Kim, Y.K., Warner, S.B., Fan, Q., Yang, C., Kyzymchuk, O., Feng, Y., Lord, J., 2011. The formation and performance of auxetic textiles. Part II: geometry and structural properties. The Journal of the Textile Institute 102 (5), 424−433.

Wang, Z., Hu, H., 2014. 3D auxetic warp-knitted spacer fabrics. Physica Status Solidi (B) 251 (2), 281−288.

Wei, G., Edwards, S., 1998. Auxeticity windows for composites. Physica A: Statistical Mechanics and Its Applications 258 (1), 5−10.

Wenchao, Z., Evans, K., 1992. A fortran program for the design of laminates with required mechanical properties. Computers & Structures 45 (5), 919−939.

Wright, J., Sloan, M., Evans, K., 2010. Tensile properties of helical auxetic structures: a numerical study. Journal of Applied Physics 108 (4), 044905.

Yeh, H., Yeh, H., Zhang, R., 1999. A study of negative Poisson's ratio in randomly oriented quasi-isotropic composite laminates. Journal of Composite Materials 33 (19), 1843−1857.

Zhang, R., Yeh, H., Yeh, H., 1998. A preliminary study of negative Poisson's ratio of laminated fiber reinforced composites. Journal of Reinforced Plastics and Composites 17 (18), 1651−1664.

Polymer nanocomposite: an advanced material for aerospace applications

8

M. Joshi, U. Chatterjee
Indian Institute of Technology, New Delhi, India

8.1   Introduction

Launching a heavy lift system into low Earth and geosynchronous orbits generally costs €5000−15,000/kg and €28,000/kg, respectively. Because of increasing oil and gas prices, the demand for lightweight materials in the aerospace industry is tremendous. Even in general aviation, fuel costs account for around 50% of the operational costs. Consequently, over the last three decades, aircraft designers began to replace metal parts with fibre-reinforced polymer (FRP) composites which were found to be an innovative and attractive material for aerospace application. FRP composites are a type of engineered material which exhibits high strength−weight and modulus−weight ratios compared with various metallic materials. The design change helped to reduce aircraft weight by more than 30%, thereby increasing fuel efficiency significantly. In addition to lower weight, these composites are also attractive to engineers because of their resistance to corrosion and fatigue compared with metals.

Polymeric composite reinforced with fibreglass, which is a glass fibre-based resin, has been used in general passenger jets since the 1950s. By the 1960s, high-stiffness boron and graphite fibres embedded in epoxy resins became available, and the US military focussed on using these materials in rudders, ailerons and other movable parts that control the motion of aircraft. Not long thereafter, boron fibres became widely used in the horizontal stabilizers of F-14 Tomcat fighter jets. And in today's F-22 fighters, carbon fibre composites and related materials compose nearly one-third of the jet's structure. Some of the sophisticated capabilities of modern military aircraft would not be possible without today's advanced composites. The V-22 (Osprey) tilt-rotor craft, for example, is able to take off, land and hover like a helicopter, as well as reorient its rotors in midair and fly like a turboprop aeroplane. That kind of aeronautical capability is due in part to the graphite−fibreglass rotors and other lightweight composite-based structures in the rotor system that are strong enough to tolerate high centrifugal forces yet remain slightly flexible. Similarly, the extreme aerial manoeuvrability of F-18 fighter jets is partly due to composites used in the aircraft's wings, flaps, vertical and horizontal stabilizers and other crucial parts.

However, in these conventional structural materials, the fibre orientation is usually in-plane (x- and y-direction), resulting in fibre-dominated material properties in these directions, whereas the matrix dominates in the z-direction. Therefore, FRPs are very

sensitive to intrinsic damage such as delamination (in particular), matrix cracking and fatigue damage. These materials also lack other required functional properties such as high electrical and thermal conductivity for electrostatic dissipation and lightning strike protection. Polymer nanocomposites (PNCs), consisting of nanomaterials dispersed into polymer matrix, have gained much interest in this field.

In the last 20 years, there has been a strong emphasis on the development of polymeric nanocomposites, where at least one of the dimensions of the filler material is of the order of a nanometre. Typical nanomaterials currently under investigation include nanoparticles, nanotubes, nanoplatelets, nanofibres, fullerenes and nanowire. In general, nanomaterials provide reinforcing efficiency because of their high aspect ratios (Mc Crum et al., 1996; Thostenson et al., 2005). The properties of a nanocomposite are greatly influenced by the size scale of its component phases and the degree of mixing between the two phases. Depending on the nature of the components used and the method of preparation, significant differences in composite properties may be obtained. Nanomaterials provide a significantly large interfacial area with the matrix and thereby at fairly low concentrations enhance the composite properties, which means lowering the product weight further. Besides, nanomaterials also can provide multifunctional properties. Many studies have reported that the mechanical, conductivity, optical, magnetic, biological and electronic properties of several inorganic nanoparticles significantly change as their size is reduced from the macroscale to the microlevel and nanolevel. In the field of nanocomposites, researches have been focussing on many diverse performance properties, including composite reinforcement, barrier properties, flame resistance, electro-optical properties, impact resistance and energy absorption applications and others.

In recent years, studies have shown the potential improvement in the properties and performance of reinforced polymer matrix materials in which nanoscale particles such as inorganic layered clay, single-walled and multiwalled carbon nanotubes (SWCNTs and MWCNTs, respectively), graphene, metal nanoparticles and others have been incorporated. This chapter presents recent worldwide research on different nanomaterial-based polymeric composites that have potential functional uses for aerospace application.

8.2 Polymeric parts in aerospace engineering: present state of the art

Aerospace is a field which demands optimum properties, in particular optimized property combinations, due to the substantial weight savings (which translate directly to cost benefits in reduced fuel consumption). Polymers possess several properties that make them useful as aerospace materials, including low density ($1.2-1.4$ g/cm^3), moderate cost, excellent corrosion resistance and high ductility (except thermosets). Some polymers are tough and transparent which makes them suitable for aircraft windows and canopies. The low-permeability property of some polymers has found application in coatings and laminations in gas-filled lighter-than-air systems. However,

polymers cannot be used on their own as structural materials because of their low stiffness, strength, creep properties and working temperature. Thus, polymers are generally used in aerospace materials in composite form. Fig. 8.1 lists some common polymers used as a matrix for aerospace composites.

Over the last three decades, FRP composites have been found to be an innovative and attractive material for aerospace application, and designers began to replace aerospace metallic parts with polymer composites. Currently, composites are used in the airframe and engine components of modern military and civilian aircraft, with polymers accounting for 40–45% of the total volume of the material. Moulded plastics and fibre–polymer composites are used extensively in the internal fittings and furniture of passenger aircraft. Polymer composites are used in various forms including sandwiched structures, moulded form, foams, laminates, radar, satellites, sensors and coatings in specific parts of the aerospace structures such as the aircraft's wings, flaps, vertical and horizontal stabilizers and so on.

Another important application of polymers is as an adhesive for joining aircraft components. It is possible to produce high-strength, durable joints using polymer adhesives without the need for fasteners such as rivets and screws. Adhesives are used to join metal-to-metal, composite-to-composite and metal-to-composite components. For example adhesives are used to bond ribs, spars and stringers to the skins of structural panels used throughout the airframe. Adhesives are also used to bond face sheets to the core of sandwich composite materials and to bond repairs to composite and metal components damaged during service. A thin layer of adhesive is used to bond together the aluminium and fibre–polymer composite sheets that produce the fibre–metal laminate called GLARE (glass-reinforced aluminium laminate), which is used in the Airbus 380 fuselage. The use of elastomers is usually confined to nonstructural aircraft parts that require high flexibility and elasticity, such as seals and gaskets.

However, polymers with metal or fibre reinforcements sometimes suffer for having high viscosities, high processing temperatures and pressure, poor creep resistance and so on. They also face problems related to higher weight, agglomeration, improper stress distribution and other factors. In the case of conventional FRP composites,
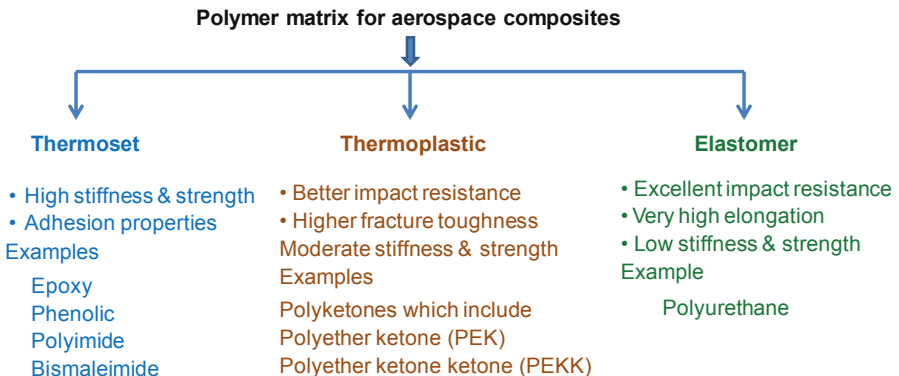
Figure 8.1 Common polymer matrix used for aerospace composites.

the fibre orientation is usually in-plane (x- and y-direction), resulting in fibre-dominated material properties in these directions whereas the matrix dominates in the z-direction. Therefore, FRPs are very sensitive to intrinsic damage such as delamination matrix cracking and fatigue damage.

8.3 Polymer nanocomposite: the leading-edge material

8.3.1 What is a nanocomposite?

PNCs have received much attention in aerospace applications over the past decade. PNCs consist of polymer matrix that has nanofillers dispersed into it. Nanofillers may be of different shapes (eg, platelets, fibres and/or spheroids), and at least one dimension must be in the range of 1−50 nm. Nanofillers provide very high interfacial area for better adhesion to polymer matrix which ultimately leads to superior property enhancement of the product. A range of nanoreinforcements with different shapes have been used to make PNCs. An important parameter for characterizing the effectiveness of reinforcement is the ratio of surface area to volume of reinforcement (Mc Crum et al., 1996). Fig. 8.2 shows a plot of surface area to volume against the aspect ratio (defined as the ratio of length to diameter) of the reinforcement.

Unlike traditional filled polymer systems, nanocomposites require relatively low dispersant loadings to achieve significant property enhancements, which makes
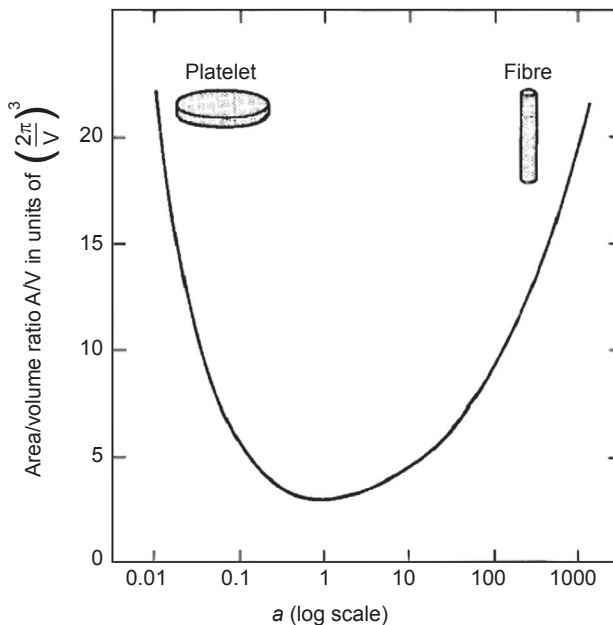
Figure 8.2 Surface area-to-volume ratio (A/V) of a cylindrical particle of given volume, plotted versus the aspect ratio (a = length/diameter).
Adapted from Mc Crum, N.G., Buckley, C.P., Bucknall, C.B., 1996. Principles of Polymer Engineering. Oxford Science, New York.
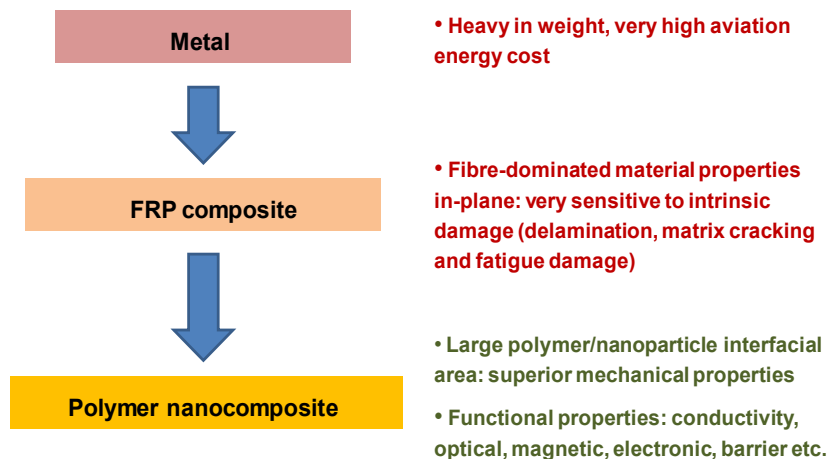
Figure 8.3 Evolution of materials for aerospace structures.

them a key candidate for aerospace applications. Besides, nanomaterial-based composites can provide various multifunctional properties, such as thermal stability, fire retardancy, electronic properties, field emission, optical properties, improved material durability, high impact resistance, energy absorption and others which are particularly significant for aerospace application (Thostenson et al., 2005; Luo and Daniel, 2003). Fig. 8.3 describes the evolution of materials for aerospace structures.

8.3.2 Synthesis routes of PNCs

Basically, there are three methods to prepare nanocomposites: solution casting, melt blending and in situ polymerization (Fig. 8.4). In solvent casting, the polymer and the nanoreinforcement are combined into a solvent and thoroughly mixed (eg, by ultra-sonication) and then the solvent is allowed to evaporate, leaving behind the nanocomposite typically as a thin film. The solvent chosen should completely dissolve the polymer as well as disperse the nanoreinforcement. The solvent used will help in the mobility of the polymer chains which in turn helps in the intercalation of the polymer chains with the layered nanoreinforcement. In the case of melt blending, an extruder or an internal mixer is used. Polymer and nanoreinforcement are added into the extruder and subjected to intensive mixing for some specific time, and then nanocomposite is extruded from the die. In this method, polymer mobility simply comes from thermal energy. In the case of in situ polymerization, initially the monomer and nanoreinforcement are mixed. The monomer is then allowed to intercalate between the silicate layers. Once the monomer is intercalated, polymerization is started. The polymerization may be due to some surface modification at the silicate surface or due to any functionalities present which catalyse the reaction (Alexandre and Dubois, 2000). There have been numerous reports on the synthesis of conducting PNCs (Fang et al., 2008; Gangopadhyay and De, 2000).
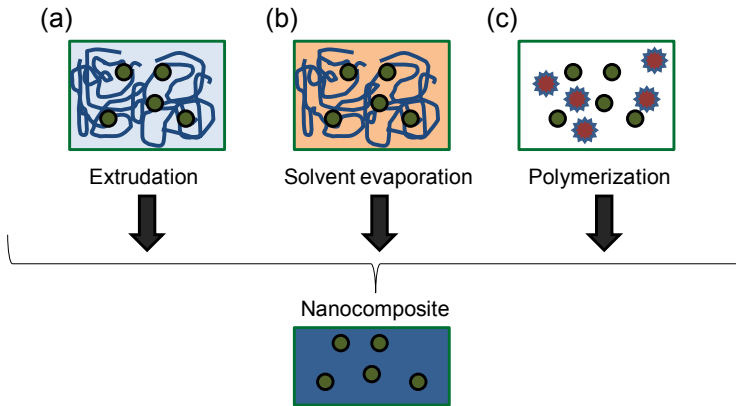
Figure 8.4 Schematic demonstration of nanocomposite synthesis. Nanoparticle dispersion in (a) polymer melt (b) polymer solution (c) monomer.

8.3.3 Modelling of nanocomposite

The interactions between nanofiller and the polymer matrix have a significant impact on the properties of nanocomposites (Ajayan et al., 2003). Various theoretical models have been considered for modelling of these materials. Molecular dynamics (MD) is the most common numerical method used for modelling of nanocomposites. Some typical examples of models are macromechanical, micromechanical and multiscale modelling. MD methods consider interaction at the atomistic scale, and apply principles of quantum mechanics and MD. These methods allow the determination of mechanical properties at the nanoscale by solving equations of motion of interacting atoms within interatomistic potentials (Rapaport, 2004). MD simulations have been applied successfully in investigation of crack propagation and fracture of individual SWCNTs and MWCNTs (Belytschko et al., 2002; Namilae, 2005) and predicting the elastic properties of carbon nanotubes (CNTs) (Cornwell and Wille, 1997). However, these techniques are computationally expensive. A brief general description and the main challenges associated with these techniques are discussed here.

8.3.3.1 Macroscopic modelling

Macroscopic modelling is a simplified approach where micro- or nanoscopic interactions between matrix and reinforcement are neglected. Properties of the composite are homogenized before the analysis, producing isotropic and homogeneous continuum (Aboudi, 1990). Effective properties like the stress−strain curve and yield point are then obtained by using mechanical testing. A big challenge when composite materials are considered is modelling the yield and failure under multiaxial loading.

8.3.3.2 Microscopic modelling

In microscale modelling, each phase of a composite is considered separately. Loading and boundary conditions are applied to both the matrix and the reinforcement. The

overall macroscopic properties of the material are then averaged and calculated as a function of the constituents' properties, using a homogenization method or direct finite element representation of a representative volume element (RVE). An important drawback of this method is the larger computation time, compared to the macroscopic approach (Aboudi, 1988). Micromechanical models have been applied in several studies to predict elastic properties of nanocomposites (Luo and Daniel, 2003; Fornes and Paul, 2003; Wu et al., 2004; Wilkinson et al., 2007; Chavarria and Paul, 2004) as well as damage and failure (Fornes and Paul, 2003; Chen et al., 2003a, 2007; Boutaleb et al., 2009).

Boutaleb et al. (2009) proposed a micromechanical analytical model in order to address the problem of stiffness and yield stress prediction in the case of nanocomposites consisting of silica nanoparticles embedded in a polymer matrix. An approach integrating the thickness of the interphase as a characteristic length scale was used. Finite element simulations were also performed in order to better understand the mechanisms occurring at the nanoscale.

8.3.3.3 Multiscale modelling

In order to predict the response of composite structures, taking into account its microstructure, a multiscale analysis can be applied. In this approach, calculations are conducted at both the macro and micro levels. At the micro level, a finite number of constituents are defined, and each is described by its own constitutive model and material properties. In contrast to the macroscopic approach, multiscale modelling is able to provide information about stresses in phases, and it allows the definition of per-phase failure. Moreover, with this formulation, influence of the filler content on the composite properties can be predicted and investigated without performing expensive material testing for each configuration.

Luo and Daniel (2003) studied properties enhancement of epoxy matrix reinforced with silicate clay particles. A three-phase model, including the epoxy matrix, the exfoliated clay nanolayers and the nanolayer clusters, was developed to account for partial exfoliation of nanolayers. The Mori−Tanaka method was applied to predict elastic properties of the material. Various parameters including the exfoliation ratio, clay layer and cluster aspect ratios, intragallery modulus, matrix modulus and matrix Poisson's ratio were taken into account. The exfoliation ratio was investigated using transmission electron micrographs, and the estimated value (10%) was included in the model. Predicted values of elastic properties were found to be in close agreement with the experimental results.

8.4 Properties of nanocomposites

Numerous studies on PNCs have demonstrated that nanofillers can provide various functional properties. Table 8.1 lists some nanomaterials with potential functional properties for aerospace applications. This section discusses the recent research performed on nanomaterials and nanocomposites that have potential for some typical properties particularly related to aerospace applications.

Table 8.1 Some nanomaterials and their functional properties related to aerospace applications

Functional properties	Nanomaterials
Mechanical, scratch resistance	Al_2O_3, SiO_2, ZrO_2
Antimicrobial	CuO, TiO_2, ZnO
Gas barrier	Nanoclays, graphene
Corrosion	Nanoclays
Electrical conductivity	CNTs, graphene, SnO_2
Fire retardancy	Nanoclays
Heat stability	Nanoclay, CNTs, ZrO_2
Ultraviolet stability	TiO_2, ZnO, $BaSO_4$, CeO_2, graphene
Impact resistance	SiO_2, TiO_2, $CaSiO_3$, Al_2O_3, CNTs, clay

8.4.1 Weight reduction

Vehicle weight is a major concern for aerospace application. Reductions in vehicle weight enable increased payload capacity that can be utilized to carry more instrumentation, supplies and/or power systems. For aeronautics, vehicle weight reduction leads to reduced fuel consumption and emissions. The current trend within the aerospace community is to maximize the use of lightweight composites in both aircraft and spacecraft. Composite utilization in the Boeing 787 is 50% compared to 7% in the Boeing 777. NASA is actively pursuing technologies to enable wider use of composites in launch vehicle dry structures and cryogenic propellant tanks.

In conventional composites, it is desirable to have a fully densified matrix since voids can act as mechanical defects resulting in premature failure and can also act as sites for environmental degradation of the composite. However, by introducing nanoscale pores or voids into a matrix in a controlled manner, it may be possible to make matrices that can sustain the same type of mechanical loads and the same durability as conventional fully dense polymer matrices. Researchers at the NASA Glenn Research Center have been working on structural polymer aerogels for use in multifunctional insulation. These nanoporous polymers have densities of the order of 0.2 g/cm^3, roughly one-fifth that of a fully dense polymer. Improvements in mechanical properties of this material could be achieved by adding nanoscale fillers (CNTs, nanoclays or graphene) to strengthen nanopore walls in these materials. Replacement of conventional carbon fibres with CNT-derived fibres having higher tensile properties will also enable significant reductions in the composite panel and, ultimately, component weight. Systems analysis indicates that utilizing a CNT fibre with a tensile strength of 10 GPa, twice that of conventional intermediate modulus fibres, would reduce the dry weight of a launch vehicle by up to 25%.

8.4.2 Strength and stiffness

Although polymer−organic nanocomposites also have a significantly higher modulus and strength than the unfilled polymer, reported results are still far below those obtained from traditional carbon fibres. However, recent work is very promising. For instance, fracture toughness (Fig. 8.5) for a 10 vol% multiwalled carbon nanotube (MWCNT)−alumina composite has been measured, indicating that it increased by 24% from 3.4 to 4.2 MPa/m^2 (Siegel et al., 2001). On characterization of CNT− polystyrene composites (Poulin et al., 2002) with the addition of only 1% nanotubes by weight (about 0.5 vol%), the authors achieved between a 36% and 42% increase in the elastic stiffness and a 25% increase in the tensile strength. They also used short-fibre composite theory to demonstrate that 10% by weight of carbon fibres (about 5 vol%) obtained in a different work (Tibbetts and McHugh, 1999) would be required to achieve the same increase in elastic modulus as achieved with 1 wt% of CNTs.

8.4.3 Thermal stability and fire retardancy

For some typical product, improved thermal management is essential to meet market-driven performance, lifetime and cost requirements. For some cases, fire management also plays a crucial role. This is particularly vital for the design of the next-generation aerospace materials with their need for enhanced functionality and
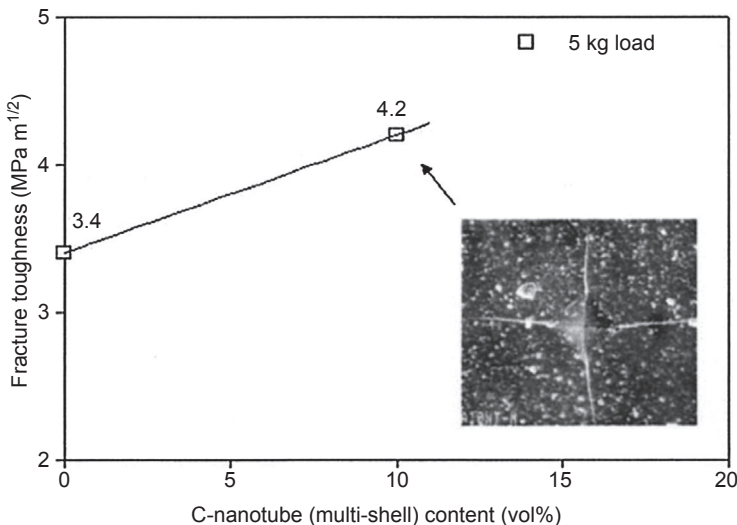
Figure 8.5 Fracture toughness of a 10 vol% MWCNT−alumina nanocomposite compared to that for the unfilled nanophase alumina. The inset shows an indent and resulting cracks.
Adapted from Siegel, R.W., Chang, S.K., Ash, B.J., Stone, J., Ajayan, P.M., Doremus, R.W., Schadler, L.S., 2001. Mechanical behavior of polymer and ceramic matrix nanocomposites. Scripta Mateialia 44 (8), 2061−2064.

increased reliability. In many cases, such as all-electric aircraft, military applications and many sensing systems, enhanced thermal stability and fire retardancy of the material are essentially required. Potential applications include microprocessors and power electronics in military appliances.

In this regard, nanoclay has been considered as a potential material, and worldwide research is progressing in this field (Leszczyńska et al., 2007; Hwu et al., 2002; Report of a DTI global watch mission (UK), 2006). Addition of clay enhances performance by acting as a superior insulator and mass transport barrier to the volatile products generated during decomposition. The clay acts as a heat barrier, which could enhance the overall thermal stability of the system and assist in the formation of char during thermal decomposition. In a nanocomposite, the temperature at which volatilization occurs is higher than for a microcomposite. Moreover, thermal oxidation of the polymer is strongly slowed in a nanocomposite with high-char yield, both by a physical barrier effect, enhanced by ablative reassembling of the silicate, and by a chemical catalytic action due to the silicate and the strongly acid sites created by thermal decomposition of the protonated amine silicate modifier. Recently, Leszczyńska et al. (2007) reviewed the thermal stability of various polymer matrices improved by montmorillonite clay and their influencing factors in detail.

The main mechanism for layered silicate is barrier formation, which influences flame spread in developing fires. However, important fire properties such as flammability or fire load are hardly influenced by adding nanoclays. Hence, combinations with aluminium hydroxide and organo-phosphorus flame retardants have been evaluated (Liang et al., 2013). Polymers that show good fire retardancy on nanocomposite formation exhibit significant intermolecular reactions, such as interchain aminolysis or acidolysis, radical recombination and hydrogen abstraction. For polymers that degrade through a radical pathway, the relative stability of the radical is the most important factor in predicting the effect that nanocomposite formation has on the reduction of the peak heat release rate. The more stable the radical produced by the polymer, the better the fire retardancy, as measured by the reduction in the peak heat release rate of the polymer−clay nanocomposite (Liang et al., 2013).

Although nanoclay is a very popular additive for thermal management and fire retardancy, other nanomaterials have also been explored in this field. Interestingly, a recent study shows that CNTs can even surpass nanoclays as effective flame-retardant additives if the carbon-based nanoparticles (single- and multiwalled nanotubes as well as carbon nanofibres (CNFs)) form a jammed network structure in the polymer matrix, so that the material as a whole behaves rheologically like a gel (Kashiwagi et al., 2005). CNTs are increasingly finding applications as thermal management materials (Zhao et al., 2006; Johnson, 2006; Hu et al., 2006). The addition of CNTs to a polymer matrix could increase the glass transition, melting and thermal decomposition temperatures due to their constraint effect on the polymer segments and chains. It is important to improve the thermal endurance of polymer composites.

However, a limiting factor in the use of CNTs is the transfer of heat flux from one nanotube to another in an efficient manner. CNTs can be woven into mats to produce a low-density, high-thermal-conductivity material. This can be put into a metal composite by pressure or squeeze casting, or epoxy can be added as a filler to give rigid mats;

however, these approaches are still at an early stage. Although expectations of CNTs are very high for their use in composites, there has been some speculation on the results they produce when mixed with polymers. For instance, CNTs are good conductors by themselves, but they may not exhibit the same level of conductivity when integrated into other materials. The problem is that CNTs vibrate at much higher frequencies than the atoms in the surrounding material, which causes the resistance to be so high that thermal conductivity is limited. A new concept of CNT dry adhesive is very attractive in terms of the potential for a high-thermal-conductivity interface. Zhao et al. (2006) recently reported the development of 'dry adhesive−Velcro', a novel CNT technology for thermal interface materials. Using chemical−vapour deposition, a dense array (Fig. 8.6) of vertically aligned MWCNTs have been synthesized on a solid surface, such as silicon (Si), and have array heights on the order of micrometres. This MWCNT dry adhesive was found to be electrically and thermally conductive (comparable to commercially available thermal paste).

Thermal management is a growing need in aerospace and defence applications alike. As devices get smaller and more powerful, the management of heat has become a serious issue. However, thermal transport in nanostructures requires an understanding of heat transport beyond that gained at the continuum level and necessitates advances in measurement methods.

8.4.4   Electronic properties

Nanocomposites research is extremely encompassing in areas such as electronics and computing, data storage and communications. In this regard, carbon-based nanomaterials are gaining much importance. CNTs are electrically conductive additives with an extremely small size and a high aspect ratio. The resulting morphology enables nanotubes to develop a conducting network within a polymer matrix at low percentage loadings, typically 1.5−4.5% by weight and ductility. Nanotubes are highly isotropic and give uniform conductivity throughout the moulded part with minimum warp (Star et al., 2003). Nano-electromechanical systems exhibit no friction; MWCNTs do not exhibit wear and can therefore serve as strong mechanical bearing since the space between the different nanotubes is on the order of nanometres, leaving no possibility of contaminants getting into the bearings. However, the properties depend on so many factors, such as the synthesis method of the nanomaterial, the aspect ratio, dispersion in the matrix, the nanomaterial's network in the matrix and so on.

Despite the excellent dispersion of CNTs and CNFs, the percolation thresholds in various systems are drastically different. Ultra-low-percolation thresholds in the range of 0.0021−0.0039 wt% and, in contrast, high-percolation thresholds in the range of 3−5 wt% have been reported in the literature (Bryning et al., 2005). Major uncertainties are associated with the type and quality of nanotubes, that is a wide variety of synthesis methods have been employed to obtain nanotubes of different sizes, aspect ratios, crystalline orientation, purity, entanglement and straightness. It has been reported that, when the aspect ratio of CNTs was reduced from 411 to 83 to 8.3 in epoxy−CNT nanocomposites, the corresponding percolation threshold increased from 0.5 to 1.5 to >4 wt%, respectively, indicating that the aspect ratio is a
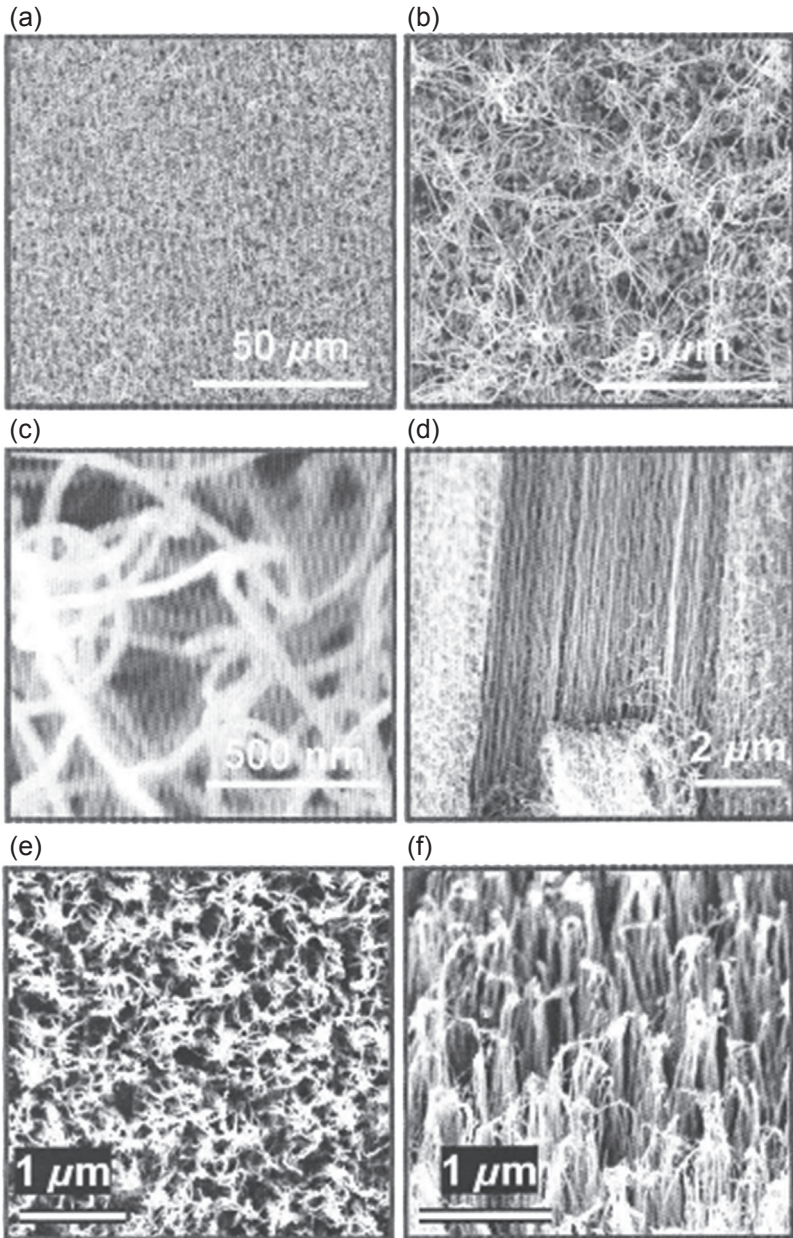
Figure 8.6 Scanning electron microscope (SEM) pictures of MWNCT arrays. (a–c) Top view of an MWCNT array with increasing magnification showing entanglement of the nanotubes at the surface. The diameters range from 20 to 30 nm. (d) Side view of the MWCNT array where a patch of the outer surface is being peeled off, showing vertical alignment of the tubes. (e, f) Top view and side view of another MWCNT array of ~40 μm array height after oxygen plasma etching. Being etched off the entangling surface layer, the MWCNTs show good vertical alignment.

Adapted from Zhao, Y., Tong, T., Delzeit, L., Kashani, A., Meyyappan, M., Majumdar, A., 2006. Interfacial energy and strength of multiwalled-carbon-nanotube-based dry adhesive. Journal of Vacuum Science & Technology B: Microelectronics and Nanometer Structures 24 (1), 331–335.

predominant factor (Bryning et al., 2005). In contrast, for an aspect ratio of 300, a percolation threshold of 0.011−0.011 vol% in epoxy−CNT nanocomposites has been reported (Kim et al., 2005). Even with an aspect ratio of 1000, Allaoui et al. (Allaoui et al., 2002) obtained a percolation threshold of 0.6 vol%. Moreover, it is also rather interesting to note that, even with the same kind of nanotubes, the percolation threshold varied (from 0.0225 to 10 wt%) depending on the matrix materials. Although the differences can be qualitatively explained based on the type and nature of the matrix−resin and the cross-linking density, concrete knowledge is still lacking. In fact, it is very difficult to control the local cross-linking density as it in turn depends on the nature of fillers, their disentanglement and their orientation (Shaffer and Windle, 1999; Sandler et al., 1992).

8.4.5 Field emission and optical properties

Due to scalability and low power consumption, field emitters are attractive candidates for a wide variety of space applications, particularly where budget is a major consideration. Field emission (FE) using CNTs has already been demonstrated as ideal for high-voltage, low-current electrical power applications such as field emission electric propulsion (FEEP), colloids, microion thrusters and perhaps even small electrodynamic (ED) tethers. CNT-based FE fits well with requirements for microsatellites, which are considered to be a viable alternative for a variety of applications, and microtechnology, by contributing to a substantial reduction of mass, volume and power requirements for small satellites and satellite subsystems (Kim et al., 2006; Krishnamoorti and Vaia, 2001; Mirfakhrai et al., 2007; Li and Xia, 2004; Xu and Huq, 2005a,b; Chen et al., 2003b).

Research on electronic devices has focussed primarily on the use of SWCNTs and MWCNTs as field emission electron sources for flat-panel displays, lamps, gas discharge tubes providing surge protection and X-ray and microwave generators. A potential applied between a nanotube-coated surface and an anode creates a high electric field due to the small radius of the nanofibre tips and the lengths of the nanofibres. The local fields cause electrons to tunnel from a nanotube tip to the tunnel. This process of nanotube-tip electron emission differs from that of bulk metals because it arises from discrete energy states instead of continuous electronic bands and its behaviour depends on the nanotube-tip structure, whether SWCNTs or MWCNTs.

The importance of electromagnetic interference (EMI) shielding has also increased in the electronics and communication industries, especially in space and military uses, due to the widespread use of packed, highly sensitive electronic devices. Kim et al. (2006) designed radar-absorbing structures (RASs) with a load-bearing ability in the X-band. Glass−epoxy plain-weave composites with excellent specific stiffness and strength, containing MWCNTs to induce dielectric loss, were fabricated. Fabrication involved impregnation of glass−epoxy plain-weave composites by mixing a matrix and MWCNTs. As the viscosity of the premixture increased rapidly above 3.0 wt%, the researchers reported that they found it difficult to maintain the uniformity of MWCNTs in the matrix. Observation of the microstructure of the composites revealed

that the uneven distribution of MWCNTs could induce high dielectric loss, which was confirmed through a measurement of permittivity.

8.4.6   Age and durability performance

Prolonged exposure of aggressive environments (eg, ultraviolet (UV) radiation, thermal exposure and oxidative and ozone atmosphere) onto any organic material causes changes in their physical, chemical and mechanical characteristics and even loss of use value. Polymer degradation in broader terms includes biodegradation, pyrolysis, oxidation and mechanical, photolytic and catalytic degradation (Pielichowski and Njuguna, 2005). Because of their chemical structure, polymers are vulnerable to harmful effects in the environment. Despite the fact that the organic UV absorber has broad applicability, it has the disadvantages of volatility and migration, due to the pure organic compositions, which not only affect the persistent performance but also lead to environment pollution. Inorganic UV absorbers, such as nano-ZnO, nano-CeO$_2$ and so on, have the advantages of good chemical stability, thermal stability, a nontoxic and odourless state, a wide wavelength range for the UV shielding and so forth (Wang et al., 2014). Exploration of self-rigidizing and self-passivating nanocomposite materials could also be useful to construct space vehicle components that are both highly resistant to space-borne particles and resistant to degradation from electromagnetic radiation, while reducing the overall weight of the spacecraft.

8.4.7   Impact resistance and energy absorption

Damage due to low- and high-velocity impact events weakens the structure of composite materials due to a continuous service load. Furthermore, an impact may generate different types of flaws before full perforation (ie, subsurface delamination, matrix cracks, fibre debonding or fracture, indentation and barely visible impact damage (BVID)). Over time, these effects can induce variations in the mechanical properties of composite structures (the primary effect of a delamination is to change the local value of the bending stiffness and the transverse-shear stiffness), leading to possible catastrophic failure. It has been reported that the energy absorption capability and related properties of polymer matrices can be engineered by adding nanoscale fillers. For example rigid nanosized particles such as SiO$_2$, TiO$_2$, CaSiO$_3$, Al$_2$O$_3$ powder, CNTs and clay nanoplatelets have been used, and some important findings have been summarized in this section.

Typical fillers for the reinforcement of polymer matrices are particles (eg, silica or aluminium oxide particles), tubes (eg, nanofibres or nanotubes) and plates (eg, nanoclay platelets). Significant enhancement of the impact strength of polymeric nanocomposites has been achieved by adding amino-functionalized MWCNTs or small amounts of SWCNTs. The sensitivity of FRPs to intrinsic damage (delamination, matrix cracking and fatigue) and their minimal multifunctionality require a significant effort to improve their performance to meet spacecraft application standards. Currently, however, there are many questions surrounding the incorporation of nanoparticles, like CNTs and CNFs, in FRPs with regard to manufacturing methodology

and structural integrity. The toughening of particle-modified semicrystalline polymers is related to the interparticle distance, s, for any type of added particle. The distance s depends on both the concentration, u, and the average size, d, of the particles.

A number of experiments have shown that fracture toughness improved with the addition of clay nanoplatelets to epoxy when the clay nanoplatelets were not fully exfoliated and intercalated clay nanoplatelets were present. Such very high improvements are not typically observed for composites reinforced with conventional microparticles. Subramaniyan and Sun (2007) reported that core−shell rubber (CSR) nanoparticles, having a soft rubber core and a glassy shell, improved the fracture toughness of an epoxy vinyl ester resin significantly more than montmorillonite (MMT) nanoclay particles with the same weight fraction. However, hybrid blends of CSR and nanoclay were found to give the best balance of toughness, modulus and strength. The same investigators highlighted that, when the nanoclay particles were used to enhance the polymer matrix in a conventional glass-fibre-reinforced composite, the interlaminar fracture toughness of the composite was less than that of the unreinforced composite. It was suggested that a possible reason for this result was the arrangement of the nanoclay particles along the fibre axis.

Two factors affect the capacity of rigid particles for energy dissipation at high loading rates:

- the ability of the dispersed particles to detach from the matrix and to initiate the local matrix shear in the vicinity of voids; and
- the size of the voids.

Therefore, the optimal minimal rigid-particle size for polymer toughening should fulfil two main requirements: to be smaller than the critical size for polymer fracture and also to have a debonding stress that is small compared with the polymer matrix yield stress.

Most of the studies that noted an increase in toughness by incorporating CNTs in polymers (both thermosets and thermoplastics) have attributed it mainly to the nanotube pull-out mechanism and the bridging of cracks in the matrix. The nanotube pull-out mechanism was inspired by conventional polymer−fibre composites where fibre−matrix debonding and fibre pull-out (including work done against sliding friction in pulling out the fibre) govern the extent of energy absorption. Hence, the very high interfacial areas in polymer−nanotube composites are expected to result in drastic improvements in the work necessary for fracture due to nanotube pull-out. To explain and confirm the pull-out mechanism, Barber et al. (2006) studied the pull-out of individual nanotubes by attaching them to the end of a scanning probe microscope (SPM) tip and pushing them into a liquid epoxy polymer (or a liquid melt of polyethylene−butene). After the polymer had solidified, the nanotube was pulled out, and the forces were recorded from the deflection of the SPM tip cantilever. Although this provided an estimate of the interfacial strength of individual nanotubes, it is not directly relevant to pull-out toughness measurement, which depends on many factors like the alignment−orientation and flexibility−entanglement nature of the nanotubes. Even by increasing the embedded length of the nanotube in the resin, the nanotube breaks instead of being pulled out from the polymer.

Nanotube-reinforced structures have up to eight times higher tensile strength and advanced energy dissipation mechanisms, so more damping can be achieved with smaller and lighter structural designs. The number of CNT walls and their size affect stress concentration in the composite, and thus short and even round particles are strongest (like diamonds etc.). However, longer fibres are flexible and may be better for damping. A CNT may act as a nanoscale spring and a crack-trapping material in composites. These damping phenomena could be multiplied when CNTs are dispersed. Orientation and geometry (waviness) of CNT particles may affect the mechanisms of energy dissipation and fracture mechanics. Maximum stiffness is achievable when the longitudinal orientation of CNTs is 90 degree. Notably, open-end CNTs do not collapse, fail or buckle due to higher stress concentrations, and many researchers have used closed-end CNT-reinforced composites. Thus, isolated SWCNTs may be desirable for damping applications due to their significant load-bearing ability because of CNT−matrix interactions.

A paper by Kireitseu et al. (2008) on the rotating fan blades of turbine engines represents another feasible aerospace or defence application. The authors considered a large rotating civil engine blade, which is typically hollow and usually has stiff rib-like metallic structures in order to increase rigidity and maintain the cross-sectional profile of the blade. They suggested a foam-filled fan where the metal structure or traditional fillers are replaced with a CNT-reinforced syntactic foam and, also, with a CNT-reinforced composite layer on the top. Results of the damping behaviour and impact toughness of the composite sandwiches showed that CNT-reinforced samples have better impact strength and vibration-damping properties over a wide temperature range. Experiments conducted using a vibrating clamped beam with the composite layers indicated up to a 200% increase in the inherent damping level and a 30% increase in the stiffness with some decrease (20−30%) in the density of the composite. The crosslinks between the nanotubes and composite layers also served to improve the load transfer within the network, resulting in improved stiffness properties. The critical issues to be considered include: the choice of nanotubes and related matrix materials for vibration damping; tailoring the nanotube−matrix interface with respect to the matrix and the orientation, dispersion and bonding of the nanotubes in the matrix. It is anticipated that significant weight, thickness and manufacturing cost reductions could be achieved in this way.

8.4.8   Tribological and anticorrosion coatings

Another major trend in the materials used in aircraft is towards nanocoatings to enhance the durability of metals. In particular, magnesium alloys, which are far lighter than steel or aluminium, are prone to corrosion, due to the high chemical reactivity of magnesium. Coatings can help prevent corrosion, but the type typically used contains chromium complexes which are a highly toxic pollutant. Materials used for these novel anticorrosion nanocoatings include silicon and boron oxides and cobalt−phosphorous nanocrystals (Voevodin et al., 1999). Nanocoatings are also now being used on turbine blades and other mechanical components which have to withstand high temperatures and friction wear. Tribological coatings can drastically lower the friction coefficient

and improve resistance to wear, which greatly improve the efficiency of the engines. Many nanostructured and nanoscale coating materials have been suggested as possible friction-modifying agents, such as carbides, nitrides, metals and various ceramics.

8.5 Case studies

With a view to provide the overview and scope of recent research and to discuss some technological and scientific approaches behind the exploration of nanocomposites in aerospace applications, a few specific case studies, performed by the nanotechnology research group at IIT Delhi, India, and supervised by Prof. Mangala Joshi, have been illustrated in this section.

8.5.1 Polyurethane-hybrid nanographite nanocomposite for microwave-absorbent applications

Conventional radar absorbent materials (RAMs) such as iron ball (carbonyl iron) and carbon black prove less effective against modern homing devices, especially those which operate at low-frequency microwaves. Hybrid nanoparticles based on ferrite are found to be more suitable for such applications. Iron (Fe)-coated carbon nanoparticles can also be successfully used for conducting, sensing and electromagnetic-shielding or radar-absorbent applications. Among the carbon nanoparticles, nanographite has potential for such applications because of its conductivity, nanomagnetism and layered structure. Therefore, nanographite coated with Fe, nickel (Ni) or chromium can be an attractive choice for microwave-absorbing material.

A recent study was performed by the nanotechnology research group at IIT Delhi, India (Bhattacharyya and Joshi, 2011, 2012), in which Fe coating was used to cover acid-functionalized nanographite by a simple and novel fluidized bed electroplating process (Fig. 8.7). The nanoparticles were further dispersed in polyurethane matrix and cast into nanocomposite films. The microwave absorption property observed in the frequency range of 300 MHz to 1.5 GHz shows that a very thin coating of Fe−Ni on nanographite helps to absorb the microwave quite efficiently. Fe−Ni-coated functionalized nanographite synthesized by this method is thus an effective microwave absorbent material and can find potential use in several defence applications as specialty coatings for fighter aircrafts and radomes, camouflage cover, nets and other coated textiles used for aerial surveillance, and others.

8.5.2 CNF-incorporated three-phase carbon−epoxy composites with enhanced mechanical, electrical and thermal properties

The high strength, high toughness and low weight of carbon−epoxy composites are some of the important properties which make them ideal for aerospace application. Reinforcements in the form of woven fabric are easy to handle and provide better
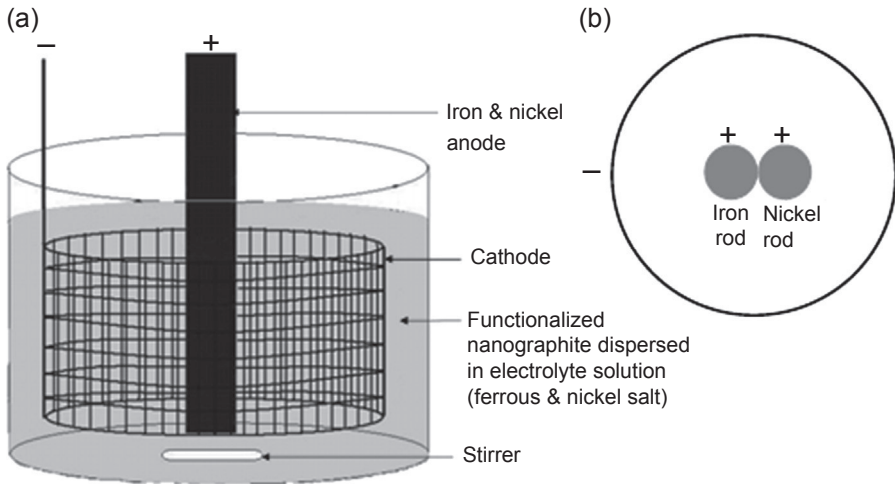
Figure 8.7 Schematic diagram of an electrolytic cell: (a) side view and (b) top view. Adapted from Bhattacharyya, A., Joshi, M., 2011. Co-deposition of Iron and Nickel on Nanographite for Microwave Absorption through Fluidized Bed Electrolysis. International Journal of Nanoscience, 10 (4), 1125−1130.

toughness and impact resistance. The properties of carbon fabric−epoxy composites strongly depend not only on the fabric properties and structure but also on the matrix properties. So many attempts have been made to improve the toughness and other properties of epoxy in order to develop high-performance carbon−epoxy composites. The toughness of epoxy was improved significantly by adding either rubbers or rigid filler particles, but at the cost of modulus, strength and thermomechanical properties. In this respect, carbon nanoparticles can be the better candidates for improving matrix properties as they provide a huge interfacial area.

A novel study in the field of carbon−epoxy composites was performed by M. Joshi et al. at IIT Delhi, India (Rana et al., 2010, 2011). In the study, a three-phase composite was developed where carbon fibres and nanofillers were used in combination to reinforce epoxy matrices. The study aimed at obtaining a homogeneous dispersion of vapour-grown CNFs (Fig. 8.8) in an epoxy resin in order to maximize the property improvement of carbon−epoxy three-phase composites. Based on this study, a suitable dispersion route was selected for the preparation of three-phase composites. Vapour-grown CNFs were uniformly dispersed in the matrix of carbon−epoxy composites using ultrasonic treatment assisted with high-speed mechanical stirring. This dispersion technique led to a significant improvement in Young's modulus and the highest improvement in tensile strength and fracture toughness of epoxy among all the dispersion routes. Dispersion of only 0.5% CNFs in the matrix improved the Young's modulus and tensile strength of carbon−epoxy composites by 37% and 18%, respectively. Similarly, compressive modulus and strength improved by 50% and 18%, respectively. The improved mechanical properties of three-phase composites are attributed to the formation of a strong interface between carbon fibres and epoxy
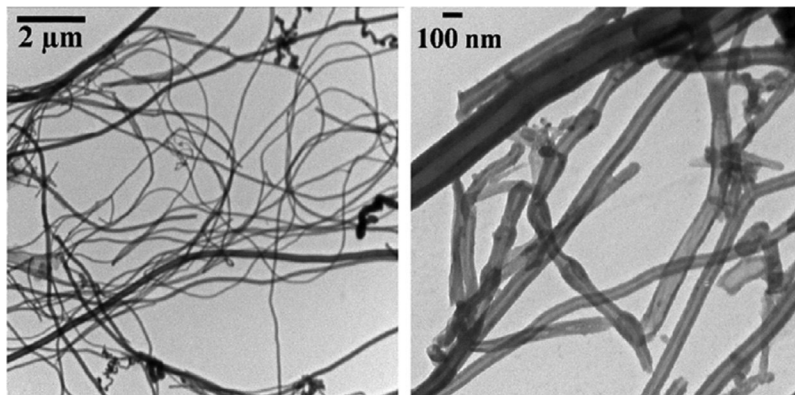
Figure 8.8 Morphology of vapour-grown CNFs under a transmission electron microscope. Adapted from Rana, S., Alagirusamy, R., Joshi, M., 2011. Development of carbon nanofibre incorporated three phase carbon/epoxy composites with enhanced mechanical, electrical and thermal properties. Composites Part A: Applied Science and Manufacturing 42 (5), 439−445.

matrix in the presence of CNFs. Due to the superior electrical and thermal conductivity of vapour-grown CNFs, their incorporation in the matrix of carbon−epoxy composites resulted in improved thermal and electrical conductivity even at very low CNF concentrations (up to 1.0%).

8.5.3 Multifunctional multilayered nanocomposite coatings and laminates for weather-resistant aerostats

An aerostat is an advanced inflatable coated or laminated textile structure that is shaped like an aircraft and floats about 3000 feet above sea level. These aerostats are used as raised platforms for various electronic payloads ranging from sophisticated airborne early-warning radar systems to very-low-frequency and low-frequency communications, active or passive electronic warfare equipment, public emergency broadcasting systems, communications relay and so on. These structures are exposed in harsh atmospheric weather for prolonged times. Unlike fixed-wing aircraft or helicopters, aerostats are 'lighter-than-air (LTA)', typically use helium gas to stay aloft and are tethered using a mooring system operated from a fixed location. A typical inflatable aerostat structure consists of a strength layer generally made up of woven textiles to provide a high strength base to the structure and a protective layer which acts as a gas barrier layer for maintaining the inflated condition of the structure for prolonged time. In such cases, the lifetime of the ultimate inflatable structure is primarily determined by the protective properties of the coating. But the use of conventional polymeric coatings (polyvinyl chloride (PVC), acrylic etc.) in these applications becomes very limited because of the coatings' poor weathering resistance, low flex fatigue, poor adhesion to substrate or high permeability to air or gases. As an alternative material for the protective layer of the aerostat, thermoplastic polyurethane (TPU)

has recently attracted more and more interest (Chattopadhyay and Raju, 2007). However, similar to other polymer materials, exposure of TPU to aggressive environments (eg, UV radiation, thermal exposure and oxidative atmosphere) for prolonged time causes changes in its physical, chemical and mechanical characteristics and even loss of use value (Boubakri et al., 2010). Conventionally, UV stabilizers such as UV absorber, hindered amine light stabilizers (HALS) and antioxidants are incorporated into the coating formulation to avoid degradation. But the conventional additives suffer from high physical loss through migration, leaching, blooming and so on. In this regard, incorporation of nanomaterials would be a novel approach. Nanomaterials not only seem to provide minimum physical loss but also may provide functional properties such as resistance to permeability of gases.

In this regard, a novel study is currently ongoing by our research group at IIT Delhi, India, to develop a multilayered coating and laminating system that incorporates advanced nanomaterials to serve multifunctional properties (Chatterjee et al., 2013, 2014, 2015).

8.6   Some commercial applications

Nanocomposites represent the frontier of high-performance materials. The growing requirement for high-performance military aerospace systems and growing demands of government-funded defence projects represent an ideal frontrunner for the commercial adoption of nanocomposite materials.

US global aerospace and defence company Lockheed Martin recently announced that the F-35 Lightning II aircraft utilizes CNTs in the wingtip fairings. The F-35 is a stealth-capable military strike fighter born out of the Joint Strike Fighter (JSF) program funded by the US Department of Defense (http://blog.luxresearchinc.com (September 2015)). The Center for Research in Advanced Materials (CIMAV), located in the Research and Technological Innovation Park (PIIT) in Monterrey, northern Mexico, has developed solar cell materials that have been reinforced with graphite nanoplatelets, especially for industrial applications (http://www.nanowerk.com (September 2015)). However, transferring any lab-scale technology towards high-volume applications is still a big challenge. Advancement in research on mass-scale synthesis of nanomaterials and their incorporation into polymers pave the way for the penetration of nanocomposites in high-volume applications, not only in aerospace but also in the automotive, oil and gas, marine, construction and wind power industries.

8.7   Conclusion

Fibre-reinforced composites which are conventionally used as aerospace materials exhibit high strength−weight and modulus−weight ratios compared with some metallic materials. However, in the last two decades, the focus has shifted towards

nanomaterial-based composites as they have shown potential improvement in their properties and can provide multifunctional performances. The current worldwide research on nanoscale particle-reinforced composites for aerospace applications can be categorized as inorganic layered clay technology, carbon material−based (SWCNT, MWCNT and CNF) technology and metal nanoparticle technology. To date, the nanoparticle reinforcement of fibre-reinforced composites or three-phase composites has also been shown to be a great possibility, but much work remains in order to understand how nanoreinforcement results in major changes in material properties.

The advantage of nanoscale compared with microscale fillers is their enormous surface area, which can act as an interface for more efficient stress transfer. One of the technological drawbacks is that mechanical reinforcement through the application of nanoparticles as a structural element in polymers, which is generally related to the degree of dispersion, impregnation in the matrix and interfacial adhesion, is more difficult to realize and still remains a challenging task. An understanding of these phenomena will facilitate their extension to the development of more advanced polymeric nanocomposite systems for high-end aerospace applications.

References

Aboudi, J., 1988. Micromechanical analysis of the strength of unidirectional fiber composites. Composites Science and Technology 33 (2), 79−96.

Aboudi, J., 1990. The nonlinear behavior of unidirectional and laminated composites-A micromechanical approach. Journal of Reinforced Plastics and Composites 9 (1), 13−32.

Ajayan, P.M., Schadler, L.S., Braun, P.V., Picu, C., Keblinski, P., 2003. Nanocomposite Science and Technology. Wiley Online Library.

Alexandre, M., Dubois, P., 2000. Polymer-layered silicate nanocomposites: preparation, properties and uses of a new class of materials. Materials Science and Engineering 28, 1−63.

Allaoui, A., Bai, S., Cheng, H.M., Bai, J.B., 2002. Mechanical and electrical properties of a MWNT/epoxy composite. Composites Science and Technology 62 (15), 1993−1998.

Barber, A.H., Cohen, S.R., Eitan, A., Schadler, L.S., Wagner, H.D., 2006. Fracture transitions at a carbon-nanotube/polymer interface. Advanced Materials 18 (1), 83−87.

Belytschko, T., Xiao, S., Schatz, G., Ruoff, R., 2002. Atomistic simulations of nanotube fracture. Physical Review B 65 (23), 235−247.

Bhattacharyya, A., Joshi, M., 2011. Co-deposition of iron and nickel on nanographite for microwave absorption through fluidized bed electrolysis. International Journal of Nanoscience 10 (4), 1125−1130.

Bhattacharyya, A., Joshi, M., 2012. Functional properties of microwave-absorbent nanocomposite coatings based on thermoplastic polyurethane-based and hybrid carbon-based nanofillers. Polymers for Advanced Technologies 23 (6), 975−983.

Boubakri, A., Guermazi, N., Elleuch, K., Ayedi, H., 2010. Study of UV-aging of thermoplastic polyurethane material. Materials Science and Engineering: A 527 (7), 1649−1654.

Boutaleb, S., Zaïri, F., Mesbah, A., Naït-Abdelaziz, M., Gloaguen, J., Boukharouba, T., Lefebvre, J., 2009. Micromechanics-based modelling of stiffness and yield stress for silica/polymer nanocomposites. International Journal of Solids and Structure 46 (7), 1716−1726.

Bryning, M.B., Islam, M.F., Kikkawa, J.M., Yodh, A.G., 2005. Very low conductivity threshold in bulk isotropic single-walled carbon nanotube-epoxy composites. Advanced Materials 17 (9), 1186−1191.

Chatterjee, U., Joshi, M., Butola, B.S., 2013. Predicting changes in TPU coating properties with weathering. In: Polymer Processing Society Asia/Australia Conference, Mumbai, India.

Chatterjee, U., Joshi, M., Butola, B.S., 2014. Weathering performance of polyurethane coatings for aerostat applications. In: International Conference on Technical Textiles and Non-wovens, New Delhi, India.

Chatterjee, U., Joshi, M., Butola, B.S., Thakre, V., Singh, G., Verma, M.K., 2015. Thermo-plastic polyurethane coatings for aerostat: influence of polyurethane chemistry and additives on weathering properties. In: International Symposium on Polymer Science and Technology: Macro 2015, Kolkata, India.

Chattopadhyay, D., Raju, K., 2007. Structural engineering of polyurethane coatings for high performance applications. Progress in Polymer Science 32 (3), 352−418.

Chavarria, F., Paul, D., 2004. Comparison of nanocomposites based on nylon 6 and nylon 66. Polymer 45 (25), 8501−8515.

Chen, J., Huang, Z., Mai, Y.W., 2003a. Constitutive relation of particulate-reinforced visco-elastic composite materials with debonded microvoids. Acta Materialia 51 (12), 3375−3384.

Chen, J., Ren, H., Ma, R., Li, X., Yang, H., Gong, Q., 2003b. Field-induced ionization and Coulomb explosion of CO_2 by intense fem to second laser pulses. International Journal of Mass Spectrometry 228 (1), 81−89.

Chen, J., Huang, Z., Zhu, J., 2007. Size effect of particles on the damage dissipation in nano-composites. Composites Science and Technology 67 (14), 2990−2996.

Cornwell, C., Wille, L., 1997. Elastic properties of single-walled carbon nanotubes in compression. Solid State Communications 101 (8), 555−558.

Fang, F.F., Choi, H.J., Joo, J.J., 2008. Conducting polymer/clay nanocomposites and their applications. Nanoscience and Nanotechnology 8 (4), 1559−1581.

Fornes, T., Paul, D., 2003. Modelling properties of nylon 6/clay nanocomposites using com-posite theories. Polymer 44 (17), 4993−5013.

Gangopadhyay, R., De, A., 2000. Conducting polymer nanocomposites: a brief overview. Chemistry of Material 12 (3), 608−622.

Hu, X.J., Padilla, A.A., Xu, J., Fisher, T.S., Goodson, K.E., 2006. 3-Omega measurements of vertically oriented carbon nanotubes on silicon. Journal of Heat Transfer 28, 1109.

Hwu, J.M., Jiang, G.J., Gao, Z.M., Xie, W., Pan, W.P., 2002. The characterization of organic modified clay and clay-filled PMMA nanocomposite. Journal of Applied Polymer Science 83 (8), 1702−1710.

Johnson, R.C., 2006. Carbon-nanotube arrays take heat off chips. Electronic Engineering Times 1423, 38.

Kashiwagi, T., Du, F., Douglas, J.F., Winey, K.I., Harris Jr., R.H., Shields, J.R., 2005. Nanoparticle networks reduce the flammability of polymer nanocomposites. Nature Materials 4 (12), 928−933.

Kim, Y.J., Shin, T.S., Choi, H.D., Kwon, J.H., Chung, Y.C., Yoon, H.G., 2005. Electrical conductivity of chemically modified multiwalled carbon nanotube/epoxy composites. Carbon 43 (1), 23−30.

Kim, C.-G., Lee, S.-E., Kang, J.-H., 2006. Fabrication and design of multi-layered radar absorbing structures of MWNT-filled glass/epoxy plain-weave composites. Composite Structures 76 (4), 397−405.

Kireitseu, M., Hui, D., Tomlinson, G., 2008. Advanced shock-resistant and vibration damping of nanoparticle-reinforced composite material. Composites Part B: Engineering 39 (1), 128−138.

Krishnamoorti, R., Vaia, R.A., 2001. Polymer nanocomposites (synthesis, characterization, and modeling). In: A.C.S. Series, vol. 804, pp. 15−25.

Leszczyńska, A., Njuguna, J., Pielichowski, K., Banerjee, J.R., 2007. Polymer/montmorillonite nanocomposites with improved thermal properties: part I. Factors influencing thermal stability and mechanisms of thermal stability improvement. Thermochimica Acta 453 (2), 75−96.

Li, D., Xia, Y., 2004. Welding and patterning in a flash. Nature Materials 3 (11), 753−754.

Liang, S., Neisius, N.M., Gaan, S., 2013. Recent developments in flame retardant polymeric coatings. Progress in Organic Coatings 76 (2), 1642−1665.

Luo, J.J., Daniel, I.M., 2003. Characterization and modelling of mechanical behavior of polymer/clay nanocomposites. Composites Science and Technology 63 (11), 1607−1616.

Mc Crum, N.G., Buckley, C.P., Bucknall, C.B., 1996. Principles of Polymer Engineering. Oxford Science, New York.

Mirfakhrai, T., Madden, J.D.W., Baughman, R.H., 2007. Polymer artificial muscles. Materials Today 10 (4), 30−38.

Namilae, S., 2005. Multiscale model to study the effect of interfaces in carbon nanotube based composites. Journal of Engineering Materials and Technology 127, 222−232.

Pielichowski, K., Njuguna, J., 2005. Thermal Degradation of Polymeric Materials. RAPRA Technologies Limited, Shawbury, Surrey, UK.

Poulin, P., Vigolo, B., Launois, P., 2002. Films and fibers of oriented single wall nanotubes. Carbon 40 (10), 1741−1749.

Rana, S., Alagirusamy, R., Joshi, M., 2010. Mechanical behavior of carbon nanofibre-reinforced epoxy composites. Journal of Applied Polymer Science 118 (4), 2276−2283.

Rana, S., Alagirusamy, R., Joshi, M., 2011. Development of carbon nanofibre incorporated three phase carbon/epoxy composites with enhanced mechanical, electrical and thermal properties. Composites Part A: Applied Science and Manufacturing 42 (5), 439−445.

Rapaport, D.C., 2004. The Art of Molecular Dynamics Simulation. Cambridge University Press, UK.

Report of a DTI global watch mission (UK), December 2006. Developments and Trends in Thermal Management Technologies − a Mission to the USA.

Sandler, J., Shaffer, M.S.P., Prasse, T., Bauhofer, W., Schulte, K., Windle, A.H., 1992. Development of a dispersion process for carbon nanotubes in an epoxy matrix and the resulting electrical properties. Polymer 40 (21), 5967−5971.

Shaffer, M.S.P., Windle, A.H., 1999. Fabrication and characterization of carbon nanotube/poly (vinyl alcohol) composites. Advanced Materials 11 (11), 937−941.

Siegel, R.W., Chang, S.K., Ash, B.J., Stone, J., Ajayan, P.M., Doremus, R.W., Schadler, L.S., 2001. Mechanical behavior of polymer and ceramic matrix nanocomposites. Scripta Mateialia 44 (8), 2061−2064.

Star, A., Liu, Y., Grant, K., Ridvan, L., Stoddart, J.F., Steuerman, D.W., Diehl, M.R., Boukai, A., Heath, J.R., 2003. Noncovalent side wall functionalization of single-walled carbon nanotubes. Macromolecules 36 (3), 553−560.

Subramaniyan, A.K., Sun, C.T., 2007. Toughening polymeric composites using nanoclay: crack tip scale effects on fracture toughness. Composites Part A: Applied Science and Manufacturing 38 (1), 34−43.

Thostenson, E., Li, C., Chou, T., 2005. Review nanocomposites in context. Journal of Composites Science & Technology 65, 491−516.

Tibbetts, G.G., McHugh, J., 1999. Mechanical properties of vapor-grown carbon fiber composites with thermoplastic matrices. Journal of Material Research 14 (7), 2871−2880.

Voevodin, A.A., ONeill, J.P., Zabinski, J.S., 1999. Nanocomposite tribological coatings for aerospace applications. Surface and Coatings Technology 116 (119), 36−45.

Wang, H., Wang, Y., Liu, D., Sun, Z., Wang, H., 2014. Effects of additives on weather-resistance properties of polyurethane films exposed to ultraviolet radiation and ozone atmosphere. Journal of Nanomaterials 2014, 1−8.

Wilkinson, A., Man, Z., Stanford, J., Matikainen, P., Clemens, M., Lees, G., Liauw, C., 2007. Tensile properties of melt intercalated polyamide 6-Montmorillonite nanocomposites. Composites Science and Technology 67 (15), 3360−3368.

Wu, Y.P., Jia, Q.X., Yu, D.S., Zhang, L.Q., 2004. Modelling Young's modulus of rubber-clay nanocomposites using composite theories. Polymer Testing 23 (8), 903−909.

Xu, N.S., Huq, S.E., 2005a. Novel cold cathode materials and applications. Materials Science and Engineering R: Reports 48 (2), 143.

Xu, N.S., Huq, S.E., 2005b. Novel cold cathode materials and applications. Materials Science and Engineering R: Reports 48 (2−5), 47−189.

Zhao, Y., Tong, T., Delzeit, L., Kashani, A., Meyyappan, M., Majumdar, A., 2006. Interfacial energy and strength of multiwalled-carbon-nanotube-based dry adhesive. Journal of Vacuum Science & Technology B: Microelectronics and Nanometer Structures 24 (1), 331−335.

Multiscale composites for aerospace engineering

9

S. Rana, S. Parveen, R. Fangueiro
School of Engineering, University of Minho, Guimarães, Portugal

9.1 Introduction

Aerospace engineering is one of the advanced technical sectors looking for innovative and high-performance materials, in order to enhance performance and safety as well as to reduce fuel consumption and cost. Multidisciplinary research and innovations in the field of materials science and engineering made it possible to develop extraordinary and multifunctional materials which are gaining tremendous attention in the high-end industrial sectors, including aerospace engineering. Advanced composite materials are one class of innovative materials with huge application potential. The possibility to combine different materials and the ease in tailoring the structure allow researchers to design composite materials with virtually any set of properties. In addition, the advancement in nanotechnology paved new pathways to develop composite materials with extraordinary properties. Different nanomaterials (ie, particles, fibres and tubes) are being utilized extensively in composite materials to achieve enhanced mechanical properties with light weight and many other essential functionalities, such as electrical and thermal conductivity, electromagnetic shielding, gas barrier properties, self-sensing abilities, self-healing properties and so on. These strong, lightweight and multifunctional composites can be the ideal materials in future for aerospace structures.

Nanocomposites developed through incorporating various nanomaterials within different matrix systems are being utilized for different industrial sectors such as medical, automobiles, electronics, food packaging and so on. However, these nanocomposites cannot meet the strength requirements for primary aerospace structures. Although some nanomaterials such as carbon nanotubes (CNTs) and carbon nanofibres (CNFs) possess remarkably higher mechanical properties as compared to conventional reinforcing materials like carbon fibres, the limitation on achieving a high volume fraction of nanomaterials in composites does not allow them to achieve high mechanical properties similar to those of conventional fibre-reinforced composites. At high volume fraction, nanomaterials are extremely difficult to disperse within the matrix and try to agglomerate, forming voids and defects in composites. Therefore, the simplest approach to achieve high mechanical performance with multifunctional properties is to develop hybrid composites that combine both conventional and nanoreinforcements. Besides their individual contribution, these reinforcements from two different scales can also have some synergistic effects. Combining reinforcements from different length scales (ie, micro, macro or nano) leads to the development of a new class of advanced composites materials, commonly known as multiscale composites (Rana et al., 2009, 2012a, 2015;
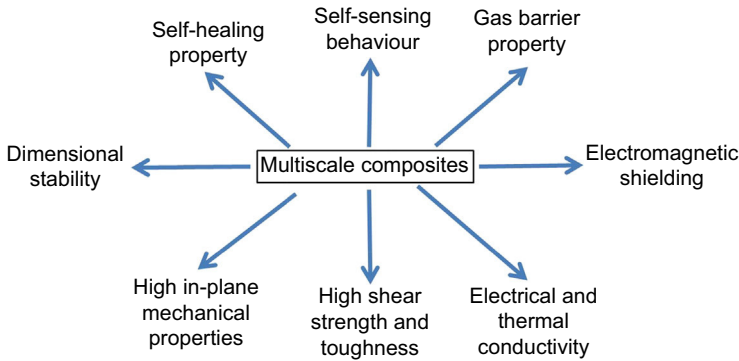
Figure 9.1 Properties of multifunctional composites.

Wang et al., 2011; Khan and Kim, 2011; Díez-Pascual et al., 2014; Rana and Fangueiro, 2015). Proper designing of multiscale composites can provide much better mechanical properties than conventional composites as well as other important characteristics such as electrical and thermal conductivity, electromagnetic shielding, damage-sensing capability and so on (Fig. 9.1), which are essential for aerospace structures.

9.2 Definition and concept

Multiscale composites can be defined as composite materials containing reinforcing elements from different length scales (ie, macro, micro and/or nano) (Rana et al., 2009, 2012a, 2015; Wang et al., 2011; Khan and Kim, 2011; Díez-Pascual et al., 2014; Rana and Fangueiro, 2015). Therefore, in principle, they are hybrid composites composed of different types of reinforcements impregnated with a matrix system. For advanced technical applications, more common are multiscale composites containing a conventional reinforcement such as glass, carbon and so on and a nanoreinforcement such as CNTs, CNFs, nanoclay or the like. Multiscale composites are commonly developed by dispersing these nanomaterials within a polymeric (or cementitious, in the case of structural applications) matrix and, subsequently, impregnating the conventional fibres with this nanodispersed resin system. However, the other route of incorporating nanomaterials within fibre, followed by their impregnation with a pure matrix, also has been tried by many researchers. These two approaches of fabricating multiscale composites are shown schematically in Fig. 9.2.

Incorporation of various nanomaterials within a fibre system can be performed by different means. Nanomaterials like CNTs and CNFs can be directly grown on the fibres during their production. Alternatively, nanomaterials can also be added to the fibre system by grafting, spraying, sizing and coating processes. The various means of incorporating nanomaterials within multiscale composites are listed here:

- Dispersion within matrix
- Growing on the fibres
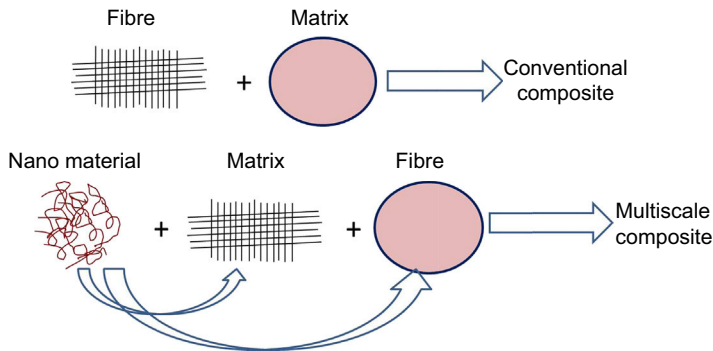
Figure 9.2 Concept of fabricating multiscale composites through different approaches.

- Transfer printing
- Grafting to the fibres
- Spraying on the fibres
- Coating the fibres
- Sizing the fibres
- Electrophoretic deposition

Each of these approaches has their own merits and demerits. Table 9.1 lists the advantages and disadvantages of the various methods to fabricate multiscale composites.

9.3 Types of nanomaterials

To date, multiscale composites have been developed using different types of nanomaterials. Some of them are nanoparticles, whereas most common are the nanomaterials with high aspect ratios such as nanofibres and nanotubes. Various nanomaterials used to fabricate multiscale composites are as follows (Rana et al., 2009, 2012a, 2015; Wang et al., 2011; Khan and Kim, 2011; Rana and Fangueiro, 2015; Díez-Pascual et al., 2014; Hussain et al., 1996; Shahid et al., 2005; Siddiqui et al., 2007; Chowdhury et al., 2006; Chisholm et al., 2005; Parveen et al., 2013). A few of these nanomaterials are presented in Fig. 9.3.

- Nano-Al_2O_3
- Nano-SiC
- Nanographite
- Nanoclay
- Nanofibre (more commonly CNFs)
- Nanotube (more commonly CNTs)

Among these nanomaterials, nanomaterials with high aspect ratios such as CNFs and CNTs were found very useful to develop multiscale composites with excellent performance. Table 9.2 shows the use of various nanomaterials in multiscale composites and the resulting improvements in performances.

Table 9.1 Different approaches for developing multiscale composites, their merits and demerits

Approaches	Merits and demerits
Dispersion	Applicable for any type of matrix and fibre system. However, the main challenge is to eliminate the nanomaterial agglomeration.
Nanomaterial growth on fibres	There is no nanomaterial agglomeration within the matrix. However, it is applicable only for nanomaterials which can be grown using the chemical vapour deposition (CVD) technique and for fibres which are resistant to the temperature of CVD.
Transfer printing	Two-step process that should be performed after nanomaterial growth by CVD. Can also be applied for polymeric fibres with lower thermal resistance.
Spraying	Simple process. During spraying, nanomaterials can agglomerate.
Coating and sizing	Simple process. Nanomaterial agglomeration is possible.
Electrophoretic deposition	Applicable for only functionalized nanomaterials and carbon fibres.
Grafting	Nanomaterials can be chemically bonded to the fibre system (ie, strong fibre−nanomaterial bonding can be achieved). Long process and fibre surface should be functionalized prior to the grafting process.

9.4 Fabrication of multiscale composites

Multiscale composites are fabricated by the following two steps:

1. Incorporation of nanomaterials (within matrix or fibre)
2. Impregnation of fibre and solidification

9.4.1 Methods of nanomaterial incorporation within matrix

Dispersion of nanomaterials is the most common method of incorporating nanomaterials in multiscale composites. Nanomaterials (especially CNFs and CNTs) usually remain in very dense agglomerates. The aim of the dispersion process is to break these agglomerates, separate the nanomaterials and distribute them homogeneously within the matrix (Rana et al., 2010a,b, 2011c). Dispersion of nanomaterials with a high aspect ratio such as CNTs is very difficult, as very strong attractive van der Waals forces exist between them. Commonly, various mechanical treatments are used to disperse CNFs and CNTs within polymeric matrices (Fiedler et al., 2006):

1. Ultrasonication
2. High-speed mechanical stirring
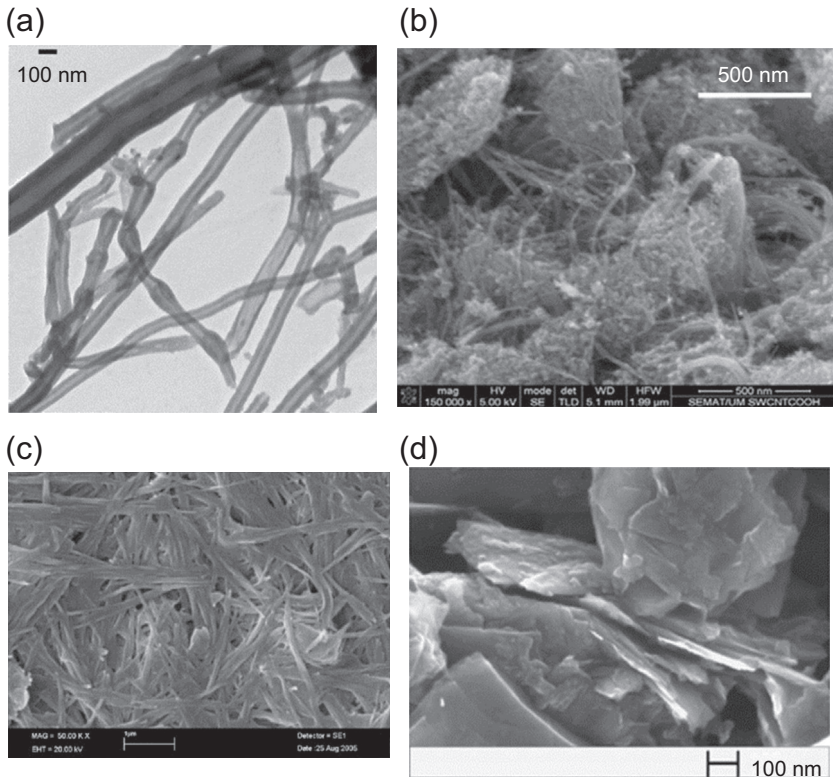
Figure 9.3 Different nanomaterials used for developing multiscale composites: (a) CNF; (b) CNT; (c) nanoclay; and (d) nanographite.
(a) Adapted from Rana, S., Alagirusamy, R., Joshi, M., 2011b. Development of carbon nanofibre incorporated three phase carbon/epoxy composites with enhanced mechanical, electrical and thermal properties. Composites Part A: Applied Science and Manufacturing 42 (5), 439−445.
(b) Adapted from Parveen, S., Rana, S., Fangueiro, R., Paiva, M.C., 2015. Microstructure and mechanical properties of carbon nanotube reinforced cementitious composites developed using a novel dispersion technique. Cement and Concrete Research, 73, 215−227. (c) Adapted from Ho, M.-W., Lam, C.-K., Lau, K.-T., Ng, D.H.L., Hui, D., 2006. Mechanical properties of epoxy-based composites using nanoclays. Composite Structures 75 (1), 415−421. (d) Adapted from Cho, J., Chen, J.Y., Daniel, I.M., 2007. Mechanical enhancement of carbon fiber/epoxy composites by graphite nanoplatelet reinforcement. Scripta Materialia 56 (8), 685−688.

3. Calendering
4. Ball milling
5. Twin-screw extrusion

Ultrasonication is the most frequently used technique for fabricating polymer matrix-based multiscale composites (Rana et al., 2011a,b, 2013; Bhattacharyya et al., 2013). The shock waves generated during the ultrasonication process separate the nano-materials from agglomerates and disperse them in the solution. Ultrasonication can be carried out in a water bath (bath sonication), or by using a probe (tip sonication) which

Table 9.2 Different functionalities that can be incorporated using various nanomaterials

Type of nanomaterials	Functionalities
Nano-Al_2O_3	Enhanced mechanical properties
Nano-TiO_2	Enhanced mechanical properties
Nanoclay	Enhanced mechanical properties and gas barrier properties
Nanographite	Enhanced mechanical properties
Carbon nanofibre	Enhanced mechanical properties, electrical and thermal conductivity, electromagnetic shielding, self-sensing and so on
Carbon nanotube	Enhanced mechanical properties, electrical and thermal conductivity, electromagnetic shielding, self-sensing and so on

can be directly introduced into the nanomaterial solution to generate localized, intense ultrasonic waves. According to the proposed mechanisms of CNT dispersion in aqueous solution, ultrasonication waves start separating the nanotubes at the end, and this facilitates the entry of surfactant molecules (Vaisman et al., 2006). CNTs are further separated along their length and go to the solution due to action of surfactant molecules (steric or electrostatic stabilization). This mechanism is shown schematically in Fig. 9.4. Therefore, usually chemical dispersants are used along with the ultrasonication

(i)   (ii)   (iii)   (iv)
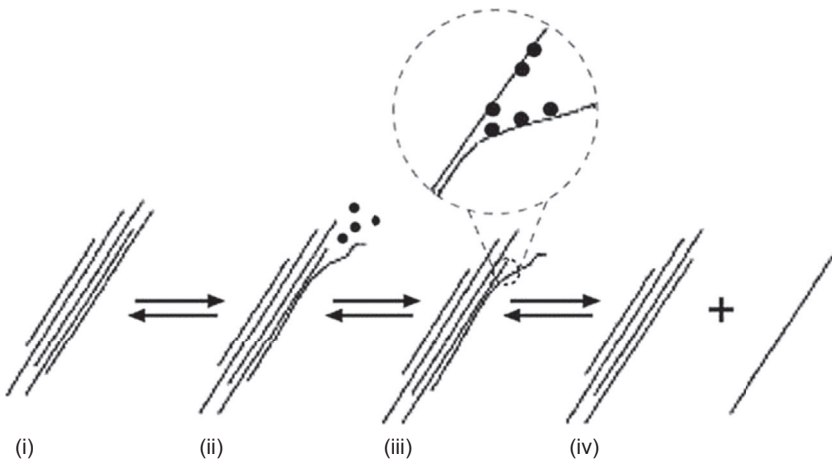
Figure 9.4 Mechanism of CNT dispersion by ultrasonication assisted by surfactant. Adapted from Vaisman, L., Daniel Wagner, H., Marom, G., 2006. The role of surfactants in dispersion of carbon nanotubes. Advances in Colloid and Interface Science 128, 37−46.
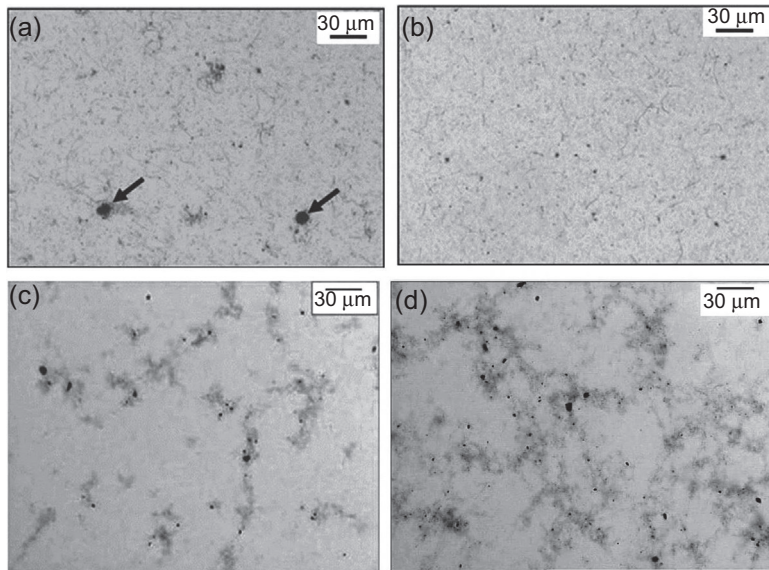
Figure 9.5 Dispersion of different nanomaterials using an ultrasonication process: (a) CNFs using 2 h of sonication; (b) CNFs using 2 h of sonication and surfactant; (c) CNTs using 10 h of sonication; and (d) CNTs using 6 h of sonication and 2 h of stirring.
Adapted from Rana, S., Alagirusamy, R., Joshi, M., 2011b. Development of carbon nanofibre incorporated three phase carbon/epoxy composites with enhanced mechanical, electrical and thermal properties. Composites Part A: Applied Science and Manufacturing 42 (5), 439−445.

process to achieve better dispersion results. Fig. 9.5(a) and (b) shows the positive influence of surfactant in dispersing CNFs in epoxy resin.

Furthermore, the presence of functional groups on the nanomaterial surface may also help in the stabilization of dispersed nanomaterials. Amine and silane functionalization are two common types of functionalization used for developing CNT-based multiscale composites (Fiedler et al., 2006; Sharma and Shukla, 2014). A scheme for amine functionalization of CNTs is shown in Fig. 9.6. Besides dispersion stabilization, functionalization also leads to formation of a strong interface between nanomaterials and the matrix through covalent bonding (Rana et al., 2012b). A strong interface helps in restricting nanomaterial pull-outs during crack growth and provides a strong crack-bridging effect.

Nanomaterials dispersion by an ultrasonication process depend strongly on several parameters. The quality of nanomaterial dispersion usually improves with ultrasonication time and energy, but at the cost of nanomaterial quality (aspect ratio, electronic properties etc.), processing time and cost. Some processing parameters such as resin viscosity and temperature of solution also influence the dispersion process, and correct control and optimization of these parameters are essential to facilitate nanomaterial dispersion without encouraging nanomaterial re-agglomeration. As ultrasonication treatment has some demerits, this process can also be combined with other mechanical techniques to reduce the treatment time and associated
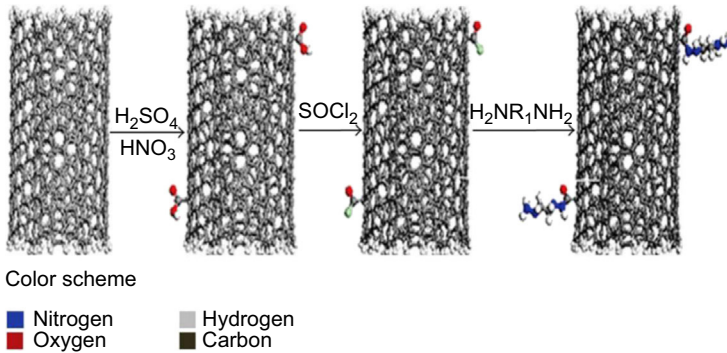
Figure 9.6 Nanomaterial functionalization for improving dispersion behaviour.
Adapted from Sharma, K., Shukla, M., 2014. Three-phase carbon fiber amine functionalized
carbon nanotubes epoxy composite: processing, characterisation, and multiscale modeling.
Journal of Nanomaterials 2014, 1−10.
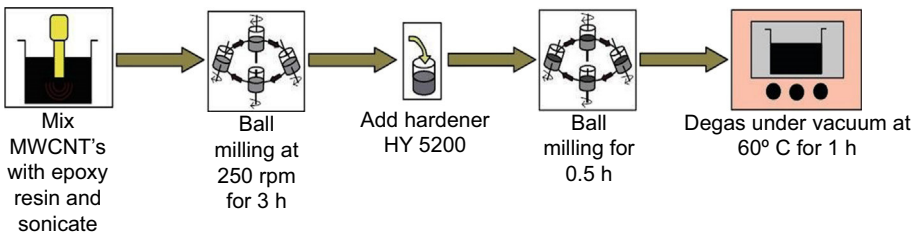
Figure 9.7 Dispersion of nanomaterials using high-speed stirring and calendering processes.
Adapted from Sharma, K., Shukla, M., 2014. Three-phase carbon fiber amine functionalized
carbon nanotubes epoxy composite: processing, characterisation, and multiscale modeling.
Journal of Nanomaterials 2014, 1−10.

problems. A route of dispersing CNTs in epoxy resin using a combination of ultra-
sonication with ball milling is presented in Fig. 9.7.

Stirring is another mechanical technique for dispersing nanomaterials within various
matrices, and it also has been utilized for fabricating multiscale composites. The disper-
sion quality during the stirring process depends strongly on the size and shape of the
propeller and the stirring speed. High-speed stirring ($\sim$4000 rpm) has been found
very effective in dispersing CNTs and CNFs in thermosetting matrices for developing
multiscale composites (Rana et al., 2011a,b). The combination of mechanical stirring
with ultrasonication has been found successful to reduce the ultrasonication time and
ensure very good dispersion quality. **Calendering** is another mechanical technique
which can be combined with ultrasonication or other mechanical treatments or can be
used alone to disperse nanomaterials in different matrices. This is an efficient technique
to produce larger amounts of nanocomposites (Fiedler et al., 2006).

In the case of thermoplastic matrices, the common approach of dispersing nanoma-
terials within the matrix is through the extrusion process (Díez-Pascual et al., 2014).
Twin-screw extrusion is usually used to disperse various nanomaterials within

thermoplastic matrices. Similar to the ultrasonication process, a number of processing parameters exist such as screw speed, profile, temperature and so on, and these decide the quality of nanomaterial dispersion within the matrix.

9.4.2 Multiscale composites fabrication by incorporating nanomaterials on the fibre surface

To avoid problems in the dispersion, multiscale composites can also be fabricated by incorporating nanomaterials directly on the fibre surface (Wicks et al., 2010; Bekyarova et al., 2007; Jiang et al., 2007; Enrique et al., 2008; He et al., 2007; Veedu et al., 2006). Fig. 9.8 shows some techniques of incorporating nanofillers on the fibre system for fabricating multiscale composites. One of the methods which has been used in research is to grow some nanomaterials like CNFs and CNTs directly on the fibre
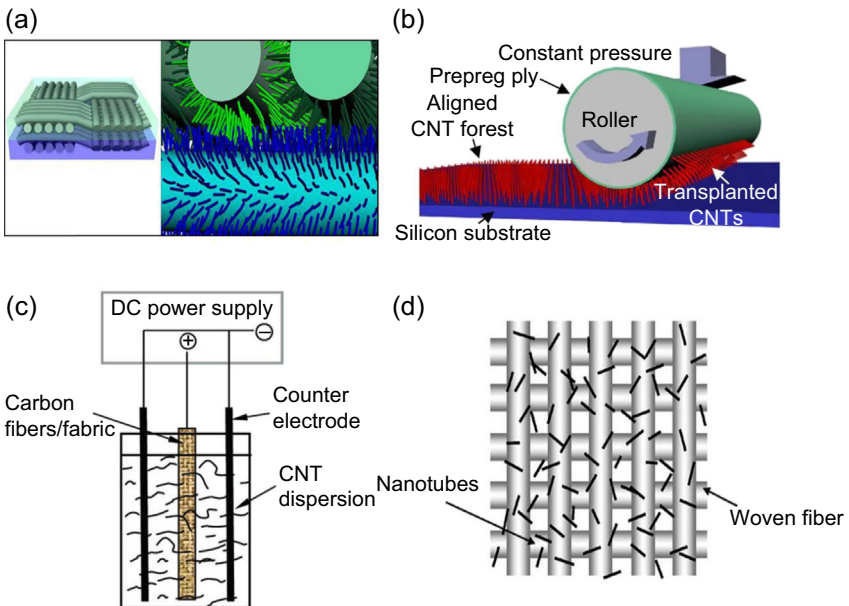
Figure 9.8 Techniques of incorporating nanomaterials on a fibre system: (a) nanomaterial growth; (b) transfer printing; (c) electrophoretic deposition; and (d) spraying process. (a) Adapted from Wicks, S.S., de Villoria, R.G., Wardle, B.L., 2010. Interlaminar and intralaminar reinforcement of composite laminates with aligned carbon nanotubes. Composites Science and Technology 70 (1), 20−28. (b) Adapted from Enrique, G.J., Wardle, B.L., Hart A.J., 2008. Joining prepreg composite interfaces with aligned carbon nanotubes. Composites Part A: Applied Science and Manufacturing, 39 (6), 1065−1070. (c) Adapted from Bekyarova, E., Thostenson, E.T., Yu, A., Kim, H., Gao, J., Tang, J., Hahn, H.T., Chou, T.W., Itkis, M.E., Haddon, R.C., 2007. Multiscale carbon nanotube−carbon fiber reinforcement for advanced epoxy composites. Langmuir 23 (7), 3970−3974. (d) Adapted from Jiang, Z., Imam, A., Crane, R., Lozano, K., Khabashesku, V.N., Barrera, E.V., 2007. Processing a glass fiber reinforced vinyl ester composite with nanotube enhancement of interlaminar shear strength. Composites Science and Technology 67 (7−8), 1509−1517.

system using the CVD technique (Fig. 9.8(a)). In this approach, the fibre system (in the form of a fabric) is first impregnated with the catalyst and used as the substrate. The carbon source gas (hydrocarbons) breaks down due to very high temperature of the reactor ($\sim 1000°C$), and growth of nanotubes is observed on the fabric. The main problem of this process is the use of very high temperature which can degrade the polymeric fibres or even carbon fibres. This leads to the development of a slightly modified approach. In this modified approach, nanomaterials are first grown on a heat-resistant metallic cloth such as alumina. In the second step, the nanotubes are transferred onto a fibrous prepreg with tacky surface by the so-called transfer printing process (Enrique et al., 2008), as shown in Fig. 9.8(b). The prepreg is rolled onto a cylinder and pressed against the alumina cloth to transfer the grown CNTs onto the fibrous prepreg.

Another simple approach to incorporate nanomaterials on the fibre surface is to spray the nanomaterial solution on the fibres before composite fabrication (Jiang et al., 2007). Although this process leads to even coating of the fibre surface with nanomaterials, considerable nanomaterial agglomeration may occur while the nanomaterials come out from the spray nozzle under pressure. Similar to spraying, another simple approach developed for incorporating nanomaterials on the fibres is dip coating the fibre in the nanomaterial solution. This process has been utilized to develop natural (jute) fibre-based multiscale composites (Zhuang et al., 2011). As shown in Fig. 9.8(c), nanomaterials like CNTs can also be deposited on the fibre surface through the electrophoresis technique (Bekyarova et al., 2007). Negatively charged functionalized CNTs are attracted to the positive carbon fibre (fabric) electrode and deposited uniformly on the fibre surface.

All methods mentioned here can only deposit the nanomaterials on the fibre surface, but they cannot form strong bonding between them. Chemical grafting is the process by which nanomaterials can be strongly adhered to a fibre surface (He et al., 2007). However, chemical grafting usually involves a long reaction scheme in which the fibre surface is first activated to form reactive sites which can then be reacted with the functionalized nanomaterials. An example of chemical grafting of CNTs on a carbon fibre surface is illustrated in Fig. 9.9. Different methods of incorporating nanomaterials on the fibre surface lead to different morphologies of deposited nanomaterials, as shown in Fig. 9.10. Nanomaterials can be deposited on single fibres or fabric surfaces, and they may be oriented or randomly deposited. The orientation and morphology of deposited nanomaterials can strongly influence the interfacial properties as well as conducting networks within the multiscale composites.

9.5 Fabrication of multiscale composites

As discussed in this chapter, the two basic steps in fabricating multiscale composites are (1) the incorporation of nanomaterials either in the fibre or matrix and (2) the fabrication of composites using a nanomaterial-incorporated fibre or matrix system. The first step has been discussed in detail in previous sections. The second step (ie, the techniques for fabrication of composites) depends on the type of matrix. In the case of a thermosetting matrix, the most common approach of fabricating multiscale
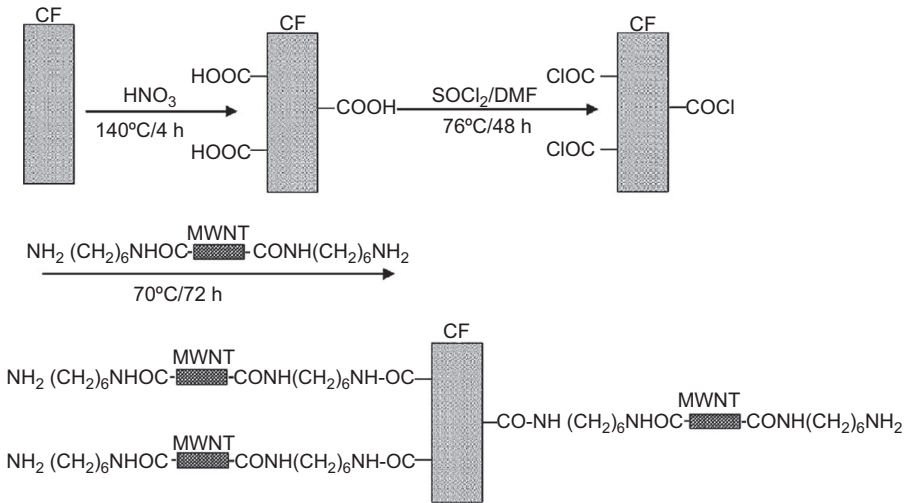
Figure 9.9 Chemical grafting of CNTs on a carbon fibre surface.
Adapted from He, X., Zhang, F., Wang, R., Liu, W., 2007. Preparation of a carbon nanotube/
carbon fiber multi-scale reinforcement by grafting multi-walled carbon nanotubes onto the
fibers. Carbon, 45 (13), 2559—2563.

composites is the vacuum-assisted resin transfer moulding (VARTM) technique (Kim et al., 2009), as shown in Fig. 9.11(a), due to its numerous advantages such as possibility to achieve high fibre volume fraction with low void content, ability to fabricate complex shapes, high production rate and less exposure of the workers to the harmful chemicals and gases. Once the nanomaterials are incorporated, the rest of the process is similar to the conventional composite fabrication process. One disadvantage of this process is the possibility of nanomaterial agglomeration within the intertow region of the fibre system (nanomaterial filtering) during resin flow under vacuum. To avoid this, the compression moulding process (Fig. 9.11(b)) can be used (Díez-Pascual et al., 2014). The process can also fabricate multiscale composites based on a thermoplastic matrix. For this purpose, thin films of nanomaterial-dispersed polymer can be prepared first using hot press or other techniques; and, subsequently, the films can be stacked together with the conventional fibre layers and consolidated under heat and pressure. Thermoplastic polymer-based multiscale composites can also be fabricated using other techniques commonly used to produce conventional fibre-reinforced thermoplastic composites (Díez-Pascual et al., 2014).

9.6 Mechanical performance of multiscale composites

Incorporation of nanomaterials within the matrix improves the mechanical properties of matrix materials. This is due to the reinforcing effect of nanomaterials possessing high mechanical properties. Nanomaterial addition can also change the morphology of the polymer matrix by changing the cross-linking density (thermosetting matrix)
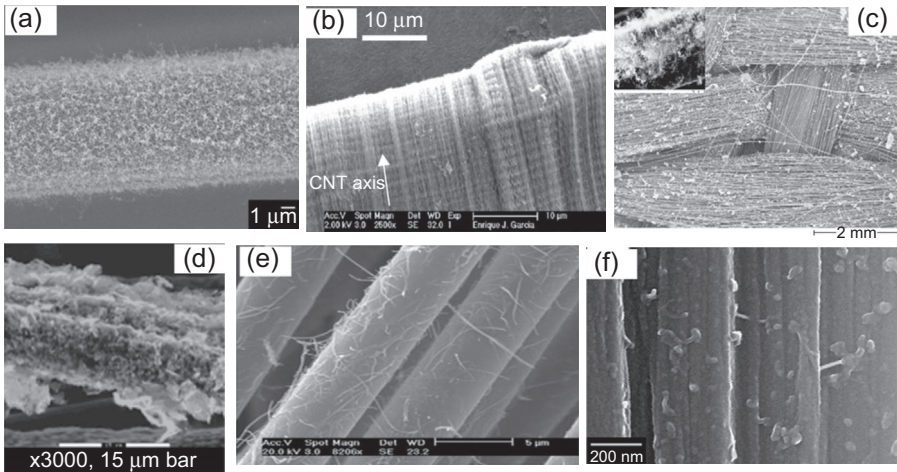
Figure 9.10 Morphology of deposited nanomaterials on a fibre surface: (a) grown CNTs on a single fibre; (b) transfer-printed CNT forests; (c) grown CNTs on a carbon fibre cloth; (d) grown nanographite on a carbon fibre surface; (e) electrophoretically deposited CNTs; and (f) chemically grafted CNTs.
(a) Adapted from Thostenson, E.T., Li, W.Z., Wang, D.Z., Ren, Z.F., Chou, T.W., 2002. Carbon nanotube/carbon fiber hybrid multiscale composites. Journal of Applied Physics 91 (9), 6034−6037. (b) Adapted from Enrique, G.J., Wardle, B.L., Hart, A.J., 2008. Joining prepreg composite interfaces with aligned carbon nanotubes. Composites Part A: Applied Science and Manufacturing 39 (6), 1065−1070. (c) Adapted from Mathur, R.B., Chatterjee, S., Singh, B.P., 2008. Growth of carbon nanotubes on carbon fibre substrates to produce hybrid/phenolic composites with improved mechanical properties. Composites Science and Technology 68 (7), 1608−1615. (d) Adapted from Park, J.K., Do, I.-H., Askeland, P., Drzal, L.T., 2008. Electrodeposition of exfoliated graphite nanoplatelets onto carbon fibers and properties of their epoxy composites. Composites Science and Technology 68 (7), 1734−1741. (e) Adapted from Bekyarova, E., Thostenson, E.T., Yu, A., Kim, H., Gao, J., Tang, J., Hahn, H.T., Chou, T.W., Itkis, M.E., Haddon, R.C., 2007. Multiscale carbon nanotube−carbon fiber reinforcement for advanced epoxy composites. Langmuir 23 (7), 3970−3974. (f) Adapted from He, X., Zhang, F., Wang, R., Liu, W., 2007. Preparation of a carbon nanotube/carbon fiber multi-scale reinforcement by grafting multi-walled carbon nanotubes onto the fibers. Carbon 45 (13), 2559−2563.

or crystallinity (thermoplastic matrix), resulting in enhancement of mechanical properties of the polymer. Nanomaterials are excellent reinforcing materials due to their small size, which provides very high surface area and strong interface with the matrix as well as reduced size of the defects. Fig. 9.12 shows how the surface−volume ratio of reinforcing materials increases with decrease in their diameter and how CNTs (particularly single-walled CNTs (SWCNTs)) possess the highest surface area due to their extremely small size (Fiedler et al., 2006). Therefore, due to their high surface area and aspect ratio as well as extraordinary mechanical properties, CNTs are considered to be the best reinforcing material for composites, and they have been extensively utilized for multiscale composites.

The reinforcement effect of nanomaterials in various matrices has been predicted using micromechanical equations (Kim et al., 2009). As for reinforcement purposes,
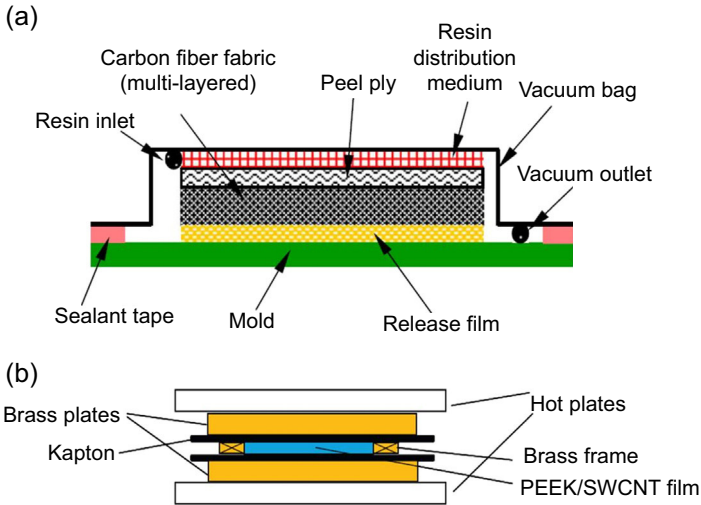
Figure 9.11 (a) Fabrication of multiscale composites using VARTM (Kim et al., 2009) and (b) compression moulding (Díez-Pascual et al., 2014).
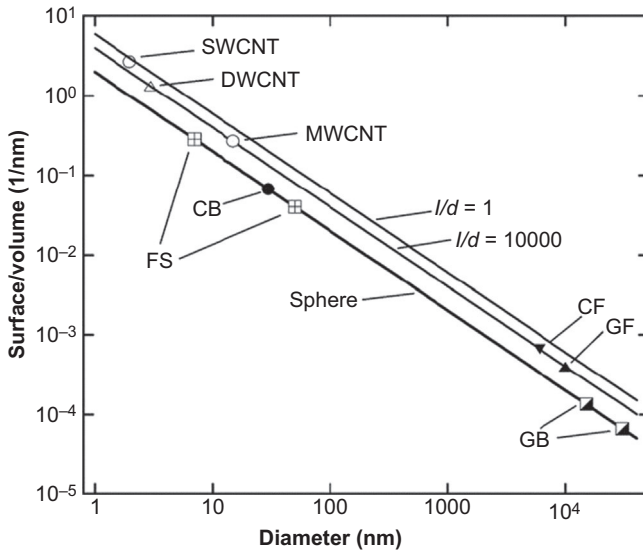
Figure 9.12 Surface−volume ratio of different nanomaterials.
Adapted from Fiedler, B., Gojny, F.H., Wichmann, M.H.G., Nolte, M.C.M., Schulte, K., 2006. Fundamental aspects of nano-reinforced composites. Composites Science and Technology 66 (16), 3115−3125.

CNTs have been extensively used, the Halpin−Tsai equation has been used to predict the tensile modulus of CNT nanocomposites as provided here:

$$E_{NC} = \left[\frac{3}{8} \frac{1 + 2\left(\frac{l_{NT}}{d_{NT}}\right)\eta_L V_{NT}}{1 - \eta_L V_{NT}} \frac{5}{8} \frac{1 + 2\eta_D V_{NT}}{1 - \eta_D V_{NT}} \right] E_{epoxy} \qquad [9.1]$$

$$\eta_L = \left(\frac{\left(\frac{E_{NT}}{E_{epoxy}} \right) - \left(\frac{d_{NT}}{4t} \right)}{\left(\frac{E_{NT}}{E_{epoxy}} \right) + \left(\frac{l_{NT}}{2t} \right)} \right) \tag{9.2}$$

$$\eta_D = \left(\frac{\left(\frac{E_{NT}}{E_{epoxy}} \right) - \left(\frac{d_{NT}}{4t} \right)}{\left(\frac{E_{NT}}{E_{epoxy}} \right) + \left(\frac{d_{NT}}{2t} \right)} \right) \tag{9.3}$$

where E, l_{NT}, d_{NT}, V_{NT} and t represent the tensile modulus, length and outer diameter of the nanotubes, nanotube volume fraction, and thickness of the graphite layer (0.34 nm), respectively.

Assuming isotropy, the shear modulus of CNT composites can be calculated from the tensile modulus using the following equation:

$$G_{NC} = \frac{E_{NC}}{2(1 + \nu)} \tag{9.4}$$

where G_{NC} is the shear modulus of the CNT composite and ν is Poisson's ratio. The mechanical properties of multiscale composites can be predicted using the micromechanics of fibre-reinforced composites. The concept of modelling multiscale composites is shown in Fig. 9.13. The mechanical properties of a nanomaterial-reinforced matrix can be first calculated using Eqs [9.1]–[9.3], and the mechanical properties of the multiscale composite can be further modelled using mechanical properties of fibre and nanoreinforced matrix systems according to the structure of the composites (woven or knitted, directionally oriented).
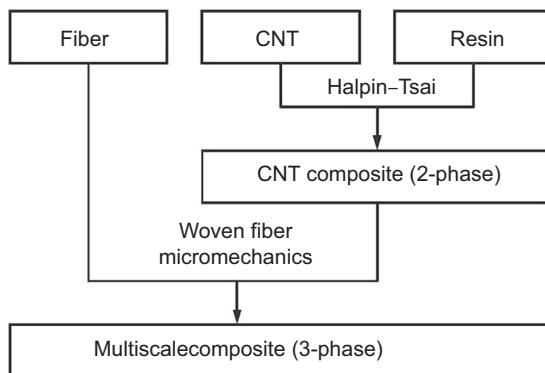
Figure 9.13 Modelling concept of multiscale composites.
Adapted from Kim, M., Park, Y.B., Okoli, O.I., Zhang, C., 2009. Processing, characterization, and modeling of carbon nanotube-reinforced multiscale composites. Composites Science and Technology 69 (3), 335–342.

9.6.1 Why does nanomaterial addition lead to better mechanical properties of conventional composites?

It is very well known that nanofillers are used in multiscale composites at low concentrations, in order to avoid agglomeration and long dispersion treatment. At this low concentration, the contribution of nanoparticles to the overall strength and stiffness of multiscale composites should be low. However, the comparison between the predicted (based on micromechanical equations) and actual elastic modulus of CNF-based carbon−epoxy multiscale composites revealed that the actual elastic modulus is much higher as compared to the predicted values (Rana et al., 2011b). This implies that incorporation of nanoreinforcements in multiscale composites has other influences besides the direct reinforcing effect. It has been observed that the fibre−matrix interface in multiscale composites is much stronger as compared to the original composite materials, as shown in Fig. 9.14. This is attributed to the increase in residual stress or interface pressure of the thermosetting matrix on the fibre surface due to nanomaterial incorporation. The change in interfacial pressure of the matrix with nanomaterial addition can be calculated using the following equation (Hussain et al., 1996):

Residual stress or interface pressure

$$P = \frac{(\alpha_m - \alpha_f)\nabla T E_m}{(1 + \nu_m) + (1 - \nu_f)E_m/E_f} \qquad [9.5]$$

where P is the residual stresses or interface pressure, α_m is the coefficient of thermal expansion of the matrix, α_f is the coefficient of thermal expansion of the fibre, ∇T is the temperature difference between T_g and room temperature, ν_m is Poisson's ratio of the matrix, ν_f is Poisson's ratio of the fibre, E_m is the elastic modulus of the matrix and E_f is the elastic modulus of the carbon fibre. Interface pressure calculated using this equation showed a significant increase in the case of multiscale composites leading to much stronger interface. The improvement in mechanical properties in case of multiscale composites is listed in Table 9.3.
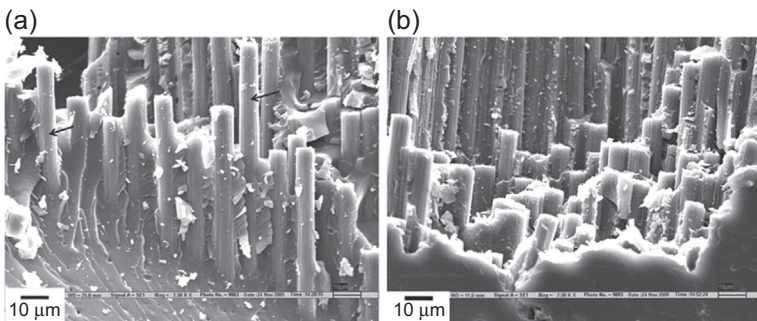
Figure 9.14 Fibre−matrix interface in (a) conventional and (b) multiscale composites.
Adapted from Rana, S., Alagirusamy, R., Joshi, M., 2011b. Development of carbon nanofibre incorporated three phase carbon/epoxy composites with enhanced mechanical, electrical and thermal properties. Composites Part A: Applied Science and Manufacturing 42 (5), 439−445.

Table 9.3 Improvement of mechanical performance of composites due to nanomaterial incorporation

Type of CNT and concentration	Fibre—matrix	Property improvement
Amino functionalized DWCNT, 0.1 and 0.3 wt%, dispersed in resin (Gojny et al., 2005)	Glass fabric—epoxy	No significant change in Young's modulus and tensile strength. Improvement of 20% in interlaminar shear strength.
MWCNT, thin-MWCNT, amine-functionalized DWCNT 0.5 wt%, dispersed in resin (Godara et al., 2009)	Carbon fibre—epoxy	No major improvement in modulus and strength. Fracture toughness improved by 80% for MWCNTs and modifying epoxy by compatibilizer.
MWCNT functionalized and nonfunctionalized 1 wt%, dispersed in resin (Qiu et al., 2007)	Glass fibre—epoxy	Improvement of 14% in tensile strength, 20% in Young's modulus and 5% in shear strength.
Silane-functionalized MWCNTs, 1 wt%, dispersed in resin (Kim et al., 2012)	Basalt—epoxy	Flexural modulus and strength increased by approximately 54% and 34%, respectively.
Silane and acid-functionalized MWCNTs, 1 wt% (Kim et al., 2012)	Basalt—epoxy	Flexural modulus, strength and fracture toughness of silane-treated CNT-based composites were, respectively, 10%, 14% and 40% greater than those of acid-treated CNT-based composites.
DWCNT-NH$_2$, 0.025—0.1 wt%, dispersed in resin (Fawad et al., 2010)	Carbon fibre—epoxy	Enhancement in flexural modulus by up to 35%, 5% improvement in flexural strength, 6% improvement in absorbed impact energy and 23% decrease in the mode I interlaminar toughness.
Amine-functionalized MWCNTs, 1 wt%, dispersed in resin (Sharma and Shukla, 2014)	Carbon fibre—epoxy	Increase in Young's modulus, interlaminar shear strength and flexural modulus by 51.46%, 39.62% and 38.04%, respectively.
SWCNT, 0.1 wt%, sprayed onto fibres in midplane ply (Jiang et al., 2007)	Glass—vinyl ester	Up to 45% increase in shear strength over control samples.
Vertically aligned CNT on prepreg surface for ply stitching, 1 vol%, transfer printing method (Enrique et al., 2008)	Carbon fibre—epoxy	Increase in fracture toughness by 1.5—2.5 times in Mode I, and 3 times in Mode II.

MWCNT, 1−2 vol% in composite, grown on fibre surface (Wicks et al., 2010)	Alumina fibre−epoxy	Improvement of steady-state toughness by 76%, in-plane tension-bearing stiffness by 19%, critical strength by 9% and ultimate strength by 5%.
CNT, 1−3 vol% in composite, grown on fibre surface (Garcia et al., 2008)	Alumina fibre−epoxy	Enhancement of 69% in interlaminar shear strength.
MWCNTs, 0.25 wt% on fibre surface, electrophoretic deposition (Bekyarova et al., 2007)	Carbon fibre−epoxy	Enhancement of interlaminar shear strength by 27%.
VCNFs, 0.5% (Rana et al., 2011b)	Carbon fibre−epoxy	Young's modulus, tensile strength, compressive modulus and compressive strength improved by 37%, 18%, 50% and 18%, respectively.
SWCNTs, 0.1% (Rana et al., 2011a)	Carbon fibre−epoxy	Young's modulus, tensile strength, compressive modulus and compressive strength improved by 95%, 31%, 76% and 41%, respectively.
PEES-wrapped laser SWCNTs, 1.0% (Ashrafi et al., 2012)	Glass fibre−PEEK	Young's modulus, tensile strength, impact strength, flexural modulus, flexural strength and interlaminar shear strength increased by 16%, 7.6%, 10%, 32.6%, 17.9% and 64.4%, respectively.
MWCNTs, 0.5% (Meszaros et al., 2011)	Basalt fibre−PA-6	Young's modulus, tensile strength, flexural modulus and flexural strength increased by 12.2%, 9%, 35.4% and 41%, respectively.
MWCNTs (Rahmanian et al., 2013)	Carbon fibre−PP	Young's modulus, tensile strength, impact strength, flexural modulus and flexural strength improved by 57%, 37.3%, 34%, 51% and 35%, respectively.
MWCNTs, 15% (Zhang, 2011)	Carbon fibre−PI	Young's modulus, tensile strength, impact strength, flexural modulus and flexural strength improved by 33.5%,125%, 75%, 36% and 29.6%, respectively.
Short MWCNTs (Qian et al., 2010)	Silica−PMMA	Interfacial shear strength improved by 150%.

DWCNT, double-walled carbon nanotube; *MWCNT*, multiwalled carbon nanotube; *PEES*, polyetherethersulfone; *PMMA*, poly(methyl methacrylate); *SWCNT*, single-walled carbon nanotube; *VCNF*, vapour-grown carbon nanofiber.

9.6.2   Improvement of matrix-dominated properties

As discussed in the previous section, incorporation of nanofillers can greatly enhance the fibre−matrix interface of fibre-reinforced composites. A direct consequence of this fact is the improvement of interlaminar shear strength of composites. An example of improving interlaminar shear strength using different types of CNT is presented in Fig. 9.15. In the case of laminated composites, the separation of plies under loading condition is one of the main failure modes. Damage of aerospace structures made with composites due to delamination already has been reported. Most of the existing methods to avoid delamination of composite layers, such as ply stitching 3D fabrics with through-thickness reinforcement, leads to reduction of in-plane mechanical properties and also increases the production cost. Therefore, multiscale composites can be a novel approach to eliminate delamination of composites without deteriorating the mechanical properties or increasing cost.

Furthermore, multiscale composites can be designed in a special way to achieve remarkable enhancement of interlaminar shear strength. One approach is to grow the nanomaterials (usually nanotubes) vertically on the ply surface so that the nanotubes can cross the interlaminar region and stitch the adjacent plies (Enrique et al., 2008). To avoid damage to fibres during nanotube growth in a CVD reactor, nanotubes can be grown first on a more thermally stable material (eg, an alumina cloth) and subsequently transferred onto the fibrous lamina through a transfer printing method.

Improvement of fracture toughness is another major advantage of multiscale composites. Dispersion of nanoscale reinforcements has been used widely to improve the fracture toughness and ductility of brittle matrices. This approach is becoming popular as the conventional methods of toughening brittle matrices (eg, using rubber particles, thermoplastics etc.) deteriorate the mechanical properties significantly.
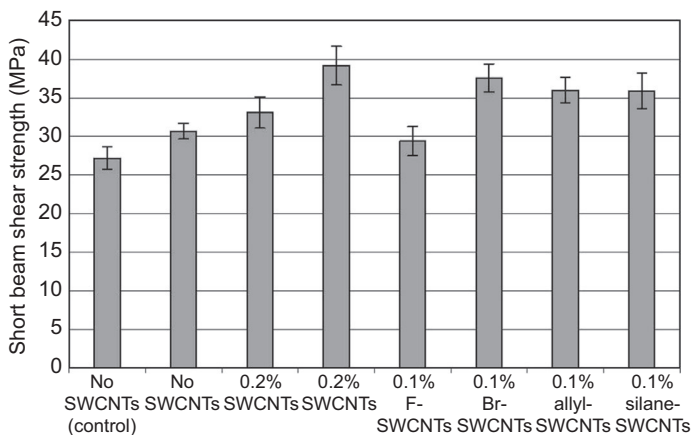
Figure 9.15 Improvement of shear strength in multiscale composites.
Adapted from Jiang, Z., Imam, A., Crane, R., Lozano, K., Khabashesku, V.N., Barrera, E.V., 2007. Processing a glass fiber reinforced vinyl ester composite with nanotube enhancement of interlaminar shear strength. Composites Science and Technology 67 (7−8), 1509−1517.
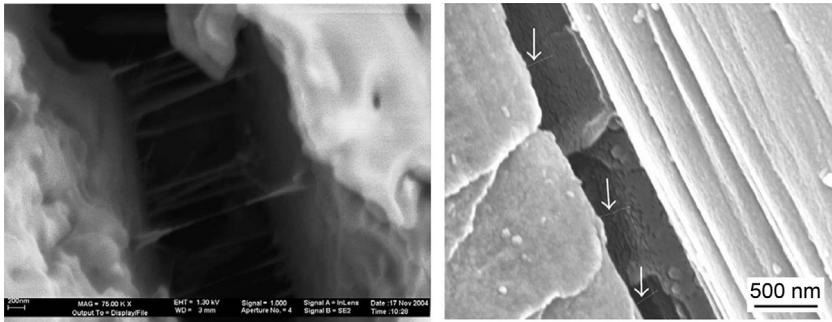
Figure 9.16 Crack-bridging effect of CNTs in multiscale composites.
Adapted from Fiedler, B., Gojny, F.H., Wichmann, M.H.G., Nolte, M.C.M. Schulte, K., 2006.
Fundamental aspects of nano-reinforced composites. Composites Science and Technology 66
(16), 3115−3125 and Fawad, I., Wong, D.W.Y., Kuwata, M., Peijs, T., 2010. Multiscale hybrid
micro-nanocomposites based on carbon nanotubes and carbon fibers. Journal of Nanomaterials
2010, 12.

Nanoscale fillers, on the other hand, improve the toughness of composites without
deteriorating the mechanical performance due to a number of toughening mecha-
nisms such as crack pinning, crack tip deflection, crack bridging and so on (Fiedler
et al., 2006). Fig. 9.16 presents the toughening mechanism of CNTs through crack
bridging. Consequently, multiscale composites with dispersed nanofillers within
the matrix possess significantly higher fracture toughness as compared to the conven-
tional composites. Improvement of fracture toughness in multiscale composites can
be noted in Table 9.3.

9.6.3 Conductivity of multiscale composites

Conductive nanofillers such as CNTs, CNFs and so on are used in various matrices
to fabricate conducting nanocomposites. It has been widely demonstrated that these
nanofillers can form conducting (electrical or thermal) paths within the matrix. Nano-
fillers like CNTs with high electrical conductivity can form a percolating network in
nonconducting matrices at very low filler concentration. Similarly, thermal conduc-
tivity can also be enhanced many times over through incorporation of nanofillers
with high thermal conductivity. Therefore, in the case of multiscale composites
with nonconducting fibre and matrix, the enhancement of conductivity is mainly
due to the improvement of conductivity of the matrix. However, in the case of multi-
scale composites containing conducting fibres such as carbon, the formation of a
three-dimensional (3D) conducting network (Fig. 9.17) is possible, as the conducting
fillers can connect the fibres, forming a well-connected conducting composite (Kim
et al., 2007). Consequently, a many-fold increase in electrical and thermal conductiv-
ity was observed in the case of multiscale composites. The improvement of conduc-
tivities of multiscale composites containing different types of fibre and matrix can be
observed in Table 9.4.

(a)   (b)
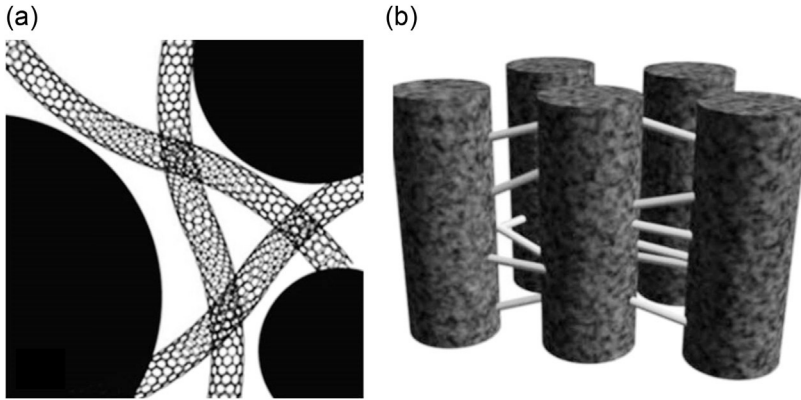
Figure 9.17 Conducting network formed by carbon fibres and CNTs.
Adapted from Zimmer, M., Cheng, Q., Li, S., Brooks, J., Liang, R., Wang, B., Zhang, C., 2012.
Comparative characterization of multiscale carbon fiber composite with long and short
MWCNTs at higher weight fractions. Journal of Nanomaterials 2012, 6 and Kim, Y.A., Kamio,
S., Tajiri, T., Hayashi, T., Song, S.M., Endo, M., Terrones, M., Dresselhaus, M.S., 2007.
Enhanced thermal conductivity of carbon fiber/phenolic resin composites by the introduction of
carbon nanotubes. Applied Physics Letters 90 (9), 093125.

Similar to mechanical properties, both thermal and electrical conductivity of multi-scale composites depend on several processing parameters. Dispersion is again one of the most important parameters influencing bulk conductivity of multiscale composites. The formation of a 3D conducting network is facilitated when nanofillers are well dispersed in the matrix. However, even deposition of CNTs on the fibre surface showed significant enhancement of electrical conductivity, as the nanotubes are trans-ferred to the matrix-rich regions near the fibre surface during composite processing and assist in forming the conducting network. Control of the alignment of nanofillers within multiscale composites is another important parameter to design multiscale com-posites with desired in-plane or out-of-plane conductivities.

9.7   Electromagnetic shielding

Multiscale composites based on CNTs have been reported to be excellent materials for electromagnetic shielding applications. Shielding of 90% electromagnetic en-ergy in the microwave range was possible using multiscale composites developed by dispersing MWCNTs in glass−epoxy composites. An increase in the shielding effectiveness was observed by increasing the thickness of the composite as well as with higher nanotube content. The enhanced electromagnetic interference (EMI) shielding efficiency of multiscale composites is attributed to the improvement of conductivity with the addition of CNTs. Conductive composites lead to shielding of electromagnetic waves, mainly due to two mechanisms: (1) reflection of electro-magnetic waves from the object charges which are forced to oscillate at the same

Table 9.4 Thermal and electrical conductivity of multiscale composites

Type of CNT and concentration	Fibre–matrix systems	Conductivity improvement
Crystalline MWCNTs, 7% (Kim et al., 2007)	Carbon fibre–phenolic resin	Thermal conductivity improved from 250 to 393 W/m K.
Aligned CNTs, 1–3% (Enrique et al., 2008)	Alumina fibre–epoxy	In-plane resistivity of $\sim 10^7$–10^8 Ohm mm and through-thickness resistivity of $\sim 10^9$ Ohm mm decreased to 10^1–10^2 Ohm mm.
SWCNTs and MWCNTs, 0.25% (Bekyarova et al., 2007)	Carbon fibre–epoxy	Out-of-plane electrical conductivity increased by 2 times for SWCNTs and 30% for MWCNTs.
SWCNTs, 0.1% (Rana et al., 2011a)	Carbon fibre–epoxy	Electrical and thermal conductivity increased from 0.034 S/m and 0.193 W/m K to 0.202 S/m and 0.343 W/m K, respectively.
VCNFs, 0.5% (Rana et al., 2011b)	Carbon fibre–epoxy	Electrical and thermal conductivity increased from 0.034 S/m and 0.193 W/m K to 0.68 S/m and 0.205 W/m K, respectively.
PEES-wrapped laser SWCNTs, 1.0% (Díez-Pascual et al., 2011)	Glass fibre–PEEK	Thermal conductivity increased by 93%.
MWCNTs, 1% (Shen et al., 2009)	Glass fibre–PA-6	Thermal conductivity increased by 90%.

MWCNT, multiwalled carbon nanotube; *PEEK*, polyether ether ketone; *PEES*, poly(1–4-phenylene ether-ether sulfone); *SWCNT*, single-walled carbon nanotube; *VCNF*, vapour-grown carbon nanofiber.

frequency as the incident wave and (b) absorption due to loss of electromagnetic energy in the form of heat owing to the oscillating charges. Absorption occurs in the volume of conducing composites, whereas refection mainly occurs from the surface of the conducting materials. However, internal reflections from the inner layers of the conducting materials are also possible. Therefore, due to the possibility of achieving high electrical conductivity at low nanomaterial content, multiscale composites present a high potential of developing EMI shielding materials for aerospace applications. Fig. 9.18 shows the shielding effectiveness of MWCNT-added glass–epoxy composites (Park et al., 2007).
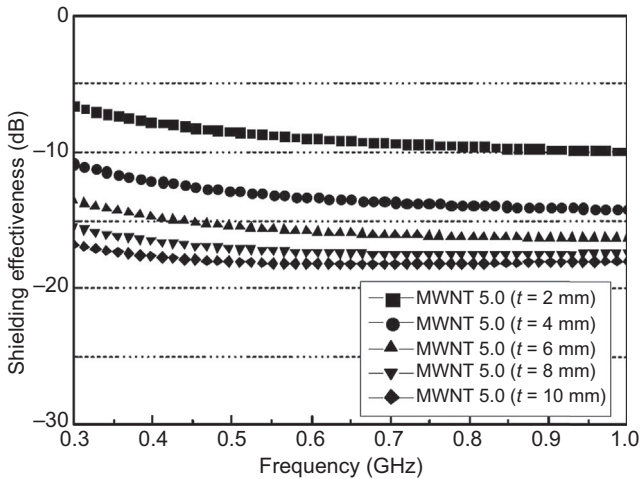
Figure 9.18 Electromagnetic shielding effectiveness of MWCNT-based multiscale composites. Adapted from Park, K.Y., Lee, S.E., Kim, C.G., Han, J.H., 2007. Application of MWNT-added glass fabric/epoxy composites to electromagnetic wave shielding enclosures. Composite Structures, 81 (3), 401−406.

9.8 Strain and damage sensing with multiscale composites

Automatic sensing of damage is very important for aerospace structures considering the safety aspect. Due to the complex structure of composite materials, it is not possible to ensure completely defect-free composites, even after stringent quality checking. Small cracks and damage, if not detected earlier, will grow with time and under loading, and they can lead to catastrophic failure and accidents. The best solution to this problem should be to detect the damage when it is in the nanoscale (or microscale) and to restrict its further growth. Different sensors (such as fibre-optic, piezoelectrics etc.) have been developed to detect strain and damage in composite materials. Alternatively, self-sensing composites have been developed to detect damage in composites without the use of external sensors (Rosado et al., 2013; Rana et al., 2014). Different self-healing approaches also have been developed to restrict the further growth of damage. In spite of these developments, most of the self-sensing composites developed until today are not able to detect nanoscale damages.

Multiscale composites can offer a huge opportunity to detect nanoscale damages as well as to effectively restrict the growth of nanolevel cracks. Nanofillers like CNTs can form well-connected electrically conducting networks. Therefore, when this network is subjected to external loading or when any damage is created, there will be a change in the CNT network at the nanoscale. As a result, the composite will show a change in electrical resistivity, which can be processed to detect the strain or analyse the location or magnitude of the damage. The microscale damage detection capability of multiscale
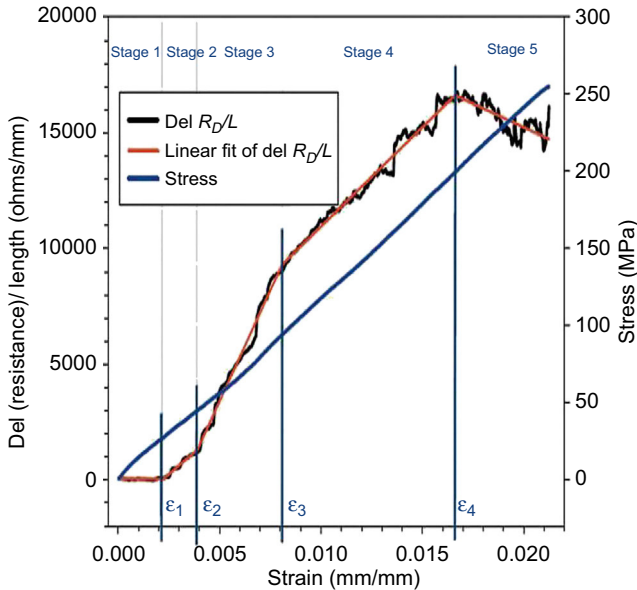
Figure 9.19 Change of resistance with tensile strain in a 3D braided multiscale composite. Adapted from Kim, K.J., Yu, W.R., Lee, J.S., Gao, L., Thostenson, E.T., Chou, T.W., Byun, J.Y., 2010. Damage characterization of 3D braided composites using carbon nanotube-based in situ sensing. Composites Part A: Applied Science and Manufacturing 41 (10), 1531−1537.

composites is illustrated in Fig. 9.19. Furthermore, as discussed in this chapter, multi-scale composites with CNTs can restrict the growth of cracks through crack-bridging mechanisms. Therefore, if CNTs are well dispersed within the matrix and a strong CNT−matrix interface is ensured (to avoid CNT pull-outs), CNTs can impose a strong hindrance on the opening and growth of cracks.

9.9 Dimensional stability of multiscale composites

Dimensional stability is another important requirement for composite materials for application in aerospace engineering. Expansion or contraction of composite layers due to temperature changes leads to the formation of cracks in the composite structure. An ideal composite for this application will be one with zero coefficient of thermal expansion (CTE). Some nanomaterials provide opportunity to fabricate composites with negligible thermal expansion or contraction due to their negative CTE, which balances the positive CTE of matrix materials. Fig. 9.20 shows the reduction of CTE in the case of multiscale composites.

Enhanced dynamic mechanical stability is another advantageous feature of multiscale composites. Under dynamic loading conditions and over a wide temperature range, multiscale composites possess higher mechanical stability as compared to the conventional
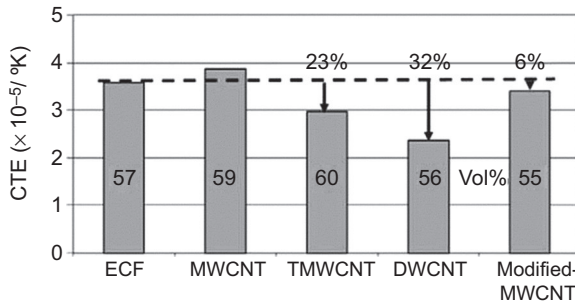
Figure 9.20 Reduction of CTE due to different types of CNTs.
Adapted from Godara, A., Mezzo, L., Luizi, F., Warrier, A., Lomov, S.V., Van Vuure, A.W., Gorbatikh, L., Moldenaers, P., Verpoest, I., 2009. Influence of carbon nanotube reinforcement on the processing and the mechanical behaviour of carbon fiber/epoxy composites. Carbon 47 (12), 2914−2923.

composites. Multiscale composites exhibit a higher storage modulus due to better interaction of nanomaterials with the polymer matrix molecules with similar dimensions. Due to this fact, improvement in glass transition temperature (T_g) also has been reported. Moreover, multiscale composites possess higher loss modulus, improving the damping characteristics of the composites.

9.10 Applications of multiscale composites in aerospace engineering

Multiscale composites can address virtually all the demands placed on aerospace materials (ie, light weight, high specific strength and stiffness, toughness, low thermal expansion coefficient and dimensional stability, electrical and thermal conductivity etc.). Any targeted sets of properties can be achieved through proper control of the structure and parameters of the multiscale composites.

As mentioned earlier, one of the major problems with composite materials is their complex structure. Any defect or flaw generated during composite manufacturing is really difficult to detect through the available testing methods. Although aircraft structures are checked thoroughly during the routine inspection through various nondestructive testing procedures, it is quite possible that some undetected flaws within the composite parts are passed, leading to subsequent growth of the flaws and failure of the structure. American Airlines Flight 587 and Airbus A300's 27 encountered this in the past. In this context, multiscale composites based on CNTs can present some distinct advantages. The growth of microflaws in multiscale composites can be restricted or be very slow due to the crack-bridging effect of CNTs, avoiding catastrophic failure and sudden accidents. In addition to that, CNTs can also detect these microflaws in advance, so timely maintenance can be undertaken. If the healing agents are also incorporated within the multiscale composites, self-repairing of the generated cracks can also be

achieved. So, multiscale composites with all these smart functionalities can develop extremely safe systems, which is highly essential for aerospace structures.

Although multiscale composites have been studied widely and the research efforts on this topic are steadily increasing, commercial application of this technology is very rare. Some reported practical applications are strong and lightweight wind turbine blades and hulls for maritime security boats made of carbon fibre composites with CNT-dispersed resin (De Volder et al., 2013). In the aerospace industry, the use of this technology has not been reported till now. Some major problems of practical implementation of these novel materials are the processing problems and associated high processing cost. The high cost of some nanomaterials like SWCNTs is also a crucial factor. Toxicity of the nanomaterials and associated special infrastructure required to handle them are the other factors restricting their full utilization. The last, but not the least, problem is the lack of proper modelling and simulation techniques to predict the behaviour of multiscale composites. Prediction methods of various properties of multiscale composites are extremely necessary to design composite structures with targeted sets of properties. Therefore, future efforts should be directed to solve the above problems related to the commercialization and practical application of multiscale composites.

9.11   Summary and conclusions

Multiscale composites are one of the most advanced types of composites, exhibiting excellent and multifunctional properties. Multiscale composites are fabricated by incorporating nanomaterials within the fibre system or matrix system (and, less frequently, between the plies of composites). Direct growth of nanomaterials, transfer printing, spraying, coating, sizing, electrophoretic deposition and so on are the different approaches of incorporating nanomaterials on the fibre system. On the other hand, nanomaterials can be incorporated within the matrix by dispersing them using various mechanical techniques such as ultrasonication, high-speed stirring, calendaring, ball milling and so on. Dispersion of nanomaterials within a matrix can be further assisted using chemical dispersants such as surfactants or nanomaterial functionalization. Multiscale composites can overcome the ever-existing problems of conventional fibre-reinforced composites such as delamination and poor z-directional mechanical properties. Additionally, they have enhanced in-plane mechanical performance, fracture toughness, impact properties, dynamic mechanical properties and thermal stability. High electrical and thermal conductivity, electromagnetic shielding, gas barrier properties, self-sensing behaviours and so on are other advantageous features of multiscale composites over conventional FRPs. However, multiscale composites are still in the research stage, and their commercial application has been rarely reported. Cost of nanomaterials, difficulties in dispersion and processing and lack of simulation and modelling techniques are some of the challenges which have to be overcome for the commercialization of these outstanding materials in various industrial sectors. Nevertheless, looking at their performance and functionalities, it is very clear that multiscale composites will be the materials of choice for future aerospace industries.

References

Ashrafi, B., Díez-Pascual, A.M., Johnson, L., Genest, M., Hind, S., Martinez-Rubi, Y., et al., 2012. Processing and properties of PEEK/glass fiber laminates: effect of addition of single-walled carbon nanotubes. Composites Part A: Applied Science and Manufacturing 43, 1267−1279.

Bekyarova, E., Thostenson, E.T., Yu, A., Kim, H., Gao, J., Tang, J., Hahn, H.T., Chou, T.W., Itkis, M.E., Haddon, R.C., 2007. Multiscale carbon nanotube−carbon fiber reinforcement for advanced epoxy composites. Langmuir 23 (7), 3970−3974.

Bhattacharyya, A., Rana, S., Parveen, S., Fangueiro, R., Alagirusamy, R., Joshi, M., 2013. Mechanical and thermal transmission properties of carbon nanofibre dispersed carbon/phenolic multi-scale composites. Journal of Applied Polymer Science 129, 2383−2392.

Chisholm, N., Mahfuz, H., Rangari, V.K., Ashfaq, A., Jeelani, S., 2005. Fabrication and mechanical characterization of carbon/SiC-epoxy nanocomposites. Composite Structures 67 (1), 115−124.

Cho, J., Chen, J.Y., Daniel, I.M., 2007. Mechanical enhancement of carbon fiber/epoxy composites by graphite nanoplatelet reinforcement. Scripta Materialia 56 (8), 685−688.

Chowdhury, F.H., Hosur, M.V., Jeelani, S., 2006. Studies on the flexural and thermomechanical properties of woven carbon/nanoclay-epoxy laminates. Materials Science and Engineering: A 421 (1-2), 298−306.

De Volder, M.F.L., et al., 2013. Carbon nanotubes: present and future commercial applications. Science 339 (6119), 535−539.

Díez-Pascual, A.M., Ashrafi, B., Naffakh, M., González-Domínguez, J.M., Johnston, A., Simard, B., et al., 2011. Influence of carbon nanotubes on the thermal, electrical and mechanical properties of poly(ether ether ketone)/glass fiber laminates. Carbon 49, 2817−2833.

Díez-Pascual, A.M., Naffakh, M., Marco, C., Gómez-Fatou, M.A., Ellis, G.J., 2014. Multiscale fiber-reinforced thermoplastic composites incorporating carbon nanotubes: a review. Current Opinion in Solid State and Materials Science 18 (2), 62−80.

Enrique, G.J., Wardle, B.L., Hart, A.J., 2008. Joining prepreg composite interfaces with aligned carbon nanotubes. Composites Part A: Applied Science and Manufacturing 39 (6), 1065−1070.

Fawad, I., Wong, D.W.Y., Kuwata, M., Peijs, T., 2010. Multiscale hybrid micro-nanocomposites based on carbon nanotubes and carbon fibers. Journal of Nanomaterials 2010, 12.

Fiedler, B., Gojny, F.H., Wichmann, M.H.G., Nolte, M.C.M., Schulte, K., 2006. Fundamental aspects of nano-reinforced composites. Composites Science and Technology 66 (16), 3115−3125.

Garcia, E.J., Wardle, B.L., Hart, A.J., Yamamoto, N., 2008. Fabrication and multifunctional properties of a hybrid laminate with aligned carbon nanotubes grown in situ. Composites Science and Technology 68 (9), 2034−2041.

Godara, A., Mezzo, L., Luizi, F., Warrier, A., Lomov, S.V., Van Vuure, A.W., Gorbatikh, L., Moldenaers, P., Verpoest, I., 2009. Influence of carbon nanotube reinforcement on the processing and the mechanical behaviour of carbon fiber/epoxy composites. Carbon 47 (12), 2914−2923.

Gojny, F.H., Wichmann, M.H.G., Fiedler, B., Bauhofer, W., Schulte, K., 2005. Influence of nano-modification on the mechanical and electrical properties of conventional fibre-reinforced composites. Composite Part A 36 (11), 1525−1535.

He, X., Zhang, F., Wang, R., Liu, W., 2007. Preparation of a carbon nanotube/carbon fiber multi-scale reinforcement by grafting multi-walled carbon nanotubes onto the fibers. Carbon 45 (13), 2559−2563.

Ho, M.-W., Lam, C.-K., Lau, K.-T., Ng, D.H.L., Hui, D., 2006. Mechanical properties of epoxy-based composites using nanoclays. Composite Structures 75 (1), 415−421.

Hussain, M., Nakahira, A., Niihara, K., 1996. Mechanical property improvement of carbon fiber reinforced epoxy composites by Al_2O_3 filler dispersion. Materials Letters 26 (3), 185−191.

Jiang, Z., Imam, A., Crane, R., Lozano, K., Khabashesku, V.N., Barrera, E.V., 2007. Processing a glass fiber reinforced vinyl ester composite with nanotube enhancement of interlaminar shear strength. Composites Science and Technology 67 (7−8), 1509−1517.

Khan, S., Kim, J.K., 2011. Impact and delamination failure of multiscale carbon nanotube-fiber reinforced polymer composites: a review. International Journal of Space Science 12 (2), 115−133.

Kim, K.J., Yu, W.R., Lee, J.S., Gao, L., Thostenson, E.T., Chou, T.W., Byun, J.Y., 2010. Damage characterization of 3D braided composites using carbon nanotube-based in situ sensing. Composites Part A: Applied Science and Manufacturing 41 (10), 1531−1537.

Kim, M.T., Rhee, K.Y., Park, S.J., Hui, D., 2012. Effects of silane-modified carbon nanotubes on flexural and fracture behaviors of carbon nanotube-modified epoxy/basalt composites. Composites Part B: Engineering 43 (5), 2298−2302.

Kim, M., Park, Y.B., Okoli, O.I., Zhang, C., 2009. Processing, characterization, and modeling of carbon nanotube-reinforced multiscale composites. Composites Science and Technology 69 (3), 335−342.

Kim, Y.A., Kamio, S., Tajiri, T., Hayashi, T., Song, S.M., Endo, M., Terrones, M., Dresselhaus, M.S., 2007. Enhanced thermal conductivity of carbon fiber/phenolic resin composites by the introduction of carbon nanotubes. Applied Physics Letters 90 (9), 093125.

Mathur, R.B., Chatterjee, S., Singh, B.P., 2008. Growth of carbon nanotubes on carbon fibre substrates to produce hybrid/phenolic composites with improved mechanical properties. Composites Science and Technology 68 (7), 1608−1615.

Meszaros, L., Gali, I.M., Czigany, T., Czvikovszky, T., 2011. Effect of nanotube content on mechanical properties of basalt fibre reinforced polyamide 6. Plastics, Rubber and Composites 40, 289−293.

Park, J.K., Do, I.-H., Askeland, P., Drzal, L.T., 2008. Electrodeposition of exfoliated graphite nanoplatelets onto carbon fibers and properties of their epoxy composites. Composites Science and Technology 68 (7), 1734−1741.

Park, K.Y., Lee, S.E., Kim, C.G., Han, J.H., 2007. Application of MWNT-added glass fabric/epoxy composites to electromagnetic wave shielding enclosures. Composite Structures 81 (3), 401−406.

Parveen, S., Rana, S., Fangueiro, R., 2013. A review on nanomaterial dispersion, microstructure and mechanical properties of carbon nanotube and nanofiber based cement composites. Journal of Nanomaterials 2013 (2013), 1−19.

Parveen, S., Rana, S., Fangueiro, R., Paiva, M.C., 2015. Microstructure and mechanical properties of carbon nanotube reinforced cementitious composites developed using a novel dispersion technique. Cement and Concrete Research 73, 215−227.

Qian, H., Bismarck, A., Greenhalgh, E.S., Shaffer, M.S.P., 2010. Carbon nanotube grafted silica fibres: characterising the interface at the single fibre level. Composites Science and Technology 70, 393−399.

Qiu, J., Zhang, C., Wang, B., Liang, R., 2007. Carbon nanotube integrated multifunctional multiscale composites. Nanotechnology 18 (27), 5708.

Rahmanian, S., Thean, K.S., Suraya, A.R., Shazed, M.A., Salleh, M.A.M., Yusoff, H.M., 2013. Carbon and glass hierarchical fibers: influence of carbon nanotubes on tensile, flexural and impact properties of short fiber reinforced composites. Materials & Design 43, 10−16.

Rana, S., Alagirusamy, R., Joshi, M., 2009. A review on carbon epoxy nanocomposites. Journal of Reinforced Plastics Composites 28, 461−487.

Rana, S., Alagirusamy, R., Joshi, M., 2010a. Mechanical behavior of carbon nanofibre-reinforced epoxy composites. Journal of Applied Polymer Science 118 (4), 2276−2283.

Rana, S., Alagirusamy, R., Joshi, M., 2010b. Mechanical properties of epoxy reinforced with homogeneously dispersed carbon nanofibre. International Journal of Plastics Technology 14 (2), 224−233.

Rana, S., Alagirusamy, R., Joshi, M., 2011a. Single-walled carbon nanotube incorporated novel three phase carbon/epoxy composite with enhanced properties. Journal of Nanoscience and Nanotechnology 11 (8), 7033−7036.

Rana, S., Alagirusamy, R., Joshi, M., 2011b. Development of carbon nanofibre incorporated three phase carbon/epoxy composites with enhanced mechanical, electrical and thermal properties. Composites Part A: Applied Science and Manufacturing 42 (5), 439−445.

Rana, S., Alagirusamy, R., Joshi, M., 2011c. Effect of carbon nanofibre dispersion on the tensile properties of epoxy nanocomposites. Journal of Composite Materials 45 (21), 2247−2256.

Rana, S., Alagirusamy, R., Joshi, M., 2012a. Carbon Nanomaterial Based Three Phase Multi-Functional Composites. Lap Lambert Academic Publishing GmbH & Co. KG, Germany.

Rana, S., Alagirusamy, R., Fangueiro, R., Joshi, M., 2012b. Effect of carbon nanofiber functionalization on the in-plane mechanical properties of carbon/epoxy multiscale composites. Journal of Applied Polymer Science 125 (3), 1951−1958.

Rana, S., Bhattacharyya, A., Parveen, S., Fangueiro, R., Alagirusamy, R., Joshi, M., 2013. Processing and performance of carbon/epoxy multi-scale composites containing carbon nanofibres and single walled carbon nanotubes. Journal of Polymer Research 20 (12), 1−11.

Rana, S., Fangueiro, R., 2015. Braided Structures and Composites: Production, Properties, Mechanics and Technical Applications. CRC Press.

Rana, S., Parveen, S., Fangueiro, R., 2015. Advanced carbon nanotube reinforced multi-scale composites. In: Bakerpur, E. (Ed.), Advanced Composite Materials: Manufacturing, Properties, and Applications. De Gruyter Open.

Rana, S., Zdraveva, E., Pereira, C., Fangueiro, R., Correia, A.G., 2014. Development of hybrid braided composite rods for reinforcement and health monitoring of structures. The Scientific World Journal 2014, 1−9.

Rosado, K.P., Rana, S., Pereira, C., Fangueiro, R., 2013. Self-sensing hybrid composite rod with braided reinforcement for structural health monitoring. Materials Science Forum 730−732, 379−384.

Shahid, N., Villate, R.G., Barron, A.R., 2005. Chemically functionalized alumina nanoparticle effect on carbon fiber/epoxy composites. Composites Science and Technology 65 (14), 2250−2258.

Sharma, K., Shukla, M., 2014. Three-phase carbon fiber amine functionalized carbon nanotubes epoxy composite: processing, characterisation, and multiscale modeling. Journal of Nanomaterials 2014, 1−10.

Shen, Z., Bateman, S., Wu, D.Y., McMahon, P., Dell'Olio, M., Gotama, J., 2009. The effects of carbon nanotubes on mechanical and thermal properties of woven glass fibre reinforced polyamide-6 nanocomposites. Composites Science and Technology 69, 239−244.

Siddiqui, N.A., Woo, R.S.C., Kim, J.K., Leung, C.C.K., Munir, A., 2007. Mode I interlaminar fracture behaviour and mechanical properties of CFRPS with nanoclay-filled epoxy matrix. Composite Part A 38 (2), 449−460.

Thostenson, E.T., Li, W.Z., Wang, D.Z., Ren, Z.F., Chou, T.W., 2002. Carbon nanotube/carbon fiber hybrid multiscale composites. Journal of Applied Physics 91 (9), 6034−6037.

Vaisman, L., Daniel Wagner, H., Marom, G., 2006. The role of surfactants in dispersion of carbon nanotubes. Advances in Colloid and Interface Science 128, 37−46.

Veedu, V.P., Cao, A., Li, X., Ma, K., Soldano, C., Kar, S., Ajayan, P.M., Nejhad, M.N.G., 2006. Multifunctional composites using reinforced laminate with carbon-nanotube forests. Nature Materials 5 (6), 457−462.

Wang, Y., Xu, Z., Chen, L., Jiao, Y., Wu, X., 2011. Multi-scale hybrid composites-based carbon nanotubes. Polymer Composites 32 (2), 159−167.

Wicks, S.S., de Villoria, R.G., Wardle, B.L., 2010. Interlaminar and intralaminar reinforcement of composite laminates with aligned carbon nanotubes. Composites Science and Technology 70 (1), 20−28.

Zhang, J.G., 2011. The effect of carbon fibers and carbon nanotubes on the mechanical properties of polyimide composites. Mechanics Compos Mater 47, 447−450.

Zhuang, R.-C., Doan, T.T.L., Liu, J.-W., Zhang, J., Gao, S.-L., Mäder, E., 2011. Multi-functional multi-walled carbon nanotube-jute fibres and composites. Carbon 49 (8), 2683−2692.

Zimmer, M., Cheng, Q., Li, S., Brooks, J., Liang, R., Wang, B., Zhang, C., 2012. Comparative characterization of multiscale carbon fiber composite with long and short MWCNTs at higher weight fractions. Journal of Nanomaterials 2012, 6.

Self-sensing structural composites in aerospace engineering

10

D.D.L. Chung
State University of New York, Buffalo, NY, United States

10.1   Introduction to self-sensing

Sensors include those for sensing strain, stress, damage, temperature and chemical processes (eg, resin curing). Sensors in the form of structural composite materials are the subject of this chapter. Due to the sensing function, these structural materials are multifunctional (Chung, 2010a,b). They are a type of smart materials, which are needed for smart structures. Multifunctional structural composites are attractive, due to the cost saving, high durability, large functional volume and design simplification associated with the use of the same material for both structural and sensing functions. A multifunctional structural composite is also attractive for the absence of mechanical property loss, which tends to occur in the case of embedded sensors, which are much larger than the diameter of carbon fibre, thereby causing bending of the carbon fibre around an embedded sensor in case of carbon fibre composites. Durability is particularly poor for attached devices, which can be detached. Embedded sensors also suffer from the difficulty (or impossibility) of repair. Examples of embedded or attached sensors include optical fibres and piezoelectric sensors.

In spite of its advantages, self-sensing has received less attention than the use of embedded or attached devices. This is due to the scientific challenge of developing self-sensing structural materials. Although much attention has been given to the mechanical properties and durability, relatively little attention has been directed to the sensing behaviour, which relates to the electrical behaviour.

Another method of sensing involves detecting the effect of damage on the vibration behaviour of the structure (Semperlotti et al., 2011). This method involves applying a load to the structure and measuring the vibration response. This method can provide damage detection, but the vibration analysis requires considerable mathematical modelling, which depends on the shape and dimensions of the structure. Furthermore, the analysis may not be adequate to indicate the location and type of the damage. In addition, the method is not effective for detecting the reversible strain.

Self-sensing is attained by exploiting the intrinsic behaviour of a structural material (Kemp, 1994; Wang, 2002). An example of such behaviour is the effect of damage on the electrical resistivity of a carbon fibre composite (Kemp, 1994; Wang, 2002; Baron and Schulte, 1988; Schulte and Baron, 1989). This effect was first reported by Baron and Schulte in 1988. Although electrical contacts and a meter are typically needed in

electrical resistance measurement and the meter needs to send a small current to the specimen under test in order to measure the resistance, the composite is the sensor. Neither the fibres nor the electrical contacts are sensors.

A variation of the resistance method of self-sensing involves the combined use of glass fibre (nonconductive) and carbon fibre in the same direction in the same composite, with the carbon fibre designed to fracture, thereby increasing the electrical resistance, while the glass fibre remains able to bear load (Nanni et al., 2006; Yoshitake et al., 2004). The resistance method is to be distinguished from self-sensing by using fibres (eg, glass fibres acting as light guides) that are themselves sensors (Brooks et al., 1997).

10.2   Electrical-resistance-based self-sensing

The measurement of electrical resistance (Singh, 2013) is most reliable for intermediate levels of resistance, such as resistance in the range from $0.1\,\Omega$ to $1\,M\Omega$. A large resistance exceeding $1\,M\Omega$ is relatively difficult to measure, due to the need for a high voltage in order to pass a current through the large resistor. Conventional meters are incapable of measuring resistances exceeding $1\,M\Omega$, due to their voltage limitation. A small resistance below $0.1\,\Omega$ poses a challenge in relation to measuring a small resistance change upon damage of the component under test. The lower limit of the resistance to be measured depends on the precision of the meter used.

Metals tend to be too conductive, so that their resistance is too low for effective sensing. The same problem applies to metal matrix composites. On the other hand, continuous carbon fibre polymer matrix composites tend to be in a resistance range that is well suited for sensing by resistance measurement. For a given composite specimen, the surface resistance is higher than the volume resistance. Obviously, the larger the specimen, the higher the resistance. For small laboratory carbon composite specimens, the surface resistance tends to be in a range that is more suitable for accurate resistance measurement than the volume resistance.

Due to the fact that carbon fibres are much more conductive electrically than the polymer matrix, the electrical conductivity of a composite is affected by damage (Kemp, 1994; Wang, 2002; Baronand Schulte, 1988; Schulte and Baron, 1989; Abry et al., 2001; Ceysson et al., 1996; Chung and Wang, 2003; Wang and Chung, 1999; Kaddour et al., 1994; Kupke et al., 2001; Mei et al., 2002; Park et al., 2014; Prabhakaran, 1990; Sugita et al., 1995). Damage in the form of fibre breakage causes the electrical conductivity in the fibre direction of the composite to decrease. On the other hand, damage in the form of delamination causes the electrical conductivity in the through-thickness direction of the composite to decrease, as explained below.

Although the polymer matrix is electrically nonconductive, the through-thickness conductivity of a composite is never zero, due to the flow of the resin during composite fabrication and the waviness of the fibre, and the consequent direct contact of fibres

that belong to adjacent laminae. The contact occurs at certain random points of the interlaminar interface. When delamination occurs, a crack occurs at this interface. This crack diminishes the extent of fibre−fibre contact, thereby causing the through-thickness conductivity of the composite to decrease.

As a consequence of the effects mentioned above, the electrical conductivity (the reciprocal of the electrical resistivity) provides an indicator of the damage. By selecting the direction of measurement of the conductivity, the type of damage can be selectively detected.

A related method of damage self-sensing involves the measurement of the capacitance in the through-thickness direction of the composite (Abry et al., 2001; Kupke et al., 2001). The capacitance decreases upon damage in the form of fibre−matrix debonding.

10.3   Electrical configurations for self-sensing

The measurement of electrical resistance usually requires electrical contacts. The accuracy tends to be lower for radiofrequency wireless methods. By placing the electrical contacts at selected regions of a structure, the resistance may be measured at selected regions. By using a two-dimensional (2D) array of voltage contacts at the surface, in addition to two current contacts also on the surface, tomography can be conducted to obtain a conductivity map, which gives information on the crack location (Hou and Lynch, 2009). An alternative method of tomography involves the use of a 2D array of current contacts along the four edges of the area being monitored (Loyola et al., 2013). This means that information on the spatial distribution of damage can be obtained by measurement of the resistivity distribution.

A related method of self-sensing involves measurement of the AC electrical impedance (Masson and Irving, 2000) instead of the DC resistance. The impedance is advantageous in that its measurement does not involve electrical polarization (Angelidis et al., 2005; Wang and Chung, 1998), which occurs during DC resistance measurement in the case of materials that are not sufficiently conductive, such as those with resistivity above $10^2 \, \Omega$ m.

An electrical contact can be made by using conductive paints, conductive adhesives or solder (Wang et al., 2007). Alternatively, an electrical contact can be made by compressing a conductive piece of solid (eg, a metal plate) against the surface of the structure; in this case, the contact is known as a pressure contact (Leong and Chung, 2004). A pressure contact is a less reliable contact than one made by using conductive paint/adhesive or solder, because the pressure contact interface consists of an array of contact points, which stem from the asperities on the two contacting surfaces. As the contact points do not amount to a substantial fraction of the geometric area of the contact interface, the resistance associated with a pressure contact tends to be relatively high. In addition, the nature and quantity of the contact points depend on the pressure, so the resistance associated with a pressure contact depends on the pressure.

In general, electrical resistance measurement can be performed using the four-probe method or the two-probe method. The four-probe method uses four electrical contacts

that are ideally lined up in the direction of the resistance measurement. The outer two contacts are for passing current, whereas the inner two contacts are for voltage measurement. In contrast, the two-probe method uses two contacts, each of which is both for passing current and for voltage measurement. The two-probe method suffers from the fact that current goes through the voltage-measuring leads, and, as a consequence, the measured voltage includes the contact potential drop. In the case that the specimen resistance is low compared to the contact resistance, the resistance obtained by using the two-probe method is highly inaccurate, as it reflects mainly the contact resistance, which is not the quantity to be measured. In the four-probe method, negligible current goes through the voltage contacts, since no current goes through an ideal voltmeter. Thus, the resistance measured by the four-probe method essentially excludes the contact resistance and thus reflects accurately the resistance of the specimen between the voltage contacts. For carbon fibre polymer matrix composites, the resistance is not high enough for the two-probe method to be reliable (Wang and Chung, 2000). Therefore, the four-probe method is recommended.

An additional problem with the two-probe method relates to the possible degradation of the electrical contacts upon strain or damage of the specimen under test. The degradation of the contacts causes the contact resistance to increase, thus affecting the resistance that is obtained by using the two-probe method (Wang et al., 2006a, 2007). In case of the four-probe method, degradation of the contacts has relatively little effect on the measured resistance, unless the degradation is excessive. The resistance obtained by using the four-probe method tends to be less noisy than that obtained by using the two-probe method (Wang et al., 2006a).

Electrical resistance usually refers to the resistance of a volume, so it is known as the volume resistance. The volume resistance should be measured with a current that goes throughout the whole cross-sectional area perpendicular to the direction of resistance measurement. In other words, the current density is uniform throughout the cross-section. To attain the uniformity, the current contacts should be such that they allow complete current penetration. As an example, consider the measurement of the resistance in a direction in the plane of a composite laminate. A current contact that allows complete current penetration can be in the form of a wire that goes through a through-hole in the direction perpendicular to the plane of the laminate. The wire must be in electrical contact with all the laminae, so it should be electrically connected to the wall of the through-hole by using a conductive adhesive or other conductive media. Silver particle−filled epoxy is a conductive adhesive that has been shown to perform well both electrically and mechanically (Wang et al., 2006a, 2007). However, this type of electrical contact suffers from its intrusiveness, as the drilling of a hole may cause some local damage to the composite.

An electrical contact that is less intrusive than the through-hole contact is a surface contact, as provided by applying a conductive medium, such as silver paint, on a surface of the composite. The conductive medium serves to connect electrically the composite surface to a lead wire that goes to a meter. In order to enhance the mechanical integrity and hygrothermal stability of the surface electrical contacts, each contact (such as one made by using silver paint) may be coated with nonconductive epoxy (Wang et al., 2007).

By using current contacts that are on the surface, the current penetration can be limited. The extent of current penetration from theses contacts depends on the proximity to these contacts within the region between the two current contacts. Within this region, the current penetration increases as the distance from either current contact increases. Thus, in the case that the current contacts are sufficiently far apart, current penetration may be complete for a part of the region between the current contacts. The extent of current penetration also depends on the degree of electrical anisotropy, the dimensions of the region for the resistance measurement, and the contact resistance. The electrical anisotropy of the composite is such that the resistivity in the through-thickness direction is higher than that in the fibre direction by several orders of magnitude. This anisotropy increases the difficulty of current penetration in the through-thickness direction. Due to the likelihood of incomplete current penetration, the resistance obtained by using current contacts that are on the same surface is referred to as the surface resistance.

Although a composite may be quasi-isotropic, the fibres are unidirectional within a lamina. The measurement of the surface resistance by using current contacts that are at two points on a composite surface is complicated by the unidirectional nature of the fibre in the surface lamina. The strong electrical anisotropy in the surface lamina causes the current to spread in the fibre direction as it travels from one current contact to the other. If the current contacts are positioned to send current in the transverse direction, current spreading is substantial in the fibre direction, due to the low resistivity in the fibre direction. If the current contacts are positioned to send current in the fibre direction, current spreading is small in the transverse direction, due to the high resistivity in the transverse direction. The extent of current spreading can be as high as 500 mm in the fibre direction (Wang and Chung, 2006a; Wang et al., 2005a). Current spreading allows the sensing of damage that is localized at a distance from the electrical contacts. An example of a type of damage that is localized is impact damage. Thus, the ability of sensing damage that is localized at a distance from the electrical contacts is better for the case in which the current contacts are positioned to send current in the transverse direction than the case in which the current contacts are positioned to send current in the fibre direction (Wang and Chung, 2006a).

In general, the volume resistance of a composite can be measured in a direction in the plane of a composite laminate, in the through-thickness direction and in an oblique direction (ie, a direction that is between the in-plane and through-thickness directions) (Wang et al., 2005b). The resistance in the plane of the composite laminate, particularly if the direction is parallel to the fibres, is sensitive to fibre breakage. The resistance in the through-thickness direction is sensitivity to delamination. The resistance in the oblique direction is sensitive to both types of damage.

The oblique resistance is particularly effective for damage sensing (Wang et al., 2005b; Wang and Chung, 2006b). It can be measured by using two surface contacts on one surface and two other surface contacts on the opposite surface, such that the two sets of contacts are not directly opposite. The distance between the two sets of contacts can be substantial. One contact in each set serves as a current contact, while the other contact in each set serves as a voltage contact. Although the current and voltage

contacts are not lined up, the current direction is close to the direction of resistance measurement.

The way that current is applied is governed by the electrical contact configuration. The configurations include the following (Wang and Chung, 2006a):

1. The current contacts are on the same surface in the plane of the laminate, so that the current is in the surface region only (Fig. 10.1(a)).
2. The current contacts are on opposite surfaces in the plane of the laminate, such that they are not directly opposite one another, thereby providing an oblique current (Fig. 10.1(b)).
3. The current contacts are on the edge surfaces (surfaces that are perpendicular to the plane of the laminate), so that the current is in the plane of the laminate and goes through the entire cross-section of the specimen (Fig. 10.1(c)).
4. The current contacts are in holes that are through the thickness of the laminate, so that the current is in the plane of the laminate and goes through the entire cross-section of the specimen (Fig. 10.1(d)).

In cases of a composite in the form of a cylinder, the electrical contacts may be circumferential or axial and may be on the inner or outer surface of the cylinder (Wang et al., 2006b). The resistance may be measured in the axial, radial, oblique or circumferential direction (Wang et al., 2006b). The circumferential resistance is particularly sensitive to damage.
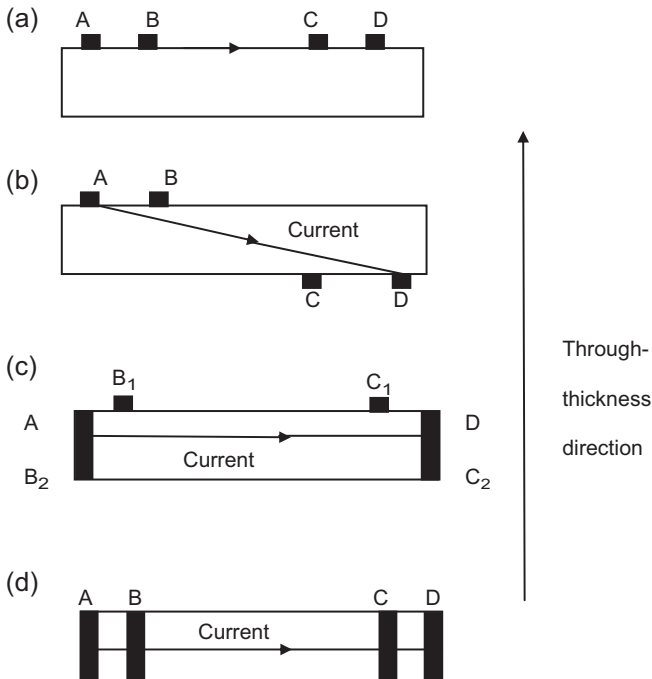
Figure 10.1 Electrical contact configurations for sensing without spatial resolution (a) Surface resistance measurement. (b) Oblique resistance measurement. (c) Volume resistance measurement using surface voltage contacts. (d) Volume resistance measurement using through-thickness voltage contacts (Chung, 2007).

Unless a substantially thick layer of the polymer matrix is present on the composite surface (due to the surface finish of the composite), removal of the surface polymer layer (eg, by mechanical polishing) prior to application of the electrical contacts is not necessary. In cases where mechanical polishing is conducted, care should be exercised so that it does not cause damage to the surface fibres.

10.4 Spatial distribution sensing

A one-dimensional (1D) resistance distribution determination, as needed for damage distribution sensing, involves a 1D array of electrical contacts, as illustrated in Fig. 10.2(a), where contacts are in the form of strips extending along the entire width of the specimen. In Fig. 10.2(a), contacts 1 and 5 are for passing current, whereas the remaining contacts are to be used two at a time (ie, 2 + 3 and 3 + 4) for voltage measurement at segments I and II, respectively (Wang and Chung, 2006a).

In order to obtain information on the damage location, the 2D resistance distribution needs to be determined. This determination ideally involves a 2D array of electrical contacts, as illustrated in Fig. 10.2(b) for the case of a 5 × 5 array (Wang and Chung, 2006a). However, in practice, the number of electrical contacts is preferably not large. Furthermore, the contacts are preferably near the edge of the specimen, as illustrated in Fig. 10.2(c), so that the electrical contacts do not interfere with the usage of the structural component. Therefore, the configuration of Fig. 10.2(c) is more suitable for practical implementation than that of Fig. 10.2(b).
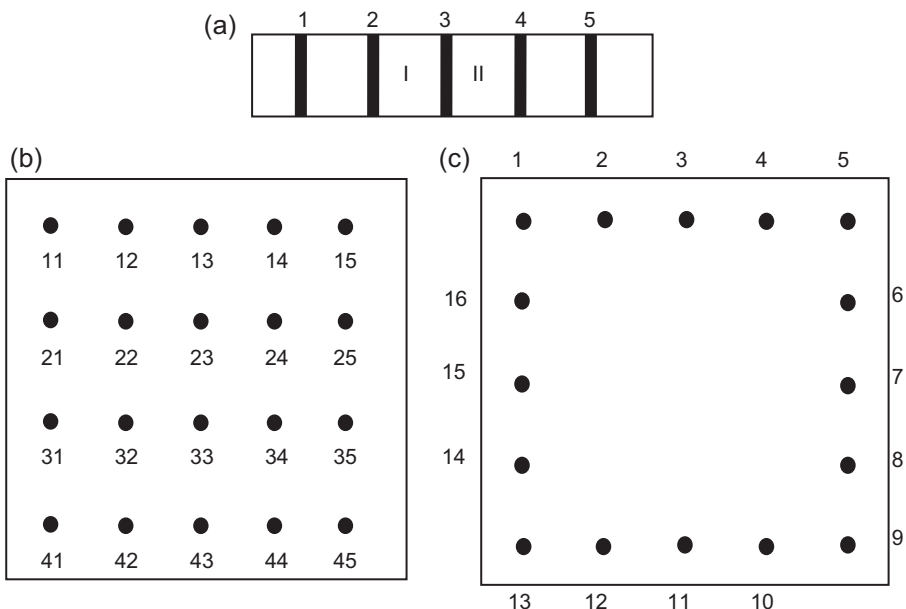
Figure 10.2 Electrical contact configurations for sensing with spatial resolution. (a) 1D resistance method. (b) 2D resistance method. (c) 2D potential method (Chung, 2007).

In order to obtain a considerable amount of information by using a rather small number of electrical contacts, the potential at each contact can be measured (say, relative to ground) for each of a number of directions of current application. This is the conventional procedure, but other procedures of collecting the potential information are possible. An example of the conventional procedure is described below (Wang and Chung, 2006a). The current is applied from 1 to 9 (Fig. 10.2(c)), and the potential is measured at each of the remaining 14 contacts. After that, the current is applied, say, from 5 to 13, while the potential is measured at each of the remaining 14 contacts. Since the current line and the potential gradient line (ie, the line connecting the two points where potential is measured) do not overlap, this 2D method does not correspond to resistance measurement, which involves overlapping of the current line and the potential gradient line. This 2D method is referred to as the potential method.

The potential method is useful for 2D sensing (Angelidis et al., 2005; Angelidis and Irving, 2007; Chu and Yum, 2001; Chung, 2007; Irving and Thiagarajan, 1998; Masson and Irving, 2000; Todoroki et al., 2004; Wang and Chung, 2006a; Wang et al., 2006c,d). However, it is less sensitive than the resistance method (Wang et al., 2004, 2006c,d), due to the distance between the current line and the potential gradient line. In the case of the resistance method, these two lines coincide. The potential method is further complicated by the current spreading, which makes truly 2D sensing impossible in the case of surface contacts (Wang and Chung, 2006a).

The electrical resistivity associated with the interlaminar interface (the weak link in a fibre laminate) is not a volume resistivity but is a contact resistivity (ie, the resistivity associated with an area (an interface) rather than a volume). The contact resistance (R_c) is related to the contact resistivity (ρ_c), which is geometry independent, by the equation

$$\rho_c = R_c A, \qquad\qquad\qquad\qquad\qquad\qquad [10.1]$$

where A is the area of concern. Eq. [10.3] means that the larger the area, the smaller the contact resistance. It indicates that the unit for the contact resistivity is $\Omega\,m^2$.

The contact resistivity may be measured by using four electrical contacts, such that two contacts (one for voltage and the other for current) are on each of the two laminae that sandwich the interlaminar interface, which serves as the sensor (Fig. 10.3) (Wang et al., 2004). By using two laminae in a cross-ply configuration (ie, the fibres in the two laminae are perpendicular) and having groups of fibres electrically connected together in each lamina, a 2D array of sensors and an $x-y$ grid of electrical connections are formed for the purpose of 2D spatially resolved sensing (Fig. 10.4) (Wang et al., 2004). Although the illustration in Fig. 10.2 is for a cross-ply configuration, the configuration can involve the laminae oriented at angles less than 90 degree.

In damage sensing utilizing continuous carbon fibre polymer matrix composites, the resistance increase that accompanies damage can be measured by DC resistance measurement (Chung, 2007), AC impedance measurement (at a frequency of 1 kHz) (Todoroki et al., 2006), measurement of the increase in oscillation frequency of an oscillation circuit attached to the composite (Matsuzaki and Todoroki, 2006) or measurement of the increase in resonant frequency of the composite which acts as an
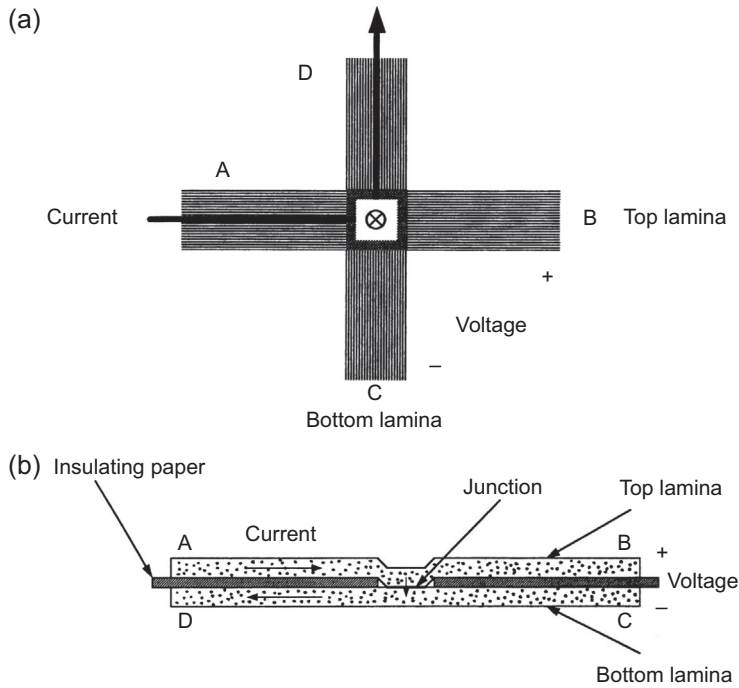
Figure 10.3 Measurement of the contact electrical resistivity of the interlaminar interface of a continuous carbon fibre polymer matrix composite using the four-probe method, with electrical contacts A and D used for passing a current and electrical contacts B and C used for voltage measurement. The contact resistivity is given by the product of the contact resistance and the contact area. (a) Cross-ply lay-up configuration. (b) Unidirectional lay-up configuration (Wang et al., 2004).

antenna (Matsuzaki et al., 2009). The frequency measurements are advantageous in that they can be conducted in a wireless fashion.

10.5 Structural composites in aerospace engineering

Composite materials are multiphase materials obtained by artificial combinations of different materials, so as to attain properties that the individual components by themselves cannot attain. The concept of improved performance is broad and includes increased strength or reinforcement of one material by the addition of another material, as well as increased toughness, decreased coefficient of thermal expansion and increased thermal or electrical conductivity.

An example of a composite material is a lightweight structural material (as used for aircraft) that is obtained by embedding continuous carbon fibres (reinforcement) in one or more orientations in a polymer matrix (binder). The fibres provide the strength and stiffness, whereas the polymer serves as the binder. Though particles can also serve as
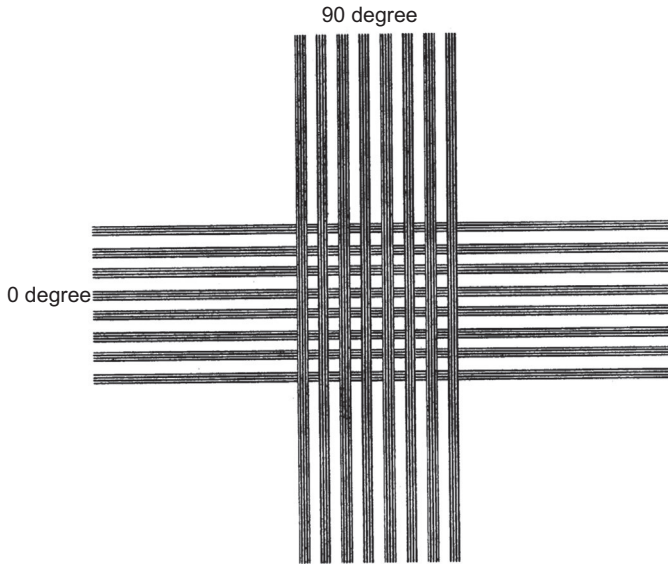
90 degree

0 degree

Figure 10.4 A 2D array of sensors, with each sensor in the form of an interlaminar interface between fibre groups that are in different directions. In this illustration, the laminae are 90 degree apart in the fibre orientation (Wang et al., 2004).

a reinforcement, they tend to be less effective than fibres. Composite materials with continuous fibres (preferably aligned to achieve a high volume fraction) are particularly attractive for their high modulus and strength.

In general, the matrix can be polymer (thermosetting or thermoplastic), metal (eg, aluminium), carbon (eg, graphite), ceramic (eg, silicon carbide) or hybrid (eg, carbon and silicon carbide). Polymer matrix materials are attractive for their low density and low cost. They are used for lightweight structures (aircraft, sporting goods, wheel chairs etc.), in addition to vibration damping, electronic enclosures, solder replacement and so on.

Metal matrix, carbon matrix and ceramic matrix composites are superior in their ability to withstand elevated temperatures and are also attractive for their low thermal expansion, but their fabrication costs are high. In addition, metal matrix composites are attractive for their high electrical and thermal conductivity and creep resistance, though they tend to suffer from galvanic corrosion.

Continuous carbon fibre carbon matrix composites (carbon−carbon composites) are dominant for high-temperature lightweight structures (such as reentry space vehicles and aircraft brakes), in spite of their tendency to be oxidized ($C + O_2 \rightarrow CO_2$) at elevated temperatures in the presence of oxygen. Continuous ceramic fibre ceramic matrix composites (ceramic−ceramic composites) are superior to carbon−carbon composites in the ability to withstand high temperatures, but they are more expensive. The chapter emphasizes polymer matrix composites with continuous fibre reinforcement, due to their wide utilization in aircraft and spacecraft.

10.6 Sensing strain or stress

10.6.1 Applications

The sensing of strain or stress is valuable for structural vibration control, load monitoring and operation monitoring. Structural vibration control is relevant because vibration involves dynamic strain, so that the sensing of vibration can be conducted by the sensing of strain.

The elastic deformation regime is to be distinguished from the plastic deformation regime that may follow the elastic deformation regime as the stress is increased beyond the elastic limit. Strain can be in the elastic deformation regime or the plastic deformation regime. In the elastic deformation regime, strain is reversible, so that it returns to zero upon unloading. In the plastic deformation regime, strain is not totally reversible. In general, the sensing of reversible strain is more challenging than that of irreversible strain. This is because the sensing of reversible strain requires a sensor that allows real-time sensing during loading, whereas the sensing of irreversible strain does not require real-time sensing.

In the elastic deformation regime, strain (which is the fractional change in dimension and describes the extent of deformation) is proportional to the stress (the force per unit area in case of tensile or compressive stress). Therefore, in this regime, strain sensors may be used as stress sensors if the proportionality constant, which is the modulus of elasticity (the ratio of stress to strain in the elastic deformation regime), is known. A stress sensor can be in the form of a strain sensor operating in the elastic deformation regime, with strain rather than stress being the quantity that relates to the sensor output (eg, electrical resistance). However, a stress sensor can be such that stress is the quantity that relates to the sensor output, as in cases in which the relationship between stress and strain is not known (Wang and Chung, 2007a).

10.6.2 Concept

Strain/stress sensors are commonly in the form of materials whose properties change in response to strain/stress. A particularly common type of strain/stress sensor is based on the concept that the electrical resistance of the sensor changes with strain, thereby allowing the measured resistance to indicate the strain. The sensor may be attached to or embedded in the structure that needs its strain measured. In this case, the sensor is often called a strain gage. The joining of the gage to the surface of the structure must be strong, so that the strain in the sensor correctly indicates the strain in the structure. For this purpose, the adhesive used for the joining must be effective when the thickness of the adhesive is small. Ineffective joining of the sensor to the structure can cause the measured strain to be lower than the actual strain in the structure. Alternatively, the structure itself may be the sensor. When the structure is the sensor, the structure is said to be self-sensing, and no sensor needs to be attached to or embedded in the structure. However, electrical contacts still need to be applied to the structure for resistance measurement.

The electrical resistivity, also known as the volume electrical resistivity, is a material property that is geometry independent. The electrical resistance (R), also known as the volume electrical resistance, relates to the electrical resistivity (ρ) by the equation

$$R = \rho l/A \tag{10.2}$$

where l is the length of the measured region in the direction of resistance measurement and A is the cross-sectional area perpendicular to the direction of resistance measurement. Eq. [10.2] means that the resistance increases with increasing l and is inversely proportional to A. It indicates that the unit for the resistivity is Ω m.

10.6.3   Approach

A particularly reliable method of resistance measurement involves the use of four electrical contacts (ideally collinear), such that the outer two contacts are for passing an electric current while the inner two contacts are for voltage measurement (Chung, 2010a; Wang and Chung, 2000; Wang et al., 2006a; Wen and Chung, 2005). This method of resistance measurement is known as the four-probe method. Its advantage stems from the fact the essentially no current goes through the voltage contacts, thus allowing the measured resistance to exclude the contact resistance. Since the contact resistance may be substantial compared to the resistance to be measured, its exclusion is important for accurate measurement of the resistance. In contrast, the two-probe method involves the use of only two electrical contacts, with each contact being used for both current passing and voltage measurement. As a consequence, the two-probe method involves a current going through the contacts, thus resulting in the measured resistance including the contact resistance. Even when the contact material is highly conductive, the contact resistance can be substantial, due to the resistance associated with the interface between the contact material and the surface of the material being evaluated. Unless the contact resistance is negligible compared to the resistance of the structure, the two-probe method is not reliable (Wang and Chung, 2000; Wang et al., 2006a; Wen and Chung, 2005).

For spatially resolved sensing, a 1D (Wang et al., 2006a) or 2D (Chung, 2007; Wen and Chung, 2006a; Wang et al., 2006c,d) array of electrical contacts can be used. In the case of 1D spatially resolved sensing, the 1D array of electrical contacts can involve the outermost two contacts being for passing current, whereas all the remaining contacts are for voltage measurement, with two of the remaining contacts used at a time (Wen and Chung, 2006a).

10.6.4   Piezoresistivity-based sensing

Strain/stress sensors based on the change of the resistance with strain/stress are of two types. The first type, known as resistive sensors, involves the resistivity not changing with strain/stress, so that the change of resistance is only due to the change in dimensions associated with the strain. The second type, known as piezoresistive sensors, involves the resistivity changing with strain/stress, so that the change in resistance is due

to both the change in resistivity and the change in dimensions. Resistive sensors are commonly in the form of metals. Piezoresistive sensors are commonly in the form of composite materials such that the filler (eg, particles and short fibres) of the composite material is more conductive than the matrix (eg, polymer and cement) of the composite material. Examples of piezoresistive composite materials include carbon black−filled polymer (Wang and Ding, 2010; Aiyar et al., 2009), CNT-filled polymer (Ciselli et al., 2010; Zhang et al., 2006), short carbon fibre−filled cement (Chung, 2002; Wen and Chung, 2000, 2001a,b, 2003, 2006a,b,c, 2007a; Zhu and Chung, 2007a), carbon black−filled cement (Xiao et al., 2010), carbon-black carbon-fibre−filled cement (Han et al., 2010a; Wen and Chung, 2007b), nickel particle−filled cement (Han et al., 2010b) and CNT-filled cement (Li et al., 2007; Han et al., 2009; Yu and Kwon, 2009).

The piezoresistive effect tends to be present to various degrees in composites with a conductive reinforcement (whether fibres or particles) and a nonconductive matrix. Upon deformation of the composite material, the microstructure changes, thus affecting the resistivity of the composite material. For example, the microstructural change involves the change in the extent of contact between the filler units. A decrease in the extent of contact commonly occurs upon tensile deformation, thus causing an increase in the resistivity; an increase in the extent of contact commonly occurs upon compressive deformation, thus causing a decrease in the resistivity. This mechanism tends to occur in composites with a ductile matrix, such as a polymer matrix (Aiyar et al., 2009; Ciselli et al., 2010; Wang and Ding, 2010). In another example, the microstructural change involves the loosening of the fibre−matrix interface upon strain, thus causing an increase in the resistivity; for example, loosening occurs upon tension (whether uniaxial tension or the tension side of a beam under flexure) and the resistivity in the tensile strain direction increases, while tightening occurs upon compression (whether uniaxial compression or the compressive side of a beam under flexure) and the resistivity in the compressive strain decreases; this mechanism tends to occur in composites with a brittle matrix, such as a cement matrix composite (Chung, 2002; Wen and Chung, 2000, 2001a,b, 2003, 2006b,c, 2007a; Zhu and Chung, 2007a).

In yet another example, the microstructural change involves the change in the degree of current penetration from the surface of a continuous carbon fibre polymer matrix composite upon flexure, so that the surface resistance changes; at the compression surface, the current penetration increases upon flexure, so that the surface resistance decreases (Fig. 10.5); at the tension surface, the current penetration decreases upon flexure, so that the surface resistance increases (Fig. 10.6) (Wang and Chung, 2006b; Wang et al., 1999; Zhu and Chung, 2007b). Flexural strain also causes the oblique resistance to increase reversibly (Wang and Chung, 2006b; Zhu and Chung, 2007b). Tensile strain in the fibre direction of the composite causes the through-thickness resistivity to increase reversibly (Wang and Chung, 1998, 2007b). Through-thickness compression causes the longitudinal resistivity to decrease reversibly (Leong et al., 2006; Wang and Chung, 2007a, 2013). These strain effects are known as piezoresistivity, which allows strain/ stress sensing (Angelidis et al., 2004; Chung and Wang, 2003; Wang and Chung, 1999, 2000, 2006a). The sensing of both strain and damage is attractive for identifying the cause of damage. The strain-sensing characteristic can be affected by damage (Wang and Chung, 2002, 2006b) and by temperature (Wang et al., 2004).
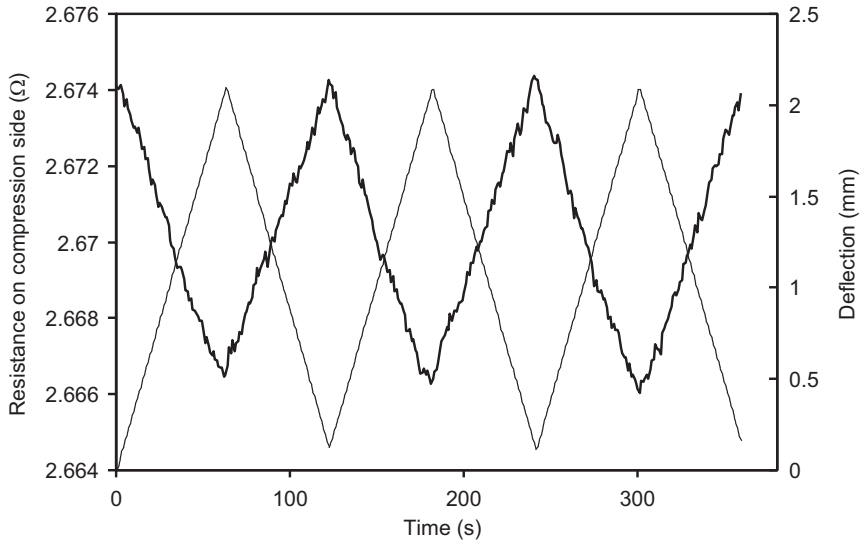
Figure 10.5 Compression surface resistance (*thick curve*) during deflection (*thin curve*) cycling at a maximum deflection of 2.098 mm (stress amplitude of 392.3 MPa) for a 24-lamina quasi-isotropic continuous carbon fibre epoxy matrix composite (Wang and Chung, 2006b).
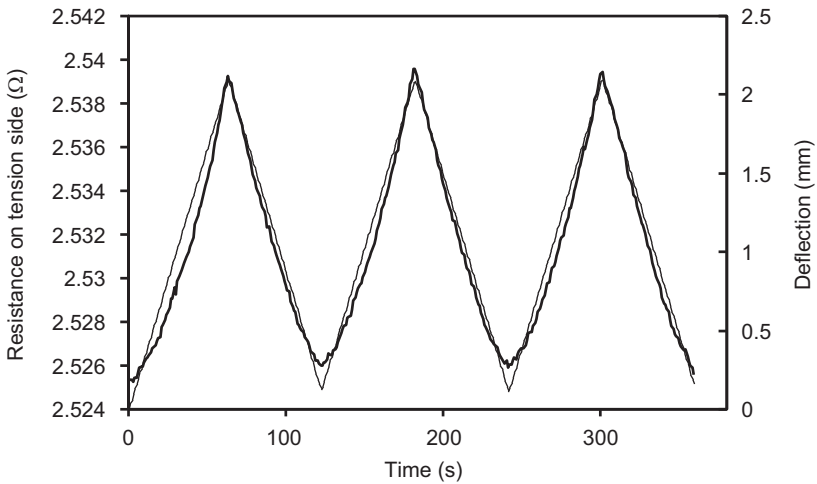
Figure 10.6 Tension surface resistance (*thick curve*) during deflection (*thin curve*) cycling at a maximum deflection of 2.098 mm (stress amplitude of 392.3 MPa) for a 24-lamina quasi-isotropic continuous carbon fibre epoxy matrix composite (Wang and Chung, 2006b).

In cases of a discontinuous reinforcement (filler) such as particles or short fibres, the sensitivity for strain sensing tends to be highest when the reinforcement volume fraction is in the vicinity of the percolation threshold, which is the volume fraction above which the reinforcement contacts one another and forms a continuous electrically conductive path. This is because the mechanism of the piezoresistivity for composites with discontinuous reinforcement commonly involves a change in the distance between the adjacent fibres or particles, and the resistivity of the composite varies most sharply with this distance when the reinforcement volume fraction is in the vicinity of the percolation threshold. In addition, a large difference in resistivity between the reinforcement and the matrix helps increase the sensitivity.

Piezoresistive sensors tend to be more sensitive than resistive sensors. The sensitivity is commonly described by the gage factor, which is defined as the fractional change in resistance per unit strain. For a resistive strain sensor, the gage factor is commonly around 2, with the exact value depending on the Poisson's ratio. For a piezoresistive strain sensor, the gage factor is commonly much higher than 2 (as high as 10^3) (Han et al., 2010b).

From Eq. [10.1], the fractional change in resistance is given by the equation

$$\delta R / R = \delta \rho / \rho + (\delta \ell / \ell)(1 + v_{12} + v_{13}), \qquad [10.3]$$

where v_{12} and v_{13} are values of the Poisson's ratio for the transverse and through-thickness strains, respectively. Positive piezoresistivity refers to the behaviour in which the resistivity increases with increasing strain (ie, $(\delta \rho / \rho)/(\delta \ell / \ell) > 0$). Negative piezoresistivity refers to the behaviour in which the resistivity decreases with increasing strain (ie, $(\delta \rho / \rho)/(\delta \ell / \ell) < 0$). Piezoresistivity is usually positive, because elongation tends to change the microstructure in such a way that the resistivity becomes higher in the direction of elongation. For example, a composite with an electrically nonconductive polymer matrix and a filler in the form of electrically conductive particles tends to exhibit positive piezoresistivity, because the distance between adjacent particles increases upon elongation of the composite, thereby decreasing the chance of touching between the adjacent particles. However, negative piezoresistivity has been reported in polymer matrix composites with continuous carbon fibres (Wang and Chung, 2007b) and those with nickel nanofibre (originally known as nickel filament) (Shui and Chung, 1997). The negative piezoresistivity is attributed to the increase in fibre and nanofibre alignment during tension.

For the purpose of effective strain sensing, a large magnitude of the gage factor (fractional change in resistance per unit strain) is desired. Eq. [10.2] shows that the gage factor depends on both the fractional change in resistivity per unit strain and the Poisson's ratio. A positive value of the gage factor does not necessarily mean that the piezoresistivity is positive, but a negative value of the gage factor necessarily means that the piezoresistivity is negative.

In order to attain a large fractional change in resistance at a particular strain, positive piezoresistivity is more desirable than negative piezoresistivity that exhibits the same magnitude of the fractional change in resistivity. When the strain is small, as is the case when the piezoresistive material is a stiff structural material, the fractional change in

resistance is essentially equal to the fractional change in resistivity. Under this circum-
stance, positive and negative piezoresistivities are equally desirable for providing a
large magnitude of the fractional change in resistance.

10.6.5 Electrical contact placement

When the structure is self-sensing, the resistance may be measured by applying current
and voltage contacts on the same surface of the structure. In this case, the measured
resistance is the surface resistance rather than the volume resistance. The surface resis-
tance depends on the extent of current penetration from the surface where the current
contacts are located. Due to the fact that the current density (current per unit
cross-sectional area) diminishes as the depth of current penetration increases and the
usually unclear profile of the current density with the depth from the surface, it is usu-
ally difficult to obtain the resistivity from the measured surface resistance. Neverthe-
less, with appropriate calibration, the surface resistance provides an indication of the
strain and stress (Wang and Chung, 2006b; Wen and Chung, 2006c).

Another method of self-sensing involves applying current contacts such that the
current density is uniform throughout the thickness of the structure. As a conse-
quence of the uniform current density, the measured resistance relates to the resis-
tivity. For the purpose of obtaining uniform current density throughout the
thickness, the current contacts may be applied at the two opposite ends of the struc-
ture, with the surface of each end being perpendicular to the direction of resistance
measurement and being entirely covered by an electrical contact. Alternatively, the
current contacts (typically in the form of a conductive mesh) may be embedded in
the structure, such that each contact extends throughout the entire cross-section of
the structure. In a less ideal method, the current contacts are applied around the
entire perimeter of the structure in two planes that are perpendicular to the direction
of resistance measurement. The configuration of the voltage contacts is less critical.
For either configuration of current contacts, the voltage contacts can be at the sur-
face, embedded inside, or be applied around the entire perimeter of the structure in
two planes that are perpendicular to the direction of resistance measurement. As
mentioned above in relation to the four-probe method of resistance measurement,
the current contacts are the outer contacts, and the voltage contacts are the inner
contacts. In the case of current contacts that are around the perimeter, the distance
between the current contact and its adjacent voltage contact must be sufficient to
allow the current density to be uniform throughout the cross-section in the region
between the two voltage contacts (Fig. 10.7) (Chung, 2010a; Zhu and Chung,
2007c).

In cases when the structure dimension is too small in the direction of resistance
measurement for the installation of four electrical contacts at four planes that are
perpendicular to the direction of resistance measurement, the four-probe method
may be carried out by using a less ideal configuration. This configuration, as illustrated
in Fig. 10.8 (Chung, 2010a), involves a current contact in the form of a hollow loop
(the large hollow rectangle in Fig. 10.8) and a voltage contact in the form of a solid
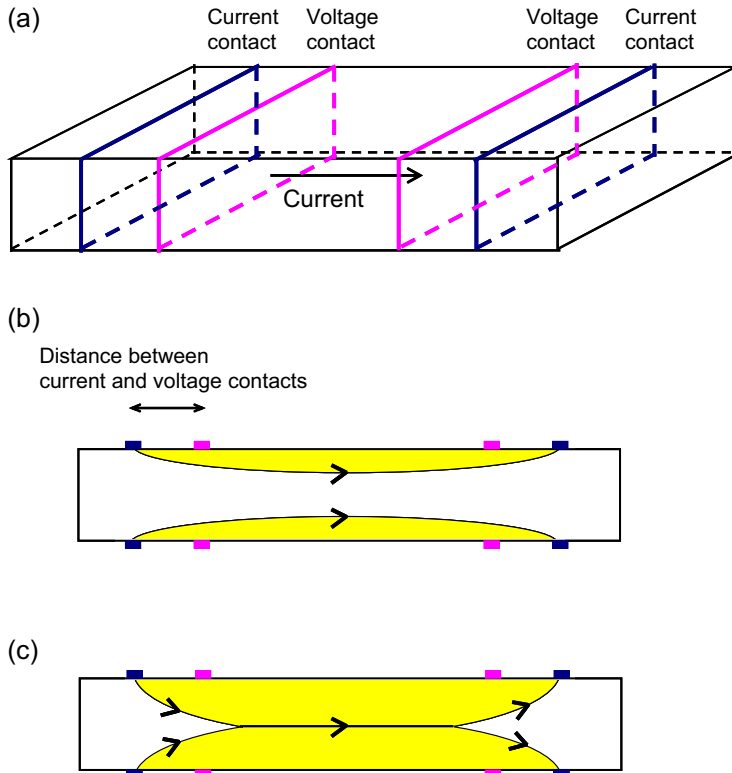
Figure 10.7 Method of volume electrical resistivity measurement involving the four-probe method, with all the electrical contacts on the surface all the way around the perimeter of the specimen. (a) 3D view. (b) Cross-sectional view showing the case of incomplete current penetration in the region between the voltage contacts. (c) Cross-sectional view showing the case of complete current penetration in the region between the voltage contacts (Chung, 2010a).

dot (the small solid rectangle in Fig. 10.8) on each of the two opposite surfaces that are perpendicular to the direction of resistance measurement.

10.6.6 Joint monitoring

Through-thickness compression is experienced in the fastening of composite panels. The monitoring of the through-thickness stress/strain is relevant to fastened joint condition monitoring. Fastened joint integrity is of practical concern due to the weakness of the composite in the through-thickness direction. This weakness is associated with the fact that the interlaminar interface is the weak link in the composite.

Through-thickness compression is encountered in the fastening of composite components. The effect of the compression is not just at the joint interface, but also within each of the components being joined.
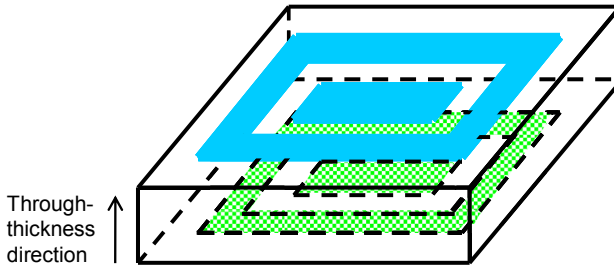
Figure 10.8 Method of volume electrical resistivity measurement involving the four-probe method, with a current contact and a voltage contact on each of two opposite surfaces. The resistance is measured in the through-thickness direction, which is perpendicular to the two opposite surfaces (Chung, 2010a).

The joint interface can be effectively monitored by measuring the contact electrical resistivity of this interface (Luo and Chung, 2000; Chung, 2001). The concept behind the joint interface monitoring stems from the notion that the joint surfaces are never perfectly smooth and, as a result, the two surfaces make contact at points. Upon compression in the direction perpendicular to the joint interface, the degree of contact changes, thereby affecting the contact resistivity of the joint interface. Fracture of some of the hillocks in the topography of either of the joint surfaces also affects the contact resistivity.

The effectiveness of resistance-based joint monitoring has been shown for a fastened joint of two carbon fibre polymer matrix composite panels. The contact resistivity of the joint interface can be achieved by using the four-probe method, with two electrical contacts (one for the current and the other for the voltage) on each of the two panels. The contact resistivity decreases with increasing through-thickness stress (Luo and Chung, 2000), due to the increased touching of the asperities on the adjoining surfaces of the two panels. The microstructure of the joint is irreversibly affected by through-thickness compressive stress at just 5% of the yield strength of the polymer matrix, as shown by irreversible decrease of the contact electrical resistivity of the joint interface.

The stress or strain in the through-thickness direction within the composite can be monitored by measuring the through-thickness or longitudinal resistance of the composite (Wang and Chung, 2013). Due to the greater complexity of the electrical contacts for through-thickness resistance measurement (Fig. 10.8) compared to those for longitudinal resistance measurement, monitoring by measuring the longitudinal resistance is easier to implement.

As shown for a continuous carbon fibre polymer matrix composite, upon through-thickness compression, the resistivity decreases in both through-thickness and longitudinal directions (Wang and Chung, 2013). Fig. 10.9 shows the variation of the through-thickness resistance with through-thickness stress during progressively increasing stress amplitude. This is because the through-thickness compression causes more fibre—fibre contact in the through-thickness direction and the increased contact enhances the conductivity in both through-thickness and longitudinal directions. The
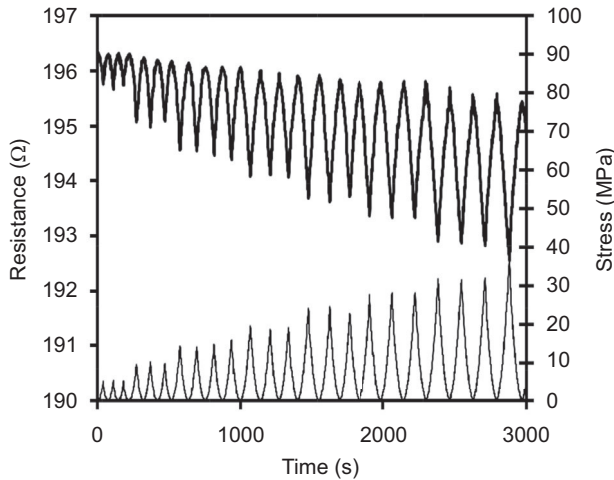
Figure 10.9 The effect of through-thickness stress (*thin lower curve*) on the through-thickness resistance (*thick upper curve*) of a continuous carbon fibre epoxy matrix composite up to a stress amplitude of 35 MPa (Wang and Chung, 2013).

longitudinal volume resistivity of a composite is diminished by the through-thickness compression, due to the decrease in the through-thickness volume resistivity (Wang and Chung, 2013). The decrease in through-thickness volume resistivity is partly due to the decrease in the contact resistivity of the interlaminar interface (Wang et al., 2004).

10.7 Sensing damage

10.7.1 Applications

Damage refers to that of a structure, which can be a bridge, pier, building, airframe, helicopter rotor, wind turbine, automobile, offshore platform, helmet and so on. Due to loading, aging (eg, corrosion and fatigue), environmental effects (eg, temperature excursions, moisture, erosion, wind and ocean waves) and extreme events (eg, earthquakes), structures degrade and the sensing of their damage before the damage becomes catastrophic is valuable for hazard mitigation and timely repair. Damage sensors are for the sensing of such damage.

10.7.2 Concept

Damage sensors can be in the form of a material that is similar in composition to the material of the structure to be sensed, such that the sensor is exposed to the same environment as the structure. Thus, the degradation of the sensor material indicates that of the structure. However, this method is limited in reliability, due to the fact that the sensor and the structure are very different in size and the extent of degradation tends

to be size dependent. A more reliable method involves the structure itself being a damage sensor; thus, the structure is said to be self-sensing. However, not all structural materials can be damage sensors. A structural material whose electrical resistivity changes with damage can be a damage sensor. The resistivity usually increases with damage, because damage commonly involves fracture or damage of certain constituents. Although it is less common, the resistivity can decrease upon minor damage, as in the case of early fatigue damage in which the degree of contact of conductive short fibres in a composite material increases due to damage of the matrix in the vicinity of the region where the fibres make increasing contact (Wang et al., 1998).

10.7.3 Approach

A continuous carbon fibre polymer matrix composite can sense its own damage, because the resistivity in the in-plane direction of the composite increases upon fibre fracture (Chung, 2007) or matrix cracking (Todoroki et al., 2006), and the resistivity in the through-thickness direction (Wang and Chung, 1998) or the oblique direction (ie, a direction between the through-thickness and in-plane directions) (Wang et al., 2005b) of the composite increases upon delamination. The carbon fibre laminates in unidirectional, cross-ply, quasi-isotropic (Chung, 2007) or woven (Hirano and Todoroki, 2007) configurations are effective for sensing minor and major damage. However, carbon fibre composites made by pultrusion are only able to sense very major damage that shortly precedes failure (Nanni et al., 2006).

A hybrid polymer matrix composite with both continuous carbon fibre and continuous glass fibre as reinforcements can also sense its own damage (Muto et al., 2001). In this hybrid composite, the carbon fibre is responsible for the sensing ability. A related hybrid composite that provides superior sensing is a continuous glass fibre composite (without carbon fibre) with one of the glass fibre tows having been coated with carbon powder (5 μm particle size), which provides the conductivity that enables sensing (Muto et al., 2001).

A continuous glass fibre polymer matrix composite containing CNTs in the matrix (Gao et al., 2010) can also sense its own damage. The CNTs render sufficient electrical conductivity to the otherwise nonconductive composite for the purpose of damage indication by resistance increase. A related damage sensor is a glass fibre (or carbon fibre) polymer matrix composite containing a CNT thread, which provides localized damage sensing (Abot et al., 2010).

In order to quantify the extent of damage that corresponds to a particular extent of resistivity change, the damage should be assessed by another method, such as the measurement of the residual elastic modulus or the residual strength of specimens made of the structural material (Chung, 2007). Because damage is usually not reversible, real-time sensing of damage is not essential. However, real-time damage sensing is attractive for immediate detection of damage for the purpose of timely repair.

The degradation of an electrical contact causes the contact resistance to increase (Wang et al., 2007). As electrical contacts may degrade as the structure degrades, the contact resistance changes as degradation occurs, thus making the four-probe method, which excludes the contact resistance from the measured resistance, highly

necessary for sensing the damage of a structure. If the two-probe method is used instead, both the damage of the structure and the damage of the electrical contacts are sensed at the same time, such that the two types of damage cannot be decoupled.

10.7.4 Self-sensing characteristics of carbon fibre polymer matrix composites

Self-sensing by electrical resistance measurement is illustrated here for carbon fibre epoxy matrix composites under flexure (three-point bending) (Wang and Chung, 2006b). The surface resistances at both the tension and compression sides of the specimen are obtained by using all four contacts on the same surface of the specimen (Fig. 10.1(a)). The oblique resistance is obtained by using two contacts on each of the two opposite surfaces (Fig. 10.1(b)). In the plane of the laminate, each electrical contact is in the form of a strip that extends in the direction perpendicular to the long dimension of the specimen (Fig. 10.2(a)). In this work, silver paint is used for making the electrical contacts. However, various contact materials can be used (Wang et al., 2007).

The surface and oblique resistances are separately and continuously measured during loading and unloading at progressively increasing stress amplitudes (Wang and Chung, 2006b). The oblique resistance after unloading decreases with increasing highest prior deflection, provided that the highest prior deflection is adequate. This effect is attributed to minor damage, which causes more fibres of one lamina to touch fibres of an adjacent lamina, thereby increasing the degree of current penetration. Thus, the oblique resistance at zero load may serve as an indicator of damage. It is a better indicator of damage than the tension/compression surface resistance, because it probes the interior of the specimen, whereas the surface resistance probes the surface region only. In general, the resistance after unloading is an attractive indicator of damage, as it allows condition monitoring at times after the damage infliction. In contrast, the resistance during loading is an indicator of damage only during the damage infliction.

Under uniaxial tension, the volume resistance of carbon fibre composite in the fibre direction (longitudinal direction) irreversibly increases upon damage (Fig. 10.10) due to fibre breakage (Wang and Chung, 1998; Park et al., 2007). The resistance may be measured by using four electrical contacts that are all around the perimeter of the specimen (Wang and Chung, 1998) or all on one surface (Park et al., 2007). Such damage during tension−tension fatigue is observed as early as halfway (50%) during the fatigue life (Fig. 10.10) (Wang and Chung, 1998). That the increase in resistance indeed signifies damage is supported by the observed decrease in the secant modulus (stress divided by strain) (Wang and Chung, 1998) as the resistance increases (Fig. 10.10). The occurrence of damage is also confirmed by simultaneous acoustic emission observation (Prasse et al., 2001).

An alternative method involves measuring the through-thickness resistance rather than the longitudinal resistance. The through-thickness resistance is sensitive to delamination, whereas the longitudinal resistance is sensitive to fibre breakage. The volume resistance in the through-thickness direction increases irreversibly upon tension−tension fatigue, due to delamination, which decreases the cross-sectional area of the
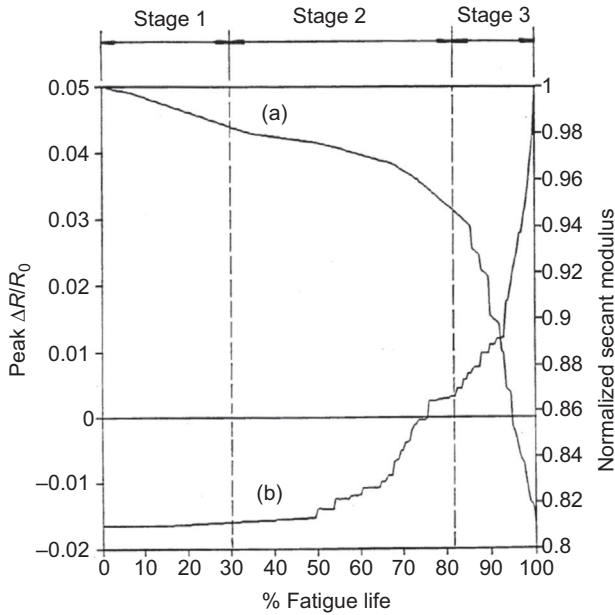
Figure 10.10 Evolution of damage in the form of fibre breakage during tension−tension fatigue, as shown by the longitudinal volume resistance: (a) normalized secant modulus and (b) the peak value of the fractional change in resistance (relative to the initial resistance) in a stress cycle. Variation of the resistance within a cycle (not shown) is due to the effect of strain rather than that of damage (Wang and Chung, 1998).

current path in the through-thickness direction. Such damage is observed as early as one-third (33%) into the fatigue life (Fig. 10.11) (Wang and Chung, 1998).

The sensing of damage inflicted by impact is practically important. Impact may be due to a bird striking an aircraft wing, a hammer being dropped accidentally or the like. Impact damage is localized, in contrast to flexural damage and tensile damage, which are spread out. The sensing of impact damage in carbon fibre composites by surface resistance measurement should be conducted by measuring the resistance in a region that contains the point of impact, unless the extent of current spreading in the chosen direction away from the point of impact is large.

Upon drop impact damage, the resistance increases irreversibly, such that the resistance increases monotonically with increasing impact energy (Angelidis and Irving, 2007; Angelidis et al., 2005; Wang et al., 2005b, 2006b), as shown in Fig. 10.12 upon impact from 0.73 to 5.08 J for the oblique resistance (Wang et al., 2005b). The trend is the same for the oblique resistance, the through-thickness resistance, the resistance of the surface receiving the impact and the resistance of the opposite surface. The directions of resistance measurement are explained in Fig. 10.1. The through-thickness resistance and the oblique resistance are more sensitive than the two surface resistances.
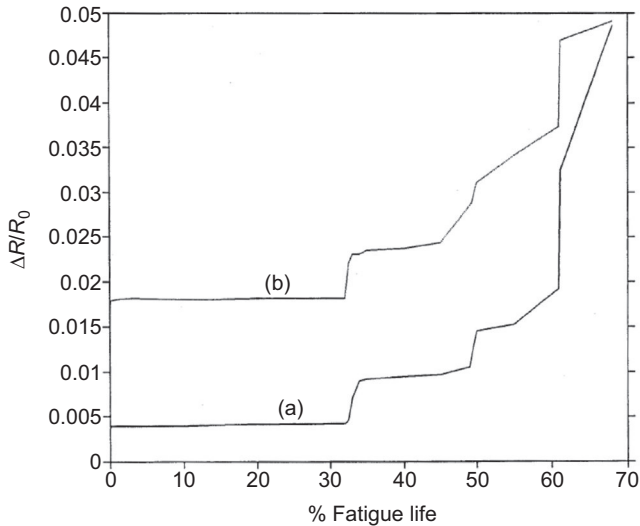
Figure 10.11 Evolution of damage in the form of delamination during tension–tension fatigue, as shown by the through-thickness volume resistance: (a) the minimum value of the fractional change in resistance (relative to the initial resistance) in a stress cycle; and (b) the maximum value of the fractional change in resistance in a stress cycle. Variation of the resistance within a cycle (not shown) is due to the effect of strain rather than that of damage (Wang and Chung, 1998).
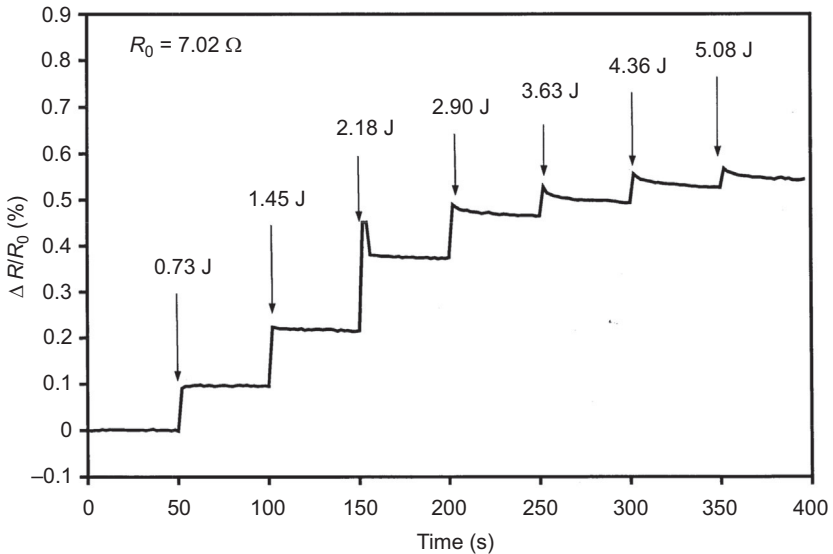
Figure 10.12 Fractional change in oblique resistance (relative to the initial resistance) versus time during impact at progressively increasing energy for a continuous carbon fibre epoxy matrix composite. The *arrows* indicate the times of the impacts (Wang et al., 2005b).

An increase in fibre volume fraction will decrease the resistivity of the composite, thereby affecting the precision of the resistance measurement. However, in a conventional structural composite, the fibre volume fraction is kept high. More significant variables are the fibre lay-up configuration and the thickness (Wang et al., 2005c).

Upon impact, the resistance of the surface receiving the impact in a longitudinal specimen segment including the point of impact increases irreversibly (Wang et al., 2005b, 2006a). However, the surface resistance of each of the two segments that are immediately next to the segment containing the point of impact decreases slightly upon impact damage (Wang et al., 2006a). The latter phenomenon, which is weak and involves the resistance decreasing, is negligible in regions that are not immediately adjacent to the segment containing the point of impact (ie, regions that are more than about 20 mm away from the point of impact).

The trend of the resistance increasing with increasing impact energy is attributed to major damage (such as delamination and fibre fracture), which is encountered by the composite specimen longitudinal segment containing the point of impact. The opposite trend, with the resistance decreasing with increasing impact energy, is relatively weak and is mainly exhibited by the segments adjacent to the segment containing the point of impact; this may be due to several reasons (Wang et al., 2006a). One possible reason relates to the distortion of the current path away from the top surface due to the major damage at the top surface nearby. This distortion can involve the current crossing from one lamina to the adjacent one, since the contact resistivity of the interlaminar interface is limited (Leong et al., 2006). The distortion results in less current at the top surface and hence a decrease of the measured resistance at the top surface. Another possible reason relates to residual stress relief in the segments adjacent to the segment containing the point of impact, due to the damage in the segment containing the point of impact. Yet another reason relates to a microstructural change associated with an irreversible increase in the degree of fibre−fibre contact across the interlaminar interface.

The effectiveness of the 2D electric potential method of impact damage sensing in a quasi-isotropic carbon fibre polymer matrix composite depends on the electrical configuration (ie, the current direction relative to the surface fibres and the electrical contact scheme) (Wang and Chung, 2006a). Oblique current application in any direction provides effective damage sensing, as shown by using electrical contacts on the opposite in-plane surfaces. In-plane current application through the entire cross-section in any direction also provides effective damage sensing, as shown by using electrical contacts that are either on the edge surfaces or in holes through the composite. In-plane surface current application is effective when the current is perpendicular to the surface fibres (due to the low resistivity in the direction of the fibres) and is ineffective when the current is parallel to the surface fibres (due to the high resistivity in the direction perpendicular to the fibres). The oblique configuration is recommended for practical implementation. In general, the potential method is reliable when (1) the resistance between the electric current line and the nearly parallel electric potential gradient line is sufficiently low, as attained when these lines are sufficiently close; and (2) the resistance between the current line and the damage location is sufficiently low, as attained when the distance of separation is sufficiently small.

10.7.5 The interlaminar interface as a sensor

The interlaminar interface is a particularly sensitive impact sensor, as the contact electrical resistivity of this interface decreases irreversibly upon impact at energy as low as 0.8 mJ $(1 \text{ mJ} = 10^{-3} \text{ J})$ (Fig. 10.13) (Wang and Chung, 2005). The irreversible
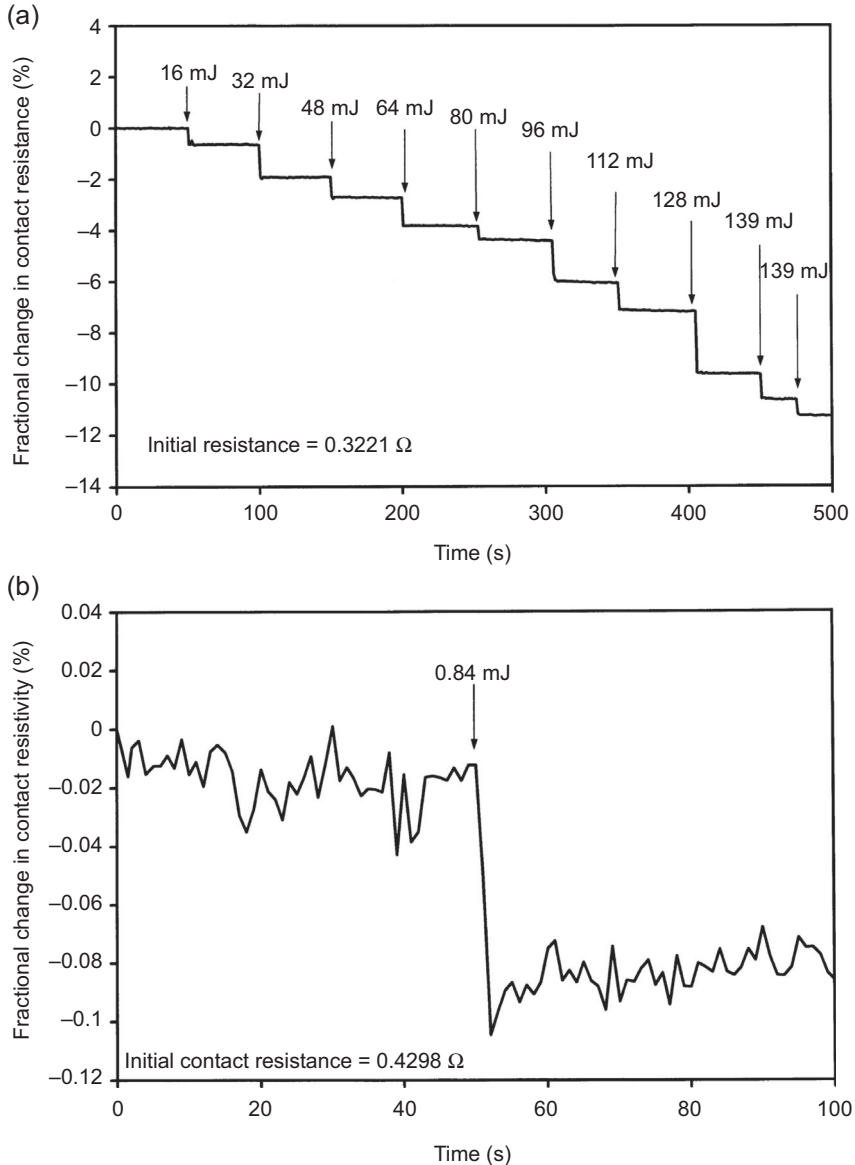
Figure 10.13 The interlaminar interface of a continuous carbon fibre epoxy matrix composite as a sensor of impact damage. (a) During impact at progressively increasing energy from 16 to 139 mJ, the contact resistivity of the interlaminar interface decreases irreversibly. The *arrows* indicate the times of the impacts. (b) During impact at 0.84 mJ (Wang and Chung, 2005).

resistance decrease is in sharp contrast to the irreversible resistance increase observed for the volume resistance (such as the oblique resistance) at much higher impact energies (Fig. 10.12). The irreversible resistance decrease of the interlaminar interface resistivity upon low-energy impact is due to the irreversible increase in the degree of fibre—fibre contact across the interlaminar interface. The effect is consistent with the partially irreversible decrease of the interlaminar interface resistivity upon uniaxial compression in the through-thickness direction, also observed for an epoxy matrix composite (Fig. 10.14(a)) (Wang et al., 2004). This is a microstructural effect rather than an effect associated with well-defined damage such as delamination or fibre breakage. Nevertheless, the microstructural effect can be considered a precursor to damage. The fact that the damage, if any, is very minor is indicated by the absence of even a shallow dent after the low-energy impact. The contact resistivity of the interlaminar interface (Wang et al., 2004) is more sensitive to subtle microstructural changes than the volume resistance in the oblique, through-thickness or longitudinal direction (Wang et al., 2005b).

Although the decrease of the contact resistivity of the interlaminar interface upon uniaxial compression in the direction perpendicular to the interface is partially reversible for a carbon fibre epoxy matrix composite (Fig. 10.14(a)), it is completely reversible for a carbon fibre nylon matrix composite (Fig. 10.14(b)). Nylon is a thermoplastic (relatively compliant), whereas epoxy is a thermoset (less compliant). Since fastening involves compression in the through-thickness direction, this difference between epoxy matrix and nylon matrix composites suggests that the latter is more resistant to fastening-related damage.

Damage due to thermal cycling is sensitively indicated by the contact electrical resistivity of the interlaminar interface. This resistivity increases abruptly upon thermal damage in a thermoset matrix composite (eg, an epoxy matrix composite), but it decreases abruptly upon thermal damage in a thermoplastic matrix composite (Wang et al., 2001). This electrical effect of thermal damage is due to matrix molecular movement in case of the thermoplastic matrix composite, and the absence of matrix molecular movement in case of the thermoset matrix composite.

10.8   Sensing temperature

10.8.1   Applications

Temperature sensing is needed for temperature control and operation control. Real-time temperature sensing is usually required. Temperature sensors are commonly thermistors and thermocouples.

10.8.2   Thermistors

A thermistor is a temperature-measuring device that is based on the notion that the electrical resistivity changes with temperature. Thermistors are commonly semiconductors or metals. For metals, the resistivity increases with increasing temperature;
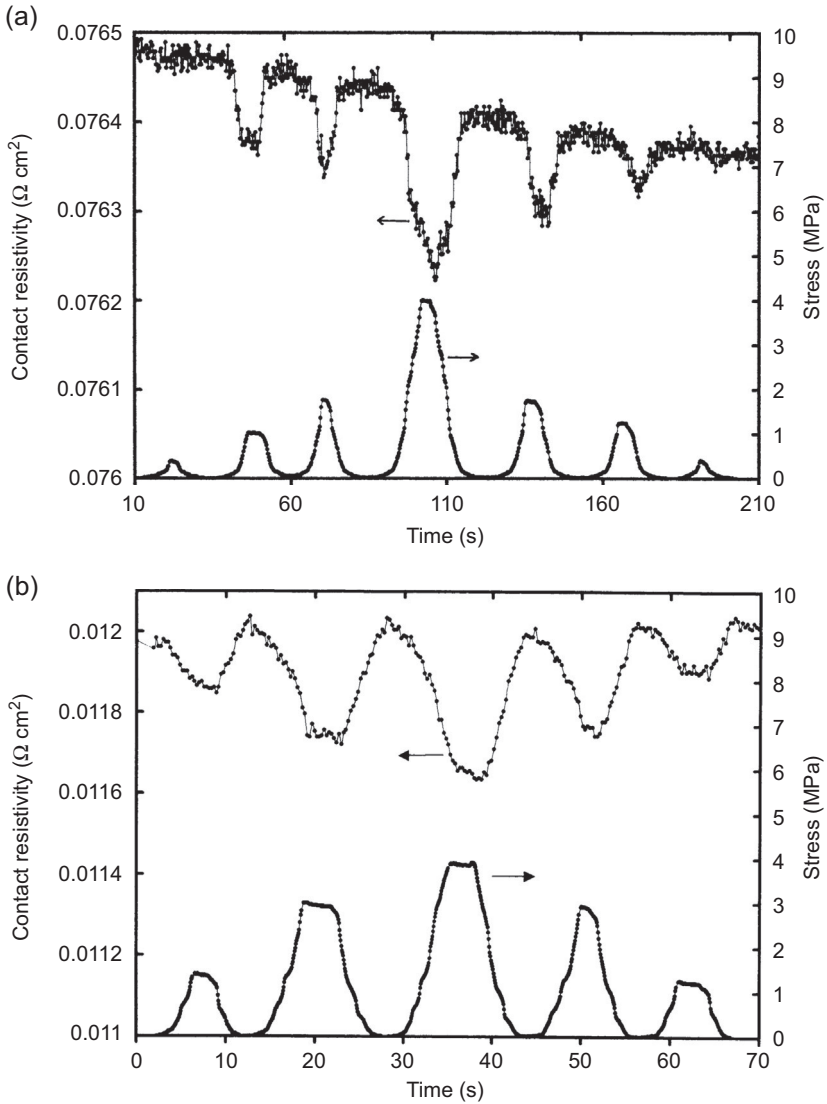
Figure 10.14 Variation of the contact electrical resistivity with time and of the stress with time during compressive stress cycling for the cross-ply interlaminar interface of a continuous carbon fibre epoxy matrix composite at different stress amplitudes up to 4 MPa. The contact resistivity decreases upon compression. (a) Epoxy matrix composite, with the resistivity decrease being partially reversible. (b) Nylon matrix composite, with the resistivity decrease being completely reversible (Wang et al., 2004).

for semiconductors, the resistivity decreases with increasing temperature. Although it is less common, thermistors can be composite materials, such as a composite material with a conductive filler and a less conductive (or nonconductive) matrix. The resistivity of the composite material changes with temperature, due to the change in microstructure with temperature. An example of a thermistor in the form of a composite material is carbon black−filled polymer (Dai et al., 2008; Xu et al., 2006); as the temperature increases, thermal expansion occurs (with the thermal expansion higher for the matrix than the filler), thus causing the extent of contact between filler units to decrease and hence an increase in resistivity of the composite material. Another example of a thermistor in the form of a composite material is the interlaminar interface of a continuous carbon fibre polymer matrix composite (Wang et al., 2004). As the temperature increases, the probability of electrons jumping from one lamina to the adjacent one increases, thus decreasing the electrical resistivity of the interlaminar interface (Fig. 10.15). By using two laminae in a cross-ply configuration (ie, the fibres in the two laminae are perpendicular) and having groups of fibres electrically connected together in each lamina, a 2D array of thermistors and a 2D grid of electrical connections are formed for the purpose of spatially resolved temperature sensing. Yet another example is short carbon fibre−filled cement (Wen et al., 1999), the resistivity of which decreases with increasing temperature due to the increase in the probability of electrons jumping from one fibre to an adjacent fibre in the composite material as the temperature increases.
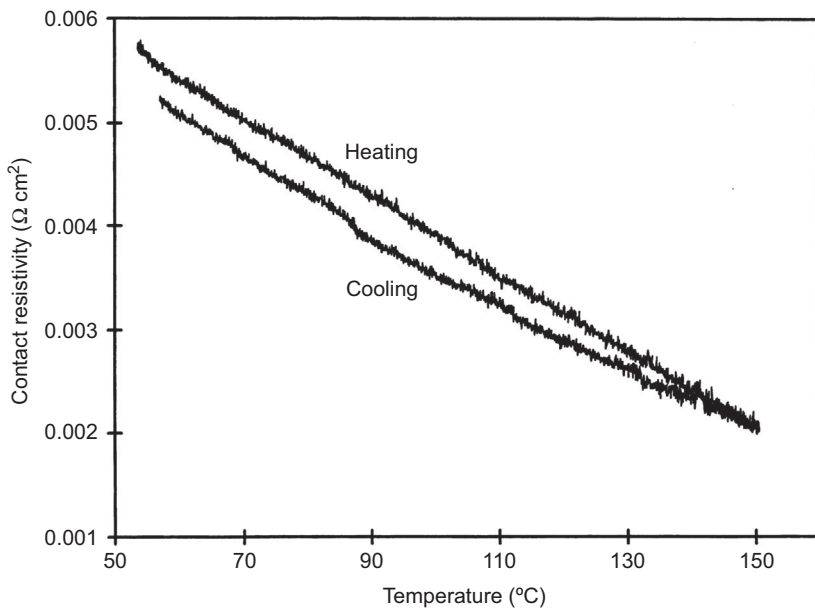
Figure 10.15 Variation of contact electrical resistivity with temperature during heating and cooling at 0.15°C/min for the cross-ply interlaminar interface of a continuous carbon fibre epoxy matrix composite (Wang et al., 2004).

10.8.3 Thermocouples

A thermocouple is a temperature-measuring device based on the Seebeck effect, which is the thermoelectric effect associated with a temperature gradient causing a voltage difference between the hot and cold points of the temperature gradient. The extent of this effect is described by the Seebeck coefficient (also known as the thermoelectric power), which is defined as the voltage difference per unit temperature difference. A thermocouple is in the form of a junction of two materials that are dissimilar in the Seebeck coefficient. In the presence of a temperature difference between the junction and the ends of the two materials away from the junction, each material experiences a voltage difference between its two ends. Due to the difference in Seebeck coefficient between these two materials, the voltage difference differs between the two materials. This results in a voltage difference between the ends of the two materials away from the junction. Thus, by measuring the voltage difference between the ends of the two materials away from the junction, the temperature of the junction can be sensed. The more dissimilar the two materials in the Seebeck coefficient are, the more sensitive the thermocouple is. Thermocouple materials are commonly metals. Although it is less common, a thermocouple can be made from composite materials. An example is a thermocouple junction in the form of a composite material is a junction between dissimilar carbon fibre laminae in a polymer matrix composite (Guerrero et al., 2002). Carbon fibres with different values of the Seebeck coefficient are used. Another example of a thermocouple junction in the form of a composite material is a junction between dissimilar cement matrix composites that are formed by pouring the corresponding dissimilar cement mixes side by side (Guerrero et al., 2002). The dissimilar cement matrix composites can be obtained by using different short conductive fibre fillers, such as carbon fibre for one mix and steel fibre for the other mix.

10.9 Sensing both strain/stress and mechanical damage

The self-sensing of both strain/stress and mechanical damage can be achieved. For example, a reversible change in the electrical resistance is used to indicate strain/stress in the elastic deformation regime, whereas an irreversible change in the resistance is used to indicate damage. A partially reversible change in the resistance indicates the occurrence of both strain and damage. Examples include carbon fibre−filled cement (Wen and Chung, 2006a,c, 2007a) and continuous carbon fibre polymer matrix composites (Wang and Chung, 2006a).

10.10 Sensing both temperature and thermal damage

The self-sensing of both temperature and thermal damage can be achieved. For example, a reversible change in the electrical resistance is used to indicate temperature, whereas an irreversible change in the resistance is used to indicate damage. A partially reversible change in the resistance indicates the occurrence of both temperature

excursion and thermal damage. Examples include continuous carbon fibre polymer matrix composites, which are particularly sensitive when the interlaminar interface is used as the sensor (Fig. 10.16) (Wang et al., 2004).

10.11 Modelling of self-sensing

An analytical model has been provided for the piezoresistive phenomenon of continuous carbon fibre polymer matrix composites under flexure (Zhu and Chung, 2007b). Damage in the form of fibre breakage, fibre–matrix debonding or delamination affects the electrical resistance, as described by a microstructure-based analytical model (Chung and Wang, 2003). The electrical effect of damage in the form of fibre breakage can be modelled by using equivalent circuits (Park et al., 2007; Schueler et al., 2001; Xia et al., 2003). The mechanical effect of damage in the form of fibre breakage can be modelled by using a mechanical network of elastic elements (Xia et al., 2003). The coupling of these electrical and mechanical models results in an analytical electromechanical model (Xia et al., 2003). Another approach involves finite element modelling, which is used to calculate the potential distribution (Angelidis and Irving, 2007) or the resistance change (Todoroki et al., 2005) associated with delamination. Furthermore, finite element modelling can be used to provide sets of data for the learning of artificial neural networks (Todoroki and Ueda, 2006). A related approach that also involves finite element modelling is electrical impedance tomography (Schueler et al., 2001).
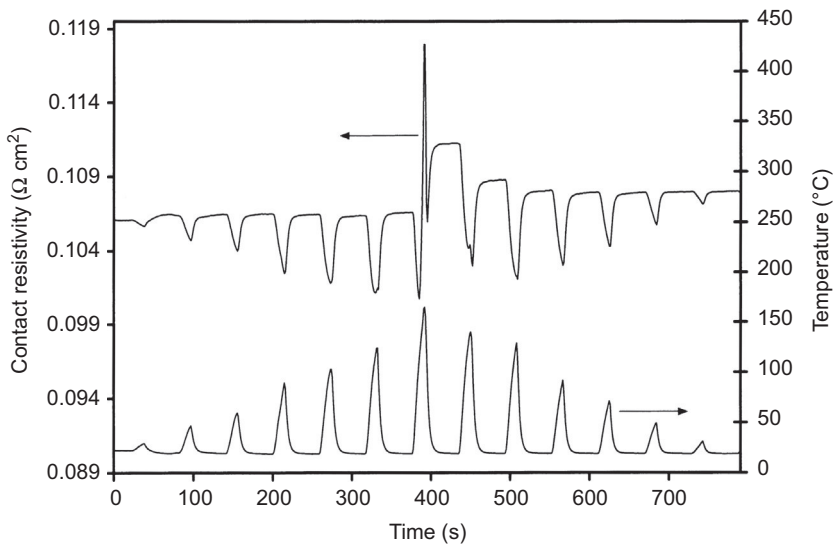
Figure 10.16 The interlaminar interface of a continuous carbon fibre epoxy matrix composite as a sensor of both temperature and thermal damage. During heating in each heating cycle, the contact resistivity of the interlaminar interface decreases, due to the interface serving as a thermistor. At the highest temperature of the hottest cycle, the contact resistivity jumps upward, due to thermal damage (Wang et al., 2004).

10.12   Applications of self-sensing composites in aerospace engineering

With the aging of aircraft, there is an increasing need for monitoring the structural health of aircraft. Timely detection of defects is key to enhancing flight safety. Structural degradation can be associated with fatigue, impact (such as impacts by birds) (Park et al., 2012), abrasion wear by hail and sand (particularly at the leading edges), indents from prop-slung pebbles (particularly on the surfaces under the wings, fuselage and gear) and so on. The monitoring pertains not only to the airframe but also to the repair, such as the bonded repair patches (Baker et al., 2009) and the fastened joints (Olsen and Rimnac, 2007). Self-sensing composites are particularly effective in the detection of minor damage, although they are also effective for detecting major damage. Competing sensing methods tend to be ineffective for the detection of very minor damage.

Structural health monitoring pertains to damage monitoring. Also of importance is the monitoring of strain or stress in the elastic regime in the absence of damage, as it relates to load monitoring and the monitoring of the normal structural operation. Self-sensing composites are particularly effective for strain/stress monitoring.

10.13   Conclusion

Structural composites that are self-sensing due to their electrical resistivity being sensitive to strain and damage include continuous carbon fibre polymer matrix composites, which are widely used for aircraft structures. The measured electrical resistance can be the volume resistance, the surface resistance or the contact resistivity of the interlaminar interface. The four-probe method rather than the two-probe method should be used for the resistance measurement.

Upon fibre fracture, the volume resistance in the fibre direction increases. Upon delamination, the volume resistance in the through-thickness direction increases. The volume resistance in the oblique direction (a direction between the longitudinal and through-thickness directions) is effective for indicating both types of damage.

The surface resistance is particularly valuable for indicating the strain and damage due to flexure, as it can be separately measured on the tension and compression surfaces associated with the flexure. The surface resistance on the tension surface increases upon flexure, due to the decrease in the degree of current penetration; the surface resistance on the compression surface decreases upon flexure, due to the increase in the degree of current penetration.

The interlaminar interface, as described by its contact resistivity, is a particularly effective sensor of the through-thickness stress, temperature, thermal damage and minor mechanical damage (such as impact damage at low energies). By having in the composite two laminae with fibres in different directions and having fibre groups (with the ends of the fibres of a group electrically connected) in each lamina, a 2D array of interlaminar interface sensors (with each sensor being the junction of a fibre group

of one lamina and a fibre group of the adjacent lamina) can be obtained for the purpose of spatially resolved sensing.

By using fibres that are electrically dissimilar (eg, p-type and n-type carbon fibres) in adjacent laminae, the composite can serve as a thermocouple. The thermocouple junction is the interlaminar interface. A 2D array of the interlaminar interface provides spatially resolved temperature sensing.

Glass fibre polymer matrix composites can be rendered self-sensing by the addition of CNTs to the matrix. Alternatively, hybrid composites involving glass fibres and carbon fibres can be self-sensing.

References

Abot, J.L., Song, Y., Vatsavaya, M.S., Medikonda, S., Kier, Z., Jayasinghe, C., Rooy, N., Shanov, V.N., Schulz, M.J., 2010. Delamination detection with carbon nanotube thread in self-sensing composite materials. Composites Science and Technology 70, 1113−1119.

Abry, J.C., Choi, Y.K., Chateauminois, A., Dalloz, B., Giraud, G., Salvia, M., 2001. In-situ monitoring of damage in CFRP laminates by means of AC and DC measurements. Composites Science and Technology 61 (6), 855−864.

Aiyar, A.R., Song, C., Kim, S., Allen, M.G., 2009. An all-polymer airflow sensor using a piezoresistive composite elastomer. Smart Materials and Structures 18, 115002.

Angelidis, N., Irving, P.E., 2007. Detection of impact damage in CFRP laminates by means of electrical potential techniques. Composites Science and Technology 67, 594−604.

Angelidis, N., Khemiri, N., Irving, P.E., 2005. Experimental and finite element study of the electrical potential technique for damage detection in CFRP laminates. Smart Materials and Structures 14, 147−154.

Angelidis, N., Wei, C.Y., Irving, P.E., 2004. The electrical resistance response of continuous carbon fibre composite laminates to mechanical strain. Composites Part A 35, 1135−1147.

Baker, A., Rajic, N., Davis, C., 2009. Towards a practical structural health monitoring technology for patched cracks in aircraft structure. Composites Part A 40A (9), 1340−1352.

Baron, C., Schulte, K., 1988. Determination of electric resistance for in-situ determination of fiber failure in carbon fiber-reinforced plastic composites. Materialpruefung 30 (11−12), 361−366.

Brooks, D., Hayes, S., Khan, N., Zolfaghar, K., Fernando, G.F., 1997. Self-sensing E-glass fiber reinforced composites. Proceedings of SPIE − The International Society for Optical Engineering 3042, 111−119.

Ceysson, O., Salvia, M., Vincent, L., 1996. Damage mechanisms characterisation of carbon fibre/epoxy composite laminates by both electrical resistance measurements and acoustic emission analysis. Scripta Materialia 34 (8), 1273−1280.

Chu, Y.-W., Yum, Y.-J., 2001. Detection of delamination in graphite/epoxy composite by electric potential method. In: Proceedings − KORUS 2001, the 5th Korea-Russia International Symposium on Science and Technology, Section 5 − Mechanics and Automotive Engineering, pp. 240−242.

Chung, D.D.L., 2001. Continuous carbon fiber polymer-matrix composites and their joints, studied by electrical measurements. Polymer Composites 22 (2), 250−270.

Chung, D.D.L., 2002. Piezoresistive cement-based materials for strain sensing. Journal of Intelligent Material Systems and Structures 13 (9), 599−609.

Chung, D.D.L., 2007. Damage detection using self-sensing concepts. Journal of Aerospace Engineering (Proceedings of the Institution of Mechanical Engineers, Part G) 221 (G4), 509−520.

Chung, D.D.L., 2010a. Functional Materials. World Scientific Pub., Singapore.

Chung, D.D.L., 2010b. Composite Materials, second ed. Springer, London.

Chung, D.D.L., Wang, S., 2003. Self-sensing of damage and strain in carbon fiber polymer-matrix structural composites by electrical resistance measurement. Polymers & Polymer Composites 11 (7), 515−525.

Ciselli, P., Lu, L., Busfield, J.J.C., Peijs, T., 2010. Piezoresistive polymer composites based on EPDM and MWNTs for strain sensing applications. e-Polymers 10 (1), 125−137.

Dai, K., Li, Z., Xu, X., 2008. Electrically conductive in situ microfibrillar composite with a selective carbon black distribution: an unusual resistivity−temperature behavior upon cooling. Polymer 49 (4), 1037−1048.

Gao, L., Chou, T., Thostenson, E.T., Zhang, Z., 2010. A comparative study of damage sensing in fiber composites using uniformly and non-uniformly dispersed carbon nanotubes. Carbon 48, 3788−3794.

Guerrero, V.H., Wang, S., Wen, S., Chung, D.D.L., 2002. Thermoelectric property tailoring by composite engineering. Journal of Materials Science 37 (19), 4127−4136.

Han, B., Han, B., Ou, J., 2010b. Novel piezoresistive composite with high sensitivity to stress/strain. Materials Science and Technology 26 (7), 865−870.

Han, B., Yu, X., Kwon, E., 2009. A self-sensing carbon nanotube/cement composite for traffic monitoring. Nanotechnology 20, 445501.

Han, B., Zhang, L., Ou, J., 2010a. Influence of water content on conductivity and piezoresistivity of cement-based material with both carbon fiber and carbon black. Journal of Wuhan University of Technology − Materials Science Edition 25 (1), 147−151.

Hou, T.-C., Lynch, J.P., 2009. Electrical impedance tomographic methods for sensing strain fields and crack damage in cementitious structures. Journal of Intelligent Material Systems and Structures 20, 1363−1379.

Hirano, Y., Todoroki, A., 2007. Damage identification of woven graphite/epoxy composite beams using the electrical resistance change method. Journal of Intelligent Material Systems and Structures 18, 253−263.

Irving, P.E., Thiagarajan, C., 1998. Fatigue damage characterization in carbon fibre composite materials using an electrical potential technique. Smart Materials and Structures 7, 456−466.

Kaddour, A.S., Al-Salehi, A.R., Al-Hassani, S.T.S., Hinton, M.J., 1994. Electrical resistance measurement technique for detecting failure in CFRP materials at high strain rates. Composites Science and Technology 51 (3), 377−385.

Kemp, M., 1994. Self-sensing composites for smart damage detection using electrical properties. Proceedings of SPIE − The International Society for Optical Engineering 2361, 136−139.

Kupke, M., Schulte, K., Schüler, R., 2001. Non-destructive testing of FRP by D.C. and A.C. electrical methods. Composites Science and Technology 61, 837−847.

Leong, C.-K., Chung, D.D.L., 2004. Pressure electrical contact improved by carbon black paste. Journal of Electronic Materials 33 (3), 203−206.

Leong, C.-K., Wang, S., Chung, D.D.L., 2006. Effect of through-thickness compression on the microstructure of carbon fiber polymer-matrix composites, as studied by electrical resistance measurement. Journal of Materials Science 41 (10), 2877−2884.

Li, G., Wang, P., Zhao, X., 2007. Pressure-sensitive properties and microstructure of carbon nanotube reinforced cement composites. Cement and Concrete Composites 29 (5), 377−382.

Luo, X., Chung, D.D.L., 2000. Material contacts under cyclic compression, studied in real time by electrical resistance measurement. Journal of Materials Science 35 (19), 4795−4802.

Loyola, B.R., La Saponara, V., Loh, K.J., Briggs, T.M., O'Bryan, G., Skinner, J.L., 2013. Spatial sensing using electrical impedance tomography. IEEE Sensors Journal 13 (6), 2357−2367.

Masson, L.C., Irving, P.E., 2000. Comparison of experimental and simulation studies of location of impact damage in polymer composites using electrical potential techniques. In: François Gobin, P., Clifford, M.F. (Eds.), Proceedings of SPIE, Fifth European Conference on Smart Structures and Materials, vol. 4073, pp. 182−193.

Matsuzaki, R., Melnykowycz, M., Todoroki, A., 2009. Antenna/sensor multifunctional composites for the wireless detection of damage. Composites Science and Technology 69, 2507−2513.

Matsuzaki, R., Todoroki, A., 2006. Wireless detection of internal delamination cracks in CFRP laminates using oscillating frequency changes. Composites Science and Technology 66, 407−416.

Mei, Z., Guerrero, V.H., Kowalik, D.P., Chung, D.D.L., 2002. Mechanical damage and strain in carbon fiber thermoplastic-matrix composite, sensed by electrical resistivity measurement. Polymer Composites 23 (3), 425−432.

Muto, N., Arai, Y., Shin, S.G., Matsubara, H., Yanagida, H., Sugita, M., Nakatsuji, T., 2001. Hybrid composites with self-diagnosing function for preventing fatal fracture. Composites Science and Technology 61, 875−883.

Nanni, F., Auricchio, F., Sarchi, F., Forte, G., Gusmano, G., 2006. Self-sensing CF-GFRP rods as mechanical reinforcement and sensors of concrete beams. Smart Materials and Structures 15, 182−186.

Olsen, K.W., Rimnac, C.M., 2007. Fatigue crack growth analyses of aerospace threaded fasteners-part III: experimental crack growth behavior. ASTM Special Technical Publication, STP 1487 (Structural Integrity of Fasteners) 17−28.

Park, H., Kong, C., Lee, K., 2012. Investigation on damage tolerance of carbon/epoxy laminate for aircraft structural design. Key Engineering Materials 488−489, 460−463 (Advances in Fracture and Damage Mechanics X).

Park, J.-M., Kwon, D.-J., Wang, Z.-J., DeVries, K.L., 2014. Review of self-sensing of damage and interfacial evaluation using electrical resistance measurements in nano/micro carbon materials-reinforced composites. Advanced Composite Materials. Pages Ahead of Print.

Park, J.-M., Hwang, T.K., Kim, H.G., Doh, Y.D., 2007. Experimental and numerical study of the electrical anisotropy in unidirectional carbon-fiber-reinforced polymer composites. Smart Materials and Structures 16 (1), 57−66.

Prabhakaran, R., 1990. Damage assessment through electrical resistance measurement in graphite fiber-reinforced composites. Experimental Techniques 14 (1), 16−20.

Prasse, T., Michel, F., Mook, G., Schulte, K., Bauhofer, W., 2001. A comparative investigation of electrical resistance and acoustic emission during cyclic loading of CFRP laminates. Composites Science and Technology 61, 831−835.

Schueler, R., Joshi, S.P., Schulte, K., 2001. Damage detection in CFRP by electrical conductivity mapping. Composites Science and Technology 61, 921−930.

Schulte, Z., Baron, C., 1989. Load and failure analyses of CFRP laminates by means of electrical resistivity measurements. Composites Science and Technology 36 (1), 63−76.

Semperlotti, F., Conlon, S.C., Barnard, A.R., 2011. Airframe structural damage detection: a non-linear structural surface intensity based technique. Journal of the Acoustical Society of America 129 (4), EL121−EL127.

Shui, X., Chung, D.D.L., 1997. A new electromechanical effect in discontinuous-filament elastomer-matrix composites. Smart Materials and Structures 6, 102−105.

Singh, Y., 2013. Electrical resistivity measurements: a review. International Journal of Modern Physics: Conference Series 22, 745−756.

Sugita, M., Yanagida, H., Muto, N., 1995. Materials design for self-diagnosis of fracture in CFGFRP composite reinforcement. Smart Materials and Structures 4 (1A), A52−A57.

Todoroki, A., Omagari, K., Shimamura, Y., Kobayashi, H., 2006. Matrix crack detection of CFRP using electrical resistance change with integrated surface probes. Composites Science and Technology 66, 1539−1545.

Todoroki, A., Tanaka, Y., Shimamura, Y., 2004. Multi-prove electric potential change method for delamination monitoring of graphite/epoxy composite plates using normalized response surfaces. Composites Science and Technology 64 (5), 749−758.

Todoroki, A., Tanaka, M., Shimamura, Y., 2005. Electrical resistance change method for monitoring delaminations of CFRP laminates: effect of spacing between electrodes. Composites Science and Technology 65, 37−46.

Todoroki, A., Ueda, M., 2006. Low-cost delamination monitoring of CFRP beams using electrical resistance changes with neural networks. Smart Materials and Structures 15, N75−N84.

Wang, D., Chung, D.D.L., 2006a. Comparative evaluation of the electrical configurations for the two-dimensional electric potential method of damage monitoring in carbon fiber polymer-matrix composite. Smart Materials and Structures 15, 1332−1344.

Wang, S., Chung, D.D.L., 2006b. Self-sensing of flexural strain and damage in carbon fiber polymer-matrix composite by electrical resistance measurement. Carbon 44 (13), 2739−2751.

Wang, D., Chung, D.D.L., 2007a. Through-thickness stress sensing of carbon fiber polymer-matrix composite by electrical resistance measurement. Smart Materials and Structures 16, 1320−1330.

Wang, S., Chung, D.D.L., 2007b. Negative piezoresistivity in continuous carbon fiber epoxy-matrix composite. Journal of Materials Science 42 (13), 4987−4995.

Wang, D., Chung, D.D.L., 2013. Through-thickness piezoresistivity in a carbon fiber polymer-matrix structural composite for electrical-resistance-based through-thickness strain sensing. Carbon 60 (1), 129−138.

Wang, D., Wang, S., Chung, D.D.L., Chung, J.H., 2006c. Comparison of the electrical resistance and potential techniques for the self-sensing of damage in carbon fiber polymer-matrix composites. Journal of Intelligent Material Systems and Structures 17 (10), 853−861.

Wang, D., Wang, S., Chung, D.D.L., Chung, J.H., 2006d. Sensitivity of the two-dimensional electric potential/resistance method for damage monitoring in carbon fiber polymer-matrix composite. Journal of Materials Science 41 (15), 4839−4846.

Wang, P., Ding, T., 2010. Conductivity and piezoresistivity of conductive carbon black filled polymer composite. Journal of Applied Polymer Science 116 (4), 2035−2039.

Wang, S., 2002. Self-sensing Structural Composite Materials (dissertation). State University of New York, Buffalo, NY, USA.

Wang, S., Chung, D.D.L., 2000. Piezoresistivity in continuous carbon fiber polymer-matrix composite. Polymer Composites 21 (1), 13−19.

Wang, S., Chung, D.D.L., 2002. Mechanical damage in carbon fiber polymer-matrix composite, studied by electrical resistance measurement. Composite Interfaces 9 (1), 51−60.

Wang, S., Chung, D.D.L., 2005. The interlaminar interface of a carbon fiber epoxy-matrix composite as an impact sensor. Journal of Materials Science 40, 1863−1867.

Wang, S., Shui, X., Fu, X., Chung, D.D.L., 1998. Early fatigue damage in carbon fiber composites, observed by electrical resistance measurement. Journal of Materials Science 33 (15), 3875−3884.

Wang, X., Fu, X., Chung, D.D.L., 1999. Strain sensing using carbon fiber. Journal of Materials Research 14 (3), 790−802.

Wang, S., Mei, Z., Chung, D.D.L., 2001. Interlaminar damage in carbon fiber polymer-matrix composites, studied by electrical resistance measurement. International Journal of Adhesion and Adhesives 21 (ER6), 465−471.

Wang, S., Chung, D.D.L., Chung, J.H., 2005a. Self-sensing of damage in carbon fiber polymer-matrix composite by measurement of the electrical resistance or potential away from the damaged region. Journal of Materials Science 40, 6463−6472.

Wang, S., Chung, D.D.L., Chung, J.H., 2005b. Impact damage of carbon fiber polymer-matrix composites, monitored by electrical resistance measurement. Composites Part A 36, 1707−1715.

Wang, S., Chung, D.D.L., Chung, J.H., 2005c. Effects of composite lay-up configuration and thickness on the damage self-sensing behavior of carbon fiber polymer-matrix composite. Journal of Materials Science 40 (2), 561−568.

Wang, S., Kowalik, D.P., Chung, D.D.L., 2004. Self-sensing attained in carbon fiber polymer-matrix structural composites by using the interlaminar interface as a sensor. Smart Materials and Structures 13 (3), 570−592.

Wang, S., Wang, D., Chung, D.D.L., Chung, J.H., 2006a. Method of sensing impact damage in carbon fiber polymer-matrix composite by electrical resistance measurement. Journal of Materials Science 41, 2281−2289.

Wang, S., Chung, D.D.L., Chung, J.H., 2006b. Self-sensing of damage in carbon fiber polymer-matrix composite cylinder by electrical resistance measurement. Journal of Intelligent Material Systems and Structures 17 (1), 57−62.

Wang, S., Pang, D.S., Chung, D.D.L., 2007. Hygrothermal stability of electrical contacts made from silver and graphite electrically conductive pastes. Journal of Electronic Materials 36 (1), 65−74.

Wang, X., Chung, D.D.L., 1998. Self-monitoring of fatigue damage and dynamic strain in carbon fiber polymer-matrix composite. Composites Part B 29B (1), 63−73.

Wang, X., Chung, D.D.L., 1999. Fiber breakage in polymer-matrix composite during static and dynamic loading, studied by electrical resistance measurement. Journal of Materials Research 14 (11), 4224−4229.

Wen, S., Chung, D.D.L., 2000. Uniaxial tension in carbon fiber reinforced cement, sensed by electrical resistivity measurement in longitudinal and transverse directions. Cement and Concrete Research 30 (8), 1289−1294.

Wen, S., Chung, D.D.L., 2001a. Uniaxial compression in carbon fiber reinforced cement, sensed by electrical resistivity measurement in longitudinal and transverse directions. Cement and Concrete Research 31 (2), 297−301.

Wen, S., Chung, D.D.L., 2001b. Carbon fiber-reinforced cement as a strain-sensing coating. Cement and Concrete Research 31 (4), 665−667.

Wen, S., Chung, D.D.L., 2003. A comparative study of steel- and carbon-fibre cement as piezoresistive strain sensors. Advances in Cement Research 15 (3), 119−128.

Wen, S., Chung, D.D.L., 2005. Strain sensing characteristics of carbon fiber reinforced cement. ACI Materials Journal 102 (4), 244−248.

Wen, S., Chung, D.D.L., 2006a. Spatially resolved self-sensing of strain and damage in carbon fiber cement. Journal of Materials Science 41 (15), 4823−4831.

Wen, S., Chung, D.D.L., 2006b. Model of piezoresistivity in carbon fiber cement. Cement and Concrete Research 36 (10), 1879−1885.

Wen, S., Chung, D.D.L., 2006c. Self-sensing of flexural damage and strain in carbon fiber reinforced cement and effect of embedded steel reinforcing bars. Carbon 44 (8), 1496−1502.

Wen, S., Chung, D.D.L., 2007a. Piezoresistivity-based strain sensing in carbon fiber reinforced cement. ACI Materials Journal 104 (2), 171−179.

Wen, S., Chung, D.D.L., 2007b. Partial replacement of carbon fiber by carbon black in multi-functional cement-matrix composites. Carbon 45 (3), 505−513.

Wen, S., Wang, S., Chung, D.D.L., 1999. Carbon fiber structural composites as thermistors. Sensors and Actuators A 78, 180−188.

Xia, Z., Okabe, T., Park, J.B., Curtin, W.A., Takeda, N., 2003. Quantitative damage detection in CFRP composites: coupled mechanical and electrical models. Composites Science and Technology 63, 1411−1422.

Xiao, H., Li, H., Ou, J., 2010. Modeling of piezoresistivity of carbon black filled cement-based composites under multi-axial strain. Sensors and Actuators A 160, 87−93.

Xu, X., Li, Z., Dai, K., Yang, M., 2006. Anomalous attenuation of the positive temperature coefficient of resistivity in a carbon-black-filled polymer composite with electrically conductive in situ microfibrils. Applied Physics Letters 89, 032105.

Yoshitake, K., Shiba, K., Suzuki, M., Sugita, M., Okuhara, Y., 2004. Damage evaluation for concrete structures using fiber reinforced composites as self-diagnosis materials. In: Udd, E., Inaudi, D. (Eds.), Smart Structures and Materials 2004: Smart Sensor Technology and Measurement Systems, Proceedings of SPIE (SPIE, Bellingham, WA), vol. 5384, pp. 89−97.

Yu, X., Kwon, E., 2009. A carbon nanotube/cement composite with piezoresistive properties. Smart Materials and Structures 18, 055010.

Zhang, W., Suhr, J., Koratkar, N., 2006. Carbon nanotube/polycarbonate composites as multifunctional strain sensors. Journal for Nanoscience and Nanotechnology 6 (4), 960−964.

Zhu, S., Chung, D.D.L., 2007a. Theory of piezoresistivity for strain sensing in carbon fiber reinforced cement under flexure. Journal of Materials Science 42 (15), 6222−6233.

Zhu, S., Chung, D.D.L., 2007b. Analytical model of piezoresistivity for strain sensing in carbon fiber polymer-matrix structural composite under flexure. Carbon 45 (8), 1606−1613.

Zhu, S., Chung, D.D.L., 2007c. Numerical assessment of the methods of measurement of the electrical resistance in carbon fiber reinforced cement. Smart Materials and Structures 16, 1164−1170.

Self-healing composites for aerospace applications

11

R. Das [1], C. Melchior [2], K.M. Karumbaiah [1]

[1]University of Auckland, Auckland, New Zealand; [2]National Polytechnic Institute of Chemical Engineering and Technology (INP-ENSIACET), Toulouse, France

11.1 Introduction

Metal alloys are being replaced by composite materials in several advanced applications, such as aerospace, automotive, marine and building components, owing to their light weight and high mechanical properties. Hence, developing damage-resistant and durable composite materials is necessary. Certainly, fibre—matrix de-bonding, matrix microcracking and impact damage are major failure modes routinely encountered in the applications of composite materials. Furthermore, deployment and maintenance of composite materials pose a challenge for critical structural parts, such as wings and fins. Hence, advanced materials and methodologies are essential to address these problems. Self-healing technology using composite materials seems to be promising, as it is designed to heal or repair fracture and damage initiation and/or propagation in structures. Self-healing composite materials prevent failure and extend the lifetime of critical structures. Maintenance of structures can be considerably simplified because of these materials, which can trigger an almost auto-repair with some of them not requiring any external intervention to start the healing process.

Self-healing composite materials are capable of auto-repairing upon initiation of damage. The early development concept of healing ability relied on mimicking living organisms, like trees and animals, which motivated research in developing self-healing materials. Self-healing materials and composites have been studied for the past few decades, specifically fuelled by the development of self-healing epoxy resin (White et al., 2002).

Self-healing mechanisms can be divided into two types, extrinsic and intrinsic healing. Extrinsic healing is based on the use of a healing agent as an additional additive, whereas intrinsic healing involves a reversible molecular bond (supramolecular chemistry) in the structure of the material. Additionally, classification can also be made based on the healing method, whether autonomic healing or non-autonomic healing (i.e., with or without external stimulus). Some of the well-known methods of developing self-healing composite materials are inclusions of microcapsules, hollow fibres or a vascular network containing healing agents (Blaiszik et al., 2008). Self-healing can also be thermally activated, using reversible interactions or dissolved thermoplastic polymers. The shape memory effect has also been used to demonstrate self-healing properties.

Self-healing composite materials include polymer matrix composites, ceramic matrix composites (CMCs), metal matrix composites (MMCs) and cementitious composites. Although research on self-healing materials is relatively new, a few commercial self-healing materials, like the Reverlink™ elastomer, are manufactured by Arkema (Cordier et al., 2008), and there are many potential applications of self-healing composites (e.g., resistant fabrics, resealing tires and long-life batteries). Self-healing coatings for corrosion protection or barrier protection have found early commercial applications.

One primary area where self-healing composites may have strong potential and already have found crucial roles is the aerospace sector. In the aerospace industry, self-healing materials have the ability to repair damage that may have occurred during a flight and increase the lifetime of the components. One key advantage of self-healing composite materials is to repair dynamic damage and maintain impact resistance. Self-healing composites can be used in various capacities (e.g., in aerospace structural parts to prevent damage and increase lifetime and also in anticorrosion and barrier coatings).

In this chapter, the primary focus is the self-healing composites that can be used in aerospace applications. Different composite materials, their manufacturing techniques, different types of self-healing concepts and various applications are presented in general and also specifically in the context of the aerospace sector. The self-healing composites can be polymer, ceramic or metal matrix composites. Initially, different self-healing concepts are explained, followed by the classification of self-healing composites. Self-healing approaches, such as microcapsules, hollow fibres, vascular network and intrinsic healing, are described in the subsequent sections. Different types of self-healing composites, such as polymer matrix composites (E-glass−epoxy and carbon fibre−epoxy), CMCs and MMCs, are then discussed. Various properties, like mechanical, corrosion and barrier protection properties, influenced by the self-healing ability of composites are briefed. Finally, applications of self-healing composites, especially in the aerospace industry, are discussed.

11.2 Self-healing concept

A self-healing material has the ability to auto-repair under a 'stimulus' when fracture or damage occurs during in-service operation either accidently or due to ageing. The 'self-healing' concept is inspired by biological systems or living beings and has been widely developed during the last decade (White et al., 2002). Additionally, a limited number of commercial applications, like the self-healing elastomer Reverlink™ (Cordier et al., 2008), have been found to date.

The most general classification of self-healing materials is based on extrinsic or intrinsic healing (Garcia and Fischer, 2014). Other forms of classification are based on autonomic healing and nonautonomic healing (Blaiszik et al., 2010). An autonomic self-healing material does not require any external trigger to initiate the self-healing

process, whereas nonautonomic materials need an external trigger, such as heat or pressure, to heal. Commonly, self-healing approaches include the use of healing agents contained in microcapsules (White et al., 2002), hollow fibres (Pang and Bond, 2005), a mesoporous network (Hamilton et al., 2010) or dissolved thermoplastics. Differences between intrinsic and extrinsic self-healing approaches are discussed in the following sections.

11.2.1 Extrinsic healing

The extrinsic healing process is based on the use of a healing agent contained in the matrix as a separate phase (White et al., 2002). The healing agent is usually in the liquid state, placed in the form of microcapsules or hollow fibres. In most approaches, the healing agent is used with a catalyst, which can also be encapsulated or dissolved in the matrix. When damage occurs, local containers are broken, and the healing agent and catalyst are released, resulting in the healing of cracks, preventing crack growth and fracture failure of the structure.

The main extrinsic healing approaches are:

1. Healing agents are contained in the form of microcapsules, and catalysts are dispersed in the matrix. In a few cases, the healing agent can also react itself; in those cases, there is no need for a catalyst to initiate the process (White et al., 2002).
2. The healing agent is contained in the form of tubes, which is essentially the same as the microcapsules, and only the shape of the container is varied (Pang and Bond, 2005).
3. The mesoporous network contains healing agents or delivers them from an external reservoir, in case of damage (Hamilton et al., 2010).

Fig. 11.1 shows a polymer composite with an encapsulated healing agent and dispersed catalyst. When the material is damaged, the healing agent flows into the crack and repairs the crack with the aid of the catalyst. In the case of hollow fibres, the healing agent is delivered or released into the cracks when damage has occurred. The extrinsic healing concept is based on the response after or at the onset of damage. Furthermore, materials using extrinsic approaches are vulnerable to repeated damage at the same location. Also, healing of structures is not possible once the healing agents are used up or containers become empty. Current research focusses on improvement of healing agents and catalysts, and on new encapsulation techniques that can react without a catalyst when released.

11.2.2 Intrinsic healing

Intrinsic healing is based on specific properties of certain materials, such as molecular structures, chemical or physical bonds. In most cases, intrinsic self-healing requires external stimuli (e.g., high temperatures). But there are few intrinsic self-healing materials which do not require any external stimuli to initiate the process of healing. Three different modes of intrinsic self-healing have been proposed (Zhang and Rong, 2012).
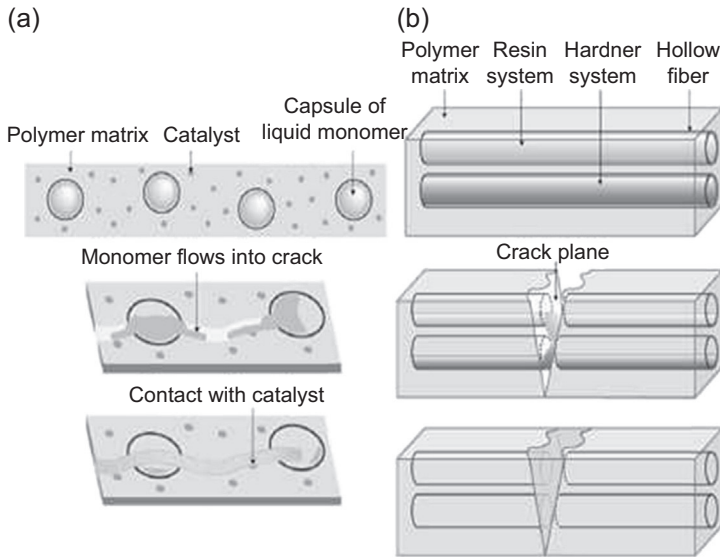
Figure 11.1 Microcapsule and hollow-fibre approaches for self-healing (Kessler, 2008).

Intrinsic self-healing can be achieved by reversible covalent bonds, thermoreversible physical interactions or supramolecular chemistry.

1. Reversible covalent chemistry implies covalent bonds that can dissociate and reassociate under damage. Such reactions mostly include ring-chain equilibrium. One widely studied example is the retro Diels−Alder (rDA) reaction (Fig. 11.2) (Park et al., 2009).
2. Research on thermoreversible physical interactions is extensive and has mainly focussed on ionomers (Varley and van der Zwaag, 2008; García et al., 2011).
3. Supramolecular chemistry is promising and has been one of the first commercial applications of self-healing polymers (Cordier et al., 2008). Reversible supramolecular interactions are low-energy interactions that have an influence on the overall properties of a material, if well designed. Possible avenues of obtaining these interactions are based on hydrogen bonding or metal coordination (Garcia and Fischer, 2014).

Fig. 11.3 shows the general mechanism of intrinsic self-healing. Reversible interactions are represented in red and blue colour. When damage occurs, a crack is formed. Intrinsic self-healing is then achieved by the recovery of the former interactions, with or without an external trigger.
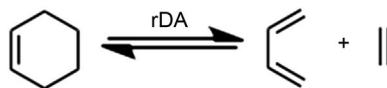
Figure 11.2 Chemical reaction of a rDA reaction (Wikipedia, 2014).
Reproduced from Kessler, M.R., 2008. 22-Self-healing composites. In: Sridharan, S. (Ed.), Delamination Behaviour of Composites. Woodhead Publishing, pp. 650−673; Blaiszik, B.J., et al., 2010. Self-Healing Polymers and Composites. Annual Review of Materials Research 40(1), 179−211.
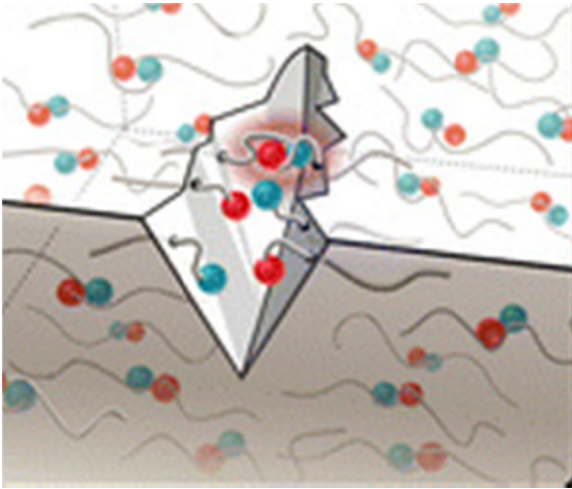
Figure 11.3 Intrinsic self-healing approach (Blaiszik et al., 2010).

11.3 Self-healing approaches

This section describes the various extrinsic and intrinsic self-healing techniques commonly used.

11.3.1 Microcapsules

Capsule-based self-healing is an extrinsic approach of self-healing as the healing agent is embedded in microcapsules. This approach has been widely studied (White et al., 2002; Keller, 2013; Yin et al., 2007).

Microcapsule-based healing consists of embedding a healing agent in microcapsules that break when cracks appear. The healing agent is then released, and crack repairing can be achieved. Commonly, a catalyst is used with the healing agent; it acts as a polymerizer in polymer composites. There are four different approaches followed to use a healing agent and catalyst: (1) The encapsulated liquid agent can be combined with a dispersed catalyst (White et al., 2002), (2) both the healing agent and the catalyst can be embedded in different capsules (Keller, 2013), (3) the healing agent can also directly react with a functionality of the matrix (Yin et al., 2007) under an external stimulus and (d) the healing agent or the catalyst can be placed in the matrix as a separate phase.

Different types of microcapsules have been manufactured and used, usually in epoxy resin matrix composites. Commonly used microcapsules are made of urea−formaldehyde (Blaiszik et al., 2008; Brown et al., 2003; Brown et al., 2004; Guadagno et al., 2010; Yang et al., 2011; Coope et al., 2011). Other types of microcapsules, such as triethylenetetramine (TETA) microcapsules for wear-resistant polymer composites (Khun et al., 2014) and poly(methyl methacrylate) (PMMA) microcapsules with high

storage and thermal stability (Li et al., 2013), have been manufactured and imple-
mented. The size of the microcapsules ranges from 25 to 250 μm. However, some
investigation has also been conducted on nanocapsules (220 nm) (Blaiszik et al.,
2008), and this showed an increase in fracture toughness per volume fraction in com-
parison with larger microcapsules.

Several encapsulation techniques have been used to prepare self-healing materials. The
research has mainly focussed on meltable dispersion, in situ and interfacial encapsulation
techniques. Meltable dispersion is the method of dispersing the healing agent in a melted
polymer to form the capsules after solidification of the polymer (Rule et al., 2005).

In situ and interfacial techniques have been used for urea–formaldehyde (Blaiszik
et al., 2008; Brown et al., 2004; Yang et al., 2011) or TETA (Khun et al., 2014) mi-
crocapsules. In this technique, the shell is developed by polymerization at the interface
of healing agent droplets and the oil-in-water emulsion. The synthesis of nanocapsules
using an ultrasonication technique can also be achieved (Blaiszik et al., 2008). The
general method of healing is demonstrated in Fig. 11.4.

11.3.2 Vascular materials

Self-healing materials that use hollow fibres or a mesoporous network are called
vascular materials (Dry and Sottos, 1993; Williams et al., 2007a,b; Toohey et al.,
2009). The approach used is an extrinsic approach and is similar to the microcapsules
approach, as the healing agent is embedded in fibres or a network of capillaries.
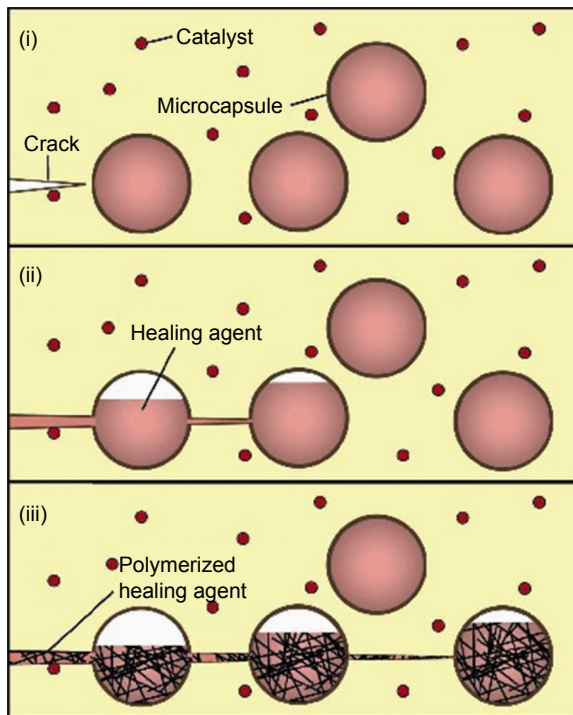
Figure 11.4 Microcapsule-based self-healing process (Garcia and Fischer, 2014).

The healing agents are released when damage occurs. Healing fibres (i.e., hollow fibres with a healing agent) have been manufactured to incorporate in fibre-reinforced polymer (FRP) composite materials, replacing some of the composite fibres. One of the main advantages of fibres over microcapsules is that fibres can be interconnected to form a network. This allows efficient delivery of the healing agent, and additionally these fibres can be networked in a way so that a large area can be healed. However, hollow fibres have a greater influence on the mechanical properties of composites than microcapsules (Fig. 11.5).

Vascular networks can be one- (1D), two- (2D) or three-dimensional (3D) systems. 1D systems were developed by Dry and Sottos (1993) on glass pipettes embedded in epoxy resins. 2D networks are an evolution of 1D systems, and are suitable for the interface between plies in laminated composites (Williams et al., 2007b). 3D systems imitate the vascular systems of living beings and are being developed to extend the lifetime of vascular self-healing composites (Toohey et al., 2009).

There are a couple of approaches to build vascular composite materials (Garcia and Fischer, 2014). The most common approach is the use of individual hollow fibres, which can replace some reinforcement fibres in FRP composite materials (Pang and Bond, 2005). Hollow fibres can be interconnected, thus forming a vascular network (Toohey et al., 2009). A novel type of hollow fibre called 'compartmented fibres' has been developed by Mookhoek et al. (2012). It has the advantages of microcapsule-based and hollow fibre−based self-healing. Indeed, using this type of fibres, a localized healing response can be activated. Another approach similar to the hollow fibre−based vascular networks is the implementation of a mesoporous network (Coope et al., 2014). Fig. 11.5 shows three different possible approaches of hollow fibre−based self-healing materials (from left to right): individual hollow fibres, compartmented fibres and interconnected fibres forming a vascular network.

A variety of techniques can be used to manufacture vascular self-healing materials, with the most common approach being the use of hollow glass fibres filled with an appropriate healing agent. For example, hollow glass fibres were filled with a healing agent containing 5% cobalt octate using the capillary action (Zainuddin et al., 2014).
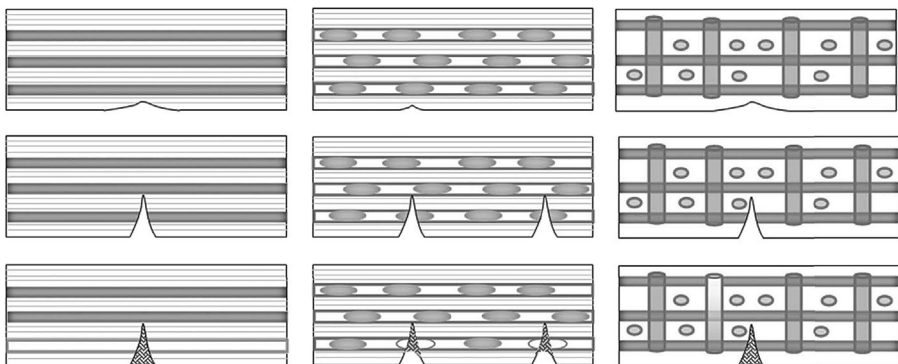
Figure 11.5 Self-healing approaches using hollow fibres (Garcia and Fischer, 2014).

These fibres were then embedded in the matrix by the vacuum-assisted resin transfer moulding (VARTM) process. However, the use of hollow glass fibres is restricted to 1D networks. In order to obtain 2D and 3D interconnected networks, steel wires as thin as 0.5 mm could be used (Coope et al., 2014; Norris et al., 2011a,b).

11.3.3 Dissolved thermoplastics

Self-healing materials based on dispersed thermoplastics use an intrinsic, thermally activated self-healing approach. The thermoplastic polymer is selected for its good compatibility and is dissolved in the polymer matrix, resulting in a homogeneous system. After damage, healing is triggered by a rise in temperature and pressure so that the thermoplastic healing agent can move and fill the cracks (Hayes et al., 2007). Researchers have tested the properties of a self-healing E-glass fibre epoxy composite containing from 5%wt to 20%wt dissolved poly(bisphenol-A-co epichlorohydrin). It has the advantage of being suitable for conventional thermosetting composites. However, there is a need for external pressure to heal the cracks, thus limiting its applications in various fields.

11.3.4 Reversible chemical reactions

Self-healing concepts can be accomplished by reversible chemical reactions due to an external trigger. The aforementioned type of self-healing concept is called an extrinsic self-healing technique, because an external stimulus such as heat or irradiation is needed to trigger the healing.

Several reversible chemical reactions have been explored for self-healing applications. The most extensively studied reactions are the rDA reactions. Fig. 11.6 shows the mechanism of polymerization and repair for DA cross-linked polymers. Chen et al. (2003) demonstrated self-healing properties of furan—maleimide polymers. Bis-maleimide tetrafuran can be used to create a thermally activated self-healing carbon fibre composite, using a DA reaction and electrical resistive heating of carbon fibres (Park et al., 2010). This composite showed nearly 100% strength recovery under certain conditions. The DA reaction was used to recover the fibre—matrix interfacial shear. This was accomplished by grafting maleimide groups in the carbon fibres that
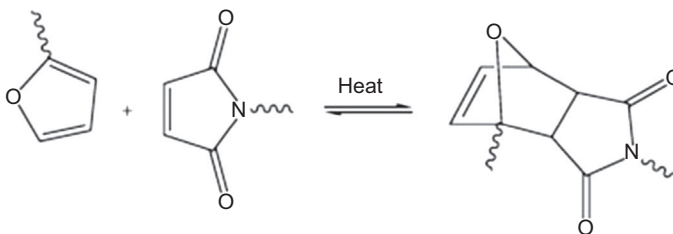
Figure 11.6 Mechanism of the Diels—Alder (DA) reaction for cross-linked polymers (Park et al., 2010).

can bond with the furans groups in the matrix (Fig. 11.7). Heating was achieved using resistivity of carbon fibres (Zhang et al., 2014). Other reversible reactions include hydrazone linkages (Deng et al., 2010) and disulphide exchange reactions (Canadell et al., 2011).

The majority of the self-healing composites that act by reversible chemical reactions still need an external heat source to start the healing process. Another way to induce self-healing is by the application of a strong light irradiation (Froimowicz et al., 2011).

11.3.5 Reversible physical interactions

Self-healing behaviours based on reversible physical interactions have been recently demonstrated. This involved the use of ionomeric polymers, which are polymers containing ionic species, such as metal salts, that can aggregate and form clusters. Owing to the formations of reversible clusters and resulting changes in the mobility of the polymeric network, they can be used in self-healing applications.

The self-healing response of poly(ethylene-comethacrylic acid) copolymers for ballistic applications has been researched (Kalista, 2007). Self-healing was triggered by the impact force. Indeed, clusters relaxations were caused by generated heat. James et al. (2014) worked on self-healing piezoelectric ceramic—polymer composites, containing zirconium titanate ceramic in a Zinc ionomer ethylene methacrylic acid (EMAA) copolymer matrix. The impact behaviour of an EMAA copolymer with
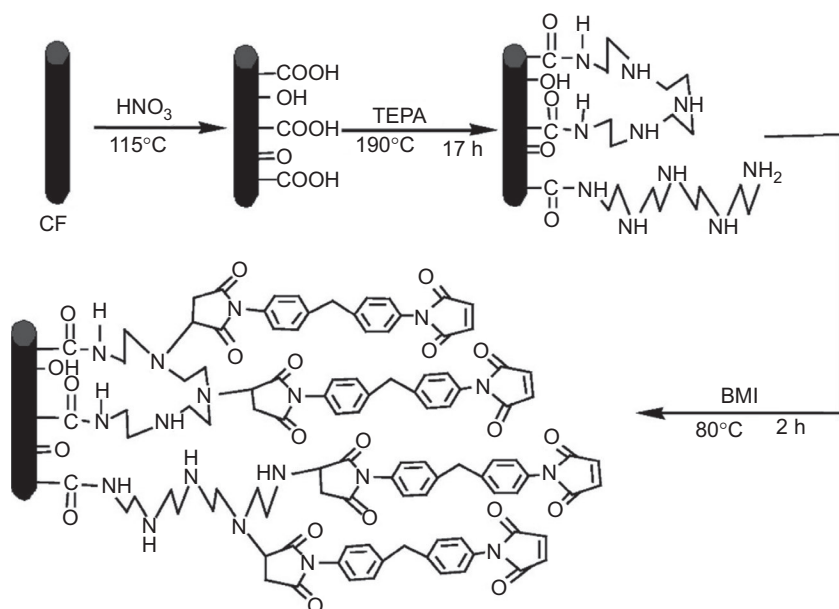
Figure 11.7 Grafting of maleimide groups on a T700-U carbon fibre surface (Zhang et al., 2014).

acid groups neutralized with sodium ions was studied to implement ionomer composites in spacecrafts for debris protection (Francesconi et al., 2013). The material developed using ionomeric polymer has good self-healing abilities and behaved better than aluminium plates under very high-velocity impacts.

11.3.6   Reversible supramolecular interactions

Reversible supramolecular interactions are interactions between molecules that are different from covalent bonds or physical interactions, such as electrostatic interactions. The interaction includes multiple hydrogen bonds, $\pi-\pi$ stacking and metal coordination.

Supramolecular interaction is a promising way to develop intrinsic self-healing composites. They are low energy and reversible, and they can have a great influence on the overall mechanical properties of the material (Fig. 11.8).

A self-healing and thermoreversible rubber from a hydrogen bond supramolecular assembly was developed in Cordier et al. (2008). Molecules forming chains through hydrogen bonding were used. The polymer could be repaired at room temperature and recovered to its initial form and elasticity. A self-healing material based on both covalent bonds and supramolecular interactions was also developed (Roy et al., 2014). Reversible supramolecular interactions were made possible by hydrogen-bonded urea groups, connected by a siloxane-based backbone while imine linkages were used as reversible covalent bonds. Light-induced self-healing properties for a metallo-supramolecular polymer using reversible coordination chemistry were also investigated. Like other intrinsic concepts, most supramolecular systems need an external trigger to heal, like pressure, light or high temperatures.

11.4   Self-healing composite constituent materials

Self-healing properties of materials have been successfully utilized to make self-healing composites. The first studies on self-healing composites were conducted on the polymer (epoxy resins)−based composites. Polymers have a good molecular mobility, which explains why the majority of the research about self-healing materials is still focussed on polymers and polymer composites. However, the interest in self-healing ceramic composites is rapidly growing. Few new concepts of self-healing have recently emerged, and self-healing MMCs appear to be promising for advanced aerospace applications. In this section, different self-healing composite materials are discussed.

11.4.1   Polymer matrix

Research in polymer-based self-healing composites in the past has been mainly focussed on composites made of epoxy matrix (White et al., 2002; Blaiszik et al., 2010; Guadagno et al., 2010; Bond et al., 2008). Recent work in the area has involved self-healing composite materials, where the composite is made of epoxy vinyl ester,
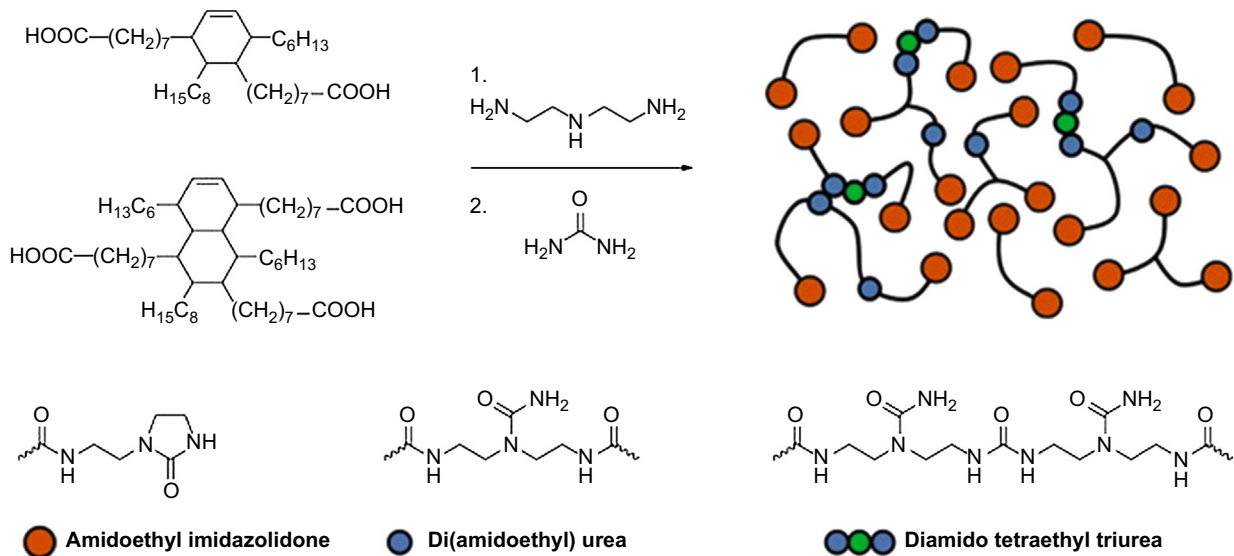
Figure 11.8 Soft (H-bond) elastomer synthesis pathway (self-healing) (de Espinosa et al., 2015).

bismaleimide tetrafuran (2MEP4F), silicones like polydimethylsiloxane (PDMS), cyclopentadiene derivatives or cyanate ester. Raw polymer and diverse composites like E-glass fibre-reinforced composites (FRCs) and carbon FRCs were also investigated. Raw polymers with embedded microcapsules or hollow fibres can also be considered as composites. Composites made of different materials with self-healing behaviours are discussed in this subsection.

11.4.1.1　Glass–epoxy fibre-reinforced polymer composites

E-glass–epoxy FRCs seem to be the first category of composite materials developed with healing capabilities, which followed the development of raw self-healing epoxy resins (White et al., 2002; Brown et al., 2003). E-glass–epoxy composites are widely used because of their light weight, affordable cost and good mechanical properties. Numerous applications for E-glass–epoxy FRC includes boats, sport cars bodies and aircraft components like radomes.

The self-healing nature of E-glass–epoxy FRCs with a dissolved poly(bisphenolA-co-epichlorohydrin) thermoplastic has been investigated (Hayes et al., 2007). The healing phenomenon used was intrinsic, as the thermoplastic polymer used was efficiently dispersed in the Araldyte epoxy matrix. A recovery of up to 70% of the virgin material properties was observed, and the observed delamination area was also reduced. In another work, self-healing woven glass fabric–reinforced epoxy composite laminates were manufactured, containing epoxy microcapsules associated with embedded $CuBr_2$(2-MeIm)4 hardener. The composite showed crack-healing properties after low-velocity impacts (Yin et al., 2008). A temperature of $140°C$ was necessary for the healing to occur. Glass fibre composites with an embedded vascular system have been developed and investigated in Norris et al. (2011a,b). The composite was made of 28-ply unidirectional laminates, and glass fibre–reinforced epoxy with 0.5 mm vascules. The suitable configuration for vascules was found to be aligned in the direction of the glass fibres. Mode I fracture toughness was not lowered by the addition of the vascular network between the composite plies. Coope et al. (2014) demonstrated self-healing for a 28-ply E-glass–epoxy unidirectional plate by incorporating a series of vascules, parallel to the fibre direction. The self-healing agent used was a Lewis acid–catalysed epoxy. This composite revealed good healing efficiency, with good strength and fracture toughness recovery. Embedded hollow glass fibres in a composite made of an SC-15 epoxy matrix reinforced with a woven (0/90) E-glass fabric has been developed (Zainuddin et al., 2014). The composite was fabricated using VARTM, and the hollow glass fibres were filled with unsaturated polyester resin using a catalytic method. The authors reported a significant improvement in the low-velocity impact properties and the filling of the cracks by the healing agent after the impact.

11.4.1.2　Carbon–epoxy fibre-reinforced polymer composites (CFRPs)

CFRPs are another category of self-healing composites that have drawn significant attention since the 2000s. Despite their high cost, this type of composite is now widely

used in advanced aerospace applications, due to the high stiffness and strength-to-weight ratios offered by these composites. Some modern civil aircrafts are now built of more than 50% CFRPs (53% of the Airbus A350XWB is made of CFRPs). Other application areas include automotive and high-end sports goods.

In general, there are fewer studies about carbon−epoxy polymer composites than about glass−epoxy polymer composites. The initial developments of self-healing carbon FRCs were noticed in the early 2000s. Kessler et al. (2003) demonstrated self-healing for a structural carbon fibre-reinforced epoxy matrix composite in 2003. The composite was made of a plain-weave carbon fabric in an EPON 828 epoxy matrix. In this study, autonomic self-healing was achieved by adding dicyclopentadiene healing agent embedded in poly-urea−formaldehyde microcapsules by in situ polymerization. Grubbs' catalyst (which are transition metal carbene complexes that are used as catalysts for olefin metathesis) was dispersed within the matrix. This composite could recover up to 80% of its virgin interlaminar fracture toughness after delamination. Norris et al. (2011b) investigated the best configuration of vascular systems in carbon FRCs. The composite was a laminate, developed of an aerospace-grade unidirectional carbon fibre−reinforced epoxy preimpregnated tape with a $[-45/90/45/0]_{2S}$ sequence. The vascular network was implemented between plies using solder wire preforms. The healing has been found to be efficient when the vascules were located between the plies. Wang et al. studied a carbon fibre−reinforced epoxy matrix composite with poly(ethylene-co-methyl acrylate) (EMA) and poly(ethylene-co-methacrylic acid) (EMAA) patches placed between the plies (Wang et al., 2012). The composite was made from rectangular prepregs. Results showed an improvement in the interlaminar fracture toughness, but a decrease in interlaminar shear strength. Additionally, EMAA has been observed to be a good choice for thermoplastic interlayer patches. Hargou et al. (2013) reported a novel ultrasonic welding method to activate EMAA in composites. The fibre−matrix interface in a carbon fibre−furan-functionalized epoxy matrix composite has been investigated (Zhang et al., 2014). Maleimide groups were grafted to carbon fibres, and the matrix was functionalized with furan groups. Healing was achieved by a thermally activated DA reaction between maleimide and furan groups. An increase in interfacial shear strength in comparison with a carbon fibre−epoxy system has been observed. Electrical resistive heating was used to activate the healing process (Park et al., 2010; Zhang et al., 2014).

11.4.1.3 Other self-healing polymer composites

Epoxy matrix−based self-healing composites have been extensively studied since the 2000s. But other types of polymers with different matrices and/or reinforcements also have been under investigation.

Autonomic self-healing of an epoxy vinyl ester matrix containing microcapsules filled with exo-dicyclopentadiene (DCPD), as well as wax-protected Grubbs' catalyst microspheres, has been investigated by Wilson et al. (2008). The DCPD−Grubbs' system proved to be a good healing agent to fill the cracks in the epoxy vinyl ester matrix. Self-healing was demonstrated to occur rapidly within 2.5 min. Park et al. (2010) synthesized a self-healing composite based on a bismaleimide tetrafuran (2MEP4F)

matrix reinforced with carbon fibres, manufactured by a vacuum-assisted injection moulding method. The lay-up sequence used for the composite was [0/90/0], and the fibre volume fraction was 0.46. In this study, healing was based on a thermally activated DA reaction using resistive heating through the carbon fibres. The work demonstrated good recovery of the strain energy after delamination, but the strength was found to be much lower than that of the virgin composite. Additionally, self-healing could not be achieved after the carbon fibres were fractured. A new poly(dimethyl siloxane) (PDMS) self-healing elastomer was developed and investigated by Keller et al. (2007). The PDMS matrix composite contained encapsulated PDMS resin associated with a separate cross-linker. A recovery of the virgin tear strength of up to 100% was reported. Furthermore, the incorporation of microspheres increases the tear strength of the material. Park et al. (2009) fabricated a two-layered composite panel made of carbon fabric and Mendomer-401, which is a thermally re-mendable cyclopentadiene derivative. The self-healing was achieved by electrical resistive heating via the carbon fabric. The suitable temperature to trigger the healing was determined by a dynamic mechanical thermal analysis. Li et al. studied a composite made of an epoxy matrix (EPON 828) with embedded strain-hardened short shape memory polyurethane (SMPU) fibres and dispersed thermoplastics particles of linear polyester (Li and Zhang, 2013). It was demonstrated that the polymer was able to self-heal wide-open cracks initiated by three-point bending tests. The healing was achieved (around at 80°C) by the combination of thermoplastic particles and the shape memory effect of SMPU.

11.4.2 Ceramic matrix

Ceramics are widely used for high-end technical applications, because of their high melting point, excellent stability and good corrosion resistance. However, such materials also undergo brittle failure, as their resistance to crack propagation is very low. Moreover, these materials are particularly sensitive to thermomechanical stresses. To overcome these problems, CMCs have been developed. CMCs consist of ceramic or metal fibres embedded into a ceramic matrix to improve the mechanical properties, such as fracture toughness, tensile strength and elongation at break.

The most common CMCs are made of a carbon, silicon carbide or aluminium oxide matrix, reinforced with carbon, silicon carbide or aluminium fibres. Different types of CMCs are C−C, C−SiC, SiC−SiC and Al_2O_3−Al_2O_3. Carbon fibre-reinforced carbon (CFRC) composites can be manufactured by gas deposition, pyrolysis, chemical reaction, sintering and electrophoretic deposition. CFRCs are used to manufacture brake discs, combustion chamber components, stator vanes, turbine blades and heat shields.

Ceramic matrix materials mainly deteriorate by oxidation. The most effective way to enhance the lifetime of such materials is, therefore, to stop or reduce oxygen diffusion within the matrix cracks by filling them or generating a protective coating. The matrix composition can be modified to enable the release of a liquid oxide to fill cracks in the case of oxygen diffusion. An example of this is the addition of boron compounds that can form B_2O_4 oxide, which is liquid over 500°C (Lamouroux et al., 1999). Inhibitors like zirconium boride can be incorporated in the matrix to stop or reduce

oxidation of the base material (McKee, 1988). In addition to these methods based on matrix modification, studies have also focussed on the development of self-healing protective coatings for CMC materials. Specifically, rare earth silicates have been used as barrier coatings for SiC—SiC composite materials (Lee et al., 2005).

A SiC—SiC fibre-reinforced ceramic composite with pyrocarbon interfacial coatings and amorphous B_4C contained in the matrix was manufactured by a chemical vapour infiltration process (Quemard et al., 2007). The samples were predamaged by a loading beyond its tensile strength, so as to create cracks in the matrix before exposure to corrosive environments. In this composite material, self-healing was due to the generation of B_2O_3 when oxidation occurs, which was able to seal the cracks, thus preventing the oxygen from further penetrating. It was found that the fibres and interfacial coatings were well protected by the self-healing, boron-containing matrix. Further work by Nualas and Rebillat, (2013) focussed on the oxidation and degradation mechanisms of the B_4C phase and the composite material as a whole. They determined the optimum temperature for self-healing to be 550°C. In another study, Zuo et al. (2012) manufactured and oxidized carbon fibre—reinforced SiC matrix ceramic composites (C—SiC). Si—B—C coatings were implemented in the matrix with the aim of obtaining self-healing behaviour. The composites were shown to have good corrosion resistance above 1000°C due to the matrix self-healing properties. The corrosion resistance of the SiC modified matrix was induced by the formation of B_2O_3 oxide, but also by borosilicate glass that sealed the matrix microcracks. Zhang et al. (2011) worked on the same type of multilayered CMCs. An improvement in the mechanical properties was established when the material was exposed to high temperatures, highlighting self-healing behaviour. Mohanty et al. fabricated Al_2O_3—SiC ceramic composites containing yttrium oxide (Y_2O_3). Microcracks were generated in the matrix using an indentation method (Mohanty et al., 2011). The self-healing property was demonstrated and was reported to be the consequence of SiC oxidation when oxygen penetrated into the cracks. The oxidation occurred under high temperatures and in the presence of additives, like Y_2O_3.

11.4.3 Metal matrix

MMCs are advanced composite materials that consist of a metallic matrix reinforced with different materials. MMCs have good mechanical properties like strength, stiffness and modulus of elasticity, along with relatively low density. However, these composites are generally much more expensive than traditional alloys and polymer matrix composites. As a consequence, their use is limited to a number of high-tech applications, such as aircraft structures, space systems and high-end sports equipment. Specifically, MMCs can be found in disc brake and landing gear components.

In most structural applications, the matrix is made up of a light metal or alloys like aluminium, magnesium or titanium. Reinforcements are usually carbon, boron or silicon carbide fibres. Particles of alumina and silicon carbide can be used so as to obtain isotropic properties.

Fig. 11.9 shows three different ways of achieving self-healing in MMCs. The use of a healing agent, containing capsules and shape memory alloy (SMA) wires, has
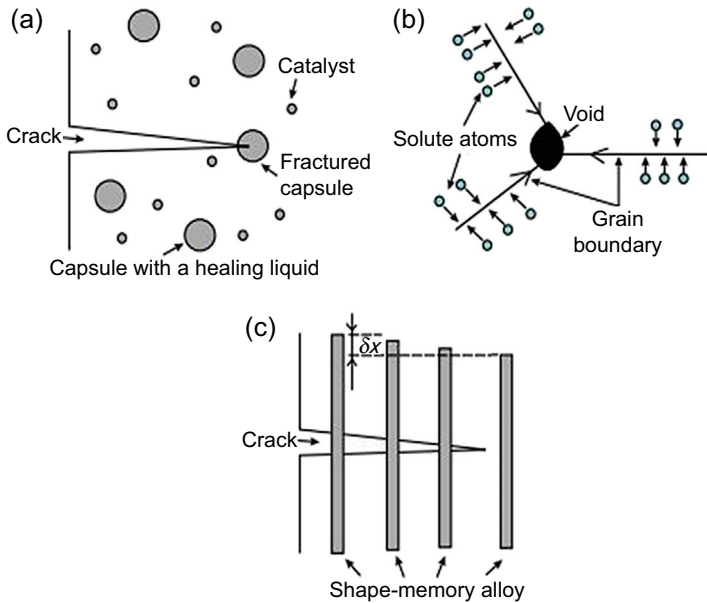
Figure 11.9 Three self-healing approaches for metallic composites (Nosonovsky and Rohatgi, 2012).

been investigated. Another possible approach is the synthesis of an oversaturated solid solution as a matrix. Atoms fill the cracks when damage occurs due to the metastable equilibrium of the solution.

Self-healing MMCs have recently been developed, although the extent of research remains far less than that for polymer matrix composites and CMCs. The studies have generally focussed on the feasibility of different approaches for implementing self-healing properties. Different concepts have been investigated in recent years, including the use of SMA fibres, low-melting point alloy containing hollow reinforcements, a supersaturated solid solution and a eutectic phase embedded in a dendritic structure.

Embedded healing agents, containing hollow reinforcements, can be used to develop a self-healing composite. Specifically, an aluminium alloy reinforced by solder alloy, containing alumina microtubes, was developed (Lucci et al., 2009). Similar to the polymer systems, the healing agents flow and fill the cracks when hollow fibres are damaged by crack propagation. The use of SMA wires in a solder matrix was assessed by Manuel (Manuel, 2007). In this study, TiNi SMA wires were embedded in a Sn-based alloy matrix containing Mg (5.7 at%) and Zn (2.7 at%) in order to obtain a high-strength self-healing MMC. The study revealed that the composite recovered 94% of its virgin tensile strength after damage, and the uniform ductility increased by 160%. To obtain greater strength and healing efficiency, the addition of a eutectic alloy with a dendritic structure at a low melting point was investigated (Nosonovsky and Rohatgi, 2012; Ruzek, 2009). The eutectic phase would melt and heal the cracks when heated, and the dendritic phase would remain solid during the healing process.

The combination of SMA wires with a metal matrix could be useful for novel self-healing metal alloys. The use of an off-eutectic phase has also been investigated (Ruzek, 2009). Off-eutectic systems had the ability to exist in solid and liquid states at the same time in equilibrium conditions. The self-healing approach was the same as eutectic and dendritic systems. The goal was to create a system that can partly melt and heal the cracks while a solid phase maintains the structural integrity of the composite. Another thermodynamic solution to create a self-healing metal composite is the use of supersaturated solid solutions as a matrix (He et al., 2010). In this concept, fatigue or damage-induced microcracks act as nucleation points for the supersaturated alloy. Cracks are therefore filled and healed when precipitation occurs naturally.

In summary, the possibilities of metal matrix self-healing composites appear to be promising, and a number of concepts have been explored to achieve efficient self-healing.

11.5 Functionality recovery in self-healing composites

Extension of service life and easy maintenance of composite structures are the main reasons behind developing self-healing technologies. Indeed, such materials are able to self-repair in case of damage, thus sensibly improving their lifespan. External intervention is not even required in the case of autonomic self-healing materials. But self-healing cannot be perfect, and damage or ageing always leads to a partial loss of the composite mechanical properties. Hence, it is important to estimate the healing efficiency for each material and each self-healing concept. Moreover, it is accepted that only a limited number of repeated damage—healing cycles can be handled by self-healing materials. Even though the properties that can be recovered by self-healing materials are diverse, healing efficiency can as defined as (Blaiszik et al., 2010):

$$\eta = \frac{f\text{healed} - f\text{damaged}}{f\text{virgin} - f\text{damaged}} \qquad [11.1]$$

where f is the property of interest.

Table 11.1 shows several healing efficiency data obtained by researchers for studies on different composite materials with different healing approaches. The properties of interest and the loading conditions are very diverse. Healing efficiency can exceed 100% because healed properties may be better than virgin properties in some cases. Additionally, Fig. 11.10 shows a comparison between pre- and posthealing of a microcrack in Mendomer40—carbon fibres (Park et al., 2009).

11.5.1 Structural integrity recovery

Research on self-healing composite materials mainly has been aimed at recovering structural integrity, rather than focussing on mechanical properties (White et al., 2002). Indeed, loss of structural integrity under service loading is a major threat to

Table 11.1 **Self-healing efficiency of some composite materials (Blaiszik et al., 2010)**

Material	Healing approach	Loading conditions	Property of interest	Healing efficiency (%)	References
Mendomer401−carbon fibres	Reversible DA reaction	Three-point bending	Strain energy	94	Park et al. (2009)
2MEP4F polymer	Reversible DA reaction	Compact tension	Fracture toughness	83	Chen et al. (2003)
Epoxy−E-glass fibres	Microcapsules	Double-cantilever beam	Fracture toughness	60	Kessler and White (2001)
Epoxy−SMA wires	Microcapsules and SMA wires	Tapered double-cantilever beam	Fracture toughness	77	Kirkby et al. (2009)
Epoxy vinyl ester	Microcapsules	Tapered double-cantilever beam	Fracture toughness	30	Wilson et al. (2008)
Epoxy−carbon fibres	Microcapsules	Width-tapered double-cantilever beam	Fracture toughness	80	Kessler et al. (2003)
Epoxy−PCL phase	Meltable phase	Single-edge notched beam	Peak fracture load	>100	Keller et al. (2007)
PDMS	Microcapsules	Tear test	Tear strength	>100	Luo et al. (2009)
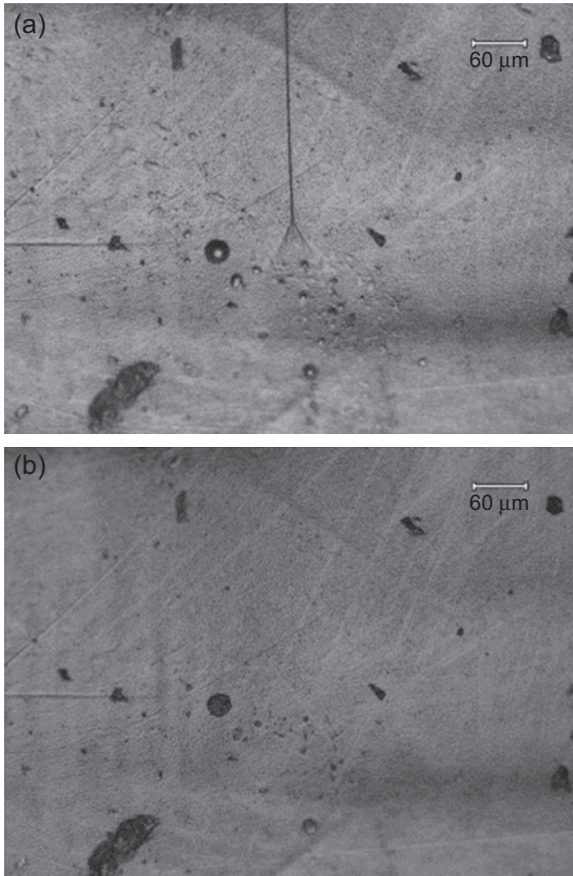
Figure 11.10 Configuration of a crack (a) before and (b) after healing (Park et al., 2009).

composites, since they are made up of different materials that respond differently to thermomechanical loadings. In particular, composite materials are subjected to matrix microcracking, delamination and fibre de-bonding. A number of studies were carried out to assess the healing efficiency on such structural damage.

Matrix microcracking can lead to wide-open cracks and then material failure. Numerous studies have been carried out to assess the efficiency of different self-healing approaches for healing the cracks. DCPD-containing microcapsules were notably used to repair fatigue cracks in epoxy matrix composites (Brown et al., 2005). As a consequence, composite fatigue life was extended by 118−213% in this research. Healing of cracks was also observed for C/Si−B−C CMCs (Zuo et al., 2012). Cracks were found to be efficiently sealed by a borosilicate glass, thus providing the composite with good resistance to oxidation. In another study, dispersed thermoplastic particles were used to heal wide-open cracks (Li and Zhang, 2013). This self-healing process is called close-then-heal, because wide-open cracks are closed

using the shape memory effect of SMPU fibres before healing. The cracks were found to be narrowed by the SMPU fibres and healed effectively. Delamination is another weakness of composites subjected to thermomechanical stresses. Recovery of structural integrity after delamination damage is a serious concern. A number of research studies have been carried out to assess the efficiency of healing on delamination damage. The concepts include the use of dissolved EMAA thermoplastic agent (Pingkarawat et al., 2012), a microvascular network (Trask et al., 2014) and mendable EMAA filaments stitching (Yang et al., 2012). Along with delamination damage, fibre de-bonding is also a potential threat to structural integrity for fibre-reinforced composite materials. Some studies have focussed on preventing or repairing such damage (Blaiszik et al., 2010; Zhang et al., 2014; Carrère and Lamon, 2003).

11.5.2   Mechanical properties recovery

Mechanical properties are the most important properties for aerospace structural materials. As a consequence, it is crucial to know the exact healing efficiency of a self-healing material from the point of view of using it for aerospace applications. Most studies about self-healing materials have focussed on mechanical properties recovery as a way of assessing self-healing efficiency; this is particularly true for fracture toughness recovery. Researchers have also assessed impact strength and fatigue resistance recovery.

11.5.2.1   Fracture property

Fracture toughness recovery can be evaluated through different mechanical tests, such as three-point bend, compact tension, double-cantilever beam, tapered double-cantilever beam and width-tapered double-cantilever beam tests. Depending on the self-healing concepts, the fracture toughness recovery rate may range from 30 to 100%.

A recovery rate of 75% of the fracture load of a microcapsules-containing epoxy resin has been observed (White et al., 2002). However, most researchers prefer fracture toughness recovery rather than peak fracture load recovery to analyse healing efficiency. The microcapsule-based healing technique has been researched and analysed since the 2000s (Mangun et al., 2010; Yuan et al., 2011a,b; Jin et al., 2012; Tripathi et al., 2014). It was demonstrated that fracture toughness recovery was highly dependent on the quantities of healing agent and catalysts utilized. Reversible DA reactions were effectively used in CFRP composites and 2MEP4F polymer systems (Park et al., 2009; Chen et al., 2003). These crosslink polymeric materials proved to heal efficiently, with recovery rates exceeding 80%.

11.5.2.2   Impact property

Impacts present critical hazards to aerospace composite structures, as impact loads can damage composite panels, which can be difficult to detect. Heavy maintenance procedures and nondestructive control methods have been developed to address these issues, but the use of self-healing composite materials could potentially be a simple and

efficient solution. A number of researchers have focussed on damage recovery after impact loading and impact properties recovery after impact. Low velocity, high velocity and repeated impacts were investigated (Zainuddin et al., 2014; Francesconi et al., 2013; Yuan et al., 2011b; Chunlin et al., 2013; Nji and Li, 2012).

Glass fibre−reinforced epoxy laminates, with embedded microcapsules, were exposed to low-velocity impact (Yuan et al., 2011b). Healing efficiency was investigated using a scanning electron microscope to calculate the reduction in damaged areas. It was shown that matrix microcracks were completely healed, and the structural damage was significantly reduced. Under low-velocity impacts, the efficiency of a healing agent, containing hollow fibres embedded in E-glass−epoxy composites, was studied (Zainuddin et al., 2014). Improvements in peak load (53%) and energy to peak load (86%) after a second impact were observed. Investigations were also carried out on high-velocity impacts. A study was carried out to identify whether a self-healing ionomeric polymer could possibly replace aluminium panels for space debris protection (Francesconi et al., 2013). It was found that damage recovery was satisfactory. Conversely, aluminium was found to have a slightly better fragmentation behaviour. Chunlin et al. (2013) manufactured self-healing sandwich composite laminates with an embedded vascular network. Specific stiffness showed good recovery after impact damage, but the composite's skin strength recovery still needed to be improved. The recovery of properties after repeated impact loading was also examined (Nji and Li, 2012). A thermoplastic composite containing shape memory polymer matrix reinforced with a 3D woven glass fibre fabric has been investigated. An automated healing at room temperature was observed after low-velocity impacts (Yuan et al., 2011b).

11.5.2.3 Fatigue property

Although polymers are not extensively used for fatigue-loading applications compared to metallic materials, structural composite materials may exhibit fatigue cracks due to cyclic mechanical loadings. Self-healing materials could be a promising solution to these cases, because these materials can heal cracks, including fatigue cracks, thus extending fatigue life.

The healing of fatigue damage in vascular epoxy composites has been investigated in Hamilton et al. (2012). The material was exposed to high levels of stress, up to 80% of the quasistatic fracture toughness. However, healing was demonstrated to be most efficient for lower loads, because the healing agent could efficiently heal the fatigue cracks. In these conditions, the rate of the crack extension was reduced by more than 80%. Neuser and Michaud (2014) focussed on the fatigue response of an epoxy matrix composite with embedded EPA-containing microcapsules and reinforced by SMA wires. The operating healing mechanism was unique to fatigue loading. EPA solvent arrested crack growth when released, and the composite toughness was improved. Additionally, SMA wires resulted in healing and recovering the structural integrity. In addition to experimental studies, some investigations were aimed at understanding the fatigue life of self-healing composites using phenomenological and physical models (Jones and Dutta, 2010).

11.5.3   Barrier and corrosion protection recovery

Corrosion resistance is a major concern for aircraft parts and especially for those exposed to external conditions. Specifically, metal alloys and polymer composites are used in fuselage parts. Moreover, engine blades and combustion chambers are subjected to very high temperatures and corrosive atmospheres, compounding the issue. A number of studies have focussed on recovering the barrier and corrosion protection properties of both coatings and bulk composite materials using self-healing concepts.

Self-healing coatings aimed at protecting aerospace-grade aluminium alloys from corrosion have been researched (García et al., 2011). The coating is based on silyl esters that react when corrosion damage occurs. Reversible disulphide links were used to recover mechanical properties of a damaged surface (Canadell et al., 2011). Mechanical properties were shown to fully recover, even after numerous healing cycles. Disulphide chemistry could be an advantage to build smart, self-healing polymer coatings. In another study, photo-induced healing was achieved for a dendritic macromonomer, and full cross-links reversibility was demonstrated (Froimowicz et al., 2011). This work paves the way towards developing self-healing aerospace coatings that could be triggered by sunlight, with no need of other external intervention. The use of microcapsules containing coatings was assessed on steel substrates (Yang et al., 2011). Epoxy-filled urea—formaldehyde microcapsules were found to efficiently protect the underlying substrate as the treated samples showed no sign of corrosion, contrary to the control steel samples. TiO_2-containing polymer composite coatings were also investigated (Yabuki et al., 2011). This concept was found to significantly increase the corrosion resistance.

11.6   Applications of self-healing composites

11.6.1   Aerospace applications

11.6.1.1   Engines

Conventional ceramic composites are now widely used in jet engines because of their excellent thermal resistance. However, sensitivity to brittle failure and impact damage reduce ceramic parts' lifespan and reliability. In addition, it is nearly impossible to use ceramic composites in mobile parts, which can be exposed to impacts, such as turbine blades. These parts are usually manufactured with nickel superalloys. But the melting point of nickel prevents engine manufacturers from being able to increase working temperatures, which limits an engine's efficiency. Hence, a number of studies have been carried out recently to assess self-healing CMCs as solutions for fixed and mobile jet engine parts.

Replacing existing ceramic composites with self-healing composites in engine combustion chambers has been attempted. Multilayered, boron-containing matrix composites were investigated as alternatives. The oxidation behaviour of the fibres and the matrix under relatively low temperatures for a SiC(f)/PyC(i)/Si—B—C(m) composite was described (Nualas and Rebillat, 2013). In self-healing ceramic

composites, the healing behaviour was due to the formation of boron oxide (B_2O_3) that can seal the matrix cracks. Investigations were also carried out under higher temperatures of $1000°C$, $1200°C$ and $1350°C$, which can typically be found in an aircraft engine combustion chamber (Liu et al., 2011).

The composite was made of a 2D-C/[SiC—(B—C)] ceramic containing boron and a boron silicon glass phase. Self-healing was achieved when the boron compounds and boron silicon glass were oxidized, which led to the formation of phases that could flow in the matrix cracks and seal them. It was found that the three-point bending strength and tensile strength increased with temperature. These results showed that the specific ceramic composite displayed a self-healing behaviour, and that it could be suited for use in aircraft combustion chambers. The use of boron was further investigated for interfacial pyrocarbon, in addition to the boron-doped matrix, to enhance self-healing properties and corrosion resistance (Fig. 11.11) (Naslain et al., 2004). In particular, a SiC—SiC fibre-reinforced ceramic composite material with a multilayered matrix containing B-doped pyrocarbon layers and B_4C and SiC layers was assessed. Boron-bearing species in the interphase layers and in the matrix itself (pyrocarbon and B_4C) give the composite a self-healing ability resulting from the formation of fluid B_2O_3 under oxidizing conditions. This type of composite is reported to have excellent corrosion resistance under mechanical loads and high temperatures and seems to be suitable for jet engine combustion chambers. Osada et al. (2014) discussed the design of self-healing ceramic composite turbine blades for jet engines. Self-healing technology would allow the use of ceramic turbine blades instead of nickel superalloy turbine blades. Indeed, current ceramic composites are sensitive to impact under external loads that can lead to blade failure. The use of ceramic blades would enable higher working temperatures, thus improving turbines' efficiency. The researchers explored nanocomposites' and multicomposites' self-healing approaches. It was demonstrated that such composites could effectively self-heal under high temperature and low oxygen partial pressure.
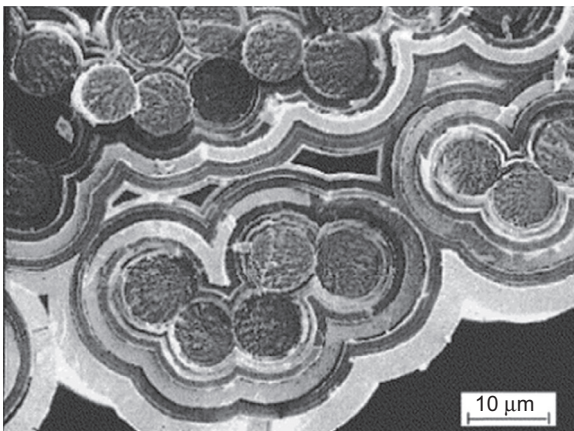
Figure 11.11 Self-healing composite showing matrix deposition around the fibres after healing (Naslain et al., 2004).

11.6.1.2 Fuselage

FRP composites are now widely used for aircraft fuselage, and the latest civil aircrafts (Boeing 787 and Airbus A350) are developed with up to 50% FRP composites by weight. However, current FRP composites are susceptible to damage under impacts, which often leads to heavier designs to meet safety requirements. Additionally, extensive maintenance is needed as impact damage on composites is difficult to detect and assess. Self-healing is one of the most promising approaches to overcome impact load vulnerability and to design low-maintenance, lightweight composite fuselages.

Studies were carried out on self-healing hollow glass fibre—epoxy composites for aerospace structural applications. In particular, a composite prepared by moulding was investigated (Tan et al., 2008). The specimens were damaged by three-point bend impact tests. Postdamage flexural tests showed a strength recovery of up to 47% after healing. The implementation of simple self-healing composites could therefore dramatically improve the resistance of aircraft composite structures to impact damage. However, most aerospace-grade composites are plastics reinforced with carbon fibres. Hence, many studies have focussed on assessing the impact and mechanical properties of carbon—epoxy self-healing composites (Bond et al., 2008; Williams et al., 2007b). In particular, Bond et al. synthesized self-healing carbon fibre—reinforced epoxy laminates to overcome the generally poor impact resistance of fibre-reinforced plastics. Two different studies about the self-healing efficiency of these composites were conducted. Initially, the flexural strength of a damaged 16-ply aerospace-grade composite with embedded 70 and 200 μm hollow glass fibres (HGFs) was investigated ($-45°/90°/45°/0°/$HGF$/-45°/90°/45°/0°/0°/45°/90°/-45°/$ HGF$/0°/45°/90°/-45°$). The results showed a 97% strength recovery after quasistatic indentation damage. The compressive strength after impact on the same composite reported an average recovery of 92% after impact damage and healing. The results revealed that the FRP composites with the healing capability can be extensively and efficiently used in aerospace fuselages as HGF self-healing composites. To improve the impact properties of self-healing polymer composites for aerospace applications, the use of superelastic shape memory NiTi alloy wires in composites with glass fabrics or carbon fabrics was investigated. The glass fabric composite laminate was a glass fibre—reinforced vinyl ester resin with a stacking sequence of $[0°, W, 90°, W, 0°, 90°, 0°]s$. The carbon composite was a vinylester resin reinforced by a carbon fabric with a stacking sequence of $[0°, W, 90°, W, 0°, 90°]s$. SMA-containing composites revealed to have a significantly higher Charpy impact energy in comparison with standard composites. However, damage tolerance of carbon composites under repeated impacts was reduced by the addition of SMA wires. So the use of SMA wires could be a promising way to render better impact resistance to aerospace glass fibre composites, but not necessarily carbon-reinforced composites. Self-healing polymer composites were also assessed as an alternative to metal alloys for protecting space structures from space debris (Francesconi et al., 2013). Particularly, an EMAA copolymer with acid groups neutralized with sodium ions was prepared. The ionomeric polymer showed excellent self-healing abilities under high-velocity impact. Additionally, polymer plates were found to be more

impact-resistant compared to typical aluminium alloy plates, although debris fragmentation properties were slightly better for aluminium plates. As a consequence, ionomeric copolymers could be used for space structure composites, in addition to materials with good fragmentation abilities. In particular, the self-healing ability in spacecraft applications could be of great importance for critical pressurized modules and reservoir-type components.

11.6.1.3 Aerostructures

As FRCs are being increasingly incorporated in aircraft structural parts, it is likely that self-healing composites will be used for such applications. Indeed, self-healing composites have a greater resistance to fatigue, because they can heal microcracks before any crack growth or extension leads to failure. Moreover, their virgin mechanical properties are sometimes higher than those of conventional composites.

A study was conducted to assess the effects of the healing components on the mechanical properties of composites to determine their use in aerospace structural applications (Guadagno et al., 2010). The studied composite was made of a DGEBA epoxy matrix with embedded DCPD-containing urea−formaldehyde microcapsules. The composite's elastic modulus was found to slightly decrease due to the addition of the catalyst in the matrix. However, a good recovery of the virgin mechanical properties after healing was evident. Most aerospace structural composites are epoxy composites. Teoh et al. (2010) carried out research on a self-healing epoxy composite with an embedded healing agent, containing HGFs. The specimens were damaged by indentation and then underwent three-point bend flexural tests. Results showed good strength recovery after healing. The investigation confirmed that self-healing HGF polymer composites could have a strong potential as future materials for aircraft structural parts. Other tests focussed on E-glass−epoxy aerospace-grade composites (Coope et al., 2014; Norris et al., 2011a). Coope et al. demonstrated self-healing for an aerospace-grade E-glass−epoxy plate by incorporating a series of vascular networks parallel to the fibres' direction. As explained in the E-glass−epoxy FRCs section, the self-healing agent was a Lewis acid−catalysed epoxy (Coope et al., 2014). The composite was found to fully recover its virgin mechanical properties. Consequently, self-healing glass−epoxy composites can be effective substitutes for aerospace fibre-reinforced polymer composites, as they have the potential to overcome current limitations. Similarly, Norris et al. (2011a) developed a glass fibre composite using an embedded vascular network to convey healing agents for incorporating self-healing FRP laminates in primary aircraft structures. The results also revealed that the addition of vascules had an insignificant effect on the fracture toughness. As a consequence, vascular self-healing FRP laminates could be a reliable solution to replace existing laminates in aerospace structural applications, besides facilitating maintenance and reducing weight through healing. Carbon fibre−reinforced polymer composites are also used widely for structural applications, especially in military and recent civil aircrafts (Airbus A350XWB and Boeing 787 Dreamliner). A carbon fibre−reinforced polymer matrix composite, combining a shape memory polymer with carbon nanotubes and a $(0°/90°/90°/0°)$ carbon fabric, was manufactured using a high-pressure

moulding process (Liu et al., 2013). The self-healing behaviour was exhibited by the polymer's reversible cross-links that rendered the system's shape memory ability. The composite was found to efficiently heal matrix cracks and regain its structural integrity after the initiation of damage under tension. Additionally, up to 72% of the virgin mechanical properties (peak load) were recovered after healing. In summary, self-healing polymer composites could replace some existing aerospace structural composites, thus enhancing aircraft damage tolerance, service life and safety.

11.6.1.4   Coatings

Coatings and paints are of crucial importance in the aerospace industry, because they protect fuselage and structural parts from external and environmental conditions that can induce corrosion damage. Self-healing coatings appear to be promising as they would automatically recover their protection ability after any damage. Self-healing coatings for protecting aerospace structures from corrosion and minor impacts can be realized with self-healing epoxy resin composites (Yang et al., 2011). Coatings are less critical than structural parts, because their failure usually does not lead to the entire structural failure. Yang et al. (2011) synthesized an epoxy resin composite coating for steel alloys with embedded urea−formaldehyde microcapsules. Microcapsules proved to be suitable for the paint application of the epoxy resin composite as they did not break apart during this step. In addition, the coated steel samples were successfully protected against corrosion even after the coating was damaged and healed.

Coatings for metallic alloys are of importance because aluminium, titanium and magnesium alloys are key materials for both civil and military aircraft and need corrosion protection. Hamdy et al. focussed on self-healing vanadia coatings for aerospace-grade aluminium (Hamdy et al., 2011a,b) and magnesium (Hamdy et al., 2011b; Hamdy and Butt, 2013) alloys, The coating was synthesized by chemical conversion on an AA2024 aluminium alloy. Vanadia coating was found to be satisfactory, especially when prepared from a 10 g/L vanadia solution. Self-healing properties are explained by the formation of a thin vanadia oxide film that prevents oxygen from further penetrating. Vanadia-containing coatings could be a good alternative to chromate coatings for aerospace-grade aluminium and magnesium alloys.

11.6.2   Other applications

Beyond aerospace structures, engines and coatings applications, the development of self-healing composites opens up a vast field of applications in automotive, high-end sports goods and a variety of industries. However, due to their high cost and complexity in manufacturing, self-healing composite materials are likely to be used only for high-tech, critical applications, such as aerospace, the nuclear industry and electronic components.

Much research has been carried out on self-healing ceramics for aircraft engines, but the use of such composites has also been investigated for solid oxide fuel cells, nuclear applications and hot coal combustion conditions (Rebillat, 2014). Self-healing

ceramics could replace existing ceramics because they are less sensitive to brittle failure and have a longer lifespan; however, the cost is a limiting factor.

Predictions of the behaviour of MMCs are complex, because of the expensive tests and cost of production. Moreover, self-healing concepts in metal are relatively new and need more investigations for practical use. However, research has led to some potential opportunities, notably for more sustainable electronic components (Nosonovsky and Rohatgi, 2012).

Self-healing polymer matrix composites can be manufactured easily and are less expensive, compared to self-healing ceramics and metals. Self-healing polymer composites are finding various applications. Notably, a number of organic coatings and paints have been investigated involving self-healing, polymer composites (García et al., 2011). Additionally, coatings for protecting ships and offshore oil platforms from seawater environments also have been researched (Yabuki et al., 2011). The efficiency of self-healing polymer composites has been evaluated for improving the lifetime of organic light-emitting diodes (OLEDs) (Lafont et al., 2012).

11.7 Summary

Self-healing composite materials have been investigated extensively since the 2000s. Numerous concepts have proved to be remarkably efficient in polymer, ceramic and metal matrix composites. These developments could pave the way to several applications, specifically in the field of aerospace. Self-healing can be achieved using healing agents containing microcapsules, vascular networks, dissolved thermoplastics and reversible interactions in polymer matrix composites. Self-healing abilities were also demonstrated for CMCs and MMCs. Self-healing composites are likely to be an important component in aerospace applications, particularly in addressing fatigue and impact resistance problems. Corrosion and barrier properties can also be efficiently recovered after healing. Applications in the aerospace sector include fuselage and aerostructures, engine blades, combustion chambers, anticorrosion coatings, smart paints and impact-resistant space structures.

References

Blaiszik, B.J., Sottos, N.R., White, S.R., 2008. Nanocapsules for self-healing materials. Composites Science and Technology 68 (3−4), 978−986.

Blaiszik, B.J., Kramer, S.L.B., Olugebefola, S.C., Moore, J.S., Sottos, N.R., White, S.R., 2010. Self-healing polymers and composites. Annual Review of Materials Research 40 (1), 179−211.

Brown, E.N., Moore, J.S., White, S.R., Sottos, N.R., 2003. Fracture and fatigue behavior of a self-healing polymer composite. In: Simon, U., et al. (Eds.), Bioinspired Nanoscale Hybrid Systems, pp. 101−106.

Brown, E.N., White, S.R., Sottos, N.R., 2004. Microcapsule induced toughening in a self-healing polymer composite. Journal of Materials Science 39 (5), 1703−1710.

Bond, I.P., Trask, R.S., Williams, H.R., 2008. Self-healing fiber-reinforced polymer composites. MRS Bulletin 33 (08), 770−774.

Brown, E.N., White, S.R., Sottos, N.R., 2005. Retardation and repair of fatigue cracks in a microcapsule toughened epoxy composite—Part II: In situ self-healing. Composites Science and Technology 65 (15−16), 2474−2480.

Cordier, P., Tournilhac, F., Soulie-Ziakovic, C., Leibler, L., 2008. Self-healing and thermor-eversible rubber from supramolecular assembly. Nature 451 (7181), 977−980.

Coope, T.S., Mayer, U.F.J., Wass, D.F., Trask, R.S., Bond, I.P., 2011. Self-healing of an epoxy resin using Scandium(III) triflate as a catalytic curing agent. Advanced Functional Materials 21 (24), 4624−4631.

Coope, T.S., Wass, D.F., Trask, R.S., Bond, I.P., 2014. Metal triflates as catalytic curing agents in self-healing fibre reinforced polymer composite materials. Macromolecular Materials and Engineering 299 (2), 208−218.

Chen, X.X., Wudl, F., Mal, A.K., Shen, H.B., Nutt, S.R., 2003. New thermally remendable highly cross-linked polymeric materials. Macromolecules 36 (6), 1802−1807.

Canadell, J., Goossens, H., Klumperman, B., 2011. Self-healing materials based on disulfide links. Macromolecules 44 (8), 2536−2541.

Carrère, P., Lamon, J., 2003. Creep behaviour of a SiC/Si-B-C composite with a self-healing multilayered matrix. Journal of the European Ceramic Society 23 (7), 1105−1114.

Chunlin, C., Kara, P., Yulong, L., 2013. Self-healing sandwich structures incorporating an interfacial layer with vascular network. Smart Materials and Structures 22 (2), 025031.

Dry, C., Sottos, N.R., 1993. Passive smart self-repair. In: Varadan, V.K. (Ed.), Polymer Matrix Composite-Materials. Smart Materials: Smart Structures and Materials 1993, vol. 1916, pp. 438−444.

Deng, G., Tang, C., Li, F., Jiang, H., Chen, Y., 2010. Covalent cross-linked polymer gels with reversible sol-gel transition and self-healing properties. Macromolecules 43 (3), 1191−1194.

de Espinosa, L.M., Fiore, G.L., Weder, C., Johan Foster, E., Simon, Y.C., 2015. Healable supramolecular polymer solids. Progress in Polymer Science 49−50.

Froimowicz, P., Frey, H., Landfester, K., 2011. Towards the generation of self-healing materials by means of a reversible photo-induced approach. Macromolecular Rapid Communications 32 (5), 468−473.

Francesconi, A., Giacomuzzo, C., Grande, A.M., Mudric, T., Zaccariotto, M., Etemadi, E., 2013. Comparison of self-healing ionomer to aluminium-alloy bumpers for protecting spacecraft equipment from space debris impacts. Advances in Space Research 51 (5), 930−940.

Garcia, S.J., Fischer, H.R., 2014. 9-Self-healing polymer systems: properties, synthesis and applications. In: Aguilar, M.R., Román, J.S. (Eds.), Smart Polymers and Their Applications. Woodhead Publishing, pp. 271−298.

García, S.J., Fischer, H.R., van der Zwaag, S., 2011. A critical appraisal of the potential of self healing polymeric coatings. Progress in Organic Coatings 72 (3), 211−221.

Guadagno, L., Longo, P., Raimondo, M., Naddeo, C., Mariconda, A., Sorrentino, A., 2010. Cure behavior and mechanical properties of structural self-healing epoxy resins. Journal of Polymer Science Part B − Polymer Physics 48 (23), 2413−2423.

Hamilton, A.R., Sottos, N.R., White, S.R., 2010. Self-healing of internal damage in synthetic vascular materials. Advanced Materials 22 (45), 5159.

Hayes, S.A., Jones, F.R., Marshiya, K., Zhang, W., 2007. A self-healing thermosetting composite material. Composites Part A: Applied Science and Manufacturing 38 (4), 1116−1120.

Hargou, K., Pingkarawat, K., Mouritz, A.P., Wang, C.H., 2013. Ultrasonic activation of mendable polymer for self-healing carbon−epoxy laminates. Composites Part B: Engineering 45 (1), 1031−1039.

He, S.M., Van Dijk, N.H., Schut, H., Peekstok, E.R., Van Der Zwaag, S., 2010. Thermally activated precipitation at deformation-induced defects in Fe-Cu and Fe-Cu-B-N alloys studied by positron annihilation spectroscopy. Physical Review B − Condensed Matter and Materials Physics 81 (9).

Hamilton, A.R., Sottos, N.R., White, S.R., 2012. Mitigation of fatigue damage in self-healing vascular materials. Polymer 53 (24), 5575−5581.

Hamdy, A.S., Doench, I., Möhwald, H., 2011a. Intelligent self-healing corrosion resistant vanadia coating for AA2024. Thin Solid Films 520 (5), 1668−1678.

Hamdy, A.S., Doench, I., Möhwald, H., 2011b. Smart self-healing anti-corrosion vanadia coating for magnesium alloys. Progress in Organic Coatings 72 (3), 387−393.

Hamdy, A.S., Butt, D.P., 2013. Novel smart stannate based coatings of self-healing functionality for AZ91D magnesium alloy. Electrochimica Acta 97, 296−303.

James, N.K., Lafont, U., van der Zwaag, S., Groen, W.A., 2014. Piezoelectric and mechanical properties of fatigue resistant, self-healing PZT-ionomer composites. Smart Materials and Structures 23 (5).

Jin, H., et al., 2012. Self-healing thermoset using encapsulated epoxy-amine healing chemistry. Polymer 53 (2), 581−587.

Jones, A.S., Dutta, H., 2010. Fatigue life modeling of self-healing polymer systems. Mechanics of Materials 42 (4), 481−490.

Kessler, M.R., 2008. 22-Self-healing composites. In: Sridharan, S. (Ed.), Delamination Behaviour of Composites. Woodhead Publishing, pp. 650−673.

Keller, M.W., 2013. Encapsulation-based self-healing polymers and composites. In: Hayes, W., Greenland, B.W. (Eds.), Healable Polymer Systems, pp. 16−61.

Khun, N.W., Sun, D.W., Huang, M.X., Yang, J.L., Yue, C.Y., 2014. Wear resistant epoxy composites with diisocyanate-based self-healing functionality. Wear 313 (1−2), 19−28.

Kalista Jr., S.J., 2007. Self-healing of poly(ethylene-co-methacrylic acid) copolymers following projectile puncture. Mechanics of Advanced Materials and Structures 14 (5), 391−397.

Kessler, M.R., Sottos, N.R., White, S.R., 2003. Self-healing structural composite materials. Composites Part A: Applied Science and Manufacturing 34 (8), 743−753.

Keller, M.W., White, S.R., Sottos, N.R., 2007. A self-healing poly(dimethyl siloxane) elastomer. Advanced Functional Materials 17 (14), 2399−2404.

Kessler, M.R., White, S.R., 2001. Self-activated healing of delamination damage in woven composites. Composites Part A: Applied Science and Manufacturing 32 (5), 683−699.

Kirkby, E.L., Michaud, V.J., Månson, J.A.E., Sottos, N.R., White, S.R., 2009. Performance of self-healing epoxy with microencapsulated healing agent and shape memory alloy wires. Polymer 50 (23), 5533−5538.

Lamouroux, F., Bertrand, S., Pailler, R., Naslain, R., Cataldi, M., 1999. Oxidation-resistant carbon-fiber-reinforced ceramic-matrix composites. Composites Science and Technology 59 (7), 1073−1085.

Lee, K.N., Fox, D.S., Bansal, N.P., 2005. Rare earth silicate environmental barrier coatings for SiC/SiC composites and Si3N4 ceramics. Journal of the European Ceramic Society 25 (10), 1705−1715.

Li, Q., Mishra, A.K., Kim, N.H., Kuila, T., Lau, K.-T., Lee, J.H., 2013. Effects of processing conditions of poly(methylmethacrylate) encapsulated liquid curing agent on the properties of self-healing composites. Composites Part B: Engineering 49, 6−15.

Li, G., Zhang, P., 2013. A self-healing particulate composite reinforced with strain hardened short shape memory polymer fibers. Polymer 54 (18), 5075−5086.

Lucci, J.M., Amano, R.S., Rohatgi, P., Schultz, B., Asme, 2009. Experiment and computational analysis of self-healing. In: An Aluminum Alloy. Imece 2008: Heat Transfer, Fluid Flows, and Thermal Systems, vol. 10 (Pts A−C), pp. 1759−1768.

Luo, X., Ou, R., Eberly, D.E., Singhal, A., Viratyaporn, W., Mather, P.T., 2009. A thermoplastic/thermoset blend exhibiting thermal mending and reversible adhesion. ACS Applied Materials & Interfaces 1 (3), 612−620.

Liu, G.-H., Cheng, L.-F., Luan, X.-G., Liu, Y.-S., 2011. Self-healing behavior of 2D-C/SiC-(B-C) composite in aero-engine combustion chamber. Journal of Inorganic Materials 26 (9), 969−973.

Liu, Y., Rajadas, A., Chattopadhyay, A., 2013. Self-healing nanocomposite using shape memory polymer and carbon nanotubes. In: Proceedings of SPIE − The International Society for Optical Engineering.

Lafont, U., van Zeijl, H., van der Zwaag, S., 2012. Increasing the reliability of solid state lighting systems via self-healing approaches: a review. Microelectronics Reliability 52 (1), 71−89.

Mookhoek, S.D., Fischer, H.R., van der Zwaag, S., 2012. Alginate fibres containing discrete liquid filled vacuoles for controlled delivery of healing agents in fibre reinforced composites. Composites Part A: Applied Science and Manufacturing 43 (12), 2176−2182.

McKee, D.W., 1988. Oxidation behavior of matrix-inhibited carbon carbon composites. Carbon 26 (5), 659−664.

Mohanty, D., Sil, A., Maiti, K., 2011. Development of input output relationships for self-healing Al_2O_3/SiC ceramic composites with Y_2O_3 additive using design of experiments. Ceramics International 37 (6), 1985−1992.

Manuel, M.V., 2007. Design of a Biomimetic Self-healing Alloy Composite. Northwestern University, Ann Arbor, p. 184.

Mangun, C.L., Mader, A.C., Sottos, N.R., White, S.R., 2010. Self-healing of a high temperature cured epoxy using poly(dimethylsiloxane) chemistry. Polymer 51 (18), 4063−4068.

Norris, C.J., Bond, I.P., Trask, R.S., 2011a. Interactions between propagating cracks and bio-inspired self-healing vascules embedded in glass fibre reinforced composites. Composites Science and Technology 71 (6), 847−853.

Norris, C.J., Bond, I.P., Trask, R.S., 2011b. The role of embedded bioinspired vasculature on damage formation in self-healing carbon fibre reinforced composites. Composites Part A: Applied Science and Manufacturing 42 (6), 639−648.

Nualas, F., Rebillat, F., 2013. A multi-scale approach of degradation mechanisms inside a SiC(f)/Si-B-C(m) based self-healing matrix composite in a dry oxidizing environment. Oxidation of Metals 80 (3−4), 279−287.

Nosonovsky, M., Rohatgi, P.K., 2012. Development of metallic and metal matrix composite self-healing materials. In: Biomimetics in Materials Science: Self-Healing, Self-Lubricating, and Self-Cleaning Materials, 152, pp. 87−122.

Nji, J., Li, G.Q., 2012. A smart polymer composite for repeatedly self-healing impact damage in fiber reinforced polymer (Frp) vessels. In: Duncan, A.J. (Ed.), Proceedings of the Asme Pressure Vessels and Piping Conference, Pvp 2011, vol. 6 (Part A and B), pp. 1221−1227.

Neuser, S., Michaud, V., 2014. Fatigue response of solvent-based self-healing smart materials. Experimental Mechanics 54 (2), 293−304.

Naslain, R., Guette, A., Rebillat, F., Pailler, R., Langlais, F., Bourrat, X., 2004. Boron-bearing species in ceramic matrix composites for long-term aerospace applications. Journal of Solid State Chemistry 177 (2), 449−456.

Osada, T., Nakao, W., Takahashi, K., Ando, K., 2014. 17-Self-crack-healing behavior in ceramic matrix composites. In: Low, I.M. (Ed.), Advances in Ceramic Matrix Composites. Woodhead Publishing, pp. 410−441.

Pang, J.W.C., Bond, I.P., 2005. A hollow fibre reinforced polymer composite encompassing self-healing and enhanced damage visibility. Composites Science and Technology 65 (11−12), 1791−1799.

Park, J.S., Kim, H.S., Hahn, H.T., 2009. Healing behavior of a matrix crack on a carbon fiber/mendomer composite. Composites Science and Technology 69 (7−8), 1082−1087.

Park, J.S., Darlington, T., Starr, A.F., Takahashi, K., Riendeau, J., Thomas Hahn, H., 2010. Multiple healing effect of thermally activated self-healing composites based on Diels−Alder reaction. Composites Science and Technology 70 (15), 2154−2159.

Pingkarawat, K., Wang, C.H., Varley, R.J., Mouritz, A.P., 2012. Self-healing of delamination cracks in mendable epoxy matrix laminates using poly[ethylene-co-(methacrylic acid)] thermoplastic. Composites Part A: Applied Science and Manufacturing 43 (8), 1301−1307.

Quemard, L., Rebillat, F., Guette, A., Tawil, H., Louchet-Pouillerie, C., 2007. Self-healing mechanisms of a SiC fiber reinforced multi-layered ceramic matrix composite in high pressure steam environments. Journal of the European Ceramic Society 27 (4), 2085−2094.

Rule, J.D., Brown, E.N., Sottos, N.R., White, S.R., Moore, J.S., 2005. Wax-protected catalyst microspheres for efficient self-healing materials. Advanced Materials 17 (2), 205.

Roy, N., Buhler, E., Lehn, J.-M., 2014. Double dynamic self-healing polymers: supramolecular and covalent dynamic polymers based on the bis-iminocarbohydrazide motif. Polymer International 63 (8), 1400−1405.

Ruzek, A.C., 2009. Synthesis and Characterization of Metallic Systems with Potential for Self-healing. University of Wisconsin-Milwaukee.

Rebillat, F., 2014. 16-Advances in self-healing ceramic matrix composites. In: Low, I.M. (Ed.), Advances in Ceramic Matrix Composites. Woodhead Publishing, pp. 369−409.

Toohey, K.S., Hansen, C.J., Lewis, J.A., White, S.R., Sottos, N.R., 2009. Delivery of two-Part Self-healing chemistry via microvascular networks. Advanced Functional Materials 19 (9), 1399−1405.

Trask, R.S., Norris, C.J., Bond, I.P., 2014. Stimuli-triggered self-healing functionality in advanced fibre-reinforced composites. Journal of Intelligent Material Systems and Structures 25 (1), 87−97.

Tripathi, M., Rahamtullah, Kumar, D., Rajagopal, C., Roy, P.K., 2014. Influence of microcapsule shell material on the mechanical behavior of epoxy composites for self-healing applications. Journal of Applied Polymer Science 131 (15), 40572.

Tan, W.C.K., Kiew, J.C., Siow, K.Y., Sim, Z.R., Poh, H.S., Taufiq, M.D., 2008. Self healing of epoxy composite for aircraft's structural applications. In: Diffusion and Defect Data Part. B: Solid State Phenomena, pp. 39−44.

Teoh, S.H., Chia, H.Y., Lee, M.S., Nasyitah, A.J.N., Luqman, H.B.S.M., Nurhidayah, S., 2010. Self healing composite for aircraft's structural application. International Journal of Modern Physics B 24 (1−2), 157−163.

Varley, R.J., van der Zwaag, S., 2008. Towards an understanding of thermally activated self-healing of an ionomer system during ballistic penetration. Acta Materialia 56 (19), 5737−5750.

White, S.R., Sottos, N.R., Geubelle, P.H., Moore, J.S., Kessler, M.R., Sriram, S.R., 2002. Autonomic healing of polymer composites (vol 409, pg 794, 2001). Nature 415 (6873), 817.

Wikipedia, 2014. Retro-Diels−Alder Reaction, Wikipedia, the Free Encyclopedia. Available from: https://en.wikipedia.org/w/index.php?title=Retro-Diels%E2%80%93Alder_reaction&oldid=632353668.

Williams, H.R., Trask, R.S., Bond, I.P., 2007a. Self-healing composite sandwich structures. Smart Materials and Structures 16 (4), 1198.

Williams, G., Trask, R., Bond, I., 2007b. A self-healing carbon fibre reinforced polymer for aerospace applications. Composites Part A: Applied Science and Manufacturing 38 (6), 1525−1532.

Wang, C.H., Sidhu, K., Yang, T., Zhang, J., Shanks, R., 2012. Interlayer self-healing and toughening of carbon fibre/epoxy composites using copolymer films. Composites Part A: Applied Science and Manufacturing 43 (3), 512−518.

Wilson, G.O., Moore, J.S., White, S.R., Sottos, N.R., Andersson, H.M., 2008. Autonomic healing of epoxy vinyl esters via ring opening metathesis polymerization. Advanced Functional Materials 18 (1), 44−52.

Yin, T., Rong, M.Z., Zhang, M.Q., Yang, G.C., 2007. Self-healing epoxy composites − preparation and effect of the healant consisting of microencapsulated epoxy and latent curing agent. Composites Science and Technology 67 (2), 201−212.

Yang, Z., Wei, Z., Le-ping, L., Hong-mei, W., Wu-jun, L., 2011. The self-healing composite anticorrosion coating. Physics Procedia 18, 216−221.

Yin, T., Rong, M.Z., Wu, J., Chen, H., Zhang, M.Q., 2008. Healing of impact damage in woven glass fabric reinforced epoxy composites. Composites Part A: Applied Science and Manufacturing 39 (9), 1479−1487.

Yang, T., Wang, C.H., Zhang, J., He, S., Mouritz, A.P., 2012. Toughening and self-healing of epoxy matrix laminates using mendable polymer stitching. Composites Science and Technology 72 (12), 1396−1401.

Yuan, Y.C., Ye, X.J., Rong, M.Z., Zhang, M.Q., Yang, G.C., Zhao, J.Q., 2011a. Self-healing epoxy composite with heat-resistant healant. ACS Applied Materials & Interfaces 3 (11), 4487−4495.

Yuan, Y.C., Ye, Y., Rong, M.Z., Chen, H., Wu, J., Zhang, M.Q., 2011b. Self-healing of low-velocity impact damage in glass fabric/epoxy composites using an epoxy-mercaptan healing agent. Smart Materials & Structures 20 (1).

Yabuki, A., Urushihara, W., Kinugasa, J., Sugano, K., 2011. Self-healing properties of TiO_2 particle-polymer composite coatings for protection of aluminum alloys against corrosion in seawater. Materials and Corrosion-Werkstoffe Und Korrosion 62 (10), 907−912.

Zhang, M., Rong, M., 2012. Design and synthesis of self-healing polymers. Science China-Chemistry 55 (5), 648−676.

Zainuddin, S., Arefin, T., Fahim, A., Hosur, M.V., Tyson, J.D., Kumar, A., 2014. Recovery and improvement in low-velocity impact properties of e-glass/epoxy composites through novel self-healing technique. Composite Structures 108, 277−286.

Zhang, W., Duchet, J., Gérard, J.F., 2014. Self-healable interfaces based on thermo-reversible Diels−Alder reactions in carbon fiber reinforced composites. Journal of Colloid and Interface Science 430, 61−68.

Zuo, X., Zhang, L., Liu, Y., Cheng, L., Xia, Y., 2012. Oxidation behaviour of two-dimensional C/SiC modified with self-healing Si−B−C coating in static air. Corrosion Science 65, 87−93.

Zhang, C., Qiao, S., Yan, K., Liu, Y., Wu, Q., Han, D., 2011. Mechanical properties of a carbon fiber reinforced self-healing multilayered matrix composite at elevated temperatures. Materials Science and Engineering: A 528 (7−8), 3073−3078.

Natural fibre and polymer matrix composites and their applications in aerospace engineering

12

P. Balakrishnan [1], M.J. John [2], L. Pothen [3], M.S. Sreekala [4], S. Thomas [1]
[1]Mahatma Gandhi University, Kottayam, Kerala, India; [2]CSIR Materials Science and Manufacturing, Port Elizabeth, South Africa; [3]Bishop Moore College, Alleppey, Kerala, India; [4]Sree Sankara College Kalady, Enakulam, Kerala, India

12.1   Introduction

Fibre-reinforced polymer (FRP) composites are the most promising and elegant materials of the present century. Their durability and integrity in various service environments can be altered by the response of its constituents (ie, fibre or polymer matrix) and the existing interface and interphase between the fibre and polymer matrix, in that particular environment. Their susceptibilities to degradation depend on the nature of the environment and the different and unique responses of each of the constituents. All these structures and components are exposed to some environment during their service life. The environmental conditions can be high and low temperatures, high humidity, ultraviolet (UV) light exposure and alkaline environment, and they may be more severe if there is a cyclic variation of temperature, hydrothermal environment and low-earth-orbit space environment (Ray and Rathore, 2014). A widespread application spectrum of FRPs covers almost every type of advanced engineering structure. Their usage includes various components in aircraft, helicopters, spacecraft, boats, ships and offshore platforms, as well as automobiles, chemical processing equipment, sports goods and civil infrastructure such as buildings and bridges (Shrive, 2006). The behaviour and performance of advanced structural FRP composites cannot be explained only in terms of the specific properties of its constituent fibre and matrix, but the existing interface and interphase between fibre and matrix have great significance as well (Guigon and Klinklin, 1994; Kuttner et al., 2013). The presence of moisture at the interface can modify interfacial adhesion, thereby affecting the mechanical performance of the FRP composites. The energy associated with UV radiation is capable of dissociating the molecule bonds in the polymer matrix and may lead to the degradation of the materials. The border surface between the fibre and the matrix is a result of the linking of constituents; it has its own morphology and chemistry and represents the critical area in fibre-reinforced composites (Guigon and Klinklin, 1994; Ray, 2004; Sethi and Ray, 2015).

The history of natural fibre composites (NFCs) began in the aerospace sector with the introduction of Gordon Aerolite which was basically flax roving

Copyright © 2016 Elsevier Ltd. All rights reserved.

impregnated with phenolic resin. The light weight, high tensile strength and stiffness of Gordon Aerolite made it suitable for use as an aircraft material. This was used for an experimental main spar of the Bristol Breinheim bomber. However, the use of the Gordon Aerolite declined with the increasing availability of newer materials.

Sandwich panels are commonly used in aircraft interiors as flooring, ceilings, galley walls, lavatories and cargo-hold liners. Recently, researchers at the Council for Scientific and Industrial Research (CSIR) in South Africa have been involved in a project in collaboration with Airbus that focuses on the development of natural fibre-reinforced thermoset sandwich panels from flax fabric—phenolic skins and a Nomex honeycomb core for use in aircraft. The panels were manufactured by compression moulding of preimpregnated composites (prepregs) at suitable temperatures to enable curing of the resin. The research work also involved the development of aqueous-based flame-retardant treatments for flax fabric to ensure that the composite panels comply with Federal Aviation Administration (FAA) regulations. In addition to primary flame retardant, the composite contained non-fibrous natural silicate fire-resistant material as well. The composite material was reported to exhibit superior flammability, smoke and toxicity properties for the aforementioned purpose (Anandjiwala et al., 2013).

In another study (Alonso-Martin et al., 2012), natural fibre-based thermoset and thermoplastic skins were developed by researchers for use as aircraft interior panels. The panels were found to possess the required flame and heat resistance, allowing easy recycling and disposal, and were cheaper and offered significant weight savings over conventional sandwich panels. The authors further stated in their patent that each kilogram of weight reduction in a typical commercial airliner provides a reduction of 0.02—0.04 kg of fuel burn per hour. The typical life of an airline can be assumed to be 100,000 h, and for every single kilogram of weight saved, a fuel burn reduction of 4 tonnes and a reduction in CO_2 emissions of 12.5 tonnes is achieved over the working life of the airliner. A typical airliner that uses aircraft interior panels made from natural fibre-reinforced panels for secondary structures such as ceilings, floors, sidewalls, bulkheads, stowage compartments and other parts in the cabin would result in a weight reduction of 200—500 kg for panels made of the inorganic resin and 100—250 kg for the panels made of the thermoplastic resin. The weight reduction also equates to a 2500—6500 tonnes reduction in CO_2 emissions during the lifetime of the airliner for panels made of the inorganic resin and a 1300—3250 tonnes reduction in CO_2 emissions during the lifetime of the airliner for panels made of the thermoplastic resin. Moreover, further CO_2 savings could be achieved at the end of the service life due to easier recycling and disposal of the sandwich panels.

Composite materials have gained popularity (despite their generally high cost) in high-performance products that need to be lightweight, yet strong enough to take high loads such as aerospace structures (tails, wings and fuselages), boat construction, bicycle frames and racing car bodies. Other uses include storage tanks and fishing rods. Natural composites (wood and fabrics) have found applications in

aircraft, from the first flight of the Wright Brothers' *Flyer 1* in North Carolina on December 17, 1903, to the plethora of uses now enjoyed by man-made (engineered) composite materials on both military and civil aircraft, in addition to more exotic applications on unmanned aerial vehicles (UAVs), space launchers and satellites. Their adoption as a major contribution to aircraft structures followed the discovery of carbon fibre at the Royal Aircraft Establishment at Farnborough, UK, in 1964. However, not until the late 1960s did these new composites start to be applied, on a demonstration basis, to military aircraft. Examples of such demonstrators were trim tabs, spoilers, rudders and doors. The most common use for polymers is the matrix phase of fibre composites. Polymers are the 'glue' used to hold together the high stiffness, high-strength fibres in fibre—polymer composites. Early manufacturing processes for lightly stressed components were small scale, involving significant elements of manual intervention in the process. They relied on the low density and high stiffness and strength of the raw materials to deliver the required performance. As the size, stress values and criticality of the parts all increased, manual input has declined dramatically, substituted by complex, sophisticated robotic machinery. The robots have delivered consistency, freedom from defects and increased processing speed to cope with the manufacture of wings and fuselage sections of large civil aircraft. However, the essentials of this prepreg route have remained unchanged, and there are still issues regarding the cost-effectiveness of this route. In parallel, manufacturing researchers are pursuing lower cost options. In this chapter, the prepreg route in its various guises will be described, and the state of the art in alternative processes contrasted with it. In the past, the principal drivers for the use of fibre-reinforced composites for aircraft components were:

- reduced weight,
- cost reduction and
- improved performance.

The emphasis has now shifted towards environmental issues. Hence, the prime drivers are now:

- reduced fuel burn,
- reduced pollution and
- reduced noise.

Taylor (2000) states that 'increasing the use of composites to replace aluminium in the manufacture of airframes brings about numerous performance advantages such as the potential for weight reduction (due to higher specific strength and modulus), increased flexibility of design (due to the ability to build performance in specific directions), greater corrosion resistance and improved fatigue resistance. Weight reduction leads to improved fuel efficiency'. Furthermore, the reduced number of fasteners on a composite structure gives a more aerodynamic surface to the aircraft compared to riveted aluminium. One of the major difficulties associated with composite manufacture is that of void formation during impregnation and cure (Lowe et al., 1995). As these gaseous voids become entrapped within the

matrix, stress concentrations can be established within the matrix. These may originate in a number of ways, including:

- During mixing of the resin formulation.
- During filling of the cavities in components of more complex shapes.
- Due to the complex nature of the textile reinforcement, because air can become entrapped in the interstices of the fabric structure. This can be particularly evident when coarse yarns (or tows) are used or in complex three-dimensional (3D) structures (eg, braided or woven), and it may be most prevalent at the tool−composite interface.
- During the complex chemical reactions which take place during the cure of thermosetting resins, as volatile gases are released and become encapsulated in the cross-linked resin (Hill and McIlhagger, 1999).

A critical requirement of any process is that it is able to minimize void formation and ensure uniform distribution of resin as well as fibres throughout the component. These are major factors, alongside cost and flexibility in manufacturing different types of components, in assessing the merits of any particular manufacturing technique. These process variations must be understood at the design stage.

Launching a heavy-lift system into low-earth and geosynchronous orbits generally costs €5000−15,000/kg and €28,000/kg, respectively. Because of increasing oil and gas prices, the demand for lightweight materials in the aerospace industry is tremendous. Even in general aviation, fuel costs account for around 50% of the operational costs. Consequently, over the last three decades, the usage of FRP composites in these applications has increased from less than 5% by structural weight (Boeing 737) to 50% (Boeing 787), contributing over 20% more fuel efficiency.

12.2   Advantages of NFCs

Natural fibres are an abundant and renewable resource, so their cost is relatively low compared with other conventional fibres. They are eco-friendly and biodegradable, and they reduce the problem of solid waste production when used to replace nondegradable fillers. Due to their inherent properties, natural fibres are flexible. Because of their nonabrasive behaviour, the filler loading within the polymer matrix can be used in larger quantities than nonorganic fillers as it is unlikely to cause damage to machinery or health during manufacturing. Natural fibres possess many advantages, such as low density, and relatively high mechanical properties, such as specific modulus and specific strength. Natural fibres have recently become more attractive to researchers as an alternative reinforcement for fibre-reinforced polymer. They are extracted from renewable sources and provide a new generation of reinforcements for polymer materials. These eco-efficient fibres have been used as substitutes for glass fibre and other synthetic polymer fibres in diverse applications. NFCs help to preserve nonrenewable resources, which are the main source for most materials used in current applications. Natural fibre-based materials are produced in smaller quantities than petroleum-based products, and their applications are directed towards different areas. Natural fibres

have a low density and can provide reinforcement capable of imparting high specific mechanical properties to a composite when compared with many synthetic fibres such as glass, carbon and Kevlar in advanced applications. As natural fibres are derived from renewable natural resources, their production requires less energy. They also eliminate many of the problems related to environmental degradation, which means that the disposal of NFCs is easier, safer and less expensive when compared with that of advanced fibre composites. NFCs also provide impressive acoustic absorption properties, which are useful in building construction. Energy consumption for the pre- and postharvesting and cultivation facets of the natural fibre separation process is lower than that of synthetic fibre production processes. The principal advantages of using natural fibres in composites are therefore lower cost, sustainability and low density.

The fibres are very often surface treated during their manufacture to prepare adhesion with the polymer matrix, whether thermosetting (epoxy, polyester, phenolic and polyimide resins) or thermoplastic (polypropylene, Nylon 6.6, PMMA and PEEK). The fibre surface is roughened by chemical etching and then coated with an appropriate size to aid bonding to the specified matrix. Whereas composite tensile strength is primarily a function of fibre properties, the ability of the matrix to both support the fibres (required for good compression strength) and provide out-of-plane strength is, in many situations, equally important. The aim of the material supplier is to provide a system with a balanced set of properties. While improvements in fibre and matrix properties can lead to improved lamina or laminate properties, the all-important field of the fibre—matrix interface must not be neglected. The load acting on the matrix has to be transferred to the reinforcement via the interface. Thus, fibres must be strongly bonded to the matrix if their high strength and stiffness are to be imparted to the composite. The fracture behaviour depends on the strength of the interface. A weak interface results in a low stiffness and strength but high resistance to fracture, whereas a strong interface produces high stiffness and strength but often a low resistance to fracture (ie, brittle behaviour). Conflict therefore exists, and the designer must select the material most nearly meeting his requirements. Other properties of a composite, such as resistance to creep, fatigue and environmental degradation, are also affected by the characteristics of the interface. In these cases, the relationship between properties and interface characteristics are generally complex, and analytical and numerical models supported by extensive experimental evidence are required.

FRP composites are prone to damage from the initiation and propagation of delaminations (ie, areas in which separation occurs in the polymer—matrix resin in which the fibres are embedded). Delaminations may also occur between the polymer and fibre layers in the form of fibre—matrix debonding. In FRP composites, delaminations are hence located in planes defined by the fibre layup, and they propagate or grow in these planes if the applied stresses are large enough (Steyer, 2013; Williams, 1989). Initiation of delaminations is typically caused by impact followed by propagation and growth due to cyclic thermomechanical service loads, or it results from manufacturing defects. Another source of delamination initiation is machining (eg, cutting) of FRP composites, as discussed in detail by Lasri et al. (2011).

Refinements in fibre process technology over the past 20 years have led to considerable improvements in tensile strength (w4.5 GPa) and in strain to fracture (more than 2%) for polyacrylonitrile-based fibres. These can now be supplied in three basic forms: high modulus (HM; E 380 GPa), intermediate modulus (IM; E 290 GPa) and high strength (HS; this has a modulus of around 230 GPa and tensile strength of 4.5 GPa). The more recent developments of the high-strength fibres have led to what are known as 'high-strain fibres', which have strain values of 2% before fracture. The tensile stress strain response is elastic up to failure, and a large amount of energy is released when the fibres break in a brittle manner. The selection of the appropriate fibre depends very much on the application. For military aircraft, both high modulus and high strength are desirable. Satellite applications, in contrast, benefit from the use of a high fibre modulus that improves stability and stiffness for reflector dishes, antennas and their supporting structures (Lasri et al., 2011). One advantage of fabrics for reinforcing purposes is their ability to drape or conform to curved surfaces without wrinkling. It is now possible, with certain types of knitting machines, to produce fibre preforms tailored to the shape of the eventual component. Generally speaking, however, the more highly convoluted each filament becomes, as at crossover points in woven fabrics or as loops in knitted fabrics, the lower its reinforcing ability.

12.3 Types of natural plant fibre

There are six basic types of natural fibres. They are classified as follows: bast fibres (jute, flax, hemp, ramie and kenaf), leaf fibres (abaca, sisal and pineapple), seed fibres (coir, cotton and kapok), core fibres (kenaf, hemp and jute), grass and reed fibres (wheat, corn and rice) and all other types (wood and roots). The natural fibre-reinforced polymer composite's performance depends on several factors, including fibres' chemical composition, cell dimensions, microfibrillar angle, defects, structure, physical properties and mechanical properties, and also the interaction of a fibre with the polymer. In order to expand the use of natural fibres for composites and improve their performance, it is essential to know the fibre characteristics. The hydrophilic nature of fibres is a major problem for all cellulose fibres if they are used as reinforcement in hydrophobic plastics such as PP, PE and so on. The moisture content of the fibres depends on the content of noncrystalline parts and the void content of the fibres. Overall, the hydrophilic nature of natural fibres influences the mechanical properties. The main disadvantages of natural fibres in reinforcement to composites are the poor compatibility between fibre and matrix and their relatively high moisture absorption. Therefore, natural fibre modifications are considered in modifying the fibre surface properties to improve their adhesion with different matrices. An exemplary strength and stiffness could be achieved with a strong interface that is very brittle in nature with easy crack propagation through the matrix and fibre. The efficiency of stress transfer from the matrix to the fibre could be reduced with a weaker interface.

Traditional fibre-reinforced composites use various types of glass, carbon, aluminium oxide and many others as reinforcing components. Natural fibres,

especially bast (bark) fibres, such as flax, hemp, jute, henequen and many others, were applied by some researchers as fibre reinforcement for composites in recent years (Phil and Soutis, 2014; Singleton et al., 2003; Rana et al., 2003; Valadez-Gonzalez et al., 1999). Advantages of natural fibres over man-made fibres include low density, low cost, recyclability and biodegradability (Oksman et al., 2003; Mohanty et al., 2005; Baley, 2002). These advantages make natural fibres potential replacements for glass fibres in composite materials. The mechanical properties of natural fibres, especially flax, hemp, jute and sisal, are very good and may compete with glass fibre in specific strength and modulus (van Voorn et al., 2001; van de Velde and Kiekens, 2002). Table 12.1 lists the mechanical properties of some natural and man-made fibres. Natural fibre-reinforced composites can be applied in the plastics, automobile and packaging industries to cut down on material cost (Frederick and Norman, 2004).

In order to expand the use of natural fibres for composites and improve their performance, it is essential to know the fibre characteristics. The physical properties of each natural fibre are critical and include the fibre dimensions, defects, strength and structure. There are several physical properties that are important to know about for each natural fibre before that fibre can be used to reach its highest potential. Fibre dimensions, defects, strength, variability, crystallinity and structure must be taken into consideration. An exemplary strength and stiffness could be achieved with a strong interface that is very brittle in nature with easy crack propagation through the matrix and fibre. The efficiency of stress transfer from the matrix to the fibre could be reduced

Table 12.1 Properties of some natural and man-made fibres

Fibre	Density (g/cm³)	Elongation (%)	Tensile strength (MPa)	Young's modulus (GPa)
Cotton	1.5−1.6	3.0−10.0	287−597	5.5−12.6
Jute	1.3−1.46	1.5−1.8	393−800	10−30
Flax	1.4−1.5	1.2−3.2	345−1500	27.6−80
Hemp	1.48	1.6	550−900	70
Ramie	1.5	2.0−3.8	220−938	44−128
Sisal	1.33−1.5	2.0−14	400−700	9.0−38.0
Coir	1.2	15.0−30.0	175−220	4.0−6.0
Softwood craft	1.5	−	1000	40.0
E-glass	2.5	2.5−3.0	2000−3500	70.0
S-glass	2.5	2.8	4570	86.0
Aramid (normal)	1.4	3.3−3.7	3000−3150	63.0−67.0
Carbon (standard)	1.4	1.4−1.8	4000	230.0−240.0

with a weaker interface. Physical methods include stretching, calendaring, thermo treatment and the production of hybrid yarns for the modification of natural fibres. Physical treatments change structural and surface properties of the fibre and thereby influence the mechanical bonding of polymers. Physical treatments do not extensively change the chemical composition of the fibres. Therefore, the interface is generally enhanced via an increased mechanical bonding between the fibre and the matrix. Cellulose fibres, which are strongly polarized, are inherently incompatible with hydrophobic polymers due to their hydrophilic nature. In many cases, it is possible to induce compatibility in two incompatible materials by introducing a third material that has properties intermediate between those of the other two. There are several coupling mechanisms in materials (eg, weak boundary layers, deformable layers, restrained layers, wettability, chemical bonding and the acid–base effect). The development of a definite theory for the mechanism of bonding using coupling agents in composites is a complex problem. The main chemical bonding theory alone is not sufficient. So the consideration of other concepts appears to be necessary. These include the morphology of the interphase, the acid–base reactions in the interface, surface energy and the wetting phenomena.

12.4   Types of matrices

High-temperature polymer blends (HTPBs) are typically used at $T \geq 140°C$ and maintain at least 25% of their room temperature (RT) properties at $154°C$. Considering their expanding applications in such sectors as the military, aerospace, transportation, electronic, health care and oil and gas industries, they need to have good processability, high mechanical performance, chemical resistance, fire retardancy and so on. FRPs are very sensitive to intrinsic damage, such as delamination (in particular), matrix cracking and fatigue damage. Several approaches have been adopted to tackle these, which include:

- improving the fracture toughness of the ply interfaces via epoxy–elastomer blends; and
- reducing the mismatch of elastic properties (and stress concentrations) at the interfaces between the laminated plies.

These materials also lack other required functional properties such as high electrical and thermal conductivity for electrostatic dissipation and lightning strike protection. Currently, it is believed that the best route to achieve multifunctional properties in a polymer is to blend it with nanoscale fillers. This is because of the three main characteristics of polymer nanocomposites:

1. reduced nanoscopic confinement of matrix polymer chains;
2. variation in properties of nanoscale inorganic constituents (many studies have reported that the mechanical, conductivity, optical, magnetic, biological and electronic properties of several inorganic nanoparticles significantly change as their size is reduced from the macroscale to the microlevel and nanolevel) and
3. nanoparticle arrangement and creation of a large polymer or particle interfacial area.

Composites are used in the airframe and engine components of modern military and civilian aircraft, with polymers accounting for 40−45% of the total volume of the material. Moulded plastics and fibre−polymer composites are used extensively in the internal fittings and furniture of passenger aircraft.

Another important application of polymers is as an adhesive for joining aircraft components. Advantages and disadvantages of different types of polymers are listed in Table 12.2. It is possible to produce high-strength, durable joints using polymer adhesives without the need for fasteners such as rivets and screws. Adhesives are used to join metal-to-metal, composite-to-composite and metal-to-composite components. For example adhesives are used to bond ribs, spars and stringers to the skins of structural panels used throughout the airframe. Adhesives are also used to bond face sheets to the core of sandwich composite materials and to bond repairs to composite and metal components damaged during service. Thin layers of adhesive are used to bond together the aluminium and fibre−polymer composite sheets that produce the fibre−metal laminate called GLARE, which is used in the Airbus 380 fuselage. The use of elastomers is usually confined to nonstructural aircraft parts that require high flexibility and elasticity, such as seals and gaskets. Polymers possess several properties that make them useful as aircraft materials, including low density ($1.2−1.4$ g cm^{-3}), moderate cost, excellent corrosion resistance and high ductility (except thermosets). Some polymers are tough and transparent which makes them suitable for aircraft windows and canopies.

Table 12.2 Comparison of the advantages and disadvantages of polymers for aircraft structural applications (Steyer, 2013)

Thermoplastic	Thermoset	Elastomer
Advantages		
• Nonreacting; no cure required • Rapid processing • High ductility • High fracture toughness • High impact resistance • Absorbs little moisture • Can be recycled	• Low processing temperature • Low viscosity • Good compression properties • Good fatigue resistance • Good creep resistance • Highly resistant to solvents • Good fibre wetting for composites	• Low processing temperature • High ductility and flexibility • High fracture toughness • High impact resistance
Disadvantages		
• Very high viscosity • High processing temperature (300−400°C) • High processing pressures • Poor creep resistance	• Long processing time • Low ductility • Low fracture toughness • Low impact resistance • Absorb moisture • Limited shelf life • Cannot be recycled	• Long processing times • Poor creep resistance • Low Young's modulus • Low tensile strength

However, polymers cannot be used on their own as structural materials because of their low stiffness, low strength, creep properties and low working temperature.

Epoxy resin is the most common thermosetting polymer used in aircraft structures. Epoxy resin is used as the matrix phase in carbon—fibre composites for aircraft structures and as an adhesive in aircraft structural joints and repairs. There are many types of epoxy resins, and the chemical structure of an epoxy resin is often used in aerospace composite materials. Epoxy resins are the polymer of choice in many aircraft applications because of their low shrinkage and low release of volatiles during curing, high strength and good durability in hot and moist environments. Epoxy resin is used extensively in aircraft composite structures, but it cannot be safely used inside cabins because of its poor fire performance. Most epoxy resins easily ignite when exposed to fire and release copious amounts of heat, smoke and fumes. Federal Aviation Administration (FAA) regulations specify the maximum limits on heat release and smoke produced by cabin materials in the event of fire, and most structural-grade epoxy resins fail to meet the specifications. Phenolic resins meet the fire regulations, and most of the internal fittings, components and furniture in passenger aircraft are made of fibreglass—phenolic composites and moulded phenolic resin (Muhammad and Mohini, 2003). The use of thermoplastics in aircraft, whether as the matrix phase of fibre—polymer composites or as a structural adhesive, is small compared with the much greater use of thermosets. Some sectors of the aerospace industry are keen to increase the use of thermoplastics in composite materials, and the number of applications is gradually increasing. Thermoplastics provide several important advantages over thermosets when used in composite materials, most notably better impact damage resistance, higher fracture toughness and higher operating temperatures. However, thermoplastics must be processed at high temperature, which makes them expensive to manufacture into aircraft composite components. Several types of thermoplastics are transparent, tough and impact resistant, which makes them well suited for aircraft windows and canopies. The thermoplastics most often used in aircraft windows are acrylic plastics and polycarbonates. Acrylic plastics are any polymer or copolymer of acrylic acid or variants thereof. An example of acrylic plastic used in aircraft windows is polymethyl methacrylate (PMMA), which is sold under commercial names such as Plexiglas and Perspex. Acrylic plastics are lighter, stronger and tougher than window glass. Polycarbonates get their name because they are polymers with functional groups linked together by carbonate groups ($-O-(C=O)-O-$) in the long molecular chain. Polycarbonates are stronger and tougher than acrylic plastics and are used when high-impact resistance is needed, such as cockpit windows and canopies. In these applications, the material must have high-impact resistance because of the risk of collision with birds (Figure 12.1). Although bird strikes do not occur at cruise altitudes, they present a serious risk at low altitudes, particularly during take-off and landing. Polycarbonate windscreens are also resistant to damage by large hailstones.

Elastomers are not suitable for use in aircraft structures because they lack stiffness and strength, but they do have exceptionally high elasticity with elongation values between 100 and several thousand per cent. This makes elastomers suitable when low stiffness and high elasticity are required, such as in aircraft tyres, seals and gaskets. Many aircraft components that require a tight seal, such as window and door seals,
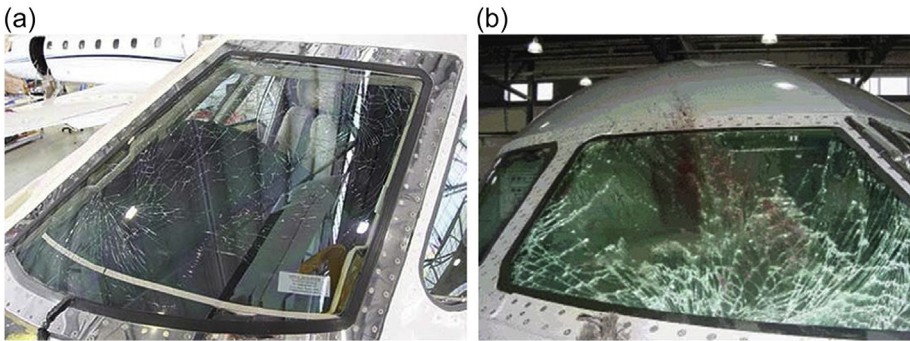
Figure 12.1 (a) Hail damage to cockpit window; and (b) bird hit damage on aircraft window.

use elastomers. These materials are used for their excellent elasticity; they can be compressed easily to make a tight seal without being damaged or permanently deformed. Although elastomers usually work well as seals and gaskets, they can gradually erode and degrade in harsh operating conditions, such as high temperatures.

12.5　Green composites

Various saleable and industrial applications of FRPs are aircrafts and spacecrafts, ships and submarines, trucks, railways, automobiles, structures and prosthetics. Due to their high specific stiffness and strength, fibre-reinforced polymer composite materials have long been used in the aerospace industry and, with increasing focus on lightweight vehicle manufacturing due to environmental legislation, automotive applications are becoming more widespread. Other notable engineering applications include pressure vessels and wastewater pipes and fittings. The need to utilize the mechanical performance of materials and to avoid unreasonable over-specification for aerospace applications was highlighted by Boeing, who estimated that it cost US$10,000 per pound (approximately UK£12,500/kg) to launch a satellite into orbit. Also of significance, when considered in terms of the levels of production and use, is that up to 40% of the fuel consumption of a road vehicle is considered to be attributable to its inertia; the effects of inertia are particularly significant on the urban test cycle. With increasing environmental pressure, some vehicle manufacturers look towards an increased use of polymer composite materials for weight savings. Another driving force for efficient design with composites in high-volume production industries is the cost of the basic material. Because of the fact that composite material has characteristics that are as good as those of conventional materials, the use of NFCs has begun gaining attractiveness in engineering applications. Properties like low density, lower material cost, renewability and environmental friendliness are most important. In the past, various studies on NFCs were carried out. Thus, the design of products using composites is an extremely essential issue, and it is imperative to know the various property-predicting factors for the design of composites. As global societies continue to grow, increasing emphasis is being placed on ensuring the sustainability of our

material systems. Topics such as greenhouse gas emissions, embodied energy, toxicity and resource depletion are being considered increasingly by material producers. Green composites deriving from renewable resources bring very promising potential to provide benefits to companies, the natural environment and end customers due to dwindling petroleum resources. The shift to more sustainable construction in the automotive industry is not only an initiative towards a more viable environment and cost-efficiency but also a demand of European regulations. The latter are playing an important role as a driving force towards sustainable materials use. According to the European Guideline 2000/53/EG issued by the European Commission, 85% of the weight of a vehicle had to be recyclable by 2005. This recyclable percentage was increased to 95% by 2015 (Mouritz, 2012). Mercedes-Benz used an epoxy matrix with the addition of jute in the door panels in its E-class vehicles back in 1996 (Koronis et al., 2013). Another paradigm of green composites' application appeared commercially in 2000, when Audi launched the A2 midrange car: the door trim panels were made of polyurethane reinforced with a mixed flax−sisal material.

Green composites fabricated using plant fibres (cellulose) and resins such as modified starches and proteins have already been demonstrated in the interiors of automobiles, whereas few examples have been shown for exteriors. Novel green composites have been tested in numerous studies in an attempt to explore their performance in several applications. The application of green composites in automobile body panels seems to be feasible because green composites have comparable mechanical performance with the synthetic ones. Conversely, green composites seem to be rather problematic due to their decomposable nature. The biodegradability issue is one problem that needs to be addressed when aiming for 100% bio-based composites application, especially when dealing with structural parts of exterior panels for future vehicles. More aspects have to be considered, such as the reproducibility of these composites' properties and their long life cycle as parts of exterior body parts. Unfortunately, to the present, bio-thermoplastics' cost is a major barrier for their generalized use in the automotive industry, but it is expected that manufacturers of these materials soon will turn up affordable solutions as their demand in industrial-scale applications will no doubt tend to decrease their prices to more affordable levels. The trend can also be reversed in the sense that the necessity for environmentally conscious solutions can overturn the value chain and put a premium price on the environmental impact of current solutions.

12.6   Limitations of natural fibres

Parallel to the advantages that natural fibres bring with their use in composites, they also have drawbacks regarding their performance, their behaviour in polymeric matrix systems and their processing. First of all, natural fibres have an inability to provide a consistent pattern of physical properties in a given year; those properties can vary from every harvesting season and/or from harvesting region based on interchangeable sun, rain and soil conditions. Additionally, these variations can be surprisingly observed

even in the same cultivation's population in between the crops. More precisely, their properties essentially depend on the locality, the part of the plant they are harvested from (leaf or stem) the maturity of the plant and how the fibres are harvested and pre-conditioned in the form of mats or chopped fibres, woven or unwoven. All these factors result in significant variation in properties compared to their synthetic fibre counterparts (glass) (Mohanty et al., 2005). Moreover, important parameters are the type of ground on which the plant grows, the amount of water the plant receives during growth, the year of the harvest and most importantly the kind of processing and production route. An approach to address this problem is to mix batches of fibres from different harvests. Blending fibres provides a hedge against variability in any single fibre crop. By having multiple suppliers of fibre and harvests, the ratio of fibres ensures relatively consistent performance in the finished part (O'Donnell et al., 2004). Alternatively, it is introduced to the market that a genetically transformed variety may guarantee products of constant quality (Brosius, 2006). One other major negative issue of natural fibres is their poor compatibility with several polymeric matrices. That may result in nonuniform dispersion of fibres within the matrix. Their high moisture sensitivity leads to severe reduction of mechanical properties and delaminating. Furthermore, low microbial resistance and susceptibility to rotting can act as restriction factors, particularly during shipment and long-term storage, as well as during composite processing (Mougin, 2006). Similar to the case of wood composites, natural fibres and plastic are like oil and water because they do not mix well. As most polymers, especially thermoplastics, are nonpolar ('hydrophobic', or repelling water) substances and not compatible with polar ('hydrophilic', or absorbing water) wood fibres, poor adhesion between polymer and fibre may result (Bismarck et al., 2005). In order to improve the affinity and adhesion between reinforcements and thermoplastic matrices in production, chemical 'coupling' or 'compatibilizing' agents have to be employed (Mougin, 2006; Bismarck et al., 2005; Ashori, 2008). Chemical coupling agents are substances, typically polymers, that are used in small quantities to treat a surface in such a way that increased bonding occurs between the treated surface and other surfaces. Another primary drawback of the use of fibres is the low processing temperature required (ie, they possess limited thermal stability). The permitted temperature is up to 200°C; above this limit, the fibres start to degrade and shrink which subsequently results in lower performance of the composite. In general, when fibres are subjected to heat, the physical and/or chemical structural changes that occur are depolymerization, hydrolysis, oxidation, dehydration, decarboxylation and recrystallization (Kim et al., 2006), which limit the variety of resins they can be blended with (Ashori, 2008). In order to avoid this processing defect, the range of temperatures as well as the processing time have to be limited (Mo et al., 2005).

12.7   Techniques for improving performance

Throughout the last 40 years of using polymer composites in the aerospace sector, designers and manufacturing engineers have progressed from relatively small, lightly

loaded components and sections of structure such as ailerons and fairings to heavily stressed and critical items such as the main wing and fuselage of the Boeing 787, the Airbus A400 M and the new Airbus A350 aircraft, which are constructed from up to 50% (53% in the case of the A350) carbon fibre-reinforced polymer composite (by weight of aircraft), and in which the main wings and fuselage are largely manufactured from composite materials. High fibre volume is essential for good aircraft structure performance. It is also important that distribution of both fibre and resin is uniform throughout the component. To illustrate, the simple rule of mixtures (ROM) approach for calculation of longitudinal modulus falls into the mechanics of materials category; the modulus of elasticity in the longitudinal direction (E_L), which is the direction of parallel fibres, is given as:

$$E_L = E_f V_f + E_m(1 - V_f) \qquad [12.1]$$

where V_f is the fibre volume fraction of the composite, E_f is the modulus of the fibre and E_m is the modulus of the resin. The typical V_f value for aerospace autoclaved prepreg components is approximately 54%, aerospace resin transfer moulding (RTM) components could be 57% and some new resin infusion and advanced pultrusion processes could be above 60%. Although the simple ROM approach predicts an increase in performance with increased V_f, in reality some important material properties such as compression after impact strength begin to diminish as the resin content becomes insufficient to support the fibres (Wielage et al., 1999). One of the major difficulties associated with composite manufacture is that of void formation during impregnation and cure (McIlhagger et al., 2014). As these gaseous voids become entrapped within the matrix, stress concentrations can be established within the matrix. These may originate in a number of ways, including:

- During mixing of the resin formulation.
- During filling of the cavities in components of more complex shapes.
- Due to the complex nature of the textile reinforcement, because air can become entrapped in the interstices of the fabric structure. This can be particularly evident when coarse yarns (or tows) are used or in complex three-dimensional (3D) structures (eg, braided or woven), and it may be most prevalent at the tool–composite interface.
- During the complex chemical reactions which take place during the cure of thermosetting resins, as volatile gases are released and become encapsulated in the cross-linked resin (Lowe et al., 1995).

Selection of both manufacturing process type and the resin or fibre system will be influenced by the specific properties required for different parts of the aircraft. High fibre strength and stiffness combined with low density are obvious general requirements for all parts of the aircraft structure. These properties have been achieved best from composites produced using layup of unidirectional prepregs coupled with autoclave curing. The high levels of composite stiffness and strength achieved by prepreg technology, combined with the low density of the constituents, make components manufactured this way suitable for wing and fuselage structures. Compression properties in particular will reduce if fibre volume fraction is low. The upper wing skin and

parts of the spar structure which are placed under compression loading will therefore benefit most from use of unidirectional prepreg material where control of fibre distribution is good.

As has been noted in this chapter, early examples of polymer composite manufacture on aircraft often used prepreg coupled with manual layup techniques, followed by an autoclave cure. This process can produce composites with straight fibres, high and uniform volume fraction and freedom from voids and porosity. Such composites thus achieve optimum stiffness and static strength. While the production cost may have been competitive with aluminium for limited production runs, generally the cost of manufacturing structures with composites via this labour-intensive route was greater than with aluminium. The performance advantages of composites in terms of stiffness and strength to weight had to be weighed against increased cost of manufacture. There has been therefore an increasing focus on reducing the cost of composite parts by reducing the costs of both materials and manufacturing processes (McIlhagger et al., 2014). Prepreg production processes for aircraft can achieve the best properties but at a relatively high cost. Alternative lower cost processes such as vacuum-assisted resin transfer moulding have been developed, but although they have superior performance in some areas such as toughness, through-thickness properties and impact resistance, they have not as yet achieved the performance levels of which prepreg route components are capable. Although smaller scale, lightly stressed components on the aircraft can be made by a variety of the lower cost techniques, the major aircraft structural elements in existing and projected aircraft of main wings, fuselage and empennage are exclusively manufactured using prepreg as the starter material and high-capital-cost robotic layup and autoclave techniques to process it. Unless raw material and process costs can be reduced, the benefits of composites will be realized only on a limited range of aircraft types (Wielage et al., 1999).

12.8   Prediction of properties: influence of factors

Lightweight structures in aerospace applications are mostly made of polymer matrix composites. The size and shape of the structure, and its usage (eg, as a primary or secondary structure in aircraft), dictate the choice of the manufacturing process. Although the early aerospace applications in defence were mainly performance driven, the cost of manufacturing today is of increasing concern. Therefore, the traditional design approach of 'defect-free' structures must be revisited. In fact, no structure is without defects; a low threshold of measurable defects is essentially what defines the 'defect-free condition'. If the cost of manufacturing is to be managed (ie, reduced in a controlled way), then the effects of defects must be assessed. This requires a mechanics-based knowledge base on characterization of defects and quantification of their effects on specific performance characteristics. Reducing cost of manufacturing further requires that the manufacturing process be quantified with parameters that can be varied to minimize cost. Voids are the most common type of matrix defects and are found in virtually all PMC parts, whether manufactured by autoclave, liquid

compression moulding or RTM. Void formation can to some extent be controlled by manufacturing process parameters such as vacuum pressure, resin viscosity, cure temperature and consolidation pressure. In one study (Harries et al., 2002), for example, void morphology and spatial distribution in a circular disc of glass—epoxy were studied in an RTM process in which the resin was injected under pressure into a mould containing fibre bundle preform. The voids were found to vary in size, shape and spatial location. Fibre defects, as noted here, are fibre misalignment and waviness, and broken fibres. In composites, where fibres are assumed to be straight, parallel and oriented in intended directions, deviations due to misalignment and waviness can reduce initial properties, particularly compression strength and stiffness, and lead to reductions in aircraft design limit load and design ultimate load capability in service. A study of the effect of fibre waviness in unidirectional composites under axial compression (Hamidi et al., 2004; Hsiao and Daniel, 1996) showed that the stiffness and strength reduced severely due to this type of defect. Stress analysis and experimental observations indicated that the interlaminar shear stress developed due to fibre waviness was responsible for delamination and subsequent failure.

Toldy et al. (2011) studied the flame retardancy of fibre-reinforced epoxy resins. As for the flame retardancy of the reference systems, the inclusion of carbon fibres into the resin resulted in a significant increase of flame-retardant performance. In case of the flame-retardant systems, outstanding LOI and UL-94 results could be achieved both for the resin and for the composite. Concerning the heat release results, the simultaneous application of flame-retardant and carbon fibres did not lead to the improvement that could be expected on the basis of additivity, due to the hindered intumescence caused by the plies of the reinforcing carbon fibres (Toldy et al., 2011)

12.9 Applications of polymers and polymer composites

Adhesives used for bonding aircraft components and sandwich composites are usually thermosets, such as epoxy resin. Adhesives must have low shrinkage during curing to avoid the formation of residual tensile stress in the bond. Correct surface preparation is essential to ensure a high-strength and durable bond is achieved with a polymer adhesive. The mechanical properties of polymers are inferior to those of aerospace structural metals, and their use is restricted to relatively low-temperature applications. Polymers transform from a hard and glassy condition to a soft and rubbery state during heating, and the maximum working temperature is defined by the heat deflection temperature or glass transition temperature. Polymers often contain additives for special functions such as colour, toughness or fire. Radar-absorbing materials (RAMs) are a special class of polymer that convert radar (electromagnetic) energy to some other form of energy (eg, heat) and thereby improve the stealth of military aircraft. RAMs must be used with other stealth technologies such as design adaptations of the aircraft shape to minimize the radar cross section. Structural components for aircraft made from fibre—polymer composites frequently comprise duroplastics shaped in prepreg and RTM processes. Celanese adds that the greatest disadvantage of this process is

the extensive drying times required for the matrix to cure. FIBRE uses prepregs that contain additional inlaid thermoplastic fibres, as well as carbon fibres, to lend structure to the window frames. These prepregs are processed to form structural inlay preforms — versions made from multiaxial fibre inlays are used to shorten cycle times. FIBRE also produced tailored fibre placement preforms parallel for precise fibre alignment. The matrix of knit and weft fibres is formed in the subsequent consolidation in a variotherm press. In this process, the Fortron PPS fibres in the prepreg ensure homogenous matrix distribution. After consolidation, the structure inlays are sprayed with short fibre-reinforced Fortron PPS to add integral stiffening or functional elements which would be much more difficult to implement with continuous fibre-reinforced materials. The combination of thermoforming and injection moulding makes the process more cost-effective and allows for higher production volumes in a shorter time (Anderson and Pratschke, 2014).

12.10 Conclusion

Fibre-reinforced composites have gained much importance nowadays in the aerospace industry due to their low weight and superior mechanical properties. Unfortunately, classic fibre-reinforced polymers often pose considerable environmental problems due to difficulty in recycling or nonbiodegradability at the end of their usable lifetime, mainly because of the compounding of miscellaneous and usually very stable fibres and matrices. In contrast, natural fibre and bio-composite materials present considerable environmental benefits due to their biodegradability and, owing to their low cost and high specific mechanical properties, have future prospects in the aerospace industry, mainly in the interior parts of the aircrafts. However, issues related to their inferior thermal and fire resistance, water absorption, degradability as well as variability in properties and their reliable prediction tools have to be solved in future for successful aerospace applications.

References

Alonso-Martin, P.P., Gonzalez-Garcia, A., Lapena-Rey, N., Fita-Bravo, S., Martinez-Sanz, V., Marti-Ferrer, F., 2012. Green aircraft interior panels and method of fabrication. US 20120148824 A1.

Anandjiwala, R., Chapple, S., John, M., Schelling, H.-J., Doecker, M., Schoke, B., 2013. A Flame-Proofed Artefact and a Method of Manufacture Thereof. Published PCT Patent Application: WO2013/084023.

Anderson, C., Pratschke, K., 2014. Fibre-reinforced composites used for cost effective aerospace window frames. Reinforced Plastics 58 (1). http://dx.doi.org/10.1016/S0034-3617(14)70013-X.

Ashori, A., 2008. Wood-plastic composites as promising green-composites for automotive industries! Bioresource Technology 99, 4661−4667.

Baley, C., 2002. Composites A: Applied Science and Manufacturing 33, 939.

Bismarck, A., Mishra, S., Lampke, T., 2005. Plant fibers as reinforcement for green composites. In: Mohanty, A.K., Misra, M., Drzal, T.L. (Eds.), Natural Fibers, Biopolymers, and Biocomposites. Crc Press-Taylor & Francis Group, Boca Raton.

Brosius, D., 2006. Natural fiber composites slowly take root. Composites Technology 12 (1), 32−37.

Frederick, T.W., Norman, W., 2004. Natural Fibers Plastics and Composites. Kluwer Academic Publishers, New York.

Guigon, M., Klinklin, E., 1994. The interface and interphase in carbon fibre-reinforced composites. Composites 25 (7), 534−539.

Hamidi, Y.K., Aktas, L., Cengiz Altan, M., 2004. Formation of microscopic voids in resin transfer molded composites. Transactions ASME Journal of Engineering Materials and Technology 126, 420−426.

Harries, C., Starnes, J., Stuart, M., 2002. Design and manufacturing of aerospace composite structures: state-of-the-art assessment. Journal of Aircraft 39, 545−560.

Hill, B.J., McIlhagger, R., 1999. Resin impregnation and prediction of fabric properties. In: Miravete, A. (Ed.), 3D Textile Reinforcements in Composite Materials. Woodhead Publishing Limited, Cambridge (UK), p. 7.

Hsiao, H.M., Daniel, I.M., 1996. Effect of fibre waviness on stiffness and strength reduction of unidirectional composites under compressive loading. Composites Science and Technology 56, 581−593.

Kim, J., Yoon, T., Mun, S., Rhee, J., Lee, J., 2006. Wood − polyethylene composites using ethylene−vinyl alcohol copolymer as adhesion promoter. Bioresource Technology 97, 494−499.

Koronis, G., Silva, A., Fontul, M., 2013. Green composites: a review of adequate materials for automotive applications. Composites Part B: Engineering 44 (1), 120−127.

Kuttner, C., Hanisch, A., Schmalz, H., Eder, M., Schlaad, H., Burgert, I., Fery, A., 2013. Influence of the polymeric interphase design on the interfacial properties of (fiber-reinforced) composites. ACS Applied Materials and Interfaces 5 (7), 2469−2478.

Lasri, L., Nouari, M., El Mansori, M., 2011. Wear resistance and induced cutting damage of aeronautical FRP components obtained by machining. Wear 271, 2542−2548. http://dx.doi.org/10.1016/j.wear.2010.11.056.

Lowe, J.R., Owen, M.J., Rudd, C.D., 1995. Void formation resin transfer molding. In: Proceedings of the 4th International Conference on Automated Composites, ICAC95. Institute of Materials, Nottingham, pp. 227−234.

McIlhagger, A., Archer, E., McIlhagger, R., 2014. Manufacturing processes for composite materials and components for aerospace applications. Polymer Composites in the Aerospace Industry 53.

Mo, X.Q., Wang, K.H., Sun, X.Z.S., 2005. Straw-based biomass and biocomposites. In: Mohanty, A.K., Misra, M., Drzal, T.L. (Eds.), Natural Fibers, Biopolymers, and Biocomposites. Crc Press-Taylor & Francis Group, Boca Raton, pp. 473−495.

Mohanty, A.K., Misra, M., Drzal, T.L., Selke, S.E., Harte, B.R., Hinrichsen, G., 2005. Natural fibers, biopolymers, and biocomposites: an introduction. In: Mohanty, A.K., Misra, M., Drzal, T.L. (Eds.), Natural Fibers, Biopolymers, and Biocomposites. Crc Press-Taylor & Francis Group, Boca Raton, pp. 1−36.

Mohanty, A.K., Misra, M., Drzal, L.T. (Eds.), 2005. Natural Fibers, Biopolymers, and Biocomposites. CRC Press.

Mougin, G., 2006. Natural Fibre Composites − Problems and Solutions. JEC Composites Magazine [cited (25)]. http://www.jeccomposites.com/news/compositesnews/challenge-natural-fibres-composite-reinforcement.

Mouritz, A., 2012. Introduction to Aerospace Materials. Royal Melbourne Institute of Technology. Woodhead Publishing, Australia, ISBN 978-1-85573-946-8.

Muhammad, P., Mohini, M.S., 2003. Resources, Conservation and Recycling 39, 325.

O'Donnell, A., Dweib, M.A., Wool, R.P., 2004. Natural fiber composites with plant oilbased resin. Composites Science and Technology 64, 1135−1145.

Oksman, K., Skrifvars, M., Selin, J.F., 2003. Natural fibers as reinforcement in poly lactic acid composites. Composites Science and Technology 63, 1317.

Phil, E., Soutis, C. (Eds.), 2014. Polymer Composites in the Aerospace Industry. Elsevier.

Rana, A.K., Mandal, S., Bandyopadhyay, S., 2003. Composites Science and Technology 63, 801.

Ray, B.C., Rathore, D., 2014. Durability and integrity studies of environmentally conditioned interfaces in fibrous polymeric composites: Critical concepts and comments. Advances in Colloid and Interface Science 209, 68−83.

Ray, B.C., 2004. Effects of crosshead velocity and sub-zero temperature on mechanical behaviour of hygrothermally conditioned glass fibre reinforced epoxy composites. Materials Science and Engineering A 379 (1), 39−44.

Sethi, S., Ray, B.C., 2015. Environmental effects on fibre reinforced polymeric composites: evolving reasons and remarks on interfacial strength and stability. Advances in Colloid and Interface Science 217, 43−67.

Shrive, N.G., 2006. The use of fibre reinforced polymers to improve seismic resistance of masonry. Construction and Building Materials 20 (4), 269−277.

Singleton, A.C.N., Baillie, C.A., Beaumont, P.W.R., Peijs, T., 2003. Composites B: Engineering 34, 519.

Steyer, T.E., 2013. Shaping the future of ceramics for aerospace applications. International Journal of Applied Ceramic Technology 10 (3), 389−394.

Taylor, A., July/August 2000. RTM material developments for improved processability and performance. SAMPE Journal 36 (4), 17e24.

Toldy, A., Szolnoki, B., Marosi, Gy, 2011. Flame retardancy of fibre-reinforced epoxy resin composites for aerospace applications. Polymer Degradation and Stability 96, 371−376.

Valadez-Gonzalez, A., Cervantes-Uc, J.M., Olayo, R., 1999. Effect of fiber surface treatment on the fiber−matrix bond strength of natural fiber reinforced composites. Composites Part B: Engineering 30 (3), 309−320.

van de Velde, K., Kiekens, P., 2002. Journal of Applied Polymer Science 83, 2634.

van Voorn, B., Smit, H.H.G., Sinke, R.J., de Klerk, B., 2001. Composites A: Applied Science and Manufacturing 32, 1271.

Wielage, B., Lampke, T., Marx, G., Nestler, K., Starke, D., 1999. Thermogravimetric and differential scanning calorimetric analysis of natural fibres and polypropylene. Thermochimica Acta 337, 169−177.

Williams, J.G., 1989. The fracture mechanics of delamination tests. Journal of Strain Analysis for Engineering Design 24 (4), 207−214.

Carbon–carbon composites in aerospace engineering

<div style="text-align:right">**13**</div>

C. Scarponi
"La Sapienza" University of Rome, Rome, Italy

13.1 Introduction

Carbon–carbon (C–C) composites are a family of advanced composite materials. They are the most advanced form of carbon and consist of fibres based on carbon precursors embedded in a carbon matrix and carbon nanotubes (CNTs) embedded in a carbon matrix. These materials are available in different shapes, from one-dimensional to n-dimensional (Fig. 13.1), depending on the raw material utilized (yarns, tapes, fabrics, knitted and braided preforms). This is the reason why the performance can be tailored depending on the applications. Originally developed for aerospace applications, today C–C composites are at the first rank among ceramic composite materials with a spectrum of properties and applications in various sectors.

The chapter highlights how C–C composites' low density, high thermal conductivity and excellent mechanical properties, also in the presence of elevated temperatures, make such materials ideal not only for aircraft brakes, rocket nozzles and re-entry nose tips, but also in most common applications such as mechanical industry and bioengineering. Moreover, in inert atmosphere, C–C composites present good chemical stability; in contrast, in the presence of an oxidizing environment, they suffer a strong
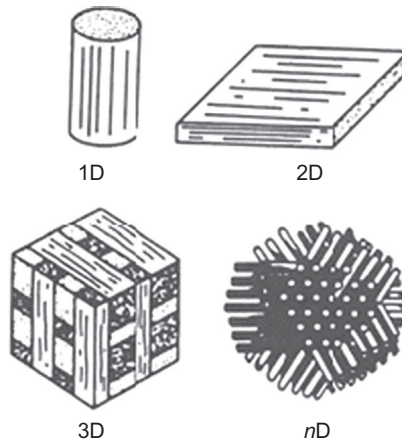
Figure 13.1 Multiple forms of carbon fibre and carbon–matrix composites.
Reproduced from Buckley, J.D., Edie, D.D., 1993. Carbon-Carbon Materials and Composites. Noyes Publications, Park Ridge, NJ, USA.

oxidation and a strong decrease of their characteristics. Therefore, it is mandatory to provide protection with coatings, which will also be discussed in this chapter.

The research on C−C materials started with the program Boeing X-20Dyna-Soar (years 1957−1963) under the responsibility of the US Air Force. The military program had the purpose of developing a sort of multimission spacecraft, to be used for reconnaissance, bombing, repairing or destroying satellites and so on. The program was abandoned before the construction of the first prototype. The technology of carbon fibres accelerated at the end of the 1960s, emerging as an innovative, high-performance material to be used for the construction of aerospace structures.

In the middle of the 1970s, C−C composites were used extensively in both the United States and Europe for the construction of Boeing 757 and Boeing 767 parts. For these applications, carbon fibres were embedded in epoxy resins. C−C composites were extensively used for missile applications, as a part of NASA's Apollo spacecraft heat shield system and numerous thermal protection systems, such as the ones used for the Space Shuttle Program. For this application, the reinforcement was used in the form of woven fabrics, and the matrix was derived from pyrolysed phenolic resin (Buckley and Edie, 1993).

As mentioned in this chapter, C−C composites consist of carbon fibre or CNTs embedded in a carbonaceous matrix. The CNT technology in a carbonaceous matrix will be described in Section 13.5. The aim of these materials is to combine the advantages of traditional fibre-reinforced composites, such as high specific strength, stiffness and in-plane toughness, with ceramics' refractory properties. A refractory material is able to resist high temperatures, preserving its mechanical and chemical properties. ASTM C71 defines such material as 'non-metallic materials having those chemical and physical properties that make them applicable for structures or as components of systems that are exposed to environments above 1000°F (811 K; 538°C)'.

The retention of mechanical properties at high temperatures, superior to any other material, has resulted in the exploitation of C−C composites as structural materials in space vehicles' heat shields, rocket nozzles and aircraft brakes. In terms of mass consumption, the main applications of C−C composites are still in high-performance braking systems. C−C composites are used not only in aerospace applications but also in other sectors, such as engine components like refractory materials, hot-pressed dies and heating elements, high-temperature fasteners, liners and tube protection coatings, guides in glass industries and so on. C−C composites have also great potential in energy sectors as polar plates for fuel cells and storage batteries (Manocha, 2003).

Applications of C−C composites in the medical field are also very promising, due to their biocompatibility and chemical inertness (Savage, 1993). In particular, the field of substitution of natural bone is still very open to experimentation: a number of different biomaterials have been used as orthopaedic implants, including polymers, metals, ceramics and composites, with variable success. Today, C−C composites are considered the most promising artificial materials for orthopaedic implants owing to their unique properties. In particular, C−C composites have a more similar elastic modulus to that of natural bone, in comparison with metallic implants (Leilei et al., 2013).

13.2   Concept of C–C composites

C–C composites consist of a fibrous carbon substrate in a carbonaceous matrix. Although both constituents are the same element, this fact does not simplify the composite's behaviour because the state of each constituent may range from carbon to graphite. Crystallographic carbon, namely graphite, consists of tightly bonded, hexagonally arranged carbon layers that are held together by weak van der Waals forces (Fig. 13.2). The bonding energy among layers is about 7 kJ/mol. The single-crystal graphite structure (hexagon) is composed of very strong covalent bonds, having energy of about 524 kJ/mol. The result is that the crystal presents a quasi-isotropic behaviour in its plane and a strong anisotropy along the direction orthogonal to the crystal's planes.

On a larger scale, carbon, in addition to its two well-defined allotropic forms (diamond and graphite), can take any number of quasi-crystalline forms ranging continuously from amorphous, glassy carbon to a highly crystalline graphite. The anisotropy of the graphite single crystal encompasses many structural forms of carbon. It ranges in the degree of preferred orientation of the crystallites and influences the porosity, among other variables. A broad range of properties is the result of this anisotropy, which is available in carbon material. In C–C composites, this range of properties can extend to both constituents.

In consideration of the variability of microstructures, base materials and different production methods (to be described below) to obtain C–C composites, it is easy to understand the high level of design flexibility and the high range of properties obtainable for these kinds of materials. In fact, the properties of the C–C composites are strongly influenced by many additional factors. From the side of fibres, the fibrous component can consist of short or long fibres, unidirectional tapes, bidirectional fabrics and woven materials (two-dimensional (2D) and three-dimensional (3D)).

The properties of carbon fibres can vary over a wide range, depending on the organic precursors and carbonization process. The precursors are rayon (nowadays practically unutilized), polyacrylonitrile (PAN) and pitch (obtained as a residue of petroleum treatment). The PAN precursor produces better performance than rayon. Depending on the process, it is possible to obtain low, medium or high-modulus fibres.

Moreover, the higher the fibre volume fraction, the higher the mechanical characteristics, up to about 60%.

The production process for carbon and graphite fibres is the same: carbonization of a pretensioned PAN precursor in inert atmosphere at high temperature (about 1600°C)
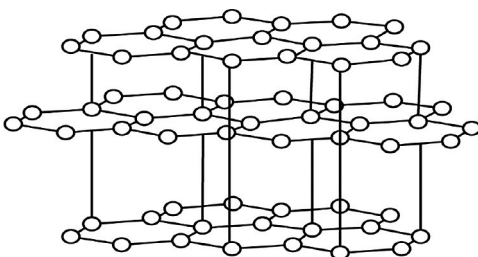
Figure 13.2 Hexagonal carbon layers held together by weak van der Waals forces (Buckley and Edie, 1993).
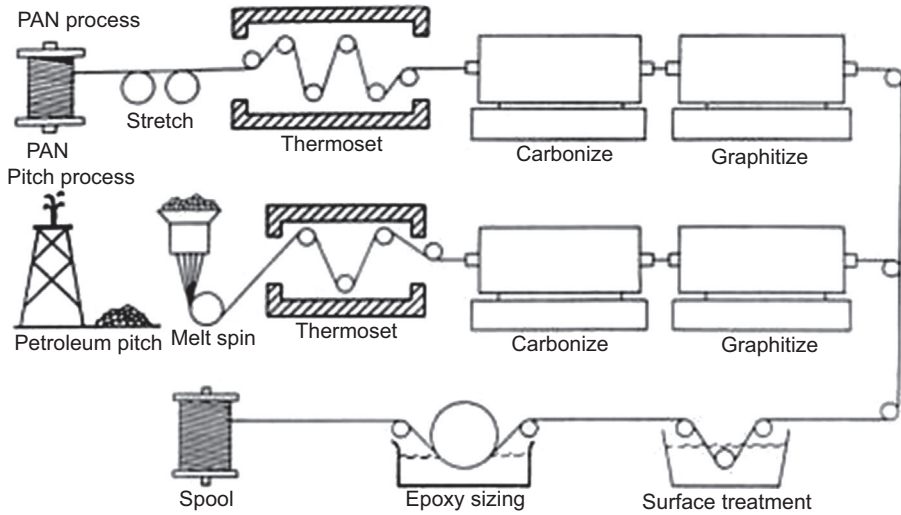
Figure 13.3 The processing sequence for PAN and mesophase pitch-based precursor carbon fibres.
Reproduced from Buckley, J.D., Edie, D.D., 1993. Carbon-Carbon Materials and Composites. Noyes Publications, Park Ridge, NJ, USA.

and graphitization at higher temperature (about 2600°C) in order to get, respectively, high-strength and high-modulus fibres. In contrast, the process used in the case of a pitch precursor is slightly different. The process is similar to the one used for glass fibres: melting, production of very thin filaments, then carbonization without tensioning. Both processes are described in Fig. 13.3.

Fibre architecture can be classified into four categories: discrete, continuous, planar interlaced (2D) and fully integrated (3D) structures (Figs. 13.4 and 13.5). In Table 13.1, the nature of the various levels of fibre architecture is summarized.

The matrix can be obtained by the carbonization of organic precursors, usually resins. The process temperature is maintained between 800°C and 1500°C. C−C is not a single material, but rather a family of materials, many combinations of which have yet to be realized and evaluated. It is easy to understand that the costs of such a family of composites are very high, so their use can be taken into account essentially for applications where the resources are justified (Buckley and Edie, 1993).

13.3 Processing of C−C materials

C−C composites are generally manufactured by two different techniques:

- Carbonization through pyrolysis of an organic matrix (both thermosetting and thermoplastic) or
- Chemical vapour deposition (CVD), by the use of a hydrocarbon gas.
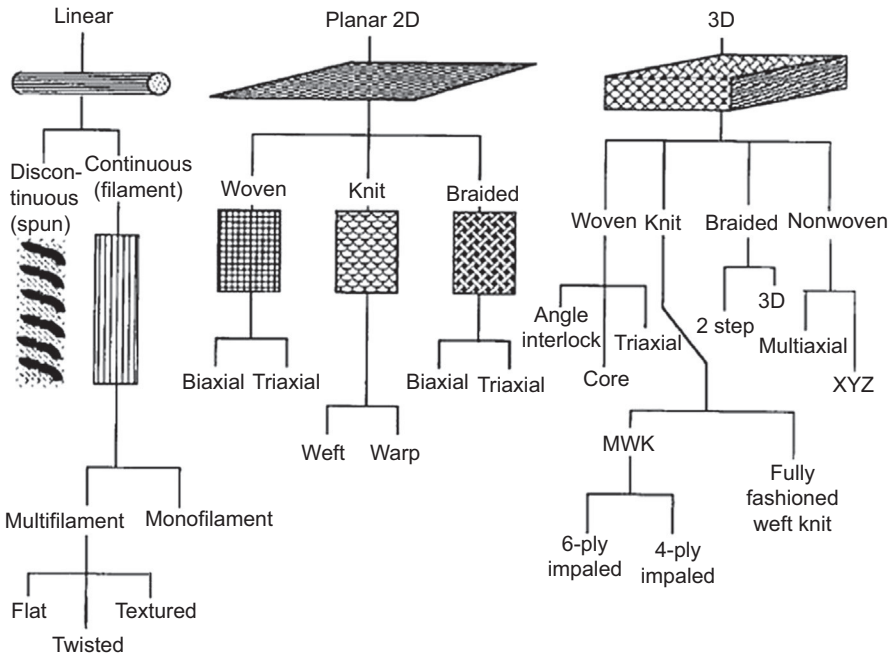
Figure 13.4 Classification of fibre architecture.
Reproduced from Buckley, J.D., Edie, D.D., 1993. Carbon-Carbon Materials and Composites, Noyes Publications, Park Ridge, NJ, USA.

Matrix pyrolysis produces two important problems:

- Shrinkage, producing porosity due to the effect of the material volume reduction and
- Residual stresses and cracks in correspondence with the matrix−fibre interface, due to gradients between the coefficients of thermal expansion (CTEs).
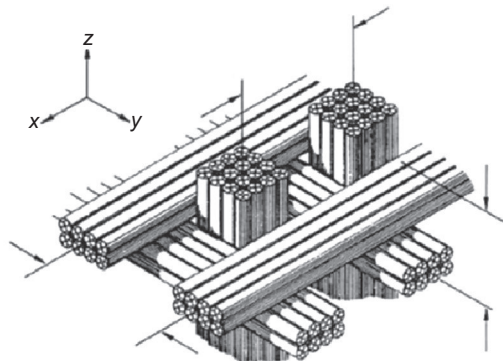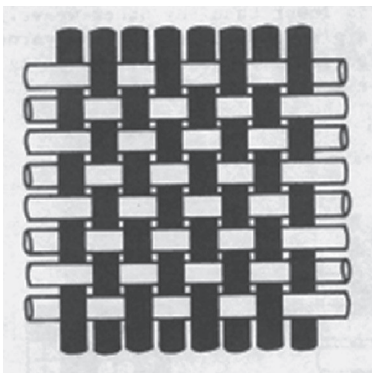
Figure 13.5 Bidirectional woven fibres and 3D constructions.
Reproduced from Savage, G. (Ed.), 1993. Carbon-Carbon Composites, Chapman & Hall.

Table 13.1 Fibre architecture for composites

Level	Reinforcement system	Textile construction	Fibre length	Fibre orientation	Fibre entanglement
I	Discrete	Chopped fibre	Discontinuous	Uncontrolled	None
II	Linear	Filament yarn	Continuous	Linear	None
III	Laminar	Simple fabric	Continuous	Planar	Planar
IV	Integrated	Advanced fabric	Continuous	3D	3D

Buckley, J.D., Edie, D.D., 1993. Carbon-Carbon Materials and Composites, Noyes Publications, Park Ridge, NJ, USA.

The aforementioned issues, together with the inherent differences of quality of the organic matrices, have a significant consequence: that, at the end of pyrolysis, usually the content and the distribution of the carbonized matrix are not satisfactory. As a result, further new cycles of impregnation and pyrolysis are necessary to obtain good quality for the part produced using this technique. The method is time-consuming and the costs are very high (Buckley and Edie, 1993).

13.4   Chemical vapour deposition

Fabrication of composite materials requires deposition of a desired matrix inside and around a fibre preform. The fibrous phase can be structured as a mat or continuous woven fibres, starting from unidirectional to multidirectional architectures. The porous structure of the preform has to be filled by the matrix and the deposition must be homogeneous. The CVD process has to provide the diffusion of the reactants through the boundary of the preform, the homogeneous penetration into the pores and finally the absorption and correct reaction. A deep description of the complex mechanisms of diffusion rate and consolidation is beyond the scope of the present book.

In the CVD process, a solid product (the matrix) nucleates and grows on a substrate (a heated fibre preform) by decomposition or reaction of gaseous species. The product is placed in a furnace, where its pores are filled with carbon, which is produced from the thermal decomposition (cracking) at high temperature (about 1250°C) of a hydrocarbon gas. This appears easy in principle, but the results are very complex in practice. Usually, the gases utilized are methane or propane.

CVD can provide superior properties to composites as compared to those made by any of the other routes, as the matrix is built up layer by layer, thus ensuring good fibre—matrix bonding and minimizing the number of defects in the structure. A further advantage of this process is that it can also be used to deposit noncarbon materials such as oxidation-protective coatings and inhibitors. However, CVD is an extremely slow and expensive process, requiring considerable operator skill and sophisticated tooling. In commercially operated processes, it is generally necessary to compromise between an ideal system and one in which the rate of carbon deposition occurs at an economically viable rate. The process can be conducted fundamentally by three different methods, schematically illustrated in Fig. 13.6: isothermal, thermal gradient and pressure gradient. CVD methods produce better mechanical characteristics, with the inconvenience of higher time and costs. However, the choice of the technology strongly depends on the application (Savage, 1993).

13.4.1   The isothermal method

The isothermal method is a technique consisting of a fibrous phase placed in a furnace and the reactant gases crossing over it (Fig. 13.7). Diffusion can start in and out of the pores. It is important to maintain the rate of the surface reaction lower than the rate of
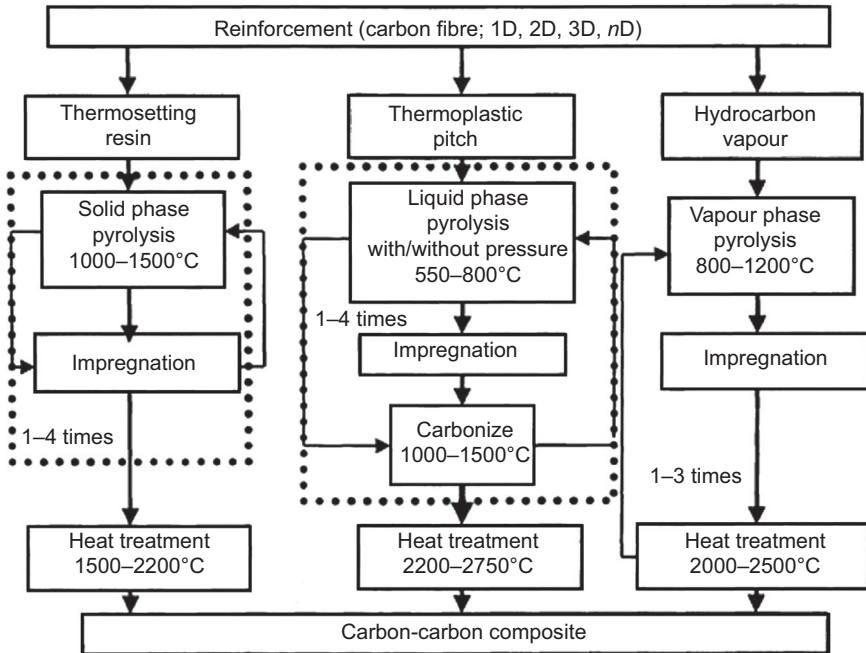
Figure 13.6 Processing of C−C composites.
Reproduced from Manocha, L.M., February/April 2003. High performance carbon−carbon composites. Sadhana 28 (Parts 1 & 2), 349−358.
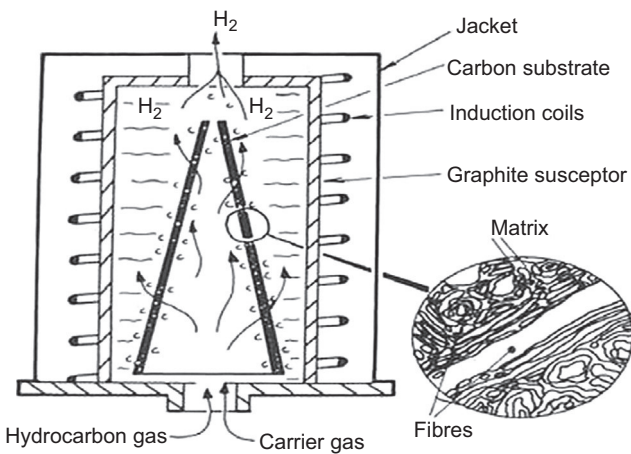
Figure 13.7 The isothermal method of CVD processing.
Reproduced from Buckley, J.D., Edie, D.D., 1993. Carbon-carbon Materials and Composites. Noyes Publications, Park Ridge, NJ, USA.
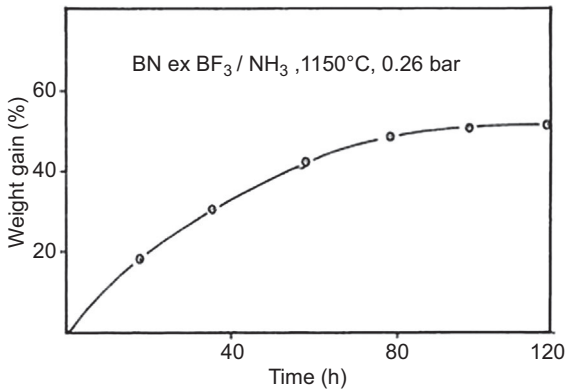
Figure 13.8 Weight gain and time for the densification of a carbon skeleton with boron nitride. Reproduced from Savage, G. (Ed.), 1993. Carbon-Carbon Composites, Chapman & Hall.

diffusion; otherwise, the pores will be sealed before the complete reaction can happen. Consequently, the weight gain rate is very slow, and the process times are very high. In addition, the densification rate slows down as the amount of porosity decreases, which does not allow full completion of the densification. The graph in Fig. 13.8 shows the amount of the weight gain in percentage with respect to time obtained for the densification of a porous C−C billet (solid to give shape to the piece) in the presence of BF_3−NH_3 (boron nitride; see Savage, 1993). It is clear how the weight gain reduces with respect to time until it reaches an asymptotic value.

This means that the parameters governing the isothermal method need to be selected as a good compromise between two conditions: obtaining well-densified materials while working in economically viable conditions as far as the deposition rate is concerned. The isothermal process, despite its limitations, remains in widespread use for the production of C−C composites. In cases in which the simultaneous production of different parts is required, a large furnace can be used for the purpose.

In practice, C−C billets are processed up to one week; in fact, the process starts for the first deposition, then the part is removed from the furnace and machined to open the surface blockage of the pores. After that, the part is repositioned into the furnace and re-densified. The cycle can be repeated three or four times, and the part can be ready for the customer in about one month.

13.4.2 The thermal gradient method

In the thermal gradient technique (Fig. 13.9), the fibrous part is supported by a mandrel, made of general solid graphite that is inductively heated. Sometimes, the part is obtained by the filament winding technique. The hottest portion of the substrate is the inside surface, directly in contact with the hot mandrel. The outer surface is exposed to a cold environment: this results in a gradient of temperature through the substrate thickness. Surface crusting is eliminated because the deposition rate is greater on the heated fibres near to the mandrel, whereas the outer fibres receive little or no deposit. Under proper infiltration conditions, carbon is first deposited on the inside
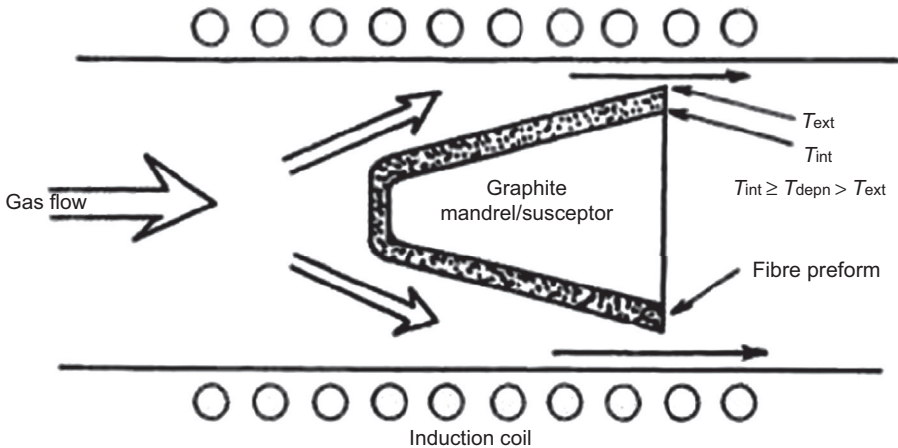
Figure 13.9 Thermal gradient method scheme.
Reproduced from Savage, G. (Ed.), 1993. Carbon-Carbon Composites, Chapman & Hall.

surface and, in a continuous process, progresses radially to the substrate, as the densi-
fied substrate itself becomes inductively heated. Infiltration is normally accomplished
at atmospheric pressure, and the mandrel is heated more or less till it reaches a temper-
ature of about 1100°C.

   Two main parameters governing the process are the conductivity of the preform and
the gas flow velocity. The best combination is low conductivity and high rate. From the
experimental point of view, a thermal gradient of 500°C in 1 cm thickness has been
obtained (Savage, 1993). With respect to the isothermal method, the thermal gradient
allows considerably higher deposition rates. The disadvantage is the limitation of pro-
cessing a single item each time.

13.4.3   The pressure gradient method

The pressure gradient method relies on forced flow of the precursor gas mixture
through the pores of the fibre preform. The fibre preform is sealed into a gas-tight
unit and heated as usual (Fig. 13.10). The resistance to gas flow of the fibre preform
produces a pressure gradient to be set up. In this process, the deposition rate increases
with time because the pressure gradient increases as the pores are filled up, just the
opposite to the previous processes described in this chapter. The deposition rate is
found to be proportional to the pressure drop across the preform.

   Although such an important result has been obtained, nevertheless the pressure
gradient method presents severe drawbacks:

- The method is confined to a single item.
- Seals must have high resistance to high temperatures and high pressures.
- Pores blockage may occur.
- Removal of the piece and surface machining could be necessary to ensure in-depth infilling.

   These are the reasons why this method is not popular for commercial use (Savage,
1993).
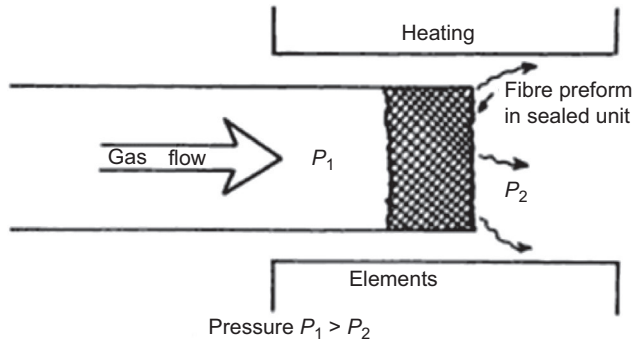
Figure 13.10 Schematic of the pressure gradient method.
Reproduced from Savage, G., 1993. Carbon-Carbon Composites, Chapman & Hall.

13.5 C−C composites from CNTs

CNTs, discovered by Sumio Iijima in 1991 (Monthioux and Kuznetsov, 2006), are an allotropic tube-shaped material made of carbon. A CNT's diameter is in the nanometric scale, ranging from <1 nm up to 50 nm, and its length is not over several microns (Wang et al., 2009). Nowadays, there are mainly two kinds of CNTs: single-walled carbon nanotubes (SWCNTs) and multiwalled carbon nanotubes (MWCNTs), as shown in Fig. 13.11. They could be employed for nanotechnology, electronics, optic and structural tasks, thanks to their higher thermal and electrical conductivity as well as mechanical properties.

Different techniques have been developed to produce them, through arc discharge, laser ablation, carbonization of an organic matrix using a pyrolysis method and CVD in vacuum or atmospheric pressure. Applications of carbon nanotubes are again at the
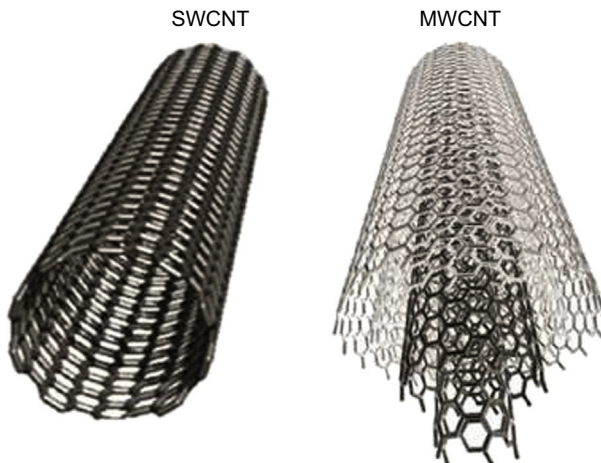
Figure 13.11 From left to right: a single-walled carbon nanotube (SWCNT) and multiwalled carbon nanotube (MWCNT).
Reproduced from Choudhary, V., Gupta, A. Polymer/Carbon Nanotube Nanocomposites, Centre for Polymer Science and Engineering Indian Institute of Technology, Delhi, India.

laboratory level, but the development of industrial applications is very promising. CNTs can be used as reinforcing structure in composite materials instead of fibres, thanks to their extraordinary mechanical properties. Standard CNTs can resist stress up to 25 GPa without deformation, and the highest stress measured is 55 GPa. The bulk modulus varies from 462 to 546 GPa (Popov et al., 2002). This is the reason why such materials can be applied for the production of special clothes, sports goods, combat jackets and space elevators as well (Edwards, 2003).

The existence of crystallographic defects, as vacancies, affects CNTs. High levels of such defects can lower the tensile strength by up to 85%. CNTs can be embedded in a carbon-based matrix. The use of classical carbonization processes (Fig. 13.12), similar to the same techniques utilized for the production of the nanotubes themselves, will create a new class of materials: C—C nanotubes, as presented in Fig. 13.13.

13.6   Structure of C—C composites

The microstructure depends on the carbonization process used, so the structure is different if the fabrication process is a CVD process using a hydrocarbon gas or the pyrolysis and eventually graphitization of a thermoset matrix or a thermoplastic matrix (Savage, 1993).
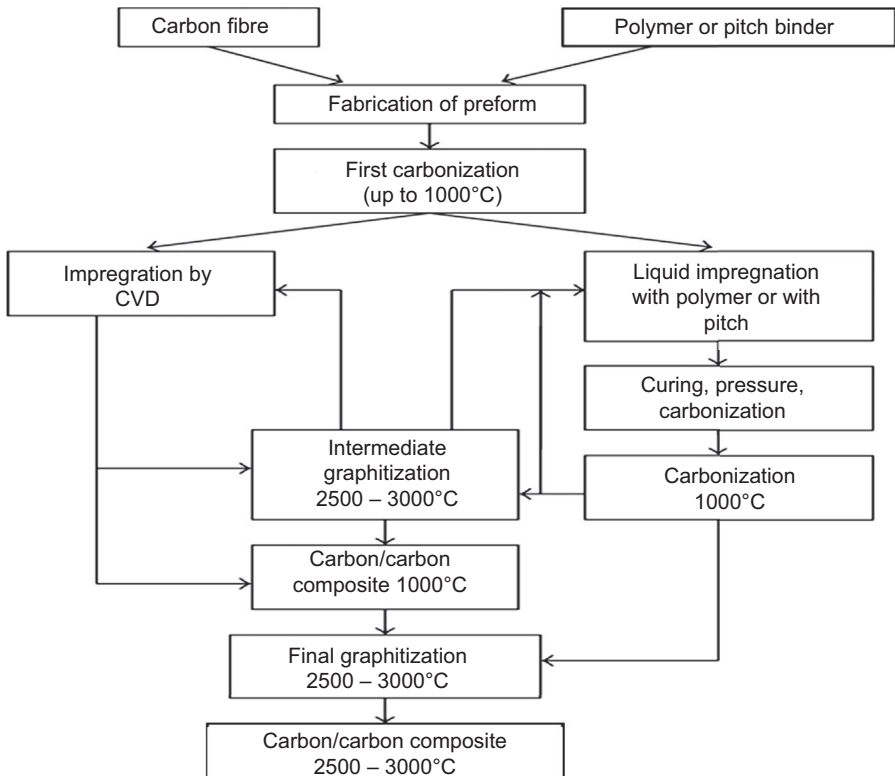
Figure 13.12 Process of manufacturing C—C composites.
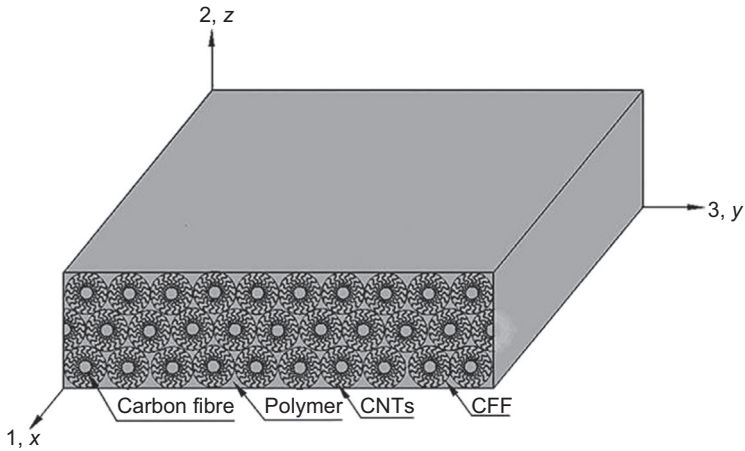
Figure 13.13 Section of a C−C composite reinforced with CNTs.

13.6.1   Pyrolysis of a thermoset matrix

In this case, the microstructure will vary dramatically, depending on the process temperature. When carbonized itself, the thermoset resin forms a glassy isotropic carbon at a temperature on the order of greater than 1000°C, but it is a graphite structure at the interface with the carbon fibres. As soon as the temperature increases to 2200°C, the anisotropy will be reduced, to disappear completely at about 2800°C, when the matrix will get the complete graphitization. At the end, the microstructure of thermoset-derived matrices is oriented in such a way that the graphite planes encircle the fibres (Savage, 1993).

13.6.2   Pyrolysis of a thermoplastic matrix

The microstructure of a pyrolysed thermoplastic matrix, such as polyether ether ketone (PEEK), usually performed under a pressure of about 10 MPa, is not affected practically by the fibre type. The matrix is organized in graphite with planes parallel to the fibres' direction (along the interphase), with high density and low porosity (Fig. 13.14) (Savage, 1993).

13.6.3   Microstructure of CVD-densified composites

Matrix deposited in the CVD process could be of three different types. The first one is the isotropic type, which consists of an optically isotropic morphology of fine particles, no more than a few microns in size. The other two kinds have optically anisotropic morphologies. The most important differences are due to the processing method: concentration and partial pressure of reactant gas and the processing temperature.

Figure 13.14 C−C composite with PEEK-derived matrix.
Reproduced from Savage, G. (Ed.), 1993. Carbon-Carbon Composites, Chapman & Hall.

The mechanisms involved in CVD are complex and still not completely understood. CVD processes produce an interphase graphitic phase without the typical shrinkage and stresses inducted by pyrolysis processes. Therefore, the mechanical characteristics are higher. The microstructures of CVD-densified composites are shown in Figs. 13.15−13.17.

250 µm
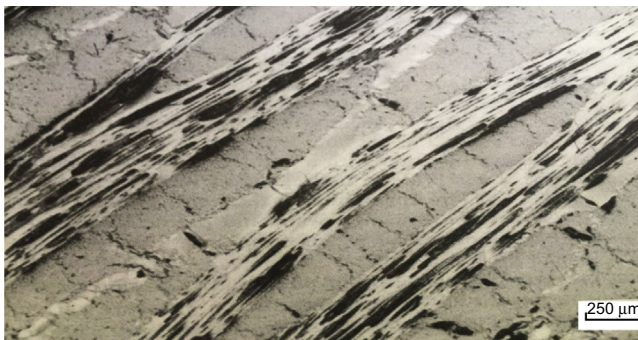
Figure 13.15 Polarized optical micrograph of a densified composite showing optical anisotropy.
Reproduced from Savage, G. (Ed.), 1993. Carbon-Carbon Composites, Chapman & Hall.
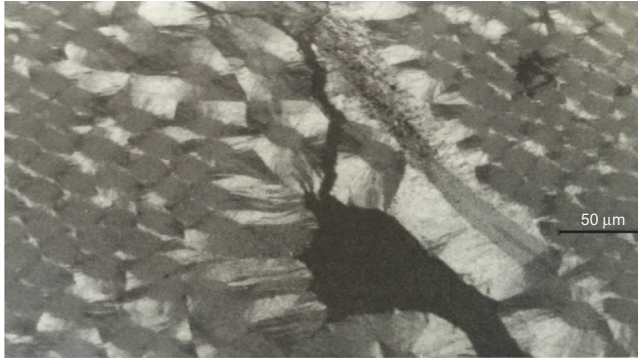
Figure 13.16 CVD detailed microstructure showing a rough lamellar matrix.
Reproduced from Savage, G. (Ed.), 1993. Carbon-Carbon Composites, Chapman & Hall.

Figure 13.17 Optical micrograph showing a microstructure of C−C composites.
Reproduced from Savage, G. (Ed.), 1993. Carbon-Carbon Composites, Chapman & Hall.

13.7 C−C properties

C−C is a family of composites whose microstructures and properties may be tailored to a great degree for a range of applications. Depending on the nature of fibres and matrices, architecture of the fibre preform, fibres−volume ratio, fabrication processes, oxidation-protective coatings, inhibitors and any other additives, the number of combinations to create different properties are almost limitless. C−C composites retain their strength at very high temperatures. High thermal conductivity and low thermal expansion give C−C composite materials an excellent resistance to thermal shock. A high heat of sublimation and low CTE for carbon and graphite result in good ablation resistance. Other advantages include chemical resistance, excellent high-temperature wear characteristics, biocompatibility, shape stability and pseudo-plastic fracture behaviour.

When C−C materials do break, they generally undergo a nonbrittle, pseudo-plastic type of fracture, rather than catastrophic failure. The deployment of C−C materials, despite their attractive properties, is severely limited, however, due to two serious

Table 13.2 **Main properties of C−C composites, GFRP and CFRP**

Property	UD HM fibres C−C composites	Epoxy-GFRP	UD HM fibres CFRP
Young's modulus	95 GPa	12.3 GPa	17 GPa
Density	1.5 g/cc	1.8 g/cc	1.6 g/cc
Shear modulus	36 GPa	30 GPa	33 GPa
Compressive strength	240 MPa	90 MPa	110 MPa
Specific heat capacity	760 J/kg K	960 kg^{-1} K^{-1}	795 kg^{-1} K^{-1}
Ultimate tensile strength	900 MPa	90 MPa	110 MPa
Thermal conductivity	40 W/m K	1.2−1.5 W/m K	15 W/m K
Thermal diffusivity	2.16 × 10^{-4} m^2/s	1.63 × 10^{-7}−1.77 × 10^{-7} m^2/s	1.6 × 10^{-7}−2.2 × 10^{-7} m^2/s
Thermal expansion	4 × 10^{-6}% K^{-1}	2.8 × 10^{-6}% K^{-1}	−1.2 × 10^{-6}% K^{-1}

Data regarding GFRP and CFRP refer to fibres ± 45 degree to loading axis, dry, room temperature, $V_f = 60\%$.
UD, unidirectional; *HM*, high modulus.

drawbacks. The materials are extremely expensive to produce, as a result of very slow and inefficient processes currently used in production. Furthermore, C−C composites oxidize at temperatures as low as 400°C, unless protected in some way. In addition, C−C exhibits low strain to failure, poor matrix properties, poor erosion resistance, lack of resistance to attack by moisture and severe difficulties with joining. For a fast reference, Table 13.2 shows the main properties of C−C composites in comparison with other materials, such as glass-fibre-reinforced plastic (GFRP) and carbon-fibre-reinforced polymer (CFRP).

13.7.1 Mechanical properties

In general, mechanical characteristics strongly depend on the fibres' architecture and content. Generally, the maximum value of the fibre content is 60% in volume. For instance, in a UD system, Young's modulus and the strength to normal stresses will be maximum along the fibre direction, following the mixture rule, and minimum in the transverse direction (Fig. 13.18).

Along the fibres, the mechanical properties of the composite are very near to the fibre properties, whereas along the transverse direction the properties are a little bit higher than the ones corresponding to the matrix itself. The strength of C−C composite materials does not generally follow the simple 'law of
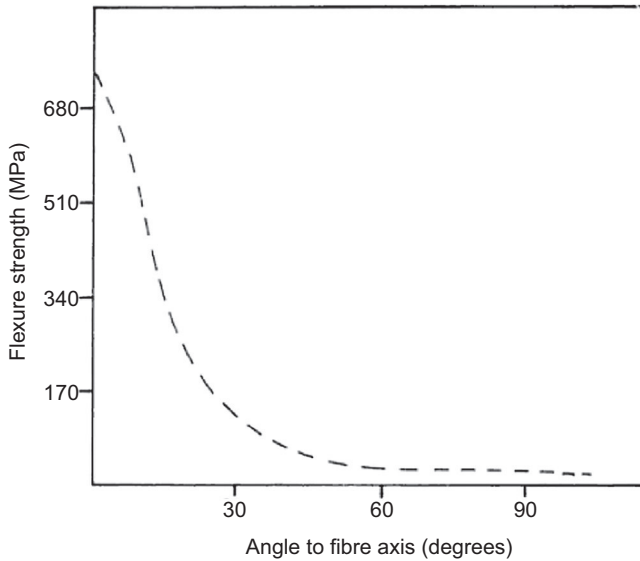
Figure 13.18 Effect of the angle between fibre axis and the load directions on the strength of a C−C composite.
Reproduced from Savage, G. (Ed.), 1993. Carbon-Carbon Composites, Chapman & Hall.

mixtures' relationship, as said above. The shrinkage due to the pyrolysis of the matrix can produce a severe decrease of the volume of about 50%. A shrinkage of this magnitude can create severe damage to the composite due to the onset of large stresses related to it. Severe thermal stresses, due to thermal expansion mismatches between fibre and matrix and between different matrix structures, result conversely in an ineffective transfer of applied loads from the matrix to the reinforcement. The result of the extended heat treatments produces weak interfacial bonding and a time-dependent deterioration of the composite during service cycles. This is the reason why simple calculations following the classical micromechanics rules yield higher results than the experimental data. Depending of materials and processes, mechanical properties of C−C tend to vary between 10% and 60% lower than the calculated values. The value frequently referred to in the scientific literature for the interlaminar shear strength is 30 MPa. One of the major assets of C−C composites is the retention of the mechanical properties at high temperatures (Fig. 13.19). Compared to the values at ambient temperature, the values of the Young's modulus and the maximum strength are higher by about 10−20% up to 1500°C.

Very little work is presented in the open literature concerning the fatigue performance of C−C composites. A Wölher diagram presented by Shunk (2001) suggests that the fatigue limit is analogous to that of steel. The infinite fatigue life is predicted as about 45−50% of the static strength in the case of 10^7 cycles under a constant cyclic sinusoidal load (Fig. 13.20).
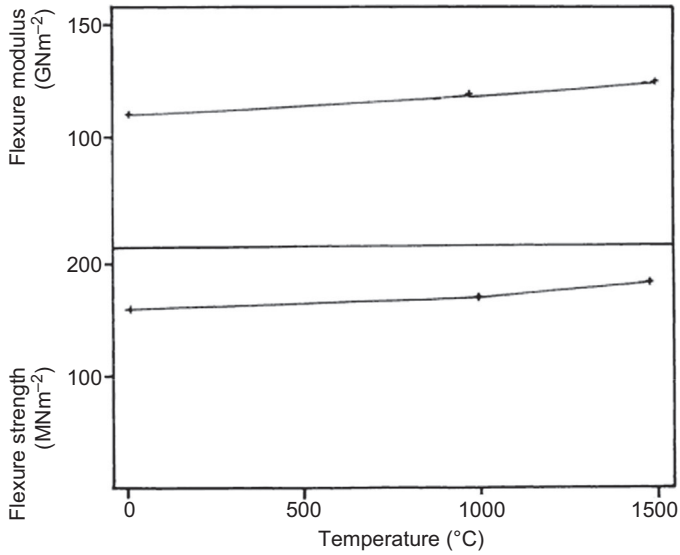
Figure 13.19 Change in flexure strength and modulus of a C−C composite made from a thermoset precursor with respect to operating temperature.
Reproduced from Savage, G. (Ed.), 1993. Carbon-Carbon Composites, Chapman & Hall.
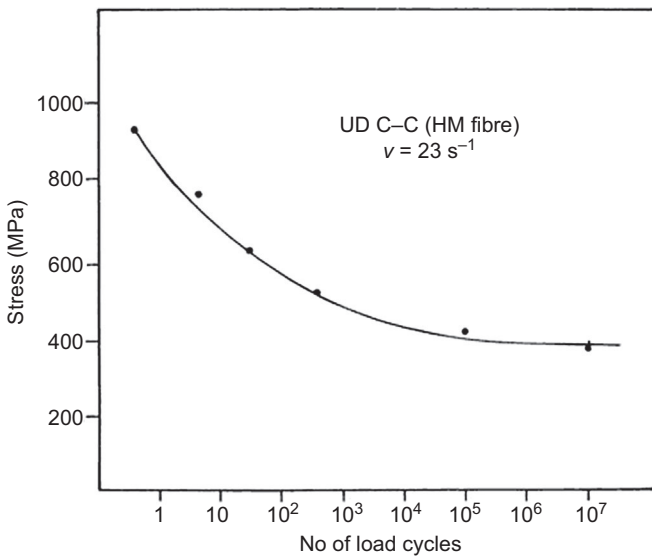
Figure 13.20 Fatigue curve for a C−C composite.
Reproduced from Savage, G. (Ed.), 1993. Carbon-Carbon Composites, Chapman & Hall.

13.7.2   Thermal properties

Next to mechanical properties, the most important characteristics of a C−C composite are thermal conduction and thermal expansion. C−C composites present the opportunity to 'tailor' thermo-physical properties into carbon materials due to the various fibre preforms, different matrices and different processes, producing different microstructures for the matrix (Savage, 1993).

13.7.2.1   Thermal conductivity

The fibres will dominate the composite thermal conductivity. The role of the matrix is different, depending on the composition (thermoset or thermoplastic) and process. The behaviour depends on the microstructure (level of crystallinity). The higher the crystallinity is, the higher the heat conduction will be. For this reason the heat conduction of thermoset glassy carbon matrices has a low thermal conductivity with respect to thermoplastic and CVD matrices, richer in graphite, presenting a higher level of crystallinity. For C−C composites, having a heterogeneous structure consisting of fibres, a matrix and pores, with the first two having a variety of microstructures, estimation of their thermal transport properties becomes complex. However, C−C materials with tailored thermal conductivities can be fabricated by the proper choice of constituents, their configuration and the processing conditions.

A comparison of thermal conductivities of C−C composites with different fibre−matrix combinations is given in Fig. 13.21. Composites with highly oriented graphitic fibres, matrices or their combination, like vapour-grown carbon fibres and matrix or mesophase pitch-based carbon fibres and matrix, exhibit very high thermal conductivities on the order of 250−350 W/m K in the fibre direction. Though these composites
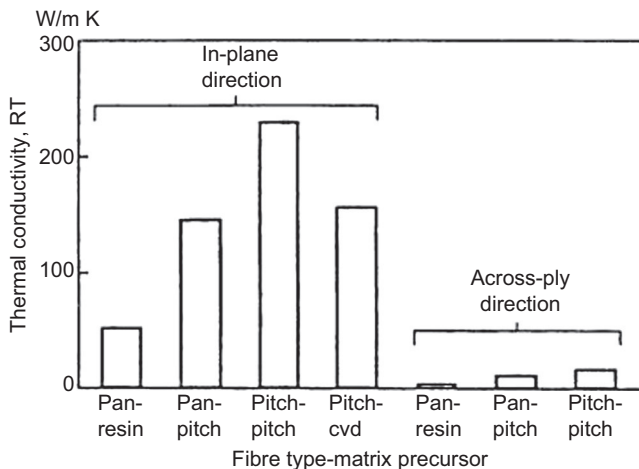
Figure 13.21 Thermal conductivity of C−C composites with different fibre−matrix combinations.
Reproduced from Savage, G. (Ed.), 1993. Carbon-Carbon Composites, Chapman & Hall.

Table 13.3 **Thermal conductivity of 3D phenolic-derived C−C materials**

Thermal conductivity (W/m K)	X−Y plane	Z-direction
At 250°C	830	55.4
At 2500°C	27.7	24.5

Table 13.4 **Thermal conductivity of 3D weave T-50 fibre with thermoplastic matrix**

Thermal conductivity (W/m K)	X−Y plane	Z-direction
At 30°C	149	246
At 1600°C	44	60

exhibit highly anisotropic character and low conductivities in transverse directions, there is always scope for improvement by varying the fibre architecture and their incorporation in different forms and ways. Thermal conductivity strongly depends on the temperature, and decreases as soon as temperature increases. Some data presented by McAllister and Lachmann (1983) are reported in Table 13.3.

Analogous data published by the Battelle Institute (McAllister & Lachmann, 1983) concerning the same parameter for a 3D weave T-50 fibre with a thermoplastic matrix are shown in Table 13.4. It is important to remember that, because of the material anisotropy, the heat conductivity coefficient is not a single parameter for the whole material, but a symmetric tensor of second-order 3×3. The matrix is therefore completely defined if six parameters are measured. It is easy to understand the difficulties in determining the full tensor. This is the reason why only some peculiar data for specific research are in the scientific literature (Savage, 1993).

13.7.2.2 Thermal expansion

Thermal expansion is an important property when using materials at high temperatures. The CTE of the composites is influenced largely by the fibre orientation. The measured values of the CTE are between 0 and 1×10^{-6}/K in the fibre direction and $6-8 \times 10^{-6}$/K in a direction perpendicular to the fibres (Manocha, 2003). Because of the material anisotropy, also the CTE is not a parameter, but a symmetric tensor of second-order 3×3. The matrix is completely defined if six parameters are measured. It is easy to understand the difficulties to conduct all the necessary tests (Savage, 1993).

13.8 Frictional properties

C−C composites have broadened the field of application of carbon-based materials in wear-related applications, from bearing seals and electrical brushes to brake pads for heavy-duty vehicles, from military, supersonic and civilian aircrafts to trucks and railways. Such applications are possible thanks to the basic tribological properties and additional high-strength and thermal conductivity characteristics of these materials. C−C composites exhibit low coefficient of friction in the fibre direction (0.3−0.5) and 0.5−0.8 in the perpendicular direction. Wear rates also follow similar trends (0.05−0.1 and 0.1−0.3 mm, respectively).

In general, for fabricating brake discs for different vehicles, different types of fibres (PAN and pitch based, with high strength and high thermal conductivity) are used in a number of configurations, either alone or in combinations with a carbon matrix derived from a different type of precursor, whether pitch or CVD. In commercial C−C brake pads, carbon fibre fabric plies are used with fibre tows inserted in the third direction and pitch−CVD route for densification. However, the choice of the constituents and processing parameters is at the discretion of the manufacturers (Manocha, 2003).

13.9 Electrical properties

When a thermoset-based C−C is heat treated to above 2800°C, there is 3D crystallite growth. The electrical conductivity, as shown in Fig. 13.22, increases correspondingly. The development of a 3D structure is seldom, if ever, observed in carbon fibres. The electrical conductivity of a C−C composite is primarily governed by the density and by the matrix microstructure, including porosity (Savage, 1993).
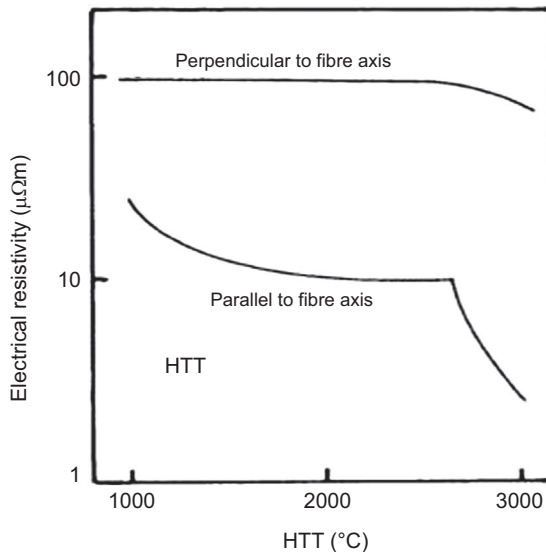
Figure 13.22 Relationship between electrical resistance and heat treatment temperature for a thermoset resin.
Reproduced from Savage, G. (Ed.), 1993. Carbon-Carbon Composites, Chapman & Hall.

13.10   Biocompatibility

Many experiments have demonstrated that elemental carbon has the best biocompatibility of all known metals. It is compatible with bones, blood and soft tissues. C−C composites can be engineered in such a way as to possess mechanical properties very similar to those of bones, thus eliminating the need for removal once the healing is complete. Materials such as C−C composites are considered 'bioactive', and there is a considerable interest in many areas of implant surgery for them. The objective is to use a material that can encourage the formation of bone rather than soft tissue at the interface (Leilei et al., 2013).

13.11   Oxidation

At temperatures above 400°C, the carbon fibres readily react with oxygen and rapidly burn away, resulting in partial or complete deterioration of the composite. The oxidative behaviour of C−C composites, which begins with gasification of carbon fibres, is followed by enlargement of pores inherently present in the composite, further aggravating the oxidation. The oxidation rate of C−C composites in air increases rapidly with increased temperature. Water vapour in air further increases the rate of oxidation. When used as a thermal protector, C−C composites are often made extremely thick to compensate for their tendency to oxidize rapidly at elevated temperatures (Advanced Composite Materials, 1986).

13.11.1   Oxidation protection of C−C composites

Carbon fibre-reinforced carbon matrix composites (C−Cs) are usually used with an antioxidation coating. For the prevention of exfoliation, high-strength bonding of the coating to the C−C substrate is often required. However, no measures have been established to determine bonding strength for thin and brittle coatings. One of the most promising measures is ceramic coating deposited on the surface of C−Cs. For example, SiC coatings are used at the nose cone and the leading edges of space shuttles.

The principal requirements for the coating material are oxidation resistance, a low evaporation rate, chemical and mechanical compatibility with the substrate, and high adhesive strength of the interface between the C−C composite and coating. The SiC coating is composed of a conversion layer and a CVD layer. The conversion layer is formed by the reaction between gas phase Si and carbon in the substrate C−Cs (Hatta et al., 2004) (Fig. 13.23). The excellent ultrahigh strength of C−C composites at temperatures above 2273 K make them the most promising candidate materials for high-temperature structural applications with advanced thermal protection. However, their oxidation above 673 K limits their applications in oxygen-containing atmosphere
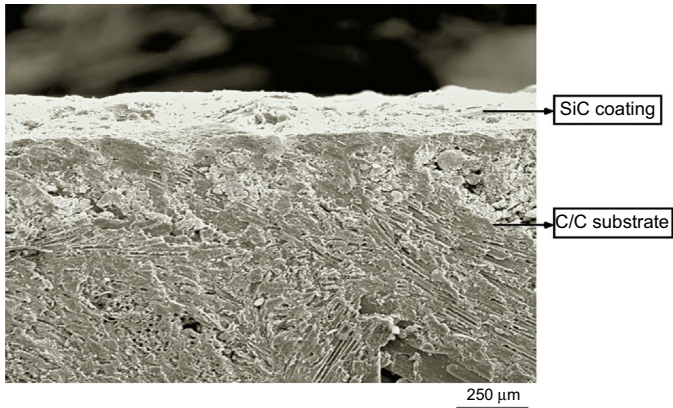
Figure 13.23 Scanning electron micrograph showing the transverse section of SiC-coated Type I C–C substrate (100×).

at high temperature, which has led to research to try to improve their oxidation resistance. A multilayer protective coating, using SiC as an internal bonding layer, has been proposed.

In the multilayer coating, $MoSi_2$ can be a useful outer-layer material, because it has a high melting point and excellent high-temperature oxidation resistance. However, the CTE mismatch between the $MoSi_2$ (8.5×10^{-6}/K) outer layer and the SiC (4.5×10^{-6}/K) bonding layer causes cracks in the protection layer and provides channels for oxygen to attach to the carbon matrix. Therefore, pure $MoSi_2$ cannot be used as the outer layer, and a multicomposition coating might be better. The CTE of $MoSi_2$ decreases with enhanced toughness by adding $Y_2Si_2O_7$ whiskers, which have low CTE and equivalent physical and chemical adaptability to SiC. To date, there are no reports of the use of $Y_2Si_2O_7$ whiskers–toughened $MoSi_2$ coating. In order to obtain a dense $Y_2Si_2O_7$–$MoSi_2$/SiC multilayer coating, a novel hydrothermal electrophoretic deposition technique was used. Influences of $Y_2Si_2O_7$ whiskers on the microstructure and oxidation resistance of the coated C–C composites were investigated.

Based on the above research, a dense and homogeneous $Y_2Si_2O_7$ whiskers–reinforced $MoSi_2$ multicomposition coating was prepared on SiC–C/C composites surface by a hydrothermal electrophoretic deposition process. Compared with $MoSi_2$ coating, $Y_2Si_2O_7$–$MoSi_2$/SiC multilayer coating possessed better oxidation protection ability for C–C composites because $Y_2Si_2O_7$ whiskers played an obvious role in decreasing the thermal expansion of $MoSi_2$ coating and increasing the toughness between the outer layer and the inner layer more effectively. The as-prepared multicomposition coating can protect C–C composites from oxidation for 100 h at 1773 K, with a weight loss of 1.22×10^{-3} g/cm^2 (Ya-Qin et al., 2011).

13.12   Applications

C−C composites, developed about three decades ago to meet the needs of the space programs, are nowadays considered high-performance engineering materials with potential application in high-temperature industries. Accordingly, steady growth also prevails in the civil market segment. In terms of mass consumption, the main applications of C−C composites are still in high-performance braking systems (Fig. 13.24). Compared to a steel brake, a C−C composite has 2.5 times higher heat capacity, reduces the weight by 40% and doubles the service life. Although the load-bearing ability of C−C composites at room temperature is not as high as that of metals, it is superior at high temperatures. This makes it the first choice for high-temperature mechanical fasteners, where this material also saves weight.

In braking applications, it is not the frictional behaviour that is of major interest, but the ability to absorb and conduct large quantities of heat in a very short period without damaging the brake assembly. These innovative materials respect all the requirements requested for space structures and are used for the production of re-entry heat shields for space vehicles and missiles and rocket nozzles, parts in gas turbine engines such as flaps, seals, liners, vanes and tail cones. Some applications of C−C composites in the space industry are shown in Fig. 13.24.

Its high purity and its resistance to heat and ionizing radiation make it a possible material for the nuclear industry. In general engineering sectors, these are used in engine components; as refractory materials; as hot-pressed dies and heating elements; as high-temperature fasteners, liners and protection tubes; as guides in glass industries and so on. For biomedical devices, C−C composites are used for prosthetic implants such as hip joint replacements and have been tested in artificial hearts for animals. C−C composites have great potential in energy sectors as polar plates for fuel cells, in storage batteries and so on. As the technology becomes more economical and viable, more and more applications will evolve (Snell et al., 2001).

(a)   (b)
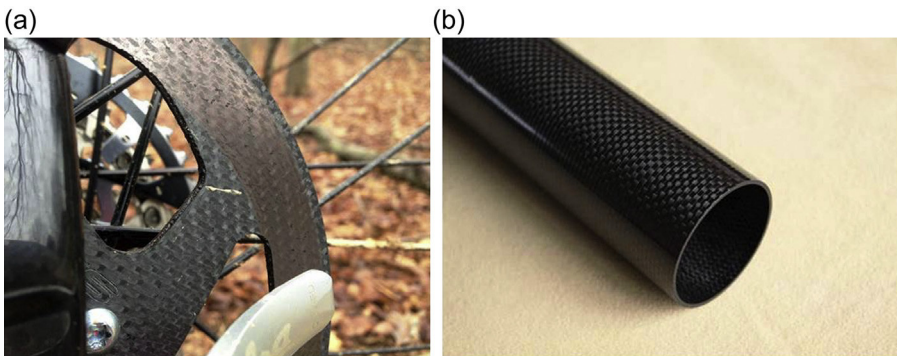
Figure 13.24 (a) C−C brake (Bikerumor); (b) C−C tube used as support of a satellite antenna feeder.
http://www.jtecrc.com/carbonfiber.html.

13.13   C—C joining

C—C composites are characterized by low density and a high strength-to-weight ratio. Thanks to these properties, C—C composites are used for different applications, such as turbine engine components and carbon brakes (Byrne, 2004), as mentioned. Joining of C—C composites need the development of appropriate techniques, with the exception of the use of mechanical fasteners, taking care of galvanic corrosion. Of course, it is not applicable to any kind of welding technique, so the better solution is to develop advanced, appropriate bonding techniques, taking into account the material itself, its geometry and the intended use for the finished part (White et al., 2007).

An important method is the so-called combustion joining (CJ) technique, based on the use of local ignition of a heterogeneous exothermic mixture. This approach can be carried out in two different ways, as illustrated in Fig. 13.25:

- *Volume combustion synthesis (VCS-CJ)*: reaction is uniform over all the volume with an external heating. The joining category of volume combustion (VCS) includes three methods: *RJ* (reactive joining), *RRW* (reactive resistance welding) and *SPS* (spark plasma sintering); and
- *Self-propagating high-temperature synthesis (SHS-CJ)*, where the reaction begins in a spot volume and the propagation throughout the volume is self-sustained.

Both SPS and RRW techniques use electrical current; in the SPS method, the electrical current promotes the reaction-sintering process, while RRW utilizes it to preheat the stack. As an example, Fig. 13.26 schematically describes the RRW process, while Figs. 13.27 and 13.28 describe, respectively, the temperature versus time and the microstructure of a joined C—C composite, corresponding to an RRW joining method.
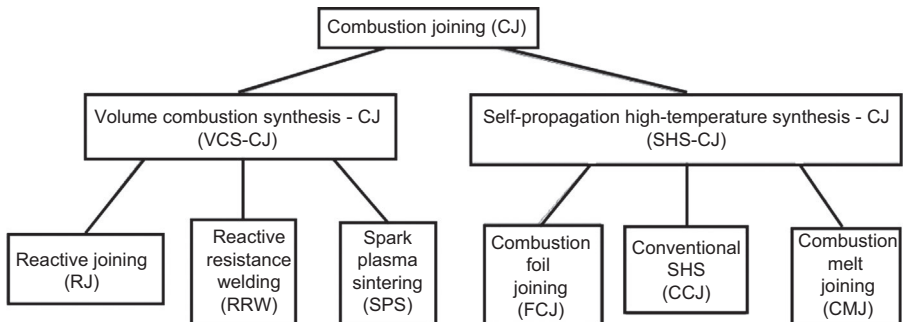
Figure 13.25 CJ classification methods.
Reproduced from White, J.D.E., Simpson, A.H., Shteinberg, A.S., Mukasyana, A.S., 2007. Combustion joining of refractory materials: carbonecarbon composites. Journal of Materials Research.
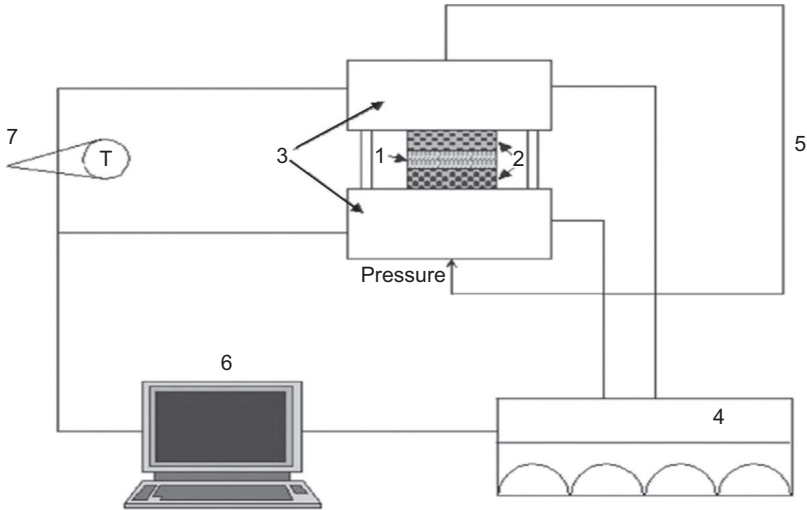
Figure 13.26 RRW joining process scheme. *T*, thermocouple.
Reproduced from White, J.D.E., Simpson, A.H., Shteinberg, A.S., Mukasyana, A.S., 2007.
Combustion joining of refractory materials: carbon−carbon composites, Journal of Materials
Research.
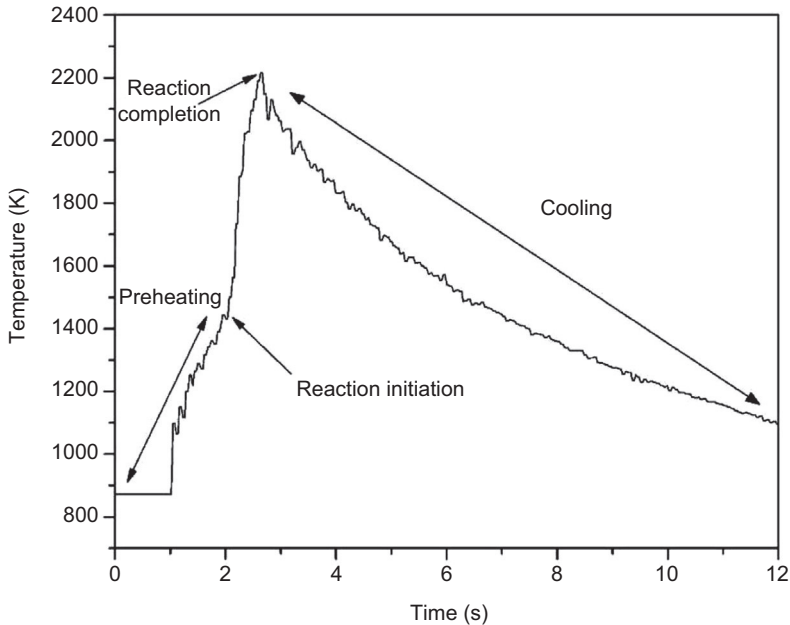
Figure 13.27 Temperature−time profile of an RRW joining method.
Reproduced from White, J.D.E., Simpson, A.H., Shteinberg, A.S., Mukasyana, A.S., 2007.
Combustion joining of refractory materials: carbon−carbon composites, Journal of Materials
Research.
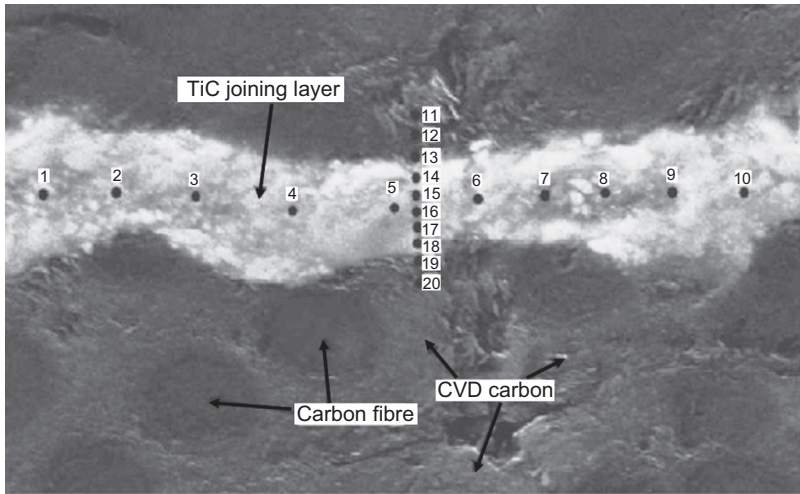
Figure 13.28 Microstructure of a joined C−C composite.
Reproduced from White, J.D.E., Simpson, A.H., Shteinberg, A.S., Mukasyana, A.S., 2007.
Combustion joining of refractory materials: carbon−carbon composites, Journal of Materials
Research.

13.14 Conclusions

C−C materials are widely used for aerospace applications, thanks to their extraordinary characteristics, such as preserving their mechanical and physical properties at very high temperatures and having a high degree of toughness and inertness. However, C−C materials have some drawbacks, consisting of costs and low efficiency of the fabrication processes, enhanced by their strong sensitivity to oxidation at temperatures lower than 400°C.

Acknowledgements

References

Advanced composite materials and structures. In: Proceedings of an International Conference [on Advanced Composite Materials and Structures] Taipei, Taiwan, Republic of China, May 19−23, 1986.

Buckley, J.D., Edie, D.D., 1993. Carbon-Carbon Materials and Composites. Noyes Publications.

Byrne, C., 2004. Modern carbon composite brake materials. Journal of Composite Materials 38, 1837.

Edwards, B.C., 2003. The space elevator: a new tool for space studies. Gravitational and Space Biology Bulletin 16 (2), 101−105.

Hatta, H., Nakayama, Y., Kogo, Y., 2004. Bonding strength of SiC coating on the surfaces of C−C composites. Advanced Composite Materials 13 (2), 141−156.

http://www.bikerumor.com/2013/04/09/first-impressions-kettle-cycles-siccc-sfl-carbon-disc-brake-rotors-more-news/.

http://www.jtecrc.com/carbonfiber.html.

Leilei, Z., Hejun, L., Kezhi, L., Zhang, S., Lu, J., Li, W., Cao, S., Wang, B., 2013. Carbon foam/hydroxyapatite coating for carbon/carbon composites: microstructure and biocompatibility. Applied Surface Science 286, 421−427.

Manocha, L.M., February/April 2003. High performance carbon−carbon composites. Sadhana 28 (Parts 1 & 2), 349−358.

McAllister, L., Lachmann, W., 1983. Fabrication of composites. In: Kelly, A., Millieko, S.T. (Eds.), Handbook of Composites 4. North Holland, p. 109.

Monthioux, M., Kuznetsov, V., 2006. Who should be given the credit for the discovery of carbon nanotubes? Carbon 44, 1621.

NASA, Getty Images, July 10, 2011.

Popov, M., Kyotani, M., Nemanich, R., Koga, Y., 2002. Superhard phase composed of single-wall carbon nanotubes. Physical Review B 65 (3), 033408.

Savage, G. (Ed.), 1993. Carbon-Carbon Composites. Chapman & Hall.

Shunk, 2001. Carbon Fiber Reinforced Carbon, Promotional Brochure.

Snell, L., Nelson, A., Molian, P., 2001. A novel laser technique for oxidation-resistant coating of carbon−carbon composite. Carbon 39, 991−999.

Wang, X., Qunqing, L., Jing, X., Zhong, J., Jinyong, W., Yan, L., Kaili, J., Fan, S., 2009. Fabrication of ultralong and electrically uniform single-walled carbon nanotubes on clean substrates. Nano Letters 9 (9), 3137−3141.

White, J.D.E., Simpson, A.H., Shteinberg, A.S., Mukasyana, A.S., 2007. Combustion joining of refractory materials: carbon−carbon composites. Journal of Materials Research.

Ya-Qin, W., Jian-Feng, H., Li-Yun, C., Xie-Rong, Z., 2011. $Y_2Si_2O_7$ whisker reinforced $MoSi_2$ multi-composition coating for SiC pre-coated carbon/carbon composites. Advanced Composite Materials 20, 125−132.

Product design for advanced composite materials in aerospace engineering

14

K.V.N. Gopal
Indian Institute of Technology Madras, Chennai, India

14.1   Introduction

Composite materials have revolutionized the design and development of modern aero-vehicles with their high specific strength and specific stiffness along with other properties. Advanced composites made from high-performance fibre-reinforced polymers (FRPs), metal matrix composites (MMCs) and ceramic matrix composites (CMCs) are used in high-performance aerospace systems to provide additional functional benefits such as temperature resistance, radar absorption and flutter suppression. Commercial aviation, understandably, lagged military aviation and the small-aircraft segment in using composites. But, in new-generation large aircraft like the Airbus A380, composites contribute nearly 25% by weight, and they contribute over 50% in more recent designs like the Boeing B787 and Airbus A350 XWB aircraft. Using composite materials in primary structural elements like the wing and fuselage provides multiple benefits like lighter aeroplanes with reduced emissions and fuel costs, lower maintenance costs and improved passenger comfort. Lightweight yet strong CMCs which can withstand very high temperatures are replacing metal components even in the hot section of next-generation commercial jet engines such as CFM's LEAP (Leading Edge Aviation Propulsion) and GE9X. Composite products can be designed in various configurations from simple bonded laminates to multidimensionally reinforcing fabric composites and advanced sandwich construction.

Advanced composites will be critical, enabling technologies in future aerospace design. The availability of resins with high strength, toughness, creep and fatigue resistance; better bonding agents; along with high performance reinforcements, improved manufacturing technology and reliable modelling techniques have accelerated the use of advanced composites in aviation. This has also created many challenges in product design. Design procedures, rules and design data which are well established for metal structures cannot be directly transplanted for composite product design. Design paradigms should include factors specific to composite materials. New standards and certification requirements are necessary. A huge design database has to be generated for various composite materials. This requires synthesis of a basic knowledge of composite materials, production techniques and the stress, deformation and failure behaviour of composites. Safety and cost competitiveness have to be key elements in any strategy for composite product design. There are many failure modes in composites, with the

initial trigger and final mode of failure being completely different and with possible interactions between different modes. The design strategy should take into account the complex failure mechanisms in composites. Particular attention should be given to the problem of joining composite elements to metal parts and its effect on the integrity of the structure.

The type of composite, constituent materials and manufacturing techniques all have considerable influence on the product design (Chawla, 2013; Mallick, 2007; Zagainov and Lozino-Lozinsky, 1996; Tsai, 1992; Gay, 2015). The immense flexibility given by the heterogeneity and controllable anisotropy of composite materials also poses significant challenges to the design process. Composite materials are not just used as replacement to metals or other conventional materials in an existing design. Advanced composite materials have opened up entirely new designs such as morphing structures which were earlier not possible with conventional materials.

14.2   Design strategy

The different stages in developing a composite product, shown schematically in Fig. 14.1, appear identical to those of metal product manufacturing but have features specific to composites and influence the design strategies for composite structures. The multiple options available at each stage make design an iterative process. In formulating the problem of the design of an aircraft structural component such as a wing or an airframe (Niu, 1988), a large number of design variables are defined, multiple constraints from different disciplines have to be satisfied by these variables and multiple objectives have to be met. Appropriate models are used to relate the constraints and objectives to the design variables. With the availability of high-performance computational tools, aircraft designers can now use techniques of **multidisciplinary design optimization** (**MDO**) at various stages of the design process.

Figure 14.1 Stages in composite product development.
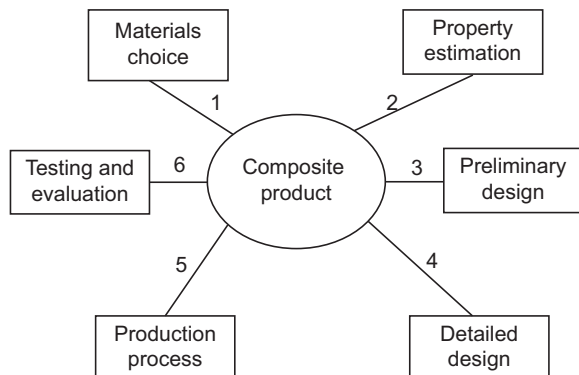
A key element of the design strategy for composite products is **materials design** or **materials engineering** (Kassapoglou, 2010; Eckold, 1994). The huge choices available in the nature and type of matrix and reinforcing elements yield composite materials with a wide variety of forms and properties which are a synergistic combination of the individual constituent properties. The designer has extensive flexibility to tailor the material system for specific objectives by analysing the performance of different material combinations. This also requires good process design to choose the most appropriate manufacturing technologies for a particular material system and end product. Unlike metals where the material science, manufacturing and design teams can remain isolated working in silos on their expertise, with advanced composites this is not a valid approach. The design strategy should allow the materials engineer, structural engineer and manufacturing specialists to work together in the design and development of every composite product. Innovations in material manufacturing can significantly shorten the design-manufacturing timelines while enhancing product quality.

The design analysis is performed in stages to minimize cost and improve efficiency. Simplified models based on experience and prior knowledge are used in preliminary design, whereas sophisticated models, needing expensive experimental and computational procedures, are restricted to the stage of detailed design. For example an aircraft wing or composite rotor blades of a helicopter can be modelled as laminated beams with minimum structural details during preliminary design. During the detailed design, they can be modelled as thin-walled closed shells with additional structural details. The load, stress and deformation predictions from the preliminary design are refined by the analysis during detailed design.

Safety and cost efficiency are equally important to aircraft manufacturers. Any design strategy for composite structures should factor in the complex failure mechanisms and anticipate possible failure scenarios during service to develop a structure that performs reliably and is also cost-effective to the operator. With advances in understanding damage and fracture in materials, **damage tolerance philosophy** is now an essential feature of aircraft design (Backman, 2005). Elements of the damage tolerance approach include health monitoring, maintenance and repair of structures. It is also important for designers to provide ways for environmentally safe end-of-cycle retirement of composite products. Design strategies need to be **innovative** and **adaptive** to incorporate the various factors influencing composite product design. Because of the interdisciplinary nature of aircraft design and production, the design process for composite parts can use the concept of concurrent engineering effectively to ensure high quality while keeping down the costs and lead times. The design strategy should enable the product design, process department and tooling departments to work together. A model-based engineering (MBE) approach can significantly improve the entire process from design to production while ensuring quality at all stages.

Uncertainty in the material data is an important issue with composite materials because of the complex microstructure and factors arising from the manufacturing processes. Enlarged scatter is observed in strength measurements of composite structures. Together with uncertainties in the loads, this has led to the use of **probabilistic**

approaches in composite product design (Chamis, 2006; Long and Narciso, 1999). Allowable probability levels (safety or failure) or probability distributions can be defined for the structure. This will then require determining probability levels for all factors influencing the failure of the structure and assessing the performance of the design.

14.3   Factors that influence product design

Several factors, specific to composite materials, influence the process of product design. These factors include:

- **Functional specification**: An aircraft design process starts right from concept studies leading to a preliminary configuration. This forms the framework for the objectives, constraints and solutions in the subsequent phases of the product design. The sources for evolving the design criteria include the airliners, aeroplane manufacturers and regulatory agencies. The system-level requirements then flow down to the individual components. The requirements for designing composite products have to be more specific than for metals. Information on the nature, magnitude and direction of the load paths is essential for composites. From the customer requirements, the functional specifications for the materials are derived. These specifications define the design of composite materials with a particular microstructure.
- **Material selection**: Based on functional specifications, the type and materials for the matrix and reinforcement have to be chosen. In the absence of sufficient property data, testing may be required for the materials. With composites, the designer can tailor the properties through change of fibre orientation or the type of reinforcement. Different types of reinforcements such as continuous fibres and nanoclay particles can be combined in a single composite material either to improve an existing set of properties or to add multifunctionality. A continuous material property gradation in a chosen direction can be achieved in a structure as in functionally graded materials. For example carbon FRPs may be lighter and possess higher strength, but glass FRP has a higher damage tolerance and is used on the Airbus A380 vertical tail plane leading edges, which are prone to damage from frequent impacts (Gay, 2015). New combinations such as aluminium-reinforced aramid (ARALL) or glass−aluminium (GLARE) fibre laminates, which provide good impact damage tolerance, have been used in aircraft structures.
- **Manufacturing process**: The design of appropriate processing techniques to manufacture a specific composite is essential to the design process. The fabrication technique and the process conditions influence the resultant composite properties, its performance and the cost of the product (Mallick, 2007). During the assembly process, attention should be given to the type of joining required between metallic parts and composite elements. The interplay between the manufacturing process and the materials together with the design factors are shown through a simple diagram in Fig. 14.2. Innovative techniques like additive manufacturing (AM) can produce parts with complex internal and external features and are being used to produce high-quality, fully functional composite material products. Techniques like fused deposition modelling (FDM) or laser sintering (LS) can create parts layer by layer from CAD data with engineering-grade thermoplastics, reducing nonrecurrent tooling costs and drastically reducing the lead time. Further developments can move these techniques from developing prototypes into the production environment. Techniques like automated tape
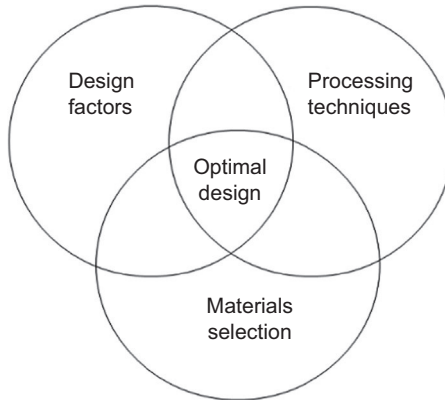
Figure 14.2 Optimal design of a composite product through interaction.

laying (ATL), used when profile is simple and regular, and automated fibre placement (AFP), which is very accurate for complex, curved shapes, are used to manufacture high-quality composite products.
- **Property estimation and analysis**: The characteristic features of a composite are its heterogeneity and anisotropy. An accurate estimation of the properties of the composite material is key to a correct analysis of the design performance. It is common in modelling for composites to replace the microstructural heterogeneity with an equivalent homogeneous and anisotropic medium for macroscopic analysis at the structural level (Kassapoglou, 2010).
- **Reliability**: While there are established factors of safety in the design of metal structures, it is not the case for composites. Design factors of safety are arrived at more often than not based on experience. At present, conservative factors are used due to relatively short experience. With greater use of composites in future, this can be expected to be less conservative.
- **Cost**: The cost of the composite product is a vital parameter in the entire design optimization procedure. With increased scale of usage, the commonly used composite materials have become competitive with conventional materials, but raw materials for advanced composites, used in niche applications, are still expensive. The costs include new manufacturing processes that may be needed and special tooling requirements for composites. But cost calculations for these applications have to consider total lifecycle costs, including reduced maintenance together with the superior performance of composite products. High-performance design tools, innovative manufacturing techniques and accurate predictive models can be used to lower the total lifecycle cost of a composite product.

14.4 Design methods

Design methods for structures range from simple empirical methods to robust deterministic and probabilistic approaches. These methods apply criteria based on strength, stiffness and stability to determine fracture mechanics−based damage tolerance, which is particularly required in critical applications such as aerospace vehicles. Empirical design is wholly unsatisfactory for composite structures.

14.4.1 Deterministic design

Stress, strain and displacement fields in the composite structure are computed from governing equations derived from mathematical models for various load-case scenarios. For complex geometries with sophisticated mathematical models, computer-based numerical techniques such as the finite element (FE) method can be used for the design analysis. These values are compared with allowable limits from different failure theories. Suitable provisions such as alternate load paths and adequate factors of safety are provided in the design to avoid catastrophic failure. In a laminated composite, final failure can occur at a significantly higher load than the load at which damage initiates. An accurate analysis of damage initiation and growth requires detailed micromechanical modelling of the fibres and matrix and the various modes of damage.

Under longitudinal tensile load, the failure mechanisms include brittle fracture of fibres, brittle fracture of fibres with pull-out and fibre pull-out with fibre−matrix debonding as represented in Fig. 14.3. The mode of failure depends on the fibre−matrix bond strength and fibre volume fraction. In compressive loading (Fig. 14.4), failure can be due to matrix cracking, fibre−matrix debonding, microbuckling of fibres and shear failure of fibres.

An alternate simplified procedure models each ply as homogeneous. In a strength-based design, a ply-by-ply failure analysis is conducted to assess the final failure load. The failure load for an individual ply is determined through an accepted failure criterion under multiaxial stress states such as the Tsai−Hill or Tsai−Wu criterion (Eqs [14.1] and [14.2]), using experimentally determined strength data, σ_{ult} (eg, ASTM D3039/D3039M for polymer matrix composite materials), to obtain the margin of safety. For an angle ply, the stresses have to be transformed into the lamina principal axes before applying the failure criterion.
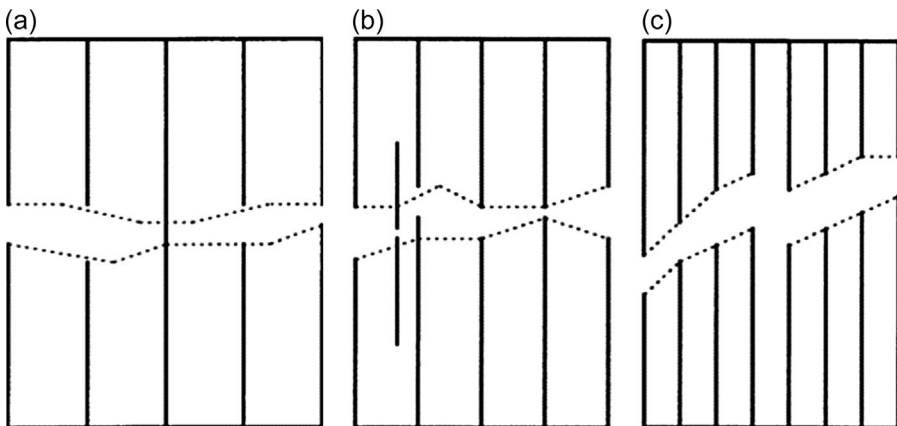
Figure 14.3 (a) Low fibre volume fraction (b) Intermediate fibre volume fraction (c) High fibre volume fraction.
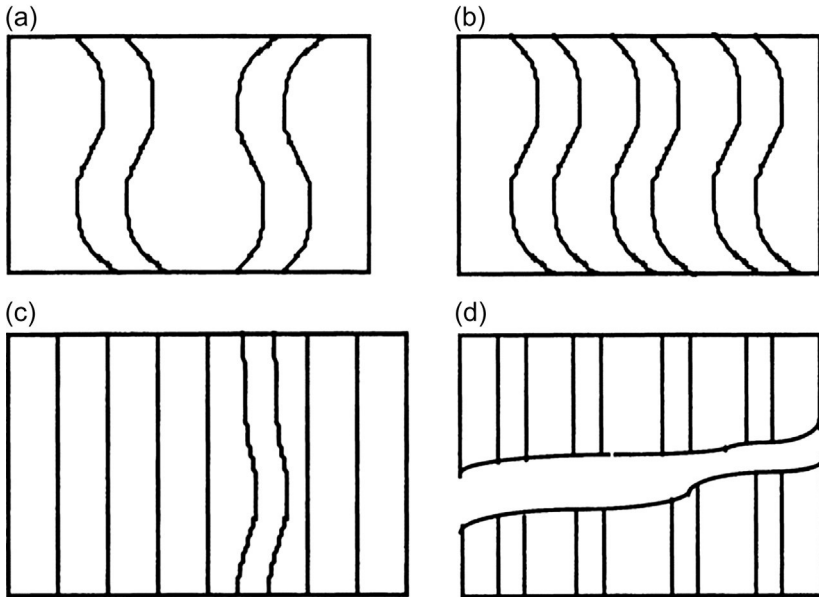
Figure 14.4 Failure modes in a unidirectional lamina under longitudinal compression. (a) Fibre microbuckling extensional mode. (b) Fibre microbuckling shear mode. (c) Transverse tensile failure of matrix. (d) Shear failure.

Tsai−Hill failure criterion:

$$\left(\frac{\sigma_1}{\sigma_{1\text{ult}}}\right)^2 - \left(\frac{\sigma_1\sigma_2}{(\sigma_{1\text{ult}})^2}\right) + \left(\frac{\sigma_2}{\sigma_{2\text{ult}}}\right)^2 + \left(\frac{\tau_{12}}{\tau_{12\text{ult}}}\right)^2 = 1 \qquad [14.1]$$

Tsai−Wu failure criterion:

$$F_1\sigma_1 + F_2\sigma_2 + F_3\sigma_1^2 + F_4\sigma_2^2 + F_5\tau_{12}^2 + F_6\sigma_1\sigma_2 = 1 \qquad [14.2]$$

Here σ_1, σ_2, τ_{12} are the failure load stress state for both criteria. The $F_1−F_6$ factors are the strength tensor components determined experimentally.

The theories give good prediction whenever there is low scatter in property values and the size effect is not significant. The Tsai−Hill failure theory considers the inter-action among the three unidirectional lamina strength parameters but does not distin-guish between tensile and compressive strengths in its equation. This can result in an underestimation of the failure stress. The Tsai−Wu failure theory is a simplification of a more general failure theory for anisotropic materials. But it is more general than the Tsai−Hill model because it distinguishes between the compressive and tensile strengths of a lamina.
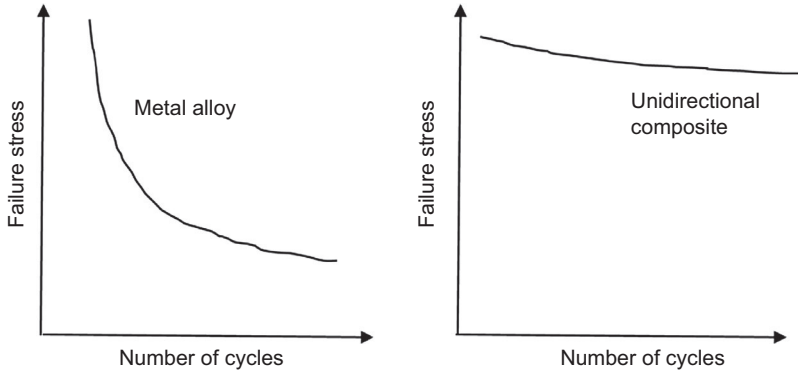
Figure 14.5 Fatigue resistance of a metal alloy and a composite.

For critical structures with low allowable margins of safety, other failure scenarios have to be examined. A fracture mechanics−based damage tolerance approach is with nondestructive testing (NDT) for crack detection to assess structural integrity in the presence of cracks. The fracture mechanics approach is used to analyse discrete damage such as inter- or intralaminar cracking, cracks in matrices and fibre−matrix debonding, which are among the common modes of failure in composites, by computing the stress fields near a crack tip, estimating the stress intensity factors (SIFs) given by Eq. [14.3] or the strain energy release rates (SERRs) given by Eq. [14.4] and comparing them with experimentally defined fracture toughness data.

$$K_I = \lim_{r \to 0} \sigma_y \sqrt{\pi a}, \quad K_I < K_{Ic}, \quad a = \text{half crack length} \tag{14.3}$$

$$G_I = \frac{K_I^2}{E'} \quad E' = E(\text{plane stress}) = \frac{E}{(1 - \nu^2)}(\text{plane strain}) \tag{14.4}$$

$$G_I < G_{Ic}$$

Three principal modes of fracture are defined: tensile, in-plane shear and out-of-plane shear modes; and failure mechanisms like delamination, matrix cracking and fibre−matrix debonding can be analysed using the methods of fracture mechanics. Fatigue failure can be modelled either through polynomial failure criteria using experimentally determined fatigue strengths or by using fracture mechanics to predict crack propagation and estimate the residual strength and life of the structure under fatigue loads. Fig. 14.5 illustrates the difference in the nature of fatigue resistance between a composite and metal alloy (Harris, 2003). This is then used to set allowable loads on the structure or to check if the design meets the requirements for the expected service loads with an adequate margin of safety.

14.4.2 Probabilistic design

In designing large-scale structures such as the fuselage or wing of an aircraft, there are several sources of uncertainty (Chamis, 2006; Long and Narciso, 1999). Uncertainty

can arise in the load prediction or in the material data. Most input parameters have a random nature. Hence, considering the load parameters, material properties and geometry as singly determined values can lead to designs with compromised reliability. The design process must take these uncertainties into consideration through appropriate methods to prevent failure in a worst-case scenario. A failure mechanism in composites like transverse matrix cracking in composites is an inherently stochastic process due to random variations of local material properties. Statistical approaches such as Weibull analysis are used to calculate parameters such as probability of failure at a particular stress level. The approach uses statistical measures for the design variables and sets reliability targets to quantify safety (risk), the sensitivity of the design variables, cost−weight reduction scenarios and optimum maintenance programmes (Chamis, 2006; Long and Narciso, 1999). At the level of a structure, this analysis has to be performed for every element to obtain the probability of failure for each failure mode and integrated over the entire domain to derive the probability of failure for the component. The use of probabilistic design allows the designer to examine areas of high localized stress more pragmatically in terms of its influence on the failure of the structure. Based on the probabilities of failure of different susceptible regions of the structure and the influence of various design variables, the composite element can be redesigned.

14.5   Design tools

Computer-based analysis and simulation have vastly increased the ability of designers to rapidly and efficiently design high-performance composite structures. Computational procedures using general purpose modelling and analysis software or special purpose in-house software allow designers to simulate and analyse all the stages of the product design and development from material selection to the manufacturing process. The analysis is run through several iterations and can include optimization methods to arrive at optimal solutions in the design space. The general sequence of analysis steps (Kollar and Springer, 2003) is shown in Fig. 14.6.

Different design tools have been developed, each tailored to different stages of the design process. Some tools are modular and allow flow of information between modules to improve efficiency. The designer has to select the appropriate tool for the particular stage of the design. The various design tools can be divided into the following categories:

- Composite configuration tools (eg, lay-up design tools)
- Basic laminate analysis
- FE software for more complex structures
- Production design tools

14.5.1   Composite configuration tools

These tools allow the user to select the type and constituents of the composite, estimate composite properties, perform laminate lay-up and stress analyses and predict the strength of the composite using simple lamina failure theories.
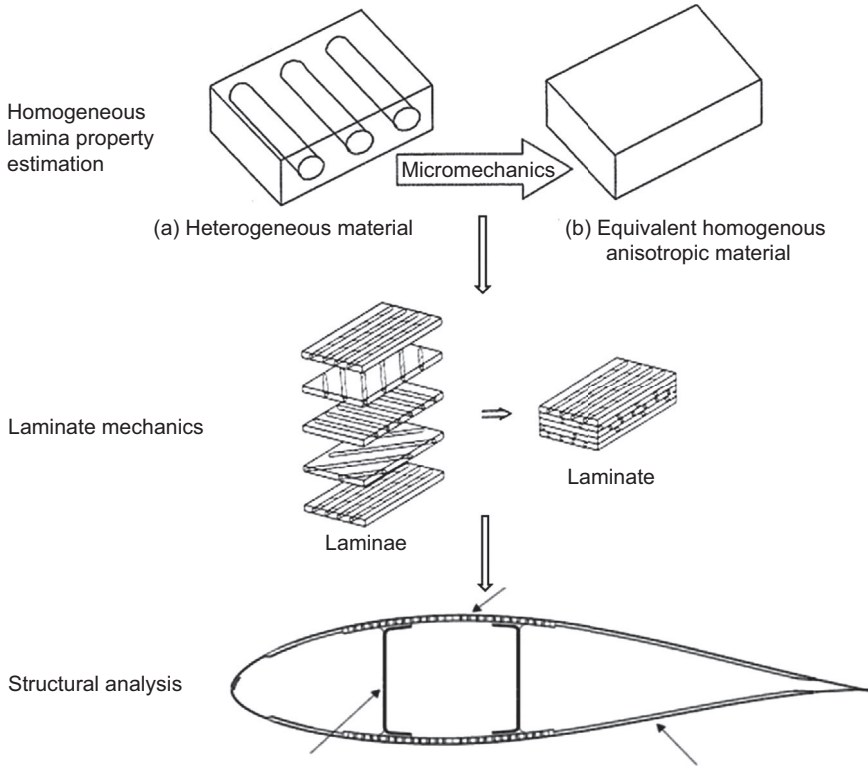
Figure 14.6 Analysis of composites at various structural scales.

1. Effective property calculations
   Among the first steps in the design process is the accurate estimation of the mechanical, thermal and hygrothermal properties of the resulting composite material system. Many simple and rigorous micromechanical theories have been proposed with varying degrees of accuracy to predict the effective composite properties. Software tools and procedures allow users to access material data from a database and predict the composite elastic constants using the micromechanical models for different types of composite, geometry and orientation of reinforcement, presence of voids in the matrix and relative amounts of each constituent.
2. Laminate design
   In laminated composites, a number of individual plies are bonded together. Each lamina can be of different thickness, and have different fibre material and fibre orientation. In a laminate design, a set of ply angles are selected as relevant to a given application. Due to manufacturing constraints, only a small discrete set of ply orientations are allowed, such as {0, ±15, ±30, ±45, ±60, ±75, ±90 degree}. A designer can use simple software tools to decide an optimal ply lay-up based on specified design constraints in terms of weight, cost, size and thickness of the laminate; individual ply thickness and any constraints on the mechanical or hygrothermal behaviour, strength and deformation. This determines the total number of plies and the proportion of each orientation in the laminate. Additionally, when the structure has zones of different thicknesses, the thickness variation is achieved

by dropping plies at specific locations. There are several design guidelines that are incorporated into the laminate design tools to decide on the stacking sequence and ply drops. The guidelines are to ensure strength and damage tolerance of the structure and avoid unwanted failure modes.

14.5.2   Basic laminate analysis

The purpose of the laminate analysis is to determine stresses and deformations in the laminates subjected to in-plane and out-of-plane mechanical loads with possible hygrothermal effects. The designer will analyse the bending, buckling and vibration response of the laminates (Kollar and Springer, 2003; Bailie et al., 1997). A ply-by-ply failure analysis can be carried out to determine the failure load and load-carrying ability of a laminate. Most design tools are capable of performing simple failure analysis using well-known failure theories. Tools are also available to check for important information like moisture diffusion, thermal conductivity and fatigue life estimation.

14.5.3   Structural analysis

For more complex composite structural elements and different types of loads, the design analysis will need powerful computational methods and software using numerical analysis methods such as FEs, boundary elements and so on. There are many commercial and free software programmes which can perform the static, dynamic and stability analysis of composite structures with advanced theoretical models. These analysis packages often have powerful pre- and postprocessing capabilities to enable the designer to model all the structural details to the required level and graphically visualize the structure's response. Using available software packages or through specially developed computational procedures based on established theories, designers can also model various failure mechanisms in composites such as fatigue or fracture and complex multiphysics problems such as fluid−structure interaction or structural−acoustic interaction in composites. Software tools are also capable of analysing difficult nonlinear problems in composites. Developers are continuously enhancing the capability of their software to model advanced material systems such as functionally graded composites, electro-magneto-elastic composites and other smart composites.

14.5.4   Production design tools

Computational tools are now available to designers to perform process simulation to optimize the manufacturing processes for the production of composites. These simulations are computationally demanding and incorporate advanced techniques like large displacement analysis, nonlinear material modelling, evolving contact surfaces and multiphysics modelling. These tools are also capable of multiprocess simulation. Software suites like ESI's Composites Simulation Suite, Siemens PLM's FiberSim[™] and CGTech's VERICUT[™] suite, among others, facilitate extensive analysis and optimization of individual manufacturing operations. Principles and theories from different

disciplines such as linear and nonlinear solid mechanics, fluid mechanics and heat transfer are used through numerical methods like FE analysis and computational fluid dynamics to model the composite manufacturing process.

14.6   Case studies in product design

Two case studies are presented here to illustrate the design challenges that occur when designing composite products for aircraft. Innovative design strategies, manufacturing techniques and sophisticated computational design tools came together to successfully build the products.

14.6.1   Case study 1: an all-composite centre wing box in the Boeing 787 Dreamliner

The centre wing box is a critical load-carrying element connecting the wings to the fuselage (Fig. 14.7). The Airbus A380 is the first aircraft with a central wing box manufactured with more than 40% composite materials, resulting in a weight savings of nearly 1.5 tonnes over the most advanced aluminium alloys. Also, the Boeing 787 Dreamliner is the first aircraft to have an all-composite centre wing box — built by Fuji Heavy Industries at Nagoya, Japan — using automated tape laying (ATL) technology (Fig. 14.8). The complete unit is 5.3 m long, 5.9 m wide and 1.2 m deep. One of the largest autoclaves ever built, measuring 7×7 m, was required to cure the centre wing box. The construction and operation of the autoclave were themselves huge challenges.

The centre box is constructed much like the outer wing, with composite skin panels stiffened by composite stringers. The composite wings of the 787 mate directly with the fuselage in a complex connection called the 'side-of-body join', instead of spars spanning the connection between the wing and fuselage as in aluminium airplanes. The stringers on the centre box inside the fuselage mate with the wing-side stringers at the wing join. The centre box had a lower part count and fewer holes than a metal counterpart. The box had varying thicknesses to suit local load requirements. But the weight-saving design introduced potential weaknesses and encountered unexpected
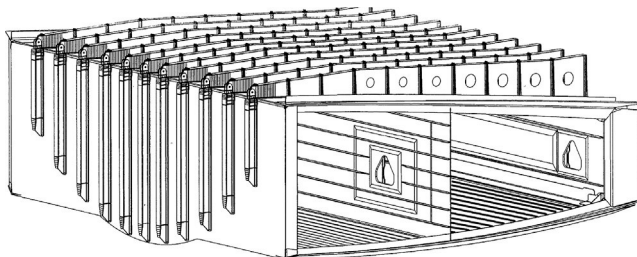
Figure 14.7 Schematic of a typical centre wing box of an aircraft.

Figure 14.8 Boeing 787 Dreamliner centre wing box before assembly.
Reproduced from www.compositesworld.com.

problems in later tests. Initial stress tests revealed cracks in the centre wing box well before the wing reached ultimate load. Engineers had to redesign the section by creating a U-shaped cutout in the end of each upper wing-skin stringer to redistribute excess load into the titanium fitting at the wing—body join. This was a particularly labour-intensive task as it had to be performed after the wing is joined. This redesign had to be validated through exhaustive testing, leading to postponement of the first flight by nearly 6 months.

14.6.2 Case study 2: a composite sliding sleeve for thrust reverser in jet engines

Sliding sleeve cascade thrust reversers (Fig. 14.9) are a common feature in most modern high-bypass-ratio jet engines, along with brakes and spoilers, to provide increased braking for an aircraft just after touchdown. On touchdown, the aft section of the engine cowl is hydraulically or electrically actuated to slide rearwards, redirecting the air in the bypass duct out through exposed cascade vanes by closing some or all of a series of blocker doors. The main structure of the translating sleeve is made of carbon fibre and other advanced composites for increased strength, noise dampening and part durability. For the Boeing 787, the particular Tier 1 supplier, Fischer Advanced Composite Components (FACC) AG, had to build the translating sleeve unit to be optimized for maximum weight reduction and minimum cost while meeting the performance specifications and stringent delivery deadlines. To achieve this, FACC proposed a completely novel manufacturing process and adopted a 3D model-based design approach integrating design, manufacturing and reporting phases of the development to reduce the design and manufacturing cycles while ensuring quality. This was possible because of the availability of powerful design tools for composite product

Figure 14.9 Sliding-type cascade
thrust reverser in a jet engine.
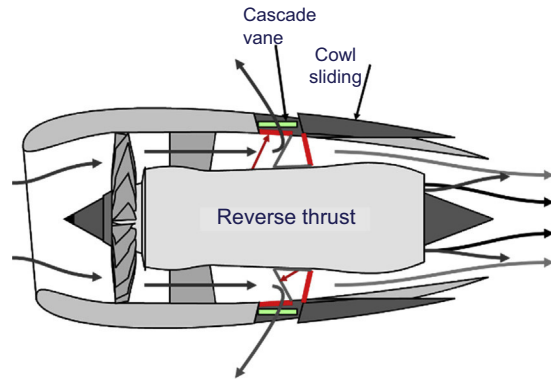
design, such as Fibersim™. The design tool allowed the complex geometric and critical
nongeometric design details to be captured in one master model, and exported the
detailed design data directly to the manufacturing machines for automated deposition,
tape laying and laser projection. The design tool also allowed the stress and aerody-
namic data from analysis tools to be shared within the model and generate stress re-
ports. This reduced the lay-up time by more than 15% and cut the delivery
timeframe by months.

14.7   Example 1: an Airbus H160 all-composite helicopter

Unveiled in March 2015, the Airbus H160 is a midsized twin-engine rotor craft
capable of carrying 12 passengers with a range of 120 nautical miles and a cruise speed
of 185 mph. The H160 features several composite-based design innovations. It is the
first-ever fully composite civil helicopter, with an airframe that is lighter, is resistant to
corrosion and fatigue and requires low maintenance. The composite body, a bearing-
less main rotor hub with innovative composite thermoplastic technology, helped
reduce weight by more than a tonne over its competitor, with improved fuel economy
and increased damage tolerance. It has the largest ever Fenestron (or fan-in-fin)
shrouded tail rotor with enhanced antitorque control efficiency, reducing exterior noise
levels by nearly 50%. The company's swept-back Blue Edge main rotor blades made
of composites allow an increase of 100 kg in the payload.

14.8   Example 2: Scaled Composites' White Knight Two

The White Knight Two (WK2) is a twin-fuselage design jet-propelled cargo aircraft
developed by Scaled Composites; it is powered by four jet engines, mounted two
on each wing. The aircraft is made entirely in carbon—epoxy to reduce the weight
of the structure. With a wingspan of about 43 m, it is the largest all-carbon aircraft

Figure 14.10 CFM Leap Engine featuring CMCs.
Reproduced from http://www.cfmaeroengines.com/engines/leap.

currently. The plane's cabling system is also carbon fibre. It is used to carry the Scaled Composites SpaceShip Two but can also provide for pre−space flight, positive G force and zero G astronaut training as well as heavy lift capability.

14.9   Example 3: CMCs for next-generation engines

The LEAP engine (Fig. 14.10) developed by CFM International, a GE Aviation and Snecma joint venture, is a revolutionary new-generation jet engine. The use of a composite cowl, carbon epoxy for the fan blades and a containment case ensured a weight saving higher than 200 kg. The blade number is reduced to 18 instead of 36. The blades are made of carbon−epoxy made from 3D woven preforms using the resin transfer moulding process. It is the first jet engine with static turbine shrouds made from refractory CMCs made from silicon carbide fibres in a silicon carbide matrix and covered with a thermal barrier coating. But engineers have now successfully tested rotating parts made from CMCs inside a GEnx demonstrator jet engine turbine. The use of CMCs in the hot section of a jet engine is a breakthrough for jet propulsion. With a density which is one-third of that of metal alloys, lightweight CMC components reduce an engine's overall weight, increasing fuel efficiency. The high-temperature properties of CMCs greatly enhance engine performance and durability.

14.10   Conclusions

Design of aerospace structures using advanced composites is a multidisciplinary activity with a strong interplay between materials, mechanics and the manufacturing

process. The wide variety in composite material systems makes materials engineering an integral feature of a composite design process. Multidisciplinary optimization is essential for efficient design and fabrication of composite structures. Ensuring damage tolerance in a composite structure is a challenge because of the complex failure mechanisms, and it requires robust analysis based on accurate mathematical models. Uncertainty in material data and environment factors requires probabilistic methods for analysis. Case studies and examples of aerospace structures show that innovation in design strategies and manufacturing techniques combined with powerful computational design simulation tools can successfully shorten the lead time and lower the cost of developing robust composite structures using advanced composites.

References

Backman, B.F., 2005. Composite Structures, Design, Safety and Innovation. Elsevier Ltd, UK.

Bailie, J.A., Ley, R.P., Pasricha, A., 1997. A Summary and Review of Composite Laminate Design Guidelines. NASA Contract NAS1-19347. Hampton, Virginia.

Chamis, C.C., December 2006. Probabilistic Design of Composite Structures, NASA/TM-2006-214660. NASA, Washington, DC.

Chawla, K.K., 2013. Composite Materials: Science and Engineering, third ed. Springer, New York.

Eckold, G., 1994. Design and Manufacture of Composite Structures. Woodhead Publishing Limited, Cambridge, England.

Gay, D., 2015. Composite Materials: Design and Applications, third ed. CRC Press, Boca Raton, FL, USA.

Harris, B. (Ed.), 2003. Fatigue in Composites. Woodhead Publishing and CRC Press LLC, Cambridge, UK.

Kassapoglou, C., 2010. Design and Analysis of Composite Structures. John Wiley & Sons, Ltd, Chichester, UK.

Kollar, L.P., Springer, G.S., 2003. Mechanics of Composite Structures. Cambridge University Press, Cambridge, UK.

Long, M.W., Narciso, J.D., June 1999. Probabilistic Design Methodology for Composite Aircraft Structures, DOT/FAA/AR-99/2. Federal Aviation Agency, Washington, DC.

Mallick, P.K., 2007. Fiber-Reinforced Composites: Materials, Manufacturing and Design, third ed. CRC Press, Boca Raton, FL, USA.

Niu, M.C.Y., 1988. Airframe Structural Design. Conmilit Press Ltd, Hong Kong.

Tsai, S.W., 1992. Theory of Composites Design, Think Composites, USA.

Zagainov, G.I., Lozino-Lozinsky, G.E., 1996. Composite Materials in Aerospace Design. Springer-Science+Business Media, B.V, Dordrecht, Netherlands.

Quality control and testing methods for advanced composite materials in aerospace engineering

15

Z. Fawaz
Ryerson University, Toronto, ON, Canada

15.1 Introduction

Aerospace structures in general and particularly those used in the construction of commercial aircrafts are subject to strict regulations aimed at ensuring their reliability and durability throughout their intended service life. The term structural integrity is often used to relate reliability and durability to a more global context where economic considerations play a major role. Part of that global context has to do specifically with measures taken by the manufacturers to validate the physical and mechanical properties of materials and therefore structures used in the building of the aerospace vehicle. This validation exercise forms an integral part of an overall quality assurance process required to ensure the structural integrity of the aerospace vehicle. By their very nature, advanced composite materials used in aerospace applications dictate a unique quality control process that begins with the very choice of the composite constituents and processing of the basic building block, often in the form of preimpregnated layers of fibres in polymeric resin, commonly referred to as prepregs. The consolidation of parts and structures from such basic building blocks, known as the cure cycle or cure process, dictates another careful quality control undertaking to ensure that the end product meets the strict quality requirements for its intended use. To this end, both destructive and nondestructive tests are conducted at various stages of the qualification process.

Section 15.2 of this chapter presents an overview of the various quality control measures deployed at each stage of the manufacturing process from the constituent materials control to process control and ultimately part consolidation controls which, in the context of advanced aerospace composites, refer principally to autoclave cure monitoring and control.

Section 15.3 discusses the various destructive tests and the corresponding testing standards typically adopted to confirm the mechanical properties of advanced composites, whereas nondestructive testing (NDT) methods are discussed in Section 15.4. Finally, Section 15.5 presents a quick overview of some relevant airworthiness considerations, and the chapter wraps up with an overall conclusion in Section 15.6.

15.2   Quality control

The term advanced aerospace composites typically refers to those materials that are made by binding high-strength and high-stiffness continuous fibres with various types of polymeric resins and consolidating the resulting bimaterial (composite) into finished parts under a prescribed cycle of temperature and pressure. The quality control process begins with controlling the raw materials used to form such advanced composites, namely, the fibres and the resin. The overall manufacturing process for advanced composites begins with the processing of fibres and resins from raw materials to obtain resins and fibres of the quality required for aerospace end-product applications. This means that the processed fibres have to meet certain minimum requirements to qualify in terms of their strength and stiffness, as well as their ability to maintain these required properties in the presence of adverse conditions such as exposure to extreme temperatures, moisture and chemicals. Similarly, the processed resins must meet certain minimum requirements to qualify, mainly in terms of their high-strength, modulus, toughness, low shrinkage, good chemical resistance, minimal curing volatility and overall ease of processing.

The constituent raw materials are subsequently converted into intermediate product forms, typically prepregs of various configurations, although certain aerospace parts are made from a direct infusion of resins into fibres without going through the intermediate preimpregnation step. The quality control process therefore depends on the chosen processing method, each having its unique control requirements. Nonetheless, for aerospace applications, the part-processing method requiring the intermediate preimpregnation product forms (prepregs) is still the predominant one. These prepregs are then further processed to obtain completed composite structures. Clearly, the overall quality control process must take into consideration the cumulative effects of the various raw materials' processing phases on the quality of the final product.

Once all required properties for the raw materials have been confirmed, the quality assurance department of the composite manufacturer will further verify that the composite fabrication processes are carried out according to engineering process specification requirements. The wide range of activities to quality-assure constituent materials and control the fabrication process is described in the following subsections.

15.2.1   Material quality control

15.2.1.1   Constituent materials control

In the case of aerospace composite materials, the manufacturer will typically specify constituent material requirements which define, among others, material inspection procedures and supplier controls that ensure that the constituent materials used in the manufacturing of a composite structure meet the engineering requirements of the original equipment manufacturer. The tests conducted by the composites manufacturer to verify the properties and performance of the received constituent materials must be standardized to ensure that production parts are manufactured with materials that

have properties equivalent to those generated from the tests conducted to establish the design allowables for this particular part or component.

Resins quality control

Resins, or what is more commonly referred to as the matrix material in a composite, are to be produced with the highest quality assurance standards in order to qualify as constituent raw materials in advanced aerospace composites. Many parameters affect resins quality and hence the performance and long-term durability of the composite. These include their chemical composition, physical state and morphology and the presence of impurities and contaminants. Testing must be performed to verify that the desired quality is obtained, and to that end tests must be carried out on the individual resin ingredients, the mixtures of ingredients and the final resin product. Among the typical tests to be carried out, the most important ones are those conducted to obtain the resin gel time, viscosity and glass transition temperature. Gel time tests provide a measurement of the time required at a given moulding temperature for a thermosetting resin to effectively solidify to a point beyond which it can no longer be considered workable. Various standardized test methods exist for the determination of gel time for resin systems, including direct probing and the use of gel timers as well as the method prescribed in the American Society for Testing and Materials (ASTM) publication ASTM D3532, which is used to obtain the gel time of resin squeezed from prepreg tape or sheet material. Fig. 15.1 shows a typical gel time testing apparatus. In this case, a low-torque, synchronous motor rotates a specially shaped stirrer in the catalysed resin or elastomer. As gelation occurs, drag exceeds torque and the motor stalls. This signals an electronic circuit which stops the clock and activates a flashing lamp. The gel time will then show on the LCD display (QUALITEST). Test methods for measuring the viscosity of resin solutions include the bubble time method described

Figure 15.1 A typical resin gel time tester.
Adapted from QUALITEST.
http://www.worldoftest.com/gel-timer.

in ASTM D1725. Finally, various test standards exist for the determination of glass transition temperature of resins, such as the one described in ASTM E1356.

Fibres quality control

Various fibre types are used in advanced aerospace composites, the most common of which are carbon−graphite fibres which are made predominately from the carbonization of polyacrylonitrile (PAN). These have highly anisotropic morphology leading to a high variability in their moduli values ranging anywhere from 100 to 800 GPa in the axial fibre direction, and around 10−30 GPa in the transverse direction. Higher moduli values can be reached, but these will require different precursors such as liquid-crystalline mesophase pitch. Besides their moduli in various directions, fibres strength is also of primary interest. Some of the standard test methods for the determination of fibres mechanical properties are listed in Table 15.1 (ASTM International). Furthermore, chemical testing to check the chemical composition of the fibres is also conducted along with surface analysis testing such as electron and X-ray spectroscopy.

Prepregs quality control

Prepregs are ready to cure resin-impregnated tow, tape, cloth or mat fibre sheets. Physical and chemical testing of uncured prepregs is required to ensure that the material adheres to quality acceptance requirements as well as for confirming processing

Table 15.1 ASTM test standards typically applicable to aerospace composites constituent materials

Test designation	Test description
C613-14	Standard test method for constituent content of composite prepreg by Soxhlet extraction
D3529M-10	Standard test method for matrix solids content and matrix content of composite prepreg
D3530-97(2008)e2	Standard test method for volatiles content of composite material prepreg
D3531/D3531M-11	Standard test method for resin flow of carbon fibre−epoxy prepreg
D3532/D3532M-12	Standard test method for gel time of carbon fibre−epoxy prepreg
D3800M-11	Standard test method for density of high-modulus fibres
D4018-11	Standard test methods for properties of continuous filament carbon and graphite fibre tows
D4102-82(2008)	Standard test method for thermal oxidative resistance of carbon fibres
D7750-12	Standard test method for cure behaviour of thermosetting resins by dynamic mechanical procedures using an encapsulated specimen rheometer

parameters. Examples of uncured prepreg quality acceptance requirements include determination and verification of fibre and resin contents, volatile and moisture contents, resin flow, gel time and tack. Furthermore, prepreg quality controls dictate testing on cured laminates to ensure the resulting properties closely match the properties used as engineering design input data. Those tests are further discussed in the next section.

A summary of some of the standard test methods applicable to aerospace composites constituent materials are listed in Table 15.1.

15.2.1.2 Procured materials controls

The main objective of the quality control measures with respect to procured materials is to confirm compliance with the engineering requirements in order to ultimately ensure the structural integrity of the part or component being manufactured. Certain material procurement controls must be set as a minimum. Those include proper identification of materials by name and specification as well as ensuring that their packaging and storage were done in such a way as to preclude damage and contamination. They also include the verification that perishable materials, prepregs and adhesives are within the allowable storage life at the time of release from storage and within the allowable work life at time of cure. Finally, procurement controls include identification of any acceptance and re-verification tests that may be required prior to the use of the procured materials (Composite Materials Handbook, 2002).

15.2.2 Process control

Processing prepreg sheets into finished composite parts is a multiphase procedure that involves laying up the sheets into moulds according to specific layering sequences, vacuum-bagging, curing and post-curing steps. Perhaps the phase that is most critical for ensuring the high quality of composite parts is the lay-up and vacuum-bagging phase shown schematically in Fig. 15.2. Laying up composite parts must be performed in clean rooms that are free of contaminants and controlled for temperature and pressure. Such an environment is required to prevent the resin in prepreg sheets from getting contaminated or degrading under any excessive heat or humidity, which will greatly affect the quality of the part being produced. Certain critical steps or operations during the lay-up phase must be closely controlled. Those critical steps follow the standard lay-up process which begins with the preparation of a clean tool surface on which a release agent is applied. The operator must ensure the cleanliness of the tool surface and verify that the release agent has been applied on it and cured properly. Extreme care must be taken to ensure that the part being manufactured is laid up within strict sizing and alignment tolerances as per the engineering drawings.

The resulting prepreg lay-up and stacking sequence must then be inspected to ensure compliance with engineering drawing requirements for number of plies and orientation. The manufacturer's paperwork should contain information on material supplier, date of production, batch number, roll number and total accumulated
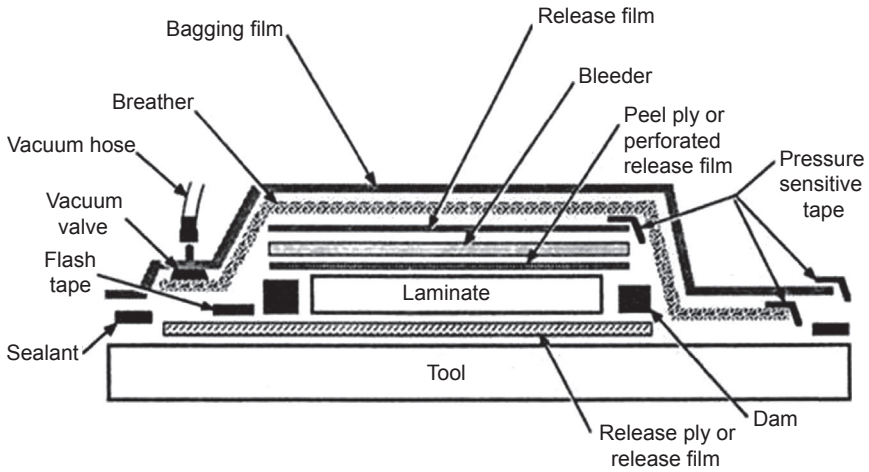
Figure 15.2 A typical vacuum-bagging setup.
Adapted from Carbonfiberguru. http://www.carbonfiberguru.com/carbon-fiber-processing-part-2-of-12-%E2%80%93-vacuum-bagging/.

hours of working life; autoclave or oven pressure, part temperatures and times; autoclave or oven load number; and part and serial numbers (Composite Materials Handbook, 2002).

15.2.2.1 Cure monitoring

Once the part is laid up, it gets vacuum bagged in preparation for autoclave curing. The vacuum-bagging step is another important step whereby care must be taken to ensure proper sealing of the bag and close monitoring to ensure that the required vacuum pressure is accurately applied. Curing begins when the vacuum-bagged part is placed inside an autoclave, as shown for example in Fig. 15.3. The autoclave is programmed to

Figure 15.3 Placement of a vacuum-bagged laminated composite part into a large autoclave.
Adapted from CompositesWorld. http://www.compositesworld.com/articles/fabrication-methods.

apply a prescribed cycle of temperature and pressure, commonly referred to as the cure cycle. A typical cure cycle for a thermosetting fibre-reinforced composite is depicted in Fig. 15.4.

Cure monitoring is the process whereby sensors are placed on or inside the part being cured to obtain information on the cure progress such as the resin viscosity, gel level and overall degree of cure. Typically, the sensors will also provide information on the direct pressure on the part as well as its temperature and degree of compaction. The information obtained from cure-monitoring sensors may be used to simply acquire part consolidation data to ensure that the prescribed cure conditions have been met. Occasionally, however, data acquired from cure-monitoring sensors may also be used to actively adjust the cure parameters during the cure cycle. The latter would require the cure-monitoring sensors to be connected to the various control channels of the autoclave through a closed feedback loop (Schubel et al., 2013).

15.2.2.2 Post-cure verifications

Depending on the criticality of the part being cured, occasionally special test panels may be consolidated along with production parts and subsequently used for physical and mechanical properties verifications. Requirement for the latter is closely tied to the structural hierarchy of the parts being produced, with parts intended for flight-critical structures being typically the subject of such requirements. The physical tests required for this verification include those to verify fibre volume, void content and ply count. Mechanical tests that may be required include 0 degree bending strength and modulus and short-beam shear strength tests.
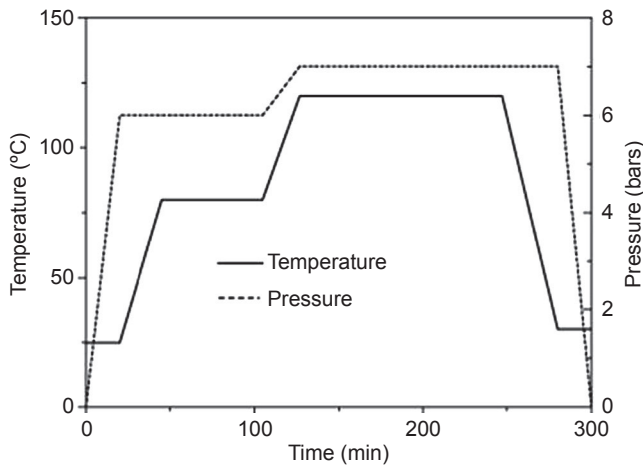
Figure 15.4 A typical autoclave cure cycle for fibre-reinforced thermosetting polymers.
Adapted from Botelho, E.C., Silva, R.A., Pardini, L.C., Rezende, M.C., 2006. A review on the development and properties of continuous fiber/epoxy/aluminum hybrid composites for aircraft structures. Materials Research 9 (3), 247−256.

The quality control process associated with aerospace composite materials procurement and manufacturing involves various quality assurance inspection and testing of the raw materials and cured parts. It all begins with quality assurance measures taken by the material supplier along with verification tests performed on the fibre and resin as separate materials. The prepreg supplier will also perform various inspections and verifications on the composite prepreg material. Once procured, the prepreg manufacturer will perform inspection and revalidation tests on the received material, conduct in-process control tests and ultimately perform nondestructive inspection tests as well as occasionally selective destructive testing on the finished parts. Those are briefly discussed in Sections 15.3 and 15.4.

15.3   Destructive testing

The need for destructive testing of aerospace composite parts arises from a stringent quality assurance philosophy that recognizes the possibility of variability in finished parts properties, inherent to this class of advanced materials. As discussed in previous sections, requirements for destructive testing begin with the need to verify the basic mechanical properties of cured parts and may go all the way to the need for testing the finished product under realistic loading scenarios to confirm its structural integrity upon such simulated conditions. A major concern in this regard is the statistically significant test results scatter associated with this class of materials, which is typically more considerable than that of their metallic counterparts (Composite Materials, 2012). The question therefore becomes one of knowing what percentage of manufactured parts would meet specification requirements; the higher that percentage, the better. Numbers representing this concept are termed measures of process capability. Typically, statistical measures, such as the standard deviation, are used to establish test result ranges that are compared to the part's engineering specification range for acceptance.

Test equipment and test methods for destructive evaluations, that are prescribed to assess product conformance, contain test and evaluation procedures that describe, among other points, the means and frequency of test equipment calibration to maintain the required accuracy and reliability of test data. Parts and products quality control documentation requirements are found in various government-adjudicated specifications such as those of the US Federal Aviation Administration (FAA) which issues the Federal Aviation Regulations (FAR) documents for commercial aircraft in the United States. For example, Part 21 ('Certification Procedures for Products and Parts') is the specific chapter that deals with commercial aircraft quality control documentation requirements (Federal Aviation).

15.3.1   Destructive testing methods

For obvious reasons, nondestructive assessment of the quality of a manufactured composite structural part is the preferred quality assurance method. However, in many instances, quality assurance may not be satisfied by nondestructive techniques

alone. In such cases, the manufacturer has to resort to destructive tests to ensure the structural integrity of a component. Occasionally, such destructive testing may simply involve dissection of the part to examine its microstructure, but more often than not mechanical testing of specimens cut from excess parts of the component or even the full-scale testing of the component itself is the dictated quality assurance method. The decision on whether to conduct destructive testing or not depends on whether a nondestructive inspection (NDI) is sufficient to assure the quality of the part. When NDI techniques are deemed inadequate for quality assurance purposes, destructive testing is then mandated. This can then take the form of either a full part dissection and subsequent microstructural examinations, which are typically the requirements when the manufacturer has little or no experience with manufacturing similar parts, or trim section testing. The latter is the preferred approach since it preserves the part and dictates that only excess sections from it be microstructurally examined or mechanically tested.

15.3.1.1   Microstructural examination

Microstructural examinations typically involve sampling out sections of the part and examining them under various optical magnifications ranging anywhere from a few-fold to as high as hundreds of thousands of times. Lower magnifications are typically associated with verifications of ply counts and stacking sequences, whereas at the high end one is looking at minute microstructural details that may shed light on the uniformity of cure or bonding between fibres and matrix. Optical microscopes will typically be used for low to mid-magnification requirements up to a few thousand times at their high end, whereas special types of microscopes such as scanning electron microscopes (SEMs) are used for magnifications up to hundreds of thousands of times. For composite parts quality assurance purposes involving such aspects as ply count or stacking sequence verifications, low-magnification microscopy is adequate. However, when aspects related to the degree and uniformity of curing or level of adhesion between constituents are being verified, higher magnification examinations, up to those afforded by advanced techniques such as SEM, are typically required. Fig. 15.5 illustrates the type of output from an SEM at two different magnifications.

Regardless of the level of magnification required, microstructural examinations typically involve carving out sample sections from the part and preparing those in a special way prior to their examination. Sample preparation methods depend on the type and level of microscopic examination being performed and generally involve polishing of the sample and embedding it in a transparent resin mould, typically epoxy, before introducing it into the microscope.

However, in the case of composite samples being prepared for SEM examinations, additional preparation steps are typically required prior to their examination. The samples are usually coated before examination with a very thin layer of a conductive material (typically gold) that will prevent charging by electrons. However, coating can potentially hide the finer surface details and is therefore not recommended for very high magnifications. Nonetheless, in most instances, coating of SEM samples is routinely performed.
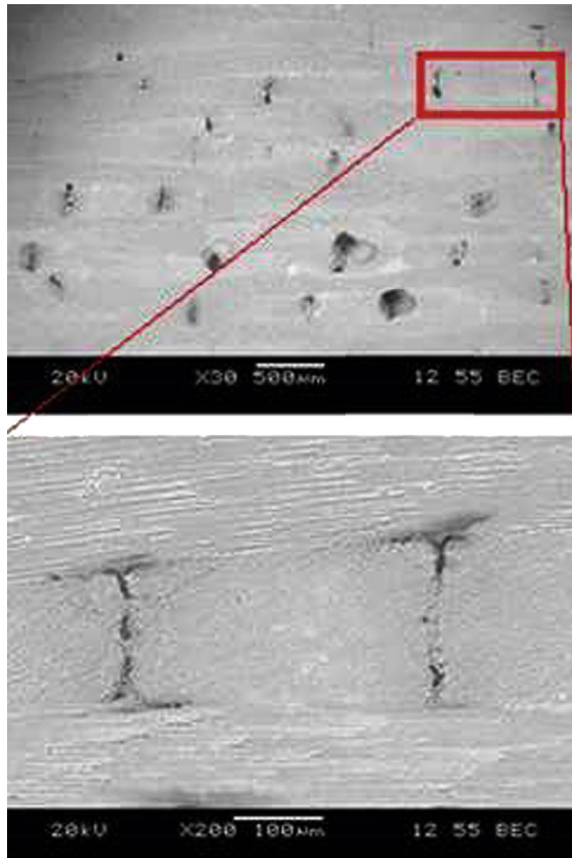
Figure 15.5 SEM images of a composite material section at two different magnifications. Courtesy of FRAMES (Facility for Research on Aerospace Materials and Engineered Structures, Ryerson University, Canada.).

15.3.1.2 Mechanical testing

Mechanical testing will typically be performed whenever a part's strength and stiffness properties are being verified under various loading scenarios, including tension, compression, bending and torsion. Test coupons are typically drawn from trim sections or separate panels cured simultaneously with the part, and subsequently cut to size and prepared for testing according to a very specific test standard applicable to the type of mechanical properties being sought. Table 15.2 lists a few of those standards that are pertinent to the type of composite materials being typically used in aerospace applications.

Mechanical testing is also required to characterize composite laminates under a wide variety of loading scenarios to generate the kind of knowledge on the behaviour and performance of such laminates that paves the way to their selection for one aerospace application or another. A wide, encompassing test program may also be

Table 15.2 ASTM test standards typically applicable to aerospace composites

Test designation	Test description
D2344/D2344M-13	Standard test method for short-beam strength of polymer matrix composite materials and their laminates
D3039/D3039M-14	Standard test method for tensile properties of polymer matrix composite materials
D3171-11	Standard test methods for constituent content of composite materials
D3410/D3410M-03(2008)	Standard test method for compressive properties of polymer matrix composite materials with unsupported gage section by shear loading
D3479/D3479M-12	Standard test method for tension−tension fatigue of polymer matrix composite materials
D3518/D3518M-13	Standard test method for in-plane shear response of polymer matrix composite materials by tensile test of a ±45 degree laminate
D3552-12	Standard test method for tensile properties of fibre-reinforced metal matrix composites
D4255/D4255M-01(2007)	Standard test method for in-plane shear properties of polymer matrix composite materials by the rail shear method
D5229/D5229M-14	Standard test method for moisture absorption properties and equilibrium conditioning of polymer matrix composite materials
D5379/D5379M-12	Standard test method for shear properties of composite materials by the V-notched beam method
D5448/D5448M-11	Standard test method for in-plane shear properties of hoop wound polymer matrix composite cylinders
D5449/D5449M-11	Standard test method for transverse compressive properties of hoop wound polymer matrix composite cylinders
D5450/D5450M-12	Standard test method for transverse tensile properties of hoop wound polymer matrix composite cylinders
D5467/D5467M-97(2010)	Standard test method for compressive properties of unidirectional polymer matrix composites using a sandwich beam
D5687/D5687M-95(2007)	Standard guide for preparation of flat composite panels with processing guidelines for specimen preparation

Continued

Table 15.2 **Continued**

Test designation	Test description
D6641/D6641M-14	Standard test method for compressive properties of polymer matrix composite materials using a combined loading compression (CLC) test fixture
D6856/D6856M-03(2008)e1	Standard guide for testing fabric-reinforced 'textile' composite materials
D7028-07e1	Standard test method for glass transition temperature (DMA Tg) of polymer matrix composites by dynamic mechanical analysis (DMA)
D7078/D7078M-12	Standard test method for shear properties of composite materials by V-notched rail shear method
D7264/D7264M-07	Standard test method for flexural properties of polymer matrix composite materials

warranted to generate empirical coefficients that form part of a generalized failure criterion for fibre-reinforced polymeric materials. Since a composite laminate's properties depend highly on its configuration, it follows that in theory an infinite number of tests may be required to fully characterize all possible configurations.

Mechanical testing of composite parts or coupons is expensive and time-consuming. The applicable test standards often call for sophisticated test equipment and auxiliaries that may only be available in highly specialized laboratories. The need for accuracy and the drive towards results repeatability dictate frequent calibrations of test equipment and high standards of quality control applicable to the test laboratory. A common quality assurance standard that is looked for when assessing the ability of a laboratory to perform mechanical testing on composites, among others, is ISO 17025. The two main areas of control in ISO 17025 are management and technical. Management controls are primarily related to the operation and effectiveness of the quality management system within the laboratory, whereas technical controls are mainly associated with the correctness and reliability of the tests and calibrations performed in the laboratory.

15.3.2 Examples of applications

One of the most common tests is the one conducted to obtain the in-plane tensile properties of aerospace composites, such as their moduli and strengths in various directions with respect to the fibres. The common standard for such a test is ASTM D3039, which describes a testing procedure to determine the in-plane tensile properties of polymer matrix composite materials reinforced by high-modulus fibres. The aerospace composite material forms of relevance to that standard are continuous fibre-reinforced composites in which the laminate is balanced and symmetric with respect to the test direction. Fig. 15.6 depicts a test coupon prepared for testing according to ASTM
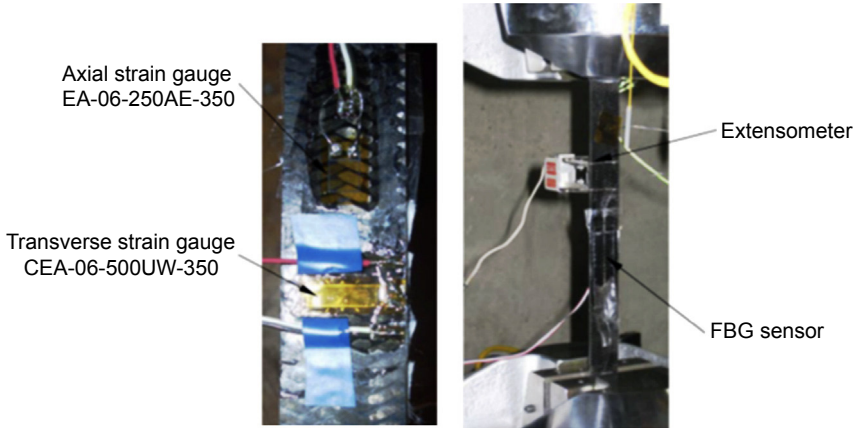
Figure 15.6 A composite materials test coupon rigged with various strain measurement sensors. Courtesy of FRAMES.

D3039. The image highlights the use of various strain sensors, such as strain gages, extensometers and fibre-optic sensors. Strain measurement on a composite test sample may present some challenges since the local strains that may be readily obtained from commonly used sensors such as strain gages may differ from strains over a larger section of the sample. Extensometers with varying gage section lengths are typically used to circumvent this shortcoming of strain gages.
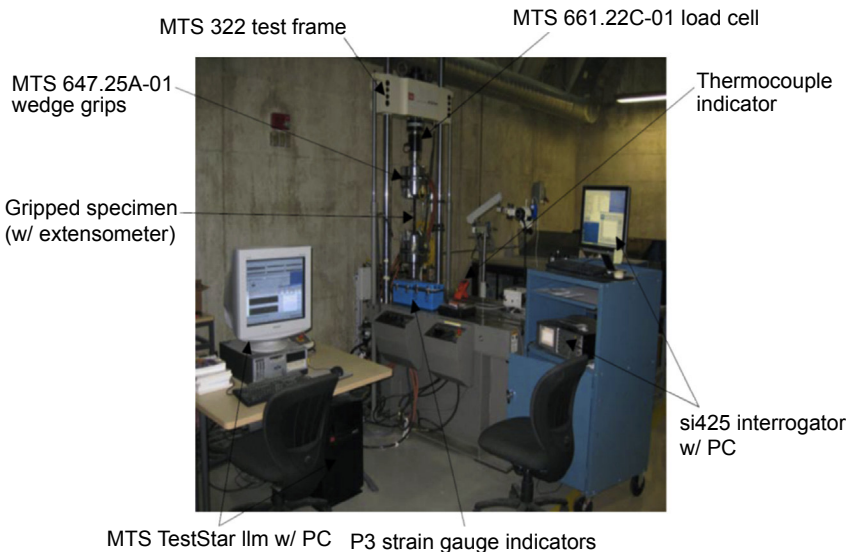
Figure 15.7 Overall setup for a composite materials coupon test. Courtesy of FRAMES.

Fig. 15.7 depicts an overall setup for a composite materials coupon test. This figure illustrates a rather elaborate test setup involving multiple hardware and software components.

In recent years, advanced composite materials have been investigated for possible use in higher temperature applications up to levels close to the materials' glass transition temperatures. For those purposes, advanced forms of polymeric matrix materials have been proposed that can maintain their mechanical integrity up to temperatures that are well above those tolerated by standard thermosetting polymers. Obviously, verifications and validations related to this class of high-temperature composites require even more sophisticated testing capabilities. Typically, heat chambers capable of generating uniform temperatures up to or beyond those required for a given high-temperature test are used. The high-temperature test environment rules out the use of certain data acquisition sensors and is limited only to those that are designed for high-temperature applications. The same goes for the coupon-gripping mechanism which has to be entirely made from heat-resisting materials if it is to be enclosed within the heat chamber, such as in the case illustrated in Fig. 15.8. Such a scenario obviously rules out the use of hydraulically actuated grips if this means that the hydraulic lines have to be exposed to the high-temperature environment.

Destructive testing is costly and time-consuming. Yet, it is often dictated when quality assurance of a manufactured composite structural part may not be satisfied by nondestructive techniques alone. In such cases, the manufacturer has to resort to destructive tests to ensure the structural integrity of a component. Occasionally, such destructive testing may simply involve dissection of the part to examine its microstructure, but more often than not mechanical testing of specimens cut from excess parts of the component or even the full-scale testing of the component itself is the
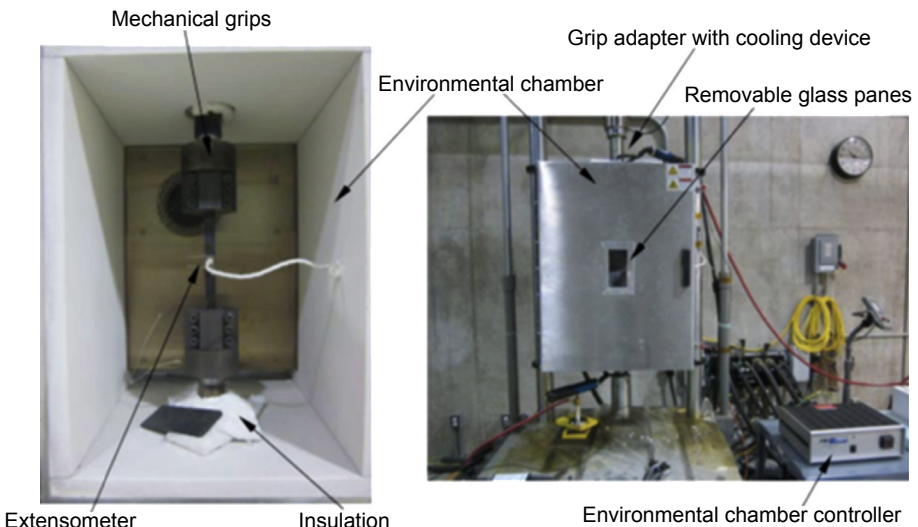
Figure 15.8 A composite coupon high-temperature test setup.
Courtesy of FRAMES.

dictated quality assurance method. Numerous methods and test standards exist to perform destructive evaluations of a composite part; the details on many of those may be found in pertinent ASTM standards such as those listed in Table 15.2.

15.4   Nondestructive testing

Unlike monolithic materials, by the very nature of their manufacturing and the associated human error elements, composites are significantly more prone to defects and anomalies. Some forms of defects, such as those related to poor bonding between the matrix and fibres or uneven infusion of the matrix materials leading to resin-poor and resin-rich areas, may lead to significant reductions in the mechanical properties of the manufactured composite part. It is therefore of paramount importance within the strict quality assurance provisions mandated by the aviation industry to routinely inspect the manufactured parts to ensure that they are devoid of any defects that may lead to unacceptable property degradation. As discussed earlier in this chapter, both destructive and nondestructive means are utilized to carry out such quality assurance provisions. Nondestructive inspection (NDI), also often referred to as NDT, is the preferred approach for obvious cost and time-related reasons. NDT techniques are useful not only for manufactured-part quality assurance purposes but also, and perhaps more importantly, for the on-site inspection of in-service components. The general approach is to thoroughly use various proven nondestructive techniques for quality assurance purposes upon the manufacturing of a composite part and to then rely on visual inspections during the service life of that part. If in-service damage is detected by visual inspections or suspected to have occurred, then more thorough NDT is conducted using a number of NDT methods suitable for field inspections. In all cases, the choice of an NDT method depends on the component material, the type of suspected or actual damage and the ability of the given NDT method to detect and quantify the said damage.

   Adequate NDT techniques allow for a rapid inspection and return to service of a part or an entire structure, thus saving tremendous amounts of time and money. The quest for powerful NDT methods that allow for accurate assessment of the damage in an aircraft structure within an increasingly damage-tolerant design philosophy has resulted in significant proliferation of NDT research and development activities (Hsu, 2008).

   ASTM defines NDT as the application of technical methods to examine materials or components in ways that do not impair future usefulness and serviceability in order to detect, locate, measure and evaluate discontinuities, defects and other imperfections; assess integrity properties and composition; and measure geometrical characteristics. Section 15.4.1 presents a summary description of the most notable NDT methods used for quality assurance purposes during the manufacturing of a composite part or for in-service inspections.

15.4.1   Conventional NDT methods

Similar to those used in other industries, the NDT techniques in the aerospace industry are based on using some form of energy such as light, heat, radiation,

electromagnetism, mechanical force or acoustic waves to assess the test object. What follows is a brief introduction to some of the widely used NDT methods in the aerospace industry and examples of their applications to composite materials.

15.4.1.1   Optical NDT

One of the simplest inspection methods commonly used to detect surface abnormalities is visual inspections by means of optical devices such as magnifying glasses, borescopes, fibrescopes and videoscopes. Visual inspection is usually sufficient for only a superficial detection of abnormalities that would require more thorough examination through more advanced NDT methods (Fahr, 2014). Fig. 15.9 shows an example of visual inspection to detect cracks and discontinuities that appear on the surface of an aircraft component. Although preferred due to its simplicity and cost efficiency, optical NDT may be of limited usefulness as a means to inspect composite parts where in-service damage and/or manufacturing flaws are embedded inside the part and therefore not visible to the surface for them to be detected via optical means.

15.4.1.2   Liquid penetrant–assisted NDT

Liquid penetrant–assisted NDT is typically used for the detection and examination of open-to-surface flaws. Penetrant materials usually contain two or more dyes that fluoresce when exposed to ultraviolet radiation. The ASTM Standard Practice for Liquid Penetrant Testing is detailed in ASTM E1417. Liquid penetrant–assisted NDT typically consists of five main stages; cleaning the test surface, applying the penetrant to the test part, dwell time, removing the excess penetrant from the part and finally inspecting the component using various means such as optical microscopy or radiography. With the latter, radiation is passed through the test object and is projected on a recording film to study the interior of the test object. The radiation is in the form of

Figure 15.9 A crack on aircraft components inspected visually.
Adapted from Industrial NDT. http://www.industrialndt.com/visual-testing.html.

either electromagnetic rays of short wavelengths (such as X-rays and gamma rays) or neutron particle radiation. The existence of defects and internal imperfections such as pores, cavities, inclusions or cracks affects the amount of radiation absorption by the test object which is projected on films or other recording media.

Application of liquid penetrant—assisted NDT to fibre-reinforced composites has to be done with care to ensure that the liquid penetrant dye does not lead to any property deterioration through interference with the constituent matrix, the fibres or the bond between them.

15.4.1.3   Ultrasonic NDT techniques

Ultrasonic NDT techniques are based on the evaluation of signals resulting from the transmission and reflection of sound waves through the test material. Applicable sonic waves are typically within a certain frequency domain, ranging anywhere from 0.5 to 50 MHz. Upon encountering a discontinuity in the test area of the composite component, a portion of the ultrasonic energy is reflected back and received by a transducer, and typically displayed on a screen in the form of electrical signals. Ultrasonic testing is one of the most common methods for NDT of aerospace composites; it is typically used to locate voids, cracks and delaminations, as well as carry out thickness measurements (Fahr and Charlesworth, 1986).

Ultrasonic inspection results are typically presented in the form of an A, B or C-scan. In an A-scan, the transmitted signal is displayed, typically on an oscilloscope in the form of a distance travelled by the signal through the component thickness versus the signal amplitude. The B-scan depicts the results of a linear scanning of the test area displayed as a time lapse between the flaw echo and the test part's front surface as a function of the position of the probe along a chosen scan line. The C-scan representation is essentially a planar view of the A-scan displacement versus amplitude information in the form of a colour map where different colours represent different levels of signal transmission. Uniform colour maps indicate uniform signal transmission and therefore no defects or at least none that are of the magnitude to affect signal transmission. Conversely, variations in colours on the map indicate the existence of signal affecting the types of flaws or defects (Fahr and Charlesworth, 1986).

15.4.2   Advanced NDT methods

The maintenance and inspection of aerospace structures made from advanced composites pose new challenges to the conventional NDT techniques. Introduction of more advanced NDT methods as well as optimization of the existing NDT techniques are key to addressing these challenges. In this subsection, some of the more advanced and optimized NDT methods used mainly in the aerospace industry are briefly introduced.

15.4.2.1   Infrared (IR) thermography

IR thermography provides a noncontact measure of the surface temperature of an object under a thermal excitation. The existence of defects and discontinuities will affect the heat flow which is related to the local differences in the surface temperature. These

temperature differences are detected by an IR camera which typically produces a colourful thermal image of the component under inspection.

There are two main types of thermography: passive thermography and active thermography. In passive thermography, the IR camera is simply pointed at the test object and the surface temperature is monitored during the normal use of the object (Montesano et al., 2013). With active thermography, the test object is heated by an external source that can be optical, mechanical, thermal or electromagnetic, and the resulting heat signature response is analysed (Riegert et al., 2006). Internal defects are displayed by mapping the surface temperature distribution or monitoring the differences in the temperature change rate. The heat may be applied to the test part either in the form of a short pulse (pulsed thermography) or in the form of a periodic excitation (lock-in thermography). This excitation can be performed through optical means or by the injection of high-power ultrasound. Fig. 15.10 shows an IR thermographic image of a mechanically cycled (fatigue) composite materials test specimen showing an area of delamination initiation.

15.4.2.2 Laser-based ultrasound techniques

In this technique, a spot on the surface of the test object is heated by a pulsed laser, causing a rapid thermal expansion of the material which in turn produces stress waves. The frequency of these waves is related to the laser-pulse rise time, which can generate ultrasonic waves through the proper pulse duration. Similar to the conventional ultrasonic method, these ultrasonic waves are reflected upon encountering internal defects and discontinuities. These waves cause a small displacement detected optically by means of a continuous-wave laser interferometer (Fahr, 2014). This method has been successfully used to inspect composite material parts of complex geometry, such as radoms, spars, wings and fuselage panels, at a speed comparable to a conventional C-scan system on flat panels (NDT). Fig. 15.11 shows the laser ultrasonic C-scan of the carbon−fiber reinforced polymer (CFRP) wing of a Falcon 10 jet.
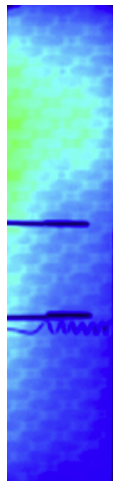
Figure 15.10 An IR thermographic image of a composite materials test specimen showing an area of delamination initiation on the top left.
Courtesy of FRAMES.

C-Scan - amplitude   C-Scan - time of flight
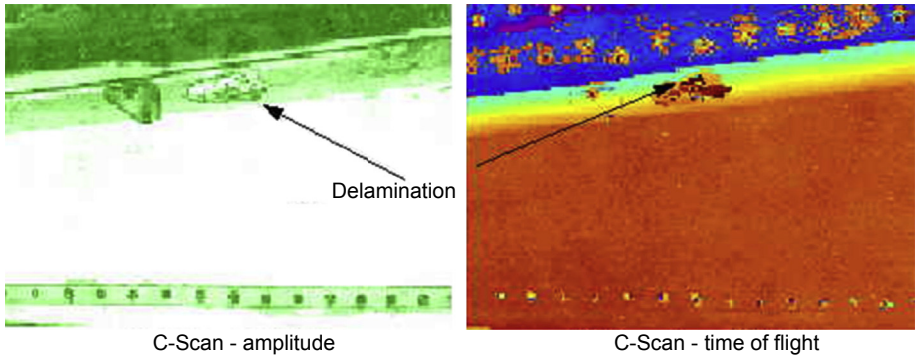
Figure 15.11 Laser ultrasonic C-scan of a Falcon 10 jet CFRP wing.
Adapted from Tretout, H., 1998. Review of advanced ultrasonic techniques for aerospace
structures. In: ECNDT, Denmark.

15.4.2.3 Laser shearography

One of the more advanced NDT methods with unique applications in aerospace is laser shearography. In this method, the surface of the test part is subjected to light from laser sources, and a shearing interferometer is used to laterally shear the reflected beam with respect to a reference beam. This leads to generating a sheared speckle image of the object that is then monitored by a charge-coupled device (CCD) camera. This NDT technique is mainly used for the inspection of composite sandwich panels with honeycomb cores and CFRP or aluminium skins in order to detect and measure the impact damage.

NDT has become an essential part of the comprehensive quality assurance philosophy and process that advanced aerospace composites are subjected to. Given their unique manufacturing methods and the inherently associated human error elements, composites are significantly more prone to defects and anomalies, which can be of a huge detriment to their structural integrity. This vulnerability is further compounded by this class of materials' inherent sensitivity to small and often barely or not visible in-service damage, such as those caused by relatively low-energy impact. It is therefore of paramount importance to have access to nondestructive inspection capabilities that are adequate for detecting those defects and damage forms in an accurate and timely fashion. Current NDT technologies, while arguably quite advanced and adequate within a research and development framework, continue to be slow and not fully optimized for in-field and maintenance types of inspections. In this regard, portability and speed of inspection continue to be among the main challenges facing NDT of aerospace composites and therefore among the key subject areas of ongoing NDT research and development efforts.

15.5 Airworthiness considerations

Airworthiness regulations are state-mandated requirements that govern aviation industry products and are meant to ensure the safe operation of flight vehicles throughout their intended service life. A key regulatory requirement in this context is to ensure

the structural integrity of a flight vehicle under all possible flight conditions, even those that may be very unlikely to occur. In this context, the retention of sufficient strength and stiffness to ensure safety throughout the life of an aerospace structure under all possible service conditions is among the main areas of regulatory concerns.

The use of advanced composite materials in airframes poses unique challenges from an airworthiness perspective. The lack of long-standing experience similar to that available for their metallic counterparts combined with the elevated degree of uncertainty associated with the structural properties and attributes of advanced composites dictate special airworthiness considerations as briefly discussed in the next two subsections.

15.5.1 Certification

Various government regulatory bodies such as the FAA or the Joint Aviation Authorities (JAA) have in place, in addition to the general regulations, special provisions that pertain specifically to the certification of composite structures. Those typically come in the form of an Advisory Circular (AC) that provides regulations and requirements that are specific to the application of composite structures, particularly those that are essential in maintaining the overall flight safety of the aircraft. In particular, the FAA's advisory circular AC No: 20−107B is the document that contains the special provisions for composite aircraft structures (Federal Aviation Administration, 2009). The circular discusses a number of issues related to the airworthiness of composite aircraft structures, including material and fabrication development, static, fatigue, damage tolerance and aeroelastic proof of structure, continued airworthiness and a number of other considerations such as crashworthiness and fire protection.

15.5.2 Design allowables

Design considerations for composite aircraft structures are primarily concerned with damage tolerance requirements. As discussed earlier in this chapter, composite structures are prone to defects such as poor bonding between the matrix and fibres, wrinkles in fibres, porosity and delamination, all of which can develop during their manufacturing process. Composite parts can also suffer damage during shipping and assembly. Furthermore, low-velocity impacts can cause barely visible yet serious damage to a composite laminate or sandwiched structure. Damage tolerance requirements specify, therefore, the ability of a structure to operate safely with such initial defects or in-service damage. As mentioned in this chapter, certification requirements are typically given in governments' Airworthiness Regulations, such as the Federal Aviation Regulations of the FAA (Parts 23 and 25) and its Advisory Circular AC 20−107B. Design allowables dictated by such regulations may be summarized as follows:

- Undamaged structure (category 1 damage) as well as damaged structures whose repair can wait (ie, damage may be tolerated until regularly scheduled maintenance) (category 2 damage) must safely withstand the limit load of the aircraft plus a 50% safety factor, that is, a limit load times 1.5, referred to as the ultimate or design load.

- Damaged structures requiring immediate repair (category 3 damage) must still be able to withstand limit load.
- Structures suffering from discrete source damage (category 4 damage) must carry 70% of limit manoeuvre loads and 40% of limit gust loads combined with maximum appropriate cabin pressure (Poe, 1996). Some examples of category 4 damage cited in AC 20−107B include rotor burst, bird strikes, tire bursts and severe in-flight hail.

With regard to damaged structures, AC 20−107B specifies that 'the extent of initially detectable damage should be established and be consistent with the inspection techniques employed during manufacture and in service'. Preference for in-service in-spections is usually given to the simple, inexpensive methods such as the optical methods discussed earlier in this chapter.

One last category of damage, designated as category 5, is the severe damage created by anomalous ground or flight events. As such, category 5 damages do not have asso-ciated damage tolerance design criteria or related structural substantiation tasks. Fig. 15.12 adopted from AC 20−107B provides a schematic diagram of design load levels associated with the various damage categories.
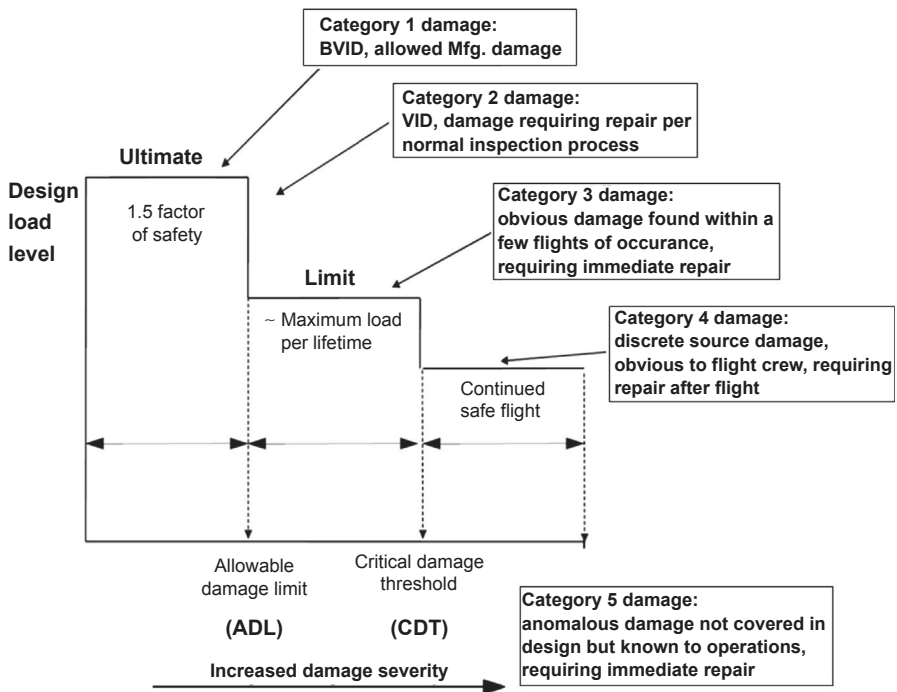
Figure 15.12 Schematic diagram of design load levels versus damage categories.
Adapted from Federal Aviation Administration: AC 20-107B − Composite Aircraft Structure, 2009. www.faa.gov/regulations_policies/advisory_circulars.

15.6   Conclusion

Due to their unique nature, advanced composite materials used in aerospace applications dictate a correspondingly unique quality control process. The process begins with ensuring that the composite constituent materials and prepreg forms meet the stringent requirements of the aerospace industry. The consolidation of parts and structures from such basic building blocks dictates another set of quality control measures to ensure that the end product meets the strict quality requirements for its intended use. This chapter has presented a brief discussion of those quality control measures and delved into a presentation of the various destructive and nondestructive tests that are conducted at various stages of the qualification process, wrapping up with a brief discussion of some relevant airworthiness considerations. As the use of advanced composites continues to proliferate at the very rapid rates that were seen in the last two decades or so, their quality control methodologies and processes will continue to evolve. A coverage like the one presented in this chapter will therefore serve as a starting point that will help set the stage for a more in-depth understanding of this very important topic.

References

ASTM International. http://www.astm.org/Standards/composite-standards.html.

Botelho, E.C., Silva, R.A., Pardini, L.C., Rezende, M.C., 2006. A review on the development and properties of continuous fiber/epoxy/aluminum hybrid composites for aircraft structures. Materials Research 9 (3), 247−256.

Composite Materials Handbook, MIL-HDBK-17-3F. Quality Control of Production Materials and Processes, vol. 3, 2002 (Chapter 3).

Composite Materials Handbook CMH-17. Polymer Matrix Composites: Guidelines for Characterization of Structural Materials, vol. 1, 2012. SAE International, ISBN 978-0-7680-7811-4.

CompositesWorld. http://www.compositesworld.com/articles/fabrication-methods.

Fahr, A., Charlesworth, A.M., 1986. An Introduction to the Ultrasonic C-Scan Inspection of Advanced Composite Materials. NRC Report: LTR-ST-1602.

Fahr, A., 2014. Aeronautical Applications of Non-destructive Testing. Destech Publications, Inc.

Federal Aviation Administration: AC 20-107B − Composite Aircraft Structure, 2009. www.faa.gov/regulations_policies/advisory_circulars.

Federal Aviation Regulations Part 21. http://www.faa-aircraft-certification.com/far-21.html.

Hsu, D.K., 2008. Nondestructive inspection of composite structures: methods and practice. In: 17th World Conference on Nondestructive Testing, October 25−28, 2008, Shanghai, China.

Industrial NDT. http://www.industrialndt.com/visual-testing.html.

Montesano, J., Fawaz, Z., Bougherara, H., 2013. Use of infrared thermography to investigate the fatigue behavior of a carbon fiber reinforced polymer composite. Composite Structures 97, 76−83.

Poe Jr., C.C., 1996. Residual Strength of Composite Aircraft Structures with Damage. In: ASM Handbook, Fatigue and Fracture, vol. 19. ASM International, pp. 920−935.

QUALITEST. http://www.worldoftest.com/gel-timer.

Riegert, G., Pflleiderer, K., GerHard, H., Solodov, I., Busse, G., 2006. Modern methods of NDT for inspection of aerospace structures. In: ECNDT.

Schubel, P.J., Crossley, R.J., Boateng, E.K.G., Hutchinson, J.R., 2013. Review of structural health and cure monitoring techniques for large wind turbine blades. Renewable Energy 51, 113−123.

Tretout, H., 1998. Review of advanced ultrasonic techniques for aerospace structures. In: ECNDT, Denmark.

Conclusions and future trends

16

S. Rana, R. Fangueiro
School of Engineering, University of Minho, Guimarães, Portugal

16.1   Summary

Fibre-reinforced composites (FRPs) have been extensively utilized in aerospace applications in military and civil aircrafts, space crafts and satellites. The main features which led to the tremendous growth of composite materials' use in aerospace structures are their light weight, high specific strength and stiffness and the possibility to tailor their shape, structure and functionalities according to requirements. In near future, FRPs, especially carbon fibre-reinforced composites, will constitute more than 50% of the weight of aircraft structures.

Different types of advanced fibrous architectures (two-dimensional (2D) and three-dimensional (3D) woven, knitted and braided) have been developed and used as preforms of composite materials. 3D fibrous architectures contain through-the-thickness yarns that improve the composite materials' z-directional properties, but at the cost of inferior in-plane mechanical properties. Therefore, although directionally oriented (DOS) 2D fibrous architectures have been employed commonly for aerospace applications, 3D fibrous architectures also have excellent prospects in the aerospace industry. Similarly, sandwich composites, developed by combining stronger skins with lightweight core materials, have high potential for aerospace applications due to their light weight and high in-plane and flexural stiffness. Currently, sandwich composites have been utilized in the fuselage of commercial aircrafts. Sandwich composites made of advanced 3D sandwich fibrous architectures with integrated face and core solve the delamination problems and may be advantageously utilized in future for aerospace parts.

Metal and ceramic matrix composites (MMCs and CMCs, respectively) are also excellent materials for aerospace structural parts. They present several advantages such as high fracture toughness, ductility, strength and stiffness, high temperature resistance, fire resistance and so on. However, these composites are highly heterogeneous systems in terms of size, shape, spatial distribution and properties of the components. Therefore, for successful utilization of CMCs and MMCs in aerospace industries, reliable modelling and simulation techniques have to be developed in order to predict the structural behaviour and various properties of the structural parts fabricated with these composite materials.

Braided composites possess several advantageous properties which make them attractive for many advanced applications, including aerospace engineering. High shear and torsional strength and stiffness, high transverse strength and modulus, damage tolerance and fatigue life, notch insensitivity, high fracture toughness and

possibility to develop complex and near-net-shape composites are some important advantages of braided composites. The rocket nozzle, fan blade containment case, aircraft propellers, stator vanes and others are some aerospace structural parts constructed using braided composites.

Auxetic composites are a new class of composite materials exhibiting a negative Poisson's ratio (ie, they extend in the transverse direction when subjected to load in the longitudinal direction). They offer several beneficial properties such as high shear modulus, synclastic curvature, high damping resistance, high fracture toughness, enhanced crack growth resistance, high energy absorption capability and so on. Looking at these properties, their utilization in aircraft structures through further research and developments in this area is highly encouraging.

Nanotechnology has made it possible to design smart and high-performance materials with enhanced as well as new functionalities. The extensive use of nanomaterials in composites is due to their high surface area resulting in better interface and reinforcement efficiency, as well as the capability of introducing new features like electrical and thermal conductivity, electromagnetic shielding, self-sensing ability, gas barrier properties, fire retardancy and so on. In the aerospace sector, composites mainly reinforced with nanoclay, carbon nanotubes (CNTs) and metal nanoparticles have been utilized. A recently announced application of nanocomposites in the aerospace industry is the use of CNT composite in the wingtip fairings.

Multiscale composites are also a special class of nanocomposites that have been developed recently. These composites are hybrid in nature, containing reinforcements from different length scales (ie, macro, micro or nano). Targeting advanced applications like aerospace, multiscale composites have been developed by introducing various nanomaterials like CNTs, carbon nanofibres, nanoclay, metal nanoparticles and so on into conventional composites either by incorporating them within the fibre surface or dispersing them within the matrix. As compared to conventional composites, multiscale composites present enhanced in-plane mechanical properties, higher fracture toughness, impact properties, fatigue resistance, thermal stability and many other functionalities as observed in the case of other nanocomposites. Multiscale composites can be fabricated using any type of fibre and matrix system and utilizing a wide range of nanomaterials, achieving a broad range of properties; therefore, they are expected to be the future materials for aerospace applications.

Self-sensing composites can be very useful for aerospace structural parts to perform continuous monitoring of strain and damage. These composites can greatly improve the safety of aerospace structures and reduce maintenance by detecting the damages at earlier stages. Different types of self-sensing composite materials for aerospace applications include continuous carbon fibre−polymer matrix composites, short carbon fibre composites, hybrid carbon fibre−carbon particle composites, carbon fibre−glass fibre composites, glass fibre−carbon nanotube composites and so on. Change in the electrical contact points under loading conditions is the main cause for the change in the electrical resistivity of these composites. Strain and damage are sensed through measuring electrical resistivity on the surface of the composites (for sensing damage due to flexure), or volume resistivity (a change in fibre direction for sensing fibre fracture, or a change in the through-thickness direction for sensing delamination or in the oblique direction for sensing both fibre fracture and delamination).

Another innovative material to enhance the safety and reduce the maintenance cost of aerospace structures is the self-healing composite materials. Self-healing composites can perform automatic repairing of damage using healing agents (within microcapsules, hollow fibres or vascular networks) within the structure of composites. The initiation or growth of cracks breaks the containers of the healing agents, and as a result, healing agents are released and the cracks are repaired automatically without any external intervention. In contrast, some mechanisms of self-healing are operated by some external stimulus such as heat, pressure, radiation and so on, such as thermoplastic healing agents and reversible physical and chemical interactions. Therefore, the self-sensing property can be utilized to detect damage and activate the self-healing mechanisms. Consequently, self-sensing, self-healing composite materials can be designed and developed to provide highly safe, durable and low-maintenance materials for aerospace applications. These composites can be utilized to recover various performances of composites, including fatigue, impact, barrier and corrosion resistance and so on.

Carbon−carbon composites are excellent materials for aerospace applications and have been already utilized in space industries for re-entry heat shields; rocket nozzles; parts of gas turbine engines such as flaps, seals, liners, vanes and tail cones; and so on. The ability to maintain mechanical and physical properties at very high temperatures, a high degree of toughness and inertness and light weight are their extraordinary characteristics which make them highly suitable for aerospace applications. However, high cost and low efficiency of the fabrication process are the technical challenges restricting their extensive use in aircrafts and other applications.

Quality control is one of the most important requirements for application of composite materials in the aerospace sector, which demands high safety. Different steps of quality control for aerospace-grade composites include characterization of fibres (density, mechanical properties, thermal oxidative resistance, chemical composition analysis, electron and X-ray spectroscopy etc.), prepregs (determination and verification of fibre and resin contents, volatile and moisture contents, resin flow, gel time and tack etc.), the manufacturing process (cure monitoring), postcure verifications (fibre volume, void content, ply count and mechanical properties) and structural parts through nondestructive (NDT) testing (optical NDT, liquid penetrant-assisted NDT, ultrasonic NDT, infrared thermography, laser-based ultrasonication techniques etc.), various destructive testing methods (fibre content determination, microstructural characterization by scanning electron microscopy, mechanical testing such as tensile, compressive, shear properties etc.), moisture absorption and so on. These quality control and characterization processes should strictly follow the norms or standards used for the aerospace industry.

16.2   Conclusion and future trends

In conclusion, several types of composite materials (ie, laminated composites, sandwich composites, braided composites, carbon−carbon composites, nanocomposites etc.) are already in use for different aerospace applications. Substantial growth in composites' use in aerospace industry can also be observed. Additionally, newly developed

composite materials such as auxetic composites, multiscale composites and so on have huge prospects for aerospace applications and will be extensively employed in future. However, the main challenge for the wide utilization of composite materials in the aerospace industry remains the affordability and reliability of these materials. A great deal of research and developments is highly essential to improve the manufacturing processes of new composites in order to obtain improved quality at lower cost. As aerospace materials should provide high safety, stringent quality control measures should be undertaken at different stages of production and use of composite materials in aerospace structures. It is extremely essential to improve the existing modelling and simulation tools and also develop new methods for the recently developed composites, in order to reduce the emphasis on destructive characterization techniques. Improvement in the existing NDT methods is also necessary. Efforts should also be directed to improve the repairing techniques in order to reduce repair time and cost. In addition, strong emphasis should be placed on developing reliable self-sensing and self-healing technologies to reduce the maintenance cost and improve the service life and safety of aerospace structures. Nevertheless, it can be forecasted that composite materials with huge flexibility in terms of materials, structure and properties will replace the metallic parts in future aerospace structures.

Further reading

Cranfield, P.E., Soutis, C., 2014. Polymer Composites in the Aerospace Industry. Woodhead Publishing.

Mouritz, A., 2012. Introduction to Aerospace Materials. Woodhead Publishing, Elsevier.

Rana, S., Fangueiro, R., 2015. Braided Structures and Composites: Production, Properties, Mechanics, and Technical Applications. CRC Press.

Rana, S., Fangueiro, R., 2016. Fibrous and Textile Materials for Composite Applications. Springer.

Zagainov, G.I., Lozino-Lozinski, G.E., 1996. Composite Materials in Aerospace Design. Springer.

Index